University of Liège
Faculty of Science

Groupe Interdisciplinaire de Génoprotéomique Appliquée
Département des Sciences de la Vie
Laboratoire d'Organogénèse et Régénération

Hormones, Simulated Microgravity and Hypergravity affect Bone and other Physiological Systems in Zebrafish Larvae

By
Jessica Aceto

A thesis submitted in fulfillment of the requirements
for the degree of Doctor of Philosophy (Life sciences)
Academic year 2014-2015

Thesis Supervisor:
Professor Marc Muller

Acknowledgement - Remerciements

Je voudrais remercier le Professeur Martial de m'avoir accueillie au sein de son laboratoire, pour ses encouragements et sa positivité.

Je remercie tout particulièrement mon Promoteur Marc Muller de m'avoir donné l'opportunité de réaliser ce doctorat au sein de son équipe et d'avoir cru en moi du début jusqu'à la fin de la concrétisation de cette thèse. De m'avoir permis de m'ouvrir au monde par les congrès et collaborations qui m'ont énormément appris scientifiquement, permis de m'affirmer et de prendre confiance en moi.

Je tiens aussi à remercier les membres de l'équipe zebrafish, tous ces collègues qui m'ont permis de réaliser la transition entre le monde des études et le monde professionnel. Un peu trop nombreux pour tous les citer. Mais chacun à leur manière m'ont apporté, au quotidien, un nouveau point de vue sur la manière de travailler et d'évoluer au sein du labo. Une attention toute particulière pour remercier Marie Winandy qui a toujours pu trouver des solutions pour mes commandes poissons assez particulières ou de dernière minute. De même, un grand merci aux étudiants que j'ai eu l'occasion d'encadrer et avec qui j'ai pu grandir en expérience aussi.

I would like to thanks all the collaborators from the ESA MAP projects. Especially, Dr. Peter Aleström, Dr. Rasoul Nourizadeh-Lillabadi from Oslo and Dr. Jack van Loon from Amsterdam, for making me so welcome in their lab, their good advices and the rich scientific experience. As well Dr. Janette A.M. Maier and Dr. Massimo Mariotti from Milan, to welcome and integrate me in their lab.

De même, j'adresse un merci tout particulier aux bioinformaticiens Raphaël Marée, Olivier Stern et Nathalie Jeanray, ainsi qu'à Nadia Dardenne, statisticienne de l'Unité de soutien méthodes en Biostatistique et Epidémiologie de l'ULG. Toutes ces personnes ont participé et rendu possible l'analyse de **toutes** ces photos de zebrafish aussi bien qualitativement que quantitativement.

Je voudrais dire un tout grand et énorme merci à tous les gens extérieur au labo qui m'ont soutenu, évidemment je veux parler de mes ami(e)s et mes parents.

Je commencerais par mes ami(e)s ; Marie-Line, Bernard, Valérie, Geoffroy, Tsvetie, Christel, Nicole et tous les autres que je n'ai pas cité. Tous ont su être à l'écoute, présent, réconfortant et motivant pour que je puisse aboutir à la fin de ce travail.

Une pensée avec un grand merci à ma marraine et ses filles qui ont toujours eu des pensées positives pour moi, même de loin.

Et finalement, **le plus grand merci** est destiné tout naturellement à mes parents pour m'avoir soutenue, re- soutenue et re re-soutenue jusqu'au bout. Cela n'a pas été rose tous les jours… Malgré cela, j'ai pu compter sur leur compréhension et présence. Ils ont toujours respecté mes choix et même en période de doutes, ils m'ont toujours encouragée à ne pas perdre mes objectifs de vue.

TABLE OF CONTENTS

Abbreviation list

µg: microgravity

µScm^{-1}: microsiemen per centimeter

1α(OH)ase: 1,25-dihydroxyvitamin D-1α-hydrolase

1,25$(OH)_2$D3:1,25-dihydroxycholecalciferol

11βHSD2: 11β-hydroxysteroid dehydrogenase type 2

25-OH-D: 25-hydroxycholecalciferol

A

ACTH: adrenocorticotropic hormone

ALP: Alkaline phosphatase

ARED: Advanced Resistive Exercise Device

B

Bglap: bone gla protein or osteocalcin

BMD: bone mineral density

BMU: Bone multicellular unit

Bsp: bone sialoprotein

C

CEVIS: cycle ergometer with vibration isolation and stabilization

cNCC: cranial neural crest cells

Col: collagen

CLINO: clinorotation

CT: calcitonin

CTR: Calcitonin receptor

CRF: corticotropin-releasing factor

CRLR: Calcitonin receptor-like receptor

CTX: C-telopeptide

CYP24a1: Cytochrome P450, family 24, subfamily A, and polypeptide 1

D

DKK1: Dickkopf factors

DMSO: dimethylsulfoxid

DNA: deoxyribonucleic acid

DPD: deoxypyridinoline

dpf: day post-fertilization

DVL: Disheveled

E

ECM: extracellular matrix

ERK: extracellular signal regulated kinase

ESA: European space agency

F

Fz: Frizzeld

G

g: gravity

GADD45B: growth arrest and DNA damage-inducible

gag: glycoaminoglycan

gapdh: glyceraldehyde-3-phosphate dehydrogenase

gfp: green fluorescent protein

GR: glucocorticoid receptor

GSK3β: glycogen synthetase kinase 3-β

H

HES: Hairy enhancer of split

Hg: hypergravity

hpf: hour post-fertilization

HPI : hypothalamus-pituitary-interrenal

I

iRED: interim resistive exercise device

Ihh: Indian Hedgehog

IPA: Ingenuity Pathway Analysis

ISH: in situ hybridization

ISS: International Space Station

J

JNK: c-Jun terminal kinase

L

LDC: large diameter centrifuge

Lrp 5/6: low density lipoprotein receptor-related protein 5 or 6

M

MCR2: melanocortin 2 receptor

MITF: microphthalmia transcription factor

Mo: Morpholino

MR: mineralocorticoid receptor

mRNA: messenger ribonucleic acid

N

NFATc1: nuclear factor activated T cells, cytoplasmic, calcineurin-dependent 1

NCC: neural crest cells

NDRG: new family of differentiation-related genes

NDRG2: N-myc downstream regulated gene 2

NTX: N-telopepetide

O

OPG: osteoprotegrin

OPPG: osteoporosis pseudoglioma

Osx: osterix

P

PPARγ2: proliferator activated receptor γ2

PTH: parathyroid hormone

PTHR1: parathyroid hormone receptor type1

PTHrP: parathyroid hormone-related protein

PYD: pyridinium or pyridinoline

R

RANK: receptor activator of nuclear factor κB

RANKL: receptor activator of nuclear factor κB ligand

RHCG: Rh Type C glycoprotein gene

RNA: ribonucleic acid

RPM: random positioning machine

rpm: rotation per minute

RT-PCR: reverse transcriptase – polymerase chain reaction

RWV: rotating wall vessel

S

SAS: space adaptation syndrome

SMS: space motion sickness

Spp1: osteopontin

STC: stanniocalcin

T

TNF: tumor necrosis factor

TRAP: tartrate-resistant acid phosphatase

TTN: titine

TVIS: vibration isolation and stabilization

U

UBB: ultimobranchial bodies

V

VitD: Vitamin D

VDR: Vitamin D receptor

Introduction

Foreword

Human has always been fascinated the mystery of space. This space conquest has begun in 1957 with the first Russian spaceflight, Sputnik 1. Then, Americans have reached the moon and walked on it in June 1969. Since then, several Gemini missions and others have followed. Human's ambitions did not stop with the construction of the International Space Station (ISS), where the mission duration extends up to 6 months or longer. The ambition still progresses with the aim of Mars exploration in 2030. However, these space explorations are not without consequences (Hughes-Fulford 2011, McCarthy 2011).

Since the very beginning of spaceflight, with short-term missions, the effects of microgravity on the astronauts became apparent, inducing several physiological problems such as vestibular troubles, loss of muscular mass, circulatory problems, as well as weariness and psychological troubles (Blaber and all, 2010; Mc Carty,2011; Fong, 2008). Unfortunately, these effects do not stop there. With long duration spaceflight from 1 to 6 month, the astronauts presented a bone loss of 1 to 2% per month, due to a decrease of bone formation and a normal or increased rate of bone resorption (Collet, Uebelhart et al. 1997, Carmeliet and Bouillon 1999). This important bone loss is called the "astronaut's osteoporosis".

The mechanisms involved in this microgravity effect on bone are unknown despite many studies attempting to explain the process. Even if the astronauts are submitted to extensive physical exercise before and during the flight, bone loss remains significant and the astronauts do not recover their previous total bone mass after a recovery period as long as the spaceflight. Therefore, the fracture risk is increased on ground after return (Collet, Uebelhart et al. 1997, Vico, Collet et al. 2000, Sibonga 2013).

Thus, if humanity want's to achieve its ambition of a manned spaceflight to Mars (where the flight duration to reach Mars takes at least 6 months, spend some time for exploration and 6 months to return to Earth), it is imperative to find solutions, among others, to prevent bone loss.

Currently, the research uses various models and methods for a better comprehension of the process of bone loss, such as bed-rest, cultured cells, hindlimb unloading (suspension by the tail) rats or fish. The present work integrates into the bone problematic using the zebrafish as a model to study cartilage and bone formation under different environmental conditions, such as drug treatment, microgravity simulation or hypergravity.

1. Microgravity and its effects on humans in space

The gravitational force is a vector composed of a magnitude and a direction facing the center of the earth. Isaac Newton has discovered the universal law of gravitation in 1665-1666 and has developed the formula to evaluate the attractive force between two bodies:

$$F_g = G_u\, Mm/d^2$$

with "M" the mass of earth, "m" the mass of the object, "d" the distance between the center of the two masses and "G_u" the universal gravitational constant = 6.67 x 10^{-11} $m^3/kg.s^2$. The higher the distance between the two bodies, the smaller the gravitational force between them. Any object on the earth's surface is submitted to a gravity force equal to 1g. The microgravity experienced during a space mission in orbit is not due to the distance between the spacecraft and earth, rather the gravitational force is decreased by the centrifugal force produced by the speed of the spacecraft in a circular orbit, actually initiating a continuous free fall (Fig. 1). Taking into consideration the mass and the gravitational force, the microgravity corresponds to 10^{-3}g on ISS, up to 10^{-5}g in the drop towers and 10^{-2}g during parabolic flight. The zero gravity (0g) is actually never reached (Morey-Holton 2003, Schmidt 2004).

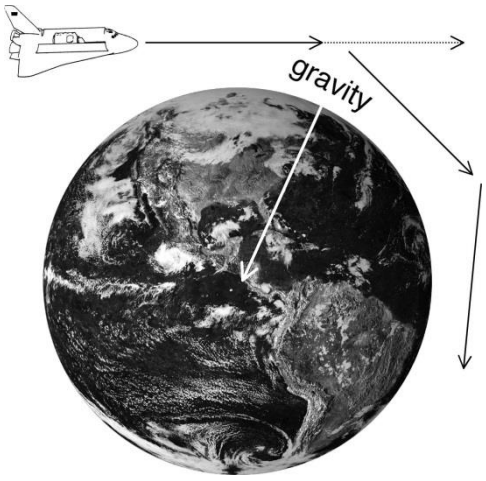

Figure 1: Forces acting on the spacecraft's trajectory leading to free fall and circling of the earth (Morey-Holton 2003).

Astronauts are also submitted to microgravity and experience several physiological effects during each flight. The human body is designed to live in 1g, not in microgravity. Here, we describe the most affected systems. The cardiovascular system endures some modifications. The fluids (blood and plasma) are shifted from the lower to the upper part of the body, inducing a face oedema during the first days in space. Higher blood volume in the head

informs the fluid volume sensors and causes a general fluid elimination through the renal system, resulting in a globally decreased blood plasma volume (Fong 2004, Vernikos and Schneider 2010). The heart rate is also decreased. After return on earth, astronauts have some difficulties to stand or walk; the fluids move rapidly from the head to the legs, inducing leg oedema. Even after short term flight, 60 to 70% of the astronauts cannot stand 10 minutes without falling into syncope (Williams, Kuipers et al. 2009).

The neurovestibular system is destabilized in microgravity due to contradictory sensory signals from the inner ear to the brain, thus producing a space adaptation syndrome (SAS). The SAS is a sensory adaptation to microgravity and is the reason of space motion sickness (SMS) symptoms like vertigo, nausea and vomiting. Proprioception is linked to the otolith organs present in the inner ear, and is very important for locomotion and position. The central nervous system needs between 1 and 3 days to adapt the visual, vestibular and sensory systems to the disorientation caused by microgravity. This adaptation is not complete and is progressive during the entire flight. Return to ground provokes again confusion in the sensory system, causing difficulties in upright standing. This instability can be further accentuated by the fluid shift from the cardiovascular system mentioned above. Moreover, the longer the duration of the mission, the longer it takes to re-adapt again to the 1g on earth (Fong 2004, Vernikos and Schneider 2010).

The musculoskeletal system also undergoes some modifications. Without gravitational load, the skeletal muscles responsible for posture and ground support lose their basic functions. This effect, added to the fluid movement into the head, leads to a decrease in bone and muscle loading (Morey-Holton 2003, Ohira, Kawano et al. 2015). The decrease of the skeletal muscle function is rapidly detectable and progresses during the entire spaceflight. All the leg muscles are affected. The postural muscles, the support muscles of the spinal cord and the neck are not useful as they are on earth and are the most affected. The muscle mass, power and velocity of contraction for these muscles are decreased, leading to muscular atrophy. The skeletal system will be affected later, due to decreased muscle load. In addition, the fluid shift and fluid loss mentioned earlier leads to increased calcium excretion, which may induce a loss of calcium from bone. The higher renal calcium excretion also increases the risk to form kidney stones (Morey-Holton 2003, Fong 2004, Vernikos and Schneider 2010, Blaber, Marcal et al. 2010).

2. Skeleton development in vertebrates

The skeletal tissue is formed by several specialized connective tissues such as cartilages, bones and tendons. The skeleton fills several important roles such as support for the whole body and attachment point for the soft organs. For example, the lower limbs are the pillars when we stand up. A further role concerns protection of the brain and the spinal cord by, respectively the cranial bones and the vertebrae. Another role involves movement through the attachment of the skeletal muscles by tendons. This connection ensures the ability to walk, catch an object or breathe. In addition, the skeletal system represents a crucial mineral storage, most importantly for calcium and phosphorus. These minerals are released into the blood circulation and distributed in the whole body. They are nearly constantly deposited and removed from bones. Finally, the bone marrow plays a role in hematopoiesis for formation of red blood cells and other blood cells (Marieb 1999).

2.1. Cartilage

Cartilage is a semi-rigid tissue. Indeed, this tissue confers rigidity and flexibility to the structures it supports. In contrast to other connective tissues, cartilage is not innervated nor vascularized. Cartilage is composed of cells, fibers and the extracellular matrix (ECM). The cells are chondroblasts (immature cells) or chondrocytes (mature cells). The ECM is composed of glycosaminoglycans (GAGs), of proteoglycans, elastic fibers, collagen type II (Col 2), and it contains up to 80% of interstitial fluid. This high level of tissue hydration allows cartilage deformation by compression and back into shape without injury.

2.1.1. Cartilage development

Cartilage generally derives from mesenchymal cells that have 2 different origins. Neural crest cells (NCC) at the level of the hindbrain form part of the cranial cartilage, while the mesoderm gives rise to the axial skeleton and the limbs. The NCC can also give rise to other tissues such as neurons, glial cells and pigment cells. Cartilage formation begins with the mesenchymal condensation. The cells form aggregates and increase their interactions. They begin to express a transcription factor, the sex determining region Y (SRY)-box9 or Sox9, and initiate differentiation of the mesenchymal cells into chondroblasts. Sox9 activates expression of collagen IIα1 (Col2a1), collagen XIα2 (Col11a2), Sox5 and Sox6. The two latter are transcription factors essential for collagen IXα1 (Col9a1) expression and the production of proteoglycans. At that stage, there are two possibilities of cartilage progression: to continue as

cartilage tissue with all the properties described above, or evolve into hypertrophic chondrocytes and induce the endochondral ossification described later. The trio Sox5, Sox6 and Sox9 are acting until chondrocyte hypertrophy. Sox9 is a negative regulator of hypertrophic chondrocytes (Quintana, zur Nieden et al. 2009, Shum and Nuckolls 2002, de Crombrugghe, Lefebvre et al. 2001).

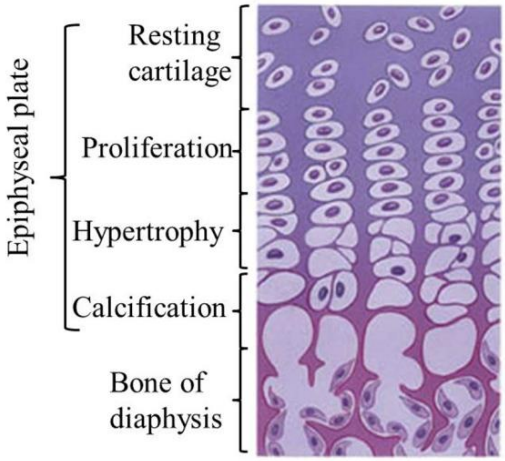

Figure 2: Cartilage development and chondrocyte differentiation with the different phases of differentiation. Adapted from https://www.boundless.com/biology/textbooks/boundless-biology-textbook/the-musculoskeletal-system-38/bone-216.

There are two different types of cartilage growth. First, the interstitial growth where the chondrocyte is present in a lacuna and can divide to form isogenic groups or produce the ECM. The cartilage develops from the inside. The second sort of cartilage development is appositional growth. The perichondrium is a connective tissue surrounding almost all cartilages and formed by two layers: an external layer composed of fibroblasts, well vascularized and playing a role in nutriment diffusion into the ECM towards the chondrocytes. The internal layer is chondrogenic. The immature cells present in this layer are able to proliferate and differentiate into chondroblasts. They synthetize the ECM and permit a growth in thickness by successive apposition (Marieb 1999).

2.1.2. Different cartilage types

There are different types of cartilage depending on the type and proportion of fibers it contains. They are all composed of the basic chondrocytes confined into the lacunae and surrounded by the ECM (Marieb 1999).

- The hyaline cartilage is the most expanded in the human body (Fig. 3A). Chondrocytes cover only 1 to 10% of this tissue, and it presents a perichondrium. The collagen matrix is

almost entirely composed of collagen type II. Chondronectin ensures the connection between the chondrocytes and the collagen fibers. The GAG is predominantly composed of chondroitin sulfate. This type of cartilage is the template for the endochondral ossification described later. It is also found in the articular cartilage, the respiratory system, the link between the ribs and the sternum, and the nasal septum.

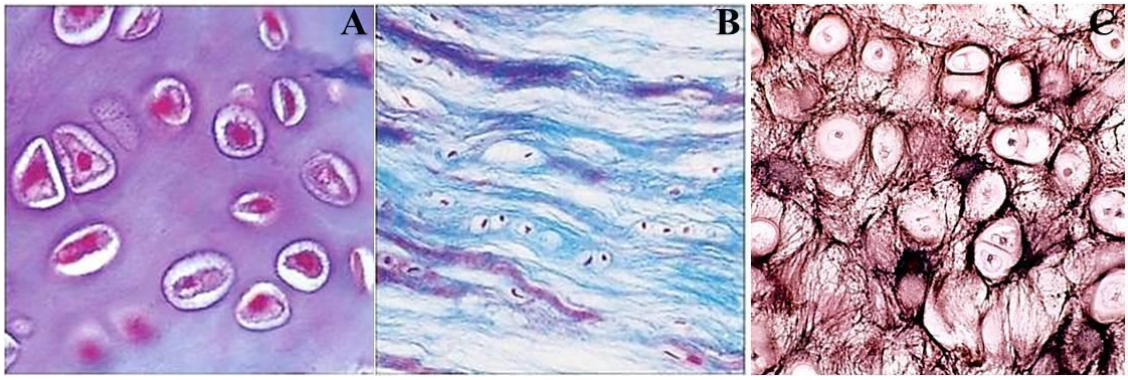

Figure 3: The different types of cartilage. A: hyaline cartilage. B: fibrous cartilage. C: elastic cartilage (Marieb 1999).

- The fibrous cartilage or fibrocartilage is based on the superposition of a row of chondrocytes alternating with an abundant row of collagen type I fibers (Fig. 3B). The ECM presents less proteoglycans. This cartilage is more resistant to pressure or stretching and is less flexible. This type of cartilage is located in the meniscus, the intervertebral discs and at the insertion of the ligaments or tendons.

-The elastic cartilage is histologically very close to the hyaline cartilage (Fig. 3C). The difference is the presence of a high level of elastin fibers. This type of cartilage has a better resistance to repeat flexion and is situated in the outer ear, a part of the Eustachian tube and the epiglottis.

2.2. Bone and its development

In contrast to cartilage, bone is a rigid, vascularized and innervated tissue. The general bone structure is formed by a periosteum surrounding the bone surface and a central part called the cancellous bone. Compared to the perichondrium in cartilage, the periosteum has two different layers: the external layer composed of an irregular, dense connective tissue, and an internal osteogenic layer. The cancellous bone is formed by bone span and can contain the hematopoietic bone marrow. Two important types of cells constitute the bone tissue:

osteoblasts and osteoclasts. The ECM is characterized by a mineralized matrix due to deposition of hydroxyapatite (calcium phosphate) crystals. The extracellular mineralized matrix is called osteoid tissue and is composed of collagen fibers almost entirely made of collagen type I (col1), proteoglycans and glycoproteins, most of which are secreted by osteoblasts (Marieb 1999). Different types of bone development exist to form the dermal and the endochondral bones.

2.2.1. Endochondral ossification

As already mentioned in the cartilage development, endochondral ossification needs a cartilage template to form the future bone (Fig. 4). The hypertrophic chondrocytes are the first step to move towards ossification. The particular status of hypertrophy involves morphological and molecular changes in chondrocytes. Morphologically, the cells are larger (Fig. 2).

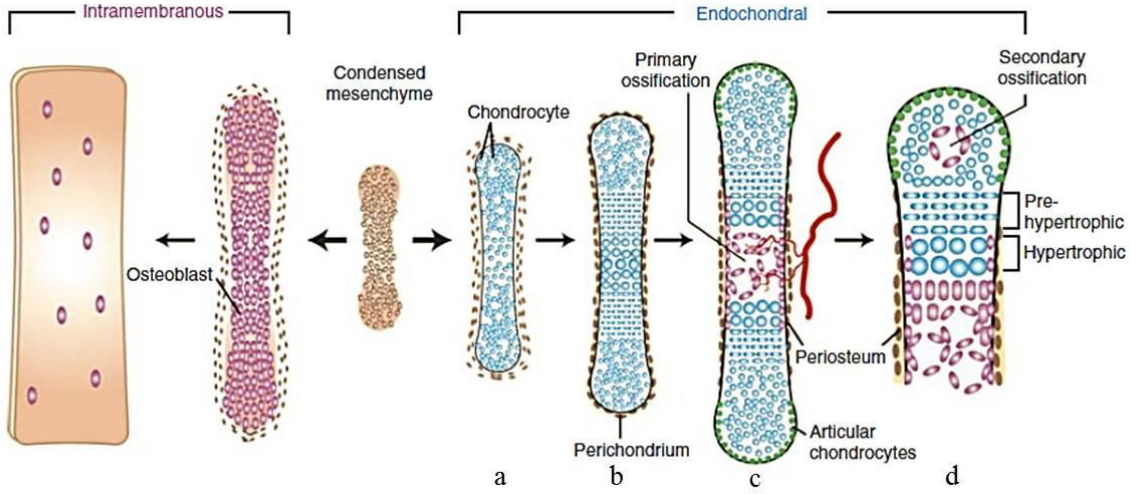

Figure 4: Scheme of the 2 types of ossification. On the right side of the condensed mesenchyme, endochondral ossification is shown with the bone collar around the cartilage (a), different stages of chondrocytes (b), blood vessel invasion and formation of the primary ossification including osteoblast colonization and secretion of osteoid (c) and the secondary ossification center in the epiphysis (d). On the left side of the condensed mesenchyme, intramembranous ossification is represented with osteoblast differentiation and direct bone formation (Regard, Zhong et al. 2012).

At the molecular level, Runt-related transcription factor 2 or Runx2 is essential to develop mature chondrocytes and for osteoblast differentiation. Runx2 is expressed in immature chondrocytes, stops proliferation of chondrocytes which then become hypertrophic. Runx3 plays the same role as Runx2, but at a lesser level and in cooperation with Runx2 to induce chondrocyte hypertrophy (Kobayashi and Kronenberg 2005, Provot and Schipani 2005).

Runx2 induces collagen X and Indian Hedgehog (Ihh) expression. Ihh is expressed in non-proliferating cells and increases chondrocyte proliferation by stimulation of the parathyroid hormone-related protein (PTHrP) production at the ends of developing bones. The negative feedback of Ihh and PTHrP delays chondrocyte hypertrophy and keeps the chondrocytes in proliferative status (Shum and Nuckolls 2002, Kronenberg 2003). Hypertrophic chondrocytes stop to express collagen II and start to express and secrete the vascular endothelial growth factor (VEGF) in the ECM to promote invasion of blood vessels in the cartilage matrix. The blood vessels provide the phosphocalcic salts into the matrix around the chondrocytes and form the calcified cartilage. Hypertrophic chondrocytes initiate apoptosis and the calcified cartilage is invaded by osteoblasts and osteoclasts from blood vessels. Finally, the cartilage is replaced by bone tissue.

The perichondrium acquires an osteogenic potential and becomes a periosteum. The mesenchymal cells differentiate into osteoblasts secreting non mineralized bone matrix, also named osteoid. This osteoid is mineralized later to form first the reticular bone and the osteoblasts differentiate into osteocytes when they are confined in the matrix (Fig. 4).

After remodeling in the central part and the periosteum, the reticular bone turns into compact, lamellar or cancellous bone (Dirckx, Van Hul et al. 2013).

2.2.2. Intramembranous ossification

This type of ossification is not built on a cartilage matrix and forms flat bones. Almost all of these flat bones are located in the cranial bones and the clavicles. These bones are also named dermal bones. Some mesenchymal cells from the vascularized connective tissue aggregate and differentiate directly into osteoblasts to create an ossification center. The bone matrix is secreted by the osteoblasts and mineralizes (Fig. 4). Later, the osteoblasts are differentiating into osteocytes, while other osteogenic cells differentiate into new osteoblasts. The bone matrix forms a trabecular network and traps the blood vessels to develop the cancellous bone. The surrounding mesenchyme cells promote external clusters to form the periosteum by the same process. The trabeculae under the periosteum continue being thicker to form woven bone. Later, this woven bone will be replaced by a denser and stronger compact bone. The internal part remains cancellous bone and its vascular tissue evolves into red marrow (Marieb 1999, Franz-Odendaal, Hall et al. 2006, Regard, Zhong et al. 2012).

2.3. Bone remodeling

2.3.1. Osteoblast formation and development into osteocytes

Ontogenetically, the skeletal tissues derive from 3 embryonic lineages: the paraxial mesoderm forms the axial skeleton (spinal column, rib cage and sternum), the neural crest cells (NCC) and the lateral plate mesoderm give rise to the craniofacial skeleton, while limbs are also derived from the lateral plate mesoderm (Ganss and Jheon 2004, Hall 2005).

Similar to chondrocytes, the osteoblasts have a mesenchymal origin. These mesenchymal stem cells are able to differentiate into several types of tissue, depending on the extracellular signals they receive and transcription factors that are induced. They become adipose tissue with the induction of PPARγ2 (proliferator activated receptor γ2), muscle tissue upon induction of MyoD, while Sox9 characterizes chondrogenesis and Runx2 is essential for osteogenesis (Marie 2001).

In the literature, several types of classification exist to distinguish the different stages of osteoblast formation until finally the osteocytes. In general, three categories are primordial: pre-osteoblasts, osteoblasts or mature osteoblasts and osteocytes. Billiard and collaborators have defined more categories by the subdivision of mature osteoblasts into early and late mature osteoblasts and an additional stage differentiating pre- and mature osteocytes. Franz-Odendaal and colleagues have described 8 categories according to their morphological observations. These additional categories have not been correlated with the expression of specific markers, such as *Alp*, *Sost*, *Dkk1*. Therefore we will use here the more simple classification. We will distinguish the general categories with each stage having its own molecular properties (Fig. 5).

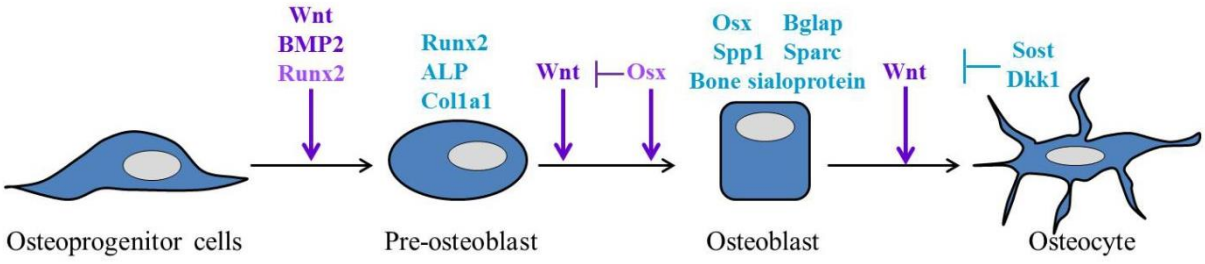

Figure 5: Osteoblast development and differentiation into osteocytes. The factors in dark purple are extrinsic signals, such as for Wnt and BMP, the others in light purple (such as Runx2 and Osx) are intrinsic or cell-autonomous signals.

Mesenchymal stem cells require the presence of BMP2 and Wnt signals to induce Runx2 expression and initiate the osteogenic precursor cell. Runx2 will be expressed during osteoblast differentiation and has an anti-proliferative effect. Osx expression follows Runx2 expression and induces osteoblast differentiation (Lian, Stein et al. 2006). Alkaline phosphatase (ALP) is also a proliferative marker. ALP, as well as collagen type 1 (col1a1) are already expressed in the pre-osteoblasts and continue in mature osteoblast (Billiard, Moran et al. 2003). These mature osteoblasts express osteocalcin (Bglap), osteopontin (Spp1), bone sialoprotein (Bsp) essential for bone matrix mineralization (Bodine, Trailsmith et al. 1996, Marie 2001, Karsenty 2008).

The main function of the osteoblast is the synthesis and the mineralization of the extracellular matrix. The osteoblasts secrete Col1a1 as well as other matrix proteins, such as osteocalcin, osteopontin, fibronectin and Bsp. Another function concerns the bone turnover by production of OPG (osteoprotegerin) and RANKL (receptor activator of nuclear factor κB ligand) released into the extracellular matrix to induce the osteoclast precursors. In consequence, the osteoblasts act also in bone turnover and bone repair. They also produce the collagenase enzyme necessary for matrix degradation (Marie 2001).

After maturation, when the osteoblasts stop to synthesize the bone matrix, they have 3 ways to evolve. First, the osteoblast can convert into quiescent cells located on the bone surface, also called lining cells. Second, they can undergo apoptosis, and third, they can become embedded into the bone matrix and differentiate into osteocytes (Dallas, Prideaux et al. 2013).

Morphologically, the osteoblasts are cuboid and form a layer of cells at the bone surface with their precursor cells. The lifespan of a human osteoblast can reach 2-3 months with a deposit of 0.5 to 1.5µm of osteoid per day. The osteocytes are the most abundant bone cell with 90% of bone cells in adults. They can be considered as a totally differentiated and specialized osteoblast (Sommerfeldt and Rubin 2001, Franz-Odendaal, Hall et al. 2006). They are smaller than osteoblasts. In 1986, Palumbo estimated a decrease of the cell body volume of about 70% between the osteoblast and the osteocyte stage. Osteocytes are trapped in the bone matrix and present a stellar form. The cellular body is confined in a lacuna of 15 to 20µm diameter. Dendritic processes penetrate the bone matrix via canals called canaliculi. The lacuna and the canaliculi form the lacunocanalicular system (Sommerfeldt and Rubin 2001, Dallas, Prideaux et al. 2013). They are regularly spaced within the bone matrix; the mechanism of this arrangement is not yet clear. Some osteocytes sacrifice themselves by apoptosis to initiate

bone remodeling. Others are viable until the death of the organism. Those have a very low turnover and develop survival mechanisms against stress resulting from aging, hypoxia, immobilization or diseases (Dallas, Prideaux et al. 2013).

The osteocytes have been considered as passive cells for a long time because they are trapped in bone matrix. Actually, they are very active and are essential for a normal function of the skeleton. The osteocytes play multiple roles due to the lacunocanalicular systems. This important system connects the osteocyte to other osteocytes, to osteoblasts and/or lining cells at the bone surface, the vascular system, and also to the bone marrow. These connections are adapted to give an access for nutriments, oxygen and to facilitate cell communication (Sommerfeldt and Rubin 2001, Santos, Bakker et al. 2009, Dallas, Prideaux et al. 2013). The osteocytes also play a role in mechanotransduction. In the 19th century, Julius Wolff was the first to identify the capability of the skeleton to adapt adaptation to mechanical loading or unloading by changing bone mass (Dallas, Prideaux et al. 2013). Osteocytes are known to be very sensitive to stress, more than osteoblasts or lining cells. The interstitial fluid in the lacunocanalicular system is submitted to changing pressure depending on the mechanical stress. This fluid flow is detected by the osteocytes. Thus, the canaliculi inform the osteocytes on the level of mechanical loading. The osteocytes produce the adequate molecules to regulate bone resorption by osteoclasts or bone formation by osteoblasts. A quick answer to mechanical loading is the release of calcium ions (You, Temiyasathit et al. 2008, Santos, Bakker et al. 2009).

2.3.1.1. Some important ossification genes

- Runx genes

Runx2 is also known as Cbfa1 and belongs to the runt-domain gene family. The *Runx2*-deficient mice (*Runx2*$^{-/-}$) do not develop any bones and die after birth by respiratory failure. Both endochondral and intramembranous ossifications are affected (Otto, Thornell et al. 1997, Komori 2006). These mice completely lack osteoblast development; they also lack hypertrophic chondrocytes but not in all skeletal structures. The Vegf, normally expressed in hypertrophic cells, is not expressed in *Runx2*$^{-/-}$ animals. Some hypertrophic chondrocytes can finally develop with a delay and calcified cartilage is visible at 17.5 days. Thus, other factors act on chondrocyte maturation (Kim, Otto et al. 1999).

Runx3, also called Aml2, plays a role in growth regulation of the gastric epithelial cells and in development of the dorsal root ganglia (Inoue, Ozaki et al. 2002, Levanon, Bettoun et al.

2002). Runx3 is also expressed in cartilage. The *Runx3*$^{-/-}$ mice are viable, however their chondrocyte maturation is delayed to finally develop a normal skeleton at neonatal stage (Yoshida, Yamamoto et al. 2004). Deficient mice with the combination *Runx2*$^{-/-}$ and *Runx3*$^{-/-}$ totally lack hypertrophic chondrocytes, they present small chondrocytes and do not express any chondrocyte maturation markers such as collagen X, Ihh, Pthr (Yoshida, Yamamoto et al. 2004). Altogether, the association of Runx2 and Runx3 is required to obtain normal chondrocyte maturation. Runx2 is crucial to determine the mesenchymal cells into osteoblastic precursors. Runx2 is also essential for osteoblast differentiation. This factor is one of the earliest genes to be expressed in osteoprogenitor cells and determines the phenotype of the osteoblast. Runx2 is regulated by phosphorylation and induces the expression of Osx (Nakashima, Zhou et al. 2002) and other target genes expressed in the mature osteoblasts such as Spp1 (Inman and Shore 2003), Bglap, Bsp, Col1a1 (Kobayashi and Kronenberg 2005).

- Osx

Osx (osterix) or Sp7 is a member of the SP transcription factor family. Osx is characterized by a three Cys(2)/His(2) zinc-finger motif (Nakashima, Zhou et al. 2002, Matsubara, Kida et al. 2008) and is expressed in all osteoblasts during endochondral and intramembranous ossification. Osx is crucial for bone development and formation. *Osx*$^{-/-}$ mice die after birth from breathing difficulties and without any bone. These null mice present a cartilage well developed for a future endochondral ossification, but mineralization cannot occur correctly and form a calcified cartilage. There is no intramembranous bone and a complete absence of a mineralized matrix. These mice do not express Bglap, Bsp or Spp1, but Runx2 expression is still present, while *Runx2* null mice do not express *Osx*. Therefore, Osx is downstream of Runx2 and is necessary for osteoblast differentiation (Nakashima, Zhou et al. 2002, Ganss and Jheon 2004, Karsenty 2008). A conditional cre/lox mouse constructed by Baek and collegues in 2009, shows an equal quantity of osteoblasts between *Osx* $^{flox/+}$;*Col1a1-Cre* and *Osx* $^{flox/-}$;*Col1a1-Cre*. However, osteoblast activity has changed. The early stage osteoblast marker Alp shows an increased expression, while the late stage osteoblast differentiation marker Bglap presents a severe decrease of its expression (Baek, Lee et al. 2009). Thus, correct Osx expression is required to continue osteoblastic differentiation and maturation. In contrast, Osx has no effect on osteoclastogenesis. All osteoclast markers are normally expressed in *Osx* null mice or the cre/lox mice (Nakashima, Zhou et al. 2002, Baek, Lee et al. 2009). Osx over-expression increases Alp, Bglap, BMP2, and Runx2 expression. Runx2

directly regulates Osx (Nishio, Dong et al. 2006, Karsenty 2008, Matsubara, Kida et al. 2008). However, Osx does not need Runx2 to be activated. BMP2 can induce Osx without Runx2 expression. This alternative pathway involves *Msx2* gene activation by BMP2, Msx2 then induces *Osx* expression (Matsubara, Kida et al. 2008). BMP2 can also activate *Osx* expression through Dlx5 (Ulsamer, Ortuno et al. 2008). Thus, BMP2 induces Osx expression using three different pathways: Runx2, Msx2 and Dlx5. Osx is required for osteoblast differentiation and has an additional regulatory role for osteoblast proliferation by inhibition of the Wnt pathway (Zhang 2012).

- Dlx genes

The Dlx gene family comprises transcription factors that contain a highly conserved homeodomain related to the Drosophila distal-less (Dll) factor. In Human and mice, the *Dlx* genes are associated in pairs: *Dlx1-2*, *Dlx3-4*, *Dlx5-6* (Simeone, Acampora et al. 1994, Merlo, Zerega et al. 2000, Li, Marijanovic et al. 2008). They have overlapping expression domains, such as in the forebrain region and in the branchial arches. Osteoblast cultured cells express different Dlx factors depending on their differentiation stage. Dlx1 and Dlx4 were not detectable, while Dlx2 expression was high earlier than the other Dlx factors, and starts to decrease at the pre-osteoblast stage. Dlx3 has its highest expression level in late stages of osteoblast differentiation and in osteocytes. Dlx3 also induces Bglap. Dlx5 and Dlx6 expression start earlier then Dlx3 in the pre-osteoblast until mature osteoblasts (Li, Marijanovic et al. 2008). These two genes present the same expression sites, but Dlx5 has generally a higher signal than Dlx6. They are both expressed in all future head bones, the trunk and limbs (Simeone, Acampora et al. 1994). Dlx5 and Dlx6 are important at different stages of bone formation. They have a redundant role as positive regulators of hypertrophic chondrocyte differentiation during endochondral ossification. Dlx5 is able to compensate completely Dlx6 in endochondral ossification. It accelerates chondrocyte hypertrophy by an extended expression of Ihh and col10a1. Dlx5 cannot induce bone mineralization, nevertheless it accelerates mineralization when the process is already begun (Zhu and Bendall 2009). The double null allele *Dlx5/6* is viable until birth, but the mice die by cerebral trauma during delivery. *Dlx5/6*$^{-/-}$ embryos show severe skeleton defects in craniofacial, limb and axial structures. The craniofacial defects are more important in the *Dlx5/6*$^{-/-}$ mouse than in the *Dlx5*$^{-/-}$. Heterozygous *Dlx5/6*$^{+/-}$ embryos are viable and do not present any anomalies (Merlo, Zerega et al. 2000, Robledo, Rajan et al. 2002), while the *Dlx5*$^{-/-}$ mice die at birth from respiratory defects. These embryos exhibit a reduction in bone volume in the total and

trabecular bone. The culture of *Dlx5*$^{-/-}$ primary osteoblasts reveals a decrease of proliferation and differentiation by a decrease of Runx2, Osx, Bglap and Bsp expression. Dlx5 is thus involved in osteoblast proliferation and differentiation, it is an indirect regulator of Runx2, a direct regulator of Osx expression and also acts on Bglap and Bsp expression (Robledo, Rajan et al. 2002, Samee, Geoffroy et al. 2008, Ulsamer, Ortuno et al. 2008). Moreover, Dlx5 is expressed in mature osteoblasts. A heterozygous *Dlx5*$^{+/-}$ mouse helped to study the Dlx5 effects at later stages (10 and 20 weeks). *Dlx5*$^{+/-}$ mice exhibit a normal morphology and a normal BMD in the whole body, including tibia and vertebrae. One exception concerns a BMD reduction in the femur, almost exclusively by a cortical thickness reduction. These mice can be partially compensated by expression of Dlx6. In contrast to embryos, older mice have no significant variation in bone formation markers. Dlx5 is also expressed in osteocytes at later stages (Robledo, Rajan et al. 2002, Samee, Geoffroy et al. 2009).

- Wnt

The denomination Wnt is a combination between wingless (*wg*), a gene involved in morphogenesis of the drosophila and the integration site (*Int*) (Burgers and Williams 2013).

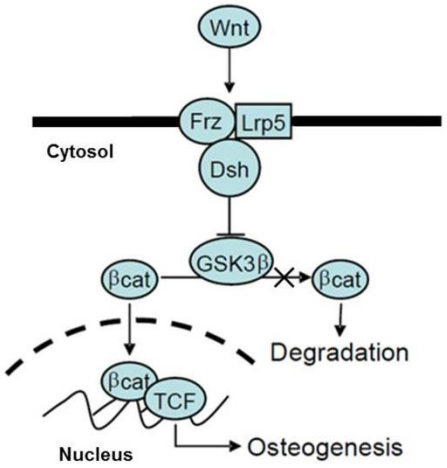

Figure 6: Wnt/β-catenin signaling (Krause and Gregory, 2012)**.**

The Wnts are a large family of 19 mammalian glycoproteins identified to date. At least three signaling pathways are described in the literature that can be initiated by Wnt factors and may have interactions between these pathways. The best understood is the canonical pathway or the Wnt/β catenin signaling (Fig. 6). The Wnt ligand binds the complex formed by the Frizzled (Fz) receptor and a member of the co-receptors "low density lipoprotein receptor-related protein" 5 or 6 (LRP5/6). This complex activates Dishevelled (Dvl) which inhibits the

activity of the glycogen synthetase kinase 3-β (GSK3β) complex, thereby protecting β-catenin from degradation. The β-catenin is stabilized and accumulated before translocation to the nucleus, where it regulates specific transcription factors (Krause and Gregory 2012, Monroe, McGee-Lawrence et al. 2012, Boudin, Fijalkowski et al. 2013)

The non-canonical Wnt pathways do act through stabilization of β-catenin. There are a minimum of 9 non-canonical pathways, but only two of them are better described (Krause and Gregory 2012). First, a calcium-dependent pathway involves the release of intracellular calcium which is important in cell migration, dorso-ventral patterning and heart development. The second is the planar cell polarity pathway and concerns cell shape control, cell fate determination and embryonic morphogenesis (Krause and Gregory 2012, Monroe, McGee-Lawrence et al. 2012, Boudin, Fijalkowski et al. 2013). The most relevant for bone metabolism is the Wnt/β catenin signaling. This pathway has different actions on osteoblast development, depending on the cell stage. In mesenchymal stem cells, Wnt/β-catenin signaling favors proliferation and inhibits differentiation. It collaborates with BMP2 signaling in the early osteogenic gene induction. Later, Wnt signaling stimulates osteoblast differentiation (de Boer, Siddappa et al. 2004, Eijken, Meijer et al. 2008, Regard, Zhong et al. 2012). Loss of function of the co-receptor Lrp5 is responsible for the osteoporosis pseudoglioma (OPPG), characterized by a low bone mass density. In contrast, a gain of function in Lrp5 induces high bone mass with an increase in the cortical thickness of long bones and cranial bones (Monroe, McGee-Lawrence et al. 2012, Boudin, Fijalkowski et al. 2013). *Lrp5*$^{-/-}$ mice present eye problems, low bone mass due to reduction of bone formation and a decrease in the number of osteoblasts (Kato, Patel et al. 2002). *Lrp6*$^{-/-}$ mice are not viable, but *Lrp5*$^{-/-}$; *Lrp6*$^{+/-}$ present a more severe bone mass reduction than *Lrp5*$^{-/-}$ alone (Holmen, Giambernardi et al. 2004). Inhibitors of Wnt signaling also illustrate the importance of Wnt signaling for a correct bone development. For example, the *Sost* gene is expressed in osteocytes and codes for sclerostin. Sclerostin binds to the Lrp5/6 receptor, blocks its interaction with the Fz receptor and thus inhibits the Wnt pathway in osteoblasts. Loss of function of the *SOST* gene causes two rare diseases, Sclerosteosis and van Buchem disease, characterized by a high bone mass due to an increased osteoblast activity (Monroe, McGee-Lawrence et al. 2012). *Sost*$^{-/-}$ mice exhibit a high bone mass phenotype, caused by an increase of the BMD, bone formation and bone strength (Li, Ominsky et al. 2008). The second Wnt inhibitor is the Dickkopf factors (DKK1). Knockout mice for *Dkk1* die after birth with severe developmental defects, while *Dkk1*$^{+/-}$ show increased bone formation, number of osteoblast

and bone mass (Morvan, Boulukos et al. 2006, Monroe, McGee-Lawrence et al. 2012). All these results support the importance of the Wnt signaling pathway in bone homeostasis.

2.3.2. Osteoclasts

The osteoclasts have a different origin from the other bone cells. They are derived from monocytes of the hematopoietic lineage. Osteoclasts are similar to macrophages, by their high capacity of migration, they are multinucleated, use several lysosomal enzymes, and they have the role of bone resorption (Sommerfeldt and Rubin 2001).

Osteoblasts express a factor essential for osteoclastogenesis. RANKL is a member of the Tumor necrosis factor (TNF) super family. RANKL secreted by the osteoblasts binds to its receptor RANK (receptor activator of nuclear factor κB) on the surface of the osteoclast precursor and stimulates its differentiation (Lacey, Timms et al. 1998, Hsu, Lacey et al. 1999, Beyer and Schett 2010). The link between RANK/RANKL promotes the recruitment of TRAF6 (TNF receptor-associated factor 6). TRAF6 activates downstream signaling pathways, for example NFkB, c-Jun terminal kinase (JNK), p38 and extracellular signal regulated kinase (ERK). As a result, RANKL initiates the activation of several transcription factors such as c-Fos, MITF (microphthalmia transcription factor) and NFATc1 (nuclear factor activated in T cells, cytoplasmic, calcineurin-dependent 1) responsible for osteoclast differentiation (Kim and Kim 2014). c-Fos is a member of the AP-1 family and is induced at early stages of osteoclast differentiation. c-Fos$^{-/-}$ mice present an important osteopetrosis and a severe defect in osteoclastogenesis (Wang, Ovitt et al. 1992, Kim and Kim 2014). Moreover, c-fos is necessary to induce NFATc1 expression (Kim and Kim 2014). MITF regulates TRAP (tartrate-resistant acid phosphatase), cathepsin K or c-fos (Kobayashi and Kronenberg 2005). NFATc1 is a major regulator of terminal osteoclast differentiation and maturation. *Nfatc1*-knockout mice present an osteopetrosis, with an important deficiency in osteoclastogenesis (Aliprantis, Ueki et al. 2008). NFATc1-deficient stem cells are unable to differentiate into osteoclasts in the presence of RANKL. At the opposite, NFATc1 addition to these deficient cells induces differentiation into osteoclasts even in absence of RANKL. NFATc1 is downstream of TRAP6 and c-Fos in the osteoclast signaling cascade (Takayanagi, Kim et al. 2002), it regulates genes specific for mature osteoclasts, such as TRAP, cathepsin K, and calcitonin receptor (Kim and Kim 2014).

A second factor, OPG or osteoprotegerin, also secreted by osteoblasts, negatively regulates osteoclastogenesis. OPG is a soluble decoy receptor for RANKL and belongs to the TNF

receptor family. OPG binding to RANKL inhibits osteoclast differentiation. *Opg*$^{-/-}$ mice show an excess of osteoclasts, causing osteoporosis (Bucay, Sarosi et al. 1998, Beyer and Schett 2010, Kim and Kim 2014).

2.3.3. Bone turnover

Bone remodeling is composed of different steps: Bone resorption by osteoclast cells, reversal, formation by the osteoblasts, mineralization and resting (Fig. 7). Usually, bone resorption takes less than 3 weeks, while bone formation takes longer, up to 2-3 months. Bone turnover takes place continuously in different parts of the skeleton, and at different time points (Henriksen, Karsdal et al. 2014). Bone remodeling causes renewal of 25% of cancellous bone and only 2 or 3% of compact bone each year (Swaminathan 2001). The balance between bone resorption and its formation is crucial to maintain healthy bone. Disruption of this balance is seen in diseases such as osteoporosis, arthritis, hyperparathyroidism, Paget's disease and bone tumors (Takayanagi, Kim et al. 2002).

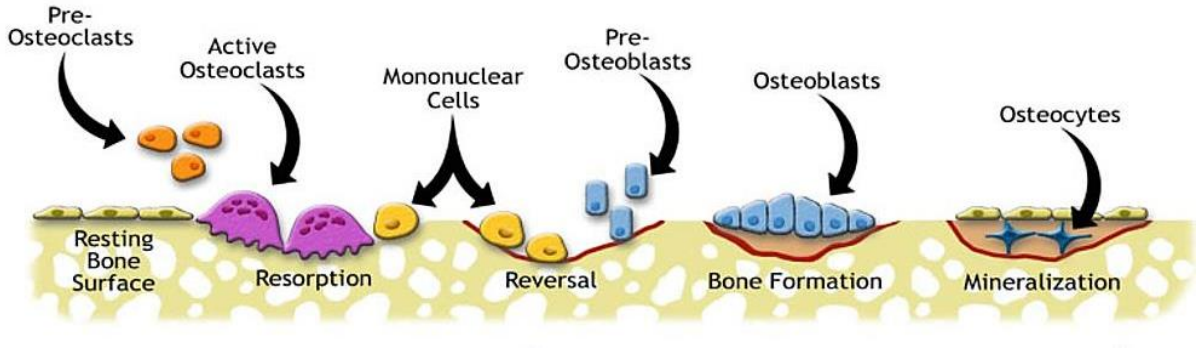

Figure 7: Scheme of the different steps in a complete bone turnover cycle (http://ns.umich.edu/Releases/2005/Feb05/bone.html).

The locations where bone remodeling occurs are called bone multi-cellular units or BMU. The human skeleton constantly presents about 1-2 x10^6 BMU (Lerner 2006). To start bone remodeling, the osteoclasts have to be activated by the RANK/RANKL coupling explained before. The osteoclast activity is cyclic, with the migration to the bone resorption site, bone degradation, detachment and restart of the same cycle at another site (Teitelbaum 2007). Resorption occurs in 2 steps: demineralization of the inorganic constituent and elimination of the organic matrix. Underneath the osteoclast, the cell surface in contact with bone becomes irregular and ruffled. Bone degradation is executed by the osteoclast's hydrolytic acid secretion to demineralize the matrix. The pH in the osteoclastic space is acid, between 2 and

4, to initiate enzyme secretion including cathepsin K and TRAP. Cathepsin K degrades collagen and other matrix proteins. At the end of bone destruction, a resorption bay is formed. The osteoclast activity can reach a resorption of 200 000 µm³ per day, they have a lifespan of 15 to 20 days (Sommerfeldt and Rubin 2001, Teitelbaum 2007, Beyer and Schett 2010). There are several bone resorption markers. The first is TRAP, present in large quantities on the osteoclast ruffled surface and in active osteoclasts. The second type of marker is the collagen cross-link molecules. The collagen is normally stabilized by cross-links formed extracellularly when the collagen is deposited into the matrix. There are 2 important cross-links: PYD (pyridinoline) and DPD (deoxypyridinoline). PYD is present in the connective tissue, in bone and has the highest concentration in cartilage. DPD is also present in different structures such as bone, dentine, aorta and ligaments. The presence of both in urine is an indicator for degradation of mature collagen. They represent 40% of free released cross-linked entities. The third marker category is the cross-linked telopeptides of collagen I, which represent the other 60%. These peptides have two possible origins, the amino-terminal end of collagen I, named NTx (N-terminal telopeptide), and the carboxyterminal end, named CTx (C-terminal telopeptide). They represent sensitive markers for bone resorption and/or modification and are more reliable than the other markers to estimate bone resorption (Swaminathan 2001).

The reversal phase corresponds to the transition between bone resorption and bone formation (Fig. 7). The osteoclasts stop to be activated and leave the resorption bay. During this phase, osteogenesis is stimulated. The reversal cells are specific to this phase and cover about 80% of the destructed surface. These cells clean the resorption bay and prepare the bone surface for bone formation (Andersen, Abdelgawad et al. 2013). Andersen and collaborators have determined the osteoblast lineage origin of the reversal cells. They express Runx2, Alp and Osx at different levels depending on their localization. The reversal cells deep inside the resorption bay, close to osteoclasts, express Runx2 and Alp. These cells are considered as early reversal cells. They are often flat cells with elongated nuclei. The reversal cells close to the bone surface and osteoblasts express also Osx. They form the late reversal cells and are more cuboid, similar to osteoblasts. Mesenchymal stem cells differentiate into pre-osteoblasts to colonize the resorption bay and permit bone formation. These osteoblasts show also the ability to clean the resorption bay. Additional studies are required to distinguish whether final bone formation derives from mesenchymal cell recruitment or reversal of cell differentiation (Andersen, Abdelgawad et al. 2013).

Bone formation is based on pre-osteoblast development and differentiation into osteocytes as described before (2.3.1) to form the osteoid tissue. The bone formation is followed by mineralization of the matrix. Some markers of bone formation are also useful. The first marker is ALP. ALPs are plasma membrane enzymes expressed in liver, kidney and bone. Their specificity is limited because bone isoforms represent 40% of the entire activity. The second marker is osteocalcin or Bglap (bone gla protein). Bglap is the major non-collagenous bone matrix protein, secreted from osteoblasts and odontoblasts. Bglap binds hydroxyapatite into the bone matrix (Swaminathan 2001). Others markers are also used as bone formation markers such as osx, col1a1.

2.4. Systemic bone regulation

The skeleton is not only regulated by local action, but also by systemic regulation. These systemic regulations include the action of estrogens, glucocorticoids, parathyroid hormone and vitamin D3. Here, we focus on the parathyroid hormone, vitamin D3 and their involvement in calcium homeostasis.

2.4.1. Parathyroid hormone

Parathyroid hormone (PTH) is a protein hormone produced by the parathyroid gland. PTH in the blood circulation binds the PTH receptor type1 (PTHR1). Another hormone, the PTHrP (PTH related peptide) presents in its N-terminal part a sequence similar to the PTH N-terminal sequence and can also bind the PTHR1 with nearly the same affinity as PTH. However, they have different roles. PTHrP regulates tissue development, including cartilage, heart and mammary gland. In contrast, PTH limits its action to bone and kidney to regulate circulating phosphate, calcium ions and Vitamin D3 (Miao, He et al. 2004, Vilardaga, Romero et al. 2011). In this study, we will only focus on the PTH effects.

PTH presents the particularity to play opposite effects on bone depending on the mode of administration. Continuous PTH promotes a catabolic effect on bone, characterized by a rapid bone turnover, an increase of osteoclast activity and a decreased bone mass, while intermittent PTH administration leads to an anabolic effect with an increase of bone formation. The detailed mechanism remains unclear. Nevertheless, the difference could be due to opposite influence on runx2. PTH induces Runx2 expression in osteoblasts, which results in an anti-apoptotic effect. This induction lasts for only 6 hours, after which the excess Runx2 is degraded by proteolysis. Continuous PTH treatment leads to one single, short anti-apoptotic

effect followed by a return to normal levels of osteoblast apoptosis. Intermittent PTH administration leads to repeated increases of Runx2 expression and thus repeated anti-apoptotic effects. The repetition delays apoptosis protects the osteoblasts from cellular death with the consequence of an increase in the number of osteoblasts (Bellido, Ali et al. 2005, Wang, Liu et al. 2005, Jilka 2007). Another possible explanation for these opposite effects results from the modification of RANKL and OPG expression during continuous PTH administration. RANKL expression is increased, while that of OPG is decreased. Thus, the RANKL/OPG ratio is increased, and bone resorption is enhanced by the increase of the osteoclast number, their differentiation and activity. The expression of bone formation markers, such as BSP, col1a1 and Bglap are reduced in continuous PTH treatment. In contrast, these markers are increased in the intermittent PTH treatment (Ma, Cain et al. 2001).

2.4.2. Vitamin D3

Vitamin D (VitD) is an essential liposoluble hormone. There are 2 forms: VitD2 called ergocalciferol of plant origin, and VitD3 named cholecalciferol of animal origin. VitD3 biosynthesis begins by food intake of the VitD2 or VitD3 forms and/or through the skin by the action of UV light. The sunlight UV converts the cholesterol precursor 7-dehydrocholesterol into pre-vitamin D3 then, in a second step, the VitD3 is obtained. VitD3 is metabolized in the liver to produce the circulating form 25-hydroxyvitamin D also named 25-hydroxycholecalciferol (25-OH-D) or calcidiol, which is the form used for storage. The active form 1,25-dihydroxycholecalciferol ($1,25(OH)_2D$) or calcitriol is generated in the kidney by the enzyme 1,25-dihydroxyvitamin D-1α-hydrolase (1α(OH)ase). This form is able to bind to the Vitamin D receptor (VDR) (Holick 1996, Bacchetta, Ranchin et al. 2010, Nguyen-Yamamoto, Bolivar et al. 2010). VitD3 has different effects on health, including a bone and calcium homeostasis role and global roles as anti-infectious, anti-inflammatory, anti-tumoral or cardiovascular protector. VitD3 disorders lead to several types of disease, such as muscle weakness, psoriasis, cancers, sclerosis or diabetes (Gennero, Moulin et al. 2004, Mithal, Wahl et al. 2009, Bacchetta, Ranchin et al. 2010).

2.4.3. Calcium homeostasis by parathyroid hormone and vitamin D3

PTH is the antagonist of calcitonin produced in the parafollicular cells of the thyroid gland. PTH is released when the circulating calcium concentration is reduced. In contrast, when the calcium level is increased, the PTH stimulus is inhibited and calcitonin secretion is induced. The latter hormone inhibits bone resorption and promotes calcium deposit into the bone matrix, thus decreasing the calcium concentration in the blood. Both PTH and calcitonin interact to maintain a normal level of calcium in the blood circulation. This interaction is important during bone development (Marieb 1999).

PTH release affects 3 different organs: bones, kidney and intestine as shown in figure 8. PTH acts after several minutes on the tubular cells of the kidney to stimulate the absorption of calcium ions. In bone, it induces the osteoclasts to degrade the bone matrix to release calcium ions and phosphates into the blood. When the hypocalcaemia is prolonged during several hours, PTH causes another action in the kidney by inducing synthesis of the VitD3 active form ($1,25(OH)_2D$). VitD3 then stimulates the intestinal absorption of calcium ions. PTH secretion returns to normal when the blood calcium reaches a normal level (Marieb 1999, Gennero, Moulin et al. 2004).

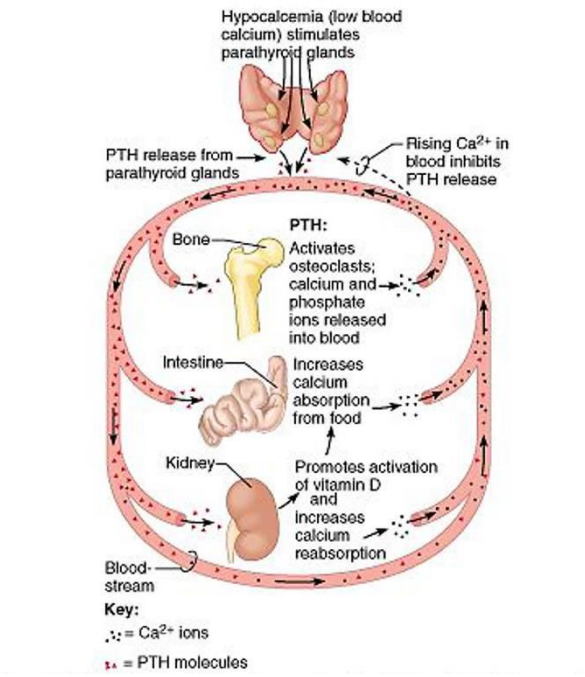

Figure 8: Effect of PTH on the three different organs to increase the calcium ion level. VitD3 active form synthesis and action on intestinal absorption (Marieb 1999)**.**

Pth null mice have normal development and are viable, despite having bone defects. The number of osteoblasts and bone mineralization are reduced in *Pth*$^{-/-}$ mice. The number of osteoclasts is also reduced by 50%. Thus, the bone turnover is very low in *Pth*$^{-/-}$ mice. The trabecular bone is decreased in *Pth*$^{-/-}$ mice, and they stay in hypocalcaemia even if they are fed with a calcium-rich diet (Miao, He et al. 2004). *Vdr* null mice exhibit bone defects with hypocalcemia due to a decrease of intestinal calcium absorption, *Vdr*$^{-/-}$ present also typical characteristics of rickets, hyperparathyroidism and osteomalacia (Amling, Priemel et al. 1999, Takeda, Yoshizawa et al. 1999). Alteration of the enzyme 1α(OH)ase, which converts VitD3 into the active form, has similar effects on the skeleton than the *Vdr* null mice (Panda, Miao et al. 2004). Both Vdr and 1α(OH)ase are also required for a normal level of PTH. The parathyroid gland is larger in both mutants and PTH levels are elevated. (Panda, Miao et al. 2004). The osteoclast number does not change even with the high levels of circulating PTH. The cartilage growth plate is larger and deformed in both mutants. (Panda, Miao et al. 2004, Nguyen-Yamamoto, Bolivar et al. 2010). Both the PTH$^{-/-}$ and the 1α(OH)ase $^{-/-}$ exhibit moderate hypocalcemia and are viable, while the double mutant PTH$^{-/-}$; 1α(OH)ase$^{-/-}$ mice present a severe hypocalcemia leading to death by tetany at 3weeks. In general, this double mutant has worse effects on bone development than the two separate mutants, such as a decrease of calcification, femur length, trabecular bone, number of osteoblasts and bone formation markers (*Runx2*, *Alp*, *Bglap*, *Col1a1*). These results suggest an interaction between PTH and VitD3 on bone formation. In contrast, Trap staining and the RANKL/Opg ratio are decreased similarly in the three mutants. There is no cooperation between PTH and VitD3 for bone resorption (Xue, Karaplis et al. 2005).

VitD3 and PTH are essential for a correct bone and calcium homeostasis. VitD3 acts essentially in kidney and intestine for calcium homeostasis, while PTH and PTHrP act also on bone for calcium homeostasis. Both have important dependent and independent roles in bone homeostasis.

2.5. Osteoporosis

Osteoporosis is defined as “a disease characterized by low bone mass and microarchitectural deterioration of bone tissue, leading to enhanced bone fragility and a consequent increase in fracture risk” (Kanis, Melton et al. 1994).

Osteoporosis is classified into 2 categories according to the osteoporotic conditions. Primary osteoporosis is due to aging and decrease of the gonadal function at menopause. This disease

is more represented in women than men. Women present 2 phases in the bone loss progression. At menopause, bone loss begins in the trabecular bones with the decrease in estrogen production, leading to an increase of bone resorption without any changes in bone formation. This phase has a peak after 4-8 years. The second phase is slower and shows a persistent bone loss in cortical and trabecular bones due to a decrease of bone formation. Usually, men experience only the slow phase, with the decrease of testosterone and estrogen levels. It is thought that the decrease of testosterone causes decreased bone formation and estrogen reduction is responsible for increased bone resorption. Secondary osteoporosis is related to other health problems, for example endocrine disorders (hyperparathyroidism, diabetes), genetic disorders, chronic pulmonary disease, glucocorticoid treatment, rheumatoid arthritis and disuse of mechanical loading including long time bed-rest, prolonged immobilization, paralysis and microgravity (Lazner, Gowen et al. 1999, Lau and Guo 2011, Giannotti, Bottai et al. 2013).

In several cases of secondary osteoporosis, the trabecular bone loss and the microarchitecture deterioration is linked to mechanical loading. As described in 2.3.1, the lacunocanalicular system of the osteocytes is important to maintain a healthy bone. The movement of interstitial fluid is induced by mechanical loading to bring nutriments and preserve osteocytes. A disruption of this mechanism leads to bone disorders (Giannotti, Bottai et al. 2013).

Normally, the BMU (basic multicellular unit) volume resorbed by osteoclasts is equal to the BMU volume reformed by the osteoblasts, however in osteoporosis, this balance is disrupted (Martin 2014). To maintain healthy bone, bone formation sites have to increase the number of osteoblasts. Actually, in post-menopausal osteoporosis, both the numbers of osteoclasts and osteoblasts are increased, causing also an increase of the bone remodeling frequency. This higher frequency decreases the osteoblasts' capacity to produce and form new and strong bone, leading to a lower volume of bone formed relative to the resorption volume. The BMU is not completely filled with new bone, resulting in structural destruction, lower bone mass and strength. The result is a negative bone or BMU balance (Lerner 2006, Martin 2014).

Dalle Carbonare and collaborators analyzed the differentiation from mesenchymal stem cells into osteoblast in osteoporosis patients compared to healthy subjects (Dalle Carbonare, Valenti et al. 2009). This study highlights several genes involved in the osteoblast alterations (Dalle Carbonare, Valenti et al. 2009). The number of mesenchymal stem cells was increased in the osteoporosis patient group, while *RUNX2*, *OSX*, *COL1A1*, *SPARC*, and *SPP1*

expressions were down-regulated and the OPG/RANKL ratio was decreased. In another study *ALP, COL1A1, MMP2, MMP9, MMP13 and NFKB* were shown to be down-regulated in post-menopausal osteoporosis patients relative to healthy persons, while *TWIST2* was upregulated (Balla, Kosa et al. 2008).

In conclusion, osteoporosis is a multifactorial disease depending on the bone remodeling balance, mechanical loading and alteration of gene expression. Several types of treatment are possible. The first type is an anti-resorptive treatment, which includes bisphosphonates, or RANKL or cathepsin K inhibitors. Bisphosphonates are widely used drugs, with the best-known being alendronate (Fosamax®), etidronate (Didocral®), risedronate (Actonel®) and zoledronic acid (Aclasta®) (http://www.osteoporosecanada.ca/losteoporose-et-vous/les-traitements-pharmacologiques/les-bisphosphonates/). This treatment decreases bone resorption and the fracture risk (Catalano, Morabito et al. 2013, Rossini, Gatti et al. 2013). Denosumab is a human monoclonal antibody that binds to RANKL with high affinity and inhibits RANKL activity. This antibody has a long-lasting action; only one injection is needed every 6 months. Odanacatib is a cathepsin K inhibitor with a half-life of 45-50 hours, thus a weekly administration is needed (Martin 2014). The second type of treatment is an anabolic treatment by intermittent PTH. The medicine is named teriparatide (Forteo ®; Elli Lilly and Company) (Burgers and Williams 2013). Administration is daily, but the PTH levels are back to normal after 3 hours. Maintaining high PTH levels for longer periods will stimulate osteoclastogenesis and bone resorption, as observed in primary hyperparathyroidism. The anabolic effect acts on the osteoblast precursors and inhibits apoptosis of osteoblasts and osteocytes. After several weeks of intermittent PTH treatment, the bone formation markers are increased, but after several months the osteoclast markers are also increased (Martin 2014). The third type of treatment targets components of the Wnt signaling pathway, such as the WNT signaling inhibitor sclerostin (SOST), expressed in osteocytes. Injection of sclerostin antibody (Romosozumab) increases the expression of bone formation markers and decreases the level of the bone resorption marker CTX after only one month. These results are similar to those obtained after 6months of intermittent PTH treatment. After one year treatment with Romosozumab, the BMD is increased to a higher level as compared to alendronate (bisphosphonate) treatment (Catalano, Morabito et al. 2013, Rossini, Gatti et al. 2013, Martin 2014). To improve the efficiency of the treatment, combinations are possible, for example intermittent PTH followed by an anti-resorption treatment or a sclerostin

antibody associated with an anti-resorption treatment (Rossini, Gatti et al. 2013, Martin 2014).

2.6. Astronaut's osteoporosis

In space, the organism of the astronauts attempts to adapt to the effects of weightlessness (microgravity). This adaptation presents some similarities with the effects of aging. Both induce physiological and functional alterations in the cardiovascular and the musculoskeletal systems. However, in particular concerning the bone system, major differences exist between space flight and aging osteoporosis:

- Stabilization and recovery of the effect on bone after space flight is observed in astronauts, not for old people.
- The effects are faster in space than on earth. Astronauts may lose in 6 months the bone mass equivalent to the loss of an entire life with aging (Vernikos and Schneider 2010, McCarthy 2011).

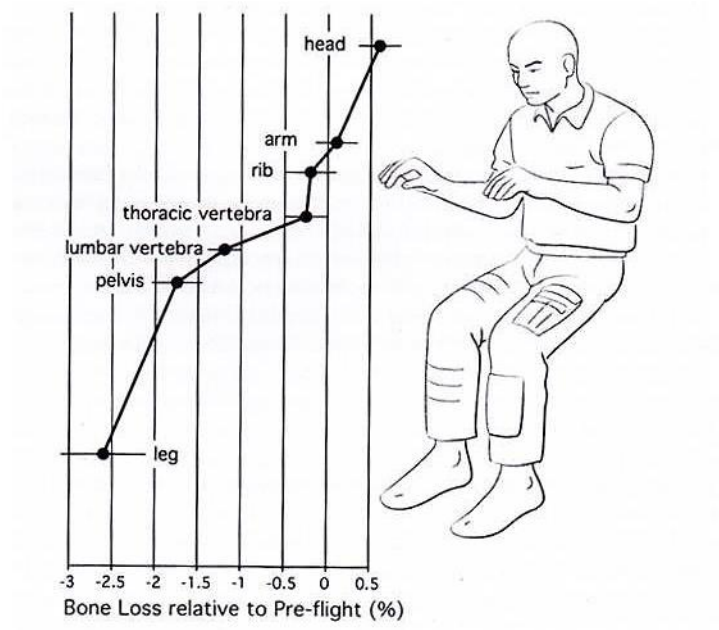

Figure 9: Percentage of bone loss based on the results observed after at least 6 month spaceflight (Beysens, Carotenuto et al. 2011).

Long-term spaceflight induces an important decrease of about 1 to 2% of bone mass and bone density per month. However, all bones are not affected at the same level. The weight-bearing bones, such as the hip, tibia, femur and vertebrae are more severely affected. Figure 9 presents the distribution of mean bone loss in the body due to microgravity. The most important problems are located in the legs, followed by the pelvis and the lumbar. Interestingly, these

results can be correlated with the fluid shift observed in space, causing higher blood pressure in the head and lower blood pressure in the legs, possibly inducing less circulating blood for bone nutrition (Alexandre 2001).

A difference is also observed between bone loss in cortical or trabecular bone. In the literature, the bone mineral density (BMD) measures are based on pre-flight and post-flight analysis. After a 1 month flight, the first altered bone is the cancellous tibia with a mean bone loss of 1.7%, while there is no change in the cortical part nor in the radius. In contrast, after 6 months spaceflight, the tibia cancellous bone loss is about 4.5% and about 2.9% in the cortical part. The radius still does not present any changes after 6 months spaceflight (Collet, Uebelhart et al. 1997, Vico, Collet et al. 2000, Carmeliet, Vico et al. 2001). Upon return to ground, the astronauts are weakened and subject to elevated fracture risk. The recovery period is longer than the duration of the flight, as even after 6 months of recovery, there is still a significant decrease of 2.5% in the trabecular tibia relative to pre-flight (Collet, Uebelhart et al. 1997, Vico, Collet et al. 2000). Sibonga and collaborators have analyzed bone loss and calculated the recovery time for 50% restoration of bone loss in 45 astronauts. They observed a bone loss of between 2 and 9%, with a greater loss in the hip and pelvis than in the lumbar spine and calcaneus. For all astronauts, it takes about 9 months after flight to obtain 50% recovery. This study agreed with that of Vico and collaborators to evaluate a recovery time longer than the duration of the spaceflight. Sibonga's calculations estimate that astronauts need about 36 months to reach the pre-flight BMD. Consequently, the astronauts have a higher fracture risk during 3 years after the flight. However, these results are variable between individual crew members, depending on nutrition, skeletal muscle reconditioning and genetics. Astronauts are on average 45years old and their bone fragility can be shown 10-15 years later, as they may present fractures at the age of 60. These fractures are premature for osteoporosis, they may well be due to the combination of irreversible deterioration after spaceflight and the effect of aging. Therefore, there is no certainty concerning a total bone recovery after long-term missions (Sibonga, Evans et al. 2007, Sibonga 2013).

The mechanism involved in microgravity-induced bone loss remains unclear. The balance between bone formation and bone resorption is disturbed, but there is controversy concerning whether only one of these processes is modified or both of them. Some authors think that only bone resorption is increased (Orwoll, Adler et al. 2013), while others argue that both bone formation and resorption are disturbed in microgravity (Fong 2004). The cellular morphology

and activity are modified in microgravity. Osteoblasts submitted to microgravity present an increased cell area and an enlarged nucleus, suggesting increased apoptosis. These morphological differences are due to the disruption of cytoskeleton components (Hughes-Fulford and Lewis 1996, Nabavi, Khandani et al. 2011, Arfat, Xiao et al. 2014). After 2 weeks in microgravity, an increase of osteocyte apoptosis is visible, which could be the consequence of increased osteoclastogenesis activation after 24 hours in space (Tamma, Colaianni et al. 2009, Arfat, Xiao et al. 2014). Bone marker analysis can be performed by comparison between pre- and post-flight astronauts in urine and blood samples. The bone formation markers ALP and Bglap are decreased after 1 to 6 months of spaceflight (Collet, Uebelhart et al. 1997, Caillot-Augusseau, Lafage-Proust et al. 1998, Smith, Wastney et al. 2005). Concerning bone resorption markers, one study saw that only PYD is increased (Collet, Uebelhart et al. 1997), while another observed that CTX and DPX are increased (Caillot-Augusseau, Lafage-Proust et al. 1998). During the recovery period after flight, all bone markers progress in the opposite direction compared to in- or immediate post-flight. Bone resorption markers decrease and bone formation markers increase (Caillot-Augusseau, Lafage-Proust et al. 1998). PTH presents a decrease of 48% during the spaceflight and an increase of 98% occurs after flight, resulting in higher than normal PTH levels. The active form of VitD3 is reduced during flight and stays low after return (Smith, Wastney et al. 2005). The calcium balance is negative, with a higher calcium excretion due to fluid loss during the first weeks in space, which may induce a bone loss during spaceflight. The calcium release from bone inhibits PTH, which is accompanied by a reduction in circulating VitD3, thus inducing a decrease of calcium absorption (Smith, Wastney et al. 2005, Smith, Heer et al. 2012). The calcium level is increased in urine during the flight and promotes the risk of renal stone formation (Morey-Holton 2003, Smith, Heer et al. 2012).

Current treatments are focused on nutrition, physical exercise and pharmacological complements. On ISS, physical training was performed on a "treadmill with vibration isolation and stabilization" (TVIS), a "cycle ergometer with vibration isolation and stabilization" (CEVIS) and resistive exercise (squat) was perfomed on the "interim resistive exercise device" (iRED) with no real improvement effect on bone loss during the long term missions. After 2008, iRED was compared to a new system of resistance training, "Advanced Resistive Exercise Device" (ARED). The bone resorption markers (NTX, CTX, PYD and DPD) were increased in both groups during flight and 30 days after flight. The bone formation markers, such as ALP, Bglap, or calcium were not significantly affected in both

groups, except for Vitamin D (active form) which decreased in both groups. The BMD in pelvis, femur, trochanter and hip is less affected in the ARED group, and the PTH level is more stable in the ARED group leading to a better bone conservation (Genc, Gopalakrishnan et al. 2010, Smith, Heer et al. 2012). A recent study showed that, on iRED and ARED, there are no differences between men and women in space. Differences were observed due to the device, not the gender. Men are sensitive to stone risk and women are more subject to BMD variations on earth. These fragilities are not modified or worse in space (Smith, Zwart et al. 2014). In addition, physical training alone is not sufficient to prevent bone loss. A specific diet increasing Vitamin D and Calcium intake is also important. One study has explored a combination of nutrition and exercise with a pharmacological therapy similar to earth osteoporosis patients. They have tested 2 drugs: Teriparatide, a recombinant form of PTH, administrated once a day by abdominal injection and Alendronate, a bisphononate. They conclude that both drugs cannot be used at high concentrations for a long time, due to important side effects such as nausea, cramps for teriparatide and acute gastrointestinal tract inflammations, petechiae, cardiac dysrhythmia, osteonecrosis of the jaw for alendronate. A perfect solution has not yet been found, but the best results seem to be obtained by a combination of 2.5hours/day physical training, a high level of teriparatide (50mcg/day) and a moderate concentration of alendronate (35mg/week) (Zobel, Del Vescovo et al. 2012). This combination contributes to a better conservation of the calcium level, but it is still not the perfect solution to protect and conserve a skeletal system as it was before flight.

3. Microgravity and hypergravity simulation experiments

The first published experiment related to gravity simulators was accomplished by Sir Thomas Andrew Knight in 1806. He studied the effect of gravity on plants using germinating bean seeds on a rotating waterwheel. The plant's roots and leaves oriented according to the gravitational vector (Knight 1806).

3.1. Clinostat

In 1879, Julius von Sachs constructed a clinostat and used this machine to study plant gravitropism. The clinostat is composed of small diameter tubes, placed horizontally and rotating around their horizontal axis at constant speed. The velocity was very slow in these experiments (from 1 to 10 rpm) and particles within a cell were rotating as described in figure 10. All particles in the clinostat are submitted to the gravitational force (1g) and to a constant rotation. When a particle is moving from position 1 to position 2, the particle is falling down

with the gravity force and follows a trajectory s1 within the rotating cell. The same process takes place while moving to position 3, 4 and back to position 1 with another vertical movement. Finally, the trajectory of the particle within a cell, instead of being vertical due to the gravity force, is circular due to the rotation of the cell (Dedolph and Dipert 1971).

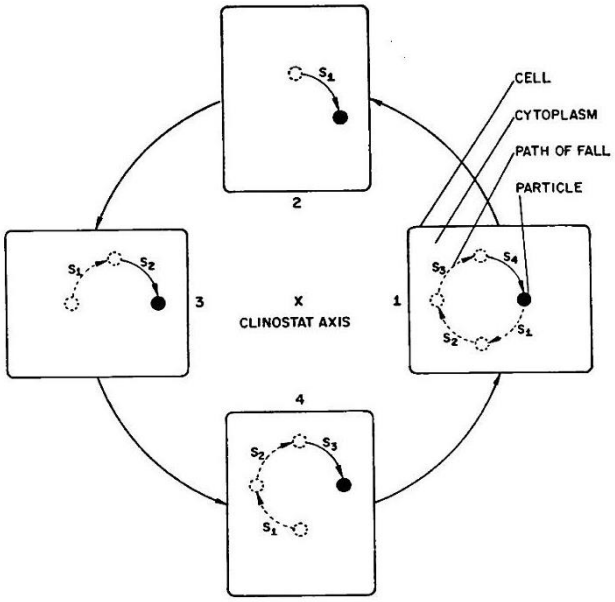

Figure 10: Particle movement inside a cell on a slow rotating clinostat (Dedolph and Dipert 1971).

In 1958, the geneticist Hermann Joseph Muller adapted the clinostat for humans to investigate the function of the statolith organ in the inner ear. The subject was placed into a cylinder and the rotation was executed around a horizontal axis. In 1965, Wolfgang Briegleb was inspired from Muller's clinostat adaptation and developed the fast rotating clinostat (Fig. 11).

Figure 11: Clinostat composed of 3 rotating tubes and 3 fixed tubes (controls).

The process is based on a higher velocity of rotation (between 60 to 90rpm) because the response time of an animal or a human to direction vector changes is shorter than in plants. The rotation has to be fast enough so that the otoliths and sensory parts are unable to respond anymore to the gravitational vector, thus inducing a spatial disorientation comparable to the disorientation experienced in microgravity (Briegleb 1992, Cogoli 1992, Klaus 2001, JJWA. 2007).

3.2. Random Positioning Machine

From the 2 dimensional clinostat described above, a 3 dimensional clinostat was derived that is composed of 2 perpendicular rotating axes. Later, in 1994, Dr Dick Mesland suggested the principle of "true random positioning". Collaboration with the European Space Agency (ESA) led to the construction of the Random Positioning Machine or RPM in 1997. The RPM executes rotation movements around two perpendicular axes that are continuously redirected at random speeds and directions.

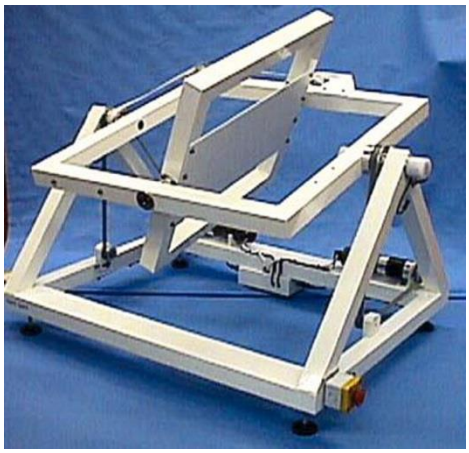

Figure 12: The Random Positioning Machin (RPM).

The device is composed of 2 independent and perpendicular frames with a central experimental platform linked to a "random walk scenario" generated by software. This orientation variation can produce effects similar to microgravity. The orientation changes are faster than the gravity response. Similar to the clinostat, the neurovestibular system is confused. In the RPM, no adaptation to the imposed reorientation of the gravity vector is possible due to the random movements. While in the clinostat, all the forces involved in the mechanism are known, the RPM still needs a better comprehension of the fluid movement in the samples (Huijser 2000, JJWA. 2007, Borst and van Loon 2009).

3.3. Rotating Wall Vessel

The Rotating Wall Vessel or RWV was created by a group of NASA's Biotechnology to improve cell culture conditions. The cells, either directly or attached to small beads, are suspended in medium filled into in a disk-shaped container, which is placed vertically and rotates around its horizontal central axis. This rotation generates a continuous sedimentation of the cells and minimizes shear force and turbulence in the fluid. Comparing the RWV to the clinostat, they both use a vessel, filled with fluid and cells, which rotates with a constant speed around a horizontal axis. However, while the clinostat tries to generate a circular trajectory of the objects to a point that they are rotating on themselves, the RWV has an opposite effect on cells with a large circular movement within the medium (Hammond and Hammond 2001, Klaus 2001).

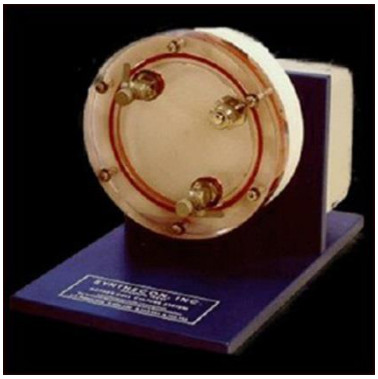

Figure 13: The Rotating Wall Vessel (RWV).

3.4. Large Diameter Centrifuge

The large diameter centrifuge or LDC has been developed by ESA to study hypergravity ranging from 1g to 20g. In contrast to the other devices detailed above, the LDC was not constructed for cultured cell only. This machine can be used for plants, animals, physics and fluid mechanism experiments, and even humans.

Figure 14: The large diameter centrifuge.

The suspended centrifuge containers ensure that the force vector resulting from the vertical gravity vector and the centrifugal force is always perpendicular to the bottom plate where the samples are placed. The advantage of the large diameter is to minimize the inertial shear force to negligible (van Loon, Folgering et al. 2003, van Loon, Folgering et al. 2004, van Loon, van Laar et al. 2009).

4. Zebrafish advantages and use as model for genomic analysis

The zebrafish (*Danio rerio*) is a small fish of 3 to 5cm living in the South of Asia, more exactly in Northern India, Northern Pakistan, Nepal and Bhutan rivers. It belongs to the bony fish class, also called teleost or *Teleostei*, in the family of *Cyprinidae*. Zebrafish present many advantages due to several characteristics such as a rapid and external development (almost all structures are developed at 48hpf), transparency of the embryos, high fecundity (one female can have more than 100 eggs per clutch). At 3 month, the zebrafish has reached its sexual maturity (Kishi, Uchiyama et al. 2003, Dahm, Geisler et al. 2005).

4.1. Genome

The zebrafish genome is organized on 25 chromosomes and contains about 30 000 genes. The zebrafish genome sequencing project started at the Wellcome Trust Sanger Institute in 2001. Currently, the whole genome is sequenced and is available in different databases such as ENSEMBL (http://www.ensembl.org/Danio_rerio/), NCBI's genome database (http://www.ncbi.nlm.nih.gov/genome/) or the Genome Reference Consortium (http://genomereference.org). The Vertebrate Genome Annotation (Vega) is based on the ENSEMBL database system to obtain common genome data and manual annotations in different species, including the zebrafish (http://vega.sanger.ac.uk). The Bioprojects database of the NCBI is another fish genomic database (http://www.ncbi.nlm.nih.gov/bioproject). About 168 different species of teleosts are included in this project. This database is almost entirely composed of transcriptome or gene expression projects (84%), and 9% of genome sequencing. The most popular model is *Danio rerio* with 37% of the Bioprojects sequences (Hubbard, Barker et al. 2002, Ashurst, Chen et al. 2005, Howe, Clark et al. 2013, Spaink, Jansen et al. 2014).

4.2. Duplication and Conservation

Whole-genome duplications occurred several times during evolution of living organisms. Two whole-genome duplications (R1 and R2) have arisen in the chordate lineage. The first

happened between the non-vertebrate chordate and the vertebrate lineage, while the second took place at the onset of jawed vertebrates. The zebrafish infraclass has arisen from a common ancestor about 340 million years ago, with a third whole-genome duplication (R3) that is not shared with the lineage leading to mammals. This additional duplication event increased the number of genes in these species, however many of these duplicates were lost. Some duplicates developed new functionalities, while others altered their expression patterns and activities. Finally, some duplicates lost part of their function by mutation and each paralog conserves part of the function of the original gene (sub-functionalization). In these cases, the 2 paralogs are conserved to preserve the complete function. About 71% of human genes are represented by at least one zebrafish ortholog, conversely 69% of zebrafish genes have a human ortholog. Zebrafish genes present generally about 80% similarity with their human homologs (Barbazuk, Korf et al. 2000, Catchen, Conery et al. 2009, Lee, Kerk et al. 2011, Howe, Clark et al. 2013).

5. Zebrafish as bone model

5.1. General structure

The head skeleton contains the earliest bones to develop and is also the most studied. The adult zebrafish skull is divided in 3 different parts: neurocranium, viscerocranium and dermatocranium. The head skeleton is composed of 74 bones in adult zebrafish. The dermatocranium possesses 29 dermal bones. The 45 endochondral bones are formed in the neurocranium and the viscerocranium. First, the head skeleton is formed by cartilage and is called the chondrocranium. After ossification, this chondrocranium becomes the osteocranium (Cubbage and Mabee 1996, Nüsslein-Volhard C 2001). The neurocranium is composed of 4 capsules (ethmoid, orbital, occipital, otic) and protects the brain and the sensory organs. The viscerocranium includes the 7 pharyngeal arches surrounding the pharynx (Fig. 15). The most anterior pair composes the mandible, the second pair forms the hyoid. The five posterior pairs of pharyngeal arches are also called branchial arches. The gills are on 3 of the posterior pharyngeal arches and the fifth carries the only teeth of the fish. Each branchial arch is formed by one transient structure named ceratobranchial in zebrafish larvae. In the juvenile (at 30 days post-fertilization or dpf), each branchial arch is divided into 5 elements; basi-, hypo-, cerato-, epi- and pharyngobranchial. The dermatocranium is the external skull part, surrounding the neurocranium and the two first pharyngeal arches (Cubbage and Mabee 1996, Nüsslein-Volhard C 2001).

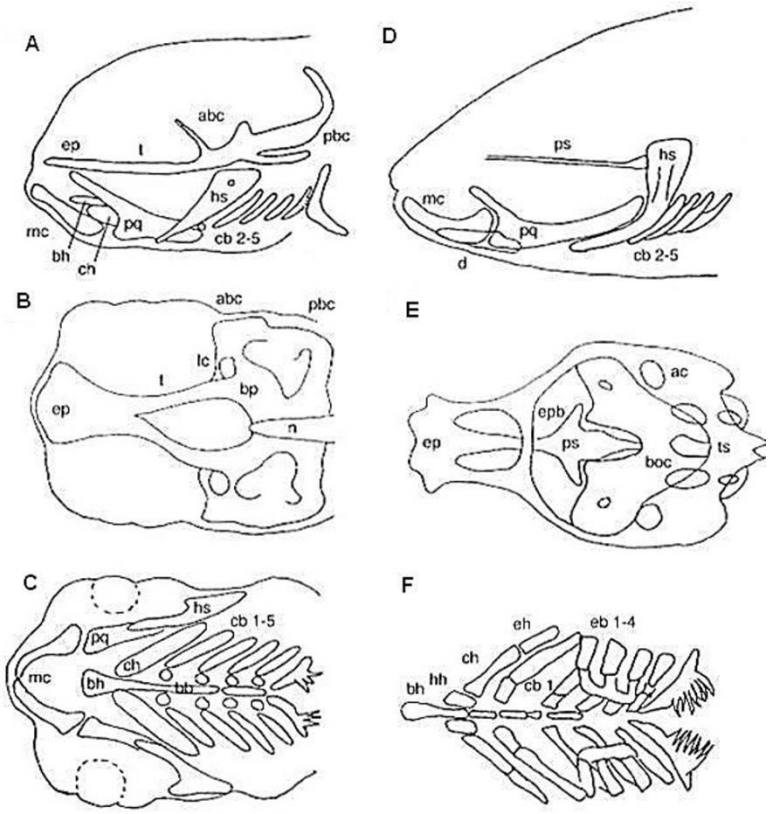

Figure 15: Schematic representation of larval (A-C) and juvenile (D-F) zebrafish skull. Lateral (A, D) and ventral (B, C, E, F) views of the viscerocranium (A, C, D, F) and neurocranium (B, E). anterior basicranial commissure (abc), auditory capsule (ac), basibranchials (bb), basihyal (bh), basioccipital (boc), basal plate (bp), ceratobranchials (cb), ceratohyal (ch), dentary (d), epibranchial (eb), epihyal (eh), ethmoid plate (ep), epiphysial bar (epb), hypohyal (hh), hyosymplectic (hs), lateral commissure (lc), Meckel's cartilage (mc), notochord (n), posterior basobranchial commissure (pbc), palatoquadrate (pq), parasphenoid (ps), trabeculae (t), tectum synopticum (ts) (Nüsslein-Volhard C 2001).

In zebrafish, the first ossification begins at 3dpf and the calcified cleithrum is observable (Gavaia, Simes et al. 2006). All the bones are formed at about 30dpf, but the zebrafish does not stop growth during its entire lifespan (Nüsslein-Volhard C 2001). In teleost fish, although they present more various types of bone, the types of ossification are closely related to those in higher vertebrates, with mainly dermal and endochondral ossification. The zebrafish is too small to present real endochondral ossification. However, two other types of ossification take place, named perichondral and parachondral ossification. Perichondral ossification is a membranous ossification surrounding the cartilage without deterioration, while parachondral ossification occurs close to the cartilage, but stays separated by the perichondrium (Meunier, Deschamps et al. 2008, Apschner, Schulte-Merker et al. 2011).

Bones are distinguished in cellular and/or acellular bone. The zebrafish contains cellular bones that possess lacunae enclosing osteocytes, in contrast to for example the medaka which

has no osteocytes (Renn, Winkler et al. 2006, Meunier, Deschamps et al. 2008, Apschner, Schulte-Merker et al. 2011).

5.2. Cartilage development

Two different types of tissue give rise to the chondrocranium, the cranial NCC and the mesoderm. The viscerocranium is formed from the NCC only. The NCCs migrate and divide into several clusters to constitute the pharyngeal arches. The first cluster gives rise to the mandible and the second to the hyoid, while the third cluster of NCC forms the 5 branchial arches (Schilling and Kimmel 1994).

The CNN differentiate into chondrocytes by the expression of several genes during chondrogenesis. *dlx2a* expression is detected already at 12hpf in NCC. Dlx2a is important for NCC migration and for the expression of other chondrogenesis factors, such as Sox9a (Sperber, Saxena et al. 2008). Bmps are also important for zebrafish cartilage and bone development. Bmp2a, Bmp2b, Bmp4 and Bmp5 are all expressed in the pharyngeal region (Holzschuh, Wada et al. 2005). In zebrafish, ectopic expression of the Bmp inhibitor Chordin causes a decrease of bone matrix-deposition and a dowregulation of both *runx2* and *sox9* genes as well as *col10a1a*, all essential for chondrocyte and osteoblast differentiation (Smith, Avaron et al. 2006). The mammalian *Sox9* gene is duplicated in zebrafish into *sox9a* and *sox9b*. Both are important for a correct cartilage formation. Their expression colocalizes in several places, such as the otic vesicle, before CNN migration, but they have also distinct expression domains. *sox9b* and *sox9a* are expressed in cNCC before migration, while only *sox9a* is expressed in cNCC after migration (Yan, Willoughby et al. 2005). The jellyfish (*jef*) mutant is sox9a deficient and totally lacks the pharyngeal cartilage. This absence of cartilage leads to severe reduction of endochondral bones. Hyomandibular and ceratohyal are missing, while others are smaller such as the dentary, maxillary and opercle (Yan, Miller et al. 2002, Yan, Willoughby et al. 2005). Sox9a, similar to the human SOX9, is crucial and has a direct effect on the *col2a1* expression. Col2a1 is also the major collagen present in cartilage, as in mammals. Sox9b is expressed in the pharyngeal region from 48hpf to at least 68hpf and is required to regulate *runx2b* expression, similar to mammals (Yan, Willoughby et al. 2005). In zebrafish, the mammalian *Runx2* gene has 2 orthologs, *runx2a* and *runx2b*. Runx2b and Runx3 are essential for correct cartilage development. Injection of morpholinos (MO) against *runx2b* leads to severe defects in the neurocranium and the pharyngeal region. Runx2b is required at different levels for skeletal development including chondrocyte maturation and

osteoblast differentiation. Runx2b morphant embryos do not develop hypertrophic cartilage. Runx2b expression depends on Runx3 expression (Flores, Lam et al. 2006). In our lab, previous studies have shown that *runx3* is expressed in the pharyngeal endoderm and initiates a regulatory cascade that induces expression of *egr1* and *sox9b*. This induction leads to repression of the follistatin a (*fsta*) gene, coding for an extracellular inhibitor of BMP signaling. As a result, the BMP factors present in the pharyngeal region are now able to induce expression of *runx2b* in the neural crest cells, thus allowing their differentiation into chondrocytes (Dalcq, Pasque et al. 2012, Larbuisson, Dalcq et al. 2013). Ihh and PTHrP are both present in zebrafish but their interactions in chondrogenesis are still not known. The mammalian *Ihh* gene has 2 orthologs *ihha* and *ihhb*. Ihha is expressed in hypertrophic chondrocytes of the cranial and fin skeleton during endochondral ossification (Avaron, Hoffman et al. 2006) and the *ihha* gene is essential for the onset of endochondral ossification (Hammond and Schulte-Merker 2009), similar to mammals. The zebrafish mutant *ihha*^{hu213} completely lacks endochondral ossification until 17dpf. At 21dpf, it appears that Ihha can be replaced by Ihhb and thus ossification can occur. PTHrP has an important role in development. PTHrP is highly expressed in muscle and cartilage. Intermediate expression levels are found in the skin, brain, kidney, gills and duodenum and very low levels are found in heart and pituitary (Abbink and Flik 2007, Guerreiro, Renfro et al. 2007). In zebrafish, there are 2 homologues; PTHrPa and PTHrPb. They present different expression patterns in the skeleton system. PTHrPa is expressed in many pharyngeal skeleton structures such as ceratobranchials, ceratohyals and teeth, while PTHrPb is only expressed in a part of the hyosymplectic and the opercle (Yan, Bhattacharya et al. 2012). PTHrP in zebrafish conserve the same function as in mammals. Morpholino knock-down of any of these two genes leads to severe defects in cartilage formation. PTHrPa morpholinos induce a decrease of *sox9b* expression and an increase of *sox9a* and *runx2b* expression, while PTHrPb morpholinos show a decrease in both *sox9* genes and an overexpression of *runx2b*. Conversely, *sox9a* and *sox9b* mutants exhibit a decrease of PTHrP expression. The double sox9a and sox9b mutant eliminated totally PTHrP expression (Yan, Bhattacharya et al. 2012).

5.3. Bone development

In zebrafish, the three bone cell types (osteoblasts, osteocytes and osteoclasts) are present. Bone development in zebrafish is similar to mammals at the level of transcription factors, pathways and matrix molecules (Renn, Winkler et al. 2006, Witten and Huysseune 2009, Apschner, Schulte-Merker et al. 2011). Both *runx2a* and *runx2b* are expressed at the early

stages of osteoblast differentiation. However, their cranial expression is already decreased around 120hpf (Li, Felber et al. 2009). Similar to mammals, *osx* is an intermediate osteoblast marker, followed by bone matrix markers such as Bglap, osteonectin, and osteopontin in mature osteoblasts (Gavaia, Simes et al. 2006, Li, Felber et al. 2009). As in mammals, Runx2b induces Bglap expression in zebrafish (Pinto, Conceicao et al. 2005). Bglap starts to be expressed at 7dpf in the 5th ceratobranchial cartilage when the teeth are already calcified. It is expressed in hypertrophic cartilage and then is restricted to cells in mineralization (Gavaia, Simes et al. 2006). In contrast to mammals, there are two bglap genes in zebrafish (*bglap1* and *bglap2*) (Laize, Viegas et al. 2006). The second bone matrix marker is Osteonectin or "secreted protein acidic cysteine-rich" (Sparc), a major non collagenic glycoprotein in the extracellular bone matrix that possesses binding sites for calcium and collagens type I, III and V (Chen, Bal et al. 1992, Bradshaw and Sage 2001, Brekken and Sage 2001). Sparc is thus important for bone calcification and mineralization in mammals. However, few studies exist concerning Sparc in zebrafish. Rotland and collegues have shown that *sparc* knockdown leads to defects in the inner ear and cartilage formation (Rotllant, Liu et al. 2008). Sparc is also essential for correct otolith development (Kang, Stevenson et al. 2008). The last glycoprotein important in bone matrix is osteopontin, also known as secreted phosphoprotein-1 (Spp1). Spp1 is regulated by Runx2 and Osx in mammals (Nakashima, Zhou et al. 2002, Inman and Shore 2003). Spp1 can bind collagen type I and Bglap (Chen, Bal et al. 1992, Ritter, Farach-Carson et al. 1992). Spp1 is an inhibitor of hydroxyapatite crystal growth and control the matrix mineralization (Boskey, Spevak et al. 2002, Gericke, Qin et al. 2005). In zebrafish, *spp1* is expressed in cells surrounding the bone matrix starting from 2 dpf . Spp1 morpholinos cause a decrease of bone deposition (Venkatesh, Lee et al. 2014), in contrast to mice lacking Spp1 that show an increase of mineralization (Boskey, Spevak et al. 2002). The collagens related to bone formation found in zebrafish are similar to those in mammals, such as Col10a1, Col1a1 and Col1a2. All these collagens are expressed in osteoblasts. The *col10a1* gene is expressed in all bone structures and is visible in both cartilage and bones (Eames, Amores et al. 2012, Kim, Lee et al. 2013). A *col1a1* mutant zebrafish presents severe bone development defects and bone fragility. This phenotype is similar to the defects observed in human skeletal dysplasia (Fisher, Jagadeeswaran et al. 2003). As described at point 2.3.1.1., murine *Dlx5* and *Dlx6* are important for a correct bone formation. In zebrafish, their homologuous genes are *dlx5a* and *dlx6a*. Both are present in the cNCC which give rise to the branchial arches and are regulated by endothelin-1 and BMP (Alexander, Zuniga et al. 2011, Zuniga, Rippen et al. 2011). Morpholino injections against *dlx5a* induce a curly tail and

deficient pectoral fins in 50% of the embryos. This phenotype is considered as moderate phenotype. More severe defects present in addition a smaller size and craniofacial defects (only 3% of the 50%). Only 6% of the *dlx6* morphants exhibit the moderate phenotype. The combined dlx5/dlx6 morphants present more severe phenotypes. The dlx5/dlx6 genes are necessary for pectoral fin formation and cleithrum differentiation (Verreijdt, Debiais-Thibaud et al. 2006, Heude, Shaikho et al. 2014). Two additional genes less studied in mammals are the two *Sox4* orthologs, *sox4a* and *sox4b*. The *Sox4* null mice die from circulation failure *in utero*, while the *Sox4* heterozygous mutant mice exhibit a decrease of bone mass and bone strength. Osx, Ocn, Col1a2 and ALP were down regulated in $Sox4^{+/-}$ mice, suggesting a decrease of bone formation (Nissen-Meyer, Jemtland et al. 2007). Sox4 is known to be expressed in hypertrophic chondrocytes of mouse hindlimbs (Reppe, Rian et al. 2000). In zebrafish, *soxa4* is known to be involved in the nervous system, while *sox4b* has a role in the pancreas and pituitary (Mavropoulos, Devos et al. 2005, Gribble, Kim et al. 2009, Quiroz, Lopez et al. 2012).

In the dermal bones, the osteoblasts express *osx* and are independent of the level of Hedgehog signaling. In contrast, endochondral bones present two populations of osteoblasts, with different sensitivities to the Hedgehog pathway. The first is similar to mammals, these osteoblasts are located at the edge of the cartilage structures and are visible from 5dpf in wild type zebrafish, but not in *ihha* mutant. These osteoblasts require a low level of hedgehog signaling to be formed. The second population is scattered within the cartilage and conserves chondrocyte morphology. They start to express *osx* and a high level of Hedgehog signaling is required for their ossification. These osteoblasts develop 3 days earlier in the *patched* mutant, where hedgehog signaling is increased relative to wild type. In contrast, they failed to develop in the *ihha* mutant, similar to the first population. Thus, *ihha* is crucial for both osteoblast populations involved in endochondral ossification (Hammond and Schulte-Merker 2009).

The osteoclasts of the zebrafish can be mononucleated or multinucleated. Actually, larvae develop only mononucleated osteoclasts, which remain predominant in juveniles. The mononucleated osteoclasts start to be active at 20dpf, as judged by TRAP analysis (Witten, Hansen et al. 2001). The first multinucleated osteoclasts appear around 40 dpf, which become predominant in adults although both types remain present during the entire fish lifespan (Witten, Hansen et al. 2001). The two categories of osteoclast induce different kinds of bone resorption; mononucleated osteoclasts produce a flat resorption bay, while the multinucleated osteoclasts form a deep resorption bay (Witten, Hansen et al. 2001). Note that recently,

expression of osteoclastic markers such as *cathepsin K*, *mmp9*, *rank* ... or the presence of TRAP enzyme was shown in zebrafish larvae at much earlier stages (Sharif, de Bakker et al. 2014).

Note that there are 3 different types of bone destruction in teleost: osteosclasia as described just before with eroded cavity formation by osteoclasts, osteocytic osteolysis and halastatic demineralization (Meunier, Deschamps et al. 2008). The osteocytic osteolysis involves osteocytes and not osteoclasts. Under particular conditions, the osteocytes are able to demineralize the bone matrix around their lacuna. This process is used to regulate calcium homeostasis. The halastatic demineralization is also named diffuse demineralization. This demineralization occurs without affecting the organic bone matrix (Meunier, Deschamps et al. 2008, Witten and Huysseune 2009).

5.4. PTH, VitD3 and calcium homeostasis

Zebrafish lack a parathyroid gland. For a long time, it was considered there were no parathyroid gland equivalent and thus no PTH. However, Okabe and Graham (2004) show that the *gcm2* gene, expressed specifically in the pharyngeal pouches and the forming parathyroid glands in mammals, is also present and expressed in zebrafish. *gcm2* expression progresses from the second pharyngeal pouch to all the pouches to finally reach the internal gill bud. This progression of expression is similar to that of the *Gcm2* gene in mammals. The internal gill bud could thus be linked to the parathyroid gland during evolution. These results suggest that *gcm2* is essential for parathyroid gland formation in the animals containing this gland, but also in teleosts which lack this gland (Okabe and Graham 2004). The zebrafish has 2 *pth* genes (*pth1*, *pth2*), one *pthrp* gene, one *pth-like* gene and 3 Pth receptor genes (*pth1r*, *pth2r*, *pth3r*). The teleost endocrine system seems actually more complex than in mammals, with different roles for Pth maybe in part due to the requirement for osmoregulation (Gensure, Ponugoti et al. 2004). The two Pths can bind and activate the human PTH/PTHrP receptor because the 34 N-terminal aa are very highly conserved between species (Guerreiro, Renfro et al. 2007). Pth is totally active and expressed also in the gills (Okabe and Graham 2004). Pth1r is very close to Pth3r, as a consequence of the gene duplication. Pth and Pthrp can bind Pth1r, but only Pth can bind Pth2r, as seen in mammals (Hoare, Rubin et al. 2000, Guerreiro, Renfro et al. 2007).

In zebrafish, the general VitD3 metabolism is also similar to that in mammals. The transformation in liver and kidney occurs with the same enzyme. A difference is the presence

of two VitD receptor genes (*vdra* and *vdrb*) in zebrafish, which display 86% of similarity overall and 97% in the binding domain. The expression of *vdra* is higher than *vdrb*, except in testis and in ovaries. Both are widely and highly expressed in intestine, kidney, transporting cells in the gill and bone of adult zebrafish. Further expression is observed in other tissues, such as the skin, olfactory organs, retina, pancreatic acinar cells, hepatocytes, brain and epithelial cells of the bile duct (Craig, Sommer et al. 2008, Craig, Zhang et al. 2012, Chun, Blatter et al. 2014).

The major difference between mammals and fish concerning calcium homeostasis is the way of calcium intake. In contrast to mammals, zebrafish find the calcium in their environment. Larvae absorb the calcium through the body skin before the development of the gills. Adult zebrafish have their calcium uptake through the gill epithelium (Guerreiro, Renfro et al. 2007, Lin, Tsai et al. 2011, Lin, Su et al. 2012). The most important sites of calcium transport are the cells in the gill epithelium and the intestine (Guerreiro, Renfro et al. 2007). The principal hormones involved in calcium homeostasis in mammals are PTH, VitD3 and calcitonin. In zebrafish, PTH and VitD3 play a similar function as in mammals. In larvae, Pth is expressed in the spinal cord and in the neuromasts of the lateral line as the calcium-sensing receptors (Lohr and Hammerschmidt 2011). Zebrafish in low calcium concentration medium exhibit an increased expression of Pth1, but not Pth2. Overexpression of Pth1, but once again not Pth2, induces a higher calcium concentration. Morpholino (MO) injections confirm these results with a decrease of the calcium level in Pth1 morphants, but no change in Pth2 morphants (Lin, Su et al. 2014). Exogenous Pth administration in zebrafish seems to have the same opposite effects depending on the mode of administration as in mammals. Continuous Pth has a catabolic effect and intermittent Pth has an anabolic effect on bone (Fleming, Sato et al. 2005). VitD3 has a positive effect on calcium absorption in the gills and intestine (Bouillon and Suda 2014). Exogenous active VitD3 increases *vdra* expression in the intestine, but not in gills. However, VitD3 affects the mineral transport in gills (Craig, Sommer et al. 2008). The exact mechanism of VitD3 on calcium regulation remains unclear. *vdra* morpholino injection decreases the calcium level, while no modification is observed in *vdrb* morphants. Exogenous VitD3 together with *vdra* MO injection confirm the role of Vdra in calcium homeostasis. Indeed, VitD3 alone or in combination with *vdrb* MO exhibit an increase of calcium concentration, while VitD3 with *vdra* MO do not present any changes. The absence of Vdra neutralizes the VitD3 effect (Lin, Su et al. 2012). Thus, Pth and VitD3 act on calcium and bone homeostasis in similar ways in zebrafish and in mammals.

Another hypocalcemic hormone is Calcitonin (Ct) which acts through 4 different receptors: Ct receptor (Ctr), and Ctr-like receptors (Crlr1, Crlr2 and Crlr3). In humans, CT is produced by the C cells of the thyroid, while in the zebrafish it is produced in the ultimobranchial bodies (UBB). Ctr and Crlr1 are expressed in the osmoregulator organs such as brain, gills, intestine, kidney, and skin. Crlr2 is expressed in spleen and Crlr3 in the heart. Zebrafish in high calcium concentration medium increase *ct* and *ctr* expression. In fact, Ct seems to exert opposite effects as shown by transgenic overexpression: at 30hpf, Ct overexpression decreases the calcium level, while at 105hpf, it increases the calcium concentration. Thus, short overexpression decrease and long term application increases the calcium level (Lafont, Wang et al. 2011, Lohr and Hammerschmidt 2011).

A last hormone acting on calcemia was discovered first in teleost before being also found in mammals: stanniocalcin (Stc). Four different Stcs were found in zebrafish: Stc1, Stc-1like, Stc2 and Stc-2 like. In low calcium concentration medium, *stc1* and *stc2* expression is decreased, while *stc1-like* and *stc2-like* expressions are unchanged in different calcium concentrations. Stc1 overexpression decreases calcium, but also Na^+, Cl^- and H^+ levels (Chou, Lin et al. 2015). Thus, this hormone is considered as hypocalcemic, but can also have a role in general ionic balance.

6. The zebrafish as model to study the effects of altered gravity.

In this study, we use the zebrafish as a model to study the effects of altered gravity. This fish, and others such as the Medaka (*Oryzias latipes*) or the goldfish (*Carassius auratus*) have been already used for several spaceflight experiments. Almost all of these spaceflight experiments concerned the effect on the vestibular system development and the otoliths, or the behavior. Otoliths, within the vestibular system, allow the animal to sense gravity and modifications in movement directions. The fish use the vestibular and the visual system to maintain their orientation and balance. In hypergravity, otolith growth and calcium incorporation is slower than in 1g (Anken, Beier et al. 2004)(Anken and all, 2004). In microgravity, the absence of gravity causes disorientation and the swimming behavior is modified. The fish are destabilized, they try to compensate by fin movements and present a looped (kinetotic) swimming. In contrast, hypergravity (3g) has no effect on the swimming behavior (Braemer W 1957, Rahmann and Anken 2000).

In the last 15 years, simulated or real altered gravity experiments on fish has progressed on different physiological systems. One of these studies concerned the possibility of fish mating

in space. A particular strain of medaka lacking any looping response (they used mainly a fixed light source for orientation) was selected for a 2 weeks Shuttle STS-65 flight. They presented a normal mating behavior and the female laid eggs whose embryonic development occurred correctly. When these fish returned on ground, they continued to breed as usual without any effect on the offspring, showing that normal development and procreation is possible in space (Ijiri 1995). Another study used a transgenic zebrafish expressing the green fluorescent protein gene (*gfp)* under the control of the β-actin promoter that was placed into a RWV. In a first experiment, beginning at the 18-20somite (20hpf) for 24hours in simulated microgravity, the *gfp* was induced in the heart, the notochord or in the entire embryo in, respectively 23.9%, 17.5%, and 8.5% of the animals (Gillette-Ferguson, Ferguson et al. 2003). A second experiment was performed with various start and end points between 8hpf and 72hpf and Gfp expression in the heart, the notochord, the eyes, the lens, the somites, the neurons and the whole embryo was monitored. No effect was observed upon treatment from 8 to 24hpf, while *gfp* expression was induced with a longer exposure until 32hpf. The highest induction was observed when the embryos were placed in simulated microgravity from 24hpf to 72hpf. After 72hpf, *gfp* expression decreased (Shimada, Sokunbi et al. 2005).

Another experiment revealed that development of the swim bladder was also disturbed in simulated microgravity, in RWV from 0 to 96hpf. The embryos developed and hatched correctly, but only 14% of the RWV embryos presented an inflated swim bladder versus 62% of the control embryos. There was no mortality, but a delay in the swimming behavior to reach the water surface and a delay in development for the swim bladder volume and the length of the embryo. This delay was not present anymore at 144hpf (Lindsey, Dumbarton et al. 2011). In a last study, Edsall and Franz-Odendaal exposed zebrafish embryos on a RWV for 12, 24, or 96 hours at key stages (10 and 12hpf) for cranial neural crest cell migration. A large part of the cranial skeleton derives from the cranial neural crest cells and they observed the skeleton at 4 months. The fish exposed for 12 and 24hours on the RWV present corrugated bones (opercle, parasphenoid) and a decrease of ossification, while the fish exposed during 96 hours were similar to the controls. Shimada and al.(Shimada, Sokunbi et al. 2005) and Edsall and al.(Edsall and Franz-Odendaal 2014) conclude that zebrafish can adapt to the effect of the RWV when they are older than 72hpf. In conclusion, all these studies demonstrate that fish, in particular zebrafish, can be used as a model to study the effect of space conditions on different physiological systems.

7. Principal objectives of this study

The general aim of our work is to use the zebrafish as a model to study bone homeostasis in spaceflight to obtain a better understanding of the mechanisms involved in adaptation to the microgravity condition.

We focused on cartilage and bone development in zebrafish larvae, mainly between 5-10dpf when ossification is actively taking place. The treated larvae were analyzed for skeletal formation, using specific staining methods for cartilage and bone extracellular matrix, and for gene expression using RT-qPCR and whole genome microarray expression analysis. The stained skeletal structures were submitted to image analysis and we developed objective and quantitative methods to evaluate the morphological and developmental modifications of the cartilage and bone skeleton. We started with chemical treatments, because the effects of VitD3 and Pth on bone are well known in mammals, but also in zebrafish (Fleming, Sato et al. 2005). Therefore, we based our study on the principle that VitD3 increases bone formation, while continuous Pth administration decreases bone development. Gene expression analysis was performed in control and treated larvae between 5dpf to 10dpf for selected bone-related genes by RT-PCR, while the microarray analysis was only performed directly after 24hour treatment, at 6dpf, to detect the early genes involved in the regulatory mechanism.

The results of these treatments were the starting point of other experiments, this time concerning gravity alterations and their effects on cartilage and bone development, but also their effects on the general physiology in zebrafish. We used 3 different microgravity simulators (clinostat, RPM and RWV). Image analysis of the skeleton and microarray analysis were performed similarly to the chemical treatments with the same goal. Our final aim was to compare the results of 3 different microgravity simulators, to select the genes involved in adaptation to microgravity, and, as an unexpected result, to select the most appropriate device to simulate microgravity using zebrafish larvae.

We finally decided to perform the same experiment on a hypergravity simulator device, a Large Diameter Centrifuge, with the expectation of opposite results. Finally, we applied another approach of simulating a microgravity effect by introducing the concept of “relative microgravity” or the “Reduced Gravity Paradigm” to induce physiological and bone alterations in the zebrafish larvae.

Results

Chapter 1

Modulation of head skeletal development and gene expression by hormones treatments.

1. Effects of drug treatments on head skeletal formation.

Our general aim is to investigate the effect of changes in gravitational conditions on zebrafish skeletal formation and general physiology. To this end, we needed to develop methods for objectively and quantitatively assessing skeleton formation in developing larvae, and to investigate gene expression using RT-PCR and whole genome micro-arrays.

To validate these different approaches, we first wanted to examine the effects of chemical treatments known to affect skeletal development. Treatment of zebrafish larvae with VitD3 was previously shown to result in enhanced bone formation, while continuous treatment with PTH led to decreased bone formation (Fleming, Sato et al. 2005). We decided to confirm these results and extend these findings by comparing the effects on skeletal formation to those on gene expression for VitD3 and continuous PTH.

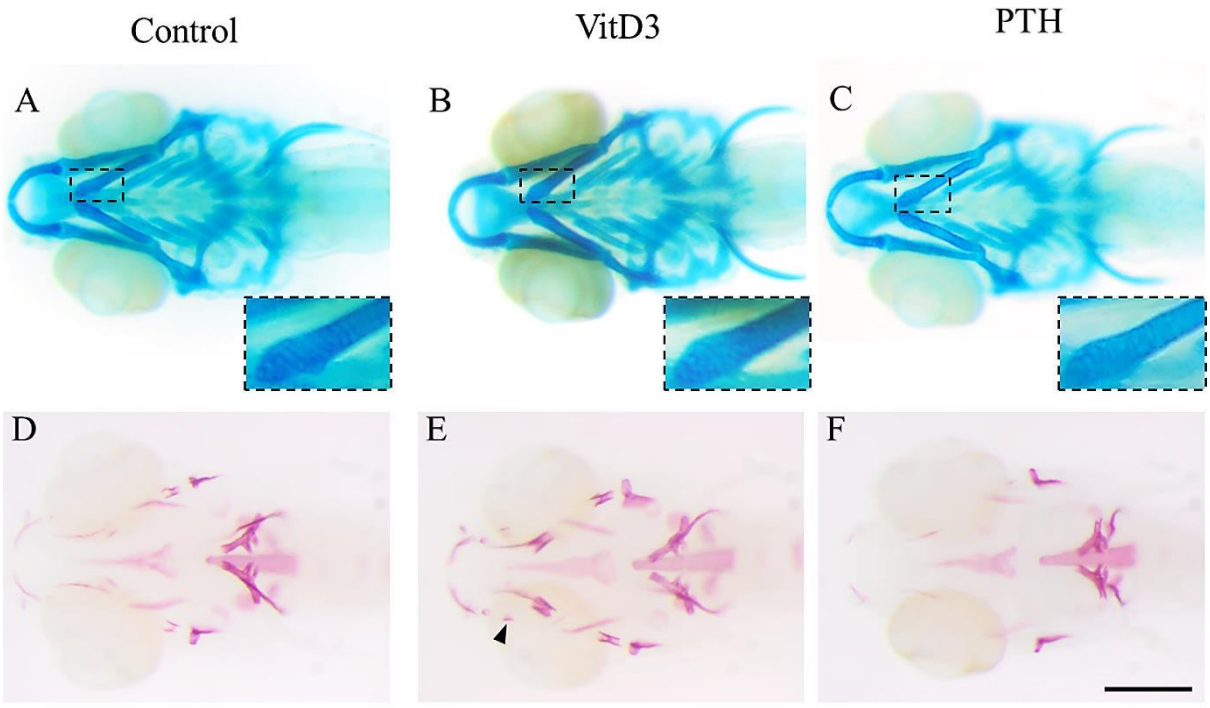

Figure 1: Cartilage and bone elements of the head skeleton in 10dpf zebrafish larvae after 5 days chemical treatments. (A-C) Alcian blue staining of cartilage. (D-F) Alizarin red staining of bone. (A,D) Controls in DMSO. (B,C) No significant effect of, respectively VitD3 and PTH on cartilage development, nor on chondrocyte shape or size (inlays showing close-up). (E) Increase of bone development after VitD3 treatment. (F) Decrease of bone development after PTH treatment. Ventral views, anterior to the left, (A-F) scale bar = 250µm.

VitD3 and PTH treatments were performed continuously from 5dpf to 10dpf, Control and treated larvae were stained by Alcian blue for cartilage extracellular matrix (ECM) and with

Alizarin red to detect the calcified bone matrix. At this stage, the head cartilage is well formed and a complete set of cartilage elements is observed (see Fig. 39 in materiel and methods or in attachment). In contrast, although ossification begins at 3dpf and the first bone structures are visible at 5dpf, the bone skeleton continues its formation until 30dpf (Nüsslein-Volhard C 2001). Nevertheless, at 10dpf, a number of bone elements are observed in the head region, the first vertebral centrae are formed, while others only begin to be calcified (for example the branchiostegal ray2) (see materiel and methods; in attachment).

In three independent experiments, 27-29 ventral view images of Alcian blue- or Alizarin red-stained larvae were obtained. After 5days of VitD3 or PTH treatment, cartilage stays unchanged as compared to the control by general observation. The structures are well formed, complete with the glycosaminoglycans present in the cartilage matrix judging from the similar staining intensity (Fig. 1A-C). In a close-up view (Fig. 1A-C, inlays), no difference could be observed in cell shape or size between the different treatments. Considering bone calcification, a general observation revealed a clear increase of bone development upon VitD3 treatment (Fig. 1E). Some structures appear in advance, such as the retroarticular (Fig. 1E arrowhead) bone and the preopercular (not shown) bone, while some other structures are thicker such as the dentary or the ceratohyal, or longer such as the branchiostegal ray2. Nevertheless, the general morphology was unchanged, In contrast, continuous PTH treatment led to a general decrease of bone formation and to a complete absence of some structures, such as the anguloarticulars and branchiostegal ray2 (Fig. 1F).

Based on these images, we applied two complementary approaches to obtain a more objective qualitative and quantitative description of the skeleton. The first one is a morphometric approach that evaluates the general aspect of the head skeleton by measuring the distances between and the relative position of all detected bone elements. The images were introduced into the CYTOMINE software (see Materials and Methods, (Marée R 2013)) and each image was annotated by positioning specific landmarks representing the different skeletal elements. For larvae stained for cartilage, 21 landmarks were defined (see materiel and methods; in attachment, Fig. C), while 29 points of interest were positioned within the Alizarin red-stained bone skeleton (see materiel and methods; in attachment, Fig. D). In these pictures, we consider the head separated horizontally in 2 parts. Some structures are unique and located on the symmetry axis, while others are paired and localized symmetrically, such as the dentary, maxilla, entopterygoid, and hyosymplectic. To facilitate recognition, these were labelled “up”

and “down”. The software then computes the distances between selected landmarks and the angles formed by lines drawn between selected points.

Morphometric analysis in VitD3-treated larvae cartilage revealed an increase of the distance between articulation (ar) "up" and "down", leading to a broader jaw as compared to untreated animals, while all the other distances remained unchanged (Fig. 2A,C; annex2). Morphometric cartilage analysis of larvae treated with PTH for 5 days revealed an increase in length of the ceratohyal cartilages (ch, Fig. 2B; annex2). Analysis of the bone skeleton after VitD3 treatment revealed a significant increase of the distance between maxillae (m, Fig. 3A; annex3), consistent with a broader jaw as already observed by cartilage morphometry. The length of the head skeleton is also increased upon VitD3 treatment with a longer distance between the anterior part of the head (an) and the notochord (n) or the parasphenoid (p). Other measures are not significantly modified (Fig. 3A,C; annex3). PTH treatment led to a significant decrease of the size of the parasphenoid (p, Fig. 3C; annex3). Some structures are missing, such as the anguloarticular (aa), branchiostegal ray2 (br2), ceratohyal (ch) and/or maxilla (m) and a significant broadening of the posterior head skeleton is revealed by the increased distance between left and right ("up" and "down") branchiostegal rays1 (br1), entopterygoids (en), and opercula (o) (Fig. 3B; annex3).

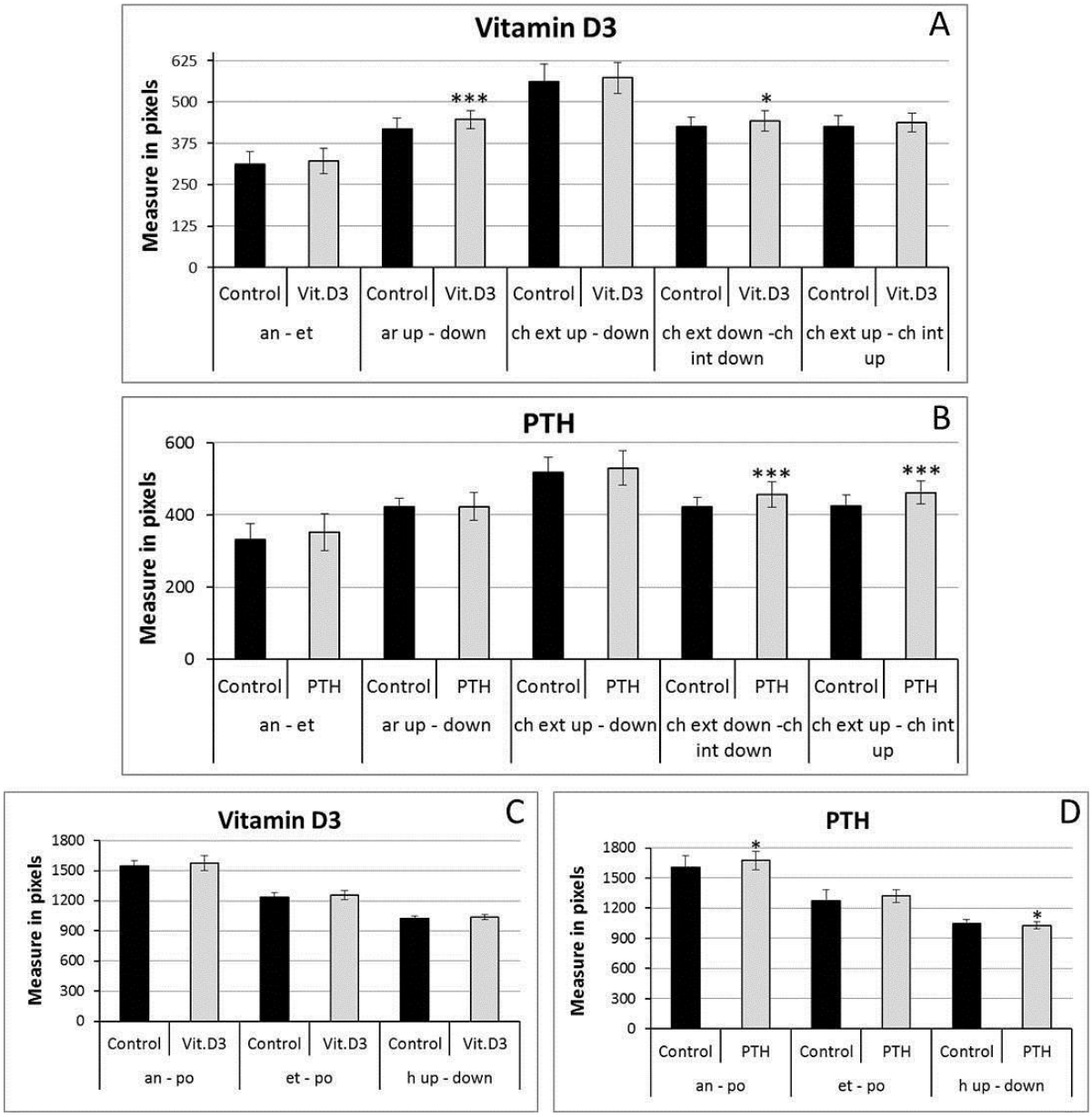

Figure 2: Morphometric analysis of cartilage staining after 5 days chemical treatments. The distances are measured in pixels, Mean ± SD and t-test analysis were calculated for each measure on at least 20 individuals, * $p < 0.05$ and *** $p < 0.001$. (A, C) Distance after VitD3 treatment, (B, D) Distance after PTH treatment, Abbreviations as in figure 1. A) Morphometric analysis in VitD3-treated larvae cartilage revealed an increase of the distance between articulation (ar) "up" and "down", leading to a broader jaw as compared to untreated animals, while (A, C) all the other distances remained unchanged. B) Morphometric cartilage analysis of larvae treated with PTH for 5 days revealed a significant increase in length of the ceratohyal cartilages only (D).

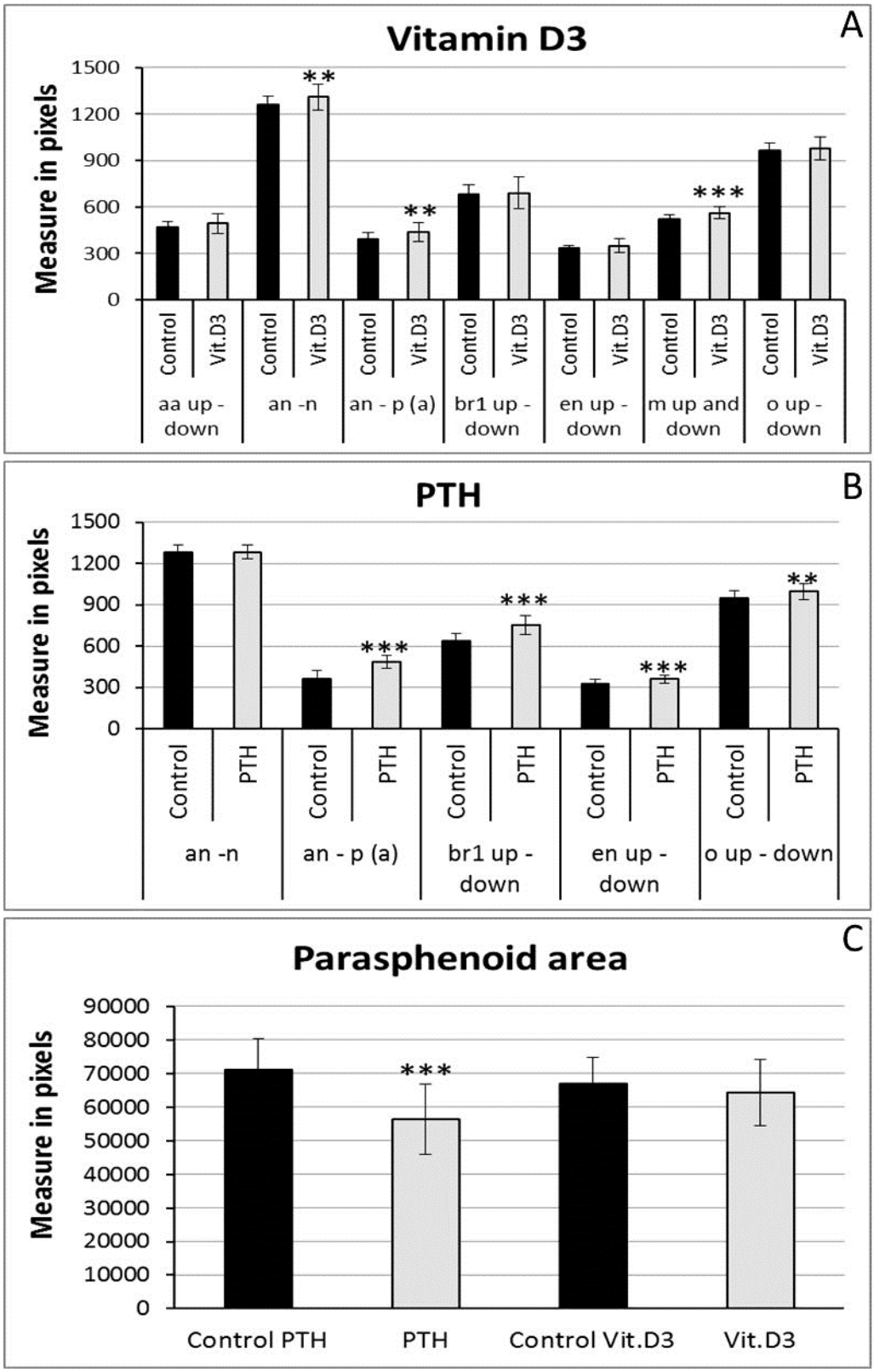

Figure 3: Morphometric analysis results of bone matrix staining after 5days chemical treatments. The distances are measured in pixels. Mean ± SD and t-test analysis were calculated for each measure on at least 20 individuals, * $p < 0.05$, ** $p < 0.01$ and *** $p < 0.001$. (A) Distances after VitD3 treatment, (B) Distances after PTH treatment, (C) Area of the parasphenoid bone results after 5 days PTH or VitD3 treatment. Abbreviations as in figure 1. A) Analysis of the bone skeleton after VitD3 treatment revealed a significant increase of the distance between maxillae (m), consistent with a

broader jaw as already observed by cartilage morphometry. The length of the head skeleton is also increased upon VitD3 treatment with a longer distance between the anterior part of the head (an) and the notochord (n), and between anterior (an) and the parasphenoid (p) bone. Other measures are not significantly modified (A, C). B) PTH treatment caused an increase of the distance between the anterior part of the head and the summit "a" of the parasphenoid, mainly due to a significant decrease of the size of the parasphenoid (p) (C).

The second approach consists in the evaluation of the intensity and progression of bone formation of the different bone structures, and their level of ossification. In each image, every bone structure is assigned a score, ranging from absent (red), early ossification (yellow), advanced (green) or over-ossified (purple) in comparison to a typical image of a control larva of the same age. The distribution of the scores obtained for the different elements in VitD3- or PTH-treated larvae and the corresponding controls is shown in Figure 5 and the results of the statistical analysis are given in Table 1 and 2.

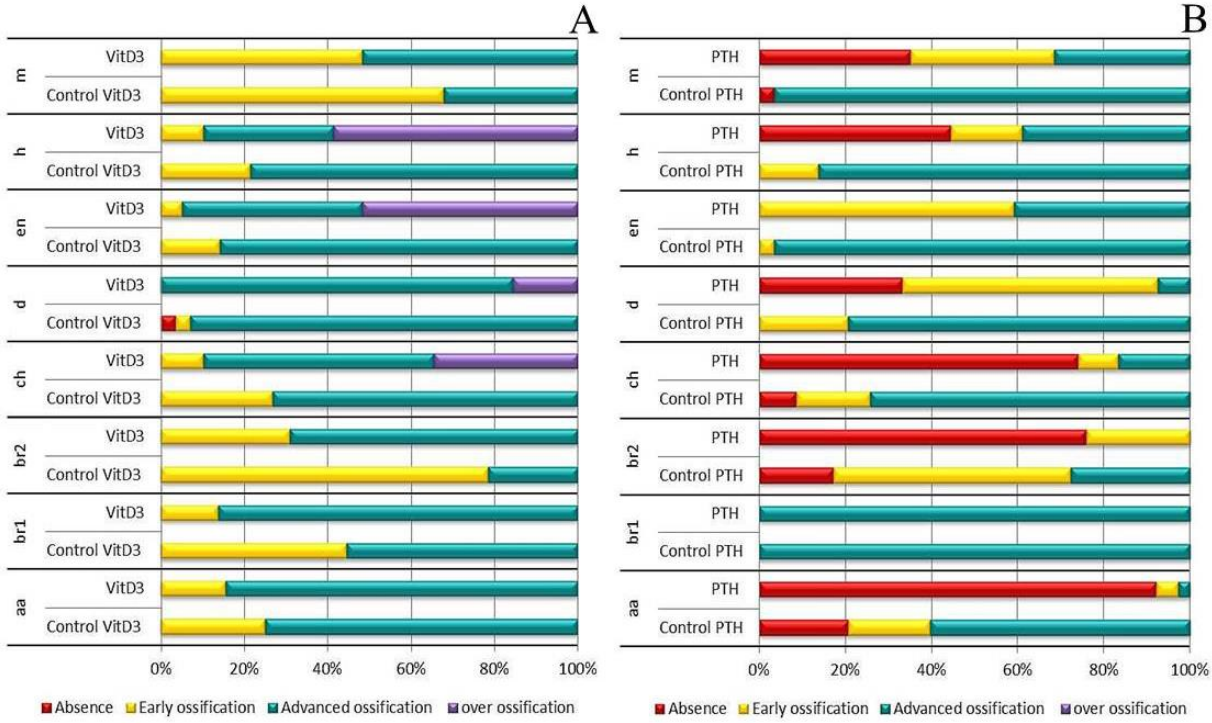

Figure 4: Extent of bone formation in 10dpf larvae after 5days chemical treatments. Bone development is classified for each element into different categories: Absent (no structure present; red), early ossification (beginning of the bone ossification; yellow), advanced ossification (the structure is present and already developed as the control; green) and over ossification (the structure is more developed compared to the control; purple). Cumulated frequencies in % are represented for each element. As no significant difference was observed for paired structures between left and right (up and down), their scores have been combined, Statistical analysis was performed by X^2 of Pearson and a logistic regression. (A) Cumulated frequency after 5days VitD3 treatment, To obtain this, values were attributed to each element according to its category and added up for each larva: 0 for absent, 1 for early, 2 for advanced, and 4 for over ossification. (B) Cumulated frequency after 5days PTH treatment.

After 5 days VitD3 treatment, all the structures are present and some are over-ossified like the hyomandibular, the entopterygoid, the dentary and the ceratohyal bones. Early (delayed) ossification is decreased for all the structures shown, as compared to controls, while advanced ossification increased in the maxilla, branchiostegal ray1, branchiostegal ray2 and anguloarticular (Fig. 4A). Statistical analysis (Table 1) reveals that only the anguloarticular and the maxilla up do not change significantly in this condition. All the other structures (br1, br2, m down, ch, d, en, hm) are significantly increased, with the hyomandibulars, entopterygoids and ceratohyals displaying the most drastic effect. These results confirm a very significant positive effect of VitD3 treatment on bone formation.

PTH treatment resulted in nearly opposite effects to VitD3. Only the entopterygoid and the branchiostegal ray1 are present in each fish (Fig. 4B) with the branchiostegal ray1 unaffected and the entopterygoid displaying 60% of early ossification in PTH-treated larvae compared to 3.45% in controls. All the other structures were absent in at least 20% of the total 27 fish analyzed. The strongest effect was seen in the anguloarticular bone with 94% of absence compared to 21% absence, 19% early ossification and 60% of advanced ossification in the controls. Specific statistical analysis confirmed that PTH treatment significantly ($p<0.001$) reduced nearly all the structures except branchiostegal ray1 (Table 2).

To obtain a global score describing the head skeleton in the different conditions, the individual structure scores in each image were added up and a mean global score was obtained showing that VitD3 treatment significantly increases bone development (from a score of 26±3 in the controls to 33±4 in the VitD3 treatment), while PTH treatment significantly decreases ossification to approximately half of untreated control (from a score of 27± 4 to 13±5.5).

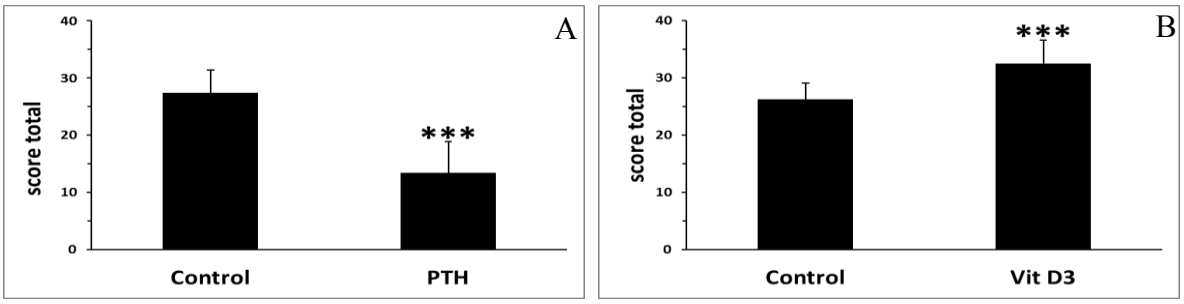

Figure 5: Global score obtained by addition of each intensity category. A) Global score of 10dpf larvae treated by PTH for 5days compare to their control. B) Global score of 10dpf larvae treated by VitD3 for 5days compare to their control.

A

Structures	Treat	N	Mean	Score of ossification (Y)		X² pearson	Logistic regression	
				early	advanced	p-value	OR (IC 95%)	p-value
anguloarticular down	Control	28	0.75	20 (71.43%)	8 (28.57%)		1	
	VitD3	29	0.86	18 (62.07%)	11 (37.93%)	0.454	1.528 (0.503-4.642)	0.455
anguloarticular up	Control	28	0.75	7 (25.00%)	21 (75.00%)		1	
	VitD3	29	0.83	5 (17.24%)	24 (82.76%)	0.473	1.600 (0.441-5.803)	0.475
branchiostegal ray1 down	Control	28	0.54	13 (46.43%)	15 (53.57%)		1	
	VitD3	29	0.86	4 (13.76%)	25 (86.24%)	**0.007**	5.417 (1.490-19.690)	**0.010**
branchiostegal ray1 up	Control	28	0.57	12 (42.86%)	16 (57.14%)		1	
	VitD3	29	0.86	4 (13.76%)	25 (86.24%)	**0.015**	4.688 (1.285-17.096)	**0.019**
branchiostegal ray2 down	Control	28	0.21	22 (78.57%)	6 (21.43%)		1	
	VitD3	29	0.59	12 (41.38%)	17 (58.62%)	**0.004**	5.194 (1.618-16.680)	**0.006**
branchiostegal ray2 up	Control	28	0.21	22 (78.57%)	6 (21.43%)		1	
	VitD3	29	0.79	6 (20.69%)	23 (79.31%)	**<0.001**	14.056 (3.933-50.232)	**<0.001**
maxilla down	Control	28	0.36	18 (64.29%)	10 (35.71%)		1	
	VitD3	29	0.66	10 (34.48%)	19 (65.25%)	**0.024**	3.420 (1.152-10.153)	**0.027**
maxilla up	Control	28	0.29	20 (71.43%)	8 (28.57%)		1	
	VitD3	29	0.38	18 (62.07%)	11 (37.93%)	0.454	1.528 (0.503-4.642)	0.455

B

Structures	Treat	N	Mean	Score of ossification (Y)			X² pearson	Ordinal logistic regression	
				early	advanced	over	p-value	OR (IC 95%)	p-value
ceratohyal down	Control	28	1.71	8 (28.57%)	20 (71.43%)	0 (0%)		1	
	VitD3	29	2.21	4 (13.79%)	15 (51.72%)	10 (34.48%)	**0.002**	6.075 (1.747-21.127)	**0.005**
ceratohyal up	Control	28	1.75	7 (25%)	21 (75%)	0 (0%)		1	
	VitD3	29	2.28	2 (6.90%)	17 (58.62%)	10 (34.48%)	**0.001**	11.764 (2. 406-57.514)	**0.002**
dentary down	Control	28	1.93	2 (7.14%)	26 (92.86%)	0 (0%)		1	
	VitD3	29	2.14	0 (0%)	25 (86.21%)	4 (13.79%	0.050	/	/
dentary up	Control	28	1.93	2 (7.14%)	26 (92.86%)	0 (0%)		1	
	VitD3	29	2.17	0 (0%)	24 (82.76%)	5 (17.24%)	**0.029**	/	/
entopterygoid down	Control	28	1.86	4 (14.29%)	24 (85.71%)	0 (0%)		1	
	VitD3	29	2.48	1 (3.45%)	13 (44.83%)	15 (51.72%)	**<0.001**	33.972 (4.040-285.690)	**0.001**
entopterygoid up	Control	28	1.86	4 (14.29%)	24 (85.71%)	0 (0%)		1	
	VitD3	29	2.45	2 (6.90%)	12 (41.38%)	15 (51.72%)	**<0.001**	16.542 (3.299-82.948)	**<0.001**
hyomandibular down	Control	28	1.82	5 (17.86%)	23 (82.14%)	0 (0%)		1	
	VitD3	29	2.41	3 (10.35%)	11 (37.93%)	15 (51.72%)	**<0.001**	11.226 (2.794-45.400)	**<0.001**
hyomandibular up	Control	28	1.75	7 (25%)	21 (75%)	0 (0%)		1	
	VitD3	29	2.54	3 (10.35%)	7 (24.14%)	19 (65.52%)	**<0.001**	19.373 (4.695-79.936)	**<0.001**

Table1: Ossification scores for individual bone elements in control and 5 days VitD3-treated larvae. (A) Bone structures distributed in 2 categories (early and advanced ossification) (B) Bone structures distributed in 3 categories (early, advanced and over ossification).

A

Structures	Treat	N	Mean	Score of ossification (Y)		X² pearson	Logistic regression	
				early	advanced	p-value	OR (IC 95%)	p-value
branchiostegal ray1 down	Control	29	1.00	0 (0%)	29 (100%)		1	
	PTH	27	0.93	2 (7.41%)	25 (92.59%)	0.136	/	0.995
branchiostegal ray1 up	Control	29	1.00	0 (0%)	29 (100%)		1	
	PTH	27	0.85	4 (14.81%)	23 (85.19%)	**0.031**	/	0.995
entopterygoid down	Control	29	0.97	1 (3.45%)	28 (96.55%)		1	
	PTH	27	0.41	16 (59.26%)	11 (40.74%)	**<0.001**	0.025 (0.003-0.208)	**<0.001**
entopterygoid up	Control	29	0.97	1 (3.45%)	28 (96.55%)		1	
	PTH	27	0.41	16 (59.26%)	11 (40.74%)	**<0.001**	0.025 (0.003-0.208)	**<0.001**

B

Structures	Treat	N	Mean	Score of ossification (Y)			X² pearson	Ordinal logistic regression	
				absence	early	advanced	p-value	OR (IC 95%)	p-value
anguloarticular down	Control	29	1.28	8 (27.59%)	5 (17.24%)	16 (55.17%)		1	
	PTH	27	0.11	25 (92.60%)	1 (3.7%)	1 (3.7%)	**<0.001**	0.031 (0.006-0.1577)	**<0.001**
anguloarticular up	Control	29	1.52	4 (13.79%)	6 (20.69%)	19 (65.52%)		1	
	PTH	27	0.04	26 (96.3%)	1 (3.7%)	0 (0%)	**<0.001**	0.006 (0.001-0.055)	**<0.001**
branchiostegal ray2 down	Control	29	1.03	6 (20.69%)	16 (55.17%)	7 (24.14%)		1	
	PTH	27	0.19	22 (81.48%)	5 (18.52%)	0 (0%)	**<0.001**	0.054 (0.014-0.201)	**<0.001**
branchiostegal ray2 up	Control	29	1.17	4 (13.79%)	16 (55.17%)	9 (31.04%)		1	
	PTH	27	0.30	19 (70.37%)	8 (29.63%)	0 (0%)	**<0.001**	0.055 (0.015-0.207)	**<0.001**
ceratohyal down	Control	29	1.66	2 (6.90%)	6 (20.69%)	21 (72.41%)		1	
	PTH	27	0.41	21 (77.78%)	1 (3.7%)	5 (18.52%)	**<0.001**	0.047 (0.013-0.169)	**<0.001**
ceratohyal up	Control	29	1.66	3 (10.35%)	4 (13.79%)	22 (75.86%)		1	
	PTH	27	0.44	19 (70.37%)	4 (14.81%)	4 (14.81%)	**<0.001**	0.052 (0.015-0.183)	**<0.001**
dentary down	Control	29	1.79	0 (0%)	6 (20.69%)	23 (79.31%)		1	
	PTH	27	0.78	8 (29.63%)	17 (62.96%)	2 (7.41%)	**<0.001**	0.018 (0.003-0.010)	**<0.001**
dentary up	Control	29	1.79	0 (0%)	6 (20.69%)	23 (79.31%)		1	
	PTH	27	0.70	10 (37.04%)	15 (55.55%)	2 (7.41%)	**<0.001**	0.018 (0.003-0.095)	**<0.001**
hyomandibular down	Control	29	1.86	0 (0%)	4 (13.79%)	25 (86.21%)		1	
	PTH	27	0.93	12 (44.44%)	5 (18.52%)	10 (37.04%)	**<0.001**	0.075 (0.020-0.282)	**<0.001**
hyomandibular up	Control	29	1.86	0 (0%)	4 (13.79%)	25 (86.21%)		1	
	PTH	27	0.96	12 (44.44%)	4 (14.81%)	11 (40.74%)	**<0.001**	0.087 (0.023-0.323)	**<0.001**
maxilla down	Control	29	1.93	1 (3.45%)	0 (0%)	28 (96.55%)		1	
	PTH	27	0.93	11 (40.74%)	7 (25.93%)	9 (33.33%)	**<0.001**	0.019 (0.002-0.163)	**<0.001**
maxilla up	Control	29	1.93	1 (3.45%)	0 (0%)	28 (96.55%)		1	
	PTH	27	1.00	8 (29.63%)	11 (40.74%)	8 (29.63%)	**<0.001**	0.017 (0.002-0.142)	**<0.001**

Table 2: Ossification scores for individual bone elements in control and 5 days PTH-treated larvae. (A) The bone structures distributed in 2 categories (early and advanced ossification) (B) The bone structures distributed in 3 categories (absent, early and advanced ossification).

2. Modification of gene expression upon drug treatment.

To gain deeper insight into the molecular mechanisms involved in the observed skeletal modifications, we analyzed the expression of several genes selected for their known function in bone formation. One class of genes codes for structural proteins such as collagens (Col1a1, Col1a2, Col10a1a) or bone specific ECM proteins such as secreted acidic cysteine rich protein (Sparc, previously named osteonectin or Osn), secreted phosphoprotein 1(Spp1, previously named osteopontin or Osp) and bone gamma-carboxyglutamate protein (Bglap, previously named osteocalcin or Ocn). The second class of interest consists of those genes coding for factors involved in regulation of cartilage and bone differentiation, including the *pth1a* gene coding for Pth as well as transcription factor genes *sox4a*, *sox4b*, *dlx5a*, *dlx6a*, *runx2b* and *osx*.

We first decided to follow the expression of these genes during the 6-10dpf period in untreated animals, using the glyceraldehyde-3-phosphate dehydrogenase (*gapdh*) house-keeping gene as reference (selected from 3 candidate housekeeping genes, see Materials and Methods). Compared to their expression at 6dpf, we observe an increase of *sparc*, *bglap*, *spp1* and *col1a1* at 7dpf, followed by a decrease at 8dpf for *sparc*, *bglap* and *spp1*, while the *col1a1* gene peaked at 8dpf and decreased its expression at later stages (Fig. 6A,D). At the opposite of col1a1, the 2 other collagens (col1a2 and col10a1) are decreased progressively from 7dpf to 10dpf (Fig. 6D). The transcription factor gene *dlx5a* displayed an expression peak at 7 and 8dpf and decreased after that, while *dlx6a* was unaffected and *osx* surprisingly revealed a 2-fold decrease from 6 to 7dpf (Fig. 6G). The *pth1a* gene expression strongly increased from 14 to 27 during the 7-9 dpf period and reach 76-fold at 10dpf, while *runx2b* displayed a 15-fold increase (Fig. 6J).

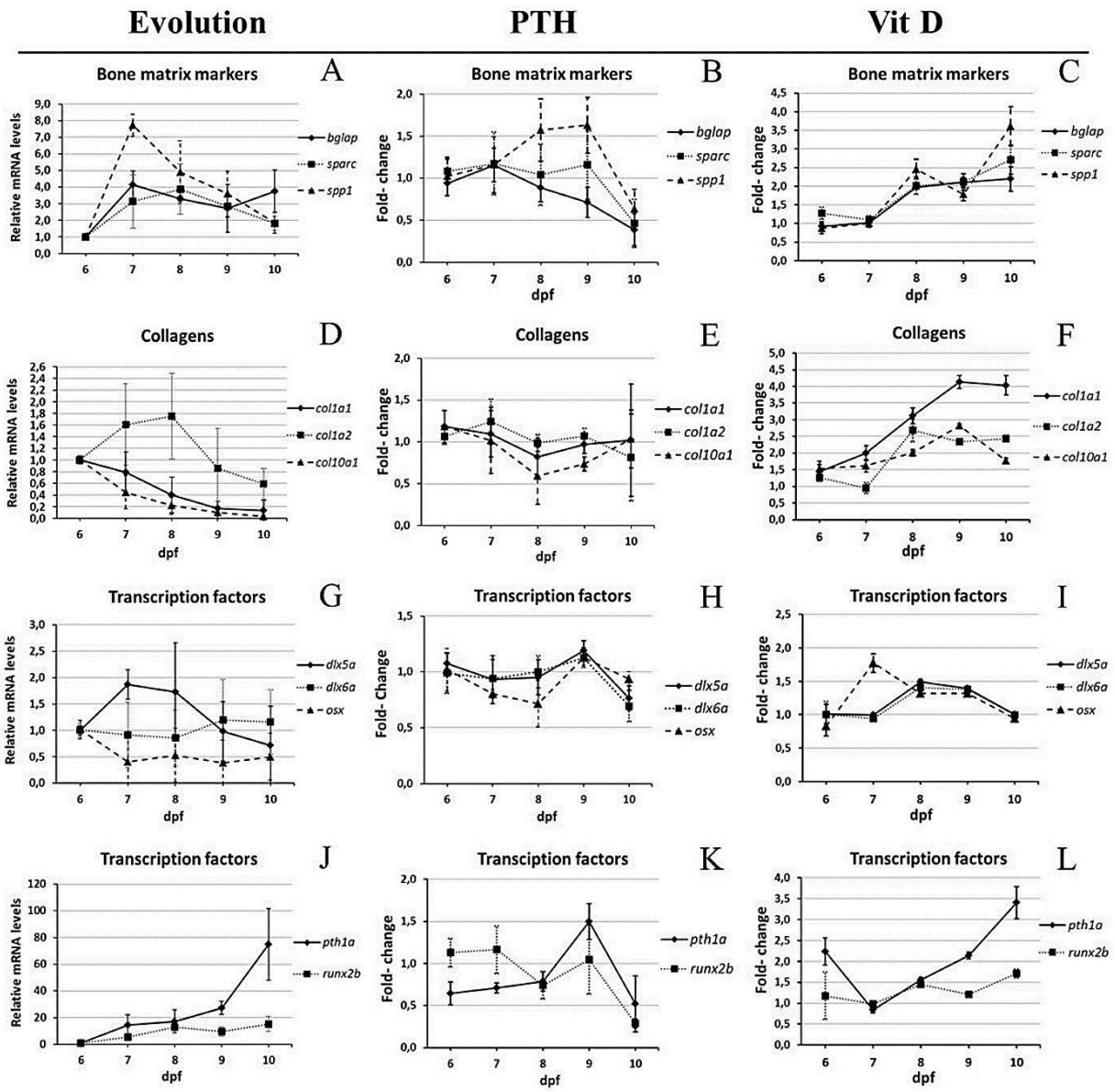

Figure 6: Expression of bone-specific genes during development between 6 and 10dpf. (A,D,G,J,M) Specific mRNA levels at 6dpf relative to the *gapdh* house-keeping gene were used as reference, and then compared to the corresponding level in larvae of different age. (B-C,E-F,H-I,K-L) Specific mRNA levels in treated larvae were determined relative to the *gapdh* reference house-keeping gene and then compared to the corresponding level in untreated controls of the same age. (A-C) Bone matrix markers *bglap*, *sparc*, *spp1*. (D-F) Collagens *col1a1*, *col1a2*, *col10a1a*. (G-I) Transcription factors *dlx5a, dlx6a* and *osx*. (J-L) Parathyroid hormone *pth1a* and transcription factor *runx2b*.

We then investigated the modulation of expression of these genes during drug treatment starting at 5dpf. Compared to untreated controls, VitD3 treatment led to a clear and significant increase in expression of all the structural protein genes: *sparc*, *bglap*, *spp1*, *col1a1* and, to a lesser extent *col1a2* and *col10a1a* (Fig. 6C, F). These results correlate well with the observed increase in bone calcification observed at 10dpf. Among the regulatory factor genes, only

pth1a revealed a strong up-regulation that increased during the treatment, while *dlx5a* and *dlx6a* were transiently induced at 8 and 9dpf. Finally, *runx2b* displayed a weak but significant increase up to 1.5-fold at 10dpf, and *osx1* was only transiently induced 2-fold at 7dpf, (Fig. 6I,L). On the other hand, relative to untreated controls, PTH treatment resulted in a transient increase of *spp1* at 8-9dpf, while *sparc*, and *bglap* were unchanged before a decrease at 10dpf (Fig. 6B). Surprisingly, no significant effect of PTH treatment was observed on the expression of the collagen genes (Fig. 6E). Among the regulatory factors, *pth1a, dlx5a, dlx6a* and *runx2b* declined at 10 dpf (Fig. 6H and K). *osx* expression remained constant (Fig. 6H).

3. Whole genome analysis of gene expression modulation by drugs.

To obtain a global view of the physiological changes caused by PTH and VitD3 treatment, we performed a microarray whole genome expression analysis. We compared 6dpf control larvae to larvae treated between 5dpf and 6dpf with the corresponding compounds, in order to capture early regulatory events rather than secondary regulations leading ultimately to the observed modulations of bone formation at 10dpf.

Four independent experiments were carried out and total RNA was extracted from control and VitD3-treated 6dpf larvae. A complete list of genes affected more than 1.3-fold (log2 fold change 0.4) by VitD3 treatment is given in the table annex 4 (p-value<0.1). Six genes were selected from the list for validation by RT-qPCR, which demonstrated the reliability of the microarray data (Table 3).

	VitD3				PTH			
	microarray		RT-PCR		microarray		RT-PCR	
Gene	Fold Change	p-value	Fold Change	p-value	Fold Change	p-value	Fold Change	p-value
cad	1.424	0.094	2.017	< 0.001				
cyp24a1	8.938	0.005	10.969	< 0.001				
igfbp1	3.782	0.004	5.250	< 0.001				
socs1	0.355	0.066	0.447	< 0.001				
slc26a3	0.525	0.028	0.654	< 0.001				
slc6a18	0.726	0.029	0.895	0.002	0.203	0.066	0.883	0.035
fgf4	0.520	0.110	0.777	< 0.001	0.450	0.079	0.831	< 0.001
mcph1					1.934	0.056	1.130	0.026
ndrg2					1.545	0.060	1.101	0.036
rxra					1.990	0.076	1.247	< 0.001
nrbp2					2.514	0.056	1.210	0.010

Table 3: Comparison of fold change values from the microarray dataset with those observed by RT-qPCR for VitD3 and PTH treatment. The fold change and statistical significance (p-values) are given from the microarray data and the RT-qPCR confirmation experiments. The data for the genes selected for confirmation of microarray results, respectively for VitD3 or PTH, are shaded in grey, s*lc6a18* and *fgf4* were chosen for their regulation by PTH and the results for VitD3 regulation are also shown.

Confirming that the VitD3 pathway was indeed activated, the most highly induced gene is *cyp24a1*, encoding a member of the cytochrome P450 superfamily of enzymes involved in the degradation of 1,25-dihydroxyvitamine D3. Modulation of the insulin pathway is indicated by the significant induction of *igfbp1* and *igf2*. According to Ingenuity Pathway Analysis (IPA; Materials and Methods), other biological functions that were affected by vitamin D treatment (Table 4) are related to lipid, small molecule, amino acid, carbohydrate and drug metabolism, followed by organismal and cardiovascular system development.

Category	p-value	Number of Genes
Lipid Metabolism	3.91E-12-1.79E-02	107
Molecular Transport	3.91E-12-1.79E-02	136
Small Molecule Biochemistry	3.91E-12-1.79E-02	155
Amino Acid Metabolism	1.53E-09-1.66E-02	46
Carbohydrate Metabolism	2.86E-09-1.71E-02	88
Vitamin and Mineral Metabolism	2.54E-07-1.3E-02	40
Energy Production	3.41E-07-1.66E-02	26
Protein Synthesis	5.67E-06-1.12E-02	81
Cellular Function and Maintenance	1.98E-05-1.65E-02	76
Free Radical Scavenging	2.08E-05-1.62E-02	33
Endocrine System Development and Function	6.95E-05-1.66E-02	35
Drug Metabolism	1.75E-04-5.66E-03	12
Cellular Development	2.21E-04-1.69E-02	59
Cellular Growth and Proliferation	2.21E-04-1.74E-02	43
Hematological System Development and Function	2.21E-04-1.74E-02	48
Cell-To-Cell Signaling and Interaction	3.6E-04-1.74E-02	30
Post-Translational Modification	3.91E-04-1.66E-02	32
Protein Degradation	3.91E-04-4.87E-03	27
Embryonic Development	3.91E-04-1.66E-02	48
Organ Development	3.91E-04-1.66E-02	50
Organismal Development	3.91E-04-1.66E-02	107
Skeletal and Muscular System Development and Function	3.91E-04-1.78E-02	57
Tissue Development	3.91E-04-1.69E-02	63
Cell Cycle	8.14E-04-1.66E-02	17
Organ Morphology	9.71E-04-1.78E-02	61
Tissue Morphology	9.86E-04-1.66E-02	90
Cell Death and Survival	1.18E-03-1.6E-02	46
Cardiovascular System Development and Function	1.22E-03-1.69E-02	72
Humoral Immune Response	1.22E-03-3.57E-03	3
Hair and Skin Development and Function	1.47E-03-1.66E-02	12
Cell Morphology	2.55E-03-1.66E-02	33
Cellular Movement	2.66E-03-1.45E-02	41
Cellular Compromise	2.77E-03-1.49E-02	13
Reproductive System Development and Function	3.03E-03-1.15E-02	41
Behavior	3.17E-03-3.17E-03	15
Digestive System Development and Function	3.17E-03-1.66E-02	52
Hepatic System Development and Function	3.19E-03-5.44E-03	17
Renal and Urological System Development and Function	3.45E-03-1.54E-02	56
Organismal Functions	3.51E-03-3.51E-03	9
Protein Trafficking	3.57E-03-3.57E-03	2
Connective Tissue Development and Function	3.59E-03-1.69E-02	33
Lymphoid Tissue Structure and Development	4.48E-03-7.35E-03	10
Gene Expression	4.67E-03-1.1E-02	10
DNA Replication. Recombination. and Repair	6.15E-03-6.15E-03	7
Nucleic Acid Metabolism	6.15E-03-6.15E-03	7
Cell-mediated Immune Response	6.97E-03-7.35E-03	5
Cellular Assembly and Organization	6.97E-03-1.66E-02	14
Hematopoiesis	6.97E-03-7.35E-03	5
Cell Signaling	7.35E-03-7.35E-03	3
Nervous System Development and Function	7.65E-03-7.65E-03	4
Visual System Development and Function	7.65E-03-1.13E-02	12

Table 4: Biological functions associated to genes affected by VitD3. Ingenuity Pathway Analysis of the list of genes affected at 6dpf after VitD3 treatment for 24 hours. Columns indicate respectively the function, the range of p-values (significance) associated to various sub-functions, and the number of genes concerned (N).

A striking feature of the affected genes list is the abundance of genes involved in molecular transport, from ion channels to ATP-dependent pumps (Table annex 4), consistent with a profound adaptation to the changes in metabolism that were also previously observed (Shih, Horng et al. 2012, Hwang and Chou 2013). Among the transcription regulatory factors, we note the decreased expression of *ppara* and of *foxo3*, involved in lipid metabolism, as well as *fosb* and *twist1*, while *klf11* and *klf13* were significantly induced (Table annex 4). As these experiments were performed using mRNA from the entire larvae, we attempted to focus on individual organ systems by filtering the affected gene set against available databases of genes involved in muscle or cartilage/bone function (GO annotation of human gene orthologs using IPA knowledge base). A network of regulatory interactions could be constructed, comprising genes common to both systems and genes specific for each organ (Fig. 7).

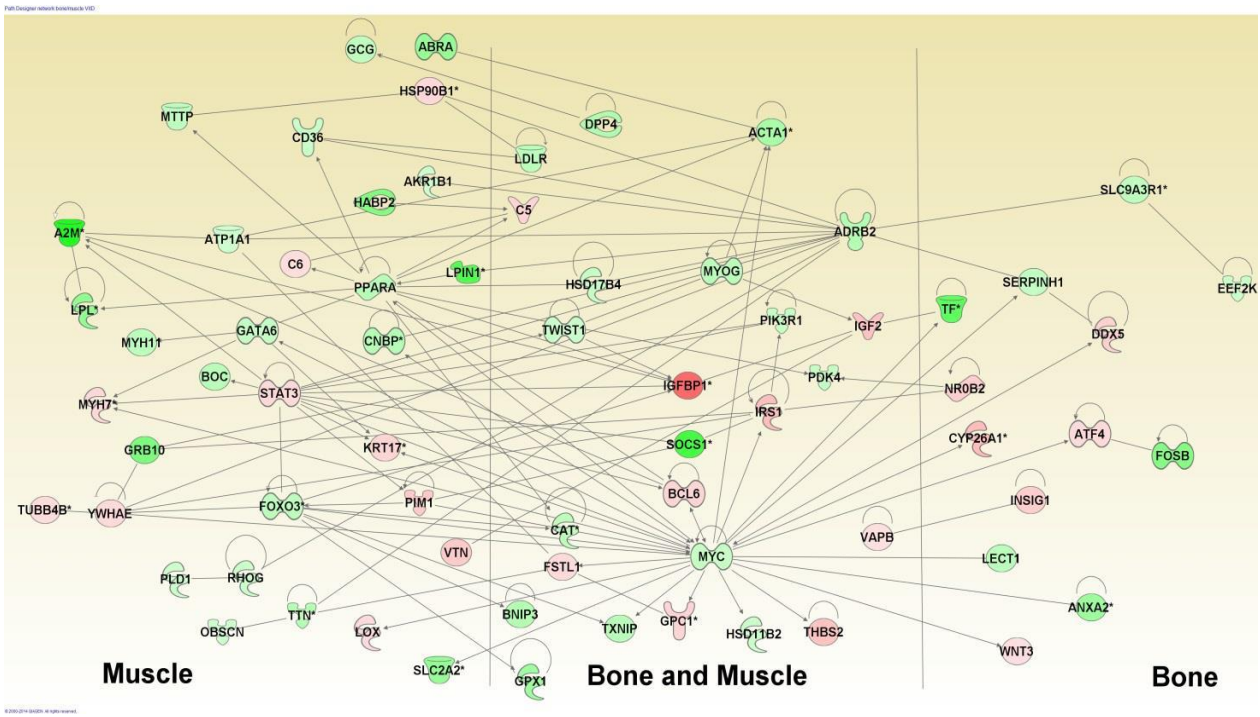

Figure 7: Gene pathways affected after VitD3 treatment between 5-6dpf. Genes filtered according to the described function for their human homologs using IPA in muscle or bone function. Genes up-regulated (red), down-regulated (green), (*) indicates that the gene is represented by two or more probes on the microarray.

Major hubs, such as the protooncogene *MYC* controlling cell proliferation, components of the insulin-like pathway such as *IGFBP1* and *IGF2*, or the cytokine receptor regulator *SOCS1* are common to both systems. Specific to muscle, regulators such as *PPARA* or *FOXO3* are down-regulated, while STAT3, mediating the cytokine receptor response, is up-regulated. Interestingly, muscle structural genes such as *TTN* (Titine) are inhibited. Other affected genes

are bone-specific transcription factors, such as *ATF4* and *FOSB*, a member of the WNT pathway (*WNT3*) or the carbohydrate (glycoprotein)-binding protein *LECT1* (Lectin1).

PTH treatment between 5dpf and 6dpf resulted in less modulation of gene expression (Table annex 5). Six genes were selected from the list to include up- and down-regulated genes for independent confirmation of the microarray expression results by RT-qPCR (Table 3). Interestingly, we observed a decrease (2.5-fold) in the expression of the endogenous *pth1a* gene (*PTH* in Table annex 5), thus confirming the previous RT-PCR results (Fig. 6K) and suggesting that the PTH treatment was effective, as the larvae exerted a compensatory response by decreasing endogenous PTH production. In rat and human osteoblastic cells, PTH receptor mRNA was shown to be down-regulated upon PTH treatment (Jongen, Willemstein-van Hove et al. 1996, Kawane, Mimura et al. 2003), in contrast we observe a significant induction (1,9-fold) of PTH receptor (*pth1rb*), suggesting more complex regulatory networks in using an *in vivo* model as opposed to *in vitro* cultures. Additional affected genes are the repressed *cyp21a2* and *hsd3b7*, indicating a decrease in steroid degradation.

The increased expression of *rxra* nuclear receptor mRNA (Table annex 5) contrasts with the observed VitD3 effects (Table annex 4), where pathways involving Rxra and its nuclear receptor dimerization partner *Ppara* were down-regulated (Table annex 4 and table 4). IPA comparison between PTH and VitD3 effects reveals that, unlike the general metabolic effects exerted by VitD3, the most prominent biological functions affected by PTH treatment were related to cell development, signaling and embryonic development (Table 5). The most highly developmentally affected systems were hematopoiesis and the skeletal, muscular and cardiovascular systems. Further analysis revealed up-regulation of a number of genes involved in or dependant on calcium metabolism, such as calreticulin (*CALR*), integrin α9 (*ITGA9*), calcitonin receptor like (*CALCRL*) or arginine vasopressin receptor a1 (*AVPR1A*).

Category	p-value	Number of Genes
Cellular Development	1.83E-04-4.02E-02	13
Connective Tissue Development and Function	1.83E-04-4.02E-02	13
Embryonic Development	1.83E-04-4.02E-02	17
Cell-To-Cell Signaling and Interaction	5.45E-04-5E-02	18
Cellular Assembly and Organization	5.45E-04-4.16E-02	13
Cellular Function and Maintenance	5.45E-04-4.16E-02	18
Hair and Skin Development and Function	5.45E-04-4.02E-02	5
Hematological System Development and Function	5.45E-04-5E-02	18
Hematopoiesis	5.45E-04-4.02E-02	5
Organ Morphology	5.45E-04-4.86E-02	22
Skeletal and Muscular System Development and Function	5.45E-04-4.02E-02	13
Tissue Development	5.45E-04-4.08E-02	25
Cellular Movement	1.15E-03-5E-02	16
Immune Cell Trafficking	1.15E-03-5E-02	15
Cell Cycle	1.78E-03-4.02E-02	10
Cell Morphology	1.78E-03-4.99E-02	19
Organ Development	1.78E-03-4.02E-02	15
Organismal Development	1.78E-03-4.86E-02	23
Respiratory System Development and Function	1.78E-03-4.02E-02	3
Tissue Morphology	1.78E-03-4.63E-02	14
Cardiovascular System Development and Function	2.65E-03-4.86E-02	16
Cellular Compromise	2.65E-03-4.02E-02	9
Cell Death and Survival	3.55E-03-4.02E-02	31
Inflammatory Response	5.07E-03-4.16E-02	13
Cellular Growth and Proliferation	5.65E-03-1.36E-02	7
Nervous System Development and Function	5.65E-03-4.02E-02	15
Small Molecule Biochemistry	6.2E-03-4.02E-02	21
Molecular Transport	7.68E-03-4.79E-02	15
Humoral Immune Response	8.35E-03-4.79E-02	5
Protein Synthesis	8.35E-03-4.79E-02	17
Cell-mediated Immune Response	8.48E-03-2.7E-02	6
Cardiovascular Disease	9.3E-03-4.49E-02	8
Digestive System Development and Function	9.3E-03-2.7E-02	3
Lymphoid Tissue Structure and Development	9.3E-03-4.49E-02	5
Carbohydrate Metabolism	1.08E-02-2.7E-02	9
Lipid Metabolism	1.11E-02-4.02E-02	8
Amino Acid Metabolism	1.36E-02-4.02E-02	2
Antimicrobial Response	1.36E-02-1.36E-02	1
Cell Signaling	1.36E-02-4.02E-02	4
Drug Metabolism	1.36E-02-2.7E-02	6
Endocrine System Development and Function	1.36E-02-1.36E-02	1
Gene Expression	1.36E-02-4.57E-02	11
Hepatic System Development and Function	1.36E-02-2.7E-02	2
Nucleic Acid Metabolism	1.36E-02-4.02E-02	5
RNA Post-Transcriptional Modification	1.36E-02-2.7E-02	1
Renal and Urological System Development and Function	1.36E-02-2.7E-02	4
Reproductive System Development and Function	1.36E-02-4.16E-02	6
Visual System Development and Function	1.36E-02-2.7E-02	2
Vitamin and Mineral Metabolism	1.36E-02-4.02E-02	4
Organismal Functions	2.18E-02-2.18E-02	2
Behavior	2.7E-02-4.02E-02	3
Free Radical Scavenging	2.7E-02-2.7E-02	1
Post-Translational Modification	2.7E-02-3.02E-02	5
Auditory and Vestibular System Development and Function	4.02E-02-4.02E-02	1
RNA Trafficking	4.02E-02-4.49E-02	2

Table 5: Biological functions associated to genes affected by PTH. Ingenuity Pathway Analysis of the list of genes affected at 6dpf after PTH treatment for 24 hours. Columns indicate respectively the function, the range of p-values (significance) associated to various sub-functions and the number of genes concerned (N).

Comparison of the genes affected by the two hormones exerting opposite effects on bone formation, VitD3 and PTH, revealed only 12 genes in common (Fig. 8A,B). Using these 12 genes allows building a regulatory network around the protooncogene *MYC* and containing several genes that are differentially regulated in these two conditions (Fig. 8B,C), suggesting opposing effects on mitochondrial (GSR), pyrimidine (CAD) or lipid metabolism (CES1).

A

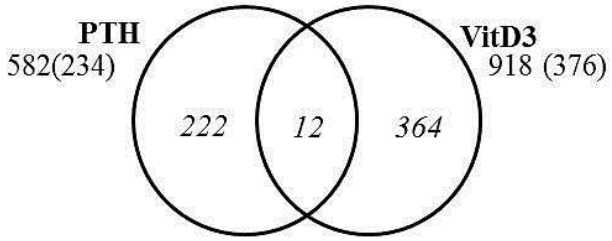

B

Common genes	VitD	PTH
C7	0,665	1,31
CAD	0,51	-1,57
CES1	**-2,104**	0,55
CPA2	-0,64	-0,65
CYP2J2	-1,015	-0,74
GSR	0,377	-0,85
HSD3B7	-0,406	-0,63
KRT17	**0,464**	0,96
MLEC	-0,396	-0,65
NRBP2	-0,477	1,33
SLC43A1	**-1,045**	0,41
SLC6A18	-0,461	-2,30

C

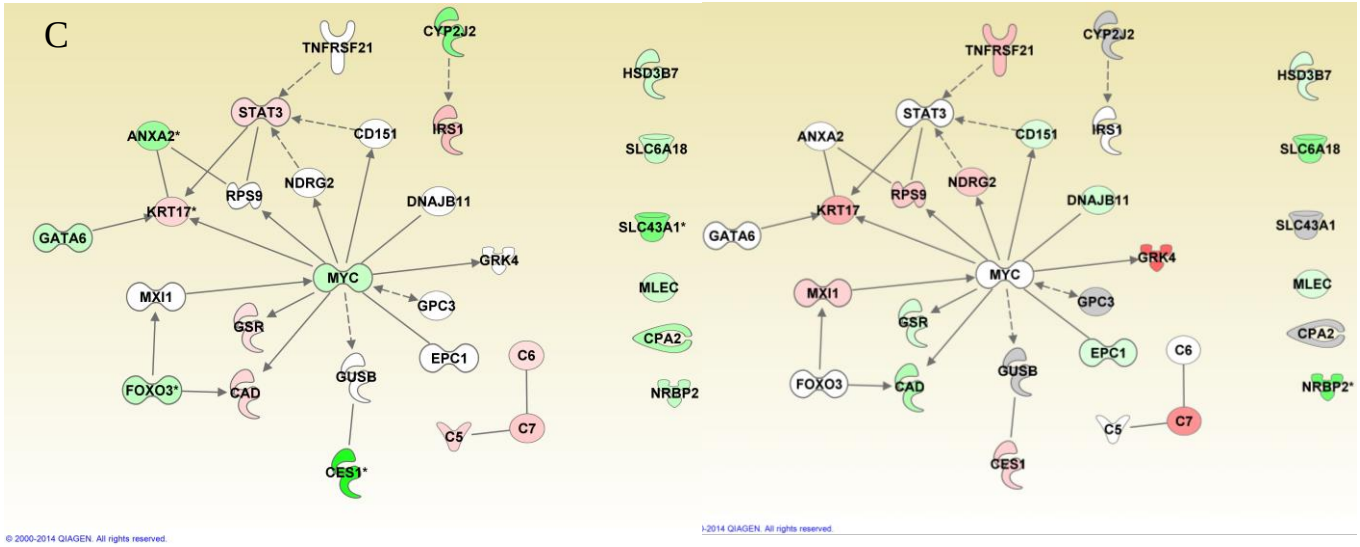

Figure 8: Comparison of genes affected after PTH or VitD3 treatment between 5-6dpf. (A) Comparison of the number of genes affected by PTH or VitD3 treatment. The number of probes resulting in different hybridization signals is given, with the numbers in parenthesis and the graph showing the numbers of IPA-annotated genes. (B) List of common genes and their respective log2(fold change) in the two conditions. (C) Network constructed using the common genes and extended using the genes affected in one of the two conditions. The color overlay indicates the fold change after VitD3 (left) or PTH (right) treatment. Genes up-regulated (red), down-regulated (green), (*) indicates that the gene is represented by two or more probes on the microarray.

4. Conclusions

In this first chapter, we detailed the image and genome analysis applied to zebrafish larvae after exposure to the hormones PTH and VitD3. Our aim was to concentrate on the effects on bone formation, therefore we chose to start the experiments at 5dpf, when perichondral ossification is taking place within all major cranial cartilage elements and intramembranous bone formation is ongoing. We evaluated the effects on cartilage and bone formation by staining these structures after several days of treatment, at 9 or 10dpf. For a more detailed, more accurate and more objective evaluation of skeletal development, we developed two different, but complimentary methods for analyzing images of stained zebrafish larvae. The first one uses a number of landmarks placed manually within the images (using the software environment CYTOMINE) and allows automatic extraction of distances and angles between these landmarks, ultimately resulting in a morphometric description of the head skeleton. The second one is based on manually assigning a developmental score to each cranial bone element within each image, enabling us to calculate a mean score for each element and a global score for each individual.

To validate these approaches, we performed two treatments of zebrafish larvae whose effects had been previously described (Fleming, Sato et al. 2005). The first treatment uses exogenous vitamin D3 (VitD3) (Lin, Su et al. 2012) to increase bone formation. Indeed, the general VitD3 metabolism in teleosts is similar to that in mammals, teleosts possess two vitamin D receptors (VDRs) and knock-down of VDRa expression causes a decrease of calcium ion uptake (Lin, Su et al. 2012). PTH and related peptides are known hypercalcemic agents in mammals, however their function is more controversial in teleosts, depending on the species (Witten and Huysseune 2009). Although teleosts do not present a parathyroid gland, they do produce PTH in the gills, probably in cells identified by the expression of *gcm2*, a gene whose orthologues are required for parathyroid development in chicken and mouse (Okabe and Graham 2004, Zajac and Danks 2008). PTH administration induced hypercalcemia in fugu (*Tetraodon nigrividans*) by inducing both osteoblast and osteoclast function and by decreasing scale calcium content (Suzuki, Danks et al. 2011). Genes homologous to the mammalian PTH-related peptides (PTHrP) were found in teleosts who were shown to be more widely expressed (Danks, D'Souza et al. 2011). These proteins increase calcium uptake in sturgeon (*Acipenser nacarii*) (Fuentes, Haond et al. 2007) and were shown to play different roles in craniofacial development in zebrafish (Yan, Bhattacharya et al. 2012). Blocking PTH signaling through the use of a PTH/PTHrP antagonist resulted in a decreased hypercalcemic

response to estradiol in sea bream (*Sparus aurata*) (Fuentes, Guerreiro et al. 2007). Finally, four stanniocalcin (*stc*) genes are present in fugu and zebrafish, only *stc1-a* expression was sensitive to the calcium concentration in water (Fuentes, Guerreiro et al. 2007, Schein, Cardoso et al. 2012) while PTHrP and Stc were shown to have opposing effects on calcium uptake in intestinal explants (Fuentes, Power et al. 2010). Depending on the mode of administration (intermittent or continuous) PTH and PTHrP were shown, respectively to increase or decrease bone formation in zebrafish (Fleming and Sato 2004).

We confirm the effects described in zebrafish on general bone formation and in addition, the combined approach allowed us give a more detailed description of these effects. Although the general morphology was preserved in both cases, VitD3 treatment lead to a broader jaw both in cartilage and bone and a longer head in bone, while PTH treatment leads to an increased length of the ceratohyal cartilage, a general decrease of ossification, a decreased length of the parasphenoid bone and a broadening of the posterior head skeleton. The discrepancy between cartilage and bone concerning the longer head probably results from the fact that the landmarks used in bone (parasphenoid and notochord) do not have a real equivalent in cartilage and may mineralize independently from it. While VitD3 treatment caused a generally significant increase in ossification of most elements, this was less prominent for the maxillary and absent for the anguloarticular. Conversely, the decrease of ossification caused by PTH treatment was significant for all elements except branchiostegal rays 1.

We then turned to studying differences in gene expression caused by the various treatments. We chose to perform these studies using mRNA from entire larvae, as methods for isolation of specific cells, such as dissection or fluorescent cell sorting might not be available in a future space experiment. First, we followed expression of bone-specific genes during normal development between 6 and 10dpf. We observed a sharp rise of mRNA coding for bone matrix proteins Sparc, Spp1, Col1a2 and a longer sharp rise of Bglap mRNA, followed by a rapid decrease after 7dpf, suggesting that the major part of the bone matrix is formed at 7dpf and that further ossification is mainly due to mineral deposition. This is consistent with the observed sharp decrease of *osx* expression, followed with some delay by *dlx5a* expression, both indicating a decrease in osteoblast differentiation. The continuous decrease in the levels of *col10a1a* mRNA could be related to the proposed inhibitory effect of this factor on biomineralization (Arias, Nakamura et al. 1997, Seitz, Rendenbach et al. 2013), while the large increase of *runx2b* and *pth1a* mRNA during the entire period could be related to some other functions of these factors (Komori, Yagi et al. 1997, Hogan, Danks et al. 2005).

Following the modulation of gene expression during chemical treatments revealed a clear upward trend for bone matrix protein-encoding genes upon VitD3 treatment and a clear downward trend during PTH treatment. These trends are consistent with the assumption that bone matrix secretion plays a functional role in the observed increase or decrease, respectively, in bone formation. Expression of *osx* is increased during the first day of VitD3 treatment and decreased during PTH treatment, again consistent with a respectively prolonged or shortened period of osteoblast differentiation, also further supported by the increase of *dlx5a*, *dlx6a*, *sox4a*, and *sox4b* expression at 8-9dpf during VitD3 treatment.

Finally, to determine the effects on whole genome gene expression of known regulators of bone formation, we chose to concentrate on mRNA levels only after one day of treatment, as we are mainly interested in regulatory events. A summary of all the genes affected by these two chemicals is shown in Table annex 6. As expected, VitD3 treatment induced *cyp24a1* expression, while PTH administration led to a decrease in endogenous *pth1a* expression. Furthermore, VitD3 treatment caused significant changes in overall metabolism, as shown by the involvement of affected genes in molecular transport or lipid metabolism. Probably for this reason, functions related to embryogenesis or organ morphology rank much lower in the list of affected pathways. These findings are consistent with previous results, obtained using a deep sequencing (RNA-seq) approach, which also showed a high proportion of metabolic pathways affected by VitD3 treatment, administered either between 2 and 6-7dpf or between 6-7dpf (Craig, Zhang et al. 2012). In contrast, PTH treatment affected less genes, but these were more involved in developmental processes. Interestingly, several genes were regulated in opposite directions upon VitD3 or PTH treatment (Fig. 8A,C), suggesting that they may be involved in the opposite effects on bone mineralization that we observed.

In conclusion, we confirmed and described more in detail the effects of VitD3 and PTH on zebrafish larvae. In our image analysis, we observed an increase of bone formation upon VitD3 treatment and a clear decrease of bone formation upon PTH treatment, similar to their actions observed in mammals (Holick 1996, Ma, Cain et al. 2001, Xue, Karaplis et al. 2005, Goltzman 2007, Peterson and Riggs 2010). The alterations observed in expression of specific bone marker genes following these treatments further support these opposite effects on bone development, and whole genome expression analysis revealed several genes and pathways that may be involved in the observed effects.

Chapter 1bis

Function of the Sox4 transcription factors in skeletal development.

1. Sox4 genes in mice and zebrafish.

The *Sox4* gene belongs to the group C class of the SOX (Sry-related HMG box containing) family of transcription factors (Kiefer 2007). The *Sox4*+/- mice exhibit a decrease in bone mass and mineralization (Nissen-Meyer, Jemtland et al. 2007). In humans, more precisely in women suffering from osteoporosis, *SOX4* expression is also decreased (Jemtland, Holden et al. 2011) and appears to be involved in maintaining the BMD (Duncan, Danoy et al. 2011). In zebrafish, there are 2 *SOX4* homologs due to the genome duplication, *sox4a* and *sox4b*. The only function known for *sox4a* concerns the regulation of neurogenesis (Gribble, Kim et al. 2009). For *sox4b*, a function was shown in the pituitary and in the pancreas (Mavropoulos, Devos et al. 2005, Quiroz, Lopez et al. 2012).

2. Expression pattern of *sox4a* and *sox4b*.

A short study was performed on both sox4 genes. *In situ* hybridization (ISH) revealed an early lateral expression of *sox4a* in two clusters in the neural crest cells and in hindbrain neurons at 24hpf and 28hpf (Fig. 9A,C). For *sox4b*, an interesting expression is observed in the pharyngeal arches at a later stage at 48hpf. At 72hpf and 96hpf, a specific expression of *sox4b* is observed in the pharyngeal region (Fig. 9B,D).

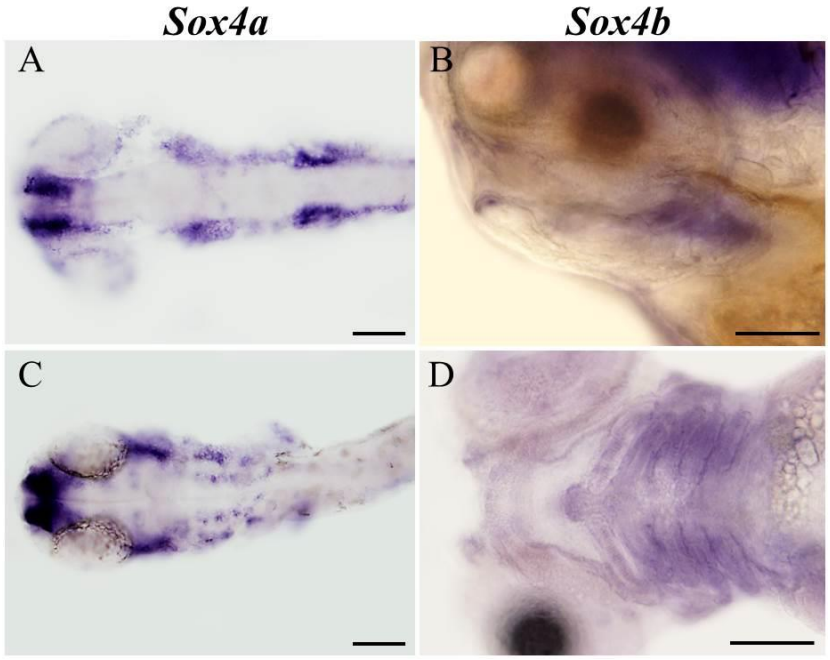

Figure 9: Both Sox4 genes expression pattern by ISH in zebrafish embryos. (A,C) *sox4a* expression pattern. (B,D) *sox4b* expression pattern. (A) *sox4a* expression at 24hpf. (B) *sox4a* expression at 28hpf. (C) *sox4b* expression at 48hpf. (D) *sox4b* expression at 96hpf in large slice. (A-D) scale bar = 100µm.

Double fluorescent ISH were also performed to more precisely define the localization of the expression of these genes. At 24hpf, *sox4a* mRNA was compared to the *dlx2a* marker for cranial cartilage precursor cells. Colocalization was observed between *sox4a* and *dlx2a* in the forebrain and in the first pharyngeal arch, the latter appearing as a "salt and pepper" distribution in the cranial neural crest cells (Fig. 10A), suggesting an expression of these two genes in two different, closely intermingled cell types, possibly representing different differentiation stages. At 48hpf, no colocalization was observed between *sox4a* and *dlx2a* (Fig. 10B), or between *sox4b* and *fli1*, a marker of the cranial neural crest and endothelial cells (Fig. 10C). At 72hpf, there is a colocalization between *sox4b* and *sox9b* in the brain and in the ventral region of the pharyngeal arches, the latter corresponding to *sox9b* expression in the pharyngeal endoderm at this stage (Fig. 10D) (Yan, Willoughby et al. 2005).

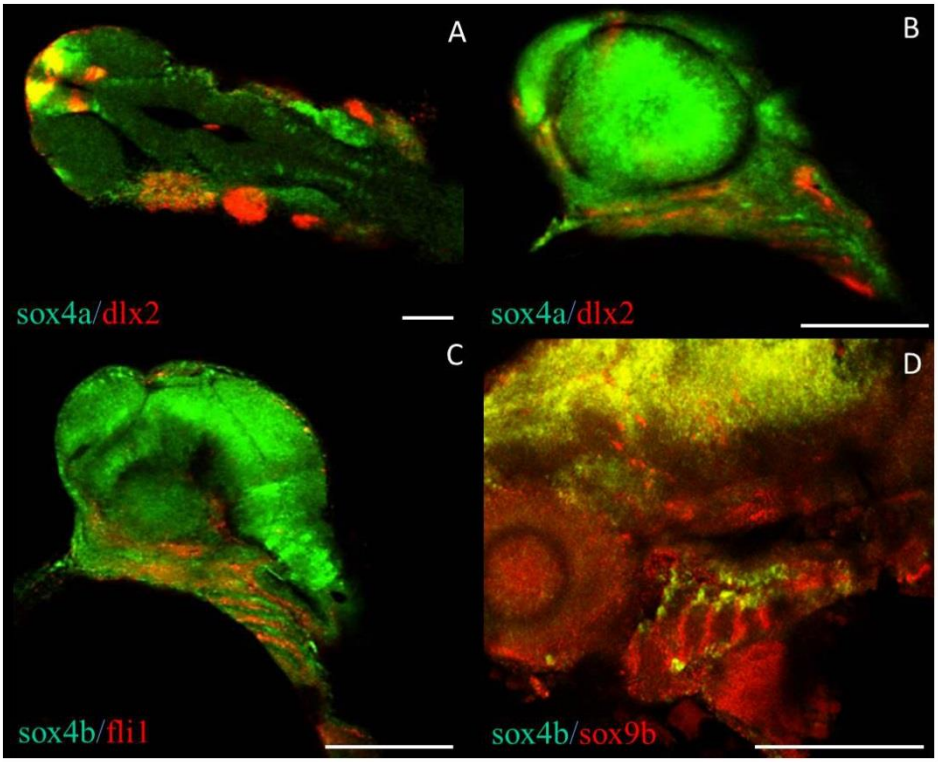

Figure 10: Double ISH with the 2 sox4 genes. (A) *sox4a* and *dlx2a* at 24hpf. (B) *sox4a* and *dlx2a* at 48hpf. (C) *sox4b* and *fli1* at 48hpf. (D) *sox4b* and *sox9b* at 72hpf. (A-D) scale bar = 100µm.

3. Expression of *sox4a* and *sox4b* during development and upon PTH or VitD3 treatment.

Taken together, these data inspired us to investigate the expression of these two genes between 5-10dpf, and during the treatments with vitD3 and PTH in order to gain a better understanding of their role on bone formation.

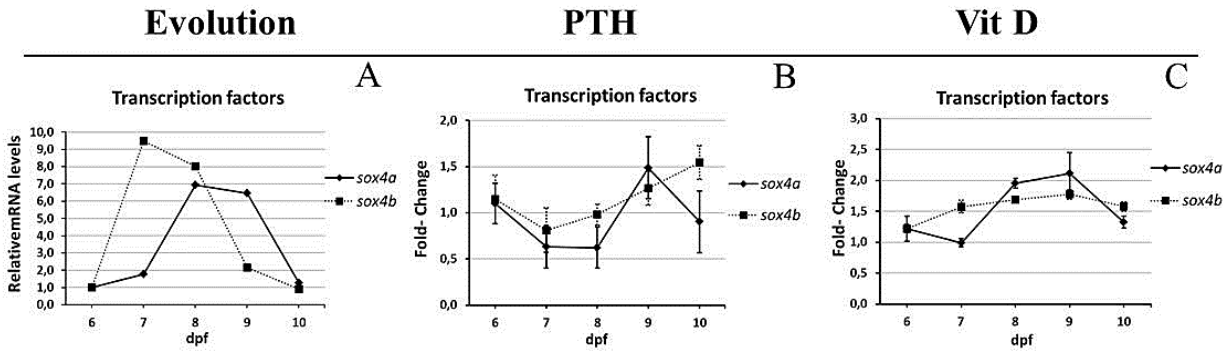

Figure 11: Expression of *sox4a* and *sox4b* genes during development between 6 and 10dpf. (A) Specific mRNA levels at 6dpf relative to the *gapdh* house-keeping gene were used as reference, and then compared to the corresponding level in larvae of different age. (B) Specific mRNA levels in PTH treated larvae were determined relative to the *gapdh* reference house-keeping gene and then compared to the corresponding level in untreated controls of the same age. (C) Specific mRNA levels in VitD3 treated larvae were determined relative to the *gapdh* reference house-keeping gene and then compared to the corresponding level in untreated controls of the same age.

In untreated larvae, both *sox4b* and *sox4a* present a transiently increased expression relative to 6dpf, starting at 9-fold for *sox4b* at 7dpf, respectively 8-fold and 7-fold for both genes at 8dpf. *sox4a* expression was still increased 6-fold at 9dpf, while *sox4b* expression declined at 9dpf and both at the end of the studied period (Fig.11A). Compared to the evolution of expression in untreated larvae, both *sox4a* and *sox4b* experience a weak, but significant (1.5- to 2-fold) increase of expression during VitD3 treatment until the end of the kinetic. The increased levels of *sox4b* mRNA between 5 and 6dpf was also observed in the microarray experiment (Fig.11C). Upon PTH treatment, *sox4a* levels decreased for the first two days and return to control levels at the end of the treatment, while *sox4b* exhibits a progressive increase from 9 to 10dpf (Fig.11A).

Thus, both treatments increase sox4b RNA expression.

4. Conclusions.

In zebrafish, little is known about the sox4 genes and their role in the skeletal system. The differences between the expression patterns of *sox4a* and *sox4b* suggest that *sox4b* would be the gene the most susceptible to play a role in bone development, with its expression from 48hpf to 5days in the pharyngeal arches. Expression of both genes is affected during the PTH or VitD3 treatment, the most significant being the clear and constant increase of *sox4b* levels during the VitD3 treatment. However, it most be noted that both genes are expressed in other tissues as well, further investigations will thus be required to determine the function of these two genes in bone formation.

Chapter 2

Modulation of head skeletal development and gene expression by microgravity simulators.

1. Head skeletal development and gene expression modulation upon microgravity simulators.

Physiological modifications in weightlessness, as experienced by astronauts during space flight, have been the subject of numerous studies. A compilation of human responses to prolonged exposure to space conditions indicates a loss of bone mineral density of about 1% per month (Nagaraja and Risin 2013). Prolonged bed rest studies confirmed this bone loss without any substantial gender differences (Morgan, Heer et al. 2014).

Animal models have also been used to gain deeper insight into the molecular mechanisms of adaptation to microgravity (Horn, van Loon et al. 2011), among which various fish species have also been used (Slenzka, Appel et al. 1995, Rahmann and Anken 2002). Here, we chose to use small zebrafish larvae in three different, commonly used approaches to simulate microgravity: clinorotation, random positioning machine (RPM) and rotating wall vessel (RWV). We compared their effect on bone formation between 5-10dpf, as well as the effect on whole genome gene expression during the first day of treatment.

2. Effects of simulated microgravity on cartilage and bone formation.

To assess the effects of several day treatments on bone formation, 5dpf larvae were maintained in the clinostat or in the RPM for 5 days. At 10dpf, control and treated larvae were stained by Alcian blue to observe the cartilage and by alizarin red to visualize calcium deposition by osteogenic cells.

After 5days in the clinostat or in RPM (Fig. 12A-D), the cartilage structures are well formed, complete and morphologically similar to the respective controls. In contrast, staining for bone structures using alizarin red, bone formation was clearly decreased in the larvae submitted to clinorotation relative to their controls (Fig. 12E,G). Several bone structures, such as anguloarticular, branchiostegal ray2, ceratohyal and dentary are absent in the 10dpf larvae after 5 days in clinorotation. In larvae subjected to RPM, only an increase in the ceratohyal was observed when compared to their controls (Fig. 12F,H).

To analyze the extent of bone formation more precisely in a qualitative and quantitative description, we applied more objective methods to the images of the stained larvae as previously described in Chapter 1. In a first, morphometric approach, each image was manually annotated using the CYTOMINE software (Marée, Stevens et al. 2013) as described in the first chapter and in the materials and methods, by defining specific landmarks indicating the

positions of the different skeletal structures. Larvae subjected to clinostat did not reveal any significant modifications in the cartilage skeleton (annex 7). In contrast, larvae stained with alizarin red revealed a clearly increased distance of the parasphenoid summit (pa) and the anterior (an) part of the larvae (Fig. 13A, annex 8), probably due to the significant decrease of the parasphenoid (p) area after clinorotation (Fig. 13B, annex 8). Note that in this case, not all the measures were possible due to the absence of several structures in many larvae, such as the anguloarticular (aa) and ceratohyal (ch) that were absent in more than 60% of the larvae investigated. In the RPM treated larvae, the only cartilage modification observed was a decrease in the length of the ceratohyals (annex 7).

The bone structures after RPM exposure are well formed, however several distances were decreased. The distance between anguloarticular up/down, entopterygoid up/down, branchiostegal ray1 up/down, and between the opercles were all significantly reduced (Fig. 13C, annex 6). The head width was thus decreased in the larvae in the RPM. The parasphenoid area was also reduced in RPM treated larvae but in contrast to clinostat, without any increase between anterior and parasphenoid distance (Fig. 13B,C; annex 8).

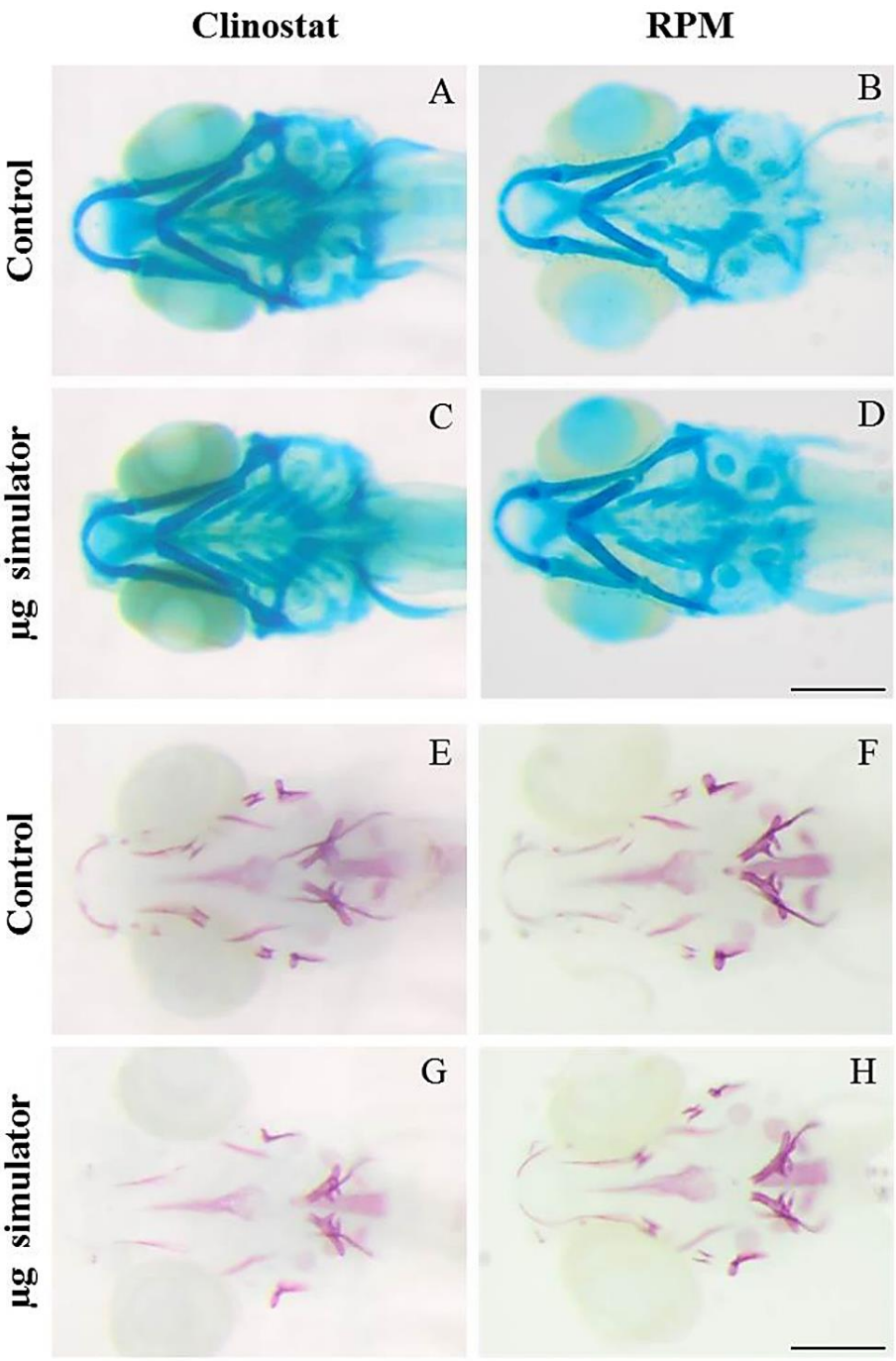

Figure 12: Effect of 5days microgravity simulation in 10dpf zebrafish larvae. (A-D) Alcian blue staining of cartilage. (E-H) Alizarin red staining of bone structures. (A,B,E,F) Controls in the respective experiments. (C,D) No effect on cartilage development after 5 days clinorotation (C) or RPM (D). Decrease of bone formation after 5days in clinostat (G), while no obvious effect on bone development after 5days RPM (H). Scale bar = 250µm.

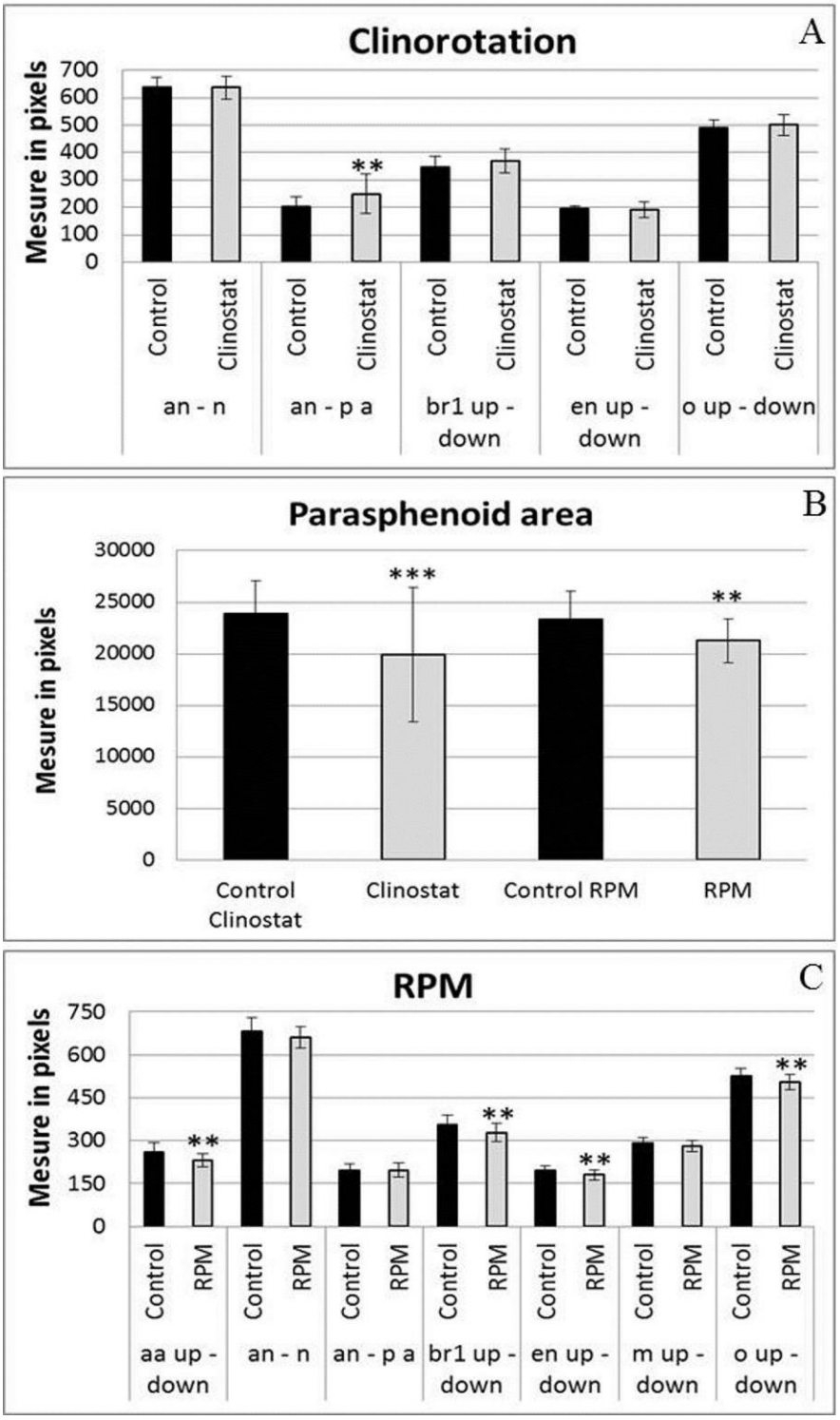

Figure 13: Morphometric analysis of head bone skeleton after 5days in microgravity simulators. The distances are measured in pixels. Mean ± SD and t-test analysis were calculated for each measure on at least 20 individuals. (A) Distances after the clinostat experiment. A significant increase of the distance between the anterior part of the larvae and the parasphenoid summit is observed. (B) The area covered by the parasphenoid is decreased upon both clinostat and RPM exposure. (C) Distances after RPM experiment. A decrease between the left and right (up-down) anguloarticulars, entopterygoids, opercles and branchiostegal rays1 is observed. * $p < 0.05$, ** $p < 0.005$ and ***$p < 0.001$.

The second method evaluates progression of bone formation in each structure, in terms of size and level of ossification through staining intensity, as also previously described in the chapter 1 and in the material and methods. A score is given to each structure according to its developmental status as absent, early ossification, advanced ossification or over-ossification. The frequency distribution of these scores reveals that exposure to clinorotation for 5 days (between 5-10dpf) leads to a significant decrease in ossification of all the structures (Fig. 14A, table 6).

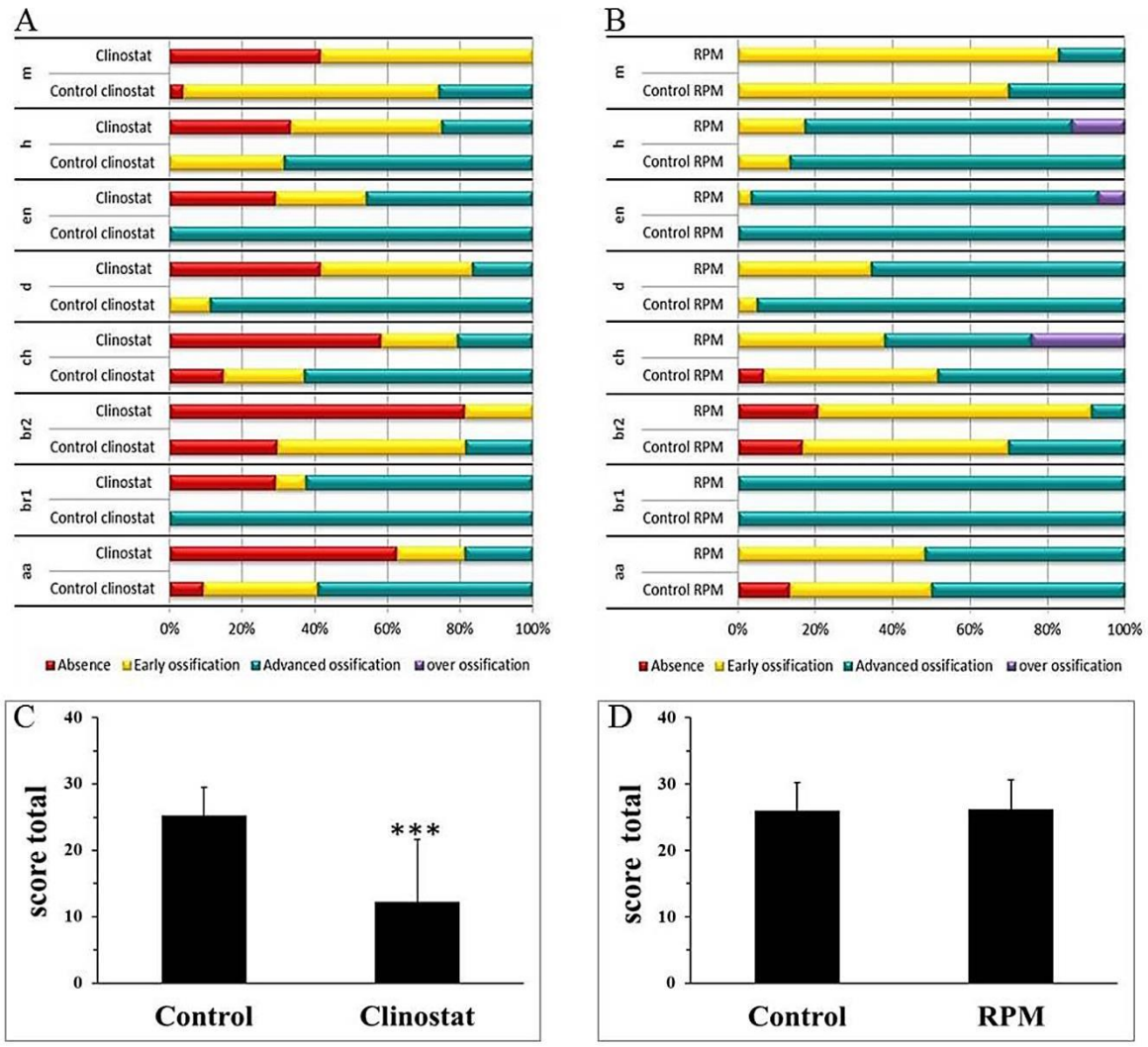

Figure14: Extent of bone formation in 10dpf larvae after 5days of microgravity simulation. Bone development is classified for each element into different categories: Absent (no structure present; red), early ossification (beginning of the bone ossification; yellow), advanced ossification (the structure is present and already developed as the control; green) and over ossification (the structure is more developed compared to the control; purple). Cumulated frequencies in % are represented for each element. As no significant difference was observed for paired structures between left and right (up and down), their scores have been combined. Statistical analysis was performed by X^2 of Pearson and a logistic regression. (A) Cumulated frequency after 5days in clinostat. (B) Cumulated frequency after 5days in RPM. (C,D) Global scores for larvae subjected to, respectively clinorotation or RPM. To obtain this, score attributed to each element were added up for each individual larva. Mean ±

SD and t-test analysis was obtained on at least 20 individuals. * $p < 0.05$, ** $p < 0.005$ and *** $p < 0.001$.

The branchiostegal ray1 and the entopterygoid structures were absent in around 25 % of the treated larvae, while they presented advanced ossification in 100% of the control larvae (Fig. 14A). The anguloarticular and the ceratohyal were absent in about 60% of the treated larvae, compared to 25% or 15%, respectively in the controls. Absence of the branchiostegal ray2 switches from 25% in controls to about 80% after clinorotation. For all structures, the frequency of larvae presenting advanced ossification decreased upon clinorotation. The statistical analysis is given in table 1. By assigning a value to the score of the structures (from 0 for absent to 3 for advanced ossification) within each larva, a global score was calculated to compare control and treated larvae. These global scores reveal a significantly decreased ossification after 5 days of clinorotation (Fig. 14C).

				Score of Y			X^2 pearson	Ordinal logistic regression	
Structures	Variable	N	Mean	absence	early	advanced	p-value	OR (IC 95%)	p-value
anguloarticular down	Control	27	1.48	3 (11.11%)	8 (29.63%)	16 (59.26%)		1	
	clinostat	24	0.54	15 (62.50%)	5 (20.83%)	4 (16.67%)	**<0.001**	0.102 (0.031-0.335)	**<0.001**
anguloarticular up	Control	27	1.52	2 (7.41%)	9 (33.33%)	16 (59.26%)		1	
	clinostat	24	0.58	15 (62.50%)	4 (16.67%)	5 (20.83%)	**<0.001**	0.104 (0.032-0.339)	**<0.001**
branchiostegal ray1 down	Control	27	2.00	0 (0%)	0 (0%)	27 (100%)		1	
	clinostat	24	1.33	7 (29.17%)	2 (8.33%)	15 (62.50%)	**0.002**	/	/
branchiostegal ray1 up	Control	27	2.00	0 (0%)	0 (0%)	27 (100%)		1	
	clinostat	24	1.33	7 (29.17%)	2 (8.33%)	15 (62.50%)	**0.002**	/	/
branchiostegal ray2 down	Control	27	0.85	9 (33.33%)	13 (48.15%)	5 (18.52%)			
	clinostat	24	0.17	20 (83.33%)	4 (16.67%)	0 (0%)	**0.001**	0.093 (0.024-0.353)	**<0.001**
branchiostegal ray2 up	Control	27	0.89	8 (29.63%)	14 (51.85%)	5 (18.52%)			
	clinostat	24	0.21	19 (79.17%)	5 (20.83%)	0 (0%)	**0.001**	0.101 (0.028-0.364)	**<0.001**
ceratohyal down	Control	27	1.48	4 (14.81%)	6 (22.22%)	17 (62.96%)		1	
	clinostat	24	0.63	14 (58.33%)	5 (20.83%)	5 (20.83%)	**0.002**	0.140 (0.045-0.438)	**<0.001**
ceratohyal up	Control	27	1.48	4 (14.81%)	6 (22.22%)	17 (62.96%)		1	
	clinostat	24	0.63	14 (58.33%)	5 (20.83%)	5 (20.83%)	**0.002**	0.140 (0.045-0.438)	**<0.001**
dentary down	Control	27	1.89	0 (0%)	3 (11.11%)	24 (88.89%)		1	
	clinostat	24	0.75	10 (41.67%)	10 (41.67%)	4 (16.67%)	**<0.001**	0.022 (0.004-0.110)	**<0.001**
dentary up	Control	27	1.89	0 (0%)	3 (11.11%)	24 (88.89%)		1	
	clinostat	24	0.75	10 (41.67%)	10 (41.67%)	4 (16.67%)	**<0.001**	0.022 (0.004-0.110)	**<0.001**
entopterygoid down	Control	27	2.00	0 (0%)	0 (0%)	27 (100%)		1	
	clinostat	24	1.17	7 (29.17%)	6 (25.00%)	11 (45.83%)	**<0.001**	/	/
entopterygoid up	Control	27	2.00	0 (0%)	0 (0%)	27 (100%)		1	
	clinostat	24	1.17	7 (29.17%)	6 (25.00%)	11 (45.83%)	**<0.001**	/	/
hyomandibular down	Control	27	1.67	0 (0%)	9 (33.33%)	18 (66.67%)		1	
	clinostat	24	0.88	9 (37.50%)	9 (37.50%)	6 (25%)	**<0.001**	0.114 (0.034-0.380)	**<0.001**
hyomandibular up	Control	27	1.70	0 (0%)	8 (29.63%)	19 (70.37%)		1	
	clinostat	24	0.96	7 (29.17%)	11 (45.83%)	6 (25%)	**<0.001**	0.109 (0.032-0.373)	**<0.001**
maxilla down	Control	27	1.22	1 (3.70%)	19 (70.37%)	7 (25.93%)		1	
	clinostat	24	0.58	10 (41.67%)	14 (58.33%)	0 (0%)	**<0.001**	0.037 (0.004-0.307)	**0.002**
maxilla up	Control	27	1.22	1 (3.70%)	19 (70.37%)	7 (25.93%)		1	
	clinostat	24	0.58	10 (41.67%)	14 (58.33%)	0 (0%)	**<0.001**	0.037 (0.004-0.307)	**0.002**

Table 6: Ossification scores for individual bone elements in 10dpf control larvae and larvae treated for 5days by clinorotation. The bone structures were classified into three

categories (absent, early, and advanced ossification). Statistical analysis was performed by X^2 of Pearson and by logistic regression.

The larvae subjected to RPM simulation between 5-10dpf developed all the structures present in the controls (Fig. 14B, table 2). The bone formation score distribution was similar to that in the controls, accordingly the global score comparison reveals no significant difference between RPM-treated and control larvae (Fig. 14D). Close inspection of the scores for individual structures confirms over-ossification of the ceratohyal in 25% and reveals increased ossification in the hyoid and entopterygoid in, respectively 14% and 7% of the RPM-treated larvae, while the dentary and branchiostegal ray 2 reveal a slight increase in the frequency of early ossification. Statistical analysis (Table 7) confirmed the significant over-ossification of the ceratohyal (p-value 0.016) and, to a lesser extent, the entopterygoid (p-value: 0.2), while the dentary and branchiostegal ray2 down revealed a slight decrease in ossification compared to the controls (table 7).

A				Score of Y		X^2 Pearson	logistic regression	
Structures	Variable	N	Mean	early	advanced	p-value	OR (IC 95%)	p-value
anguloarticular down	Control	30	0.87	4 (13.33%)	26 (86.67%)		1	
	RPM	29	1.00	0 (0%)	29 (100%)	0.042	/	0.995
anguloarticular up	Control	30	0.50	15 (50%)	15 (50%)		1	
	RPM	29	0.58	14 (48.28%)	15 (51.72%)	0.895	1.071 (0.386-2.975)	0.895
branchiostegal ray1 down	Control	30	1.00	30 (100%)	0 (0%)		1	
	RPM	29	1.00	29 (100%)	0 (0%)	/	/	/
branchiostegal ray1 up	Control	30	1.00	30 (100%)	0 (0%)		1	
	RPM	29	1.00	29 (100%)	0 (0%)	/	/	/
branchiostegal ray2 down	Control	30	0.30	21 (70.00%)	9 (30.00%)		1	
	RPM	29	0.07	27 (93.10%)	2 (6.90%)	**0.023**	0.17 (0.034-0.886)	**0.035**
branchiostegal ray2 up	Control	30	0.30	21 (70.00%)	9 (30.00%)		1	
	RPM	29	0.10	26 (89.66%)	3 (10.34%)	0.061	0.269 (0.065-1.122)	0.072
dentary down	Control	30	0.90	3 (10.00%)	27 (90.00%)		1	
	RPM	29	0.66	10 (34.48%)	19 (65.52%)	**0.023**	0.211 (0.051-0.871)	**0.031**
dentary up	Control	30	0.90	3 (10.00%)	27 (90.00%)		1	
	RPM	29	0.66	10 (34.48%)	19 (65.52%)	**0.023**	0.211 (0.051-0.871)	**0.031**
maxilla down	Control	30	0.33	20 (66.67%)	10 (33.33%)		1	
	RPM	29	0.17	24 (82.76%)	5 (17.24%)	0.156	0.417 (0.122-1.421)	0.162
maxilla up	Control	30	0.27	22 (73.33%)	8 (26.67%)		1	
	RPM	29	0.17	24 (82.76%)	5 (17.24%)	0.383	0.573 (0.163-2.016)	0.386

B				Score of Y			X^2 Pearson	Ordinal logistic regression	
Structures	Variable	N	Mean	early	advanced	over	p-value	OR (IC 95%)	p-value
ceratohyal down	Control	30	1.47	16 (53.33%)	14 (46.67%)	0 (0%)		1	
	RPM	29	1.86	11 (37.93%)	11 (37.93%)	7 (24.14%)	**0.016**	2.721 (0.995-7.440)	0.051
ceratohyal up	Control	30	1.50	15 (50%)	15 (50%)	0 (0%)		1	
	RPM	29	1.86	11 (37.93%)	11 (37.93%)	7 (24.14%)	**0.016**	2.467 (0.908-6.705)	0.077
entopterygoid down	Control	30	2.00	0 (0%)	30 (100%)	0 (0%)		1	
	RPM	29	2.03	1 (3.45%)	26 (89.66%)	2 (6.90%)	0.195	2.099 (0.179-24.569)	0.555
entopterygoid up	Control	30	2.00	0 (0%)	30 (100%)	0 (0%)		1	
	RPM	29	2.03	1 (3.45%)	26 (89.66%)	2 (6.90%)	0.195	2.099 (0.179-24.569)	0.555
hyomandibular down	Control	30	1.87	4 (13.33%)	26 (86.67%)	0 (0%)		1	
	RPM	29	1.97	5 (17.24%)	20 (68.97%)	4 (13.79%)	0.087	1.604 (0.461-5.582)	0.458
hyomandibular up	Control	30	1.87	4 (13.33%)	26 (86.67%)	0 (0%)		1	
	RPM	29	1.97	5 (17.24%)	20 (68.97%)	4 (13.79%)	0.087	1.604 (0.461-5.582)	0.458

Table 7: Ossification scores for individual bone elements in 10dpf control larvae and larvae treated for 5days by RPM. (A) The bone structures were classified into two categories (early, and advanced ossification). (B) The bone structures were classified into three categories (early,

advanced, and over ossification). Statistical analysis was performed by X^2 of Pearson and by logistic regression.

3. Effects of simulated microgravity on stress in larvae

Stress can induce bone loss (Feng and McDonald 2011, Henning, Park et al. 2011, Weinstein 2012, Santamaria, Bello et al. 2015), therefore we decided to evaluate the stress status in the larvae. Stress inputs activate the hypothalamus-pituitary-interrenal (HPI) axis and finally result in the production of cortisone (Fig. 15).

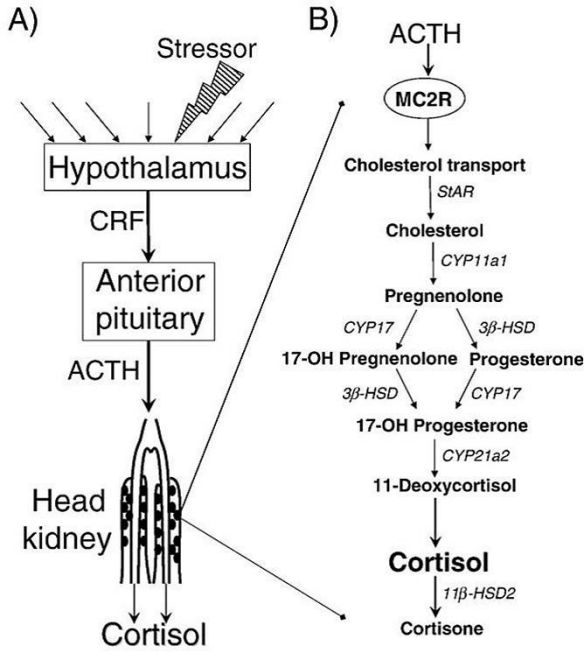

Figure 15: Hypothalamus–pituitary–interrenal (HPI) axis. A) Schematic overview of the anatomy and signaling cascade. B) Cortisol synthesis within an interrenal cell is stimulated by ACTH. A series of enzymatic reactions then leads to the synthesis of cortisone and its release into the circulation (Alsop and Vijayan 2009).

Actually, stress signals induce the hypothamalic neurons to secrete the corticotropin-releasing factor (CRF), which stimulates the release of adrenocorticotropic hormone (ACTH) from the pituitary into the circulation. ACTH binds to the melanocortin 2 receptor (MCR2) expressed in mammals in the adrenal gland. However, fish lack this gland and the corticosteroidogenic cells are present in the head kidney of the fish, called interrenal tissue. The interrenal cells produce the cortisol and secrete it into the blood circulation (Alsop and Vijayan 2008, Aluru and Vijayan 2008, Alsop and Vijayan 2009, Aluru and Vijayan 2009). The final step is the activation of cortisol into cortisone by the 11β-hydroxysteroid dehydrogenase type 2 (11βHSD2) enzyme (Alsop and Vijayan 2009). Cortisol binds 2 types of receptors; the mineralocorticoid receptor (MR) in the kidney or the glucocorticoid receptor (GR) present in

the target tissues. Zebrafish possess only a single gene for CRF ACTH and GR in contrast to other teleosts which contain duplicates. This suggests that zebrafish lost their duplicates in the past (Alsop and Vijayan 2009). The GR has 2 variants (GRα and GRβ) very similar to humans. Cortisol binds GRα with high affinity, while it binds GRβ with low affinity without trans-activation activity (Alsop and Vijayan 2009).

In a first experiment, we wanted to confirm that an excess of cortisol would result in impaired bone formation in zebrafish larvae. Therefore, we used the synthetic glucocorticoid hormone dexamethasone, to observe the effect of dexamethasone treatment for 5 days (from 5 to 10dpf) on the cartilage and bone systems (Fig. 16). Image analysis was performed as previously described.

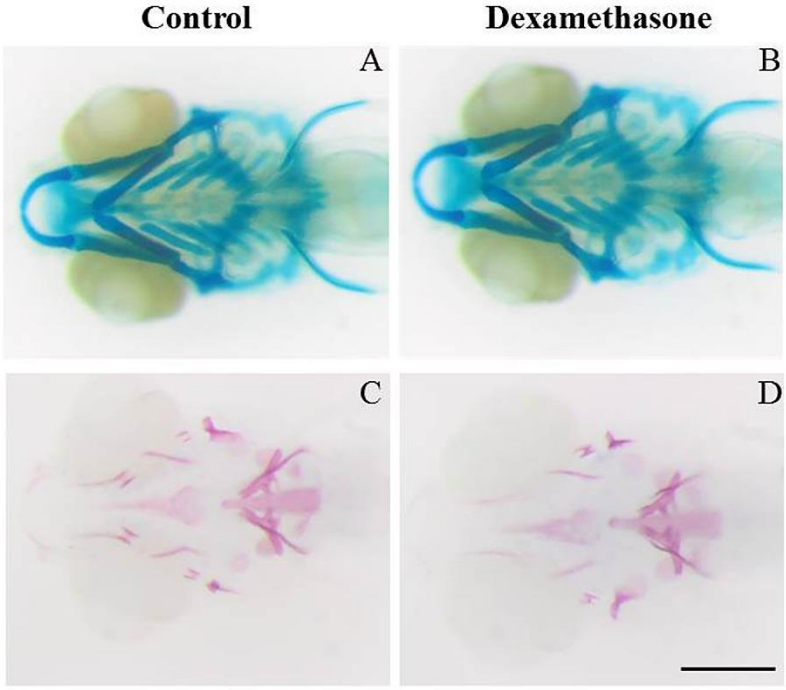

Figure 16: Cartilage and bone elements of the head skeleton in 10dpf zebrafish larvae after 5 days chemical treatments. (A-B) Alcian blue staining of cartilage. (C-D) Alizarin red staining of bone. (A,C) Controls in DMSO. (B) No significant effect of dexamethasone on cartilage development. (D) Decrease of bone development after 10mg/l dexamethasone treatment. Ventral views, anterior to the left, (A-D) scale bar = 250µm.

In preliminary experiments, we first tested several concentrations (2.55µM-25.48µM corresponding to 1 or 10mg/l) of dexamethasone; only the highest tested concentration (25.48µM) lead to skeletal defects, as assessed by visual inspection (Hillegass, Villano et al. 2007). We then exposed 5dpf larvae for 5days to continuous dexamethasone 25.48µM. In 10dpf treated larvae, the cartilage appears very similar to the controls (Fig. 16A,B). There is not effect on already formed cartilage. In contrast, bone formation is clearly affected by the

dexamethasone treatment. Several structures are delayed and some are absent, such as the maxilla or the anguloarticular bone (Fig. 16C,D). Based on these images, we applied the image analysis methods previously described. First, the morphometric approach confirmed that fish cartilage after 5days dexamethasone treatment does not exhibit any significant changes (annex 9). The bone skeleton analysis revealed a significant decrease in the distance between the opercles (o) and between the anterior part of the head (an) and the notochord, suggesting both a narrower and a shorter head after dexamethasone treatment (Fig. 17A).

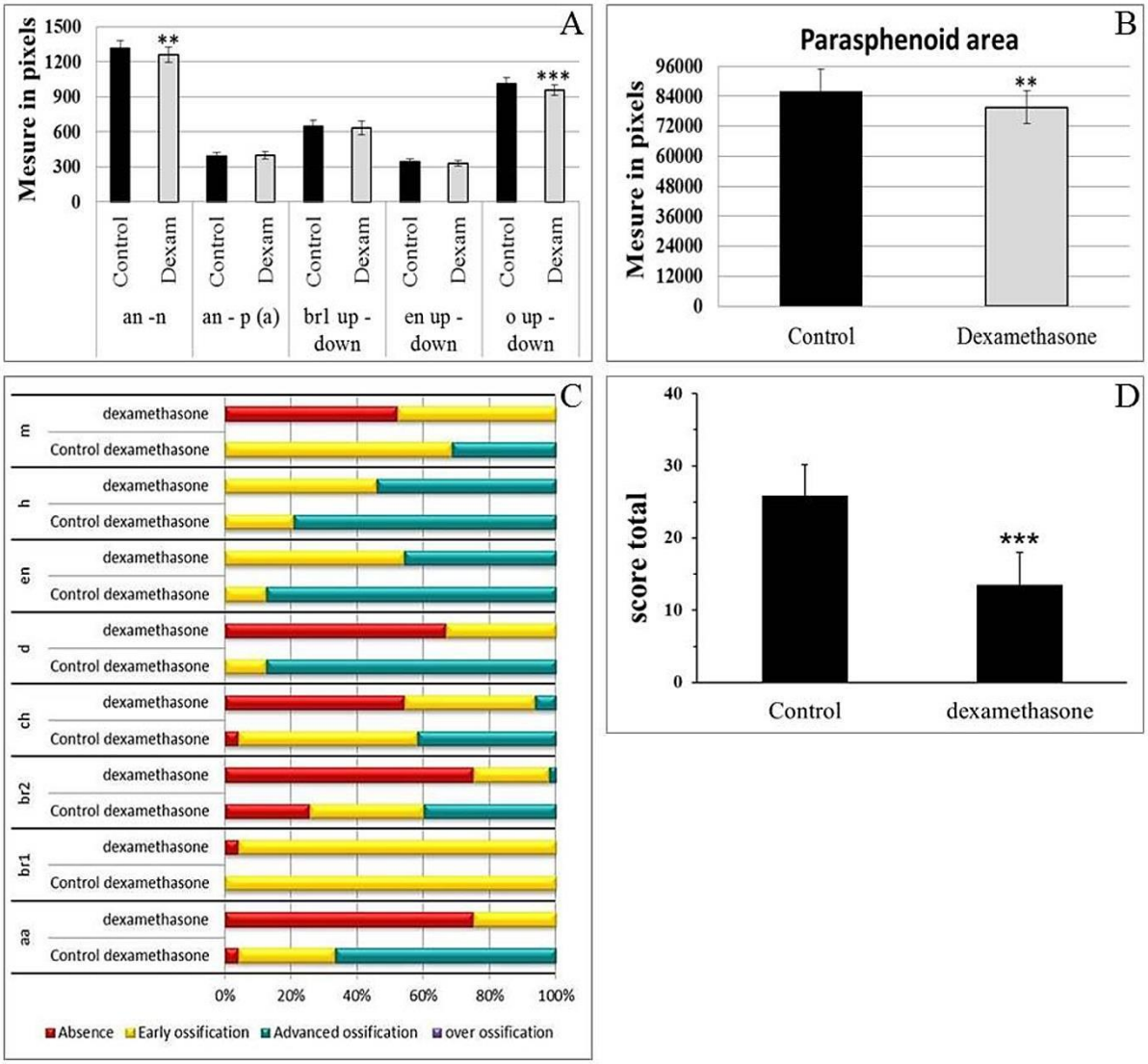

Figure 14: Bone formation in 10dpf zebrafish larvae after 5days dexamethasone treatment. (A,B) Morphometric analysis: The distances are measured in pixels. Mean ± SD and t-test analysis were calculated for each measure on at least 20 individuals. The only significant modification is a decrease of the distance between branchiostegal rays1.** $p < 0.005$ and ***$p < 0.001$. (C,D) Extent of bone formation in dexamethasone-treated larvae compared to controls for individual elements (C) or global score (Mean ± SD) (D).

The second analysis, evaluating the level of ossification of the different bone structures, resulted in similar conclusions. The frequency distribution (Fig. 17C) reveals a general delay in ossification upon dexamethasone treatments, except for the branchiostegal ray1 (br1).

A

				Score of Y		X^2 pearson	Logistic regression	
Structures	Variable	N	Mean	early	advanced	p-value	OR (IC 95%)	p-value
entopterygoid down	Control	24	0,88	3 (12,50%)	21 (87,50%)		1	
	dexamethasone	24	0,46	13 (54,17%)	11 (45,83%)	**0,002**	0,121 (0,028-0,516)	**0,004**
entopterygoid up	Control	24	0,88	3 (12,50%)	21 (87,50%)		1	
	dexamethasone	24	0,46	13 (54,17%)	11 (45,83%)	**0,002**	0,121 (0,028-0,516)	**0,004**
hyomandibular down	Control	24	0,79	5 (20,83%)	19 (79,17%)		1	
	dexamethasone	24	0,46	13 (54,17%)	11 (45,83%)	**0,017**	0,223 (0,062-0,794)	**0,021**
hyomandibular up	Control	24	0,79	5 (20,83%)	19 (79,17%)		1	
	dexamethasone	24	0,54	11 (45,83%)	13 (54,17%)	0,066	0,311 (0,087-1,108)	0,072

B

				Score of Y			X^2 pearson	Ordinal logistic regression	
Structures	Variable	N	Mean	absence	early	advanced	p-value	OR (IC 95%)	p-value
anguloarticular down	Control	24	1,63	1 (4,17%)	7 (29,17%)	16 (66,67%)		1	
	dexamethasone	24	0,25	18 (75,00%)	6 (25,00%)	0 (0,00%)	**<0,001**	0,008 (0,001-0,078)	**<0,001**
anguloarticular up	Control	24	1,63	1 (4,17%)	7 (29,17%)	16 (66,67%)		1	
	dexamethasone	24	0,25	18 (75,00%)	6 (25,00%)	0 (0,00%)	**<0,001**	0,008 (0,001-0,078)	**<0,001**
branchiostegal ray1 down	Control	24	2,00	0 (0,00%)	24 (100%)	0 (0,00%)		1	
	dexamethasone	24	1,96	1 (4,17%)	23 (95,83%)	0 (0,00%)	0,312	/	0,997
branchiostegal ray1 up	Control	24	2,00	0 (0,00%)	24 (100%)	0 (0,00%)		1	
	dexamethasone	24	1,96	1 (4,17%)	23 (95,83%)	0 (0,00%)	0,312	/	0,997
branchiostegal ray2 down	Control	24	1,08	5 (20,83%)	12 (50,00%)	7 (29,17%)		1	
	dexamethasone	24	0,25	18 (75,00%)	6 (25,00%)	0 (0,00%)	**<0,001**	0,073 (0,019-0,280)	**<0,001**
branchiostegal ray2 up	Control	24	1,13	4 (16,67%)	13 (54,17%)	7 (29,17%)		1	
	dexamethasone	24	0,29	18 (75,00%)	5 (20,83%)	1 (4,17%)	**<0,001**	0,072 (0,019-0,276)	**<0,001**
ceratohyal down	Control	24	1,38	1 (4,17%)	13 (54,17%)	10 (41,67%)		1	
	dexamethasone	24	0,54	13 (54,17%)	9 (37,50%)	2 (8,33%)	**<0,001**	0,071 (0,017-0,293)	**<0,001**
ceratohyal up	Control	24	1,38	1 (4,17%)	13 (54,17%)	10 (41,67%)		1	
	dexamethasone	24	0,50	13 (54,17%)	10 (41,67%)	1 (4,17%)	**<0,001**	0,046 (0,009-0,235)	**<0,001**
dentary down	Control	24	1,88	0 (0,00%)	3 (12,50%)	21 (87,50%)		1	
	dexamethasone	24	0,33	16 (66,67%)	8 (33,33%)	0 (0,00%)	**<0,001**	/	/
dentary up	Control	24	1,88	0 (0,00%)	3 (12,50%)	21 (87,50%)		1	
	dexamethasone	24	0,33	16 (66,67%)	8 (33,33%)	0 (0,00%)	**<0,001**	/	/
maxilla down	Control	24	1,33	0 (0,00%)	16 (66,67%)	8 (33,33%)		1	
	dexamethasone	24	0,46	13 (54,17%)	11 (45,83%)	0 (0,00%)	**<0,001**	/	/
maxilla up	Control	24	1,29	0 (0,00%)	17 (70,83%)	7 (29,17%)		1	
	dexamethasone	24	0,50	12 (50,00%)	12 (50,00%)	0 (0,00%)	**<0,001**	/	/

Table 8: Ossification scores for individual bone elements in 10dpf control larvae and larvae treated for 5days by dexamethasone. (A) Bone structures distributed in 2 categories (early and advanced ossification) (B) Bone structures distributed in 3 categories (early, advanced and over ossification).

The more precise statistical analysis confirms these observations with a decrease of bone development in all the present structures. Only the branchiostegal ray1 (br1) and the hyomandibular (h) up are not significantly different compared to the controls (Table 8).

In a second experiment, we wanted to investigate whether microgravity simulation actually causes stress in the zebrafish larvae. To evaluate the stress status of 6dpf larvae after 1 day treatment by simulated microgravity, we determined the whole body cortisol levels in 15 larvae directly after sacrifice. We begin to compare two different methods to collect and euthanize the larvae. The first consists in adding 4 g/l tricaine to the larvae, as recommended in 0.04g/l.… and resulting in rapid anesthesia followed by death after 2-3 minutes (low tricaine). The second consists in collecting the larvae in a small volume of E3 medium followed by addition of 1.6g/l of tricaine (high tricaine). We observed a significant increase of cortisol levels in the larvae sacrificed after previous anesthesia by the lower concentration of tricaine (Fig. 18A), probably due to the acute stress induced by anesthesia.

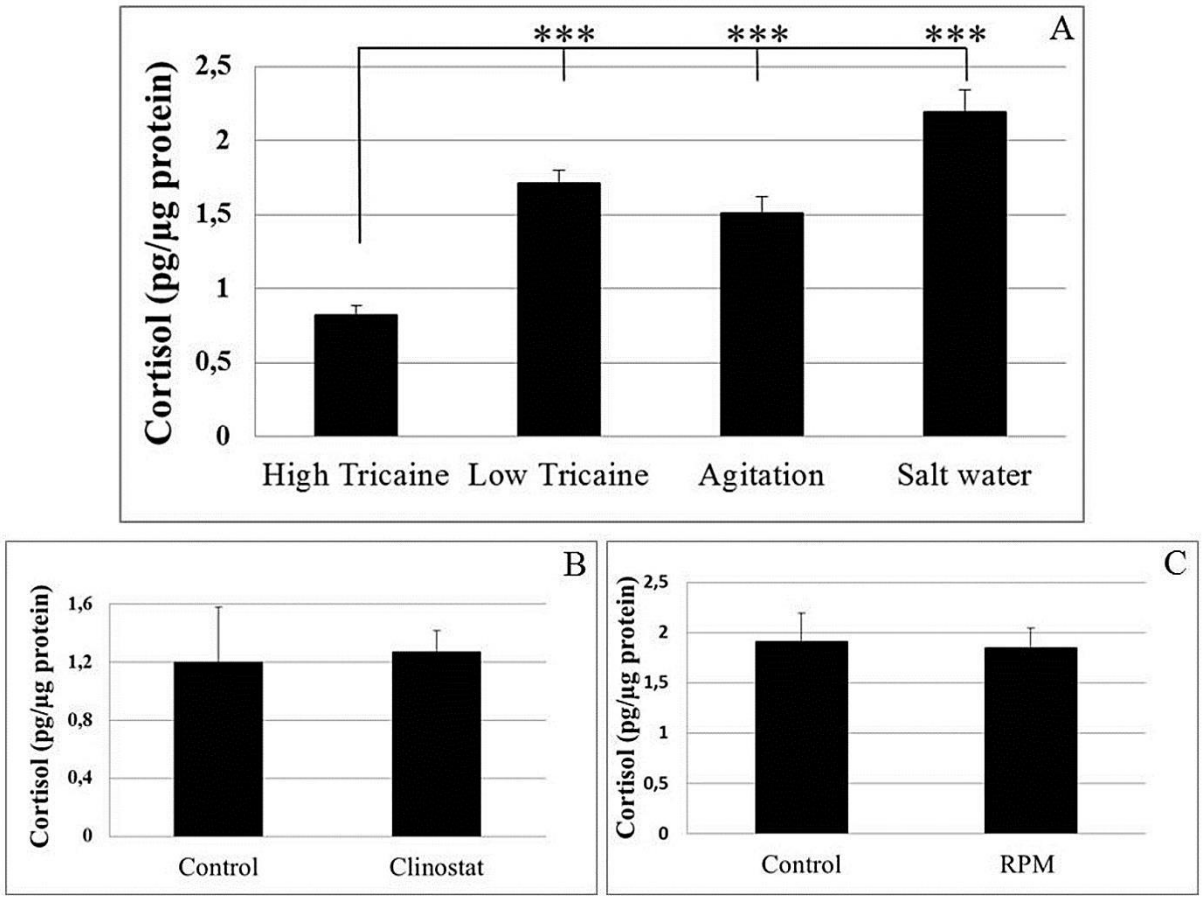

Figure 18: Stress evaluation by cortisol assay. (A) Negative and positive controls. Tricaine, agitation and salt water increase significantly the cortisol level compare to pursuit. (B) No change in cortisol level in clinostat compare to their control. (C) No change in cortisol level in RPM compare to their control. ***$p < 0.001$.

Consequently, all experiments were performed using the higher tricaine concentration for larvae sacrifice. We then performed two positive control experiments by using two different methods known to induce acute stress in zebrafish larvae: the first consists in intense agitation for 30s in 5 ml medium followed by 5 min rest before sacrifice at high tricaine concentration (Alsop and Vijayan 2008), while the second exposes the larvae to a 1.75g/l NaCl solution for 5 min before leaving them for recovery for 5 min in E3 and sacrifice (Alderman and Bernier 2009). Both stress conditions lead to a significant increase in cortisol levels, as expected, that were interestingly similar to the levels observed under low tricaine conditions (Fig. 18A). Finally, we determined the cortisol levels in 6dpf larvae after one day in simulated microgravity. No difference was measured between the larvae subjected to clinorotation or RPM as compared to their respective controls. (Fig. 18B, C). Note that in the RPM experiment, we observed a significantly higher basal cortisol level already in the control larvae, which remained similar in the treated larvae. These elevated levels are probably due to the noise and vibrations sensed by the control larvae that were placed into the same incubator, although not subjected to the random movements of the RPM device. These results demonstrate that the larvae placed into one of these 2 microgravity simulators are not stressed compared to their respective controls. Thus, any modification observed is most likely related to the effect of simulated microgravity and not stress.

4. Rotating wall vessel

Another recently developed device for placing cultured cells or tissues into simulated microgravity is the so-called Rotating Wall Vessel (RWV) device (Goodwin, Jessup et al. 1992, Spaulding, Jessup et al. 1993, Unsworth and Lelkes 1998, Grimm, Wehland et al. 2014). We placed 5dpf zebrafish larvae into the rotating disk, while control larvae were placed into the same disk but kept immobile in the same incubator. After staining for bone elements, we noticed a higher variability in the extent of ossification between individual larvae and between experiments (Fig. 19A,B and C, D, see also the high incidence of absent elements in Fig. 19E and Fig. 19G; annex 8c), however the larvae subjected to RWV did not present any obvious changes in bone formation between the treated and controls (Fig. 19A-D; annex 8c). Similarly, morphometric analysis did not reveal any significant changes between the treated and the control larvae, only a slight decrease of the distance between branchiostegal ray1 up and down was observed (Fig. 19E,F; annex 8c). Similarly, no significant difference was observed in the extent of ossification, both on individual elements (Fig. 19G, annex 10) and on the global scores (Fig. 19H).

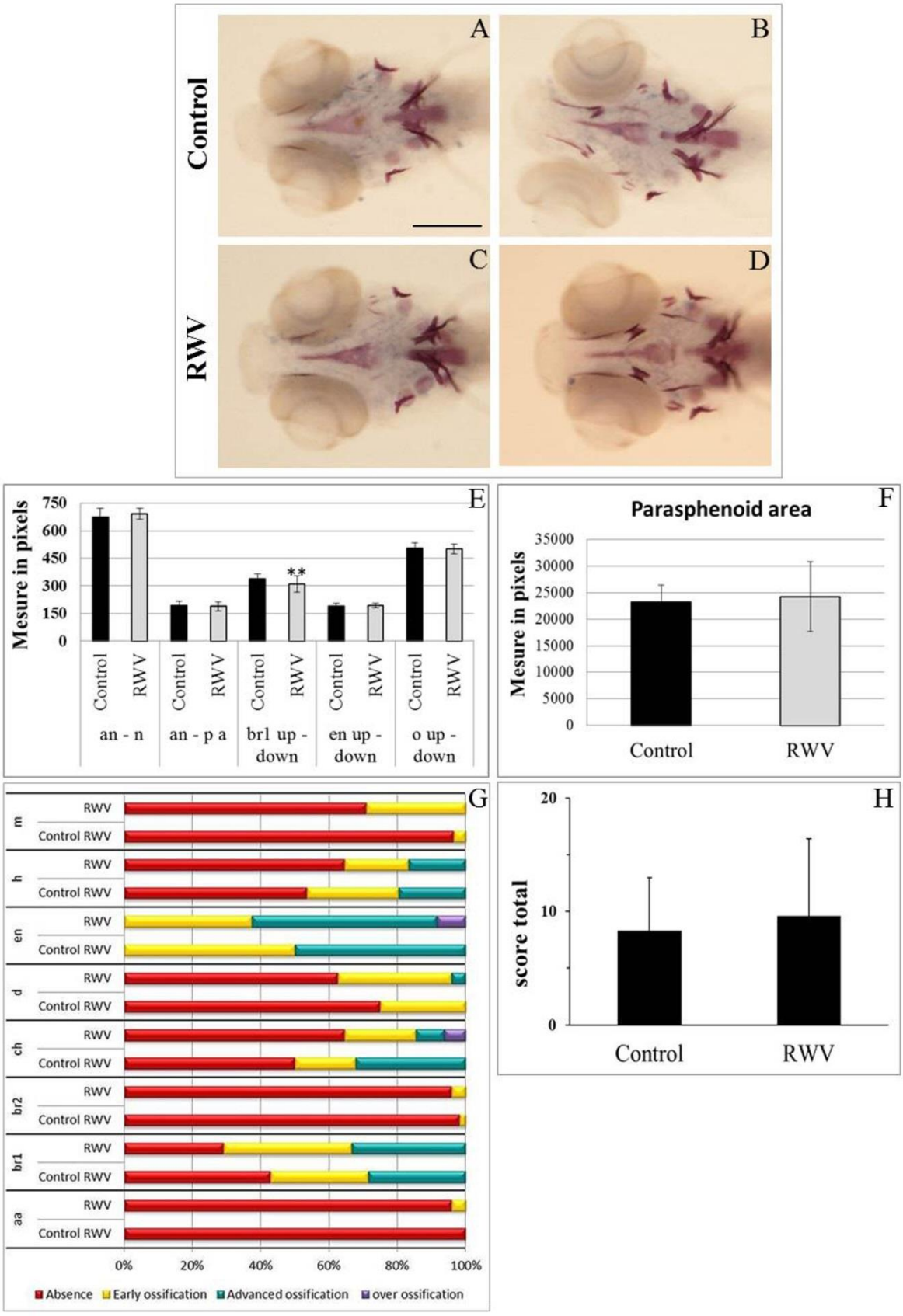

Figure 19: Bone formation in 10dpf zebrafish larvae after 5days RWV treatment. (A-D) Alizarin red staining of bone extracellular matrix in control (A, B) or RWV-treated (C,D) larvae in two independent experiments. (E,F) Morphometric analysis: The distances are measured in pixels.

Mean ± SD and t-test analysis were calculated for each measure on at least 20 individuals. The only significant modification is a decrease of the distance between branchiostegal rays1.** $p < 0.005$ and ***$p < 0.001$. (G,H) Extent of bone formation in RWV-treated larvae compared to controls for individual elements (G) or global score (Mean ± SD) (H).

5. Effects of simulated microgravity on gene expression

To obtain a global view of the physiological changes caused by simulated microgravity, we performed a microarray whole genome expression analysis. We compared 6dpf control larvae to larvae exposed between 5dpf and 6dpf to clinorotation, RPM or RWV, in order to capture early regulatory events rather then secondary regulations leading ultimately to the observed modulations of bone formation at 10dpf. Four independent experiments were carried out, using 70 larvae for each experimental condition, on the RWV and RPM devices. For clinorotation (CLINO), due to the small volume available in the rotating tubes, only 15 larvae were run in parallel in three tubes; thus each control or rotated sample consisted of a pool from 4 different experiments to reach a sample size of 60 larvae. Total RNA was extracted from 6dpf control larvae and larvae that experienced microgravity simulation, reverse transcribed into cDNA and used as probes for gene expression microarray analysis.

A list of genes affected more than 1.4-fold ($|\log2$ fold change$|>0.49$) by each simulation device was extracted and introduced into the Ingenuity Pathway Analysis software (IPA; Materials and Methods) for further analysis. Respectively 208, 170, and 353 genes were significantly affected in the CLINO, RPM, and RWV experiment, of which respectively 66, 63, and 184 genes found an annotation in IPA (Fig. 20).

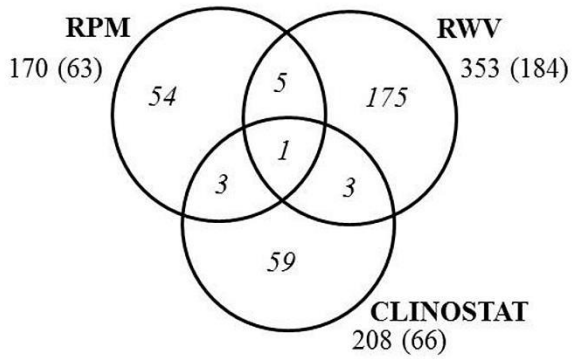

Figure 20: Genes whose expression is affected by the different approaches to simulate microgravity. The absolute number of probes resulting in a statistically significant hybridization signal is given for each condition. In parentheses, the corresponding number of genes with an annotation in IPA is given, while the Venn diagram represents the number of genes unique to each condition and genes common to any two or all three conditions.

The full list of these genes is given in Tables annex 11 (CLINO), annex 12 (RPM), and annex 13 (RWV). 11 genes were selected from the lists for validation by RT-qPCR, which demonstrated the reliability of the microarray data (Table 9).

	CLINO		RPM		RWV	
Genes	**RT-PCR**	**Microarray**	**RT-PCR**	**Microarray**	**RT-PCR**	**Microarray**
col10a1	**0.85±0.1**		**0.91±0.1**		**1.53±0.3**	1.45
cyp24a1	1.1±0.2		1.17±0.4		**2.00±0.3**	1.53
rhcg2a	**1.50±0.3**	1.77	**1.16±0.1**		**1.40±0.3**	1.47
rhcga	**0.84±0.2**		**3.04±0.4**	1.71	**1.50±0.2**	2.38
fos b	**0.47±0.8**	0.67				
igfr2	**0.87±0.1**	0.32				
ndrg2	**1.44± 0.2**	1.57				
ehf			**0.54±0.1**	0.53		
elf3			**0.62±0.1**	0.52		
igfbp1					**1.56±0.4**	1.57
socs3					**1.54±0.4**	1.62

Table 9: Comparison of fold change values from the microarray dataset with those observed by RT-qPCR for CLINO, RPM, and RWV treatment. The fold change is given from the microarray data and the RT-qPCR confirmation experiments. For microarray data, only significant fold-change values are shown. For RT-PCR data, bold-type indicates significant changes in expression ($p<0.05$).

In general, it appears that the number of significantly affected genes is relatively low, indicating that microgravity simulation has no major immediate impact on general physiology. The most highly affected gene in CLINO (Table annex 11) is *AXIN2* (log2 fold -3.48), indicating a down-regulation of the Wnt pathway, while the most highly up-regulated gene is *HES1* that is involved in NOTCH signaling (Kageyama and Ohtsuka 1999). Construction of interaction pathways using IPA (Fig. 21A) revealed a small pathway centered around FGF2, and the increased expression of *CYP19A1*, required for estrogen synthesis, and its effect on lipoprotein metabolism. Exposure to the RPM device led to increased expression of the *NOTCH1* and *WNT3A* signaling proteins and the *RUNX1* transcription factor, while expression of the transcriptional regulators *MED23*, *HOXB9*, *ELF3*, and *EHF* was decreased (Table annex 12). Pathway construction (Fig. 21B) revealed two networks centered around NOTCH1 and WNT3A, as well as a connection between transcription factors BARX2 and SRF. Exposure to the RWV induced the *CYP24A1* gene (Table annex 13), encoding a member of the cytochrome P450 superfamily of enzymes involved in the degradation of 1,25-dihydroxyvitamine D3, indicating that the VitD3 pathway was activated. Further, RWV exposure induced expression of the JAK/STAT pathway regulators *SOCS1* and *SOCS3*, while

expression of the matrix metalloprotease genes *MMP8* and *MMP9* was decreased. Using the RWV data set, a large network of interacting genes could be constructed (Fig. 21C), that was centered around JUN.

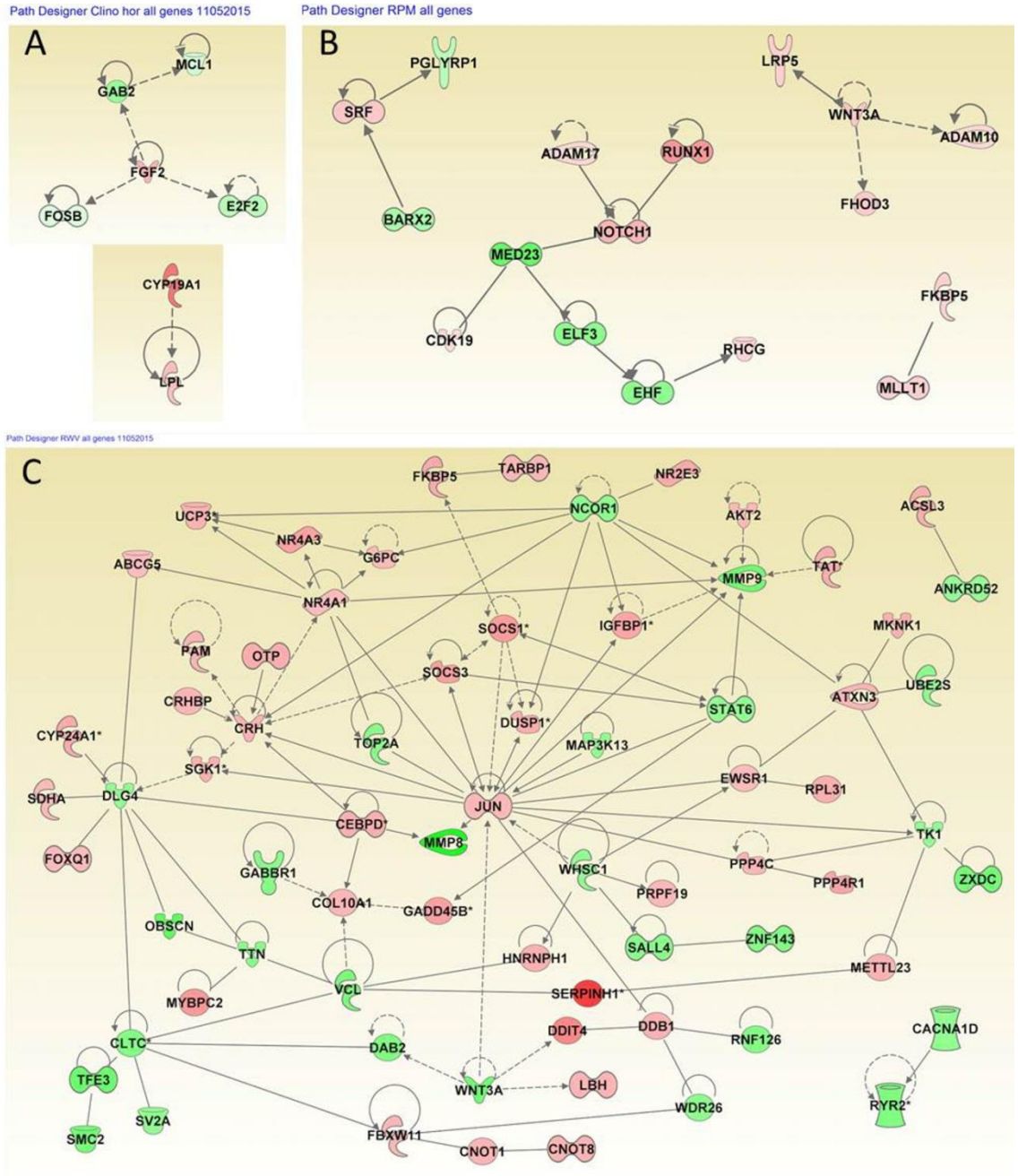

Figure 21: Network of genes affected in the different simulated microgravity experiments. Network of genes affected in **(**A) CLINO, (B) RPM, and (C) RWV conditions. Color overlay indicates the fold change relative to the respective controls. Genes up-regulated (red), down-regulated (green), (*) indicates that the gene is represented by two or more probes on the microarray.

Comparison of the three data sets revealed only one gene whose expression was affected in each of the three microgravity simulation approaches, coding for the ammonium transporter Rh Type C glycoprotein RHCG (Table 10). In zebrafish, at least two homologs have been

identified for this human gene identified in IPA, *rhcga* and *rhcg2a*. Interestingly, exposure to CLINO induced *rhcg2a* expression, RPM exposure induced *rhcga* expression while in the RWV experiment, both genes were up-regulated (Table 10). 11 additional genes were common two only two of the tested conditions (Table 10).

Symbol	Entrez Gene Name	Log Ratio (CLINO)	Log Ratio (RPM)	Log Ratio (RWV)
RHCG	Rh family. C glycoprotein	0.82	0.78	1.51
P2RY13	purinergic receptor P2Y. G-protein coupled. 13	-1.50		0.59
RYR2	ryanodine receptor 2 (cardiac)	-1.37		-0.57
GADD45B	growth arrest and DNA-damage-inducible. beta	-0.56		0.69
CXCR3	chemokine (C-X-C motif) receptor 3	1.85	-1.04	
DMBX1	diencephalon/mesencephalon homeobox 1	1.10	0.96	
KLHL38	kelch-like family member 38	1.01	-1.42	
WNT3A	wingless-type MMTV integration site family. member 3A		1.07	-0.63
FKBP5	FK506 binding protein 5		0.84	0.63
ACSL6	acyl-CoA synthetase long-chain family member 6		0.76	1.35
SERPINH1	serpin peptidase inhibitor. clade H (heat shock protein 47). member 1. (collagen binding protein 1)		0.76	1.40
Sult5a1	sulfotransferase family 5A. member 1		-1.81	-0.81

Table 10: Genes expression affected by the different approaches to simulate microgravity. Gene symbol, Entrez gene name and Log Ratio between expression levels in treated and control larvae in the indicated conditions.

One important aspect of our study is the fact that we investigated gene expression using mRNA from the entire larvae. When we focused on individual organ systems by filtering the affected gene sets against available databases of genes involved in specific functions (GO annotation of human gene orthologs using IPA knowledge base), networks of regulatory interactions could be constructed for each system. Major hubs were identified such as JUN, FOSB, STAT6, and NOTCH1, that connected to different affected genes in each tested condition (Fig. 22, 23, 24). Specific to bone, HOXB9 is connected to FGF2 and ELF3 is connected to JUN, while in the cardiovascular system ELF3 connected to NOTCH1 through MED23 (Fig. 24). Components of the insulin-like pathway such as IGF2R and IGFBP1, or the cytokine receptor regulators SOCS3 and SOCS1 are represented, while the ryanodin receptor RYR2 was only present in CLINO and RWV. Interestingly, the muscle structural gene *TTN* (Titine) was inhibited in RWV.

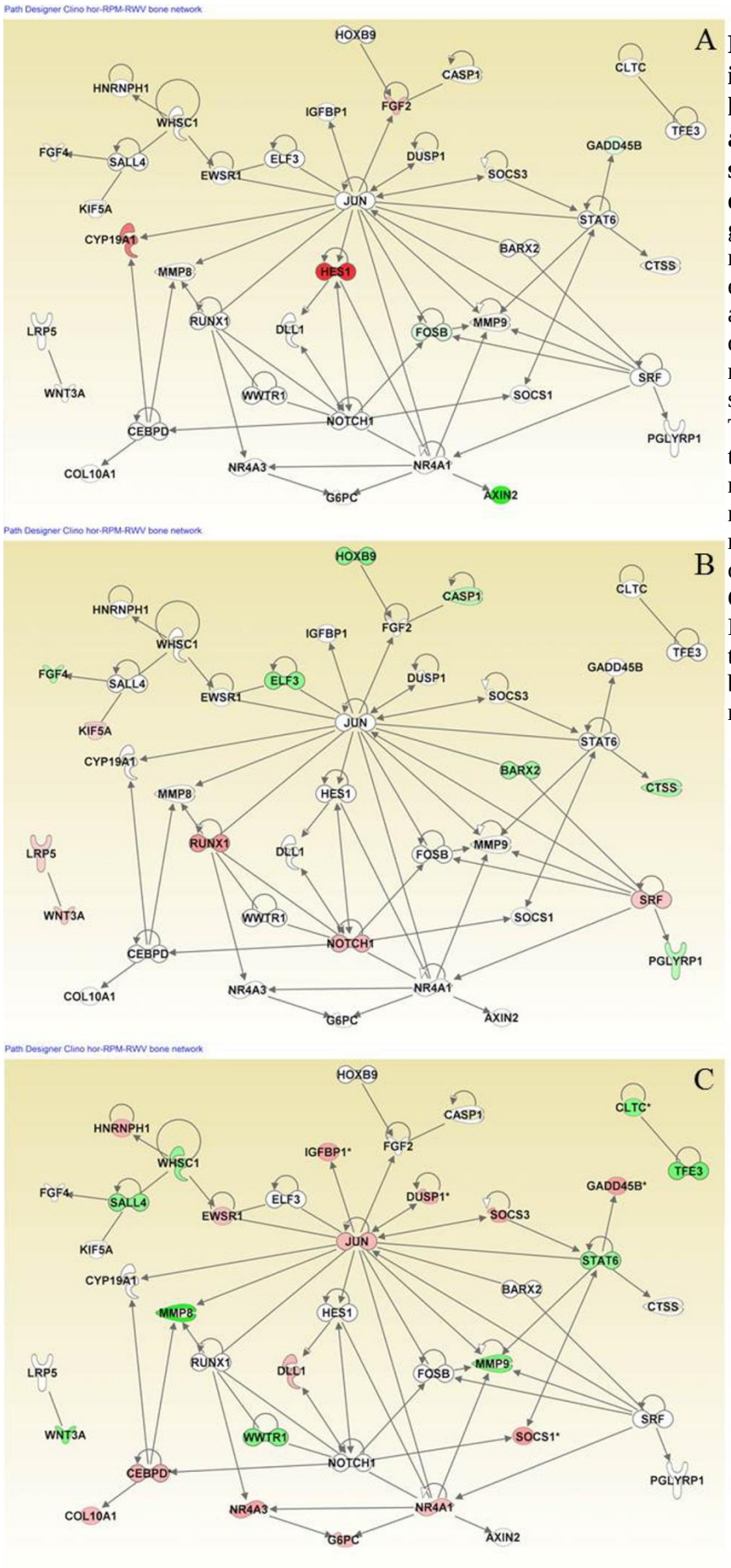

Figure 22: Gene network involved in bone homeostasis and genes affected in the different simulated microgravity experiments. The lists of genes affected in the microgravity simulation experiments were combined and filtered according to the described function for their mammalian homologs in the skeletal system using IPA. The color overlay indicates the fold change relative to the respective controls (up-regulated genes in red, down-regulated genes in green) observed, respectively in **(**A) CLINO, (B) RPM, and (C) RWV conditions.(*) indicates that the gene is represented by two or more probes on the microarray.

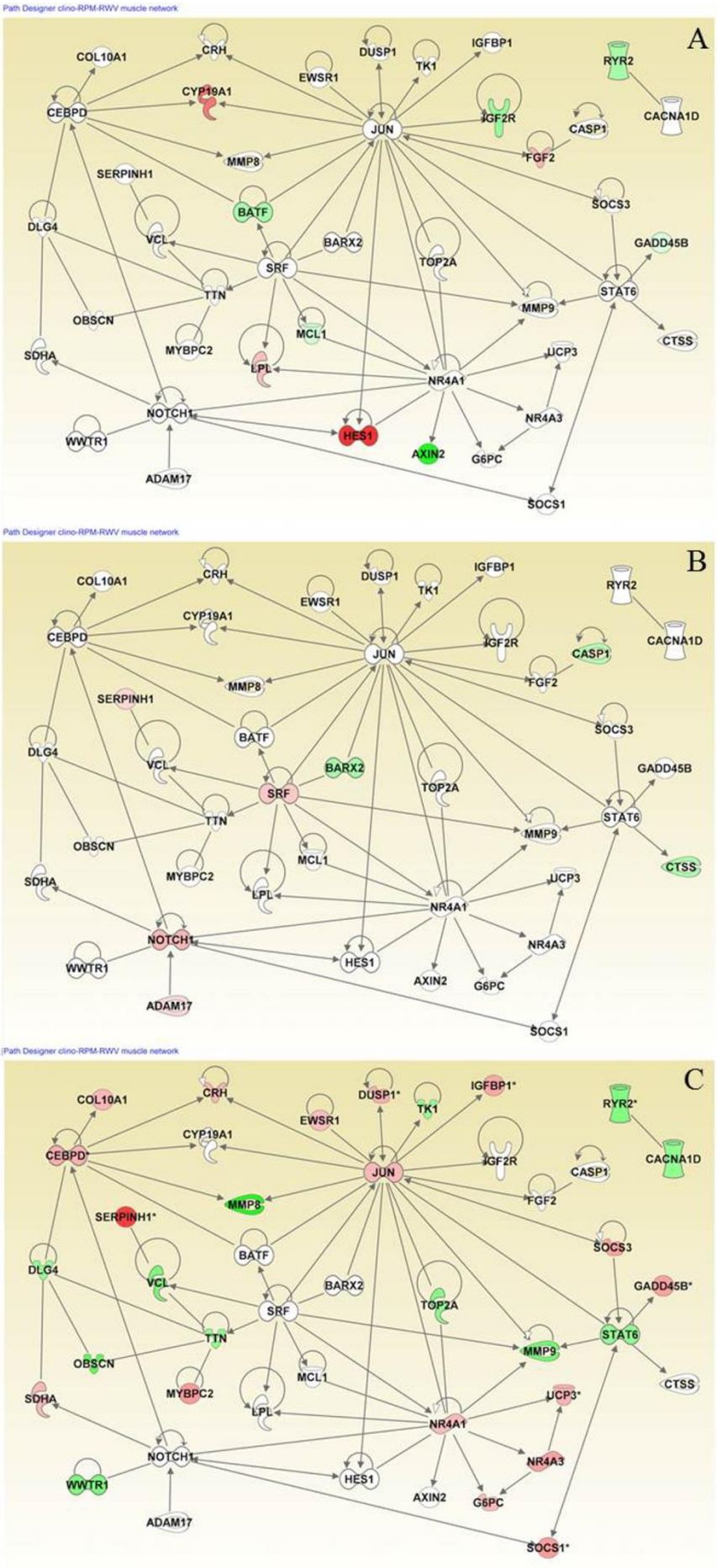

Figure 23: Gene network involved in the muscular system and genes affected in the different simulated microgravity experiments. The lists of genes affected in the microgravity simulation experiments were combined and filtered according to the described function for their mammalian homologs in the muscular system using IPA. The color overlay indicates the fold change relative to the respective controls (up-regulated genes in red, down-regulated genes in green) observed, respectively in **(**A) CLINO, (B) RPM, and (C) RWV conditions. (*) indicates that the gene is represented by two or more probes on the microarray.

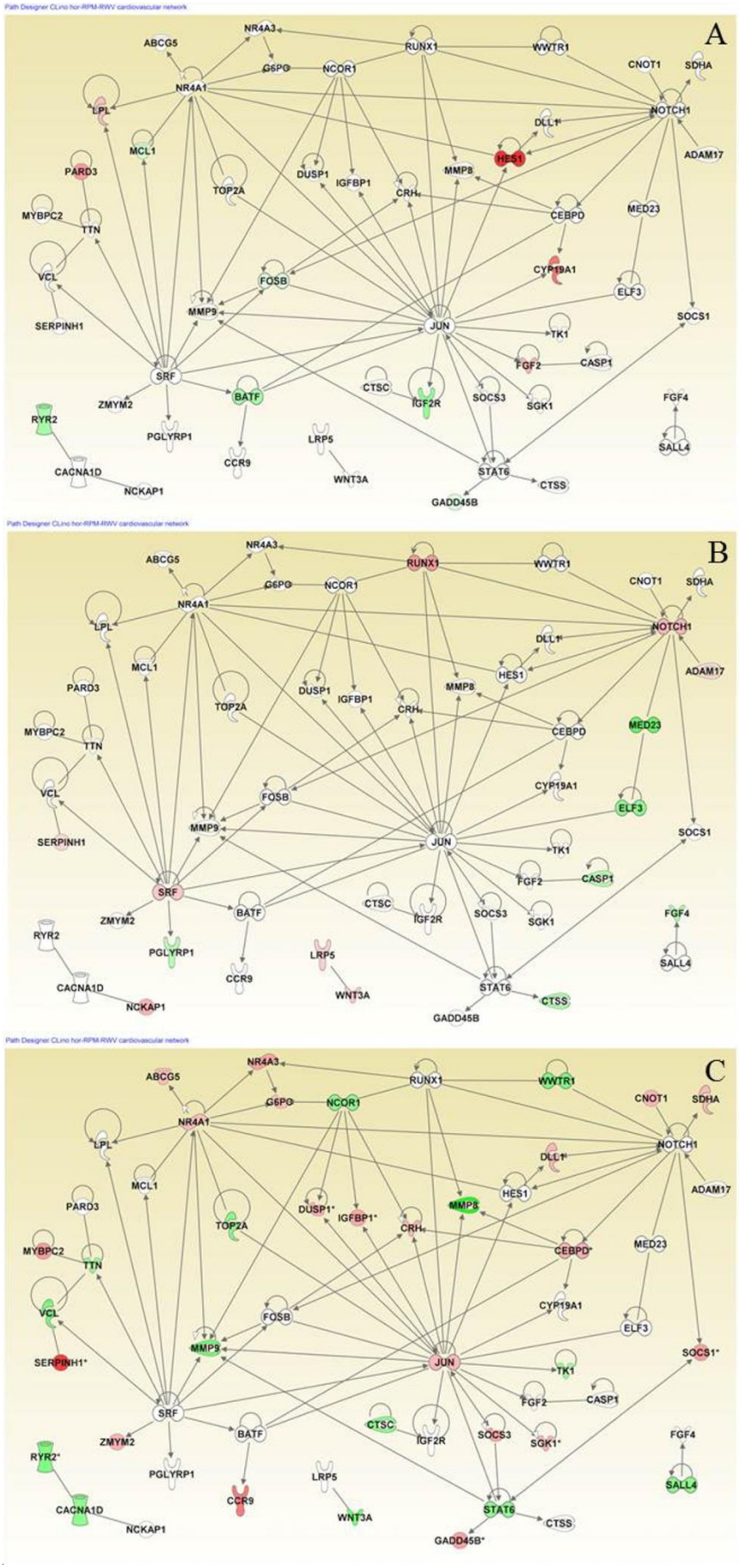

Figure 24: Gene network involved in the cardiovascular system and genes affected in the different simulated microgravity experiments. The lists of genes affected in the microgravity simulation experiments were combined and filtered according to the described function for their mammalian homologs in the cardiovascular system using IPA. The color overlay indicates the fold change relative to the respective controls (up-regulated genes in red, down-regulated genes in green) observed, respectively in **(**A) CLINO, (B) RPM, and (C) RWV conditions. (*) indicates that the gene is represented by two or more probes on the microarray.

Ingenuity Pathway Analysis (IPA; Materials and Methods) was used to compare the biological functions and regulatory pathways that were affected by the different microgravity simulation approaches. Among the "canonical pathways" affected (Table 11), the retinoid X receptor RXR is prominent in its common role for FXR/RXR, VDR/RXR and FXR/RXR signaling. All three approaches acted on IL-6, Notch, VDR, Hif1ß, LPS/IL-1 and Notch signaling, while many other pathways were only affected by RPM and/or RWV such as Matrix metalloproteases, TR/RXR, JAK/Stat, or IGF-1 signaling (Table 11).

Canonical Pathway	CLINO	RPM	RWV
Atherosclerosis Signaling	1.42		1.44
FXR/RXR Activation	1.11		1.62
IL-6 Signaling	1.06	1.17	1.54
Notch Signaling	0.75	1.91	0.43
ATM Signaling	0.57		1.42
VDR/RXR Activation	0.55	0.60	1.37
LXR/RXR Activation	0.47		1.78
HIF1ß Signaling	0.40	0.45	1.50
LPS/IL-1 Mediated Inhibition of RXR Function	0.29	0.33	1.55
Wnt/ß-catenin Signaling	0.24	1.44	0.49
Regulation of the Epithelial-Mesenchymal Transition Pathway		1.96	0.37
Death Receptor Signaling		1.30	
Inhibition of Angiogenesis by TSP1			2.20
IL-17A Signaling in Fibroblasts		0.94	1.37
PXR/RXR Activation			1.77
Acute Phase Response Signaling		0.90	1.58
IL-22 Signaling			1.50
Inhibition of Matrix Metalloproteases		2.15	1.33
LPS-stimulated MAPK Signaling		1.33	0.21
Huntington's Disease Signaling			2.66
TR/RXR Activation			2.61
Role of JAK family kinases in IL-6-type Cytokine Signaling			1.50
PEDF Signaling		1.36	0.22
Erythropoietin Signaling		0.53	1.83
IL-4 Signaling			1.47
Glucocorticoid Receptor Signaling		0.55	2.10
Airway Pathology in Chronic Obstructive Pulmonary Disease			2.79
PCP pathway		1.46	0.72
Role of JAK1 and JAK3 in Œ≥c Cytokine Signaling			1.58
JAK/Stat Signaling			2.67
IGF-1 Signaling		0.42	2.00
IL-2 Signaling			1.55

Table 11: Canonical pathways affected by the different approaches to simulate microgravity. Ingenuity Pathway Analysis of the lists of genes affected at 6dpf after 1 day CLINO, RPM or RWV each time compared to the corresponding controls. The numbers represent –Log(p-value) for significance that the corresponding list of genes affects the indicated pathway.

When we classified the affected genes according to their involvement in specific "Disease and Biological Functions", a striking difference became apparent between the three approaches

(Table 12). While CLINO affected morphology, size and resorption of bone as well as the quantity of osteoclasts, bone and blood cells, RPM and RWV affected hematopoietic system development, RPM revealed more relevant effects on stem and progenitor cells and skin, somite and cardiovascular system development, and RWV acted on anxiety, adipogenesis, osteoclastogenesis, gestation and mortality.

Diseases and Bio Functions	CLINO	RPM	RWV
growth of arteriole	4.31		
quantity of bone cells	4.17		
morphology of trabecula	4.16		
quantity of blood cells	3.84	1.89	
morphology of bone	3.41		
quantity of cells	3.20		2.42
morphology of trabecular bone	3.15		
resorption of bone	3.05		
quantity of osteoclasts	2.96		
quantity of leukocytes	2.88	1.87	
abnormal morphology of body cavity	2.86		
size of bone	2.80		
quantity of lymphocytes	2.77		
abnormal morphology of endometrium	2.77		
neurogenesis of embryonic tissue	2.68		
contractility of heart	2.64		
abnormal morphology of trabecula	2.59		
development of hematopoietic system		4.38	1.82
development of lymph follicle		4.03	
quantity of progenitor cells		3.46	
network formation of endothelial cells		3.44	
development of somites		3.01	
morphogenesis of skin		2.91	
quantity of neural stem cells		2.89	
development of cardiovascular system		2.88	
somitogenesis		2.88	
morphogenesis of foregut		2.80	
morphogenesis of bone		2.62	
anxiety			3.32
adipogenesis			3.20
osteoclastogenesis			2.98
gestation			2.59
morphogenesis of mammary gland			2.59
mortality			2.52

Table 12: Diseases and Biological functions affected by the different approaches to simulate microgravity. Ingenuity Pathway Analysis of the lists of genes affected at 6dpf after 1 day CLINO, RPM or RWV each time compared to the corresponding controls. The numbers represent –Log(p-value) for significance that the corresponding list of genes affects the indicated biological function.

A similar observation can be made when classifying the more generic "Disease and Biological Function" terms according to their relevance (Table annex 14). "Connective Tissue

Disorders", Skeletal and Muscular Disorders, and "Connective Tissue Development and Function" ranked on position 2, 5, and 11, respectively for CLINO, while "Hematological System Development and Function", "Hematopoiesis" and "Cancer" ranked highest in RPM and "Cellular Development" and "Cellular Growth and Proliferation" and "Endocrine System Development and Function" were on top position for RWV. The discrepancy between the different microgravity simulation approaches becomes fully apparent when analyzing the different data sets for putative upstream regulators and the predicted change in activity of these regulators (Table annex 15). Especially when comparing CLINO and RWV, most common proposed regulators are modulated in opposite directions, as best illustrated by the affected genes regulated by CREB1 (Fig. 25).

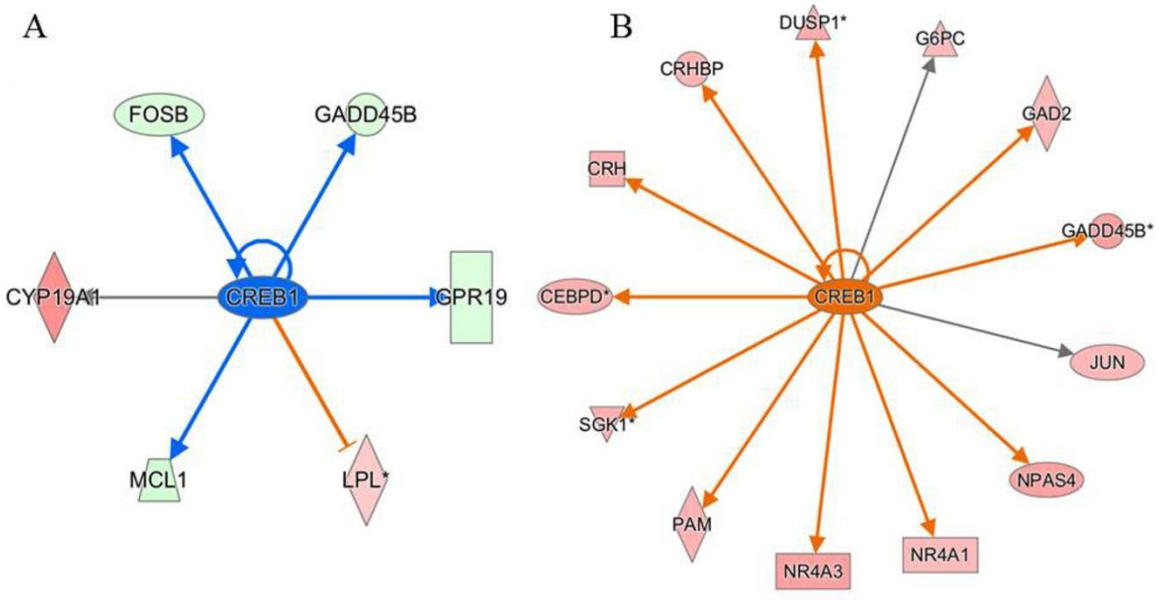

Figure 25: Genes connected to the upstream regulator CREB1 predicted by Ingenuity Pathway Analysis. (A) CREB1 activity is predicted to be down-regulated in CLINO condition (blue color). (B) CREB1 activity is predicted to be up-regulated in RWV conditions. Blue or orange lines indicate, respectively inhibition or activation of expression consistent with the prediction, grey arrow indicates that no information is available (inconsistent findings would be in yellow). Arrows indicate an interaction activating, while stop-lines indicate an interaction inhibiting expression of the target gene. Red overlay color indicates increased gene expression, while green overlay indicates decreased gene expression in the corresponding experiment.

The observed changes in gene expression are consistent with a decrease in CREB1 activity in CLINO, but highly consistent with an increased activity of CREB1 in RWV. Interestingly, the RPM data set is often more coherent with the CLINO data, although the most relevant CLINO regulators are not represented.

6. Conclusions

Here, we used devices traditionally used for studying the effects of simulated microgravity on microorganisms or cell cultures can be adapted to the study of this vertebrate model system. We used various approaches to simulate microgravity, including the 2D clinostat (CLINO), Random positioning machine (RPM) and the Rotating Wall Vessel (RWV). To our knowledge, this is the first time that these three different approaches were tested on the same model in a parallel study.

We first concentrated on the effects of simulated microgravity on bone formation. In zebrafish, ossification starts in the head skeleton at 3dpf, however extensive bone mineralization is observed beyond 4-5dpf, therefore we chose 5dpf as starting point for the microgravity simulation experiments. Simulation was continued for several days in order to observe the effect on skeletal formation at 9-10dpf, modifications in the head cartilage and bone skeleton were assessed using the described morphometric and extent of ossification methods in the previous chapter. Assessment of the distances between the different landmarks in the cartilage skeleton revealed no or very minor (in RPM) changes in morphology due to microgravity simulation.

In contrast, the morphology of the head bone skeleton was affected by microgravity simulation. Clinorotation caused a significant decrease of the parasphenoid area, in line with the general decrease in ossification in these conditions . The parasphenoid area was also reduced in RPM conditions, albeit to a lesser extent, while the distance between several paired bone elements (anguloarticular, branchiostegal rays1, entopterygoids, and opercles) was significantly reduced. A similar, albeit weaker effect was observed in RWV conditions, with only a slight decrease of the distance between branchiostegal rays1. Such a narrowing of the head skeleton was not observed for the cartilage elements that the dermal skeleton might be more responsive to changes in environment at these stages. Evaluation of the extent of ossification for individual elements revealed that clinorotation for 5 days caused a significant decrease in ossification of individual bone elements, and on the global score.

In contrast to the results in clinorotation, both RPM and RWV did not result in a significant change in the global extent of ossification, while three (in RPM) or two (in RWV) bone elements revealed over-ossification in some individuals. This intriguing discrepancy probably results from the specific model organism used here. Indeed, in contrast to microorganisms growing in suspension and cell cultures or even plant shoots fixed on a supporting medium,

zebrafish larvae are free-swimming individuals. Visual inspection during the different simulation experiments revealed that the unpredictable movements of the RPM, or the larger diameter rotation of the RWV led to increased swimming behavior in the larvae, while the continuous rotation of the water column during clinorotation allowed a more natural, mainly resting behavior. In addition, in the clinostat, we observed that immobile larvae were indeed following the rotating movement, while swimming larvae tended to compensate the rotating environment in order to keep their level. Thus, our assumption is that the water movements in RPM and RWV will trigger swimming behavior in the zebrafish larvae, thereby disturbing the intended microgravity simulation effect as was already previously suggested (Brungs, Hauslage et al. 2011, Herranz, Anken et al. 2013). Furthermore, induced swimming could possibly even cause an unwanted physical training, or muscle loading effect. Such a training effect could explain the increased ossification observed in some elements, similar to the accelerated bone formation previously observed after intense swim training in a constant flow device (Fiaz, Leon-Kloosterziel et al. 2012). Previously published experiments exposing zebrafish embryos of different stages to RWV simulation support these conclusions. One study analyzed the expression of selected genes of larvae exposed to RWV during various periods during the first three days of development and showed that none of the early effects was observed in larvae treated after 72hpf, when all the larvae have hatched and are freely swimming (Shimada, Sokunbi et al. 2005, Edsall and Franz-Odendaal 2014). Similarly, analysis of bone defects in adult zebrafish caused by early exposure to RWV were shown to be absent when the treated larvae were older than 48hpf during the treatment (Edsall and Franz-Odendaal 2014).Future experiments may reveal whether these disturbing effects can be overcome by embedding the larvae in a gel or a fine glass fiber mesh. Taken together, we conclude that clinorotation is probably the most appropriate approach to simulate microgravity on free-swimming aquatic organisms.

The observation that bone formation was decreased upon clinorotation raised the question concerning a possible involvement of stress in this effect. Loss of bone mineral density was shown in U. S. military during combat missions (Henning, Park et al. 2011) or during glucocorticoid treatment of inflammatory diseases (Feng and McDonald 2011, Weinstein 2012). Similarly, increased bone resorption was shown in atlantic bluefin tuna (*thynnus thynnus*) when reared in captivity which was partly attributed to stress (Santamaria, Bello et al. 2015). On the other hand, the level of stress during space missions was assessed by performing cortisol measurements before, during and post-flight. The cortisol levels do not significantly

change between the samples (Caillot-Augusseau, Lafage-Proust et al. 1998). Another study found an identical cortisol level in animals in space and in control animals on earth (Carmeliet, Vico et al. 2001). These results suggest that the bone loss observed in astronauts is not due to stress. Nevertheless, we could not exclude that the zebrafish larvae would experience stress when placed into the microgravity simulation devices. No increase in cortisol levels was observed in larvae after undergoing 1 day simulation on CLINO or RPM, one causing decreased bone formation and the other one not. Thus, these results strongly argue against the possibility that the decreased bone formation in CLINO may be due to stress.

Finally, we chose to analyze the changes in gene expression caused by the different microgravity simulation approaches after only one day of treatment, as we were mainly interested in early regulatory events rather than in secondary events such as clearly decreased bone formation. In general, the number of affected genes was low, and interestingly only one gene was common to all three experiments. This common gene actually represents two zebrafish homologs of the human *RHCG* Rh Type C glycoprotein gene, coding for an ammonium transporter protein. Whose up-regulation was correlated with increased ammonium secretion in zebrafish larvae (Nakada, Hoshijima et al. 2007). Previously, expression of *rhcga* in zebrafish was shown mainly in mitochondrion-rich cells of the yolk sac and gills during larval stages, and in adult gills and kidney (Nakada, Hoshijima et al. 2007). Larval expression increased in correlation with increased ammonia excretion during development, which probably reflects the increased ammonia detoxification required from the amino acid metabolism due to consumption of the yolk (Bucking, Lemoine et al. 2013). It is unclear whether *rhcg2a* may play a similar role, however it is interesting to note that exposure to CLINO induced *rhcg2a* and reduced *rhcga* expression, RPM exposure induced *rhcga* expression while in the RWV experiment, both genes were up-regulated (Table 9). This observation suggests that increased ammonium production may be caused by the rotating/moving environment during microgravity simulation, which seems to be highest in RWV conditions. The lack of other genes commonly affected by the three microgravity simulation approaches is further substantiated when analyzing affected diseases and biological functions, affected pathways, and, most dramatically when searching for putative upstream regulators suggested by the obtained gene lists. Indeed, clinorotation appeared to induce very different physiological processes, or the same process in opposite directions, relative to RPM or RWV (Table annex15, Fig. 25). This observation further supports the conclusion that the three different microgravity simulation devices actually cause very different adaptation

reactions. Only CLINO resulted in a clearly decreased bone formation and changes expression of genes more specifically involved in biological functions related to bone formation (Table 12, Table 14), thus it appears most plausible that clinorotation is the most appropriate device to simulate microgravity on ground.

Among the genes affected by CLINO, a small molecular network could be constructed containing the *FOSB*, *FGF2*, *E2F2*, *GAB2* and *MCL1* genes (Fig. 21). FOSB is a member of the FOS family of leucine zipper transcription factors, which can heterodimerize with JUN family members to form the AP1 complex, well known to control cell proliferation, differentiation and transformation. Decreased expression of c-Fos in microgravity was shown in osteoblastic cells (Sato, Hamazaki et al. 1999, Hughes-Fulford, Rodenacker et al. 2006), while in murine carcimona cells decreased induction of *c-Fos* and *c-Jun* was shown in microgravity (de Groot, Rijken et al. 1990, de Groot, Rijken et al. 1991). Other genes specifically affected by clinorotation are *GAB2*, a GRB2-associated binding protein involved in signal transduction through tyrosine kinase (RTK) or non-RTK receptors (Wohrle, Daly et al. 2009) and required for allergic reactions, mast cell growth in bone marrow, bone homeostasis and heart function (Wohrle, Daly et al. 2009), the *BCL-2*-related *MCL1* involved in control of cell survival (Yang-Yen 2006), and E2F2 controlling the cell cycle (Denis, Vaziri et al. 2000, Wu, Timmers et al. 2001). Finally, the sex steroid aromatase gene *CYP19A1*, converting androgens into estrogens (Simpson, Clyne et al. 2002), is up-regulated after clinorotation.

In conclusion, we show here for the first time that zebrafish larvae experiencing simulated microgravity by clinorotation, but not by RPM or RWV, in early life stages between 5-10dpf exhibit decreased bone formation in the head. This decrease in skeleton ossification was not preceded by decreased cartilage formation, and was not due to increased stress.

Chapter 3

Modulation of head skeletal development and gene expression by hypergravity.

1. Effects of hypergravity on bone and general development.

In this chapter, we intended to complement our studies in microgravity detailed in the previous chapter by applying the opposite effect, we investigated the effects due to increased gravity using the large diameter centrifuge (LDC) at the European Space Agency, ESA (Noordwijk, Netherlands). In a first experiment, zebrafish larvae were grown at normal gravity (1g) until 5dpf. One half of the population was brought to 3g hypergravity in the LDC for another 4 days, while the other half was kept at 1g (Fig. 26).

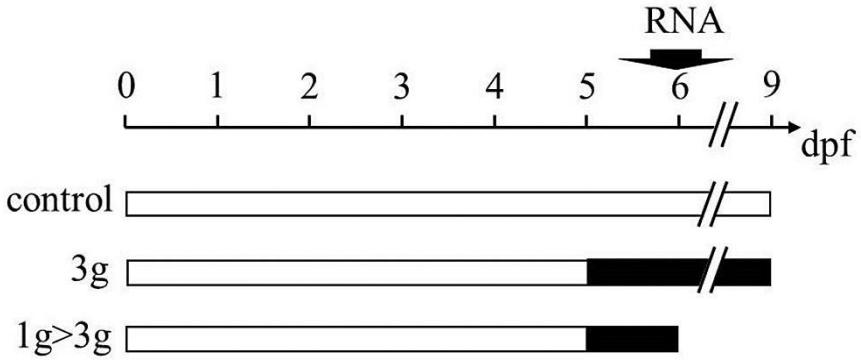

Figure 26: Schematic overview of hypergravity experiments. Larvae are placed at hypergravity at 5dpf until 9dpf (3g), while (control) larvae are kept at normal gravity for 9 days. Total mRNA was extracted at 6dpf and batches of larvae were fixed at 9dpf for Alizarin red staining of bone matrix.

At 9dpf, the larvae were stained with Alizarin red for bone matrix (Fig. 27A,B) and analyzed as described above. No difference was observed between the two samples when total length of the larvae or size of the eye or lens was determined (not shown). In the morphometric analysis, the 3g larvae present a larger head skeleton with a significant increase of the distance between the 2 anguloarticular bones, branchiostegal rays1, entopterygoid and the opercle (Fig. 27C; annex16A). In bone formation analysis (Fig. 28A, Table 13), the anguloarticular, branchiostegal ray2 and hyomandibular presented a clear over ossification, while the ceratohyal presented a significantly higher proportion of advanced ossification. In contrast, the dentary, maxilla and entopterygoid were not significantly affected (Fig. 28A). The global score obtained by addition of the scores of all the separate structures revealed a significant increase of bone formation (from a score of 23± 4 to 27± 5.5) (Fig. 28B). A clearly weaker calcification was observed in the otoliths. More than 60% of the controls show 2 pairs of dark otoliths (Fig. 27A,B and Fig. 28C) compared to only lightly stained otoliths in the 3g group.

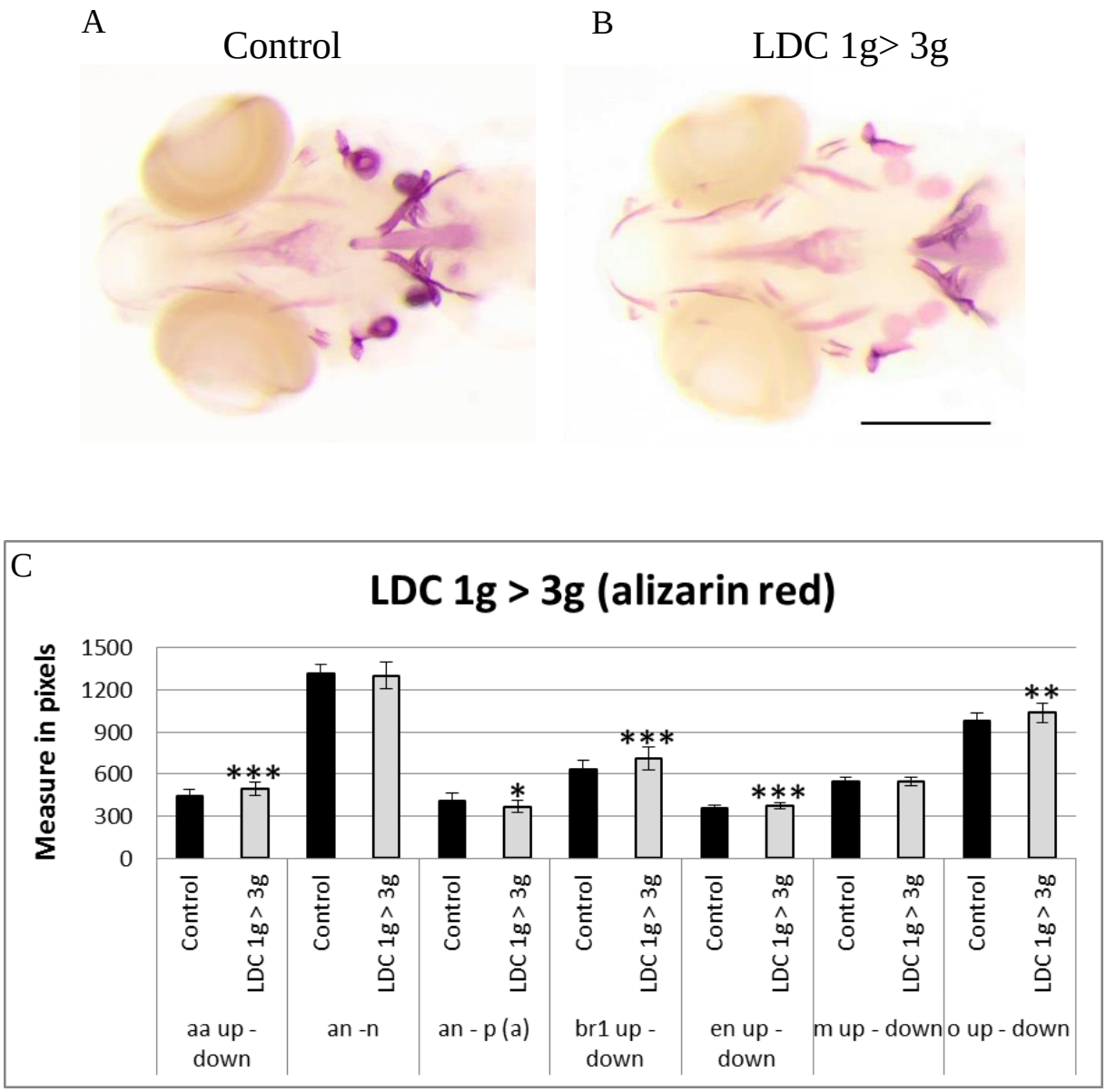

Figure 27: Effect of 3g hypergravity between 5-9dpf on bone formation (A,B). Alizarin red staining of 9dpf control larvae (A) and larvae treated for 4 days in 3g hypergravity after 5 days at 1g (B). Ventral view, anterior to the left. (C) Comparison of morphometric measurements for some selected distances within the heads of control and 3g-treated larvae. Mean ± SD and t-test analysis were calculated for each measure on at least 20 individuals. * $p < 0.05$, ** $p < 0.01$ and ***$p < 0.001$.

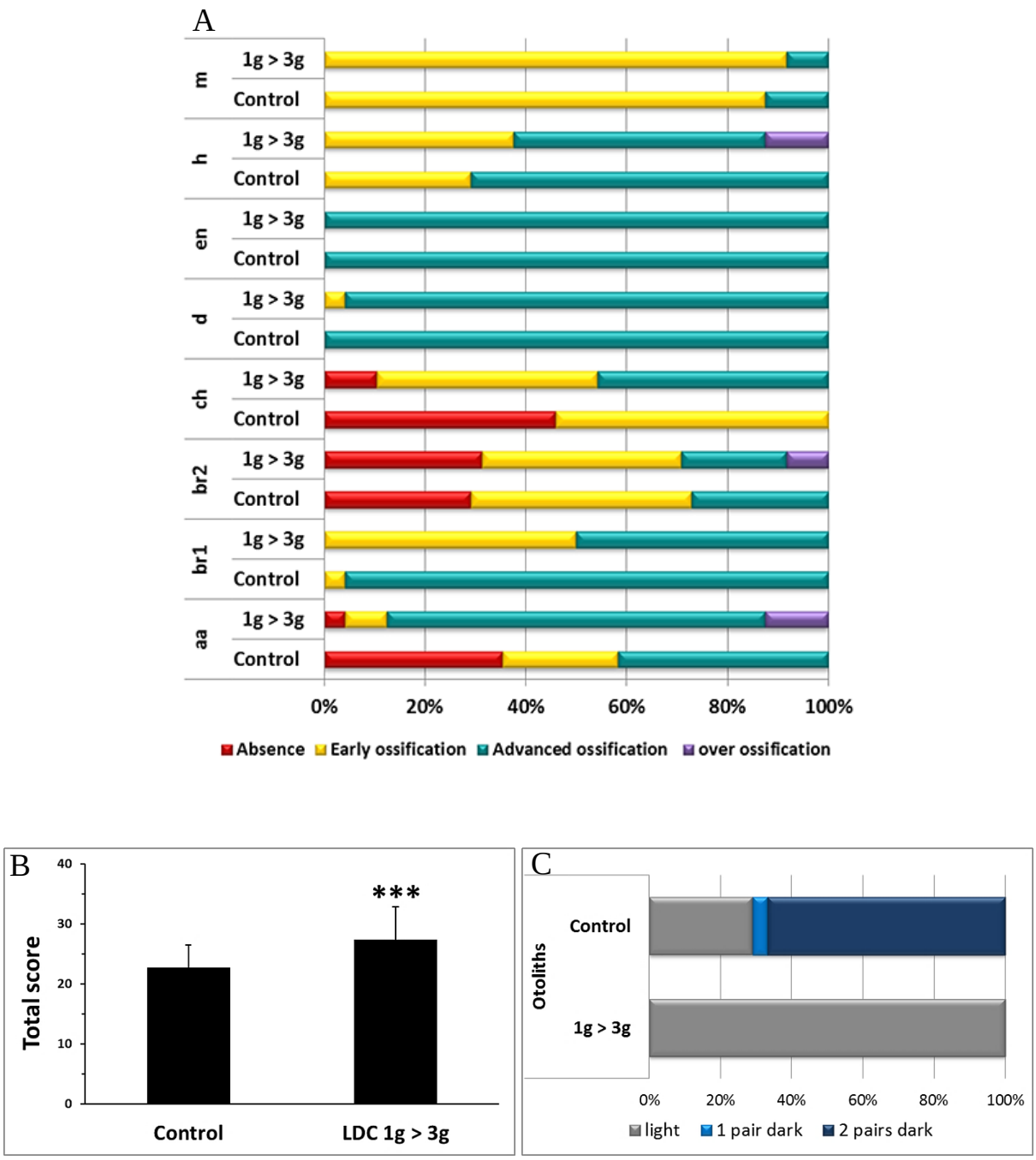

Figure 28: Changes in the extent of bone formation in hypergravity experiments. (A) Cumulated frequency after 3g between 5-9dpf. Bone development is classified for each element into different categories: Absent (no structure present; red), early ossification (beginning of the bone ossification; yellow), advanced ossification (the structure is present and already developed as the control; green) and over ossification (the structure is more developed compared to the control; purple). Cumulated frequencies in % are represented for each element. As no significant difference was observed for paired structures between left and right (up and down), their scores have been combined. Statistical analysis was performed by X^2 of Pearson and a logistic regression. (B) Global score for bone formation in control and 3g treated larvae. (C) Comparison of cumulated frequencies of, respectively light, 1 pair dark or two pairs dark otoliths in control and 3g treated larvae. For abbreviations see legend to Figure 1.

A

Structures	Treat	N	Mean	Score of ossificaiton (Y) early	Score of ossificaiton (Y) advanced	X² pearson p-value	Logistic regression OR (IC 95%)	Logistic regression p-value
branchiostegal ray1 down	Control	24	0.96	3 (12.50%)	21 (87.50%)		1	
	LDC 1g > 3g	24	1.00	0 (0%)	24 (100%)	0.074	/	0.995
branchiostegal ray1 up	Control	24	0.96	3 (12.50%)	21 (87.50%)		1	
	LDC 1g > 3g	24	1.00	0 (0%)	24 (100%)	0.074	/	0.995
dentary down	Control	24	1.00	0 (0%)	24 (100%)		1	
	LDC 1g > 3g	24	0.96	1 (4.17%)	23 (95.83%)	0.312	/	0.995
dentary up	Control	24	1.00	0 (0%)	24 (100%)		1	
	LDC 1g > 3g	24	0.96	1 (4.17%)	23 (95.83%)	0.312	/	0.995
entopterygoid down	Control	24	1.00	0 (0%)	24 (100%)		1	
	LDC 1g > 3g	24	1.00	0 (0%)	24 (100%)	/	/	/
entopterygoid up	Control	24	1.00	0 (0%)	24 (100%)		1	
	LDC 3 g	24	1.00	0 (0%)	24 (100%)	/	/	/
hyomandibular down	Control	24	0.71	7 (29.17%)	17 (70.83%)		1	
	LDC 1g > 3g	24	0.63	9 (37.50%)	15 (62.50%)	0.540	0.686 (0.205-2.295)	0.541
hyomandibular up	Control	24	0.71	7 (29.17%)	17 (70.83%)		1	
	LDC 3 g	24	0.63	9 (37.50%)	15 (62.50%)	0.540	0.686 (0.205-2.295)	0.541
maxilla down	Control	24	0.13	21 (87.50%)	3 (12.50%)		1	
	LDC 1g > 3g	24	0.08	22 (91.67%)	2 (8.33%)	0.637	0.636 (0.096-4.197)	0.639
maxilla up	Control	24	0.13	21 (87.50%)	3 (12.50%)		1	
	LDC 1g > 3g	24	0.08	22 (91.67%)	2 (8.33%)	0.637	0.636 (0.096-4.197)	0.639

B

Structures	Treat	N	Mean	Score of ossificaiton (Y) absence	Score of ossificaiton (Y) early	Score of ossificaiton (Y) advanced	X² pearson p-value	Ordinal logistic regression OR (IC 95%)	Ordinal logistic regression p-value
anguloarticular down	Control	24	1.08	8 (33.33%)	6 (25.00%)	10 (41.67%)		1	
	LDC 1g > 3g	24	1.83	1 (4.17%)	2 (8.33%)	21 (87.50%)	**0.003**	9.993 (2.360-42.315)	**0.002**
anguloarticular up	Control	24	1.04	9 (37.50%)	5 (20.83%)	10 (41.67%)		1	
	LDC 3 g	24	1.83	1 (4.17%)	2 (8.33%)	21 (87.50%)	**0.003**	10.249 (2.413-43.538)	**0.002**
branchiostegal ray2 down	Control	24	0.92	7 (29.17%)	12 (50.00%)	5 (20.83%)		1	
	LDC 1g > 3g	24	0.96	8 (33.33%)	9 (37.50%)	7 (29.17%)	0.661	1.094 (0.382-3.129)	0.867
branchiostegal ray2 up	Control	24	1.04	7 (29.17%)	9 (37.50%)	8 (33.33%)		1	
	LDC 3 g	24	1.00	7 (29.17%)	10 (41.67%)	7 (29.17%)	0.942	0.904 (0.319-2.568)	0.850
ceratohyal down	Control	24	0.54	11 (45.83%)	13 (54.17%)	0 (0.00%)		1	
	LDC 1g > 3g	24	1.33	3 (12.50%)	10 (41.67%)	11 (4583%)	**<0.001**	12.584 (3.063-51.701)	**<0.001**
ceratohyal up	Control	24	0.54	11 (45.8%)	13 (54.17%)	0 (0.00%)		1	
	LDC 1g > 3g	24	1.38	2 (8.33%)	11 (45.83%)	11 (45.83%)	**<0.001**	19.388 (3.831-98.128)	**<0.001**

Table 13: Ossification scores for individual bone elements in control and 3g-treated larvae between days 5-6dpf. The fraction (in %) of larvae presenting the indicated score for each element is given. together with the statistical evaluation of a significant difference compared to control. **(**A) The bone structures distributed in 2 categories (early and advanced ossification) (B) The bone structures distributed in 3 categories (absent, early and advanced ossification).

In addition, total mRNA was extracted from the larvae at 6dpf and whole genome gene expression was compared between larvae exposed for 1 day to 3g and 1g controls. The number of genes found to be modulated by hypergravity was 499, although the extent of induction or repression was surprisingly low (Table annex 17), but significant as confirmed by RT-qPCR for 5 selected genes (Table 31).

	Microarray		RT-PCR	
Gene	**Fold Change**	**p-value**	**Fold Change**	**p-value**
nr1d1	0.447	0.058	0.518	< 0.001
rhcg	0.68	0.046	0.779	< 0.001
socs1	0.564	0.045	0.544	< 0.001
spry4	0.674	0.064	0.739	< 0.001
txnip	1.88	0.058	2.555	< 0.001

Table 14: Comparison of fold change values from the microarray dataset with those observed by RT-qPCR for larvae placed at 3g between 5 and 6dpf (1g>3g) relative to control. The fold change and statistical significance (p-values) are given from the microarray data and the RT-qPCR confirmation experiments.

Interestingly, among the affected biological functions (Table 15), cellular and organism developmental processes ranked highest, only molecular transport appears in second position. More specifically, development and function of the skeletal and muscular system and connective tissue ranked highest, followed by the nervous and endocrine systems and finally hematological and cardiovascular systems. Among the specifically affected genes, many transporter and ion channel genes are present, reminiscent of the observations after VitD3 treatment. Interestingly, among the transcription factors, vitamin D receptor (*vdr*) is weakly, but significantly down-regulated, similar to the nuclear receptor *pparg*. Other prominent transcription factor genes are the homeo-box containing *pou3f3* and its potential partners *meis1* and *onecut1*. Construction of specific networks in three different organ systems using IPA (Fig. 29) revealed the inhibition of hubs like *MYC*, *PPARG*, vitamin D receptor (*VDR*), *NFKBIA* inhibitor in all systems, but also an extensive network specific to the cardiovascular system with. Interestingly, a down-regulation of the growth factor receptor/Ras mediator gene *GRB*2 was observed.

Category	p-value	Number of Genes
Cellular Growth and Proliferation	2.42^{E-07}-9.08^{E-03}	66
Molecular Transport	3.83^{E-07}-9.08^{E-03}	46
Cellular Development	3.53^{E-06}-9.08^{E-03}	64
Embryonic Development	1.44^{E-05}-9.08^{E-03}	36
Cell Death and Survival	2.1^{E-05}-9.08^{E-03}	66
Organ Development	2.51^{E-05}-5.47^{E-03}	29
Organismal Development	2.51^{E-05}-9.08^{E-03}	57
Skeletal and Muscular System Development and Function	2.51^{E-05}-9.08^{E-03}	25
Tissue Development	2.51^{E-05}-9.08^{E-03}	50
Connective Tissue Development and Function	3.48^{E-05}-9.08^{E-03}	22
Nervous System Development and Function	3.98^{E-05}-9.08^{E-03}	14
Endocrine System Development and Function	5.3^{E-05}-9.04^{E-03}	19
Lipid Metabolism	5.3^{E-05}-9.08^{E-03}	23
Small Molecule Biochemistry	5.3^{E-05}-9.08^{E-03}	39
Gene Expression	6.34^{E-05}-9.08^{E-03}	46
Organismal Survival	7.23^{E-05}-5.31^{E-03}	49
Cell Morphology	8.19^{E-05}-9.08^{E-03}	40
Hair and Skin Development and Function	1.16^{E-04}-9.08^{E-03}	14
Renal and Urological System Development and Function	1.97^{E-04}-1.67^{E-03}	11
Reproductive System Development and Function	1.97^{E-04}-9.08^{E-03}	12
Tissue Morphology	1.98^{E-04}-9.04^{E-03}	44
Cell Cycle	2.44^{E-04}-9.08^{E-03}	25
Cell-To-Cell Signaling and Interaction	2.67^{E-04}-9.08^{E-03}	19
Cellular Assembly and Organization	2.67^{E-04}-9.08^{E-03}	11
Cellular Movement	4.34^{E-04}-9.08^{E-03}	40
Hematological System Development and Function	4.37^{E-04}-9.08^{E-03}	34
Hematopoiesis	4.37^{E-04}-8.39^{E-03}	23
Cellular Function and Maintenance	4.86^{E-04}-9.08^{E-03}	13
Carbohydrate Metabolism	6.66^{E-04}-9.08^{E-03}	23
Organ Morphology	8.7^{E-04}-9.08^{E-03}	24
Lymphoid Tissue Structure and Development	1.06^{E-03}-8.47^{E-03}	7
Cardiovascular System Development and Function	1.14^{E-03}-9.08^{E-03}	29
Amino Acid Metabolism	1.67^{E-03}-9.08^{E-03}	8
Vitamin and Mineral Metabolism	1.83^{E-03}-9.08^{E-03}	8
DNA Replication. Recombination. and Repair	1.91^{E-03}-6.16^{E-03}	15
Digestive System Development and Function	2.26^{E-03}-9.08^{E-03}	17
Behavior	2.28^{E-03}-2.28^{E-03}	5
Hepatic System Development and Function	2.8^{E-03}-2.8^{E-03}	7
Respiratory System Development and Function	2.83^{E-03}-4.27^{E-03}	2
Nucleic Acid Metabolism	4.27^{E-03}-9.08^{E-03}	2
Protein Synthesis	4.27^{E-03}-9.04^{E-03}	25
Humoral Immune Response	6.71^{E-03}-6.71^{E-03}	7
Post-Translational Modification	6.94^{E-03}-6.94^{E-03}	2
Immune Cell Trafficking	7.97^{E-03}-9.08^{E-03}	13
Free Radical Scavenging	8.78^{E-03}-8.78^{E-03}	12
Cell-mediated Immune Response	9.08^{E-03}-9.08^{E-03}	1
Cellular Compromise	9.08^{E-03}-9.08^{E-03}	1
Cellular Response to Therapeutics	9.08^{E-03}-9.08^{E-03}	1
Drug Metabolism	9.08^{E-03}-9.08^{E-03}	4

Table 15: Biological functions associated to genes affected by hypergravity between 5-6dpf (1g>3g). Ingenuity Pathway Analysis of the list of genes affected at 6dpf after 3g hypergravity

treatment for 24 hours (1g>3g). Columns indicate respectively the category of function, the range of p-values (significance) associated to various sub-functions, and the number of genes concerned.

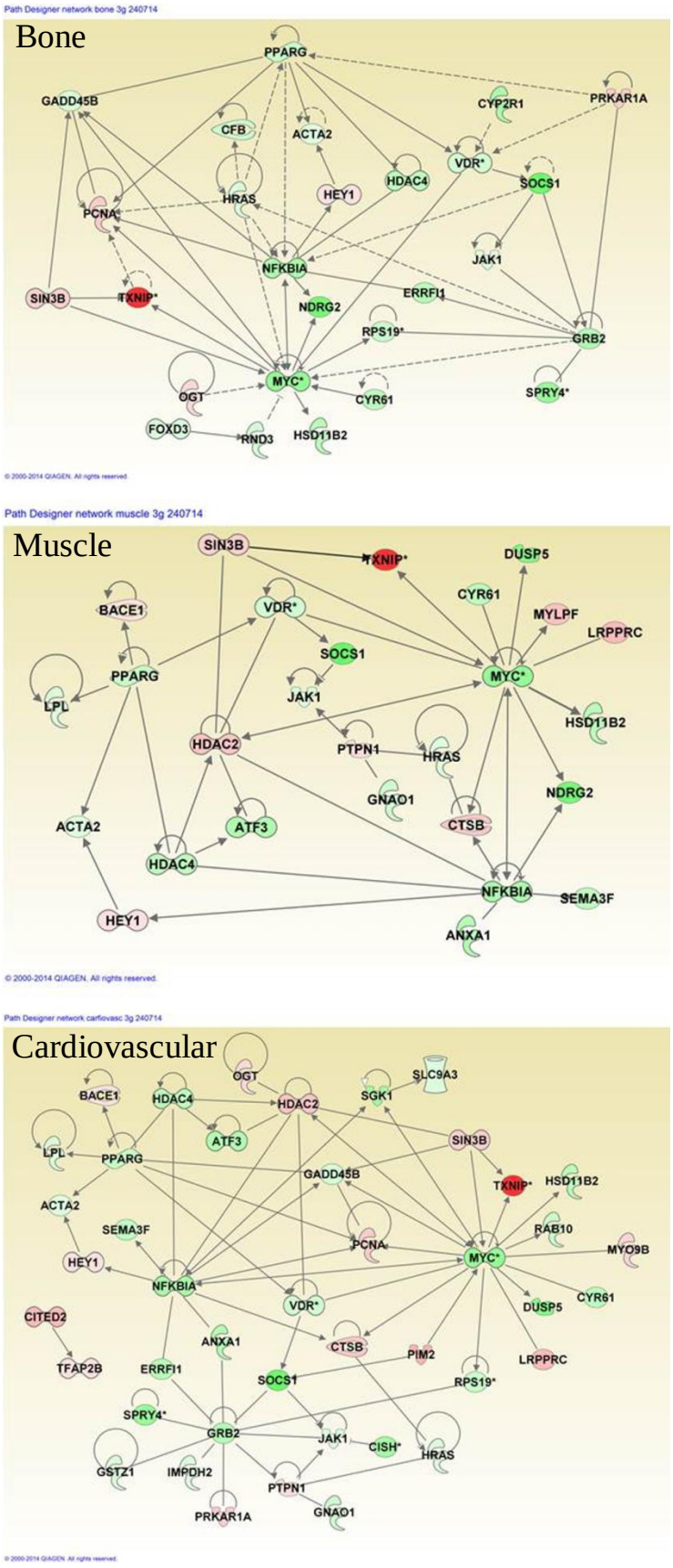

Figure 29: Regulatory networks related to different tissues after 3g hypergravity between 5-6dpf. Genes filtered according to the described function for their human homologs using IPA in bone, muscle, or cardiovascular system function. Genes up-regulated (red), down-regulated (green), (*) indicates that the gene is represented by two or more probes on the microarray.

2. Effects of "relative microgravity" on bone and general development.

As an approach to investigate some of the effects on zebrafish physiology to be expected when going into real microgravity, we applied a protocol that we would qualify as "Reduced Gravity Paradigm" or "relative microgravity". The principle is to grow the zebrafish larvae for a defined period (5 days) in a hypergravity environment (in this case 3g), before returning them to normal gravity for one additional day (Fig. 30). The effect of this decrease in gravity on bone formation and gene expression was then investigated.

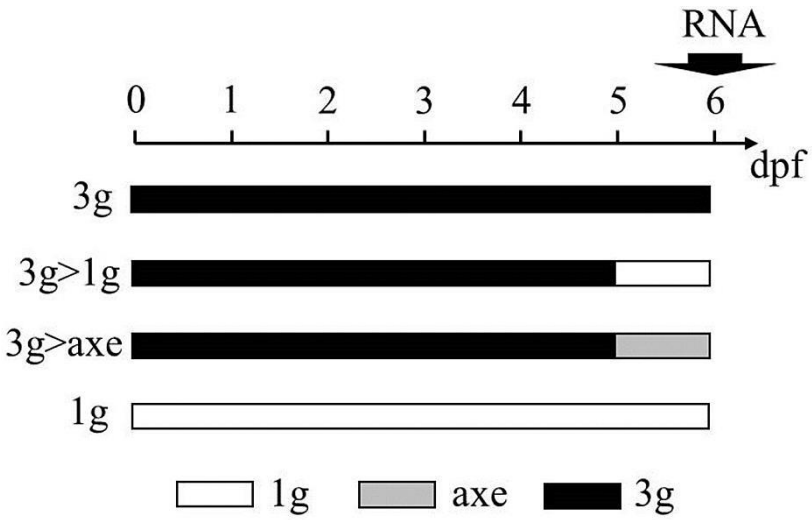

Figure 30: Schematic overview of the relative microgravity experiment. Experiment in which the control larvae were placed at 3g and kept at 3g until 6dpf (3g), or returned at 5dpf to 1g outside (3g>1g) or on the axis of the centrifuge (3g>axe) for one day. An additional batch of larvae was kept at normal gravity until 6dpf (1g). RNA extraction and Alizarin red staining are performed at 6dpf.

Zebrafish fertilized eggs were subjected at 4hpf to 3g hypergravity until 5dpf. For comparison, a parallel batch was grown at normal gravity outside of the centrifuge chamber (1g). The morphology of the embryos and larvae was monitored every day by microscopic observation, no striking effect was observed on developmental processes such as segmentation, organogenesis or hatching time. Only a clearly decreased (delayed) pigmentation was observed at 24hpf (Fig. 31A.B), which was rapidly resolved as pigmentation was indistinguishable in 1g and 3g embryos at 2dpf.

At 5dpf, the larvae exposed for 5 days to 3g in the LDC. were separated in three distinct batches, one was left in the LDC for another day (3g) while the other two were returned to normal gravity for one day. One batch was kept in a separate incubator outside of the centrifuge chamber (3g>1g); the other was placed in an incubator positioned on the axis of the LDC (3g>axe), in order to maintain a rotation movement without increasing the gravitational

force. The 1g batch continued to grow at normal gravity outside of the centrifuge chamber for the entire 6 days.

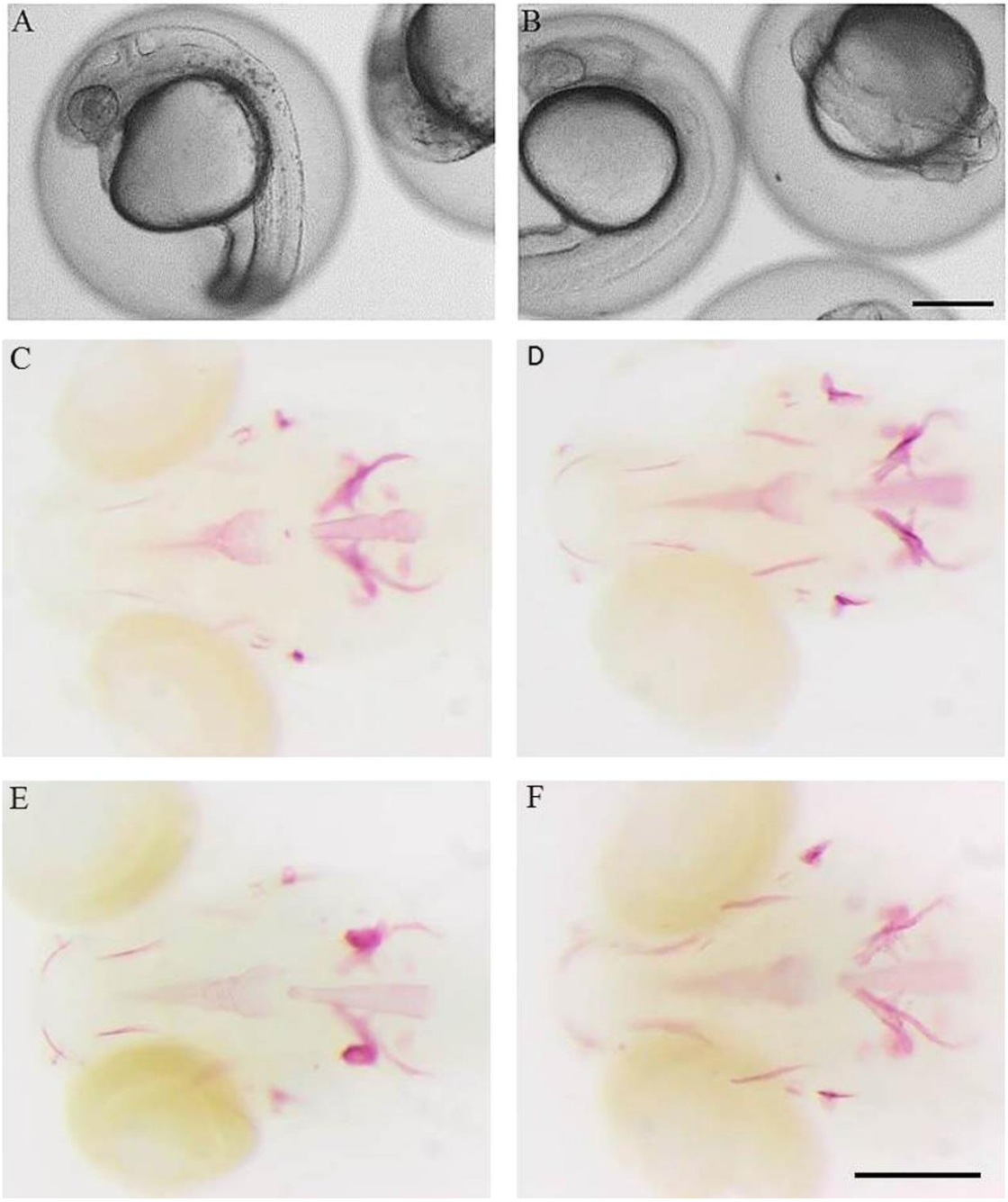

Figure 31: Effect of "relative microgravity" between 5-6dpf on bone formation. (A, B) comparison of pigmentation at 24hpf in 1g (A) and 3g (B) larvae. (C-F) Alizarin red staining of larvae kept at 1g until 6dpf (1g, C). control larvae kept at 3g until 6dpf (3g, D). larvae kept at 3g until 5dpf and returned to 1g off the centrifuge (3g>1g, E) or on the axis (3g>axe, F). Ventral view, anterior to the left.

At 6dpf, all larvae were collected and stained for calcified structures using Alizarin red. Compared to larvae grown for 6 days at 1g, the bone structures in the head of all 3g exposed larvae appeared more intense (Fig. 31C-F). Morphological analysis revealed a significant

increase in the distance between branchiostegal rays 1, entopterygoid and opercle, and an increase in the parasphenoid area (Fig. 32A.B; annex16B). The global score obtained was significantly increased in all samples exposed to 3g for 5 or 6 days (Fig. 32C) and corroborate the intensity increase observed in the Fig. 31C-F.

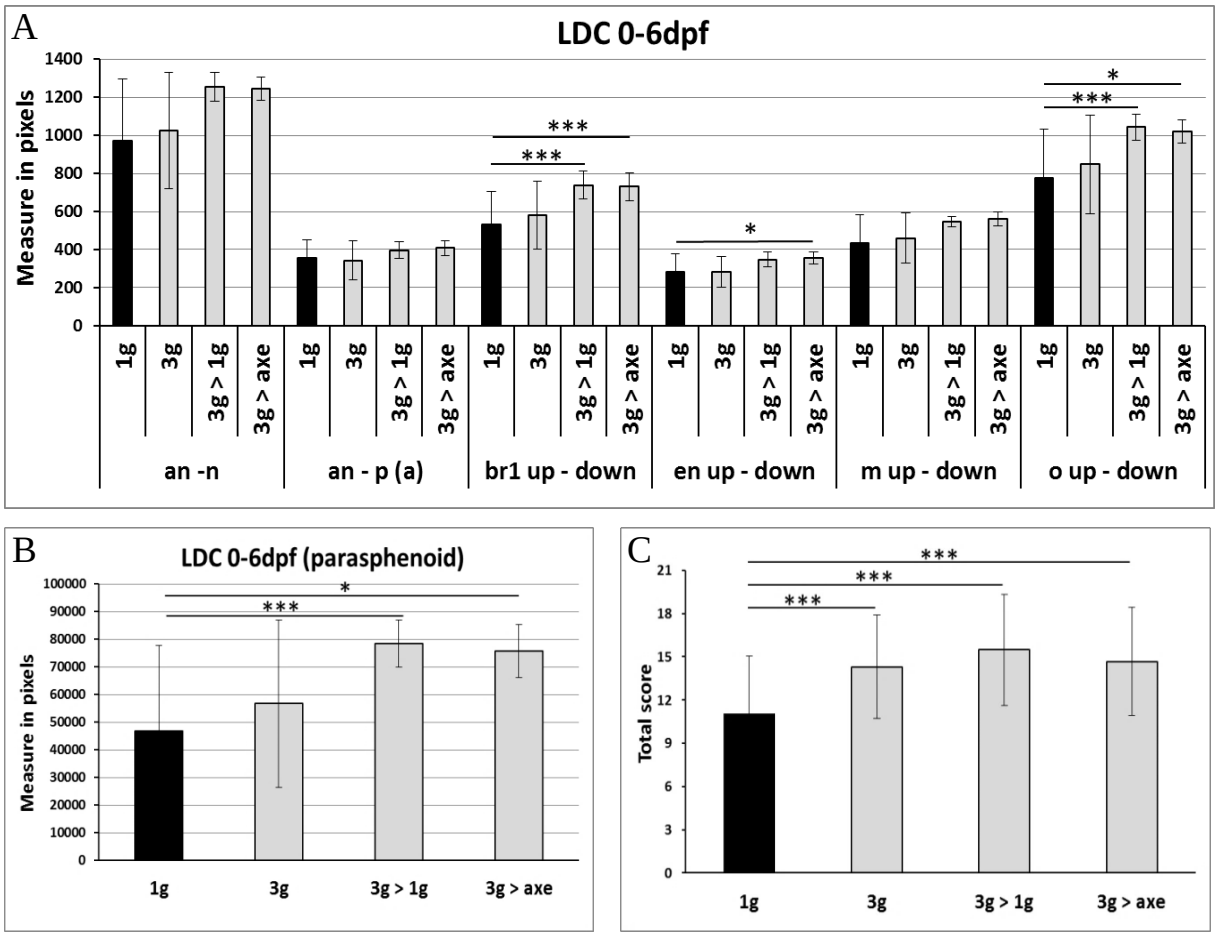

Figure 32: Morphometric analysis of bone elements at 6dpf after "relative microgravity". The distances are measured in pixels. Mean ± SD and t-test analysis were calculated for each measure on at least 20 individuals. **(**A) Distances between the different cranial bone elements. (B) Area of the parasphenoid bone. * $p < 0.05$ and *** $p < 0.001$. For abbreviations see legend to Figure in attachement. (C) Bone formation progression analysis of bone elements at 6dpf after "relative microgravity". Global scores for bone formation in control and the different treated larvae.

The complete statistical analysis supports these results specifically in the anguloarticular, maxillary and, to a lesser extent the ceratohyal, hyomandibular and branchiostegal ray 1 structures (Table 16).

A

Structures	Treat	N	Mean	Score of ossification (Y) early	Score of ossification (Y) advanced	X² Pearson p-value	Logistic regression OR (IC 95%)	Logistic regression p-value	Logistic regression global p-value
branchiostegal ray1 down	3g	33	0.97	1 (3.03%)	32 96.97%)	**<0.001**	2.783 (0.238-32.556)	0.415	**0.039**
	3g > 1g	25	0.68	8 (32.00%)	17 (68%)		0.185 (0.035-0.983)	0.048	
	3g > axe	25	1.00	0 (0%)	25 (100%)		/	0.995	
	1g	25	0.92	2 (8.00%)	23 (92%)		1.00		
branchiostegal ray1 up	3g	33	0.97	1 (3.03%)	32 (97%)	**0.009**	2.783 (0.238-32.556)	0.415	0.147
	3g > 1g	25	0.76	6 (24.00%)	19 (76%)		0.275 (0.050-1.525)	0.140	
	3g > axe	25	1.00	0 (0%)	25 (100%)		/	0.995	
	1g	25	0.92	2 (8.00%)	23 (92%)		1.00		
dentary down	3g	33	0.73	9 (27.27%)	24 (72.7%)	**0.001**	2.461 (0.822-7.370)	0.842	0.190
	3g > 1g	25	1.00	0 (0%)	25 (100%)		/	0.107	
	3g > axe	25	0.80	5 (20%)	20 (80%)		3.692 (1.052-12.957)	0.995	
	1g	25	0.52	12 (48%)	13 (52%)		1.00		
dentary up	3g	33	0.73	9 (27.27%)	24 (72.7%)	**0.001**	2.461 (0.822-7.370)	0.842	0.190
	3g > 1g	25	1.00	0 (0%)	25 (100%)		/	0.107	
	3g > axe	25	0.80	5 (20%)	20 (80%)		3.692 (1.052-12.957)	0.995	
	1g	25	0.52	12 (48%)	13 (52%)		1.00		
entopterygoid down	3g	33	0.88	4 (12.12%)	29 (88%)	0.075	3.412 (0.892-13.046)	0.079	0.098
	3g > 1g	25	0.72	7 (28.00%)	18 (72%)		1.210 (0.360-4.065)	0.073	
	3g > axe	25	0.92	2 (8.00%)	23 (92%)		5.412 (1.017-28.791)	0.758	
	1g	25	0.76	8 (32.00%)	17 (68%)		1.00		
entopterygoid up	3g	33	0.88	4 (12.12%)	29 (88%)	0.226	2.819 (0.0722-11.01)	0.136	0.246
	3g > 1g	25	0.72	7 (28.00%)	18 (72%)		1.000 (0.291-3.437)	1.000	
	3g > axe	25	0.88	3 (12.00%)	22 (88%)		2.852 (0.643-12.642)	0.168	
	1g	25	0.80	7 (28.00%)	18 (72%)		1.00		

B

Structures	Treat	N	Mean	Score of ossification (Y) absence	Score of ossification (Y) early	Score of ossification (Y) advanced	X² pearson p-value	Ordinal logistic regression OR (IC 95%)	Ordinal logistic regression p-value	Ordinal logistic regression global p-value
anguloarticular down	3g	33	1.12	11 (33.33%)	7 (21.21%)	15 (45.45%)	**0.005**	0.50 (0.19-1.35)	0.171	**0.045**
	3g > 1g	25	1.24	8 (32%)	3 (12%)	14 (56%)		0.38 (0.13-1.09)	0.072	
	3g > axe	25	1.44	7(28%)	0 (0%)	18 (72%)		0.21 (0.07-0.63)	0.006	
	1g	25	0.76	11 (44%)	9 (36%)	5 (20%)		1.00		
anguloarticular up	3g	33	1.09	12 (36.36%)	6 (18.18%)	15 (45.45%)	**0.008**	0.49 (0.18-1.33)	0.164	**0.035**
	3g > 1g	25	1.24	8 (32%)	3 (12%)	14 (56%)		0.35 (0.12-1.03)	0.057	
	3g > axe	25	1.44	7 (28%)	0 (0%)	18 (72%)		0.19 (0.06-0.60)	0.004	
	1g	25	0.72	12 (48%)	8 (32%)	5 (20%)		1.00		
branchiostegal ray2 down	3g	33	0.21	26 (78.79%)	7 (21.21%)	0 (0%)	0.169	0.93 (0.26-3.38)	0.912	0.405
	3g > 1g	25	0.08	24 (96%)	0 (0%)	1 (4%)		5.68 (0.63-51.07)	0.121	
	3g > axe	25	0.2	20(80%)	5 (20%)	0 (0%)		1.00 (0.25-4.01)	1.000	
	1g	25	0.2	20(80%)	5 (20%)	0 (0%)		1.00		
branchiostegal ray2 up	3g	33	0.24	26 (76.47%)	8 (23.53%)	0 (0%)	0.247	0.99 (0.29-3.34)	0.983	0.432
	3g > 1g	25	0.12	23 (92%)	1(4%)	1(4%)		3.43 (0.63-18.64)	0.153	
	3g > axe	25	0.16	21 (84%)	4 (16%)	0 (0%)		1.65 (0.40-6.76)	0.489	
	1g	25	0.24	19 (76%)	6 (24%)	0 (0%)		1.00		
ceratohyal down	3g	33	0.57	20 (60.61%)	7 (21.21%)	6 (18.18%)	**0.003**	0.74 (0.25-2.18)	0.587	0.078
	3g > 1g	25	1	12 (48%)	1 (4%)	12 (48%)		0.30 (0.10-0.91)	0.033	
	3g > axe	25	0.48	18 (72%)	2 (8%)	5 (20%)		1.08 (0.33-3.55)	0.894	
	1g	25	0.57	16 (64%)	8 (32%)	1 (4%)		1.00		
ceratohyal up	3g	33	0.67	18 (54.54%)	8 (24.24%)	7 (21.21%)	**0.011**	0.52 (0.18-1.53)	0.236	0.082
	3g > 1g	25	1.04	11 (44%)	2 (8%)	12 (48%)		0.24 (0.08-074)	0.013	
	3g > axe	25	0.64	16 (64%)	2 (8%)	7 (28%)		0.62 (019-1.97)	0.416	
	1g	25	0.36	17 (68%)	7 (28%)	1(4%)		1.00		
hyomandibular down	3g	33	1.88	0 (0%)	4 (12.12%)	29 (87.88%)	0.080	0.21 (0.06-0.78)	0.020	0.083
	3g > 1g	25	1.52	4 (16%)	4 (16%)	17 (68%)		0.83 (0.27-2.57)	0.751	
	3g > axe	25	1.52	2 (8%)	8 (32%)	15 (60%)		1.00 (0.33-3.03)	1.000	
	1g	25	1.52	2 (8%)	8 (32%)	15 (60%)		1.00		
hyomandibular up	3g	33	1.91	0 (0%)	3 (9.09%)	30 (90.91%)	0.174	0.18 (0.04-0.76)	0.020	0.140
	3g > 1g	25	1.64	3 (12%)	3 (12%)	19 (76%)		0.63 (0.19-2.09)	0.448	
	3g > axe	25	1.72	1(4%)	5 (20%)	19 (76%)		0.56 (0.17-1.91)	0.358	
	1g	25	1.56	2 (8%)	7 (28%)	16 (64%)		1.00		
maxilla down	3g	33	1.64	3 (9.09%)	6 (18.18%)	24 (72.73%)	**0.005**	0.24 (0.08-0.69)	0.008	**0.001**
	3g > 1g	25	1.76	2 (8%)	2 (8%)	21 (84%)		0.13 (0.03-0.46)	0.002	
	3g > axe	25	1.8	1 (4%)	3 (12%)	21 (84%)		0.12 (0.03-0.44)	0.001	
	1g	25	1.12	6 (24%)	10 (40%)	9 (36%)		1.00		
maxilla up	3g	33	1.57	5 (15.15%)	4 (12.12%)	24 (72.73%)	**0.001**	0.29 (0.10-0.82)	0.019	**0.003**
	3g > 1g	25	1.84	2 (8%)	0 (0%)	23 (92%)		0.07 (0.01-0.33)	0.001	
	3g > axe	25	1.68	2 (8%)	4 (16%)	19 (76%)		0.22 (0.07-0.72)	0.012	
	1g	25	1.12	6 (24%)	10 (40%)	9 (36%)		1.00		

Table 16: Ossification scores for individual bone elements in larvae placed at 1g or 3g for 6 days or returned to 1g the last day. The fraction (in %) of larvae presenting the indicated score for each element is given. together with the statistical evaluation of a significant difference compared to control. (A) The bone structures distributed in 2 categories (early and advanced ossification). (B) The bone structures distributed in 3 categories (absent, early and advanced ossification)

2.1. A central gene network is rapidly activated in reduced gravity.

At 6dpf, all larvae were collected and used for mRNA extraction. Gene expression was determined by micro-array analysis, larvae exposed to 3g for the entire 6 days were chosen as control. The tables annex 18 to 20 are the lists of all affected genes in larvae left at respectively 1g, 3g>axe and 3g>1g relative to those left at 3g for 6 days. The tables indicate the human homolog of the gene, its "Entrez" gene name, the log ratio of 1g, 3g>axe, or 3g>1g larvae compared to larvae kept at 3g between 0 and 6dpf, the presence of duplicate probes on the microarray (D) and the type of protein it encodes. Genes are arranged according to their type and in alphabetical order.

Relative to this hypergravity sample, a remarkable similarity was observed in the biological functions affected in the normal gravity larvae (Table annex 21). Among the top ten functions modulated in each condition we found, on the one hand cell growth and proliferation, development, death and survival, organization and function, on the other hand embryonic and organismal (organ) development with a focus on connective tissue and cardiovascular development in the 6 days control at 1g. Only 3g>axe larvae presented 7 affected genes related to "auditory and vestibular system", possibly related to their stay on a purely rotating position.

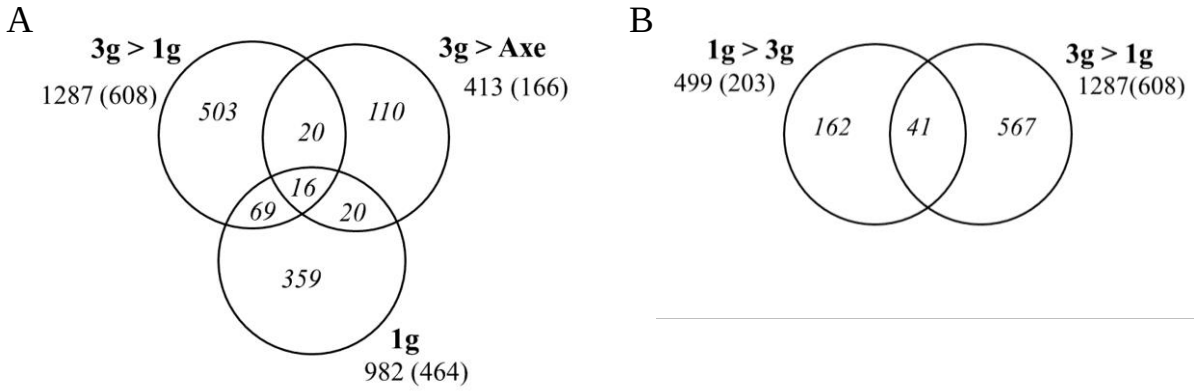

Figure 33: Number of genes affected in the various hypergravity experiments. The absolute number of probes resulting in a statistically significant hybridization signal is given for each condition. In parentheses, the corresponding number of genes with an annotation in IPA is given, while the Venn diagrams represent the number of genes unique to each condition and genes common

to two or three conditions. (A) The relative microgravity experiment. (B) Comparison between hypergravity (1g>3g) and the relative microgravity condition (3g>1g).

When comparing the affected genes in the three conditions, it appears that 16 genes are common to all three (Fig. 33A), while 20 genes are common only to the 1g samples between days 5 and 6 (3g>1g and 3g>axe). Respectively, 69 and 20 genes are common between the static 1g for 1 day (3g>1g) or rotating 1g (3g>axe) for 1 day and the larvae having spent all 6 days at 1g (1g). Several genes, mostly common to all three conditions, were selected and the modulation of their expression was confirmed by RT-qPCR (Table 17).

	1g (Inc)				**3g>axe**				**3g>1g**			
	microarray		**RT-PCR**		**microarray**		**RT-PCR**		**microarray**		**RT-PCR**	
Gene	**FC**	**p-value**	**FC**	**p-value**	**FC**	**p-value**	**FC**	**p-value**	**FC**	**p-value**	**FC**	**p-value**
btg2	0.232	0.029	0.206	< 0.001	0.353	0.048	0.335	< 0.001	0.220	0.014	0.134	< 0.001
cebpb	0.386	0.022	0.323	< 0.001	0.395	0.033	0.326	< 0.001	0.462	0.030	0.351	< 0.001
fos	0.173	0.029	0.056	< 0.001	0.247	0.098	0.202	< 0.001	0.134	0.023	0.050	< 0.001
fos b	0.229	0.009	0.494	< 0.001	0.253	0.088	0.879	< 0.001	0.237	0.036	0.311	< 0.001
klf2a	0.616	0.087	0.476	< 0.001			0.820	< 0.001	0.533	0.010	0.419	< 0.001
socs3a	0.177	0.029	0.177	< 0.001	0.244	0.085	0.289	< 0.001	0.146	0.004	0.132	< 0.001

Table 17: Comparison of fold change (FC) values from the microarray dataset with those observed by RT-qPCR in the "relative microgravity" experiments. The fold change and statistical significance (p-values) are given from the microarray data and the RT-qPCR confirmation experiments. In the 3g>axe experiment, the human KLF2 gene in table S12 is actually the *klf2b* zebrafish ortholog, in contrast to the *klf2a* ortholog shown here.

Regulatory networks were constructed using the genes common to all three conditions, but also using those common to the 1g for one day condition (3g>1g and 3g>1axe) (Fig. 34). Strikingly, a network composed of 7 genes (FOS, FOSB, EGR1, EDN1, SOCS3, GADD45B, KLF2) that were affected in exactly the same manner in all three conditions could be constructed, indicating that they represent a central network that is affected by gravitational conditions. Most importantly, these central genes were affected to the same extent, relative to the 3g for 6 days control, whether the larvae were kept at 1g during the entire experiment or only for the last day, suggesting that their expression levels are specific to this gravitational condition and are rapidly (within one day) adapted to new conditions. Five additional genes (*MVP*, *HBE1*, *HES5*, *SOX10*, *LGALS3BP*) were only affected after 1 day at lower gravity (both 3g>1g and 3g>1axe), indicating that they may be actually involved in the mechanism for rapid adaptation to lower gravity.

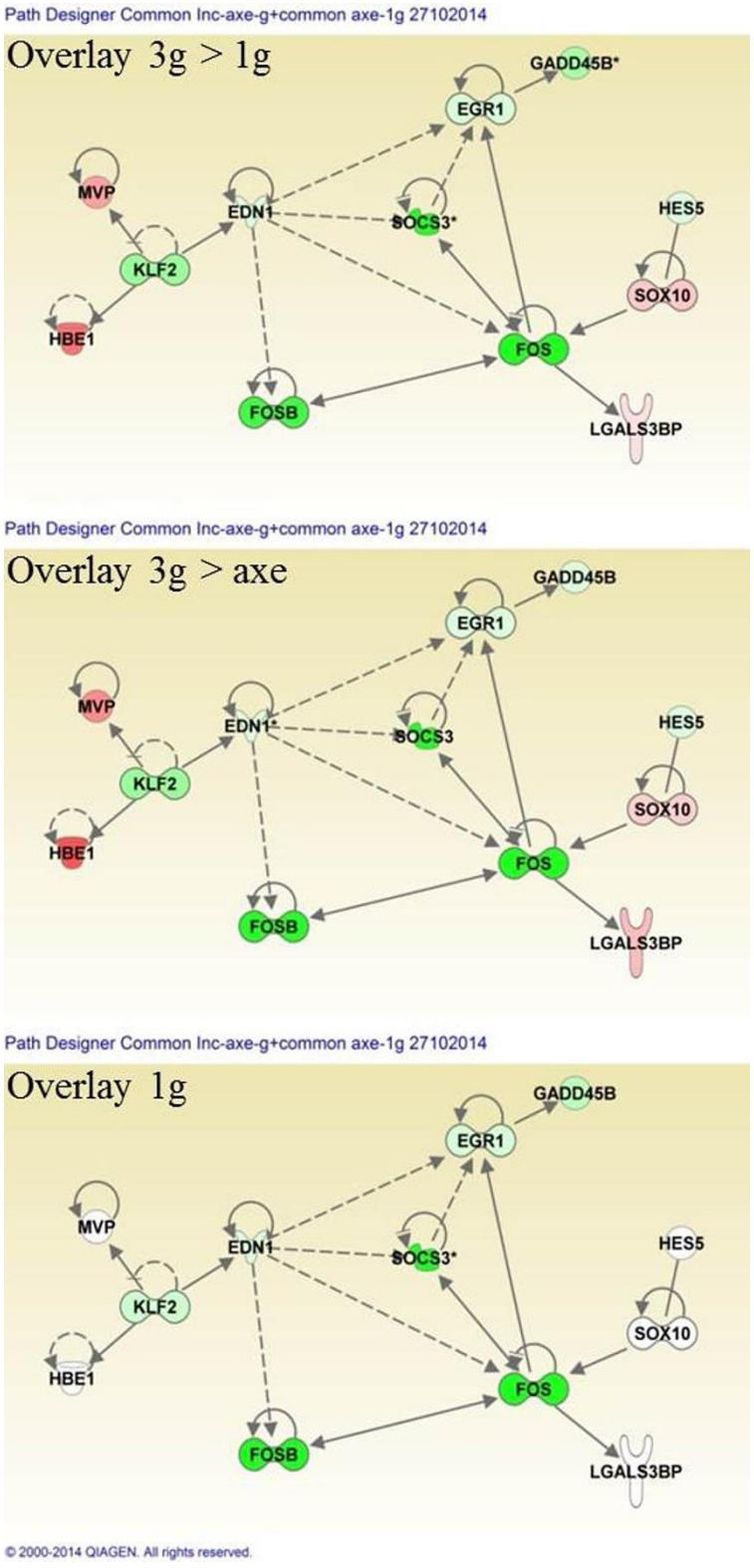

Figure 34: Network of genes affected in "relative microgravity" experiments. A network was constructed using the genes common to all three experiments, or the genes common only to 3g>1g and 3g>axe. Color overlay indicates the fold change relative to the 3g sample taken as control. Genes up-regulated (red), down-regulated (green), (*) indicates that the gene is represented by two or more probes on the microarray.

Further analyses were performed using all the genes common to any two of the conditions (Fig. 35).

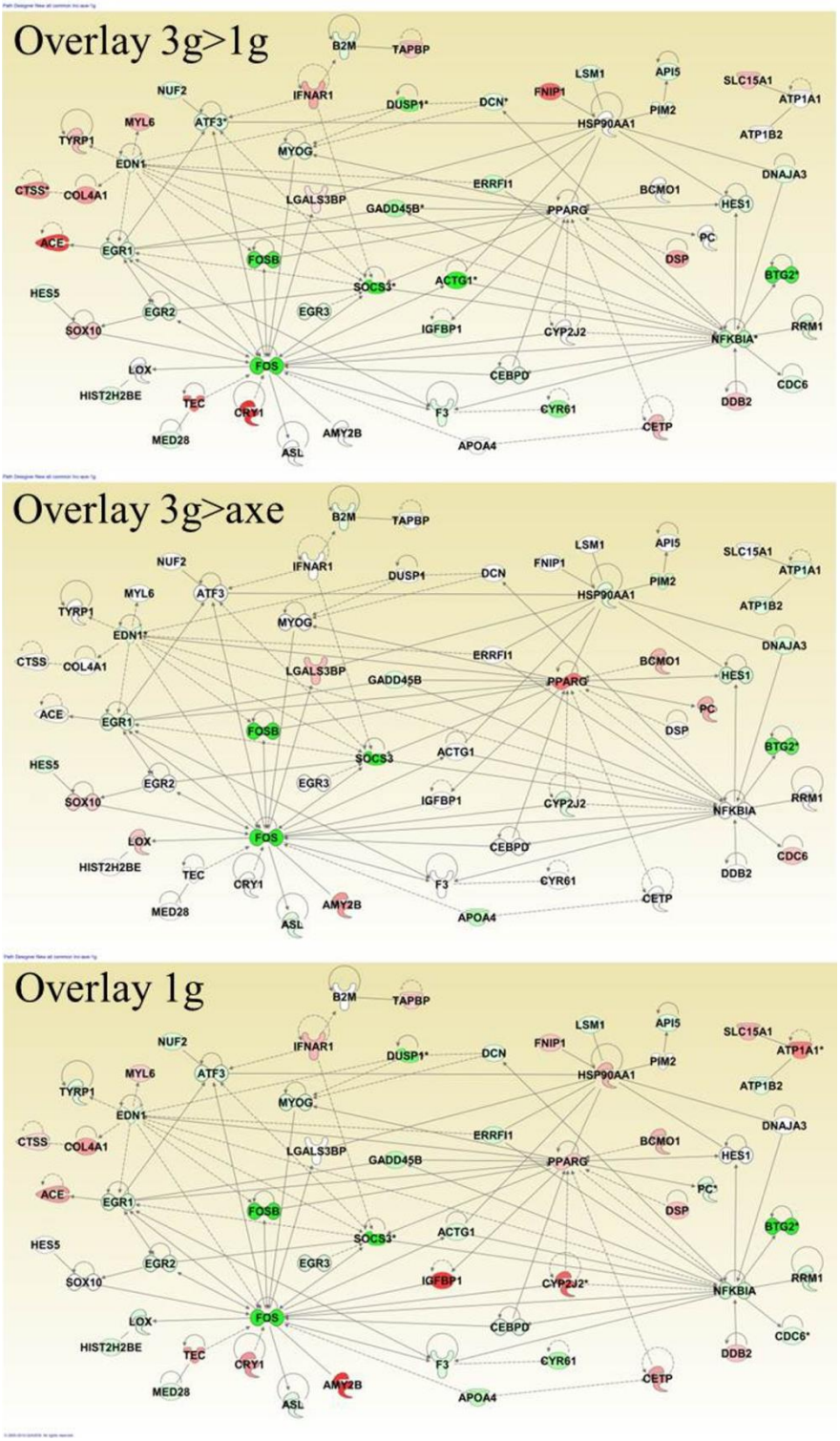

Figure 35: Network of genes affected in "relative microgravity" experiments. A network was constructed using the genes common to any two of the three experiments. The color overlay indicates the fold change in each experiment (1g, 3g>1g and 3g>axe) relative to the 3g sample taken as control. Genes up-regulated (red), down-regulated (green), (*) indicates that the gene is represented by two or more probes on the microarray.

By extending the network that way, other nodes become apparent, such as the nuclear receptor PPARG, the protein chaperone HSP90AA1 and the regulatory peptide endothelin (EDN1) (Fig. 35). Expression of *NFKBIA*, a target gene for the NFkB pathway coding for an inhibitor of this pathway. was decreased in two conditions, potentially causing the decreased expression of the antiproliferative factor BTG2 (Farioli-Vecchioli, Saraulli et al. 2009)

observed in all three conditions. Another analysis was performed according to their potential function in individual organ systems (Fig. 36).

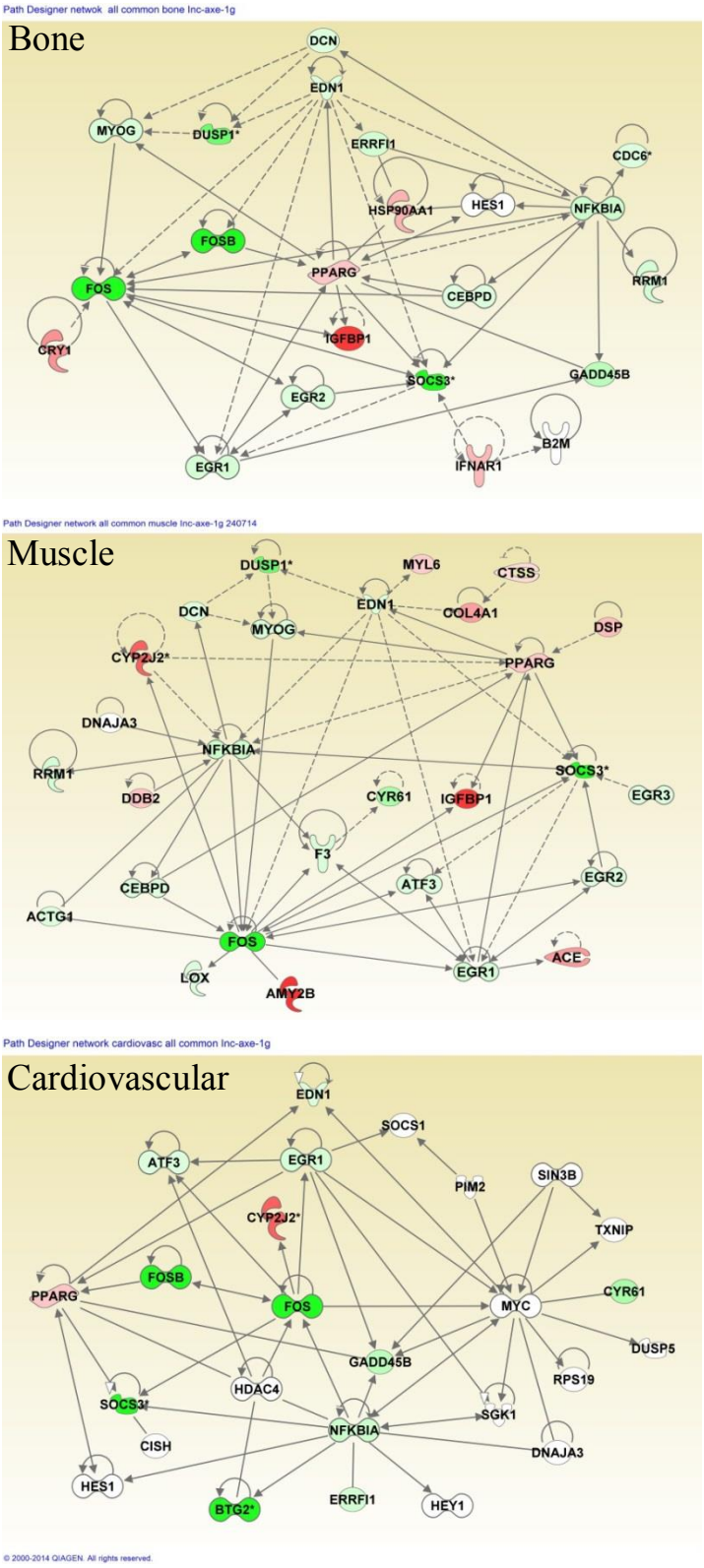

Figure 36: Tissue-specific networks of genes affected in "relative microgravity" experiments. Networks were constructed using the genes common to any two of the three experiments and filtered according to the described function for their human homologs using IPA in bone, muscle or cardiovascular system function. The color overlay indicates the fold change in the 1g experiment (1g, 3g>1g and 3g>axe) relative to the 3g sample taken as control. Genes up-regulated (red), down-regulated (green) and (*) indicates that the gene is represented by two or more probes on the microarray.

Finally we compared the genes affected in the 1g>3g experiment, which experienced a shift from 1g to 3g on day 5, with those affected in the 3g>1g experiment where the larvae were

returned to 1g after 5 days at 3g. Among the affected genes, 41 were common to both experiments (Fig. 33B) that could be assembled in a regulatory network (Fig. 37).

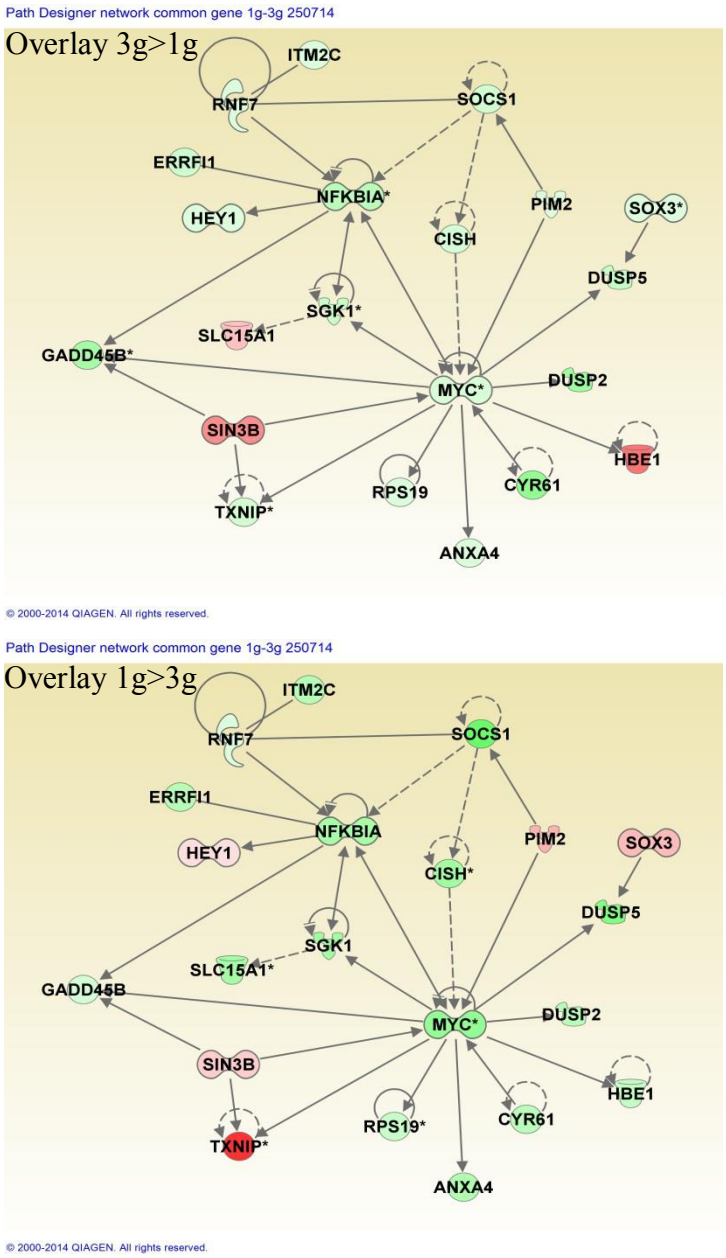

Figure 37: Network of genes affected in "relative microgravity" (3g>1g) and 3g between 5-6dpf (1g>3g) experiments. A network was constructed using the genes common to the 3g>1g from the relative microgravity experiment and 1g>3g from the hypergravity experiment. The color overlay indicates the fold change in each experiment relative to the respective control: control is 1g for the 1g>3g, and 3g for the 3g>1g experiment. Genes up-regulated (red), down-regulated (green), (*) indicates that the gene is represented by two or more probes on the microarray.

Two regulatory genes attracted our attention due to their increased expression in the 3g environment (note the fold change relative to the 1g control in the 1g>3g. and relative to the 3g sample in the 3g>1g experiment): SOX3 is a transcription factor shown to be involved in neural. pituitary and craniofacial development (Dattani 2005), while the *HEY1* gene is a target of Notch signaling and was shown to regulate bone homeostasis (Salie, Kneissel et al. 2010). Two other genes, coding for embryonic hemoglobin HBE1 and the oligopeptide transporter SLC15A1 were down-regulated at 3g.

3. Conclusions

When we applied the previously described methods of morphological analysis to larvae subjected to hypergravity, we observed a broadening of the entire head skeleton (increased distance between symmetrically paired elements), for both types of treatment: 3g between 5-9dpf (1g>3g experiment, Fig. 27A-C), and 3g between 0 and 6dpf (experiments 3g, 3g>1g and 3g>axe, Fig. 31). Similarly, the developmental scoring method allowed a more differentiated description of the observed effects. Increased ossification was significant only in the anguloarticular and ceratohyal after 3g treatment between 5-9dpf (1g>3g), but extended to the maxillary in the earlier treatments from 0-5 or 6dpf. Understanding of the molecular mechanisms underlying these differential effects on the various skeletal elements and their morphology will require further investigation. Importantly, exposing the larvae for 6 days to 3g (3g condition) or returning them to 1g for the last day (3g>1g and 3g>axe) did not significantly affect bone formation, indicating that 1 day of altered gravity is not sufficient to cause or revert morphological changes in the skeleton.

Exposure to 3g starting at 5dpf (1g>3g condition) led to increased bone calcification in the anguloarticular and ceratohyals at 9dpf (Fig. 27), while the otoliths were clearly less stained. The decrease in otolith calcification by hypergravity was already previously described (Sebastian, Esseling et al. 2001, Beier, Anken et al. 2002) and was proposed to involve a regulatory mechanism linking gravity sensing to the production of carbonic anhydrase and other matrix proteins in the inner ear (Horn 2003, Anken, Beier et al. 2004, Anken 2006). Thus, the decrease in otolith calcification after prolonged exposure to 3g was expected, but it also emphasizes the specificity of the observed increase in ossification.

During early exposure to 3g (in the "relative microgravity" experiments), we observed a transient delay in pigmentation at 24hpf, which was rapidly resorbed at 48hpf. This finding is reminiscent of the transient decrease in the number of melanocytes that was observed at 24hpf during early exposure to simulated microgravity using a Rotating Wall Vessel device (Edsall and Franz-Odendaal 2014). It is at present unclear whether a common mechanism may explain such a similar delay both in hypergravity and in simulated microgravity.

When comparing genes and pathways affected by hypergravity, cellular growth and proliferation functions ranked very high, followed by cellular, tissue and organismal development (Table 15; annex 21). Among the canonical pathways affected (Table annex 22),

we found those involving IGF, as already mentioned, and those involving pituitary hormones Prl and Gh as well as nuclear receptors. Interestingly, finer analysis of the affected biological functions revealed that all hypergravity conditions acted on organism survival and cell apoptosis (Table annex23), although no effect on larval survival or growth was observed in our experiments. Affected regulatory networks comprise PPARG, involved in adipocyte differentiation and regulating blood glucose uptake, consistent with the presence of other genes connected to insulin function. This observation may be related to previous experiments in rodents that showed a decrease in fat mass in hypergravity (Van Loon 2001, Van Loon, Tanck et al. 2005). Another gene consistently induced by hypergravity in mammals is the *Hsp70* stress response gene (Van Loon 2001, Van Loon, Tanck et al. 2005). In zebrafish kept for the first two days at 3g. increased expression of a fluorescent reporter transgene *hsp70-gfp* hypergravity was shown mainly in the lens (Shimada and Moorman 2006), however no induction of the *hsp70* gene was observed here, probably due to the later observation stages. This indicates that older fish larvae are probably less stressed by hypergravity than are mammalian systems. Note that changes in the *fli1-gfp* transgene expression were also only observed for exposures before 24hpf (Moorman, Shimada et al. 2007).

The c-FOS gene was first described as the cellular homolog of the viral oncogene causing murine osteosarcoma (van Straaten, Muller et al. 1983), while gene knock-out mice suffered from severe defects in bone development and haematopoiesis (Wang, Ovitt et al. 1992). First microgravity experiments in murine carcinoma cells revealed a decreased induction of c-Fos and its heterodimeric partner c-Jun by growth factors (de Groot, Rijken et al. 1990, de Groot, Rijken et al. 1991). Decreased c-Fos expression in microgravity was also observed in osteoblastic cells (Hughes-Fulford, Tjandrawinata et al. 1998, Sato, Hamazaki et al. 1999), while exposure to intense hypergravity (50-90g) caused an increased expression of c-Fos and Egr1 (Nose and Shibanuma 1994). More moderate hypergravity conditions (3g) also revealed rapid (36 min) induction of c-Fos expression in osteoblasts (Fitzgerald and Hughes-Fulford 1996), while both hypergravity loading and unloading caused increased expression in rat brains (Fuller, Murakami et al. 1994, Gustave Dit Duflo, Gestreau et al. 2000). This latter c-Fos induction was then considered as an indicator for neural activity in specific brain regions, in particular those related to vestibular sensing and processing (Pompeiano, d'Ascanio et al. 2002, Nakagawa, Uno et al. 2003, Kaufman 2005).

Here, we also show that exposure of zebrafish embryos to 3g hypergravity during the first 5-6 days of development leads to increased expression of *fos*, as part of a regulatory network

composed of 6 other genes (*fosb*, *egr1*, *edn1*, *socs3a*, *gadd45b*, *klf2a*) that are induced in all 3g conditions. Among these, the *fos* homolog *fosb* and the Zn-finger transcription factor gene *egr1* belong to the immediate-early class of genes that are rapidly induced by growth factors. In mouse, FosB knock-out leads to behavioral defects (Brown, Ye et al. 1996), while Egr1 null mice display sterility, impaired growth and pituitary development (Lee, Sadovsky et al. 1996, Topilko, Schneider-Maunoury et al. 1998). Egr1 was also rapidly induced in osteoblast cells upon mechanical stress (Granet, Boutahar et al. 2001). In zebrafish (Close, Toro et al. 2002), *egr1* was shown to be part of a regulatory cascade controlling cartilage development (Dalcq, Pasque et al. 2012) that is induced by Fgf signaling (Larbuisson, Dalcq et al. 2013). Edn1 is a vasoconstrictor peptide whose absence causes elevated blood pressure and craniofacial abnormalities (Kurihara, Kurihara et al. 1994) in mouse, while a zebrafish *edn1* mutant displayed mainly defects in cranial cartilage development (Piotrowski, Schilling et al. 1996, Miller, Schilling et al. 2000). Socs3 is a suppressor of cytokine signaling; in mouse it was shown to inhibit placental and fetal liver erythropoiesis (Roberts, Robb et al. 2001), while a zebrafish mutant in the paralog *socs3a* was deficient in hair cell development and regeneration in the inner ear and the lateral line neuromasts (Liang, Wang et al. 2012). Gadd45b is a factor causing growth arrest upon DNA-damage, but also involved in hematopoiesis and immune response (Lu, Ferrandino et al. 2004). Finally, loss of the *Klf2* gene in mouse causes defects in vascular, skeletal and craniofacial development and in erythropoiesis (Wani, Means et al. 1998), while a zebrafish *klf2a* mutant displayed impaired cardiac valve development due to a deficient response to blood flow (Vermot, Forouhar et al. 2009). Klf2a was further shown to be required for nitric oxyde (NO) synthesis during artery and hematopoietic stem cell development (Wang, Zhang et al. 2011), a process that is also highly involved in bone development (Henrotin, Bruckner et al. 2003, Saura, Tarin et al. 2010, Renn, Pruvot et al. 2014). Taken together, the network formed by these seven genes that are up-regulated in 3g conditions carries the potential to affect most processes that are known to be influenced by gravitational changes; from vestibular gravity sensing to hematopoiesis, immune response, vascular system and finally the skeletal system as was illustrated here. Moreover, this network is activated not only in larvae grown at 3g relative to larvae grown at 1g for 6 days, but also relative to larvae grown at 3g for 5 days and then returned to 1g for only one day (Fig. 34). Increased expression of this gene network appears to be specific for hypergravity, while expression rapidly returns to normal after 1 day at 1g.

Five genes could be connected to this regulatory network that were specifically up-regulated (*MVP*, *HBE1*, *SOX10*, *LGALS3BP*) or down-regulated (*HES5*) after return to 1g conditions for 1 day (Fig. 31). In mouse, Sox10 knock-out leads to neurological defects (Britsch, Goerich et al. 2001), while *sox10* mutant zebrafish are deficient in melanocyte pigmentation and inner ear development (Malicki, Schier et al. 1996, Whitfield, Granato et al. 1996, Dutton, Abbas et al. 2009). Similarly, Hes5 was shown to regulate neurogenesis (Cau, Gradwohl et al. 2000), but also human cartilage differentiation under the control of Notch signaling (Karlsson, Jonsson et al. 2007). Lgals3bp was shown to play a role in immune response and cell adhesion (Trahey and Weissman 1999). HBE1 codes for one of the embryonic hemoglobins, suggesting alterations in oxygen transport under different gravity conditions. MVP is a component of the ribonucleoprotein "vault" structures involved in nucleo-cytoplasmic transport and signal transduction (Zheng, Sumizawa et al. 2005). Interestingly, loss of function studies for Mvp in zebrafish revealed defects in brain development and the response to mechanical stimulus (touch) (Blaker-Lee, Gupta et al. 2012). The precise role of these genes in detection of decreased gravity and signal transmission to other physiological systems remains to be established.

Comparison of the 1g>3g and the 3g>1g experiments revealed the increased expression in hypergravity of two regulatory genes. SOX3 and HEY1, which both may play a role in bone development and/or homeostasis (Dattani 2005, Salie, Kneissel et al. 2010), while HBE1 and SLC15A1 were down-regulated at 3g. Interestingly, only HBE1 is also regulated in the 3g>axe experiment, further supporting a general effect on oxygen transport, while only GADD45B expression was affected in all 3g experiments. None of the other genes composing the common regulatory network in "relative microgravity" was affected in the 1g>3g experiment. Actually, the overall effect of 1 day exposure to 3g was surprisingly small at the genome level, compared to the other hypergravity experiments (Tables annex17-20), a result that is reminiscent of that observed previously in mammalian renal cells (Hammond, Benes et al. 2000). This observation suggests that the "Reduced Gravity Paradigm" is not simply a reversed hypergravity experiment, but rather that it represents a specific experimental condition. Future experiments will reveal whether this approach may be considered as a good approximation of microgravity.

Discussion

Zebrafish present remarkable degrees of similarity with mammals in the molecular mechanisms involved in their developmental biology and physiology. Moreover, their ease of husbandry, high fecundity, and small size paves the way for a possible future space experiment, triggering the proposal of their use for the study of gravitational biology (Goerlich, Renn et al. 2005, Aceto, Muller et al. 2008, Muller, Aceto et al. 2008, Aceto, Nourizadeh-Lilladadi et al. 2009, Muller, Dalcq et al. 2009, Muller, Dalcq et al. 2010, Horn, van Loon et al. 2011). In the case of human astronauts, bone loss is mainly observed in the weight-bearing bones (Collet, Uebelhart et al. 1997, Vico, Collet et al. 2000). The first signs of degradation are located in the tibia trabecular bone, it later continues to worsen in the trabecular bone and finally progress also in the cortical bone (Collet, Uebelhart et al. 1997). In contrast, the notion of weight-bearing bones is less clear in zebrafish, thus the effect of altered gravity on bones could be more general. In this study, we focused on the head skeleton, because bone development begins in the head of the larvae (Nüsslein-Volhard C 2001, Gavaia, Simes et al. 2006).

We decided to explore the effect of several microgravity simulation devices known in the Space research field (CLINO, RPM and RWV) and also the effect of hypergravity on zebrafish larvae. We started our investigations by setting up an approach to objectively characterize cranial skeletal development in zebrafish larvae using morphometric image analysis and applied this method to further characterize the effects of VitD3 and PTH on cartilage and bone formation. This analysis confirmed the anabolic effect of VitD3 and revealed that VitD3 treatment conserves the general skeletal morphology, but leads to a longer head and a larger jaw. Bone calcification is stronger for most elements, and some elements calcify earlier. In contrast, continuous PTH treatment leads to a general decrease of ossification. PTH treatment conserves the general cartilage morphology except for an increased length of the ceratohyal, while in bone some structures are missing and the parasphenoid is significantly decreased (Fig. 35A,B).

Furthermore, we have followed the expression of selected bone-related genes: One class of genes codes for collagens (Col1a1, Col1a2 and Col10a1a) or bone-specific ECM proteins such as Sparc, Spp1and Bglap. In mammals, Col10a1 is important for chondrocyte hypertrophy (Karsenty 2008). Unlike in mammals, *col10a1a* is expressed in both chondrocytes and osteoblasts in zebrafish (Kim, Lee et al. 2013). The *col1a1a* zebrafish mutant exhibits severe bone defects and fragility (Fisher, Jagadeeswaran et al. 2003). Sparc is important for bone mineralization and calcification by its calcium binding site (Chen, Bal et

al. 1992) and defects in Sparc lead to bone mass decrease (Bradshaw and Sage 2001). Similar to Sparc, Spp1 has high affinity for calcium and is involved in bone mineralization (Chen, Bal et al. 1992, Ritter, Farach-Carson et al. 1992). Spp1 null mice exhibit an increase in bone mineralization (Boskey, Spevak et al. 2002). Bglap is a crucial gene for bone mineralization and is expressed first in hypertrophic cartilage, then in mineralization cells (Gavaia, Simes et al. 2006, Laize, Viegas et al. 2006).

The second class of interest are factors involved in regulation of cartilage and bone differentiation, including the *pth1a* gene coding for Pth as well as transcription factor genes *sox4a*, *sox4b*, *dlx5a*, *dlx6a*, *runx2b* and *osx*. Osx is required for bone formation. *Osx* null mice exhibit only cartilage, but no bone, leading to calcified cartilage (Nakashima, Zhou et al. 2002, Karsenty 2008). Runx2 is a central gene for bone development, its deficiency leads to severe defects in both endochondral and intramembranous ossifications (Otto, Thornell et al. 1997, Kim, Otto et al. 1999). Dlx5/6 null mice present severely affected skeleton (Robledo, Rajan et al. 2002). In zebrafish, morpholino injection against *dlx5a/6a* causes defects in the cleithrum formation and a clear decrease of *runx2b* and *col10a1a* expression (Heude, Shaikho et al. 2014). The last two genes are *sox4a* and *sox4b* studied in our lab. We are still investigating a potential bone function of sox4b, because sox4 null mice show a clear decrease in bone mass and strength (Nissen-Meyer, Jemtland et al. 2007).

We followed the expression of all these genes during the 5 days of VitD3 or PTH treatment. These results reveal a significant increase upon VitD3 treatment in the expression of all the first class, structural bone genes: *sparc*, *bglap*, *spp1*, *col1a1* and, to a lesser extent *col1a2* and *col10a1a*. In the second class, the expression of the regulatory genes *pth1a* and *runx2b* is also well increased. The up-regulation of all these genes upon VitD3 treatment is in line with an increase of bone formation, due to their function during bone development. In contrast, PTH treatment did not lead to a significant decrease in expression of all these genes during the treatment, only at the end of the treatment the mRNA levels for *sparc, bglap, spp1, pth1a and runx2b* decreased significantly. Again, these observations are in line with the observed decrease in bone mineralization observed upon PTH treatment, although the inhibitory effects on the mRNA levels seem to be slower than the increase due to VitD3. This could be due to the stability of the mRNA, which delays detection of decreased expression Taken together, these observations are consistent with the observed increase or decrease in bone formation at 10dpf.

The last two genes that we studied during these treatments are *sox4a* and *sox4b*. The expression of *sox4a* is increased at 8-9dpf in VitD3, but variable in PTH with a decrease at 7-8dpf followed by an increase at 9dpf and unchanged at the end of the treatment. *sox4b* expression is more constant, with a regular increase from 7 to 10dpf in the VitD3 treatment and a progressive increase at 9 and 10dpf. The expression pattern of *sox4b* seems interesting with an expression in the pharyngeal arches, but it should be noted that both genes are expressed in other tissues, that are not related to bone formation. Thus, the changes in expression that we observed may well be related to some other function. The Sox4b topic continues to be studied in our lab by my colleague Joerg Renn, who has constructed a transgenic zebrafish line expressing a truncated, dominant-negative version of Sox4b (Sox4bΔC) under the control of a heat-shock inducible promoter. Unfortunately, no consistent bone effect was observed until now on these transgenic zebrafish after induction of expression of the dominant-negative Sox4 mutant at different stages, which might be due to insufficient expression of the mutant. These genes clearly need further studies to know their function in cartilage and bone development.

The image analysis in the different microgravity simulators revealed clearly different effects on bone formation. Only the clinostat caused a general decrease in bone formation in all the structures present at 10dpf (Fig. 38D) and the absence of several structures compared to the controls. The evaluation of each structure ossification revealed that clinorotation for 5 days caused a significant decrease in ossification of individual bone elements, and on the global score. In contrast to the clinostat, the RPM caused an increase of ossification in two different structures, the dentary (d) and the branchiostegal ray2 (br2) (Fig. 38E) and lead to a significant decrease in the width of the head (decreased distance between aa, en, br1, o). The only similarity between CLINO and RPM is the decrease of the parasphenoid area, although this decrease is stronger in CLINO and probably explains the increased distance between the anterior (an) part of the larvae and the summit a of the parasphenoid that is not seen in the RPM. In striking contrast, the RWV experiment yielded totally different results compared to CLINO and RPM. The only effect observed in the morphometric analysis is a slight decrease of the distance between the branchiostegal rays1 (br1), while the evaluation of bone formation per structure indicates a higher bone formation in the maxilla (m) (Fig. 38F).

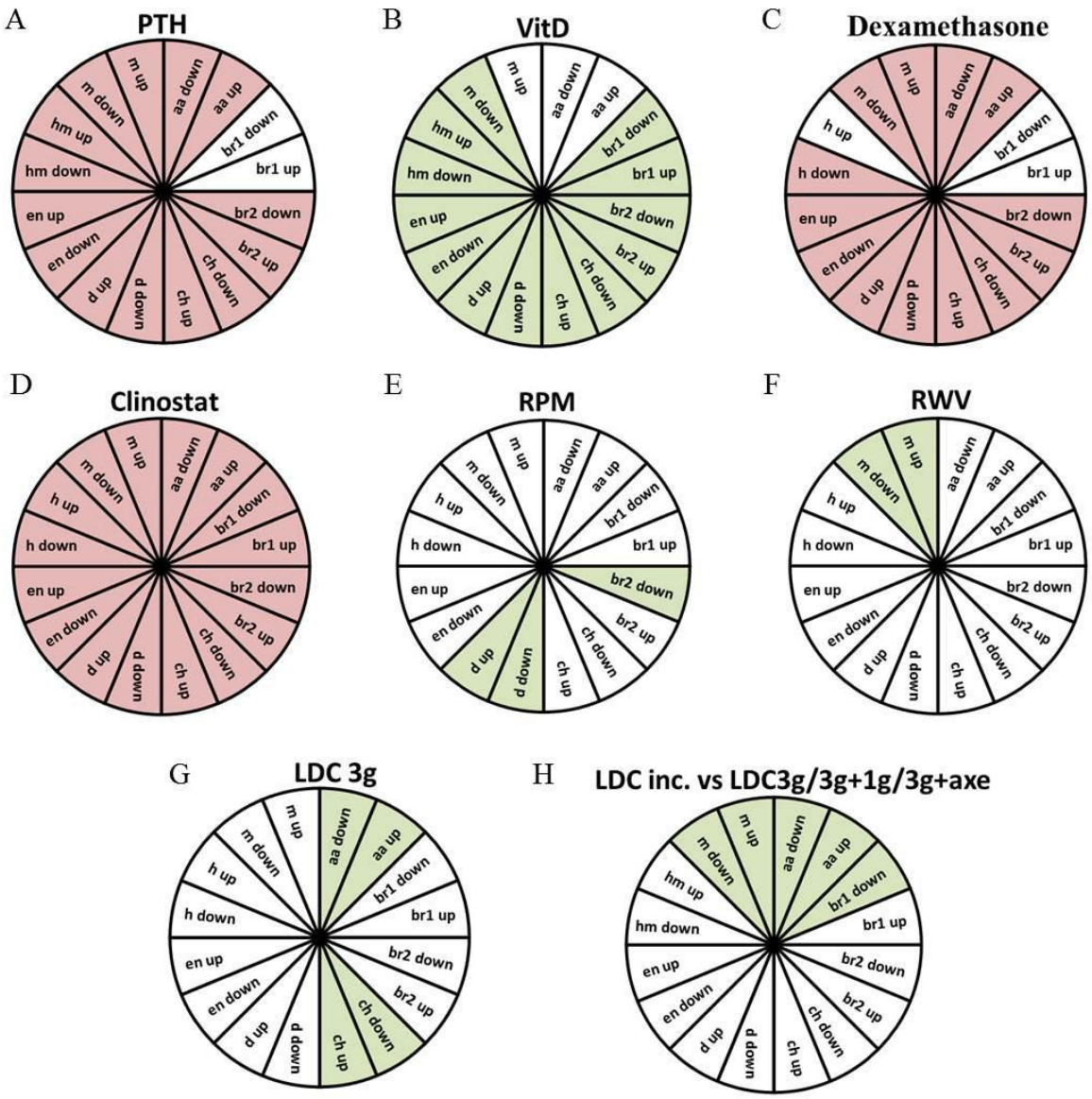

Figure 38: Summary graphs comparing the bone formation scores for each structure in the different experiments. Statistical analysis was performed by X^2 of Pearson and a logistic regression. In red, the scores are significantly increased. In green, the scores are significantly decreased. (A) PTH. (B) VitD3. (C) Dexamethasone. (D) Clinostat. (E) RPM. (F) RWV. (G)3g hypergravity between 5-6dpf. (H) "Relative microgravity"**.** For abbreviations see legend on the figure in attachment.

In contrast to the results in clinorotation, both RPM and RWV did not result in a significant change in ossification and three (in RPM) or two (in RWV) bone elements revealed over-ossification in some individuals. These differences in effects caused by the microgravity simulation devices are further supported by the gene expression analysis (see below). Thus, at this stage, it appears that clinorotation is probably the most appropriate approach to simulate microgravity. These results highlight the fact that we used an entire organism in these devices.

These machines are used with cell cultures or even plant shoots fixed on a supporting medium. Here, we used zebrafish larvae and at 5dpf they are free-swimming individuals. Behavior observations during the experiments suggest an imcreased swimming behavior in RPM and RWV, while in clinorotation the behavior seems more natural with the larvae simply following the rotating movement. Thus, we believe that the water movements in RPM and RWV will induce swimming behavior in the zebrafish larvae and possibly a physical training, thereby disturbing the intended microgravity simulation effect as was already previously suggested (Brungs, Hauslage et al. 2011, Herranz, Anken et al. 2013). This can be related to a muscle loading effect and explain the increased ossification observed. Bone formation is known to be increased in swim training devices (Fiaz, Leon-Kloosterziel et al. 2012). Two studies on zebrafish support these conclusions. The first study exposed larvae on RWV during various periods and they showed that no effect was observed in larvae treated after 72hpf (stage when all larvae have left the chorion and are free swimming) (Shimada, Sokunbi et al. 2005). The second study observed bone anomalies in adult zebrafish caused by RWV treatment during early stages, but again these defects are absent when the treated embryos were older than 48hpf (Edsall and Franz-Odendaal 2014). Taken together, we conclude that clinorotation is probably the most appropriate approach to simulate microgravity for free-swimming aquatic larvae.

Interestingly, the 3g hypergravity experiments consistently revealed an increase in the global calcification score, suggesting an increase of bone formation (Fig. 28B). Cumulated frequency and statistical analysis reveal that four structures, the anguloarticular (aa), ceratohyal (ch), branchiostegal ray2 (br2) and hyomandibular (h), were significantly increased (Fig. 28.A and table 13). The morphometric analysis reveals an increase in the head width with the length increase between the aa, en, br1 and o. Taken together, the 3g results suggest a local increase in bone formation under hypergravity conditions. This increase is in line with our expectations if we consider that microgravity induces a decrease and hypergravity an increase of bone development.

In the context of bone formation, the "relative microgravity" experiments present an important difference in the period of treatment compared to the other experiments. Indeed, the relative microgravity were performed through early exposure to 3g (from 0 to 5 or 6dpf) while the other experiments start at 5dpf. We observed a transient delay in pigmentation at 24hpf, which was rapidly resorbed at 48hpf. A similar effect was observed in a previous study during early exposure to RWV (Edsall and Franz-Odendaal 2014), however it is unclear why both hypergravity and simulated microgravity would induce both a delay in pigmentation. The

"relative microgravity" morphometric analysis reveals an increase of the distance between br1, en and o. The global ossification score is also increased, as well as the individual scores for m, aa and br1 (Fig. 38H). The observed effects are the same for larvae having spent 6 days at 3g or larvae that had been returned to 1g during the last day, indicating that this one day is insufficient to generate differences in bone formation between the conditions. In addition, at the opposite of the CLINO and the RPM, the parasphenoid area is increased in 3g>1g and 3g>axe compared to the 1g conditions, the 3g from 0 to 6 dpf did not allow a conclusion due to high variability. Most importantly, these analyses reveal similarities in the effects of 3g hypergravity independent of the difference in the treatment period. Nearly all the effects observed in hypergravity, between 0 to 6dpf or between 5-10dpf, are the exact opposite from CLINO. Once more, clinorotation appears as the best approach to simulate microgravity on zebrafish larvae. Moreover, RPM and RWV are both more close to the hypergravity results. Further analysis would be helpful to compare the different effects on bone formation. For example, we could test an extended period of "relative microgravity" by exposing larvae from 0 to 10days at 3g compared to 5 days at 3g followed by 5 additional days at 1g.

In general, in all the different conditions (PTH, VitD3, CLINO and RPM and hypergravity), the morphometric analysis revealed no or very minor modifications in the cartilage structures. These results suggest that cartilage is not influenced by the various treatments. However, the cartilage system is already developed at the beginning of the treatment (5dpf) indicating that cranial cartilage morphology is not affected by mechanical constraints, at least past a certain stage. In this context, it is interesting to note that also inhibition of the Fgf or Bmp signaling pathways in zebrafish larvae older than 2 days did not affect cartilage formation (Dalcq, Pasque et al. 2012, Larbuisson, Dalcq et al. 2013, Windhausen, Squifflet et al. 2015). In contrast, the bone system starts its development at 3dpf and is still in formation even at 10dpf, corresponding to the end of the different treatments. Since they are developing, the treatments act directly on the structures growth and exhibit higher effect on bone development. Early exposure to microgravity in a RWV revealed morphological changes in the cartilage skeleton (Edsall and Franz-Odendaal 2014), it would be interesting to see whether early exposure to hypergravity would also cause deformities.

The decrease of bone formation caused by clinorotation raised the question concerning a possible effect due to stress experienced by the larvae during the experiment. Indeed, endogenous excess cortisol or glucocorticoid therapy is known to induce secondary osteoporosis if they are over-dosed or taken on long-term to treat inflammatory diseases

(Graves and Lukert 2004, Hong, Chen et al. 2008, Sbaihi, Rousseau et al. 2009). A natural glucocorticoid produced in mammals, but also in fish by the HPI axis during high stress is thus the cortisol (Alsop and Vijayan 2008, Silverman and Sternberg 2012). Although clinorotation is probably the most gentle microgravity simulation device, we nevertheless measured the cortisol content in larvae after treatment and showed that neither CLINO nor RPM generated a significant stress response. Our results are thus due to the effect of the specific condition on the device and not due to stress. This is consistent with several studies that have previously shown that astronauts are submitted to changes in cortisol level neither before, nor during or after the flight (Caillot-Augusseau, Lafage-Proust et al. 1998, Carmeliet, Vico et al. 2001). Their bone loss is due to the weightlessness environment.

Despite the fact that we did not observe an increase in cortisol levels, we decided to evaluate the effect of glucocorticoid on bone development. Here, we used dexamethasone, a synthetic glucocorticoid, to observe the defect in bone formation on larvae in these conditions. The morphometric analysis revealed a decrease of the distance between the opercle (o) and also a decrease of the length of the head with a shorter distance between anterior (an) and the notochord (n). The ossification score analysis exhibit a general significant decrease for all structures except for branchiostegal ray1 (br1) and hyomandibular up (h up) (Fig. 38C) leading to a clear decrease visible on fig.13C and D. We thus conclude that high levels of glucocorticoids can indeed induce a decrease in bone formation in developing zebrafish larvae, however we also need to emphasize that the dexamethasone concentration leading to these defects was relatively high (25 µM in the E3 medium).

After defining the effects of hormonal treatments, microgravity simulation and hypergravity on bone formation, we decided to analyze the modifications in gene expression at the whole genome level to gain insight into the molecular mechanisms involved. As we were mainly interested in regulatory events, we analyzed the transcriptomes in each case after 1 day treatments, to avoid observation of secondary events. Treatments were started on 5dpf larvae and mRNAs were extracted at 6dpf. In addition, we implemented a new type of hypergravity experiment, the “relative microgravity” or “Reduced Gravity Paradigm”, which consisted in growing the larvae for 5 days at 3g, before returning them at 1g for 1 day. Taken together, these results allow highlighting various genes by their modifications in several experiments. For example, RHCG (Rh Type C glycoprotein gene) is the only gene common to the 3 microgravity simulators. As previously discussed, up-regulation of this ammonium transporter could indicate an increase in ammonium secretion, maybe caused by the movement induced

by the microgravity simulation (Nakada, Hoshijima et al. 2007). Another gene affected in different conditions, such as clinostat, hypergravity but also in RWV and in relative microgravity was *GADD45B* (growth arrest and DNA damage-inducible). GADD45B is down-regulated in all these conditions except an up-regulation in RWV. GADD45B is involved in hematopoiesis and immune response, but also in chondrocyte differentiation (Lu, Ferrandino et al. 2004, Ijiri, Zerbini et al. 2005, Goldring, Otero et al. 2008, Zenmyo, Tanimoto et al. 2010). *GADD45B* is down-regulated in osteoarthritic bone (Hopwood, Tsykin et al. 2007), similar to what we observed in CLINO, hypergravity and relative µg. At the opposite, Gadd45B is up-regulated in murine skeletal muscle after space-flight or hindlimb suspension (Allen, Bandstra et al. 2009). In cartilage, GADD45B is known to induce *Col10a1* and *MMP13* expression and is involved in chondrosarcoma (Ijiri, Zerbini et al. 2005, Tsuchimochi, Otero et al. 2010, Zenmyo, Tanimoto et al. 2010). In our experiments, *col10a1* is also regulated in the same direction as *gadd45b* in CLINO and RWV. This gene is clearly known to be crucial to form hypertrophic chondrocyte (Eames, Amores et al. 2012, Kim, Lee et al. 2013).

Another gene affected in various experiments is *NDRG2* (N-myc downstream regulated gene 2) This gene belongs to the *NDRG* (new family of differentiation-related genes) family composed of 4 members (Kang, Jung et al. 2011). *NDRG2* is mostly expressed in brain, heart, kidney, skeletal muscle, and somites (Zhu, Zhao et al. 2012). NDRG2 is involved in cancer and metastasis, its down-regulation in several cancers, such as liver, thyroid, pancreatic and prostatic cancer, suggest a possible function in tumor suppression (Gao, Wu et al. 2011). NDRG2 overexpression contributes to inhibit the cell's capacity for proliferation and invasion (*in vitro*) and contributes to suppress liver cancer metastasis (Gao, Wu et al. 2011). NDRG2 can also play a role more related to the skeleton and skeletal muscle system by its function in regulation of vertebral morphogenesis during somite differentiation (Zhu, Zhao et al. 2012). *Ndrg*$^{-/-}$ mice present vertebral defects and Ndrg2 overexpression in chondrocytes or osteoblasts lead to different defects such as supplementary ribs on the lombar1 (Zhu, Zhao et al. 2012). Concerning gravitational effects, a spaceflight experiment using bone marrow macrophages has shown an increase of NDRG2 in the macrophages (Ortega, Lu et al. 2012). In our experiments, *ndrg2* is down-regulated at 3g in the 1g>3g experiment and in simulated microgravity in clinorotation, but increased upon 1 day PTH treatment. These variable regulations probably reflect the complex roles of this factor in various physiological systems

under the different conditions, and do not a clear assignment of a specific role in skeletal development.

Several genes from our gene expression analyses are involved in calcium metabolism. Quite obviously, many of these genes are altered in the hormone treatments, as both hormones are known to act on calcium levels. In VitD3, they are all down-regulated (CALCOCO1, RGN, KCNMB2, STC2 and OBSCN) except the calcium channel CACNA2D2, which is up-regulated. In PTH, we find other genes also involved in calcium regulation but the effect is, as expected, just opposite to that of the VitD3 treatment. The calcium channel CACNB1 is down-regulated and all the other genes, such as CALR, CALCRL, CAB39 and EFCAB4B, are up-regulated. Interestingly, some calcium regulatory genes are also modified in the altered gravity experiments. In CLINO, *CALCOCO1* is up-regulated and in RWV, *OBSCN* is down-regulated, while in VitD3, both genes are down-regulated. These results correlate well with the observed effects on bone formation, decreased in CLINO and increased in RWV and VitD3. In the relative µg experiments, the results are less clear. In 1g, the calcium channels CACNA2D2, CACNG6 are both up-regulated, while in 3g>1g, CACNG1 and CACNG6 are down-regulated. However, EFACB14 is up-regulated in both 3g>axe and 3g>1g. Some further investigation is needed to understand these differences in the relative µg.

Two other interesting genes are *FOS* and *FOSB*. The CLINO experiment affects a small molecular network containing the *FOSB* gene (Fig. 18A). Interestingly, *FOSB* and *FOS* were also included in a network that was described in chapter 3 in the 7 common genes affected by relative microgravity. In both cases, *fosb* expression was decreased in the lower gravity condition. Expression of truncated versions of FosB was shown in mice to cause osteosclerosis and increased expression of osteoblast marker genes (Sabatakos, Rowe et al. 2008). Taken together, these observations point to a central network comprising members of the FOS factors whose global expression may serve as an indicator for gravity conditions. Note that *fosb* expression was also decreased after VitD3 treatment.

Other genes appear to be more specifically regulated by different gravity conditions. We show that the bone-related *HESI* (Hairy enhancer of split) gene is strongly up-regulated in a bone-related network by CLINO (Fig. 19A), while this gene and HES5 are down-regulated in relative µg in 3g>1g and 3g>axe. Both genes, coding for helix-loop-helix transcription factors, are involved in the control of neural stem cell differentiation (Hatakeyama, Bessho et al. 2004), *HES5* was shown to be regulated during cartilage differentiation (Karlsson, Jonsson

et al. 2007) while *HES1* is involved in development of the digestive system (Crosnier, Stamataki et al. 2006). HES1 and HES5 are downstream effectors of Notch signaling (Zanotti and Canalis 2010, Zanotti and Canalis 2012, Zanotti and Canalis 2013), which is very important for bone development and remodeling by suppressing the differentiation of skeletal cells (Zanotti and Canalis 2010, Zanotti and Canalis 2012, Zanotti and Canalis 2013). In our study, *NOTCH1* expression is up-regulated in RPM, but in the other experiments, Notch signaling is also affected as indicated by the changes in expression of its target genes, such as *HES1* in CLINO, *HES1* and *HES5* in relative µg, up-regulation of *HEY1* in hypergravity and a down-regulation in relative µg (3g>1g). These changes could be, at least in part, related to the observed effects on bone formation.

SOCS1 and SOCS3 are two genes from the Suppressors of cytokine signaling family (SOCS) composed of 8 members (Ferla, Aboraia et al. 2014, Ahmed, Larkin et al. 2015). SOCS1 and SOCS3 are important for T cell regulation in the immune system (Elliott and Johnston 2004, Ahmed, Larkin et al. 2015). $Socs1^{-/-}$ mice die within 3weeks after birth with fatal inflammatory disease (Johnston 2004). $Socs3^{-/-}$ mice die during mid-gestation by a placental insufficiency. The role of Socs3 in the placenta is still not clear. SOCS3 deficiency activates STAT3 and leads to chronic inflammatory disease such as arthritis or Crohn's disease (Elliott and Johnston 2004). In our genomic analysis, *socs1* and *socs3* are both up-regulated in RWV, down-regulated in relative µg, in hypergravity, and VitD3. Moreover, *Socs3* has been shown to be up-regulated during mouse osteoclast differentiation in RWV (Sambandam, Blanchard et al. 2010).

Interestingly, an important gene involved in VitD3 metabolism is also affected in several of our experiments. The active form of VitD3 ($1,25(OH)_2D3$) or calcitriol is catabolized by the 24-hydroxylase or CYP24a1 enzyme (Cytochrome P450, family 24, subfamily A, and polypeptide 1) mainly in the kidney but also in intestine, bone and parathyroid at a smaller level (Ferla, Aboraia et al. 2014, Ono 2014, Ormsby, Findlay et al. 2014). Mutation of *CYP24A1* induces Idiopathic Infantile Hypercalcemia (IIH) (Cools, Goemaere et al. 2015). In our results, CYP24a1 is increased in relative microgravity, RWV and in VitD3, suggesting once more that RWV has effects similar to VitD3 treatment.

Few data have been published concerning whole genome gene expression studies in microgravity (Pardo, Patel et al. 2005, Versari, Klein-Nulend et al. 2013, Versari, Longinotti et al. 2013, Neutelings, Nusgens et al. 2015). Compared to clinorotation of zebrafish larvae for 1

day, no gene commonly affected was found in human adipose tissue-derived mesenchymal stem cells (AT-MSC) kept for 14 days on RPM (Versari, Klein-Nulend et al. 2013), human umbilical vascular endothelial cells (HUVEC) exposed to space conditions for 7 days (Versari, Longinotti et al. 2013) or in the skin of mice that spent 3 months in space (Neutelings, Nusgens et al. 2015). Murine 2T3 osteoblast precursor cells cultured for 3 days on an RPM revealed decreased expression of IGF-1 and IGF-2 (Pardo, Patel et al. 2005), possibly related to the decreased expression of IGF2R observed here. Other genes whose expression was affected in 2T3 cells, such as decreased expression of BMPs, PTHR or RUNX2, may reflect secondary events after 3 days in microgravity, rather than the regulatory events that were investigated in the zebrafish experiments.

Despite the few investigations related to our experiments, these results support the conclusion that the three different microgravity simulation devices actually cause very different adaptation reactions. Only CLINO resulted in a clearly decreased bone formation and changes expression of genes more specifically involved in biological functions related to bone formation (Table12, Table annex14), thus it appears most plausible that clinorotation is the most appropriate device to simulate microgravity on ground. A similar conclusion was also reached when comparing otolith growth in cichlids placed on clinorotation or RWV (Brungs, Hauslage et al. 2011). However, a previous study investigated bone formation in adult zebrafish after having exposed the embryos to simulated microgravity in a RWV during the first two days (between 10-22hpf, or 12-36hpf) (Edsall and Franz-Odendaal 2014). An abnormal parasphenoid phenotype was observed in adult (4 months-old) fish, although no obvious defect was observed at earlier stages (10-, 35-, or 65dpf). The authors suggest that early exposure to RWV causes subtle defects in the cranial neural crest cells, as also suggested by the observed transient defects in pigmentation and the transient differences observed in 10dpf skulls (Edsall and Franz-Odendaal 2014), or on the positioning of the parasphenoid that would cause these late onset defects. Here, we show that clinorotation starting at 5dpf causes a significant decrease of the calcified parasphenoid area and a general decrease of calcification in all major cranial bones at 10dpf, without changes in the general morphology. This result is consistent with previous experiments exposing mouse fetal long bones for 4 days to space conditions (Van Loon, Bervoets et al. 1995) that revealed decreased mineralization, but no change in growth or collagen synthesis.

The clinorotation results are also in line with the well-established bone loss experienced by astronauts in space or bed rest studies (Nagaraja and Risin 2013, Morgan, Heer et al. 2014),

and with the space experiments performed on rats (Morey and Baylink 1978, Wronski, Morey-Holton et al. 1987, Vico, Chappard et al. 1988, Turner, Evans et al. 1995) or mouse (Tavella, Ruggiu et al. 2012). Microgravity-caused effects ranged from decreased trabecular numbers (Vico, Chappard et al. 1988, Tavella, Ruggiu et al. 2012) and thickness (Vico, Chappard et al. 1988) in tibia, a decreased mineral content and number of osteoblasts (Wronski and Morey 1983, Wronski, Morey-Holton et al. 1987, Turner, Evans et al. 1995). In human astronauts, a decrease of the bone formation markers (type I procollagen propeptide and bone alkaline phosphatase) decreased, while bone resorption markers such as the procollagen C-telopeptide increased during space flight (Caillot-Augusseau, Lafage-Proust et al. 1998, Caillot-Augusseau, Vico et al. 2000). The decreased bone formation observed during microgravity simulation by clinorotation, as well as the increased bone formation due to hypergravity, strongly indicate that skeleton formation in zebrafish between 5-10dpf is a good model to study gravitational effects on bone metabolism. One important difference is however apparent: only weight bearing bones are significantly affected by microgravity in humans or rodents (Vico, Chappard et al. 1988, Tavella, Ruggiu et al. 2012, Nagaraja and Risin 2013), while most cranial bone elements appear to be affected by gravitational changes in zebrafish larvae. It is unlikely that these effects result from changes in muscle strain, as is generally accepted for the mammalian weight-bearing bones, further experiments will be required to better understand this general sensitivity to gravitational conditions of the developing zebrafish bones.

The clinorotation is in our conclusion the best microgravity simulator for ground simulation with an entire organism, the zebrafish larvae. However, microgravity is defined as gravity below 10^{-6}g and biological processes are already affected at 10^{-3}g, as can be found for example on ISS. The correct term to define this condition would be weightlessness. Concerning the microgravity simulators such as the clinostat, RPM, or RWV, the gravitational vector is compensated by several forces. Actually, gravity is still present, only the influence and the effect of this force are changed or abrogated. In consequence, these devices are not really microgravity simulators, however they are able to simulate for example the neurovestibular system disturbance also present in space (Briegleb 1992, Van Loon 2007).

Finally, how can we be sure that clinorotation is the best “microgravity simulator”? Our assumption is that it is the spontaneous or induced movements of the zebrafish larvae that mainly disturb the microgravity effect in RPM and RWV, and may induce a training effect. To verify this hypothesis and eventually study the real effect of these devices on larvae, it is possible to use mutant larvae, such as the *nic1* mutant which are paralyzed but develop

normally (Sepich, Wegner et al. 1998). Other alternatives such as the dropping tower and also the parabolic flight can induce real weightlessness, but only for a very short time. These devices can be an answer to our research with real weightlessness, but it would be impossible to place the larvae during 24hours in weightlessness. Finally, the real answer to our questions requests a spaceflight with zebrafish larvae. This project is in progress and maybe realizable in a near future. In parallel to this flight project, future experiments could be performed using simulated microgravity or hypergravity to further investigate the molecular mechanisms involved in the effects that we describe here. We could use the fluorescent zebrafish line *Tg(osx-mCherry)* for live detection of osteoblasts during these experiments. Thus, after the structures analysis by our morphology analysis, we can go further to analyze the changes specifically in bone cells during these experiments. Another live detection method of osteoblast activity is the nitric oxide detection. This method performed on transgenic zebrafish or in combination with alizarin red staining allows the colocalization and the characterization of bone structures and osteoblast activity (Renn, Pruvot et al. 2014). The transgenic zebrafish lines can also be used to isolate fluorescent osteoblasts by FACS and analyze gene expression specifically in osteoblasts, rather than in whole embryos as performed here. Other transgenic lines can be used for other specific cells in other organs such as muscles, blood vessels or in the immune system.

Materials and Methods

1. Animal procedures

Zebrafish (Danio rerio) were maintained under standard conditions (Westerfield 2007) in the GIGA zebrafish facility (licence LA2610359). Briefly, zebrafish (*Danio rerio*) of the AB strain were reared in a recirculating system from Techniplast, Italy at a maximal density of 7 fish/l. The water characteristics were as follows: pH = 7.4, conductivity = 500 µScm-1, temperature = 28°C. The light cycle was controlled (14 h light, 10 h dark). Fish were fed twice daily with dry powder (ZM fish food®) adapted to their age and once daily with fresh *Artemia salina* nauplii (ZM fish food®). Larvae aged less than 14 days were also fed twice daily with a live paramecia culture. Wild type embryos were used and staged according to (Kimmel, Ballard et al. 1995).

The day before breeding, wild-type adult male and female zebrafish were set up in several breeding tanks, separated by a clear plastic wall. After the light was turned on the next morning, walls are removed, eggs are generated by natural mating and collected from 30 minutes to 2 hours after spawning. After sorting, clean eggs are moved to Petri dishes and incubated at 28°C in E3 medium (5 mM Na Cl, 0.17 mM KCl, 0.33 mM $CaCl_2$, 0.33 mM $MgSO_4$, 0.00001 % Methylene Blue). All protocols for experiments were evaluated by the Institutional Animal Care and Use Committee of the University of Liège and approved under the file numbers 568, 1074, and 1264 (licence LA 1610002).

2. Hormone treatments

Parathyroid hormone (PTH; Merck-Calbiochem®, Overijse, Belgium) stock solution (1µg/ml) was prepared in DMSO and stored in aliquots at -20°C. Vitamin D3 (cholecalciferol, VitD3; Sigma®-Aldrich, Diegem, Belgium) stock solution (200µl/ml) in DMSO was stored in aliquots at -20°C for maximum one month.

The treatment protocol was inspired by Fleming and collaborators experiments (Fleming, Sato et al. 2005). Larvae at 5dpf were transferred into a 6 well plate (Millipore) containing E3 medium supplemented with the required chemical or vehicle (DMSO) as negative control. The medium was changed every day at the same time. Final concentrations in E3 were at 10ng/ml for PTH and 200ng/ml for VitD3. Each well contained 20 fish in 4ml. They were treated for 1day (n=50-60 larvae) to perform microarrays and for 5days, from 5 to 9 or 10dpf, to observe the longer-term effects of treatments by different staining (n=20-30 larvae). Plates were placed into the dark and incubated at 28°C. The larvae were euthanized by tricaine overdose (0.048% w/v) and directly submitted to an RNA extraction at 6dpf (for microarrays)

or a 4% para-formaldehyde (PFA; Sigma®-Aldrich, Diegem, Belgium) fixation at 6, 9 or 10dpf (for staining).

3. Microgravity simulation experiments

3.1. Clinostat

The clinostat device (benchtop 2D clinostat) (van Loon, Veldhuijzen et al. 1999) was used to simulate the microgravity condition. This instrument allows parallel positioning of 6 horizontal tubes, of which 3 are rotating at a precisely controlled constant speed of 60 rpm, while 3 others are kept immobile to serve as control. As the tubes have to be hermetically closed during the experiment, we carried out preliminary experiments to determine a density of 1 larva/ml as maximal to avoid health and behavioral (slow movements) effects. In each tube, 5 larvae of 5dpf were placed into 5ml of freshly prepared and oxygenated E3 medium. The medium was changed every 24hours to renew the oxygen level. The clinostat was placed in the zebrafish facility (room temperature 26°C) and covered by an aluminum paper to keep the larvae in the dark, isolated from possible visual clues concerning the rotation. This procedure resulted in an increase of the temperature to 28°C. Visual inspection just after setup revealed that the water column within the rotating tubes followed the movement without turbulence, as well as the immobile larvae.

3.2. Random positioning machine

The Random Positioning Machine (RPM) (Dutch Space, Leiden, NL) is a 3-dimensional microgravity simulation device (Mesland, Anton et al. 1996, Van Loon 2007). It is composed of an experimental platform that is itself rotating, and mounted onto a frame able to rotate independently around a perpendicular axis. The random variations of speed and directions are computer-controlled to reach the global abolition of gravity force. The entire frame is placed into an incubator to control the temperature at 28°C and to ensure darkness, in order to avoid visual clues concerning the movements. The 5dpf larvae were placed into 15ml falcon tubes in E3 medium. The medium was changed every 24hours. As the clinorotation experiment, the RPM was running during 24 hours for microarray analysis and until 9days for image analysis.

3.3. Rotating wall vessel

The Rotating Wall Vessel (RWV) allows to place 4 rotating discs at the same time. The discs have a diameter of 6 cm and are composed of a gaz-permeable material. The discs were filled with 10ml E3 and 60 larvae of 5dpf were added into each disc. The discs on the RWV were rotating at a constant speed of 28rpm. In parallel, other discs were placed horizontally near the RWV to serve as control. All these experiments were performed in the dark, inside an

incubator at 28°C. As for the Clinorotation or the RPM, a part of this experiment was performed during 24hours for microarray analysis and until 10dpf for image analysis. The medium was also changed every 24hours.

4. Hypergravity experiments in the Large Diameter Centrifuge

A Large Diameter Centrifuge (LDC) was used for hypergravity experiments. It is composed of a central axis linked to 2 perpendicular arms, each arm terminating in 2 opposing gondolas where it is possible to install an incubator containing the samples. The arms provide an 8m diameter for rotation and can provide centrifugal forces of maximum 20g. The zebrafish larvae were incubated in 20 ml E3 in a Petri dish placed in an incubator within a gondola for 3g experiments, and placed either in an incubator on the centrifuge axis (axe) or outside of the centrifuge for 1g controls. In this setting, the medium represents less then 5 mm of water column and thus the 3g acceleration causes an increase in hydrostatic pressure of maximum 0.0015 bar, as compared to the 1bar atmospheric pressure (Van Loon 2007).

5. Stress experiment

5.1. Dexamethasone

The protocol was inspired by the previously published experiments (Hillegass, Villano et al. 2007). The dexamethasone solution was diluted to obtain a concentration of 1mg/ml and divided in small aliquots to store them at -20°C. The final dilution in E3 was at 10ng/ml (25.48µM). Larvae at 5dpf were transferred into a 6 well plate (Millipore) containing E3 medium containing the dexamethasone solution or the vehicle only as negative control (0.1% ethanol). Each well contained 20 larvae in 4ml. The medium was changed every day at the same hour. Plates were placed into the dark and incubated at 28°C. The larvae were treated from 5 to 10dpf. Then, they were anesthetized by tricaine and fixed by 4% PFA at 10dpf for subsequent staining.

5.2. Cortisol stress response

This experiment was adapted from the literature (Alsop and Vijayan 2008, Alderman and Bernier 2009). Each condition contained 15 fish of 6dpf to obtain comparable samples and was prepared in triplicates. Positive control larvae were stressed by 2 different techniques. First, the larvae were placed into a 20ml container and swirled during 30 seconds in 5ml water. Then, they were placed 5min in an incubator at 28°C (Alsop and Vijayan 2008). Finally, they were frozen in liquid nitrogen and stored at -80°C. This condition is called “agitation”. The second positive control was adapted from (Alderman and Bernier 2009) and consisted in placing the

larvae for 5min in salt water of 1.75g/100ml, followed by 5min in E3 at 28°C before freezing them in liquid nitrogen and storing at -80°C. This condition is called “salt water”.

The negative controls were obtained in two different ways. First, a standard procedure called “high tricaine” that consists in catching the larvae alive in the Petri dish before placing them into an Eppendorf tube, where tricaine at 0.04 g/l is added to kill them. The second consists in adding tricaine at 1.6 g/l into the Petri dish, waiting until the larvae are immobile and unresponsive and then placing them into an Eppendorf tube and frozen in liquid nitrogen. This method is called “low tricaine” in our results.

5.3. Cortisol measurement

15 larvae per condition were homogenized in 1mlof cold PBS (pH= 7,4) using a Potter. Then, 500µl of homogenate served for cortisol extraction into 3ml of diethyl ether. This extraction is repeated three times before the ether is evaporated to dryness in a waterbath at 45°C under a nitrogen flow (Alsop and Vijayan 2008).

After evaporation, eluates were dissolved in 500µl enzyme immunoassay (EIA) buffer. Cortisol was quantified using a cortisol EIA kit (Cayman Chemical Co., Ann Arbor, MI) composed of a colorimetric 96-well enzyme immunoassay. Normalization to the protein concentration of each homogenate was performed using the Micro BCA^{TM} Protein Assay kit (Thermo Scientific, Pierce Biotechnology, Rockford, IL). The cortisol data were adjusted to the cortisol extraction efficiency (= 93% as determined from a spiked negative control); the detection limit was 12 pg cortisol/ml (Alsop and Vijayan 2008, Alderman and Bernier 2009).

6. Staining methods

Acid-free protocols were adapted (Walker and Kimmel 2007) to perform Alcian blue (8 GX Sigma®-Aldrich, Diegem, Belgium) staining of cartilage structures and Alizarin red S (Sigma®-Aldrich, Diegem, Belgium) staining of calcified structures. At 6, 9 or 10dpf, the larvae were fixed in 4% PFA for 2h at room temperature and rinsed several times with PBST.

Cartilage was stained overnight in 10 mM $MgCl_2$, 80% EtOH and 0.04% Alcian blue. The larvae were washed in different concentrations of ethanol (80%, 50%, 25%) to remove excess staining. Pigmentation was bleached in a H_2O_2 solution (H_2O_2 3%, KOH 0.5%) and finally the larvae were rinsed 3 times in a solution of 25% glycerol / 0.1% KOH and 50% glycerol, 0.1% KOH and finally stored in this solution at 4°C.

During acid-free bone structure staining with Alizarin red, bleaching was performed immediately after fixation, before the staining. After the bleaching, long rinses (at least 20min each) in a 25% glycerol, 0.1% KOH solution are necessary to prevent the fading of the staining. The larvae are stained in a 0.05% Alizarin red solution in water for 30min in the dark on low agitation, rinsed in a 50% glycerol, 0.1% KOH solution to remove excess staining and kept at 4°C in the same solution.

Images of stained larvae (n=20-30 larvae) were obtained on a binocular (Olympus, cell B software).

7. Image analysis

Image analysis was performed on the pictures of larvae stained with Alcian blue for cartilage or Alizarin red for bone. Individual cartilage and bone elements were identified according to (Cubbage and Mabee 1996, Kimmel, Miller et al. 1998, Schilling 2002, Verreijdt, Debiais-Thibaud et al. 2006, Li, Felber et al. 2009). For morphometric analysis, images were uploaded into the CYTOMINE environment (Marée, Stevens et al. 2013) and manually annotated by positioning 21 landmarks for larvae stained for cartilage (Fig. 39C) as previously defined in the CYTOMINE ontology. 29 landmarks were placed for larvae stained for bone in hormonal treatments (Fig. 39D), of which 15 were selected for the hypergravity experiments. The program then defines the positions of all selected landmarks and computes all the distances (in pixels) and angles (in radian) of all the possibilities between two points of interest. These data were exported into an Excel file and a selection of interesting measures was conducted by performing principal component analysis on data obtained from differently treated larvae to identify invariable or redundant measures. The measures selected were: for cartilage (Alcian blue): Anterior to Ethmoid plate, Anterior to Posterior, Articulation down to Articulation up, Ceratohyal ext. down to Ceratohyal ext. up, Ceratohyal ext. down to Ceratohyal int. down, Ceratohyal ext. up to Ceratohyal int. up, Ethmoid plate to Posterior, Hyosymplectic down to Hyosymplectic up; and for bone (Alizarin red): Anguloarticular down to Anguloarticular up, Anterior to Notochord, Anterior to Parasphenoid a, Branchiostegal ray 1 down to Branchiostegal ray 1 up, Entopterygoid down to Entopterygoid up, Maxilla down to Maxilla up, Opercle down to Opercle up, Parasphenoid a to Parasphenoid b , Parasphenoid b to Parasphenoid c, area of the parasphenoid triangle: parasphenoid a, b, and c, and finally the angles between parasphenoid a and b, a and c, b and c. Statistics were performed using

GraphPad Prism5. A t-test was used for control versus treatment experiments, while a one way ANOVA was used for multiple comparisons.

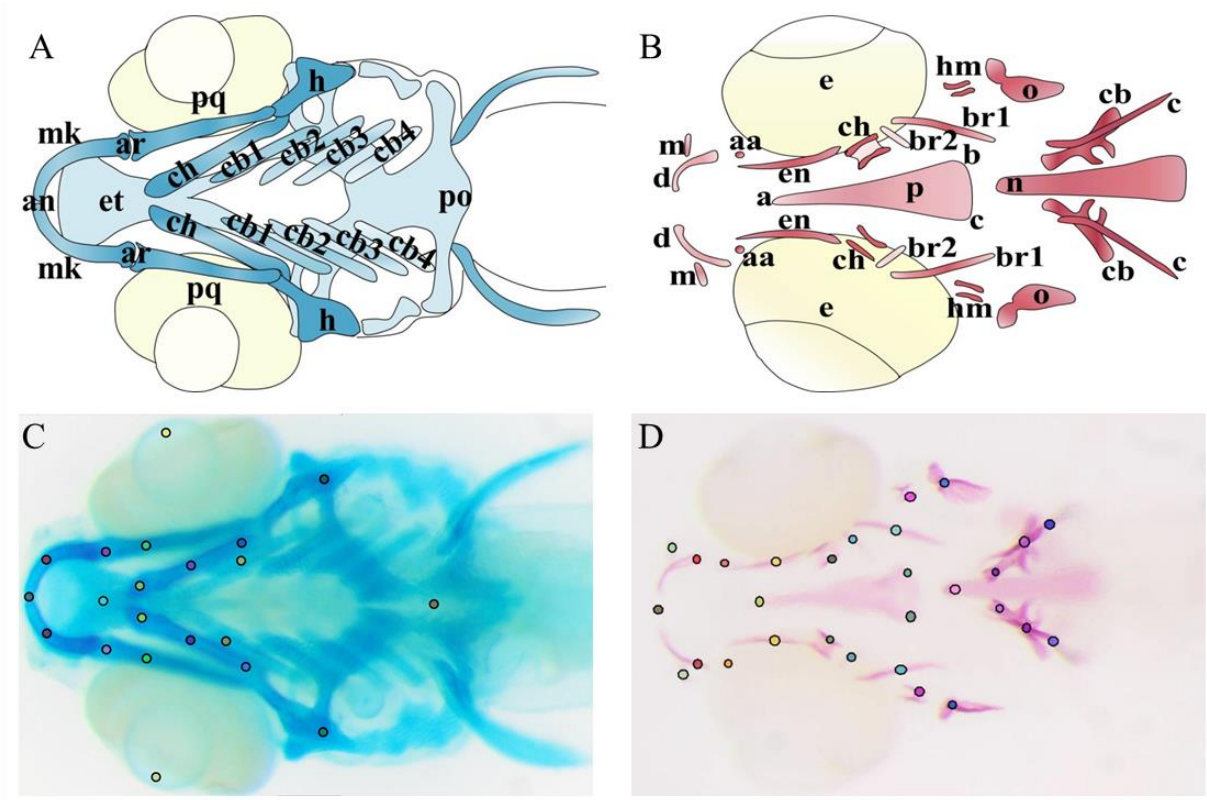

Figure 39: Cartilage and bone elements of the head skeleton in 10dpf zebrafish. (A) Schematic representation of the different head cartilage elements, anterior limit (an), articulation (ar), ceratobranchial pairs 1 to 4 (cb1-4), ceratohyal (ch), ethmoid plate (et), hyosymplectic (h), Meckel's cartilage (mk), palatoquadrate (pq), posterior limit (po), (B) Schematic representation of the different cranial bone elements with 29 landmarks used for chemicals treatments and 15 landmarks for the 3g and the relative-hypergravity. The 15 landmarks are anguloarticular (aa), anterior (an), branchiostegal ray1 (br1), entopterygoid (en), maxilla (m), notochord (n), opercle (o), parasphenoid (p), Note that the parasphenoid is a triangular bone defined by its anterior summit (a) and two posterior summits (b,c), The 29 landmarks include the 15 named before with branchiostegal ray2 (br2), cleithrum (c), ceratobranchial 5 (cb), ceratohyal (ch), dentary (d), hyomandibular (hm). (C) Alcian blue staining of head cartilage representing the landmarks used for morphometry. (D) Alizarin red staining of cranial bones representing the landmarks used for morphometry.

Morphometric analysis did not inform about the extent of ossification within each larva. Thus, a systematic structure analysis was generated. Each bone structure was classified based on the progress of development into one of the four following categories: absent, early ossification, advanced ossification and over ossification. When values were considered as quantitative, comparison between two groups (control versus chemical treatment or hypergravity in 1g>3g) was assessed by a Student t-test, while comparison between different treatments ("relative microgravity" experiment) was assessed by an analysis of variance (ANOVA). A contingency table considered ordinal values distributed among the 4 classes (from absent to over

ossification) or only 3 classes when one class was not present in the sample. Association between classes and treatment was assessed by X^2 test and by an ordinal logistic regression and the odds ratio (OR). The "relative microgravity" experiment was analyzed in addition by grouping the 3g, 3g>1g and 3g>axe versus the 1g sample. Statistical analyses were performed using the Statistica Software (version 10). Results were considered statistically significant at the 5% critical level ($p < 0.05$).

8. Single and fluorescent double whole-mount in situ hybridization

Single and fluorescent double whole-mount in situ hybridization on zebrafish embryos Single hybridizations and detections were carried out as previously described (Hauptmann and Gerster 1994) on wild-type embryos. Anti-sense RNA probes were prepared by transcribing linearized cDNA clones with SP6, T7, or T3 polymerase using digoxigenin or fluorescein labeling mix (Roche). Fluorescent double hybridizations were performed by adapting various fluorescent in situ hybridization protocols to the zebrafish (Denkers, Garcia-Villalba et al. 2004, Zhou and Vize 2004). Before the hybridization, zebrafish embryos were incubated in 2% H2O2 during 40 min for endogenous peroxydase inactivation, just prior to proteinaseK treatment. For the hybridization, anti-sense probes were prepared using digoxigenin labeling mix (Roche) or DNP-11-UTP ribonucleotides (TSAi Plus system, Perkin Elmer). The embryos were blocked in 100 mM Tris –HCl pH 7.5, 150 mM NaCl (TNT buffer) with 0.5% Blocking Reagent (Perkin Elmer). For the detection, we used pre-absorbed HRP-coupled antidigoxigenin (Roche) or HRP-coupled anti-DNP antibodies (Perkin Elmer). The embryos were then extensively washed in TNT buffer. The revelation was performed by incubating embryos during 40 min in tyramide-FITC and tyramide-Cy3 prepared according to Peter Vize's protocol (Zhou and Vize 2004) at a final dilution of 1/50 in 1 Amplification Reagent (Perkin Elmer). Embryos were then conserved in TNT buffer. The sox4a probe was generated from KpnI-linearized fb82f08, using SP6 RNA polymerase. The sox4b probe was synthesized by transcription from pCRIIRTOPOR-sox4b linearized with HindIII and using T7 RNA polymerase.

9. RNA extraction and reverse transcription

Larvae at 6dpf, after 24h treatment, were used for RNA extraction. Total RNA was extracted of 60 larvae per experiment using Trizol, followed by the RNeasy Mini kit (Qiagen, Hilden, Germany) according to the manufacturer's instructions and conserved at -80 degrees. They were treated with Rnase-free Dnase Set (Qiagen, Hilden, Germany). After extraction, the quality and concentration of total RNA was evaluated by electrophoresis on capillary gel and

the ratio of absorbance at 260/280nm by spectrophotometer (Bioanalyzer 2100, Agilent Technologies, Diegem, Belgium). Synthesis of cDNA was performed from 1µg of total RNA, which was reverse transcribed (Transcriptor iScript^{TM} cDNA Synthesis Kit, Bio-Rad, Nazareth, Belgium) according to the manufacturer's instructions.

10. Real Time-PCR

Gene-specific oligonucleotide primers were designed using the Primer3 software to span exon-exon junctions to avoid detection of genomic DNA contamination (see Table S1 for primer sequences) and synthesized by Eurogentec (Seraing, Belgium) or Integrated DNA Technology (Leuven, Belgium). cDNA was used as template for quantitative Real-Time PCR with the SensiMix^{TM} SYBR Kit (Bioline, London, UK), containing Sybr green. Reactions were performed on an Applied Biosystems 7900 HT sequences Detection System (Applied Biosystems, Foster City, CA) using the onboard software (SDS 2.4). Purity of the amplicons was checked by melting curves at the end of each reaction. Ct values were exported from the onboard software as a text file and imported into a customized Microsoft excel spreadsheet. 1 µl of the RT reaction (1/20 of the total cDNA) was added to 1X SYBR green master mix (Bioline, London, UK), 150 nmol of each primer in 15 µl total volume. Samples were run in triplicate in optically clear 384-well plates (ABgene), sealed with optical adhesive film (Applied Biosystems). "No template" controls were run for all reactions, and all RNA preparations were subjected to sham reverse transcription to check for the absence of genomic DNA amplification. The relative transcript level of each gene was obtained by the $2^{-\Delta\Delta Ct}$ method (Pfaffl 2001) and normalized relative to the *gapdh* (glyceraldehyde-3-phosphate deshydrogenase) housekeeping gene chosen from a panel of 3 genes (*gapdh*, *ef1-a*, *ß-actin*) as the most stably expressed throughout our experiments (not shown). Data from biological replicates were averaged and are shown as mean normalized gene expression ± SD.

Cycling parameters: 50°C x 2 min, 95°C x 10 min, then 40 cycles of the following 95°C x 15 s, 62°C x 20 s. A melting temperature-determining dissociation step was performed at 95°C x 15 s, 60°C x 15 s, and 95°C x 15 s at the end of the amplification phase.

11. Microarray expression experiments

For microarray expression analysis, four replicates from each treatment (control and drug or gravity treatment) were analyzed in 2+2 dye-swap hybridizations. One µg total RNA was linearly amplified one round and labeled, using Amino Allyl Message Amp II aRNA amplification kit (Ambion-Life Technologies, Gent, Belgium) as previously described (Nourizadeh-Lillabadi, Lyche et al. 2009). Five µg of the resulting antisense RNA (aRNA)

from the exposed and control groups was labeled either with Cy3-dUTP or Cy5-dUTP (GE Healthcare Bio-Sciences AB, Uppsala, Sweden). The labeled targets were examined for amplification yield and incorporation efficiency by measuring the aRNA concentration at 260 nm, Cy3 incorporation at 550 nm, and Cy5 at 650 nm using Nanodrop (Thermoscientific, Wilmington, DE, USA). A good aRNA probe had a labeling efficiency of 30–50 fluorochromes every 1000 bases. One to 5 µg of each labeled aRNA target was mixed, 9 µl 25× fragmentation buffer (Agilent Technologies, Diegem, Belgium) added, and the final volume adjusted to 225 µl with RNase-free H2O followed by incubation for 30 min at 60°C. The hybridization solution was prepared by adding 220.5 µl of 2× hybridization buffer (Agilent Technologies, Diegem, Belgium) and 4.5 µl sonicated herring sperm DNA (10 µg/µl; Promega, Madison, WI, USA) to the labeled target aRNA. Microarray slides (4x44K zebrafish V2 or V3, Agilent Technologies, Diegem, Belgium) were prehybridized at 42°C, 60 min using 0.1% bovine serum albumin (BSA) Fraction V, 5× SSC, and 0.1% sodium dodecyl sulfate (SDS). Hybridization was performed at 60°C for 16 h using gasket slides, hybridization chamber, and oven (Agilent Technologies, Diegem, Belgium) according to Agilent 60-mer oligo microarray processing protocol. Microarray slides were then washed 3 × 5 min in 0.5 × SSC, 0.01% SDS (first wash at 42°C and next two at room temperature). Finally, slides were washed 3 times in room temp with 0.06× SSC and dried immediately by centrifugation at 800×g for 1 min.

Microarray slides were scanned using a GenePix 4000B (Axon instrument, Foster City, CA). Scanning was performed at a level just before saturation of several spots. Raw data generated from Genepix were imported into the Bioconductor package LIMMA and corrected for background (Smyth and Speed 2003). For within-array and between-array normalization, print tip Loess and scale were used, respectively (Smyth and Speed 2003). An empirical Bayes moderated t-test (Smyth and Speed 2003, Smyth, Michaud et al. 2005) was applied to detect differently expressed genes across treated and control samples. The p values were corrected for multiple testing using the Benjamini–Hochberg (BH) (Benjamini and Hochberg 1995) method and p-values <0.1 were selected as differently expressed genes. The generated gene list was further filtered for genes with low intensity and with small changes in expression. In the averaged normalized MA-Plot, the majority of genes were clustered in between M values of ±0.4 (fold change ±1.3) and selected to be threshold criteria for differently expressed gene list. The VitD3 and RWV data were obtained on a SureScan Dx

instrument (Agilent Technologies, Diegem, Belgium) and analyzed using the GeneSpring software (Agilent Technologies, Diegem, Belgium) by applying the same settings.

Raw data and complete lists of analyzed data are publicly available at Arrayexpress (https://www.ebi.ac.uk/arrayexpress/).

12. Ingenuity Pathway Analysis.

For pathway and biological function analysis of significantly differently expressed genes, Ingenuity pathway analyses (IPA®, QIAGEN Redwood City; http://www.ingenuity.com) were used. The lists with differently expressed genes generated by the microarray analysis were translated into mammalian (human, mouse, and rat) orthologs using the Unigene & Gene Ontology Annotation Tool and uploaded to IPA. The IPA software is an online exploratory tool with a curated database for over 20,000 mammalian genes and 1.9 million published literature references. IPA's database together with EntrezGene, Gene Ontology, etc., integrates transcriptomics data with mining techniques to predict and build gene networks, pathways, and biological function clusters. The output results are given scores and p-values that are computed based on the number of uploaded genes in the cluster or network and the size of the network or cluster in the Ingenuity knowledge database. Fisher's exact test is used to determine the probability that each associated biological function is due to chance alone. Scores for IPA networks are the negative logarithm of the p-value, indicating the likelihood of the focus genes (genes uploaded to IPA) in a network being found together due to random chance. Scores of 2 or higher have at least a 99% likelihood of not being generated by chance alone.

In some cases, activation z-scores are used in the statistical analysis. This score identifies upstream regulators or pathways that can explain the observed gene expression changes in the dataset, by taking into account the direction (induced or reduced expression) and extent of change, and based on regulations known from the entire IPA database. Z-scores >2 predict activation of the upstream regulator, z-score <-2 predict inhibition.

Annexes

Annex 1: List of primers.

Experiments	Primer	Forward (5' -> 3')	Reverse (5' -> 3')
Housekeeping gene	gadph	GTGGAGTCTACTGGTGTCTTC	GTGCAGGAGGCATTGCTTACA
VitD3 and PTH	bglap	TCTTCCTGACTCCTCAGATACTAAAC	TTCCAGCCCTCTTCTGTCTC
	col1a1	CACAGAAGACCGGACCCTAC	CTTTGAGGCGAGGGAAGTT
	col1a2	CGTACTTGCCGTGACATCAG	GTCTGGCCAGTAGAGAAGTCG
	col10a1	TGCCCATGGTGAGAGATATG	GTGCCTGGTTCTCCTGCTAC
	dlx5a	CCAATACCACGGAGTCAATG	GCTGTGGAGTATGAGCCGTA
	dlx6a	AATCACCGTTTCCAGCAGAC	CGCCTTGTTTCAACAGCTTC
	osx	AAATCAGCTCGTGGTTCTGG	GCTGTGGACAGGTTTCTTCC
	pth1a	CAGGCCTCTGAGAAGCAAAC	GTTTCATCTGCAGCCAGTCC
	runx2b	GTGGCCACTTACCACAGAGC	TCGGAGAGTCATCCAGCTT
	sparc	AGGTGGAGACCGGAGAGTTT	CCCTTCTTGCAGTGATGGTT
	spp1	CGCCACAGTCTTCTGTGTACC	TTGAACAATTACAAGCTCTTCTGAG
VitD3 confirmation	cad	TCATTGGCGCAAAGACATAC	ACCCGTGATTCTGAGAGGTG
	cyp24a1	TGGAGATCAAACCATGGAAAG	CCGTCCAGCTTCATGACTTC
	fgf4	AAATCACCGGCGTACACAAC	CGTAAAGCTTCCCTTTGCTG
	igfbp1	TCCCGAGAGCTGGAGACC	AGCAGGTGATGCAGTGAGC
	slc26a3	AAGCCTACCGCAAACACAAG	CTTCATCCACCCAATGACAG
	slc6a18	AATGGGACAACAAGGTCCAG	CAGGTACGGGATCAGAAACG
	socs1	TGTATTGCCTGCTCTTGGAG	TGATTCCCTTCCACTGAACTG
PTH confirmation	fgf4	AAATCACCGGCGTACACAAC	CGTAAAGCTTCCCTTTGCTG
	mcph1	TACGCCAGCTCTGAAAAACC	AACATTCGGAGTTGGTCAGC
	ndrg2	AAGCACCAAACCTGCTCAAC	CTCGTACGGAGCCTGATCTC
	nrbp2	GCATCGAGAGTGCGTACTTG	TCCACCTGCATCAGGTCCTC
	rxra	GAGTGGGCGAAGAGGATTC	CCTGTGGCCAACAGTATTCC
	slc6a18	AATGGGACAACAAGGTCCAG	CAGGTACGGGATCAGAAACG
Clinostat Horizontal	fos b	TGCCGCTAAGTGTAGGAACC	CAGGCGCTCTTTCTCCTTC
	igfr2	CTTCGGATGACAGCCTATGG	ACAGACCGCACTTCCTTCTC
	mcph1	TACGCCAGCTCTGAAAAACC	AACATTCGGAGTTGGTCAGC
	ndrg2	AGCCTCGACAGGAACAACAC	AGCCATCTTGAGGAATGAGG
RPM	ehf	CCAGCCTAGCTCCATATTGC	TCTCGGATGAACTCCCAAAG
	elf3	GGAGTTGGGCAATCTGCTAC	TGGAGGGAAATGAGTTCTGC
	klf2	TGCACTTTTTCTGGATGTGG	TCCCAACTGCAATGATAGGG
RWV	igfbp1	TCCCGAGAGCTGGAGACC	AGCAGGTGATGCAGTGAGC
	socs3	GGGAAGACAAGAGCCGAGAC	ACACACCAAACCCTGAGCTG
Clinostat vertical	btg2	GGTGTTCAGAGACGGACTCG	GAGGGTCCATTTCATGGTTG
	fos b	TGCCGCTAAGTGTAGGAACC	CAGGCGCTCTTTCTCCTTC
	socs3	GGGAAGACAAGAGCCGAGAC	ACACACCAAACCCTGAGCTG
Confirmation in the Clinostat – RPM and RWV	col10a1	TGCCCATGGTGAGAGATATG	GTGCCTGGTTCTCCTGCTAC
	col1a2	CGTACTTGCCGTGACATCAG	GTCTGGCCAGTAGAGAAGTCG
	cyp24a1	TGGAGATCAAACCATGGAAAG	CCGTCCAGCTTCATGACTTC
	rhcga	CACCAGCGACATCGAGAAC	AGAAAGTTGAAGCCCACTGC
	rhcg2a	ATGCAAGGCTGGTTTCATTC	CAACCAGCCACACAGAAATC
Hypergravity 3g	nr1d1	CCGCAGTAGACACGAACAAC	CGAAGCAGGGTTGTGTAAGG
	rhcg	CGAGGAGGCAGACACTAACTG	CAGGAAGGTCATGAGGAACC
	socs1	TGTATTGCCTGCTCTTGGAG	TGATTCCCTTCCACTGAACTG
	spry4	ATCGCAACGACCTGTTCATC	AATGTGGTGAGGAACCCTTG
	txnip	GAGTCGGATGCGCTAAAGTC	CAGGCCTGAGAGTGATGGAG
Relative microgravity	btg2	GGTGTTCAGAGACGGACTCG	GAGGGTCCATTTCATGGTTG
	cebpb	TATGCAAGCAGCCAGTCAAC	TGGTACTGGGGCAAAGAGTC
	fos	GGTATTACCCGCTCAACCAG	TGACAGTTGGCACGAAAGAG
	fos b	TGCCGCTAAGTGTAGGAACC	CAGGCGCTCTTTCTCCTTC
	klf2	TGCACTTTTTCTGGATGTGG	TCCCAACTGCAATGATAGGG
	socs3	GGGAAGACAAGAGCCGAGAC	ACACACCAAACCCTGAGCTG

Annex 2: Morphometric analysis of cartilage staining after 5 days chemical treatments. A) VitD3. B) PTH.

A)

Measures	Variable	N	Mean	SD	t-test	p-value
Distance from anterior to ethmoid plate	Control	31	310.9	39.515		
	VitD3	29	320.7	38.272	0.972	0.335
Distance from anterior to posterior	Control	31	1545	56.317		
	VitD3	29	1575	73.543	1.809	0.076
Distance between articulation up and down	Control	31	417.6	34.617		
	VitD3	29	446.2	26.479	3.575	**0.001**
Distance between ceratohyal extern up and down	Control	31	560.8	54.211		
	VitD3	29	573	46.951	0.926	0.358
Distance between ceratohyal extern down and ceratohyal interne down	Control	31	424.2	30.502		
	VitD3	29	442.7	31.658	2.306	**0.025**
Distance between ceratohyal extern up and ceratohyal interne up	Control	31	425	33.554		
	VitD3	29	437.5	28.958	1.536	0.130
Distance from ethmoid plate to posterior	Control	31	1234	45.045		
	VitD3	29	1255	45.402	1.775	0.081
Distance between hyosymplectic up and down	Control	31	1027	21.992		
	VitD3	29	1035	24.864	1.311	0.195

B)

Measures	Variable	N	Mean	SD	t-test	p-value
Distance from anterior to ethmoid plate	Control	27	332	43.023		
	PTH	27	352.1	51.553	1.562	0.124
Distance from anterior to posterior	Control	27	1607	116.205		
	PTH	27	1674	93.267	2.326	**0.024**
Distance between articulation up and down	Control	27	422.1	23.700		
	PTH	27	423.4	39.286	0.150	0.882
Distance between ceratohyal extern up and down	Control	27	517.8	42.101		
	PTH	27	529.4	47.852	0.939	0.352
Distance between ceratohyal extern down and ceratohyal interne down	Control	27	422.7	25.761		
	PTH	27	455.5	34.946	3.935	**<0.001**
Distance between ceratohyal extern up and ceratohyal interne up	Control	27	424.2	30.818		
	PTH	27	461.6	31.515	4.409	**<0.001**
Distance from ethmoid plate to posterior	Control	27	1275	105.337		
	PTH	27	1322	62.540	1.975	0.054
Distance between hyosymplectic up and down	Control	27	1050	35.035		
	PTH	27	1029	35.736	2.178	**0.034**

Annex 3: Morphometric analysis of bone staining after 5 days chemical treatments. A) VitD3. B) PTH.

A)

Measures	Variable	N	Mean	SD	t-test	p-value
Distance between anguloarticular up and down	Control	28	471.8	33.498		
	VitD3	29	494.1	64.269	1 .631	0.109
Distance from anterior to notochord	Control	28	1259	57.947		
	VitD3	29	1311	83.214	2 .736	**0.008**
Distance from anterior to parasphenoid a	Control	28	389.5	46.610		
	VitD3	29	437.1	60.610	3 .318	**0.002**
Distance between branchiostegal ray1 up and down	Control	28	679.8	61.497		
	VitD3	29	690.6	104.412	0 .471	0.639
Distance between entopterygoid up and down	Control	28	333.2	20.546		
	VitD3	29	350.6	43.093	1 .931	0.059
Distance between maxilla up and down	Control	28	523.6	29.286		
	VitD3	29	562.5	39.448	4 .218	**<0 .001**
Distance between opercle up and down	Control	28	964.4	47.249		
	VitD3	29	978.2	73.215	0 .846	0.401
Triangle area of the parasphenoid	Control	28	66930	7809.626		
	VitD3	29	64410	9835.053	1 .070	0.289

B)

Measures	Variable	N	Mean	SD	t-test	p-value
Distance between anguloarticular up and down	Control	29	/	/		
	PTH	27	/	/	/	/
Distance from anterior to notochord	Control	29	1281	53.805		
	PTH	27	1283	52.719	0.105	0.917
Distance from anterior to parasphenoid a	Control	29	362.9	61.381		
	PTH	27	483.6	49.454	8.235	**<0.001**
Distance between branchiostegal ray1 up and down	Control	29	638.9	49.064		
	PTH	27	752.6	70.613	5.237	**<0.001**
Distance between entopterygoid up and down	Control	29	328	30.734		
	PTH	27	359	31.208	3.801	**<0.001**
Distance between maxilla up and down	Control	29	/	/		
	PTH	27	/	/	/	/
Distance between opercle up and down	Control	29	949.3	49.133		
	PTH	27	994.5	57.491	3.210	**0.002**
Triangle area of the parasphenoid	Control	29	71130	9182.696		
	PTH	27	56350	10371.666	5.747	**<0.001**

Annex 4: VitD3 microarrays by entrez gene name.

Symbol	Entrez Gene Name	Log Ratio VitD3	p-value	N	Type(s)
A2M	alpha-2-macroglobulin	-1,165	5,01E-02	D	transporter
A2M	alpha-2-macroglobulin	-1,793	6,14E-02	D	transporter
ACTR6	ARP6 actin-related protein 6 homolog (yeast)	-0,644	2,70E-02		transporter
AP1S1	adaptor-related protein complex 1, sigma 1 subunit	0,736	5,82E-02		transporter
APOA4	apolipoprotein A-IV	-1,756	1,63E-02	D	transporter
APOA4	apolipoprotein A-IV	-0,647	8,52E-02	D	transporter
APOA4	apolipoprotein A-IV	-1,392	1,22E-02	D	transporter
APOA4	apolipoprotein A-IV	-0,681	9,49E-02	D	transporter
ATP1A1	ATPase, Na+/K+ transporting, alpha 1 polypeptide	-0,385	7,00E-02		transporter
ATP2B3	ATPase, Ca++ transporting, plasma membrane 3	0,425	7,17E-02		transporter
ATP9B	ATPase, class II, type 9B	0,431	5,68E-02		transporter
CACNA2D2	calcium channel, voltage-dependent, alpha 2/delta subunit 2	0,384	4,79E-02		ion channel
CNGA3	cyclic nucleotide gated channel alpha 3	-0,613	4,55E-02		ion channel
FABP2	fatty acid binding protein 2, intestinal	-0,752	5,78E-02	D	transporter
FABP2	fatty acid binding protein 2, intestinal	-0,805	3,76E-02	D	transporter
FOLR1	folate receptor 1 (adult)	-1,087	2,01E-02	D	transporter
FOLR1	folate receptor 1 (adult)	-0,896	3,04E-02	D	transporter
GJB3	gap junction protein, beta 3, 31kDa	-0,483	6,57E-02		transporter
HBZ	hemoglobin, zeta	-0,594	4,10E-02	D	transporter
HBZ	hemoglobin, zeta	-0,488	3,19E-02	D	transporter
HBZ	hemoglobin, zeta	-0,629	9,27E-02	D	transporter
HBZ	hemoglobin, zeta	-0,669	8,67E-02	D	transporter
HBZ	hemoglobin, zeta	-0,673	9,16E-02	D	transporter
KCNMB2	potassium large conductance calcium-activated channel, subfamily M, beta member 2	-0,630	5,61E-02		ion channel
LDLR	low density lipoprotein receptor	-0,530	3,25E-02		transporter
MTTP	microsomal triglyceride transfer protein	-0,512	8,32E-02		transporter
PDZD3	PDZ domain containing 3	-0,903	5,77E-02		transporter
PEA15	phosphoprotein enriched in astrocytes 15	0,408	3,50E-02		transporter
PLLP	plasmolipin	-0,428	5,22E-02		transporter
Rrbp1	ribosome binding protein 1	-0,401	2,77E-02		transporter
SCN4B	sodium channel, voltage-gated, type IV, beta subunit	-0,412	3,16E-02		ion channel
SERINC5	serine incorporator 5	0,379	5,07E-02		transporter
SLC10A3	solute carrier family 10, member 3	0,474	9,07E-03		transporter
SLC11A2	solute carrier family 11 (proton-coupled divalent metal ion transporter), member 2	0,401	3,39E-02		transporter
SLC16A2	solute carrier family 16, member 2 (thyroid hormone transporter)	0,834	5,93E-02		transporter
SLC25A15	solute carrier family 25 (mitochondrial carrier; ornithine transporter) member 15	0,498	4,11E-02		transporter
SLC25A43	solute carrier family 25, member 43	-0,686	9,15E-02		transporter
SLC26A3	solute carrier family 26 (anion exchanger), member 3	-0,929	2,80E-02		transporter
SLC27A2	solute carrier family 27 (fatty acid transporter), member 2	-0,549	2,12E-02		transporter
SLC28A2	solute carrier family 28 (concentrative nucleoside transporter), member 2	-0,868	3,93E-02	D	transporter
SLC28A2	solute carrier family 28 (concentrative nucleoside transporter), member 2	-0,526	7,42E-02	D	transporter
SLC2A2	solute carrier family 2 (facilitated glucose transporter), member 2	-0,543	2,87E-02	D	transporter
SLC2A2	solute carrier family 2 (facilitated glucose transporter), member 2	-0,830	8,52E-02	D	transporter
SLC35A1	solute carrier family 35 (CMP-sialic acid transporter), member A1	0,420	6,18E-02		transporter
SLC37A4	solute carrier family 37 (glucose-6-phosphate transporter), member 4	-0,400	9,73E-02		transporter
SLC43A1	solute carrier family 43 (amino acid system L transporter), member 1	-1,042	2,47E-02	D	transporter
SLC43A1	solute carrier family 43 (amino acid system L transporter), member 1	-0,998	1,09E-02	D	transporter
SLC43A1	solute carrier family 43 (amino acid system L transporter), member 1	-1,069	3,46E-02	D	transporter
SLC43A1	solute carrier family 43 (amino acid system L transporter), member 1	-1,074	3,80E-02	D	transporter
SLC5A2	solute carrier family 5 (sodium/glucose cotransporter), member 2	-0,451	5,70E-02		transporter
SLC5A9	solute carrier family 5 (sodium/sugar cotransporter), member 9	-0,744	2,82E-02		transporter
SLC6A18	solute carrier family 6 (neutral amino acid transporter), member 18	-0,461	2,93E-02		transporter

SLC6A19	solute carrier family 6 (neutral amino acid transporter), member 19	-0,769	2,22E-02		transporter
SLC6A9	solute carrier family 6 (neurotransmitter transporter, glycine), member 9	0,390	6,83E-02		transporter
SLC7A3	solute carrier family 7 (cationic amino acid transporter, y+ system), member 3	0,465	7,70E-02		transporter
SYT15	synaptotagmin XV	-0,380	5,80E-02		transporter
TCN2	transcobalamin II	-0,476	5,10E-02		transporter
TF	transferrin	-1,122	1,45E-02	D	transporter
TF	transferrin	-1,179	2,34E-02	D	transporter
TF	transferrin	-1,289	9,25E-03	D	transporter
TF	transferrin	-0,959	1,04E-02	D	transporter
TF	transferrin	-1,132	1,15E-02	D	transporter
TF	transferrin	-1,152	3,26E-02	D	transporter
TF	transferrin	-1,138	9,54E-03	D	transporter
Tmed11	transmembrane emp24 protein transport domain containing	-0,717	3,17E-02		transporter
TTPA	tocopherol (alpha) transfer protein	-0,426	9,78E-02		transporter
TTYH3	tweety family member 3	0,402	7,16E-02		ion channel
ZP3	zona pellucida glycoprotein 3 (sperm receptor)	-0,788	3,73E-02		transporter
ABRA	actin-binding Rho activating protein	-0,848	7,28E-02		transcription regulator
ANKRD33	ankyrin repeat domain 33	-0,547	7,27E-02		transcription regulator
ATF4	activating transcription factor 4	0,453	9,66E-02		transcription regulator
BCL6	B-cell CLL/lymphoma 6	0,525	4,10E-02		transcription regulator
CALCOCO1	calcium binding and coiled-coil domain 1	-1,011	8,40E-02		transcription regulator
CNBP	CCHC-type zinc finger, nucleic acid binding protein	-0,585	2,01E-02	D	transcription regulator
CNBP	CCHC-type zinc finger, nucleic acid binding protein	-0,531	3,29E-02	D	transcription regulator
CNBP	CCHC-type zinc finger, nucleic acid binding protein	-0,468	5,01E-02	D	transcription regulator
ETV4	ets variant 4	0,423	4,87E-02		transcription regulator
FOSB	FBJ murine osteosarcoma viral oncogene homolog B	-0,988	7,37E-02		transcription regulator
FOXK1	forkhead box K1	0,426	6,79E-02		transcription regulator
FOXO3	forkhead box O3	-0,386	4,34E-02	D	transcription regulator
FOXO3	forkhead box O3	-0,507	7,90E-02	D	transcription regulator
FOXO3	forkhead box O3	-0,401	4,36E-02	D	transcription regulator
FOXQ1	forkhead box Q1	0,692	4,92E-02		transcription regulator
GATA6	GATA binding protein 6	-0,460	8,38E-02		transcription regulator
GSPT1	G1 to S phase transition 1	0,438	8,68E-02		translation regulator
HIF3A	hypoxia inducible factor 3, alpha subunit	0,476	2,53E-02	D	transcription regulator
HIF3A	hypoxia inducible factor 3, alpha subunit	0,482	6,22E-02	D	transcription regulator
HIF3A	hypoxia inducible factor 3, alpha subunit	0,387	8,16E-02	D	transcription regulator
KLF11	Kruppel-like factor 11	1,451	2,42E-02	D	transcription regulator
KLF11	Kruppel-like factor 11	2,629	8,99E-03	D	transcription regulator
KLF13	Kruppel-like factor 13	1,185	2,28E-02	D	transcription regulator
KLF13	Kruppel-like factor 13	1,032	3,64E-02	D	transcription regulator
MEIS2	Meis homeobox 2	0,393	3,99E-02		transcription regulator
MYC	v-myc avian myelocytomatosis viral oncogene homolog	-0,443	8,64E-02		transcription regulator
MYOG	myogenin (myogenic factor 4)	-0,545	1,07E-02		transcription

					regulator
NCOA4	nuclear receptor coactivator 4	0,464	3,89E-02	D	transcription regulator
NCOA4	nuclear receptor coactivator 4	0,467	3,06E-02	D	transcription regulator
NR0B2	nuclear receptor subfamily 0, group B, member 2	0,631	2,65E-02		ligand-dependent nuclear receptor
NRARP	NOTCH-regulated ankyrin repeat protein	0,528	8,64E-02	D	transcription regulator
NRARP	NOTCH-regulated ankyrin repeat protein	0,473	8,63E-02	D	transcription regulator
PPARA	peroxisome proliferator-activated receptor alpha	-0,556	2,94E-02		ligand-dependent nuclear receptor
RYBP	RING1 and YY1 binding protein	0,707	4,61E-02	D	transcription regulator
RYBP	RING1 and YY1 binding protein	0,548	7,74E-02	D	transcription regulator
SMARCC1	SWI/SNF related, matrix associated, actin dependent regulator of chromatin, subfamily c, member 1	0,516	8,92E-02	D	transcription regulator
SMARCC1	SWI/SNF related, matrix associated, actin dependent regulator of chromatin, subfamily c, member 1	0,578	6,43E-02	D	transcription regulator
SOX4	SRY (sex determining region Y)-box 4	0,459	4,76E-02	D	transcription regulator
SOX4	SRY (sex determining region Y)-box 4	0,395	2,72E-02	D	transcription regulator
SOX4	SRY (sex determining region Y)-box 4	0,480	9,74E-02	D	transcription regulator
STAT3	signal transducer and activator of transcription 3 (acute-phase response factor)	0,471	1,22E-02		transcription regulator
TWIST1	twist family bHLH transcription factor 1	-0,416	7,22E-02		transcription regulator
ZNF423	zinc finger protein 423	0,557	5,30E-02		transcription regulator
ADRB2	adrenoceptor beta 2, surface	-0,603	2,52E-02		G-protein coupled receptor
CD36	CD36 molecule (thrombospondin receptor)	-0,421	7,09E-02		transmembrane receptor
CUBN	cubilin (intrinsic factor-cobalamin receptor)	-0,444	3,16E-02		transmembrane receptor
GPC1	glypican 1	0,535	2,44E-02	D	transmembrane receptor
GPC1	glypican 1	0,376	2,86E-02	D	transmembrane receptor
GPR112	G protein-coupled receptor 112	-0,595	7,88E-02		G-protein coupled receptor
GPR139	G protein-coupled receptor 139	0,556	3,32E-03		G-protein coupled receptor
ITGB4	integrin, beta 4	0,535	2,90E-02		transmembrane receptor
LYVE1	lymphatic vessel endothelial hyaluronan receptor 1	0,806	6,75E-02		transmembrane receptor
OPN1LW	opsin 1 (cone pigments), long-wave-sensitive	-1,538	3,33E-03		G-protein coupled receptor
OPRL1	opiate receptor-like 1	-0,613	4,39E-02		G-protein coupled receptor
PGRMC1	progesterone receptor membrane component 1	-0,388	4,56E-02		transmembrane receptor
RELT	RELT tumor necrosis factor receptor	0,460	6,03E-02		transmembrane receptor
C5	complement component 5	0,543	8,88E-04		cytokine
EBI3	Epstein-Barr virus induced 3	-1,268	3,77E-02	D	cytokine
EBI3	Epstein-Barr virus induced 3	-1,512	3,66E-02	D	cytokine
IGF2	insulin-like growth factor 2 (somatomedin A)	0,761	9,30E-03		growth factor
PDGFC	platelet derived growth factor C	0,592	8,87E-02		growth factor
BAIAP2	BAI1-associated protein 2	0,381	3,52E-03		kinase

BCKDK	branched chain ketoacid dehydrogenase kinase	-0,413	7,09E-02		kinase
CDKN3	cyclin-dependent kinase inhibitor 3	-0,445	6,96E-02		phosphatase
CHKA	choline kinase alpha	-0,509	4,48E-02		kinase
EEF2K	eukaryotic elongation factor-2 kinase	-0,414	2,01E-02		kinase
FBP1	fructose-1,6-bisphosphatase 1	-0,551	8,30E-02	D	phosphatase
FBP1	fructose-1,6-bisphosphatase 1	-0,384	8,33E-02	D	phosphatase
FBP1	fructose-1,6-bisphosphatase 1	-0,556	7,13E-02	D	phosphatase
GNE	glucosamine (UDP-N-acetyl)-2-epimerase/N-acetylmannosamine kinase	-0,400	3,30E-02		kinase
GRK7	G protein-coupled receptor kinase 7	-0,752	6,95E-02	D	kinase
GRK7	G protein-coupled receptor kinase 7	-0,618	8,45E-02	D	kinase
LPIN1	lipin 1	-1,165	6,70E-02	D	phosphatase
LPIN1	lipin 1	-1,208	6,14E-02	D	phosphatase
LPIN1	lipin 1	-1,370	6,74E-02	D	phosphatase
MEX3B	mex-3 RNA binding family member B	0,548	8,21E-02	D	kinase
MEX3B	mex-3 RNA binding family member B	0,508	6,91E-02	D	kinase
NRBP2	nuclear receptor binding protein 2	-0,477	7,35E-02		kinase
OBSCN	obscurin, cytoskeletal calmodulin and titin-interacting RhoGEF	-0,382	5,35E-02		kinase
PCK1	phosphoenolpyruvate carboxykinase 1 (soluble)	0,511	8,54E-02	D	kinase
PCK1	phosphoenolpyruvate carboxykinase 1 (soluble)	0,577	8,54E-02	D	kinase
PCK2	phosphoenolpyruvate carboxykinase 2 (mitochondrial)	-0,632	1,94E-02	D	kinase
PCK2	phosphoenolpyruvate carboxykinase 2 (mitochondrial)	-0,668	2,59E-02	D	kinase
PDK2	pyruvate dehydrogenase kinase, isozyme 2	-0,622	1,45E-02	D	kinase
PDK2	pyruvate dehydrogenase kinase, isozyme 2	-0,700	3,27E-02	D	kinase
PDK2	pyruvate dehydrogenase kinase, isozyme 2	-0,475	5,08E-02	D	kinase
PDK4	pyruvate dehydrogenase kinase, isozyme 4	-0,455	4,37E-02		kinase
PHKA1	phosphorylase kinase, alpha 1 (muscle)	-0,449	5,97E-02		kinase
PIK3R1	phosphoinositide-3-kinase, regulatory subunit 1 (alpha)	-0,450	9,29E-02		kinase
PIM1	pim-1 oncogene	0,678	2,57E-02		kinase
PKLR	pyruvate kinase, liver and RBC	-0,759	6,79E-02	D	kinase
PKLR	pyruvate kinase, liver and RBC	-0,688	8,46E-02	D	kinase
PKLR	pyruvate kinase, liver and RBC	-0,701	9,77E-02	D	kinase
PKLR	pyruvate kinase, liver and RBC	-0,874	1,17E-02	D	kinase
PPM1H	protein phosphatase, Mg2+/Mn2+ dependent, 1H	0,446	2,87E-02		phosphatase
PPP4C	protein phosphatase 4, catalytic subunit	0,401	7,85E-03		phosphatase
PTP4A3	protein tyrosine phosphatase type IVA, member 3	0,583	4,67E-02	D	phosphatase
PTP4A3	protein tyrosine phosphatase type IVA, member 3	0,478	6,33E-02	D	phosphatase
STK19	serine/threonine kinase 19	-0,456	3,89E-02		kinase
STK39	serine threonine kinase 39	-0,426	6,98E-03	D	kinase
STK39	serine threonine kinase 39	-0,545	4,04E-02	D	kinase
TPK1	thiamin pyrophosphokinase 1	-0,481	1,69E-02		kinase
TTN	titin	-0,522	6,08E-03	D	kinase
TTN	titin	-0,424	6,24E-02	D	kinase
TTN	titin	-0,578	3,95E-02	D	kinase
TTN	titin	-0,375	2,22E-02	D	kinase
TWF2	twinfilin actin-binding protein 2	-0,418	5,80E-02		kinase
ACE2	angiotensin I converting enzyme 2	-0,407	5,38E-02		peptidase
ANPEP	alanyl (membrane) aminopeptidase	-0,444	1,22E-02		peptidase
CNDP2	CNDP dipeptidase 2 (metallopeptidase M20 family)	-0,540	4,32E-02		peptidase
CPA2	carboxypeptidase A2 (pancreatic)	-0,640	8,02E-02		peptidase
CTRB2	chymotrypsinogen B2	-0,791	4,38E-02		peptidase
CTSH	cathepsin H	-0,407	3,05E-02		peptidase
CTSS	cathepsin S	0,377	4,77E-02		peptidase
DPP4	dipeptidyl-peptidase 4	-0,628	4,78E-02		peptidase
EPHX1	epoxide hydrolase 1, microsomal (xenobiotic)	-0,725	9,10E-03	D	peptidase
EPHX1	epoxide hydrolase 1, microsomal (xenobiotic)	-0,625	1,93E-02	D	peptidase
F7	coagulation factor VII (serum prothrombin conversion accelerator)	-0,569	6,00E-02		peptidase
F9	coagulation factor IX	0,668	9,22E-03		peptidase
HABP2	hyaluronan binding protein 2	-1,004	6,57E-02		peptidase
LONP1	lon peptidase 1, mitochondrial	0,447	7,49E-02		peptidase
MMP11	matrix metallopeptidase 11 (stromelysin 3)	0,883	5,26E-03		peptidase

PAPPA	pregnancy-associated plasma protein A, pappalysin 1	0,723	3,21E-02	D	peptidase
PAPPA	pregnancy-associated plasma protein A, pappalysin 1	0,588	4,75E-02	D	peptidase
PEPD	peptidase D	-0,461	6,22E-02	D	peptidase
PEPD	peptidase D	-0,407	4,87E-03	D	peptidase
TMPRSS13	transmembrane protease, serine 13	0,378	3,67E-02		peptidase
USP14	ubiquitin specific peptidase 14 (tRNA-guanine transglycosylase)	0,491	5,08E-03		peptidase
USP37	ubiquitin specific peptidase 37	0,387	8,75E-02		peptidase
AASDHPPT	aminoadipate-semialdehyde dehydrogenase-phosphopantetheinyl transferase	-0,541	4,88E-02	D	enzyme
AASDHPPT	aminoadipate-semialdehyde dehydrogenase-phosphopantetheinyl transferase	-0,609	5,49E-02	D	enzyme
ACAA1	acetyl-CoA acyltransferase 1	-0,413	2,26E-02	D	enzyme
ACAA1	acetyl-CoA acyltransferase 1	-0,473	3,14E-02	D	enzyme
ACADS	acyl-CoA dehydrogenase, C-2 to C-3 short chain	-0,389	2,18E-02		enzyme
ACOX1	acyl-CoA oxidase 1, palmitoyl	-0,845	6,53E-02		enzyme
ACSF2	acyl-CoA synthetase family member 2	-0,494	2,08E-02		enzyme
ACSL3	acyl-CoA synthetase long-chain family member 3	0,467	6,01E-02		enzyme
ACTA1	actin, alpha 1, skeletal muscle	-0,526	3,90E-02	D	other
ACTA1	actin, alpha 1, skeletal muscle	-0,621	8,67E-02	D	other
ACTA1	actin, alpha 1, skeletal muscle	-0,628	3,00E-02	D	other
ACTA1	actin, alpha 1, skeletal muscle	-0,446	4,16E-02	D	other
ACTA1	actin, alpha 1, skeletal muscle	-0,694	7,54E-02	D	other
ACTA1	actin, alpha 1, skeletal muscle	-0,591	1,61E-02	D	other
AGMAT	agmatine ureohydrolase (agmatinase)	-0,429	5,74E-02		enzyme
AKR1B1	aldo-keto reductase family 1, member B1 (aldose reductase)	-0,385	3,86E-02		enzyme
ALAS2	aminolevulinate, delta-, synthase 2	-0,682	4,22E-02	D	enzyme
ALAS2	aminolevulinate, delta-, synthase 2	-0,565	7,58E-02	D	enzyme
ALDH4A1	aldehyde dehydrogenase 4 family, member A1	-0,460	1,67E-02		enzyme
ANXA2	annexin A2	-0,786	7,11E-02	D	other
ANXA2	annexin A2	-0,597	3,78E-02	D	other
ANXA2	annexin A2	-0,660	6,56E-02	D	other
AOC1	amine oxidase, copper containing 1	-0,684	4,09E-02		enzyme
ARMC2	armadillo repeat containing 2	-0,495	7,47E-02		other
ARRDC2	arrestin domain containing 2	0,376	3,89E-02		other
ATAD2B	ATPase family, AAA domain containing 2B	0,446	5,54E-02		other
ATAD3A	ATPase family, AAA domain containing 3A	0,380	5,92E-03		other
BCAT2	branched chain amino-acid transaminase 2, mitochondrial	-0,638	2,30E-02	D	enzyme
BCAT2	branched chain amino-acid transaminase 2, mitochondrial	-0,636	4,97E-02	D	enzyme
BCAT2	branched chain amino-acid transaminase 2, mitochondrial	-0,453	8,24E-02	D	enzyme
BNIP3	BCL2/adenovirus E1B 19kDa interacting protein 3	-0,599	4,91E-02		other
BOC	BOC cell adhesion associated, oncogene regulated	-0,556	2,27E-02		other
C4orf33	chromosome 4 open reading frame 33	-0,376	3,97E-02		other
C6	complement component 6	0,418	5,60E-03		other
C7	complement component 7	0,665	8,71E-02		other
CA7	carbonic anhydrase VII	-0,566	4,59E-02		enzyme
CAD	carbamoyl-phosphate synthetase 2, aspartate transcarbamylase, and dihydroorotase	0,510	9,35E-02		enzyme
CADPS	Ca++-dependent secretion activator	-0,443	8,96E-02		other
CAT	catalase	-0,515	1,71E-02	D	enzyme
CAT	catalase	-0,423	8,00E-02	D	enzyme
CCBL2	cysteine conjugate-beta lyase 2	-0,381	4,82E-02		enzyme
CCDC125	coiled-coil domain containing 125	-0,380	7,53E-02		other
CEACAM20	carcinoembryonic antigen-related cell adhesion molecule 20	-0,549	6,26E-02		other
CEP85	centrosomal protein 85kDa	-0,511	9,95E-02		other
CES1	carboxylesterase 1	-2,047	4,85E-02	D	enzyme
CES1	carboxylesterase 1	-2,244	4,64E-02	D	enzyme
CFH	complement factor H	-1,151	7,01E-02		other
CHD8	chromodomain helicase DNA binding protein 8	0,382	3,18E-02		enzyme
CHPT1	choline phosphotransferase 1	-0,441	2,47E-02		enzyme
CHST2	carbohydrate (N-acetylglucosamine-6-O) sulfotransferase 2	-0,429	7,11E-02		enzyme
CISH	cytokine inducible SH2-containing protein	-1,615	7,77E-02	D	other
CISH	cytokine inducible SH2-containing protein	-1,269	3,92E-02	D	other

CISH	cytokine inducible SH2-containing protein	-1,294	5,72E-02	D	other
CISH	cytokine inducible SH2-containing protein	-1,261	4,79E-02	D	other
CISH	cytokine inducible SH2-containing protein	-1,779	4,33E-02	D	other
CISH	cytokine inducible SH2-containing protein	-1,260	3,41E-02	D	other
CISH	cytokine inducible SH2-containing protein	-0,983	6,59E-02	D	other
CLEC4E	C-type lectin domain family 4, member E	0,422	7,50E-02	D	other
CLEC4E	C-type lectin domain family 4, member E	0,443	7,01E-02	D	other
COL9A2	collagen, type IX, alpha 2	-0,417	5,61E-02		other
CREB3L3	cAMP responsive element binding protein 3-like 3	-0,475	1,42E-02		other
CROT	carnitine O-octanoyltransferase	-1,574	5,98E-02		enzyme
CTDSPL	CTD (carboxy-terminal domain, RNA polymerase II, polypeptide A) small phosphatase-like	0,496	1,93E-02	D	other
CTDSPL	CTD (carboxy-terminal domain, RNA polymerase II, polypeptide A) small phosphatase-like	0,558	5,62E-02	D	other
CTH	cystathionase (cystathionine gamma-lyase)	-0,581	3,92E-02	D	enzyme
CTH	cystathionase (cystathionine gamma-lyase)	-0,536	7,30E-02	D	enzyme
CUZD1	CUB and zona pellucida-like domains 1	-0,562	7,23E-02	D	other
CUZD1	CUB and zona pellucida-like domains 1	-0,629	4,81E-02	D	other
CYB5R2	cytochrome b5 reductase 2	-0,437	2,99E-02		enzyme
CYP24A1	cytochrome P450, family 24, subfamily A, polypeptide 1	2,955	2,87E-03	D	enzyme
CYP24A1	cytochrome P450, family 24, subfamily A, polypeptide 1	3,160	5,18E-03	D	enzyme
CYP26A1	cytochrome P450, family 26, subfamily A, polypeptide 1	0,830	5,03E-02	D	enzyme
CYP26A1	cytochrome P450, family 26, subfamily A, polypeptide 1	0,779	2,02E-02	D	enzyme
CYP27A1	cytochrome P450, family 27, subfamily A, polypeptide 1	-0,477	7,42E-02		enzyme
Cyp2ac1	cytochrome P450, family 2, subfamily ac, polypeptide 1	0,836	1,74E-02	D	other
Cyp2ac1	cytochrome P450, family 2, subfamily ac, polypeptide 1	-0,639	9,50E-02	D	other
Cyp2ac1	cytochrome P450, family 2, subfamily ac, polypeptide 1	1,134	1,52E-02	D	other
Cyp2ac1	cytochrome P450, family 2, subfamily ac, polypeptide 1	-0,605	1,88E-02	D	other
Cyp2ac1	cytochrome P450, family 2, subfamily ac, polypeptide 1	1,069	8,69E-02	D	other
Cyp2g1	cytochrome P450, family 2, subfamily g, polypeptide 1	-0,375	5,17E-02	D	enzyme
Cyp2g1	cytochrome P450, family 2, subfamily g, polypeptide 1	-0,457	9,67E-02	D	enzyme
CYP2J2	cytochrome P450, family 2, subfamily J, polypeptide 2	-1,015	6,16E-02		enzyme
CYP3A7	cytochrome P450, family 3, subfamily A, polypeptide 7	-0,911	8,51E-02	D	enzyme
CYP3A7	cytochrome P450, family 3, subfamily A, polypeptide 7	-0,414	2,54E-02	D	enzyme
CYP8B1	cytochrome P450, family 8, subfamily B, polypeptide 1	-0,686	2,20E-02		enzyme
D1Pas1	DNA segment, Chr 1, Pasteur Institute 1	0,411	1,52E-02		other
DAO	D-amino-acid oxidase	-0,464	1,11E-02	D	enzyme
DAO	D-amino-acid oxidase	-0,576	5,06E-02	D	enzyme
DBT	dihydrolipoamide branched chain transacylase E2	-0,458	2,62E-02	D	enzyme
DBT	dihydrolipoamide branched chain transacylase E2	-0,422	4,47E-02	D	enzyme
DCLRE1B	DNA cross-link repair 1B	-0,422	3,50E-02		enzyme
DCT	dopachrome tautomerase	-0,431	1,24E-02	D	enzyme
DCT	dopachrome tautomerase	-0,410	3,93E-02	D	enzyme
DDC	dopa decarboxylase (aromatic L-amino acid decarboxylase)	-0,542	9,33E-02		enzyme
DDT	D-dopachrome tautomerase	-0,627	4,14E-02		enzyme
DDX5	DEAD (Asp-Glu-Ala-Asp) box helicase 5	0,576	9,21E-02		enzyme
DECR1	2,4-dienoyl CoA reductase 1, mitochondrial	-0,562	4,76E-02		enzyme
DHRS13	dehydrogenase/reductase (SDR family) member 13	-0,607	9,83E-02		enzyme
DHTKD1	dehydrogenase E1 and transketolase domain containing 1	-1,004	5,69E-02	D	enzyme
DHTKD1	dehydrogenase E1 and transketolase domain containing 1	-0,830	6,43E-02	D	enzyme
DHX32	DEAH (Asp-Glu-Ala-His) box polypeptide 32	0,733	2,25E-02		enzyme
DIO1	deiodinase, iodothyronine, type I	-0,573	4,26E-03	D	enzyme
DIO1	deiodinase, iodothyronine, type I	-0,609	8,94E-02	D	enzyme
DMGDH	dimethylglycine dehydrogenase	-0,462	1,64E-02		enzyme
DMRT1	doublesex and mab-3 related transcription factor 1	-0,834	2,21E-02		other
DNAJC4	DnaJ (Hsp40) homolog, subfamily C, member 4	-0,446	8,95E-02		other
DNMT3A	DNA (cytosine-5-)-methyltransferase 3 alpha	0,516	9,87E-03		enzyme
DOLPP1	dolichyldiphosphatase 1	0,390	4,27E-02		enzyme
DPYS	dihydropyrimidinase	-0,402	7,06E-02		enzyme
ELOVL2	ELOVL fatty acid elongase 2	-0,449	3,45E-02		enzyme
ETNPPL	ethanolamine-phosphate phospho-lyase	-0,751	9,08E-02		enzyme
FADS6	fatty acid desaturase 6	1,083	3,19E-02		enzyme

FAM131C	family with sequence similarity 131, member C	0,503	6,11E-02		other
FAM13A	family with sequence similarity 13, member A	-0,421	2,66E-02		other
FAM46C	family with sequence similarity 46, member C	-0,601	3,17E-02	D	other
FAM46C	family with sequence similarity 46, member C	-0,443	1,38E-02	D	other
FBXO2	F-box protein 2	-0,613	2,09E-03		enzyme
FCGBP	Fc fragment of IgG binding protein	-0,687	5,23E-02		other
FSTL1	follistatin-like 1	0,455	9,56E-03		other
GADD45A	growth arrest and DNA-damage-inducible, alpha	0,396	9,17E-02	D	other
GADD45A	growth arrest and DNA-damage-inducible, alpha	-0,941	4,59E-02	D	other
GADD45A	growth arrest and DNA-damage-inducible, alpha	-0,844	4,88E-02	D	other
GATM	glycine amidinotransferase (L-arginine:glycine amidinotransferase)	0,435	4,89E-02	D	enzyme
GATM	glycine amidinotransferase (L-arginine:glycine amidinotransferase)	0,377	5,33E-02	D	enzyme
GATM	glycine amidinotransferase (L-arginine:glycine amidinotransferase)	0,417	4,60E-02	D	enzyme
GCAT	glycine C-acetyltransferase	-0,904	2,06E-02		enzyme
GCG	glucagon	-0,492	2,42E-02		other
GCHFR	GTP cyclohydrolase I feedback regulator	-0,928	4,35E-02		other
GDA	guanine deaminase	-0,524	5,50E-02		enzyme
GGCT	gamma-glutamylcyclotransferase	0,627	3,80E-02		enzyme
GLDC	glycine dehydrogenase (decarboxylating)	-0,505	6,31E-02	D	enzyme
GLDC	glycine dehydrogenase (decarboxylating)	-0,586	2,13E-02	D	enzyme
GLDC	glycine dehydrogenase (decarboxylating)	-0,515	4,58E-02	D	enzyme
GNG10	guanine nucleotide binding protein (G protein), gamma 10	-0,561	7,18E-03		enzyme
GNPDA2	glucosamine-6-phosphate deaminase 2	0,813	2,85E-02		enzyme
GOT2	glutamic-oxaloacetic transaminase 2, mitochondrial	-0,468	2,78E-02		enzyme
GPT	glutamic-pyruvate transaminase (alanine aminotransferase)	0,392	5,25E-02	D	enzyme
GPT	glutamic-pyruvate transaminase (alanine aminotransferase)	0,590	6,83E-02	D	enzyme
GPT	glutamic-pyruvate transaminase (alanine aminotransferase)	0,490	3,04E-02	D	enzyme
GPT	glutamic-pyruvate transaminase (alanine aminotransferase)	0,632	9,35E-02	D	enzyme
GPX1	glutathione peroxidase 1	-0,770	2,77E-02		enzyme
GRB10	growth factor receptor-bound protein 10	-1,053	2,88E-02		other
GSR	glutathione reductase	0,377	6,52E-02		enzyme
GSTK1	glutathione S-transferase kappa 1	-0,415	1,97E-02		enzyme
GSTO1	glutathione S-transferase omega 1	-0,470	7,39E-02		enzyme
Gstt3	glutathione S-transferase, theta 3	0,410	1,45E-02		enzyme
HADH	hydroxyacyl-CoA dehydrogenase	-0,409	1,09E-02		enzyme
HAGH	hydroxyacylglutathione hydrolase	-0,501	2,77E-02		enzyme
HAO2	hydroxyacid oxidase 2 (long chain)	-0,441	6,52E-02		enzyme
HGD	homogentisate 1,2-dioxygenase	-0,534	7,20E-02		enzyme
HMCES	5-hydroxymethylcytosine (hmC) binding, ES cell-specific	-0,540	6,37E-02		other
HMGCL	3-hydroxymethyl-3-methylglutaryl-CoA lyase	-0,374	2,07E-02		enzyme
HNMT	histamine N-methyltransferase	-0,431	1,15E-02		enzyme
HPD	4-hydroxyphenylpyruvate dioxygenase	-0,543	8,16E-02		enzyme
HSD11B1L	hydroxysteroid (11-beta) dehydrogenase 1-like	-0,698	4,07E-02		other
HSD11B2	hydroxysteroid (11-beta) dehydrogenase 2	-0,408	5,70E-02		enzyme
HSD17B4	hydroxysteroid (17-beta) dehydrogenase 4	-0,450	4,12E-02		enzyme
HSD3B7	hydroxy-delta-5-steroid dehydrogenase, 3 beta- and steroid delta-isomerase 7	-0,406	4,16E-02		enzyme
HSP90B1	heat shock protein 90kDa beta (Grp94), member 1	0,467	7,45E-02	D	other
HSP90B1	heat shock protein 90kDa beta (Grp94), member 1	0,486	4,70E-02	D	other
IFRD1	interferon-related developmental regulator 1	0,507	3,92E-02		other
IGFBP1	insulin-like growth factor binding protein 1	1,077	3,38E-02	D	other
IGFBP1	insulin-like growth factor binding protein 1	1,774	4,67E-03	D	other
IGFBP1	insulin-like growth factor binding protein 1	1,109	2,40E-02	D	other
IGFBP1	insulin-like growth factor binding protein 1	1,120	4,72E-02	D	other
IGFBP1	insulin-like growth factor binding protein 1	1,919	3,90E-03	D	other
ING5	inhibitor of growth family, member 5	-0,734	4,22E-02		other
INSIG1	insulin induced gene 1	0,616	4,79E-02		other
IRS1	insulin receptor substrate 1	0,816	2,28E-03		enzyme
ITIH3	inter-alpha-trypsin inhibitor heavy chain 3	-0,514	9,64E-02	D	other
ITIH3	inter-alpha-trypsin inhibitor heavy chain 3	-0,528	5,99E-02	D	other

ITLN1	intelectin 1 (galactofuranose binding)	-1,274	4,88E-02		other
JAKMIP1	janus kinase and microtubule interacting protein 1	0,546	1,39E-03		other
KIAA1324	KIAA1324	-0,623	8,12E-02		other
KRT17	keratin 17	0,499	2,06E-02	D	other
KRT17	keratin 17	0,444	8,65E-02	D	other
KRT17	keratin 17	0,393	7,13E-02	D	other
KRT17	keratin 17	0,520	2,04E-02	D	other
LCT	lactase	-1,104	3,59E-02		enzyme
LECT1	leukocyte cell derived chemotaxin 1	-0,532	9,60E-02		other
LOC285556	uncharacterized LOC285556	0,570	8,68E-02		other
LOX	lysyl oxidase	0,459	6,99E-02		enzyme
LPL	lipoprotein lipase	-0,851	6,88E-02	D	enzyme
LPL	lipoprotein lipase	-0,865	9,87E-02	D	enzyme
MALRD1	MAM and LDL receptor class A domain containing 1	-0,909	3,42E-02		other
MBOAT4	membrane bound O-acyltransferase domain containing 4	-0,404	7,76E-02		enzyme
MCM7	minichromosome maintenance complex component 7	0,373	5,31E-02		enzyme
Mettl21e	methyltransferase like 21E	-0,381	9,44E-02		other
METTL7A	methyltransferase like 7A	-0,512	1,11E-02		other
MFSD4	major facilitator superfamily domain containing 4	-0,447	5,27E-02		other
MID1	midline 1 (Opitz/BBB syndrome)	0,400	5,27E-02		other
MIOX	myo-inositol oxygenase	1,245	1,48E-02		enzyme
MLEC	malectin	-0,396	2,20E-02		other
MOCS1	molybdenum cofactor synthesis 1	-0,755	6,52E-02		other
MOGAT1	monoacylglycerol O-acyltransferase 1	-0,395	9,35E-02	D	enzyme
MOGAT1	monoacylglycerol O-acyltransferase 1	-0,588	4,41E-02	D	enzyme
MOV10L1	Mov10l1, Moloney leukemia virus 10-like 1, homolog (mouse)	0,518	4,63E-03		enzyme
MYH11	myosin, heavy chain 11, smooth muscle	-0,524	8,62E-02		other
MYH7	myosin, heavy chain 7, cardiac muscle, beta	0,479	7,96E-02	D	enzyme
MYH7	myosin, heavy chain 7, cardiac muscle, beta	0,441	7,32E-02	D	enzyme
MYL3	myosin, light chain 3, alkali; ventricular, skeletal, slow	-0,396	4,13E-02		other
NEFL	neurofilament, light polypeptide	0,483	5,76E-02	D	other
NEFL	neurofilament, light polypeptide	0,497	3,51E-02	D	other
NEFL	neurofilament, light polypeptide	0,562	6,86E-02	D	other
NEIL1	nei endonuclease VIII-like 1 (E, coli)	-0,373	5,13E-02		enzyme
NEURL2	neuralized E3 ubiquitin protein ligase 2	-0,459	3,82E-02	D	other
NEURL2	neuralized E3 ubiquitin protein ligase 2	-0,492	3,83E-02	D	other
NID1	nidogen 1	-0,453	8,81E-02	D	other
NID1	nidogen 1	-0,674	5,18E-02	D	other
NIPSNAP3A	nipsnap homolog 3A (C, elegans)	-0,391	6,85E-02		other
NLGN4Y	neuroligin 4, Y-linked	0,380	9,36E-02		enzyme
NPHP3	nephronophthisis 3 (adolescent)	-0,420	4,03E-02		other
NUDT16	nudix (nucleoside diphosphate linked moiety X)-type motif 16	-0,420	6,90E-02		enzyme
OLFM4	olfactomedin 4	-0,842	4,73E-02	D	other
OLFM4	olfactomedin 4	-0,811	2,84E-03	D	other
OXCT1	3-oxoacid CoA transferase 1	0,526	6,58E-02		enzyme
PARD3	par-3 family cell polarity regulator	0,456	6,19E-02		other
PARN	poly(A)-specific ribonuclease	0,439	2,73E-02		enzyme
PBLD	phenazine biosynthesis-like protein domain containing	-0,592	9,02E-02	D	enzyme
PBLD	phenazine biosynthesis-like protein domain containing	-1,348	6,88E-02	D	enzyme
PBLD	phenazine biosynthesis-like protein domain containing	-0,630	1,21E-02	D	enzyme
PCCA	propionyl CoA carboxylase, alpha polypeptide	-0,377	2,84E-02		enzyme
PDF	peptide deformylase (mitochondrial)	0,704	4,78E-02		enzyme
PDLIM5	PDZ and LIM domain 5	0,555	2,57E-02		other
PGM1	phosphoglucomutase 1	-0,511	5,01E-02		enzyme
PKHD1L1	polycystic kidney and hepatic disease 1 (autosomal recessive)-like 1	0,483	7,58E-02	D	other
PKHD1L1	polycystic kidney and hepatic disease 1 (autosomal recessive)-like 1	0,437	3,40E-02	D	other
PLA1A	phospholipase A1 member A	-0,393	5,29E-02		enzyme
PLD1	phospholipase D1, phosphatidylcholine-specific	-0,380	1,92E-02		enzyme
PLEKHS1	pleckstrin homology domain containing, family S member 1	0,605	1,79E-02	D	other
PLEKHS1	pleckstrin homology domain containing, family S member 1	0,480	4,20E-03	D	other

Plscr2	phospholipid scramblase 2	-0,541	4,32E-02		other
PLTP	phospholipid transfer protein	1,264	8,09E-02		enzyme
POPDC3	popeye domain containing 3	-0,460	6,40E-03		other
PPAT	phosphoribosyl pyrophosphate amidotransferase	0,495	5,02E-04		enzyme
PPDPF	pancreatic progenitor cell differentiation and proliferation factor	0,451	6,11E-02		other
PRAF2	PRA1 domain family, member 2	-0,461	5,63E-02		other
PRRC2B	proline-rich coiled-coil 2B	0,455	1,60E-03		other
PRTFDC1	phosphoribosyl transferase domain containing 1	-0,464	6,13E-02		enzyme
PTGR2	prostaglandin reductase 2	-0,460	1,87E-02		enzyme
PTS	6-pyruvoyltetrahydropterin synthase	-0,818	6,19E-02		enzyme
PURG	purine-rich element binding protein G	1,842	6,83E-02		other
PYGB	phosphorylase, glycogen; brain	-0,475	5,29E-02		enzyme
RCL1	RNA terminal phosphate cyclase-like 1	0,378	8,17E-02		enzyme
RCVRN	recoverin	-0,432	7,17E-02		other
RGN	regucalcin	-0,492	6,19E-02		enzyme
RGS21	regulator of G-protein signaling 21	-0,516	8,80E-02		other
RHOG	ras homolog family member G	-0,401	9,83E-02		enzyme
RND2	Rho family GTPase 2	0,437	2,96E-02	D	enzyme
RND2	Rho family GTPase 2	0,690	1,08E-02	D	enzyme
RPE65	retinal pigment epithelium-specific protein 65kDa	-1,279	1,31E-02		enzyme
SC5D	sterol-C5-desaturase	0,680	2,80E-02		enzyme
SEPP1	selenoprotein P, plasma, 1	-0,420	8,57E-02		other
SERPINB6	serpin peptidase inhibitor, clade B (ovalbumin), member 6	-0,532	5,78E-02		other
SERPINH1	serpin peptidase inhibitor, clade H (heat shock protein 47), member 1, (collagen binding protein 1)	-0,467	6,14E-02		other
SESN1	sestrin 1	-0,811	3,88E-02	D	other
SESN1	sestrin 1	-0,697	5,81E-02	D	other
SESN1	sestrin 1	-0,780	5,69E-02	D	other
SH2D4A	SH2 domain containing 4A	0,531	7,18E-02		other
SLC16A12	solute carrier family 16, member 12	0,999	3,26E-02		other
SLC25A38	solute carrier family 25, member 38	-1,258	8,13E-02		other
SLC25A47	solute carrier family 25, member 47	-0,721	1,18E-02		other
SLC9A3R1	solute carrier family 9, subfamily A (NHE3, cation proton antiporter 3), member 3 regulator 1	-0,513	5,78E-02	D	other
SLC9A3R1	solute carrier family 9, subfamily A (NHE3, cation proton antiporter 3), member 3 regulator 1	-0,510	9,15E-02	D	other
SMPDL3B	sphingomyelin phosphodiesterase, acid-like 3B	-0,782	5,74E-02		enzyme
SNRNP25	small nuclear ribonucleoprotein 25kDa (U11/U12)	-0,392	7,20E-02		other
SOCS1	suppressor of cytokine signaling 1	-1,494	6,57E-02	D	other
SOCS1	suppressor of cytokine signaling 1	-1,321	6,60E-02	D	other
STC2	stanniocalcin 2	-1,754	1,51E-02		other
STEAP4	STEAP family member 4	0,529	5,57E-02		enzyme
STRA6	stimulated by retinoic acid 6	-0,477	3,85E-02	D	other
STRA6	stimulated by retinoic acid 6	-0,566	2,60E-02	D	other
SUCLG2	succinate-CoA ligase, GDP-forming, beta subunit	-0,419	1,63E-02		enzyme
SULT1C2	sulfotransferase family, cytosolic, 1C, member 2	-0,709	5,34E-02		enzyme
SULT2B1	sulfotransferase family, cytosolic, 2B, member 1	1,185	1,48E-02	D	enzyme
SULT2B1	sulfotransferase family, cytosolic, 2B, member 1	1,216	6,97E-03	D	enzyme
SULT2B1	sulfotransferase family, cytosolic, 2B, member 1	0,418	2,75E-02	D	enzyme
SULT2B1	sulfotransferase family, cytosolic, 2B, member 1	0,604	1,65E-02	D	enzyme
TAT	tyrosine aminotransferase	1,603	1,43E-02	D	enzyme
TAT	tyrosine aminotransferase	1,403	1,16E-02	D	enzyme
TAT	tyrosine aminotransferase	1,291	9,73E-03	D	enzyme
TAT	tyrosine aminotransferase	1,309	3,22E-03	D	enzyme
TAT	tyrosine aminotransferase	1,522	6,46E-03	D	enzyme
TECTB	tectorin beta	0,802	7,69E-02	D	other
TECTB	tectorin beta	0,897	8,15E-02	D	other
TES	testis derived transcript (3 LIM domains)	0,376	7,17E-02		other
THBS2	thrombospondin 2	0,747	4,31E-02		other
TM4SF5	transmembrane 4 L six family member 5	-0,563	3,76E-02		other
TMEM150B	transmembrane protein 150B	-0,761	6,28E-02		other
TMEM205	transmembrane protein 205	-0,422	9,97E-03		other

TMEM263	transmembrane protein 263	0,872	5,33E-02		other
TMOD4	tropomodulin 4 (muscle)	-0,456	1,97E-02		other
TMX4	thioredoxin-related transmembrane protein 4	0,383	8,02E-02		enzyme
TNNI2	troponin I type 2 (skeletal, fast)	-0,403	9,93E-02		enzyme
TP53INP1	tumor protein p53 inducible nuclear protein 1	0,429	5,74E-02		other
TREH	trehalase (brush-border membrane glycoprotein)	-0,550	7,09E-02	D	enzyme
TREH	trehalase (brush-border membrane glycoprotein)	-0,632	7,69E-02	D	enzyme
TRIM3	tripartite motif containing 3	-0,425	9,17E-02		other
TSPAN1	tetraspanin 1	-0,929	3,23E-02	D	other
TSPAN1	tetraspanin 1	-0,943	4,74E-02	D	other
TTC36	tetratricopeptide repeat domain 36	-0,420	6,46E-02		other
TTC38	tetratricopeptide repeat domain 38	-0,440	2,03E-02		other
TTC7A	tetratricopeptide repeat domain 7A	-0,426	1,23E-02		other
TUBA8	tubulin, alpha 8	0,399	9,95E-02		other
TUBB4B	tubulin, beta 4B class IVb	0,405	1,80E-02	D	other
TUBB4B	tubulin, beta 4B class IVb	0,434	4,56E-03	D	other
TUBB4B	tubulin, beta 4B class IVb	0,379	3,67E-02	D	other
TXNIP	thioredoxin interacting protein	-0,553	4,73E-02		other
UGDH	UDP-glucose 6-dehydrogenase	-0,523	3,32E-02		enzyme
UGT1A1	UDP glucuronosyltransferase 1 family, polypeptide A1	-0,922	1,56E-02	D	enzyme
UGT1A1	UDP glucuronosyltransferase 1 family, polypeptide A1	-0,864	7,69E-03	D	enzyme
UGT2A3	UDP glucuronosyltransferase 2 family, polypeptide A3	-0,398	4,79E-02		enzyme
UPB1	ureidopropionase, beta	-0,399	2,83E-02		enzyme
URAD	ureidoimidazoline (2-oxo-4-hydroxy-4-carboxy-5-) decarboxylase	-0,677	7,23E-02		enzyme
USH1C	Usher syndrome 1C (autosomal recessive, severe)	-0,820	2,63E-02		other
VAPB	VAMP (vesicle-associated membrane protein)-associated protein B and C	0,388	4,41E-02		other
VASN	vasorin	0,469	1,28E-02		other
VIL1	villin 1	-0,589	3,05E-02	D	other
VIL1	villin 1	-0,491	3,11E-02	D	other
VIL1	villin 1	-0,556	5,08E-02	D	other
VTN	vitronectin	0,649	1,11E-02		other
WNT3	wingless-type MMTV integration site family, member 3	0,408	2,90E-02		other
WSB1	WD repeat and SOCS box containing 1	-0,492	1,34E-02		other
YWHAE	tyrosine 3-monooxygenase/tryptophan 5-monooxygenase activation protein, epsilon	0,454	5,15E-02		other
ZNF729	zinc finger protein 729	-0,465	5,26E-02		other

Annex 5: PTH microarrays by entrez gene name.

Symbol	Entrez Gene Name	Log Ratio PTH	p-value	N	Type(s)
BET1L	Bet1 golgi vesicular membrane trafficking protein-like	1,210	7,53E-02		transporter
CACNB1	calcium channel, voltage-dependent, beta 1 subunit	-1,060	7,90E-02		ion channel
CLCN1	chloride channel, voltage-sensitive 1	0,797	5,64E-02		ion channel
COMMD1	copper metabolism (Murr1) domain containing 1	0,545	8,50E-02		transporter
GJA9	gap junction protein, alpha 9, 59kDa	1,750	9,39E-02		transporter
KCNK18	potassium channel, subfamily K, member 18	1,040	6,67E-02		ion channel
MB	myoglobin	-0,656	9,39E-02		transporter
MTX1	metaxin 1	-0,415	5,90E-02		transporter
NXF1	nuclear RNA export factor 1	-0,902	7,90E-02		transporter
P2RX7	purinergic receptor P2X, ligand-gated ion channel, 7	-1,420	8,96E-02		ion channel
PANX1	pannexin 1	-1,060	9,58E-02		transporter
RPH3A	rabphilin 3A homolog (mouse)	0,836	4,94E-02		transporter
SLC12A3	solute carrier family 12 (sodium/chloride transporter), member 3	-0,763	5,64E-02		transporter
SLC18A3	solute carrier family 18 (vesicular acetylcholine transporter), member 3	-1,930	5,58E-02		transporter
SLC43A1	solute carrier family 43 (amino acid system L transporter), member 1	0,405	9,81E-02		transporter
SLC6A18	solute carrier family 6 (neutral amino acid transporter), member 18	-2,300	6,63E-02		transporter
SLC7A10	solute carrier family 7 (neutral amino acid transporter light chain, asc system), member 10	-1,100	5,64E-02		transporter
SLC9A6	solute carrier family 9, subfamily A (NHE6, cation proton antiporter 6), member 6	-0,985	7,90E-02		transporter
SMC4	structural maintenance of chromosomes 4	0,376	7,83E-02		transporter
AATF	apoptosis antagonizing transcription factor	-1,050	6,63E-02		transcription regulator
CALR	calreticulin	1,060	6,36E-02		transcription regulator
DMBX1	diencephalon/mesencephalon homeobox 1	0,721	9,09E-02		transcription regulator
EEF2	eukaryotic translation elongation factor 2	0,722	9,81E-02		translation regulator
EGR1	early growth response 1	-0,725	9,91E-02		transcription regulator
EPC1	enhancer of polycomb homolog 1 (Drosophila)	-0,698	7,95E-02		transcription regulator
ESR2	estrogen receptor 2 (ER beta)	-1,250	9,81E-02		ligand-dependent nuclear receptor
FOXB2	forkhead box B2	-1,080	5,89E-02		transcription regulator
GATA4	GATA binding protein 4	0,879	8,83E-02		transcription regulator
HOXA5	homeobox A5	-0,515	7,90E-02		transcription regulator
INSM2	insulinoma-associated 2	0,732	7,64E-02		transcription regulator
IRX6	iroquois homeobox 6	0,631	7,90E-02		transcription regulator
JARID2	jumonji, AT rich interactive domain 2	-1,400	9,95E-02		transcription regulator
LDB2	LIM domain binding 2	0,597	4,94E-02	D	transcription regulator
LDB2	LIM domain binding 2	1,330	5,64E-02	D	transcription regulator
LRCH4	leucine-rich repeats and calponin homology (CH) domain containing 4	1,030	5,47E-02		transcription regulator
MXI1	MAX interactor 1, dimerization protein	0,530	7,90E-02		transcription regulator
NKX3-2	NK3 homeobox 2	0,697	7,14E-02		transcription regulator
PDLIM1	PDZ and LIM domain 1	-0,943	9,27E-02		transcription regulator
PTRF	polymerase I and transcript release factor	0,480	8,88E-02		transcription regulator
RPS9	ribosomal protein S9	0,613	7,19E-02		translation regulator

RXRA	retinoid X receptor, alpha	0,993	7,64E-02		ligand-dependent nuclear receptor
TAF1	TAF1 RNA polymerase II, TATA box binding protein (TBP)-associated factor, 250kDa	0,416	7,96E-02		transcription regulator
TOX2	TOX high mobility group box family member 2	0,604	7,83E-02		transcription regulator
ACKR3	atypical chemokine receptor 3	-2,210	6,67E-02		G-protein coupled receptor
AVPR1A	arginine vasopressin receptor 1A	2,150	4,94E-02		G-protein coupled receptor
CALCRL	calcitonin receptor-like	0,735	7,74E-02		G-protein coupled receptor
CHRM2	cholinergic receptor, muscarinic 2	0,500	9,48E-02		G-protein coupled receptor
CHRNA6	cholinergic receptor, nicotinic, alpha 6 (neuronal)	-2,090	6,63E-02		transmembrane receptor
GFRA1	GDNF family receptor alpha 1	1,200	9,81E-02		transmembrane receptor
GPR132	G protein-coupled receptor 132	0,973	8,14E-02		G-protein coupled receptor
HLA-B	major histocompatibility complex, class I, B	0,469	6,75E-02		transmembrane receptor
ILDR1	immunoglobulin-like domain containing receptor 1	0,788	6,63E-02		transmembrane receptor
ITGA4	integrin, alpha 4 (antigen CD49D, alpha 4 subunit of VLA-4 receptor)	0,758	8,50E-02		transmembrane receptor
LHCGR	luteinizing hormone/choriogonadotropin receptor	-1,130	9,91E-02		G-protein coupled receptor
LY75	lymphocyte antigen 75	-1,390	5,90E-02		transmembrane receptor
OR8G5	olfactory receptor, family 8, subfamily G, member 5	-2,060	9,02E-02		G-protein coupled receptor
PTHR1	parathyroid hormone receptor	0,908	6,85E-02		G-protein coupled receptor
TNFRSF1A	tumor necrosis factor receptor superfamily, member 1A	1,010	7,74E-02		transmembrane receptor
TNFRSF21	tumor necrosis factor receptor superfamily, member 21	0,782	4,94E-02		transmembrane receptor
FAM3C	family with sequence similarity 3, member C	-0,477	9,09E-02		cytokine
FGF4	fibroblast growth factor 4	-1,150	7,87E-02		growth factor
GDF9	growth differentiation factor 9	-1,900	7,90E-02		growth factor
IGF1	insulin-like growth factor 1 (somatomedin C)	1,460	8,88E-02		growth factor
INHBB	inhibin, beta B	-0,830	9,02E-02		growth factor
AK3	adenylate kinase 3	-0,557	9,09E-02		kinase
COASY	CoA synthase	-1,430	9,81E-02		kinase
DAPK3	death-associated protein kinase 3	-1,300	4,94E-02		kinase
DCLK2	doublecortin-like kinase 2	1,240	7,39E-02		kinase
EPHB2	EPH receptor B2	1,540	9,81E-02		kinase
GRK4	G protein-coupled receptor kinase 4	1,840	5,60E-02		kinase
ILKAP	integrin-linked kinase-associated serine/threonine phosphatase	-0,707	5,58E-02		phosphatase
NAGK	N-acetylglucosamine kinase	-0,816	8,83E-02		kinase
NME2	NME/NM23 nucleoside diphosphate kinase 2	0,743	8,21E-02		kinase
NRBP2	nuclear receptor binding protein 2	1,330	5,64E-02	D	kinase
RPS6KA2	ribosomal protein S6 kinase, 90kDa, polypeptide 2	-0,735	6,63E-02		kinase
SGK1	serum/glucocorticoid regulated kinase 1	-0,505	7,96E-02		kinase
SYNJ1	synaptojanin 1	-2,670	8,55E-02		phosphatase
Afg3l1	AFG3(ATPase family gene 3)-like 1 (yeast)	-4,740	3,48E-02		peptidase
CPA2	carboxypeptidase A2 (pancreatic)	-0,647	9,81E-02		peptidase
IDE	insulin-degrading enzyme	-0,623	9,09E-02		peptidase
RHBDL2	rhomboid, veinlet-like 2 (Drosophila)	-0,679	9,26E-02		peptidase
SPPL2A	signal peptide peptidase like 2A	0,542	6,63E-02		peptidase
USP24	ubiquitin specific peptidase 24	1,240	6,63E-02		peptidase
ABI1	abl-interactor 1	1,040	7,14E-02		other
ADAP2	ArfGAP with dual PH domains 2	-0,726	4,94E-02		other
ALKBH5	alkB, alkylation repair homolog 5 (E, coli)	-0,900	6,63E-02		enzyme
ANLN	anillin, actin binding protein	-1,370	8,50E-02		other
ARGLU1	arginine and glutamate rich 1	0,595	9,81E-02		other

ARHGEF11	Rho guanine nucleotide exchange factor (GEF) 11	0,750	5,97E-02	other
ARHGEF19	Rho guanine nucleotide exchange factor (GEF) 19	1,420	7,80E-02	other
ARL8B	ADP-ribosylation factor-like 8B	1,270	9,39E-02	enzyme
ARPC5	actin related protein 2/3 complex, subunit 5, 16kDa	-1,050	5,64E-02	other
ARRB2	arrestin, beta 2	-0,684	6,63E-02	other
ASPN	asporin	1,670	5,50E-02	other
ASRGL1	asparaginase like 1	-0,765	4,94E-02	enzyme
AXIN1	axin 1	0,404	9,81E-02	other
C15orf41	chromosome 15 open reading frame 41	-0,815	7,83E-02	other
C2orf40	chromosome 2 open reading frame 40	1,060	9,69E-02	other
C2orf47	chromosome 2 open reading frame 47	-0,951	6,61E-02	other
C3orf58	chromosome 3 open reading frame 58	-0,676	5,58E-02	other
C4orf29	chromosome 4 open reading frame 29	-0,904	3,48E-02	other
C7	complement component 7	1,310	4,94E-02	other
CA8	carbonic anhydrase VIII	-0,650	8,50E-02	enzyme
CAB39	calcium binding protein 39	1,540	9,51E-02	enzyme
CABLES2	Cdk5 and Abl enzyme substrate 2	0,543	8,50E-02	other
CABLES2	Cdk5 and Abl enzyme substrate 2	-2,030	9,69E-02	other
CAD	carbamoyl-phosphate synthetase 2, aspartate transcarbamylase, and dihydroorotase	-1,570	6,78E-02	enzyme
CARS	cysteinyl-tRNA synthetase	-0,417	9,09E-02	enzyme
CBY1	chibby homolog 1 (Drosophila)	2,390	4,94E-02	other
CCDC62	coiled-coil domain containing 62	0,495	9,16E-02	other
CD151	CD151 molecule (Raph blood group)	-0,709	5,64E-02	other
CDC34	cell division cycle 34	-0,878	6,85E-02	enzyme
CDIPT	CDP-diacylglycerol--inositol 3-phosphatidyltransferase	-0,583	8,83E-02	enzyme
CES1	carboxylesterase 1	0,555	4,94E-02	enzyme
CHD4	chromodomain helicase DNA binding protein 4	0,425	9,39E-02	enzyme
CNPY3	canopy FGF signaling regulator 3	-0,699	5,64E-02	other
CPLX2	complexin 2	0,392	9,69E-02	other
CS	citrate synthase	-0,682	8,83E-02	enzyme
CWC22	CWC22 spliceosome-associated protein homolog (S, cerevisiae)	0,924	8,45E-02	other
CYP21A2	cytochrome P450, family 21, subfamily A, polypeptide 2	-1,260	5,89E-02	enzyme
CYP2J2	cytochrome P450, family 2, subfamily J, polypeptide 2	-0,742	9,81E-02	enzyme
DCPS	decapping enzyme, scavenger	-0,982	9,39E-02	enzyme
DCTN1	dynactin 1	0,694	6,63E-02	other
DENND5A	DENN/MADD domain containing 5A	-1,240	7,96E-02	other
DNAJB11	DnaJ (Hsp40) homolog, subfamily B, member 11	-0,892	4,94E-02	other
DNASE1L3	deoxyribonuclease I-like 3	-0,544	8,83E-02	enzyme
EFCAB4B	EF-hand calcium binding domain 4B	1,590	6,63E-02	other
EFEMP1	EGF containing fibulin-like extracellular matrix protein 1	-2,240	7,64E-02	enzyme
EFNA1	ephrin-A1	0,450	8,44E-02	other
FAIM	Fas apoptotic inhibitory molecule	1,940	7,74E-02	other
FAM177A1	family with sequence similarity 177, member A1	-0,469	7,80E-02	other
FBLN1	fibulin 1	0,742	8,50E-02	other
FOXRED1	FAD-dependent oxidoreductase domain containing 1	-0,846	7,80E-02	other
GALNT2	polypeptide N-acetylgalactosaminyltransferase 2	-0,808	7,95E-02	enzyme
GLB1	galactosidase, beta 1	1,370	5,64E-02	enzyme
GLB1L	galactosidase, beta 1-like	0,654	9,09E-02	other
Gm16500	predicted gene 16500	-0,625	5,58E-02	other
GNAL	guanine nucleotide binding protein (G protein), alpha activating activity polypeptide, olfactory type	-0,768	9,37E-02	enzyme
GPAM	glycerol-3-phosphate acyltransferase, mitochondrial	0,894	9,39E-02	enzyme
GPC3	glypican 3	0,521	9,81E-02	other
GRAMD1B	GRAM domain containing 1B	0,924	4,94E-02	other
GRAMD1C	GRAM domain containing 1C	-0,553	4,94E-02	other
GSR	glutathione reductase	-0,847	5,64E-02	enzyme
GUCA1A	guanylate cyclase activator 1A (retina)	0,659	8,18E-02	other
GUSB	glucuronidase, beta	0,544	7,97E-02	enzyme

HARS	histidyl-tRNA synthetase	-0,929	5,64E-02	enzyme
HAUS6	HAUS augmin-like complex, subunit 6	-1,550	5,58E-02	other
HDC	histidine decarboxylase	0,796	9,16E-02	enzyme
HIST2H2AB	histone cluster 2, H2ab	2,200	5,64E-02	other
HLA-A	major histocompatibility complex, class I, A	-1,210	9,31E-02	other
Hmga2	high mobility group AT-hook 2	0,749	5,64E-02	enzyme
HSD3B7	hydroxy-delta-5-steroid dehydrogenase, 3 beta- and steroid delta-isomerase 7	-0,626	6,85E-02	enzyme
ISM2	isthmin 2	-1,630	8,83E-02	other
ITGA9	integrin, alpha 9	1,620	6,61E-02	other
KIAA1324L	KIAA1324-like	0,789	6,84E-02	other
KIF23	kinesin family member 23	1,440	6,99E-02	other
KLHDC8A	kelch domain containing 8A	0,569	7,96E-02	other
KLHL40	kelch-like family member 40	-1,080	8,45E-02	other
KRT17	keratin 17	0,961	7,64E-02	other
L3HYPDH	L-3-hydroxyproline dehydratase (trans-)	0,984	7,64E-02	enzyme
LCTL	lactase-like	-1,250	5,64E-02	enzyme
LGI1	leucine-rich, glioma inactivated 1	-1,340	6,63E-02	other
LIPH	lipase, member H	-0,666	7,39E-02	enzyme
LOC102551489	protein unc-13 homolog C-like	0,615	5,47E-02	other
LOC391722	myosin regulatory light chain 12B-like	0,561	9,39E-02	other
MARVELD1	MARVEL domain containing 1	0,596	9,81E-02	other
MCPH1	microcephalin 1	0,952	5,58E-02	other
MFAP3L	microfibrillar-associated protein 3-like	-0,835	5,64E-02	other
MLEC	malectin	-0,645	7,14E-02	other
MOCOS	molybdenum cofactor sulfurase	1,700	7,90E-02	enzyme
MRPL41	mitochondrial ribosomal protein L41	-0,438	7,14E-02	other
MSI2	musashi RNA-binding protein 2	0,945	9,81E-02	other
MTSS1	metastasis suppressor 1	-0,852	9,76E-02	other
MYO1G	myosin IG	-1,330	9,96E-02	other
NDRG2	NDRG family member 2	0,628	5,97E-02	other
OSBPL2	oxysterol binding protein-like 2	-1,130	9,16E-02	other
PALM2	paralemmin 2	1,120	7,64E-02	other
PAPL	iron/zinc purple acid phosphatase-like protein	0,867	9,69E-02	enzyme
PARP14	poly (ADP-ribose) polymerase family, member 14	0,765	5,58E-02	other
PDIA4	protein disulfide isomerase family A, member 4	-0,652	5,67E-02	enzyme
PDZD8	PDZ domain containing 8	0,876	9,03E-02	other
PHLDA2	pleckstrin homology-like domain, family A, member 2	-0,853	5,64E-02	other
PLA2G12A	phospholipase A2, group XIIA	0,779	9,39E-02	enzyme
PPIL2	peptidylprolyl isomerase (cyclophilin)-like 2	-0,408	7,90E-02	enzyme
PPP1R14C	protein phosphatase 1, regulatory (inhibitor) subunit 14C	-1,640	5,64E-02	other
PRMT1	protein arginine methyltransferase 1	-0,971	5,90E-02	enzyme
PSMD5	proteasome (prosome, macropain) 26S subunit, non-ATPase, 5	-0,915	7,70E-02	other
PTGES	prostaglandin E synthase	0,509	9,70E-02	enzyme
PTGES	prostaglandin E synthase	1,510	9,81E-02	enzyme
PTH1	parathyroid hormone	-1,320	4,94E-02	other
PTX3	pentraxin 3, long	1,820	3,48E-02	other
RAD21	RAD21 homolog (S, pombe)	1,570	6,75E-02	other
RALGDS	ral guanine nucleotide dissociation stimulator	-0,985	4,94E-02	other
RBM18	RNA binding motif protein 18	-0,655	6,72E-02	other
RHOF	ras homolog family member F (in filopodia)	-1,700	4,94E-02	enzyme
RIT1	Ras-like without CAAX 1	1,050	9,16E-02	enzyme
RPAP1	RNA polymerase II associated protein 1	-1,220	9,81E-02	other
RPL23	ribosomal protein L23	0,705	9,39E-02	other
RPL27A	ribosomal protein L27a	0,977	7,90E-02	other
RPUSD1	RNA pseudouridylate synthase domain containing 1	-0,862	5,64E-02	enzyme
SAG	S-antigen; retina and pineal gland (arrestin)	0,517	7,64E-02	other
SASH1	SAM and SH3 domain containing 1	1,970	9,25E-02	other

SCARB2	scavenger receptor class B, member 2	1,360	7,64E-02		other
SERPINE1	serpin peptidase inhibitor, clade E (nexin, plasminogen activator inhibitor type 1), member 1	-0,981	9,81E-02		other
SGCG	sarcoglycan, gamma (35kDa dystrophin-associated glycoprotein)	-1,510	3,48E-02		other
SHISA2	shisa family member 2	0,907	6,63E-02		other
SLC25A51	solute carrier family 25, member 51	-0,658	8,20E-02		other
SLC43A3	solute carrier family 43, member 3	-1,330	3,48E-02		other
SMURF2	SMAD specific E3 ubiquitin protein ligase 2	-3,370	9,30E-02		enzyme
SPTLC3	serine palmitoyltransferase, long chain base subunit 3	-1,180	6,85E-02		enzyme
SRSF1	serine/arginine-rich splicing factor 1	-0,577	7,87E-02	D	other
SRSF1	serine/arginine-rich splicing factor 1	-0,529	7,90E-02	D	other
SSB	Sjogren syndrome antigen B (autoantigen La)	-0,657	6,41E-02		enzyme
ST6GAL2	ST6 beta-galactosamide alpha-2,6-sialyltranferase 2	0,645	7,63E-02		enzyme
ST8SIA2	ST8 alpha-N-acetyl-neuraminide alpha-2,8-sialyltransferase 2	0,641	7,95E-02		enzyme
TANGO2	transport and golgi organization 2 homolog (Drosophila)	-1,460	5,58E-02		other
TBC1D1	TBC1 (tre-2/USP6, BUB2, cdc16) domain family, member 1	1,990	5,50E-02		other
TFPI	tissue factor pathway inhibitor (lipoprotein-associated coagulation inhibitor)	-2,390	5,64E-02		other
TGFBRAP1	transforming growth factor, beta receptor associated protein 1	0,705	6,75E-02		other
THOC2	THO complex 2	0,491	7,74E-02		other
TMEM181	transmembrane protein 181	2,470	4,94E-02		other
TMEM30B	transmembrane protein 30B	-1,070	9,39E-02		other
TMEM87B	transmembrane protein 87B	0,501	9,26E-02		other
TMX3	thioredoxin-related transmembrane protein 3	0,600	6,63E-02		enzyme
TPD52L1	tumor protein D52-like 1	-0,544	9,81E-02		other
TSPEAR	thrombospondin-type laminin G domain and EAR repeats	0,741	7,58E-02		other
TTC14	tetratricopeptide repeat domain 14	-0,712	6,85E-02		other
Ttc39a	tetratricopeptide repeat domain 39A	-0,906	7,14E-02		other
TXNRD3	thioredoxin reductase 3	-1,490	9,37E-02		enzyme
UNC93B1	unc-93 homolog B1 (C, elegans)	0,698	9,39E-02		other
USP32	ubiquitin specific peptidase 32	0,805	7,74E-02		enzyme
VPS37B	vacuolar protein sorting 37 homolog B (S, cerevisiae)	0,758	5,58E-02		other
VSNL1	visinin-like 1	0,441	9,25E-02		other
WDR5	WD repeat domain 5	-1,400	9,09E-02		other
XAF1	XIAP associated factor 1	0,857	6,63E-02		other
ZC3H6	zinc finger CCCH-type containing 6	0,961	8,28E-02		other
ZNF346	zinc finger protein 346	0,867	9,39E-02		other
ZNF729	zinc finger protein 729	-1,320	6,85E-02	D	other
ZNF729	zinc finger protein 729	-0,981	8,50E-02	D	other
ZNF729	zinc finger protein 729	2,170	9,16E-02	D	other

Annex 6: VitD3 and PTH Heat map.

Symbol	Entrez Gene Name	PTH	VitD3
FOSB	FBJ murine osteosarcoma viral oncogene homolog B		-0.99
FOXQ1	forkhead box Q1		0.69
EGR1	early growth response 1	-0.73	
ZNF729	zinc finger protein 729	-1.32	-0.47
CYP2J2	cytochrome P450. family 2. subfamily J. polypeptide 2	-0.74	-1.02
APOA4	apolipoprotein A-IV		-1.76
SLC6A19	solute carrier family 6 (neutral amino acid transporter). member 19		-0.77
OPN1LW	opsin 1 (cone pigments). long-wave-sensitive		-1.54
MYOG	myogenin (myogenic factor 4)		-0.55
WDR5	WD repeat domain 5	-1.40	
STK39	serine threonine kinase 39		-0.55
LOX	lysyl oxidase		0.46
SPPL2A	signal peptide peptidase like 2A	0.54	
TTC7A	tetratricopeptide repeat domain 7A		-0.43
ATP1A1	ATPase. Na+/K+ transporting. alpha 1 polypeptide		-0.39
IGFBP1	insulin-like growth factor binding protein 1		1.92
NPAS4	neuronal PAS domain protein 4		
SOCS1	suppressor of cytokine signaling 1		-1.49
CISH	cytokine inducible SH2-containing protein		-1.78
TXNIP	thioredoxin interacting protein		-0.55
SGK1	serum/glucocorticoid regulated kinase 1	-0.51	
MYC	v-myc avian myelocytomatosis viral oncogene homolog		-0.44
ARRDC2	arrestin domain containing 2		0.38
CPA2	carboxypeptidase A2 (pancreatic)	-0.65	-0.64
LECT1	leukocyte cell derived chemotaxin 1		-0.53
TUBA8	tubulin. alpha 8		0.40
BCKDK	branched chain ketoacid dehydrogenase kinase		-0.41
KLF11	Kruppel-like factor 11		2.63
KIF23	kinesin family member 23	1.44	
DBT	dihydrolipoamide branched chain transacylase E2		-0.46
ANLN	anillin. actin binding protein	-1.37	
SRSF1	serine/arginine-rich splicing factor 1	-0.58	
HADH	hydroxyacyl-CoA dehydrogenase		-0.41
SLC37A4	solute carrier family 37 (glucose-6-phosphate transporter). member 4		-0.40
PPP4C	protein phosphatase 4. catalytic subunit		0.40
FCGBP	Fc fragment of IgG binding protein		-0.69
SSB	Sjogren syndrome antigen B (autoantigen La)	-0.66	
PGM1	phosphoglucomutase 1		-0.51
TUBB4B	tubulin. beta 4B class IVb		0.43
HSP90B1	heat shock protein 90kDa beta (Grp94). member 1		0.49
C2orf40	chromosome 2 open reading frame 40	1.06	
DNAJB11	DnaJ (Hsp40) homolog. subfamily B. member 11	-0.89	

DDC	dopa decarboxylase (aromatic L-amino acid decarboxylase)		**-0.54**
FAIM	Fas apoptotic inhibitory molecule	**1.94**	
ACKR3	atypical chemokine receptor 3	**-2.21**	
STC2	stanniocalcin 2		**-1.75**
LCTL	lactase-like	**-1.25**	
GADD45A	growth arrest and DNA-damage-inducible. alpha		**-0.94**
HABP2	hyaluronan binding protein 2		**-1.00**
TSPAN1	tetraspanin 1		**-0.94**
ACTA1	actin. alpha 1. skeletal muscle		**-0.69**
C2orf47	chromosome 2 open reading frame 47	**-0.95**	
PDK2	pyruvate dehydrogenase kinase. isozyme 2		**-0.70**
TMX3	thioredoxin-related transmembrane protein 3	**0.60**	
SERPINH1	serpin peptidase inhibitor. clade H (heat shock protein 47). member 1. (collagen binding protein 1)		**-0.47**
CALCRL	calcitonin receptor-like	**0.74**	
TNFRSF21	tumor necrosis factor receptor superfamily. member 21	**0.78**	
CNBP	CCHC-type zinc finger. nucleic acid binding protein		**-0.59**
VTN	vitronectin		**0.65**
VIL1	villin 1		**-0.59**
MYH11	myosin. heavy chain 11. smooth muscle		**-0.52**
ILDR1	immunoglobulin-like domain containing receptor 1	**0.79**	
ACTR6	ARP6 actin-related protein 6 homolog (yeast)		**-0.64**
ADRB2	adrenoceptor beta 2. surface		**-0.60**
PARN	poly(A)-specific ribonuclease		**0.44**
TREH	trehalase (brush-border membrane glycoprotein)		**-0.63**
GOT2	glutamic-oxaloacetic transaminase 2. mitochondrial		**-0.47**
TMOD4	tropomodulin 4 (muscle)		**-0.46**
GJB3	gap junction protein. beta 3. 31kDa		**-0.48**
ACAA1	acetyl-CoA acyltransferase 1		**-0.47**
NCOA4	nuclear receptor coactivator 4		**0.47**
TWF2	twinfilin actin-binding protein 2		**-0.42**
GNE	glucosamine (UDP-N-acetyl)-2-epimerase/N-acetylmannosamine kinase		**-0.40**
POPDC3	popeye domain containing 3		**-0.46**
CCBL2	cysteine conjugate-beta lyase 2		**-0.38**
FOXK1	forkhead box K1		**0.43**
ACOX1	acyl-CoA oxidase 1. palmitoyl		**-0.85**
SLC25A47	solute carrier family 25. member 47		**-0.72**
EEF2	eukaryotic translation elongation factor 2	**0.72**	
CYP27A1	cytochrome P450. family 27. subfamily A. polypeptide 1		**-0.48**
NID1	nidogen 1		**-0.67**
PDLIM1	PDZ and LIM domain 1	**-0.94**	
ETNPPL	ethanolamine-phosphate phospho-lyase		**-0.75**
TMPRSS13	transmembrane protease. serine 13		**0.38**
SMPDL3B	sphingomyelin phosphodiesterase. acid-like 3B		**-0.78**
INSIG1	insulin induced gene 1		**0.62**
CACNA2D2	calcium channel. voltage-dependent. alpha 2/delta subunit 2		**0.38**

MOGAT1	monoacylglycerol O-acyltransferase 1		**-0.59**
HGD	homogentisate 1.2-dioxygenase		**-0.53**
SERPINB6	serpin peptidase inhibitor. clade B (ovalbumin). member 6		**-0.53**
CTRB2	chymotrypsinogen B2		**-0.79**
HSD17B4	hydroxysteroid (17-beta) dehydrogenase 4		**-0.45**
TAT	tyrosine aminotransferase		**1.60**
CYP24A1	cytochrome P450. family 24. subfamily A. polypeptide 1		**3.16**
NDRG2	NDRG family member 2	**0.63**	
GRK7	G protein-coupled receptor kinase 7		**-0.75**
SLC25A43	solute carrier family 25. member 43		**-0.69**
LPL	lipoprotein lipase		**-0.87**
CTDSPL	CTD (carboxy-terminal domain. RNA polymerase II. polypeptide A) small phosphatase-like		**0.56**
ALAS2	5'-aminolevulinate synthase 2		**-0.68**
HSD11B2	hydroxysteroid (11-beta) dehydrogenase 2		**-0.41**
BOC	BOC cell adhesion associated. oncogene regulated		**-0.56**
GUSB	glucuronidase. beta	**0.54**	
ANKRD33	ankyrin repeat domain 33		**-0.55**
USP14	ubiquitin specific peptidase 14 (tRNA-guanine transglycosylase)		**0.49**
ALDH4A1	aldehyde dehydrogenase 4 family. member A1		**-0.46**
USP37	ubiquitin specific peptidase 37		**0.39**
NRBP2	nuclear receptor binding protein 2	**-3.12**	**-0.48**
CES1	carboxylesterase 1	**0.56**	**-2.24**
SLC6A18	solute carrier family 6 (neutral amino acid transporter). member 18	**-2.30**	**-0.46**
CAD	carbamoyl-phosphate synthetase 2. aspartate transcarbamylase. and dihydroorotase	**-1.57**	**0.51**
C7	complement component 7	**1.31**	**0.67**
KRT17	keratin 17. type I	**0.96**	**0.52**
SLC43A1	solute carrier family 43 (amino acid system L transporter). member 1	**0.41**	**-1.07**
GSR	glutathione reductase	**-0.85**	**0.38**
MLEC	malectin	**-0.65**	**-0.40**
HSD3B7	hydroxy-delta-5-steroid dehydrogenase. 3 beta- and steroid delta-isomerase 7	**-0.63**	**-0.41**

Annex 7: Morphometric analysis of cartilage staining after 5 days microgravity simulators. A) Clinostat. B) RPM.

A)

Measures	**Variable**	**N**	**Mean**	**SD**	**t-test**	**p-value**
Distance from anterior to ethmoid plate	Control	24	376.2	55.681		
	Clinostat	25	411.8	50.954	2.363	**0.022**
Distance from anterior to posterior	Control	24	1625	45.098		
	Clinostat	25	1633	67.083	0.484	0.630
Distance between articulation up and down	Control	24	465.9	38.617		
	Clinostat	25	465.2	45.117	0.053	0.958
Distance between ceratohyal extern up and down	Control	24	681.1	70.198		
	Clinostat	25	706	78.676	1.097	0.278
Distance between ceratohyal extern down and ceratohyal interne down	Control	24	532	29.903		
	Clinostat	25	523.9	30.263	0.865	0.392
Distance between ceratohyal extern up and ceratohyal interne up	Control	24	532.4	24.437		
	Clinostat	25	528.7	34.196	0.435	0.665
Distance from ethmoid plate to posterior	Control	24	1194	47.739		
	Clinostat	25	1173	61.763	1.314	0.195
Distance between hyosymplectic up and down	Control	24	1076	26.185		
	Clinostat	25	1084	31.152	0.964	0.340

B)

Measures	**Variable**	**N**	**Mean**	**SD**	**t-test**	**p-value**
Distance from anterior to ethmoid plate	Control	29	385.1	36.891		
	RPM	30	372.1	62.310	0.922	0.360
Distance from anterior to posterior	Control	29	1632	91.184		
	RPM	30	1623	105.545	0.339	0.736
Distance between articulation up and down	Control	29	473.3	49.918		
	RPM	30	471.9	41.770	0.113	0.910
Distance between ceratohyal extern up and down	Control	29	697.6	51.436		
	RPM	30	693.7	67.678	0.195	0.846
Distance between ceratohyal extern down and ceratohyal interne down	Control	29	534.6	26.655		
	RPM	30	506.8	44.482	3.049	**0.004**
Distance between ceratohyal extern up and ceratohyal interne up	Control	29	549.9	33.447		
	RPM	30	505.9	39.659	4.774	**0.000**
Distance from ethmoid plate to posterior	Control	29	1247	69.180		
	RPM	30	1250	68.886	0.216	0.830
Distance between hyosymplectic up and down	Control	29	1080	37.482		
	RPM	30	1090	37.284	1.037	0.304

Annex 8: Morphometric analysis of bone staining after 5 days microgravity simulators. A) Clinostat. B) RPM. C) RWV.

A)

Measures	Variable	N	Mean	SD	t-test	p-value
Distance between anguloarticular up and down	Control	27	/	/	/	/
	Clinostat	24	/	/	/	/
Distance from anterior to notochord	Control	27	638.3	36.239		
	Clinostat	24	637.3	41.773	0.090	0.928
Distance from anterior to parasphenoid a	Control	27	202.6	35.032		
	Clinostat	24	248.7	72.270	2.952	**0.005**
Distance between branchiostegal ray1 up and down	Control	27	345	42.170		
	Clinostat	24	368.7	44.562	1.956	0.056
Distance between entopterygoid up and down	Control	27	194.4	11.318		
	Clinostat	24	190.6	28.914	0.641	0.524
Distance between maxilla up and down	Control	27	/	/	/	/
	Clinostat	24	/	/	/	/
Distance between opercle up and down	Control	27	490.6	28.818		
	Clinostat	24	500.6	37.871	1.069	0.291
Triangle area of the parasphenoid	Control	27	23850	3215.886		
	Clinostat	24	19930	6535.947	2.737	**0.009**

B)

Measures	Variable	N	Mean	SD	t-test	p-value
Distance between anguloarticular up and down	Control	30	258.8	32.876		
	RPM	29	230.8	23.531	3.723	**0.001**
Distance from anterior to notochord	Control	30	682.5	47.012		
	RPM	29	661.3	36.392	1.980	0.052
Distance from anterior to parasphenoid a	Control	30	194.7	25.402		
	RPM	29	197.3	23.999	0.404	0.688
Distance between branchiostegal ray1 up and down	Control	30	355.8	33.301		
	RPM	29	328.4	30.676	3.254	**0.002**
Distance between entopterygoid up and down	Control	30	195	17.070		
	RPM	29	181.1	18.107	3.131	**0.003**
Distance between maxilla up and down	Control	30	291.1	21.691		
	RPM	29	280.5	19.285	2.011	0.049
Distance between opercle up and down	Control	30	527	23.678		
	RPM	29	505.5	26.229	3.229	**0.002**
Triangle area of the parasphenoid	Control	30	23370	2680.592		
	RPM	29	21270	2144.052	3.288	**0.002**

C)

Measures	Variable	N	Mean	SD	t-test	p-value
Distance between anguloarticular up and down	Control	28	/	/		
	RWV	24	/	/	/	/
Distance from anterior to notochord	Control	28	675.7	46.324		
	RWV	24	693.3	30.069	1.545	0.129
Distance from anterior to parasphenoid a	Control	28	194.4	21.456		
	RWV	24	189.2	23.983	0.812	0.421
Distance between branchiostegal ray1 up and down	Control	28	337	27.094		
	RWV	24	309	44.133	3.548	**0.001**
Distance between entopterygoid up and down	Control	28	189.6	16.674		
	RWV	24	193.3	12.825	0.859	0.395
Distance between maxilla up and down	Control	28	/	/		
	RWV	24	/	/	/	/
Distance between opercule up and down	Control	28	505.9	29.439		
	RWV	24	500.2	25.916	0.720	0.475
Triangle area of the parasphenoid	Control	28	23204.5	4373.509		
	RWV	24	24259.6	3464.506	0.926	0.359

Annex 9: Morphometric analysis of bone staining after 5 days dexamethasone treatment. A) Cartilage results. B) Bone results.

A)

Measures	Variable	N	Mean	SD	t-test	p-value
Distance from anterior to ethmoid plate	Control	21	330	32.852		
	Dexamethasone	20	332.9	30.370	0.292	0.772
Distance from anterior to posterior	Control	21	1600	57.918		
	Dexamethasone	20	1583	39.869	1.101	0.278
Distance between articulation up and down	Control	21	439.5	21.987		
	Dexamethasone	20	425.1	34.624	1.593	0.119
Distance between ceratohyal extern up and down	Control	21	605.6	46.698		
	Dexamethasone	20	590.9	55.919	0.916	0.365
Distance between ceratohyal extern down and ceratohyal interne down	Control	21	523.3	30.558		
	Dexamethasone	20	512	24.046	1.315	0.196
Distance between ceratohyal extern up and ceratohyal interne up	Control	21	517.6	22.616		
	Dexamethasone	20	510.5	19.474	1.070	0.291
Distance from ethmoid plate to posterior	Control	21	1273	51.110		
	Dexamethasone	20	1255	37.450	1.287	0.206
Distance between hyosymplectic up and down	Control	21	1040	28.072		
	Dexamethasone	20	1035	24.900	0.596	0.555

B)

Measures	Variable	N	Mean	SD	t-test	p-value
Distance between anguloarticular up and down	Control	24	/	/		
	Dexamethasone	24	/	/	/	/
Distance from anterior to notochord	Control	24	1320	63.228		
	Dexamethasone	24	1261	67.252	3.138	**0.003**
Distance from anterior to parasphenoid a	Control	24	390.4	29.522		
	Dexamethasone	24	399	31.588	0.968	0.338
Distance between branchiostegal ray1 up and down	Control	24	647.7	54.092		
	Dexamethasone	24	634	59.700	0.831	0.410
Distance between entopterygoid up and down	Control	24	340.5	27.088		
	Dexamethasone	24	328.2	22.001	1.720	0.092
Distance between maxilla up and down	Control	24	/	/		
	Dexamethasone	24	/	/	/	/
Distance between opercule up and down	Control	24	1013	49.510		
	Dexamethasone	24	955.8	45.001	4.199	**<0.001**
Triangle area of the parasphenoid	Control	24	85870	9067.170		
	Dexamethasone	24	79500	6524.896	2.793	**0.008**

Annex 10: Recapitulative table of statistical analysis of RWV in bone evolution image analysis.

A

				Score of Y		X^2 pearson	logistic regression	
Structures	Variable	N	Mean	early	advanced	p-value	OR (IC 95%)	p-value
anguloarticular down	Control	28	0.00	28 (100%)	0 (0%)		1	
	RWV	24	0.00	24 (100%)	0 (0%)	/	/	/
anguloarticular up	Control	28	0.00	28 (100%)	0 (0%)		1	
	RWV	24	0.00	24 (100%)	0 (0%)	/	/	/
branchiostegal ray2 down	Control	28	0.00	28 (100%)	0 (0%)		1	
	RWV	24	0.00	24 (100%)	0 (0%)	/	/	/
branchiostegal ray2 up	Control	28	0.00	28 (100%)	0 (0%)		1	
	RWV	24	0.00	24 (100%)	0 (0%)	/	/	/
entopterygoid down	Control	28	0.50	14 (50.00%)	14 (50.00%)		1	
	RWV	24	0.64	9 (37.50%)	15 (62.50%)	0.366	0.600 (0.198-1.820)	0.367
entopterygoid up	Control	28	0.50	14 (50.00%)	14 (50.00%)		1	
	RWV	24	0.64	9 (37.50%)	15 (62.50%)	0.366	0.600 (0.198-1.820)	0.367

B

				Score of Y			X^2 pearson	ordinal logistic regression	
Structures	Variable	N	Mean	absence	early	advanced	p-value	OR (IC 95%)	p-value
branchiostegal ray1 down	Control	28	0.87	12 (42.86%)	8 (28.57%)	8 (28.57%)		1	
	RWV	24	1.05	7 (29.17%)	9 (37.50%)	8 (33.33%)	0.585	1.53 (0.557-4.183)	0.411
branchiostegal ray1 up	Control	28	0.87	12 (42.86%)	8 (28.57%)	8 (28.57%)		1	
	RWV	24	1.05	7 (29.17%)	9 (37.50%)	8 (33.33%)	0.585	1.53 (0.557-4.183)	0.411
ceratohyal down	Control	28	0.73	14 (50.00%)	6 (21.43%)	8 (28.57%)		1	
	RWV	24	0.68	16 (66.67%)	1 (4.17%)	7 (29.17%)	0.175	0.632 (0.553-1.867)	0.407
ceratohyal up	Control	28	0.80	14 (50.00%)	4 (14.29%)	10 (35.71%)		1	
	RWV	24	0.64	16 (66.67%)	2 (8.33%)	6 (25.00%)	0.472	0.531 (0.178-1.585)	0.257
dentary down	Control	28	0.27	21 (75.00%)	7 (25.00%)	0 (0.00%)		1	
	RWV	24	0.41	15 (62.50%)	8 (33.33%)	1 (4.17%)	0.413	1.883 (0.575-6.163)	0.296
dentary up	Control	28	0.27	21 (75.00%)	7 (25.00%)	0 (0.00%)		1	
	RWV	24	0.41	15 (62.50%)	8 (33.33%)	1 (4.17%)	0.413	1.883 (0.575-6.163)	0.296
hyomandibular down	Control	28	0.57	16 (57.14%)	7 (25.00%)	5 (17.86%)		1	
	RWV	24	0.59	15 (62.50%)	5 (20.83%)	4 (16.67%)	0.919	0.825 (0.280-2.429)	0.727
hyomandibular up	Control	28	0.67	14 (50.00%)	8 (28.57%)	6 (21.43%)		1	
	RWV	24	0.55	16 (66.67%)	4 (16.67%)	4 (16.67%)	0.457	0.547 (0.185-1.621)	0.277
maxilla down	Control	28	0.03	27 (96.43%)	1 (3.57%)	0 (0.00%)		1	
	RWV	24	0.32	17 (70.83%)	7 (29.17%)	0 (0.00%)	**0.011**	11.118 (1.255-98.491)	**0.030**
maxilla up	Control	28	0.03	27 (96.43%)	1 (3.57%)	0 (0.00%)		1	
	RWV	24	0.32	17 (70.83%)	7 (29.17%)	0 (0.00%)	**0.011**	11.118 (1.255-98.491)	**0.030**

Annex 11: CLINO microarrays by entrez gene name.

Symbol	Entrez Gene Name	log Ratio	B-value	Type(s)
AIFM3	apoptosis-inducing factor, mitochondrion-associated, 3	1.870	4.09E00	enzyme
ATP2B3	ATPase, Ca++ transporting, plasma membrane 3	1.050	2.09E-01	transporter
ATP6AP1	ATPase, H+ transporting, lysosomal accessory protein 1	0.722	2.04E-01	transporter
AXIN2	axin 2	-3.480	4.09E-01	other
BATF	basic leucine zipper transcription factor, ATF-like	-1.380	1.41E00	transcription regulator
BTBD16	BTB (POZ) domain containing 16	1.610	8.31E-01	other
C1orf27	chromosome 1 open reading frame 27	1.810	4.75E-01	other
CALCOCO1	calcium binding and coiled-coil domain 1	1.010	4.06E-01	transcription regulator
CENPM	centromere protein M	-0.605	6.17E-01	other
CHD5	chromodomain helicase DNA binding protein 5	-0.648	1.13E00	enzyme
CRYGS	crystallin, gamma S	1.030	5.43E-01	other
CXCR3	chemokine (C-X-C motif) receptor 3	1.850	3.76E-01	G-protein coupled receptor
CYP19A1	cytochrome P450, family 19, subfamily A, polypeptide 1	1.340	3.75E00	enzyme
DMBX1	diencephalon/mesencephalon homeobox 1	1.100	3.58E-01	transcription regulator
DUPD1	dual specificity phosphatase and pro isomerase domain containing 1	-1.320	1.20E00	enzyme
E2F2	E2F transcription factor 2	-1.110	1.27E00	transcription regulator
EEA1	early endosome antigen 1	-1.710	5.07E-01	other
EFR3B	EFR3 homolog B (S. cerevisiae)	-0.850	7.37E-01	other
EGLN3	egl-9 family hypoxia-inducible factor 3	-0.615	1.22E00	enzyme
ELOVL1	ELOVL fatty acid elongase 1	-0.628	1.28E00	enzyme
FAM212A	family with sequence similarity 212, member A	0.800	5.24E-02	other
FGF2	fibroblast growth factor 2 (basic)	0.732	2.04E-01	growth factor
FOSB	FBJ murine osteosarcoma viral oncogene homolog B	-0.576	6.51E-01	transcription regulator
GAB2	GRB2-associated binding protein 2	-1.620	3.13E-01	other
GADD45B	growth arrest and DNA-damage-inducible, beta	-0.561	5.60E-01	other
GPR19	G protein-coupled receptor 19	-0.512	3.37E-01	G-protein coupled receptor
HELB	helicase (DNA) B	0.659	3.47E-03	enzyme
HES1	hes family bHLH transcription factor 1	2.010	9.21E-02	transcription regulator
HOXB6	homeobox B6	1.230	2.51E-01	transcription regulator
IGF2R	insulin-like growth factor 2 receptor	-1.610	7.30E-01	transmembrane receptor
IQGAP2	IQ motif containing GTPase activating protein 2	1.190	4.72E-01	other
JPH3	junctophilin 3	1.390	8.04E-02	ion channel
KIAA0101	KIAA0101	-0.618	8.48E-01	other
KIAA0556	KIAA0556	-1.090	3.01E-01	other
KLHL14	kelch-like family member 14	0.577	2.84E-01	other
KLHL38	kelch-like family member 38	1.010	1.84E-01	other
LPL	lipoprotein lipase	0.628	6.51E-01	enzyme
MAD2L1BP	MAD2L1 binding protein	-0.757	8.77E-01	other
MAPKAPK3	mitogen-activated protein kinase-activated protein kinase 3	1.110	3.05E-01	kinase
MASP2	mannan-binding lectin serine peptidase 2	-1.140	1.24E00	peptidase
MCL1	myeloid cell leukemia 1	-0.698	1.67E-01	transporter
MOCOS	molybdenum cofactor sulfurase	0.870	1.35E00	enzyme
MORN4	MORN repeat containing 4	1.920	5.37E-01	other
NDRG2	NDRG family member 2	0.649	4.09E-01	other
NUF2	NUF2, NDC80 kinetochore complex component	-0.674	1.78E00	other
P2RY13	purinergic receptor P2Y, G-protein coupled, 13	-1.500	1.78E00	G-protein coupled receptor
PARD3	par-3 family cell polarity regulator	0.987	6.98E-01	other
PTPRJ	protein tyrosine phosphatase, receptor type, J	1.910	2.30E00	phosphatase
RALGAPB	Ral GTPase activating protein, beta subunit (non-catalytic)	0.995	7.01E-01	other
RANBP10	RAN binding protein 10	1.550	3.49E-01	other
RHCG	Rh family, C glycoprotein	0.825	2.41E00	transporter
RNPEPL1	arginyl aminopeptidase (aminopeptidase B)-like 1	1.500	2.36E00	peptidase
RYR2	ryanodine receptor 2 (cardiac)	-1.370	4.26E-01	ion channel
SETD5	SET domain containing 5	-1.250	1.23E00	other
SLC35D1	solute carrier family 35 (UDP-GlcA/UDP-GalNAc transporter), member D1	-1.370	1.94E00	transporter
SLIT3	slit homolog 3 (Drosophila)	0.879	5.46E-01	other
SMG6	SMG6 nonsense mediated mRNA decay factor	1.360	5.00E-01	enzyme
TELO2	telomere maintenance 2	-1.730	2.38E-01	other
TESK2	testis-specific kinase 2	1.540	2.20E-02	kinase
TPCN2	two pore segment channel 2	1.720	3.55E-01	ion channel
TPMT	thiopurine S-methyltransferase	-0.908	2.50E00	enzyme
TYW5	tRNA-yW synthesizing protein 5	0.783	1.46E00	enzyme
ZMYM4	zinc finger, MYM-type 4	0.902	4.55E-01	other

Annex 12: RPM microarrays by entrez gene name.

Symbol	Entrez Gene Name	Log Ratio	B-value	Type(s)
ACIN1	apoptotic chromatin condensation inducer 1	0.738	3.14E-01	enzyme
ACSL6	acyl-CoA synthetase long-chain family member 6	0.762	5.20E-02	enzyme
ADAM10	ADAM metallopeptidase domain 10	0.735	4.04E-01	peptidase
ADAM17	ADAM metallopeptidase domain 17	0.770	7.48E-02	peptidase
ADAT2	adenosine deaminase, tRNA-specific 2	3.750	1.50E00	enzyme
APC2	adenomatosis polyposis coli 2	0.721	1.28E-02	enzyme
ARGLU1	arginine and glutamate rich 1	0.597	2.93E00	other
ARHGEF17	Rho guanine nucleotide exchange factor (GEF) 17	1.020	1.07E00	other
ARL14	ADP-ribosylation factor-like 14	1.630	8.03E-01	other
BARX2	BARX homeobox 2	-0.728	1.95E-01	transcription regulator
CARD9	caspase recruitment domain family, member 9	-0.607	1.01E00	other
CASP1	caspase 1, apoptosis-related cysteine peptidase	-0.617	1.86E00	peptidase
CDK19	cyclin-dependent kinase 19	0.688	9.80E-02	kinase
CES1	carboxylesterase 1	0.572	3.23E00	enzyme
CFB	complement factor B	-0.584	1.29E-02	peptidase
CTSS	cathepsin S	-0.693	2.14E00	peptidase
CXCR3	chemokine (C-X-C motif) receptor 3	-1.040	7.77E-02	G-protein coupled receptor
DAAM1	dishevelled associated activator of morphogenesis 1	0.702	5.60E-01	other
DMBX1	diencephalon/mesencephalon homeobox 1	0.965	1.79E00	transcription regulator
EHF	ets homologous factor	-0.912	3.69E00	transcription regulator
ELF3	E74-like factor 3 (ets domain transcription factor, epithelial-specific)	-0.932	2.45E00	transcription regulator
ERAP1	endoplasmic reticulum aminopeptidase 1	-0.592	1.29E00	peptidase
FAM46A	family with sequence similarity 46, member A	0.952	5.45E-01	other
FGF4	fibroblast growth factor 4	-0.683	2.93E-02	growth factor
FHOD3	formin homology 2 domain containing 3	0.972	1.40E-01	other
FKBP5	FK506 binding protein 5	0.845	2.61E-02	enzyme
GPR142	G protein-coupled receptor 142	1.850	2.43E-02	G-protein coupled receptor
HOXB9	homeobox B9	-0.952	1.26E00	transcription regulator
INHBB	inhibin, beta B	0.665	1.06E00	growth factor
IPPK	inositol 1,3,4,5,6-pentakisphosphate 2-kinase	0.702	2.69E-01	kinase
IQCJ-SCHIP1	IQCJ-SCHIP1 readthrough	0.952	1.85E00	other
KIF5A	kinesin family member 5A	0.825	1.32E-01	transporter
KLHL38	kelch-like family member 38	-1.420	2.42E-01	other
LRP5	low density lipoprotein receptor-related protein 5	0.891	1.47E00	transmembrane receptor
MAPK6	mitogen-activated protein kinase 6	0.673	8.71E-01	kinase
MED23	mediator complex subunit 23	-1.260	4.03E-01	transcription regulator
MLLT1	myeloid/lymphoid or mixed-lineage leukemia (trithorax homolog, Drosophila); translocated to, 1	0.851	4.60E-01	transcription regulator
MPEG1	macrophage expressed 1	-0.992	1.27E-01	other
NAALADL1	N-acetylated alpha-linked acidic dipeptidase-like 1	0.745	1.63E-01	peptidase
NCKAP1	NCK-associated protein 1	1.390	2.70E00	other
NFKBIE	nuclear factor of kappa light polypeptide gene enhancer in B-cells inhibitor, epsilon	-0.529	2.92E-01	transcription regulator
NOTCH1	notch 1	1.360	7.36E-01	transcription regulator
PDZD4	PDZ domain containing 4	0.964	1.34E00	other
PGLYRP1	peptidoglycan recognition protein 1	-0.570	2.10E-01	transmembrane receptor
PIGK	phosphatidylinositol glycan anchor biosynthesis, class K	3.520	3.12E00	peptidase
RAB11FIP4	RAB11 family interacting protein 4 (class II)	0.584	7.87E-01	other
RAB3A	RAB3A, member RAS oncogene family	1.160	4.27E00	enzyme
RAPH1	Ras association (RalGDS/AF-6) and pleckstrin homology domains 1	1.360	1.08E00	other
RBM47	RNA binding motif protein 47	0.798	2.65E-01	other
RHCG	Rh family, C glycoprotein	0.777	1.37E-01	transporter
RUNX1	runt-related transcription factor 1	1.860	6.58E-01	transcription regulator
SCARB2	scavenger receptor class B, member 2	0.704	1.80E00	other
SERPINH1	serpin peptidase inhibitor, clade H (heat shock protein 47), member 1, (collagen binding protein 1)	0.761	2.49E-01	other
SLC16A6	solute carrier family 16, member 6	1.730	1.71E00	transporter

SLC38A4	solute carrier family 38, member 4	0.845	2.68E-01	transporter
SLC44A5	solute carrier family 44, member 5	1.250	1.47E00	transporter
SPEF2	sperm flagellar 2	-1.340	3.22E-01	other
SRF	serum response factor (c-fos serum response element-binding transcription factor)	1.010	4.90E-01	transcription regulator
Sult5a1	sulfotransferase family 5A, member 1	-1.810	3.99E00	other
Vmn2r1	vomeronasal 2, receptor 1	-1.280	1.01E-01	other
WNT3A	wingless-type MMTV integration site family, member 3A	1.070	4.30E-01	cytokine
XAF1	XIAP associated factor 1	-0.782	1.39E00	other

Annex 13: RWV microarrays by entrez gene name.

Symbol	Entrez Gene Name	Log Ratio	p-value	Type(s)
ABCA2	ATP-binding cassette, sub-family A (ABC1), member 2	-0.525	2.53E-01	transporter
ABCG5	ATP-binding cassette, sub-family G (WHITE), member 5	0.487	9.03E-02	transporter
ACSL3	acyl-CoA synthetase long-chain family member 3	0.599	1.61E-01	enzyme
ACSL6	acyl-CoA synthetase long-chain family member 6	1.350	2.29E-01	enzyme
ADPGK	ADP-dependent glucokinase	-0.536	3.10E-02	kinase
AHNAK	AHNAK nucleoprotein	-0.516	1.20E-01	other
AKT2	v-akt murine thymoma viral oncogene homolog 2	0.517	2.02E-01	kinase
ALDH7A1	aldehyde dehydrogenase 7 family, member A1	0.486	2.74E-01	enzyme
ANKRD52	ankyrin repeat domain 52	-0.486	1.06E-01	transcription regulator
ANKRD9	ankyrin repeat domain 9	0.604	1.42E-02	other
ARFGEF2	ADP-ribosylation factor guanine nucleotide-exchange factor 2 (brefeldin A-inhibited)	0.589	1.51E-01	other
ARHGAP27	Rho GTPase activating protein 27	-0.498	1.52E-01	other
ARHGAP6	Rho GTPase activating protein 6	-0.720	8.47E-02	other
ARL5C	ADP-ribosylation factor-like 5C	0.504	8.16E-02	other
ARRDC2	arrestin domain containing 2	0.547	2.39E-03	other
ARRDC2	arrestin domain containing 2	0.521	2.64E-03	other
ARRDC2	arrestin domain containing 2	0.515	9.84E-03	other
ATXN3	ataxin 3	0.547	1.22E-01	peptidase
BIN3	bridging integrator 3	-0.590	1.16E-01	other
BOC	BOC cell adhesion associated, oncogene regulated	-0.694	1.93E-02	other
C15orf59	chromosome 15 open reading frame 59	0.621	2.42E-01	other
C1orf95	chromosome 1 open reading frame 95	-0.645	9.21E-02	other
CACNA1D	calcium channel, voltage-dependent, L type, alpha 1D subunit	-0.489	2.59E-02	ion channel
CCR9	chemokine (C-C motif) receptor 9	0.964	9.61E-02	G-protein coupled receptor
CDK14	cyclin-dependent kinase 14	-0.605	1.31E-01	kinase
CEBPD	CCAAT/enhancer binding protein (C/EBP), delta	0.592	5.72E-02	transcription regulator
CEBPD	CCAAT/enhancer binding protein (C/EBP), delta	0.563	3.00E-02	transcription regulator
CEBPD	CCAAT/enhancer binding protein (C/EBP), delta	0.488	1.49E-01	transcription regulator
CFH	complement factor H	-0.549	2.15E-02	other
CHAC1	ChaC glutathione-specific gamma-glutamylcyclotransferase 1	0.557	5.52E-02	other
CHAC1	ChaC glutathione-specific gamma-glutamylcyclotransferase 1	0.546	5.57E-02	other
CIRH1A	cirrhosis, autosomal recessive 1A (cirhin)	0.554	5.09E-02	other
CLTC	clathrin, heavy chain (Hc)	-0.559	7.13E-02	other
CLTC	clathrin, heavy chain (Hc)	-0.506	1.86E-01	other
CNOT1	CCR4-NOT transcription complex, subunit 1	0.545	2.07E-01	other
CNOT8	CCR4-NOT transcription complex, subunit 8	0.553	2.50E-03	transcription regulator
COL10A1	collagen, type X, alpha 1	0.537	2.55E-02	other
COL6A3	collagen, type VI, alpha 3	-0.509	9.84E-02	other
COQ10B	coenzyme Q10 homolog B (S. cerevisiae)	0.675	4.16E-02	other
CORO1C	coronin, actin binding protein, 1C	-0.519	1.91E-01	other
CRH	corticotropin releasing hormone	0.555	3.91E-03	cytokine
CRHBP	corticotropin releasing hormone binding protein	0.543	1.04E-01	other
CTSC	cathepsin C	-0.540	2.33E-01	peptidase
CUZD1	CUB and zona pellucida-like domains 1	0.673	7.58E-02	other
CYP24A1	cytochrome P450, family 24, subfamily A, polypeptide 1	0.617	1.61E-01	enzyme
CYP24A1	cytochrome P450, family 24, subfamily A, polypeptide 1	0.585	1.15E-01	enzyme
Cyp2ac1	cytochrome P450, family 2, subfamily ac, polypeptide 1	0.814	2.72E-02	other
Cyp2ac1	cytochrome P450, family 2, subfamily ac, polypeptide 1	0.697	1.92E-02	other
DAB2	Dab, mitogen-responsive phosphoprotein, homolog 2 (Drosophila)	-0.575	2.72E-01	other
DDB1	damage-specific DNA binding protein 1, 127kDa	0.562	3.31E-01	other
DDIT4	DNA-damage-inducible transcript 4	0.869	8.80E-02	other
DLG4	discs, large homolog 4 (Drosophila)	-0.500	3.85E-01	kinase
DLL1	delta-like 1 (Drosophila)	0.522	1.85E-01	enzyme

Dmd	dystrophin	-0.526	9.86E-02	other
DNAJC19	DnaJ (Hsp40) homolog, subfamily C, member 19	0.573	5.43E-02	other
DUSP1	dual specificity phosphatase 1	0.602	8.31E-02	phosphatase
DUSP1	dual specificity phosphatase 1	0.571	3.01E-02	phosphatase
EBPL	emopamil binding protein-like	-0.706	1.53E-01	enzyme
EIF4EBP3	eukaryotic translation initiation factor 4E binding protein 3	0.910	3.92E-02	other
ENTPD8	ectonucleoside triphosphate diphosphohydrolase 8	0.598	1.32E-02	enzyme
EVI5L	ecotropic viral integration site 5-like	-0.553	9.30E-02	other
EVPL	envoplakin	-0.556	9.54E-02	other
EWSR1	EWS RNA-binding protein 1	0.492	3.79E-01	other
FAM126B	family with sequence similarity 126, member B	0.489	2.94E-01	other
FAM46C	family with sequence similarity 46, member C	0.623	5.53E-02	other
FAM89B	family with sequence similarity 89, member B	0.500	2.93E-01	other
FAM91A1	family with sequence similarity 91, member A1	0.564	2.37E-01	other
FBXW11	F-box and WD repeat domain containing 11	0.529	1.61E-01	enzyme
FGD1	FYVE, RhoGEF and PH domain containing 1	-0.492	1.38E-01	other
FKBP5	FK506 binding protein 5	0.629	1.63E-01	enzyme
FLOT2	flotillin 2	-0.577	2.06E-01	other
FOXJ1	forkhead box J1	0.608	8.10E-02	transcription regulator
FOXQ1	forkhead box Q1	0.499	6.23E-02	transcription regulator
G6PC	glucose-6-phosphatase, catalytic subunit	0.507	5.70E-02	phosphatase
GABBR1	gamma-aminobutyric acid (GABA) B receptor, 1	-0.543	1.96E-01	G-protein coupled receptor
GAD2	glutamate decarboxylase 2 (pancreatic islets and brain, 65kDa)	0.525	2.91E-01	enzyme
GADD45B	growth arrest and DNA-damage-inducible, beta	0.693	1.03E-02	other
GADD45B	growth arrest and DNA-damage-inducible, beta	0.589	3.19E-02	other
GIPC1	GIPC PDZ domain containing family, member 1	-0.505	8.42E-02	other
GPHB5	glycoprotein hormone beta 5	-0.773	4.22E-02	other
HNRNPH1	heterogeneous nuclear ribonucleoprotein H1 (H)	0.573	3.60E-01	other
HPX	hemopexin	0.727	5.47E-02	transporter
HPX	hemopexin	0.563	1.97E-02	transporter
HPX	hemopexin	0.503	1.19E-02	transporter
HSD17B12	hydroxysteroid (17-beta) dehydrogenase 12	0.559	1.80E-01	enzyme
HSPA14	heat shock 70kDa protein 14	0.486	1.37E-01	peptidase
IGFBP1	insulin-like growth factor binding protein 1	0.652	1.02E-02	other
IGFBP1	insulin-like growth factor binding protein 1	0.648	5.19E-02	other
INSM1	insulinoma-associated 1	0.565	1.80E-01	transcription regulator
IPO5	importin 5	-0.526	3.99E-01	transporter
IVNS1ABP	influenza virus NS1A binding protein	0.796	2.39E-01	other
JUN	jun proto-oncogene	0.519	1.40E-01	transcription regulator
KCMF1	potassium channel modulatory factor 1	0.535	2.26E-01	other
LBH	limb bud and heart development	0.548	6.90E-02	transcription regulator
LIPG	lipase, endothelial	0.524	2.40E-02	enzyme
LOXL1	lysyl oxidase-like 1	-0.556	1.94E-02	enzyme
LTA4H	leukotriene A4 hydrolase	0.494	2.75E-01	enzyme
LYRM2	LYR motif containing 2	0.533	1.87E-01	other
MAP3K13	mitogen-activated protein kinase kinase kinase 13	-0.504	2.55E-01	kinase
MBNL2	muscleblind-like splicing regulator 2	-0.539	2.10E-01	other
MBNL2	muscleblind-like splicing regulator 2	-0.518	1.38E-01	other
MBNL2	muscleblind-like splicing regulator 2	-0.518	1.38E-01	other
METTL11B	methyltransferase like 11B	-0.705	1.90E-03	other
METTL23	methyltransferase like 23	0.562	8.12E-03	other
MGAT5	mannosyl (alpha-1,6-)-glycoprotein beta-1,6-N-acetyl-glucosaminyltransferase	-0.489	1.23E-01	enzyme
MIP	major intrinsic protein of lens fiber	0.497	3.15E-01	transporter
MKNK1	MAP kinase interacting serine/threonine kinase 1	0.590	5.47E-02	kinase
MKRN2	makorin ring finger protein 2	0.521	3.00E-01	other
MMP8	matrix metallopeptidase 8 (neutrophil collagenase)	-1.017	2.62E-01	peptidase
MMP9	matrix metallopeptidase 9 (gelatinase B, 92kDa gelatinase, 92kDa type IV collagenase)	-0.650	2.81E-01	peptidase
Mslnl	mesothelin-like	0.540	4.24E-02	other
Mslnl	mesothelin-like	0.489	1.38E-01	other
MTHFD1L	methylenetetrahydrofolate dehydrogenase (NADP+ dependent) 1-like	-0.769	1.23E-01	enzyme
MTRF1	mitochondrial translational release factor 1	0.495	9.44E-02	translation regulator
MYADM	myeloid-associated differentiation marker	-0.524	1.03E-01	other

MYBPC2	myosin binding protein C, fast type	0.745	1.43E-01	other
NAA40	N(alpha)-acetyltransferase 40, NatD catalytic subunit	0.579	1.81E-01	other
NAPEPLD	N-acyl phosphatidylethanolamine phospholipase D	0.513	1.71E-01	enzyme
NCOR1	nuclear receptor corepressor 1	-0.518	2.19E-01	transcription regulator
NDRG3	NDRG family member 3	0.540	2.25E-01	other
NDRG3	NDRG family member 3	0.527	2.30E-01	other
NDRG3	NDRG family member 3	0.494	1.93E-01	other
NDRG4	NDRG family member 4	0.554	3.37E-01	other
NOP14	NOP14 nucleolar protein	0.563	1.35E-01	other
NPAS4	neuronal PAS domain protein 4	0.679	1.55E-01	transcription regulator
NR2E3	nuclear receptor subfamily 2, group E, member 3	0.619	1.04E-01	ligand-dependent nuclear receptor
NR4A1	nuclear receptor subfamily 4, group A, member 1	0.496	2.23E-02	ligand-dependent nuclear receptor
NR4A3	nuclear receptor subfamily 4, group A, member 3	0.688	2.80E-02	ligand-dependent nuclear receptor
NUDT17	nudix (nucleoside diphosphate linked moiety X)-type motif 17	0.509	1.89E-01	other
OBSCN	obscurin, cytoskeletal calmodulin and titin-interacting RhoGEF	-0.732	7.81E-02	kinase
OLFML2B	olfactomedin-like 2B	-0.756	4.77E-02	other
OTP	orthopedia homeobox	0.606	3.05E-01	transcription regulator
P2RY13	purinergic receptor P2Y, G-protein coupled, 13	0.591	3.78E-01	G-protein coupled receptor
PAIP2B	poly(A) binding protein interacting protein 2B	0.874	2.49E-01	translation regulator
PAM	peptidylglycine alpha-amidating monooxygenase	0.551	2.46E-01	enzyme
PDK2	pyruvate dehydrogenase kinase, isozyme 2	0.585	1.92E-01	kinase
PEPD	peptidase D	0.503	2.01E-01	peptidase
PFN4	profilin family, member 4	0.616	1.35E-01	other
PLB1	phospholipase B1	0.539	1.29E-01	enzyme
PPP4C	protein phosphatase 4, catalytic subunit	0.532	3.92E-01	phosphatase
PPP4R1	protein phosphatase 4, regulatory subunit 1	0.666	2.98E-01	phosphatase
PRPF19	pre-mRNA processing factor 19	0.530	1.47E-01	other
RAP1A	RAP1A, member of RAS oncogene family	-0.497	1.53E-01	enzyme
RELN	reelin	0.492	2.03E-01	peptidase
RGS21	regulator of G-protein signaling 21	0.498	1.46E-01	other
RHCG	Rh family, C glycoprotein	1.511	6.94E-02	transporter
RHCG	Rh family, C glycoprotein	1.250	2.57E-02	transporter
RHCG	Rh family, C glycoprotein	1.057	4.88E-03	transporter
RHCG	Rh family, C glycoprotein	0.802	4.64E-02	transporter
RHCG	Rh family, C glycoprotein	0.561	2.79E-02	transporter
RNF126	ring finger protein 126	-0.549	9.57E-02	other
RPE65	retinal pigment epithelium-specific protein 65kDa	-0.664	9.88E-02	enzyme
RPL31	ribosomal protein L31	0.588	6.48E-02	other
RYR2	ryanodine receptor 2 (cardiac)	-0.567	1.69E-01	ion channel
RYR2	ryanodine receptor 2 (cardiac)	-0.505	5.00E-02	ion channel
RYR2	ryanodine receptor 2 (cardiac)	-0.490	1.62E-01	ion channel
SALL4	spalt-like transcription factor 4	-0.530	2.10E-01	transcription regulator
SDHA	succinate dehydrogenase complex, subunit A, flavoprotein (Fp)	0.512	1.56E-01	enzyme
SERPINH1	serpin peptidase inhibitor, clade H (heat shock protein 47), member 1, (collagen binding protein 1)	1.401	1.37E-01	other
SERPINH1	serpin peptidase inhibitor, clade H (heat shock protein 47), member 1, (collagen binding protein 1)	0.512	6.09E-02	other
SGCD	sarcoglycan, delta (35kDa dystrophin-associated glycoprotein)	-0.612	1.84E-01	other
SGCD	sarcoglycan, delta (35kDa dystrophin-associated glycoprotein)	-0.493	1.11E-01	other
SGK1	serum/glucocorticoid regulated kinase 1	0.573	1.48E-01	kinase
SGK1	serum/glucocorticoid regulated kinase 1	0.494	1.86E-01	kinase
SLC17A7	solute carrier family 17 (vesicular glutamate transporter), member 7	-0.488	3.56E-02	transporter
SLC18A3	solute carrier family 18 (vesicular acetylcholine transporter), member 3	0.830	3.25E-01	transporter
SLC25A39	solute carrier family 25, member 39	0.587	1.60E-01	other
SLC25A43	solute carrier family 25, member 43	0.631	7.91E-02	transporter
Slc47a2	solute carrier family 47, member 2	0.525	2.16E-01	transporter
SLC7A5	solute carrier family 7 (amino acid transporter light	-0.521	9.77E-02	transporter

	chain, L system), member 5			
SLMO2	slowmo homolog 2 (Drosophila)	0.600	3.92E-02	other
SMC2	structural maintenance of chromosomes 2	-0.613	3.06E-01	transporter
SOCS1	suppressor of cytokine signaling 1	0.721	5.37E-04	other
SOCS1	suppressor of cytokine signaling 1	0.691	4.97E-03	other
SOCS3	suppressor of cytokine signaling 3	0.697	6.85E-02	phosphatase
SPG11	spastic paraplegia 11 (autosomal recessive)	0.603	1.79E-01	other
SPTBN2	spectrin, beta, non-erythrocytic 2	-0.616	1.45E-01	other
ST8SIA6	ST8 alpha-N-acetyl-neuraminide alpha-2,8-sialyltransferase 6	-0.531	1.06E-01	enzyme
STAT6	signal transducer and activator of transcription 6, interleukin-4 induced	-0.498	1.77E-01	transcription regulator
STX4	syntaxin 4	-0.486	2.10E-01	transporter
Sult5a1	sulfotransferase family 5A, member 1	-0.810	2.18E-02	other
SV2A	synaptic vesicle glycoprotein 2A	-0.490	2.19E-01	transporter
TARBP1	TAR (HIV-1) RNA binding protein 1	0.537	7.19E-02	transcription regulator
TAT	tyrosine aminotransferase	0.613	7.58E-02	enzyme
TAT	tyrosine aminotransferase	0.553	1.40E-02	enzyme
TAT	tyrosine aminotransferase	0.551	9.74E-02	enzyme
TDO2	tryptophan 2,3-dioxygenase	0.536	3.42E-03	enzyme
TFE3	transcription factor binding to IGHM enhancer 3	-0.660	2.53E-01	transcription regulator
TK1	thymidine kinase 1, soluble	-0.486	5.51E-02	kinase
TM6SF2	transmembrane 6 superfamily member 2	-0.514	9.62E-02	other
TMEM175	transmembrane protein 175	0.587	1.98E-01	other
TMEM19	transmembrane protein 19	0.488	2.47E-01	other
TMUB1	transmembrane and ubiquitin-like domain containing 1	0.643	1.62E-01	other
TOP2A	topoisomerase (DNA) II alpha 170kDa	-0.534	3.77E-04	enzyme
TP53I11	tumor protein p53 inducible protein 11	-0.490	1.35E-01	other
TTN	titin	-0.532	5.91E-02	kinase
TTYH1	tweety family member 1	-0.621	1.18E-02	ion channel
UACA	uveal autoantigen with coiled-coil domains and ankyrin repeats	-0.500	6.88E-03	other
UBE2S	ubiquitin-conjugating enzyme E2S	-0.521	2.24E-01	enzyme
UCP3	uncoupling protein 3 (mitochondrial, proton carrier)	0.565	6.69E-02	transporter
UCP3	uncoupling protein 3 (mitochondrial, proton carrier)	0.546	7.84E-02	transporter
UCP3	uncoupling protein 3 (mitochondrial, proton carrier)	0.507	1.36E-01	transporter
UCP3	uncoupling protein 3 (mitochondrial, proton carrier)	0.507	1.36E-01	transporter
ULK2	unc-51 like autophagy activating kinase 2	0.501	3.87E-02	kinase
USP44	ubiquitin specific peptidase 44	0.526	9.48E-02	peptidase
VCL	vinculin	-0.602	1.34E-01	enzyme
VPS28	vacuolar protein sorting 28 homolog (S. cerevisiae)	0.500	2.48E-01	transporter
WBSCR16	Williams-Beuren syndrome chromosome region 16	0.497	2.53E-01	other
WDR26	WD repeat domain 26	-0.513	1.69E-01	other
WHSC1	Wolf-Hirschhorn syndrome candidate 1	-0.498	1.11E-01	enzyme
WNT3A	wingless-type MMTV integration site family, member 3A	-0.632	1.74E-01	cytokine
WWTR1	WW domain containing transcription regulator 1	-0.596	1.43E-01	transcription regulator
ZBED4	zinc finger, BED-type containing 4	0.553	2.41E-01	other
ZDHHC9	zinc finger, DHHC-type containing 9	0.624	2.03E-01	enzyme
ZMYM2	zinc finger, MYM-type 2	0.565	2.31E-01	other
ZNF143	zinc finger protein 143	-0.565	1.47E-01	transcription regulator
ZXDC	ZXD family zinc finger C	-0.629	1.24E-01	transcription regulator

Annex 14: Microgravity microarrays (CLINO, RPM, RWV) by category.

Category	CLINOSTAT	RPM	RWV
Cell Death and Survival	1	38	12
Connective Tissue Disorders	2	20	7
Immunological Disease	3	33	9
Inflammatory Disease	4	21	10
Skeletal and Muscular Disorders	5	22	11
Cancer	6	3	13
Tumor Morphology	7	15	37
Cellular Development	8	4	1
Cellular Function and Maintenance	9	17	18
Cellular Movement	10	9	36
Connective Tissue Development and Function	11	44	29
Hepatic System Development and Function	12	74	24
Tissue Development	13	27	21
Cellular Growth and Proliferation	14	13	2
Embryonic Development	15	5	32
Neurological Disease	16	40	30
Organ Development	17	7	26
Organismal Development	18	8	34
Renal and Urological System Development and Function	19	50	52
Reproductive System Development and Function	20	51	49
Hematological System Development and Function	21	1	5
Tissue Morphology	22	14	57
Hematological Disease	23	35	63
Cardiovascular Disease	24	52	16
Organismal Injury and Abnormalities	25	49	14
Cell Cycle	26	30	35
Protein Synthesis	27	37	48
Cell Signaling	28	55	
Small Molecule Biochemistry	29	43	41
Vitamin and Mineral Metabolism	30		67
Organ Morphology	31	29	51
Cell Morphology	32	25	60
Hematopoiesis	33	2	6
Cardiovascular System Development and Function	34	16	50
Nervous System Development and Function	35	48	58
Molecular Transport	36	42	40
Hair and Skin Development and Function	37	28	73
Skeletal and Muscular System Development and Function	38	45	20
Cellular Assembly and Organization	39	26	17
Reproductive System Disease	40	63	15
Gene Expression	41	47	66
DNA Replication, Recombination, and Repair	42	67	71
Endocrine System Development and Function	43	73	3
Gastrointestinal Disease	44	32	23
Hepatic System Disease	45		25
Lymphoid Tissue Structure and Development	46	6	33
Amino Acid Metabolism	47	70	59
Auditory Disease	48	71	
Auditory and Vestibular System Development and Function	49	72	
Behavior	50	66	27
Cell-To-Cell Signaling and Interaction	51	23	47
Cell-mediated Immune Response	52	10	31
Cellular Compromise	53	39	70
Dermatological Diseases and Conditions	54	18	8
Developmental Disorder	55	56	53
Digestive System Development and Function	56		22
Drug Metabolism	57	57	61
Endocrine System Disorders	58	31	69
Energy Production	59		45
Hereditary Disorder	60	58	46
Humoral Immune Response	61	19	74
Immune Cell Trafficking	62	11	43
Infectious Disease	63	59	54

Inflammatory Response	64	24	4
Lipid Metabolism	65	41	39
Metabolic Disease	66	34	64
Nucleic Acid Metabolism	67		
Ophthalmic Disease	68	60	19
Post-Translational Modification	69	12	76
Protein Degradation	70	36	77
Visual System Development and Function	71	69	62
Renal and Urological Disease	72	62	65
Carbohydrate Metabolism	73	54	28
Organismal Survival	74	65	55
Cellular Response to Therapeutics	75		
Respiratory Disease	76	46	38

Annex 15: Microgravity (CLINO, RPM, RWV) Heat map.

Upstream reg.	CLINOSTAT	RPM	RWV
CREB1	**-2.19**		**3.24**
TCR	**-1.99**		**2.20**
IL12 (complex)	**-1.70**		**2.42**
IL6	**-1.39**		**2.43**
IL1B	**-0.39**	**-1.02**	**2.41**
IL10		**1.98**	**1.70**
NFkB (complex)		**-1.54**	**1.55**
EGF	**-1.03**	**-0.39**	**1.61**
HIF1A	**-1.41**		**1.62**
Growth hormone			**2.76**
IFNG		**-1.79**	**0.87**
IL1		**-1.00**	**1.65**
IL2	**1.00**		**1.45**
TLR9			**2.42**
CEBPB			**2.41**
LIF			**2.40**
IL4	**-1.00**		**1.39**
LDL			**2.37**
PDGF BB			**2.33**
AGT	**1.97**		**0.34**
TNF		**-1.37**	**0.93**
STK11			**2.24**
NFKBIA			**2.22**
TLR3			**2.20**
PPARG			**2.13**
IL6ST			**2.00**
NCOR1			**-2.00**
NR5A2			**1.98**
CRH			**1.98**
CREM	**-1.97**		
CTNNB1			**1.97**
IFNB1		**-1.96**	
CD40LG	**-0.85**	**1.09**	
MAPK14			**1.93**
Pkc(s)			**1.89**
NR3C1			**1.89**
STAT3			**1.83**
FOXO1			**1.82**
F2		**1.34**	**0.46**
PTH			**1.80**
POMC			**1.75**
Vegf	**-1.00**	**0.65**	
FSH			**1.62**
EGR2			**1.60**
LEP			**1.56**
P38 MAPK			**1.50**
Hdac			**-1.48**

SOCS1			**-1.46**
Creb			**1.43**
MTOR			**1.34**
FGF2			**1.34**
STAT1			**1.33**
RUNX2	**1.25**		
TGFB1		**0.81**	**0.40**

Annex 16: Morphometric analysis of bone staining after 5 days relative microgravity. A) Hypergravity (1g>3g). B) Relative microgravity (3g, 3g<1g, 3g>axe, 1g).

A)

Measures	Variable	N	Mean	SD	t-test	p-value
Distance between anguloarticular up and down	Control	24	440.5	48.307		
	1g > 3g	24	495.4	47.607	3.965	**<0.001**
Distance from anterior to notochord	Control	24	1312	68.801		
	1g > 3g	24	1300	95.294	0.514	0.610
Distance from anterior to parasphenoid a	Control	24	407.2	57.249		
	1g > 3g	24	368.8	45.839	2.559	**0.014**
Distance between branchiostegal ray1 up and down	Control	24	633.5	67.031		
	1g > 3g	24	710.7	84.974	3.492	**0.001**
Distance between entopterygoid up and down	Control	24	354.6	19.230		
	1g > 3g	24	375.6	22.524	3.470	**0.001**
Distance between maxilla up and down	Control	24	543.8	32.352		
	1g > 3g	24	550.3	29.804	0.718	0.477
Distance between opercle up and down	Control	24	981.8	49.643		
	1g > 3g	24	1038	69.188	3.224	**0.002**
Triangle area of the parasphenoid	Control	24	85760	10106.464		
	1g > 3g	24	90360	9593.111	1.620	0.112

B)

Measures	Variable	N	Mean	SD	anova	p-value
Distance from anterior to notochord	3g	33	1024	304,9	=	**0,008**
	3g > 1g	25	1253	74,76	=	
	3g > axe	25	1246	60,30	=	
	1g	25	972,4	324,6		
Distance from anterior to parasphenoid a	3g	33	342,9	103,7	=	0,077
	3g > 1g	25	396,7	43,35	=	
	3g > axe	25	407,4	37,66	=	
	1g	25	354,6	98,67		
Distance between branchiostegal ray1 up and down	3g	33	579,3	178,6	=	**<0.001**
	3g > 1g	25	738,3	73,69	***	
	3g > axe	25	729,6	73,63	***	
	1g	25	529,6	174,2		
Distance between entopterygoid up and down	3g	33	284,1	80,18	=	**0,001**
	3g > 1g	25	348,4	37,37	=	
	3g > axe	25	355,3	30,46	*	
	1g	25	284,2	95,86		
Distance between maxilla up and down	3g	33	460,6	133,4	=	**0,048**
	3g > 1g	25	545,6	28,31	=	
	3g > axe	25	560,5	36,76	=	
	1g	25	433,8	149,2		
Distance between opercule up and down	3g	33	848,0	258,0	=	**<0,001**
	3g > 1g	25	1043	68,04	***	
	3g > axe	25	1020	60,79	*	
	1g	25	776,1	254,4		
Triangle area of the parasphenoid	3g	33	56690	30290	=	**<0,001**
	3g > 1g	25	78410	8486	***	
	3g > axe	25	75840	9570	*	
	1g	25	46760	31000		

Annex 17: Hypergravity microarrays by entrez gene name.

Symbol	Entrez Gene Name	Log Ratio 1g>3g	p-value	D	Type(s)
ABCA5	ATP-binding cassette. sub-family A (ABC1). member 5	-0.223	8.38E-02		transporter
APOA4	apolipoprotein A-IV	-0.353	9.57E-02		transporter
AQP3	aquaporin 3 (Gill blood group)	-0.166	7.48E-02		transporter
HBE1	hemoglobin. epsilon 1	-0.311	7.58E-02		transporter
KCND3	potassium voltage-gated channel. Shal-related subfamily. member 3	-0.252	4.52E-02	D	ion channel
KCND3	potassium voltage-gated channel. Shal-related subfamily. member 3	-0.195	8.61E-02	D	ion channel
KPNA4	karyopherin alpha 4 (importin alpha 3)	0.149	8.59E-02		transporter
NUP133	nucleoporin 133kDa	0.188	8.61E-02	D	transporter
NUP133	nucleoporin 133kDa	0.182	9.53E-02	D	transporter
REEP5	receptor accessory protein 5	-0.280	6.37E-02		transporter
RHCG	Rh family. C glycoprotein	-0.556	4.61E-02		transporter
SCN5A	sodium channel. voltage-gated. type V. alpha subunit	-0.253	7.07E-02		ion channel
SEC23B	Sec23 homolog B (S. cerevisiae)	-0.251	7.34E-02		transporter
SEH1L	SEH1-like (S. cerevisiae)	-0.174	7.69E-02		transporter
SLC15A1	solute carrier family 15 (oligopeptide transporter). member 1	-0.485	5.01E-02	D	transporter
SLC15A1	solute carrier family 15 (oligopeptide transporter). member 1	-0.487	8.61E-02	D	transporter
SLC25A26	solute carrier family 25 (S-adenosylmethionine carrier). member 26	-0.114	7.99E-02		transporter
SLC25A43	solute carrier family 25. member 43	-0.496	6.86E-02		transporter
SLC5A6	solute carrier family 5 (sodium/multivitamin and iodide cotransporter). member 6	0.101	9.94E-02		transporter
SLC6A19	solute carrier family 6 (neutral amino acid transporter). member 19	-0.185	6.64E-02		transporter
SLC9A3	solute carrier family 9. subfamily A (NHE3. cation proton antiporter 3). member 3	-0.183	9.20E-02		ion channel
SYT11	synaptotagmin XI	-0.302	5.97E-02		transporter
VDAC3	voltage-dependent anion channel 3	-0.155	8.43E-02		ion channel
VPS9D1	VPS9 domain containing 1	-0.167	9.22E-02		transporter
ANKRD33	ankyrin repeat domain 33	-0.135	6.71E-02		transcription regulator
ATF3	activating transcription factor 3	-0.433	8.23E-02		transcription regulator
CITED2	Cbp/p300-interacting transactivator. with Glu/Asp-rich carboxy-terminal domain. 2	0.310	8.61E-02		transcription regulator
EIF5	eukaryotic translation initiation factor 5	0.222	6.64E-02		translation regulator
FOXD3	forkhead box D3	-0.213	4.52E-02		transcription regulator
FOXP4	forkhead box P4	-0.233	6.64E-02		transcription regulator
HDAC2	histone deacetylase 2	0.261	7.07E-02		transcription regulator
HDAC4	histone deacetylase 4	-0.371	6.30E-02		transcription regulator
HEY1	hes-related family bHLH transcription factor with YRPW motif 1	0.130	7.05E-02		transcription regulator
KLF7	Kruppel-like factor 7 (ubiquitous)	-0.203	5.97E-02		transcription regulator
MEIS1	Meis homeobox 1	-0.264	5.79E-02		transcription regulator
MYC	v-myc avian myelocytomatosis viral oncogene homolog	-0.587	3.95E-02	D	transcription regulator
MYC	v-myc avian myelocytomatosis viral oncogene homolog	-0.567	4.52E-02	D	transcription regulator
NFKBIA	nuclear factor of kappa light polypeptide gene enhancer in B-cells inhibitor. alpha	-0.475	4.52E-02		transcription regulator
NR1D1	nuclear receptor subfamily 1. group D. member 1	-1.161	5.79E-02		ligand-dependent nuclear receptor
ONECUT1	one cut homeobox 1	-0.097	9.67E-02		transcription regulator
POU3F3	POU class 3 homeobox 3	0.144	7.29E-02		transcription regulator
PPARG	peroxisome proliferator-activated receptor gamma	-0.318	9.08E-02		ligand-dependent nuclear receptor
PURA	purine-rich element binding protein A	-0.304	7.75E-02		transcription regulator
SHOX	short stature homeobox	-0.261	5.77E-02		transcription regulator
SIN3B	SIN3 transcription regulator family member B	0.216	6.79E-02		transcription regulator
SOX3	SRY (sex determining region Y)-box 3	0.298	9.51E-02		transcription regulator
TANC2	tetratricopeptide repeat. ankyrin repeat and coiled-coil containing 2	-0.155	6.64E-02		transcription regulator
TFAP2B	transcription factor AP-2 beta (activating enhancer binding protein 2 beta)	0.144	9.16E-02		transcription regulator

TOB1	transducer of ERBB2. 1	-0.325	7.13E-02		transcription regulator
VDR	vitamin D (1.25- dihydroxyvitamin D3) receptor	-0.245	5.77E-02	D	transcription regulator
VDR	vitamin D (1.25- dihydroxyvitamin D3) receptor	-0.240	6.75E-02	D	transcription regulator
ANTXR2	anthrax toxin receptor 2	-0.235	6.81E-02		transmembrane receptor
CLK4	CDC-like kinase 4	0.615	9.30E-02		kinase
CSNK1A1L	casein kinase 1. alpha 1-like	-0.237	8.43E-02		kinase
DUSP2	dual specificity phosphatase 2	-0.388	4.52E-02		phosphatase
DUSP5	dual specificity phosphatase 5	-0.695	8.43E-02		phosphatase
GRK7	G protein-coupled receptor kinase 7	-0.541	4.52E-02		kinase
IP6K2	inositol hexakisphosphate kinase 2	0.256	4.52E-02		kinase
JAK1	Janus kinase 1	-0.198	8.51E-02		kinase
MAPK4	mitogen-activated protein kinase 4	-0.111	9.30E-02		kinase
NT5C3A	5'-nucleotidase. cytosolic IIIA	0.259	6.64E-02	D	phosphatase
NT5C3A	5'-nucleotidase. cytosolic IIIA	0.264	6.95E-02	D	phosphatase
PFKFB4	6-phosphofructo-2-kinase/fructose-2.6-biphosphatase 4	-0.473	6.64E-02		kinase
PHKG1	phosphorylase kinase. gamma 1 (muscle)	-0.220	9.94E-02		kinase
PIM2	pim-2 oncogene	0.335	9.30E-02		kinase
PRKAR1A	protein kinase. cAMP-dependent. regulatory. type I. alpha	0.236	7.13E-02		kinase
PTPN1	protein tyrosine phosphatase. non-receptor type 1	0.163	7.63E-02		phosphatase
SGK1	serum/glucocorticoid regulated kinase 1	-0.517	7.07E-02		kinase
STK35	serine/threonine kinase 35	-0.634	6.30E-02		kinase
STRADA	STE20-related kinase adaptor alpha	0.177	7.07E-02		kinase
BACE1	beta-site APP-cleaving enzyme 1	0.118	8.57E-02		peptidase
CFB	complement factor B	-0.281	5.79E-02		peptidase
CTSB	cathepsin B	0.247	6.11E-02		peptidase
ENDOU	endonuclease. polyU-specific	-0.139	6.64E-02		peptidase
UCHL5	ubiquitin carboxyl-terminal hydrolase L5	0.120	9.76E-02		peptidase
USP14	ubiquitin specific peptidase 14 (tRNA-guanine transglycosylase)	0.150	9.22E-02		peptidase
USP37	ubiquitin specific peptidase 37	0.207	6.79E-02		peptidase
ACBD6	acyl-CoA binding domain containing 6	0.182	6.81E-02		other
ACTA2	actin. alpha 2. smooth muscle. aorta	-0.141	6.64E-02		other
ADD3	adducin 3 (gamma)	-0.185	8.98E-02		other
AHCY	adenosylhomocysteinase	0.149	8.98E-02		enzyme
ALAS2	aminolevulinate. delta-. synthase 2	-0.111	9.94E-02		enzyme
ALDH4A1	aldehyde dehydrogenase 4 family. member A1	-0.134	8.43E-02		enzyme
ALDH8A1	aldehyde dehydrogenase 8 family. member A1	-0.202	4.89E-02		enzyme
ANXA1	annexin A1	-0.416	5.29E-02		enzyme
ANXA4	annexin A4	-0.421	4.52E-02		other
ARL5C	ADP-ribosylation factor-like 5C	-0.700	5.19E-02		other
ARR3	arrestin 3. retinal (X-arrestin)	-0.236	6.95E-02		other
ARRDC2	arrestin domain containing 2	-0.427	6.08E-02		other
ATG10	autophagy related 10	-0.108	8.43E-02		enzyme
ATL2	atlastin GTPase 2	0.214	8.43E-02		other
B3GAT2	beta-1.3-glucuronyltransferase 2 (glucuronosyltransferase S)	-0.315	4.52E-02		enzyme
BCMO1	beta-carotene 15.15'-monooxygenase 1	-0.126	7.07E-02		enzyme
BLOC1S6	biogenesis of lysosomal organelles complex-1. subunit 6. pallidin	-0.252	8.43E-02		other
BOC	BOC cell adhesion associated. oncogene regulated	-0.167	5.74E-02		other
C10orf54	chromosome 10 open reading frame 54	-0.116	7.69E-02		other
CA10	carbonic anhydrase X	-0.274	4.52E-02	D	enzyme
CA10	carbonic anhydrase X	-0.246	6.37E-02	D	enzyme
CA10	carbonic anhydrase X	-0.328	6.64E-02	D	enzyme
CAPG	capping protein (actin filament). gelsolin-like	-0.182	6.64E-02		other
CCDC124	coiled-coil domain containing 124	-0.240	5.77E-02		other
CCDC85C	coiled-coil domain containing 85C	-0.323	8.70E-02		other
CDH7	cadherin 7. type 2	-0.190	5.77E-02		other
CEP63	centrosomal protein 63kDa	0.233	5.23E-02		other
CISH	cytokine inducible SH2-containing protein	-0.410	4.52E-02	D	other
CISH	cytokine inducible SH2-containing protein	-0.510	7.75E-02	D	other
CLDN9	claudin 9	-0.349	9.67E-02		other
CRHBP	corticotropin releasing hormone binding protein	-0.220	5.72E-02		other

CSDC2	cold shock domain containing C2. RNA binding	-0.190	6.64E-02		other
CTDSPL	CTD (carboxy-terminal domain. RNA polymerase II. polypeptide A) small phosphatase-like	-0.253	5.81E-02		other
CYP2AC1	cytochrome P450. family 2. subfamily ac. polypeptide 1	0.114	8.43E-02		other
CYP2J2	cytochrome P450. family 2. subfamily J. polypeptide 2	0.424	6.37E-02		enzyme
CYP2R1	cytochrome P450. family 2. subfamily R. polypeptide 1	-0.465	7.48E-02		enzyme
CYR61	cysteine-rich. angiogenic inducer. 61	-0.369	5.77E-02		other
DDX18	DEAD (Asp-Glu-Ala-Asp) box polypeptide 18	0.214	8.68E-02		enzyme
DDX51	DEAD (Asp-Glu-Ala-Asp) box polypeptide 51	0.179	7.95E-02		enzyme
ELOVL1	ELOVL fatty acid elongase 1	-0.305	4.52E-02		enzyme
EMC1	ER membrane protein complex subunit 1	0.220	5.43E-02		other
ERGIC2	ERGIC and golgi 2	-0.161	6.41E-02		other
ERRFI1	ERBB receptor feedback inhibitor 1	-0.390	6.41E-02		other
FAM78B	family with sequence similarity 78. member B	-0.241	7.69E-02		other
FBLN7	fibulin 7	-0.216	5.77E-02		other
FBXL3	F-box and leucine-rich repeat protein 3	-0.310	6.81E-02		enzyme
FITM2	fat storage-inducing transmembrane protein 2	-0.179	9.94E-02		other
FKBP5	FK506 binding protein 5	-1.230	6.86E-02		enzyme
FUCA1	fucosidase. alpha-L- 1. tissue	-0.265	7.07E-02		enzyme
GADD45B	growth arrest and DNA-damage-inducible. beta	-0.230	9.08E-02		other
GBP1	guanylate binding protein 1. interferon-inducible	0.128	8.51E-02		enzyme
GNAO1	guanine nucleotide binding protein (G protein). alpha activating activity polypeptide O	-0.278	8.43E-02		enzyme
GOT1	glutamic-oxaloacetic transaminase 1. soluble	0.218	6.95E-02		enzyme
GPR137C	G protein-coupled receptor 137C	-0.329	5.16E-02		other
GRB2	growth factor receptor-bound protein 2	-0.417	3.03E-02		other
GSTZ1	glutathione S-transferase zeta 1	-0.211	6.39E-02		enzyme
GUSB	glucuronidase. beta	-0.147	9.30E-02		enzyme
HRAS	Harvey rat sarcoma viral oncogene homolog	-0.190	8.43E-02		enzyme
HRSP12	heat-responsive protein 12	-0.162	6.81E-02		other
HSD11B2	hydroxysteroid (11-beta) dehydrogenase 2	-0.383	4.52E-02		enzyme
HSD17B12	hydroxysteroid (17-beta) dehydrogenase 12	-0.404	3.58E-02		enzyme
IGHMBP2	immunoglobulin mu binding protein 2	0.170	6.81E-02		enzyme
IMPACT	impact RWD domain protein	-0.106	8.60E-02		other
IMPDH2	IMP (inosine 5'-monophosphate) dehydrogenase 2	-0.149	6.86E-02		enzyme
ITM2C	integral membrane protein 2C	-0.401	4.52E-02		other
KCTD5	potassium channel tetramerization domain containing 5	-0.346	9.94E-02		other
KDSR	3-ketodihydrosphingosine reductase	-0.147	8.21E-02		enzyme
LPL	lipoprotein lipase	-0.197	6.64E-02		enzyme
LRIT3	leucine-rich repeat. immunoglobulin-like and transmembrane domains 3	-0.167	6.37E-02		other
LRPPRC	leucine-rich pentatricopeptide repeat containing	0.305	6.97E-02		other
MBOAT2	membrane bound O-acyltransferase domain containing 2	0.189	5.81E-02		enzyme
MED18	mediator complex subunit 18	0.222	7.01E-02	D	other
MED18	mediator complex subunit 18	0.243	7.07E-02	D	other
MGST1	microsomal glutathione S-transferase 1	-0.207	6.97E-02		enzyme
MIDN	midnolin	-0.619	6.05E-02		other
MKLN1	muskelin 1. intracellular mediator containing kelch motifs	0.183	8.61E-02		other
MTMR10	myotubularin related protein 10	0.264	8.98E-02		other
MTR	5-methyltetrahydrofolate-homocysteine methyltransferase	0.152	8.21E-02	D	enzyme
MTR	5-methyltetrahydrofolate-homocysteine methyltransferase	0.227	8.43E-02	D	enzyme
MYLPF	myosin light chain. phosphorylatable. fast skeletal muscle	0.280	4.72E-02		other
MYO9B	myosin IXB	0.190	5.18E-02		enzyme
NAP1L1	nucleosome assembly protein 1-like 1	-0.227	4.61E-02	D	other
NAP1L1	nucleosome assembly protein 1-like 1	-0.234	5.43E-02	D	other
NDC1	NDC1 transmembrane nucleoporin	0.160	6.81E-02		other
NDRG2	NDRG family member 2	-0.754	8.23E-02		other
NDUFAF5	NADH dehydrogenase (ubiquinone) complex I. assembly factor 5	-0.150	6.20E-02		other
NHLH2	nescient helix loop helix 2	-0.096	9.66E-02		other
NSA2	NSA2 ribosome biogenesis homolog (S. cerevisiae)	-0.347	6.45E-02		other
OGT	O-linked N-acetylglucosamine (GlcNAc) transferase	0.169	7.13E-02		enzyme
OLIG3	oligodendrocyte transcription factor 3	0.174	6.64E-02		other

ORC4	origin recognition complex. subunit 4	0.124	7.69E-02		other
PCDH7	protocadherin 7	-0.269	6.64E-02		other
PCDHA8	protocadherin alpha 8	-0.253	8.61E-02		other
PCNA	proliferating cell nuclear antigen	0.225	4.52E-02		enzyme
PDE6C	phosphodiesterase 6C. cGMP-specific. cone. alpha prime	0.371	8.43E-02		enzyme
PHF10	PHD finger protein 10	0.143	6.64E-02		other
PHYHIPL	phytanoyl-CoA 2-hydroxylase interacting protein-like	-0.368	5.77E-02		other
PRPF39	pre-mRNA processing factor 39	0.240	9.16E-02		other
PRPF4	pre-mRNA processing factor 4	0.129	9.91E-02		other
PRPF40A	PRP40 pre-mRNA processing factor 40 homolog A (S. cerevisiae)	0.113	9.51E-02		other
PSMD11	proteasome (prosome. macropain) 26S subunit. non-ATPase. 11	0.173	7.07E-02		other
PTCD3	pentatricopeptide repeat domain 3	0.258	4.52E-02	D	other
PTCD3	pentatricopeptide repeat domain 3	0.203	5.77E-02	D	other
PTCD3	pentatricopeptide repeat domain 3	0.253	5.81E-02	D	other
PTCD3	pentatricopeptide repeat domain 3	0.176	8.51E-02	D	other
PVALB	parvalbumin	-0.290	4.52E-02		other
PWP1	PWP1 homolog (S. cerevisiae)	0.275	4.52E-02	D	other
PWP1	PWP1 homolog (S. cerevisiae)	0.241	5.77E-02	D	other
RAB10	RAB10. member RAS oncogene family	-0.292	6.78E-02		enzyme
RABGGTB	Rab geranylgeranyltransferase. beta subunit	0.143	9.30E-02		enzyme
RFNG	RFNG O-fucosylpeptide 3-beta-N-acetylglucosaminyltransferase	0.219	9.78E-02		enzyme
RND3	Rho family GTPase 3	-0.236	8.43E-02		enzyme
RNF180	ring finger protein 180	0.197	7.07E-02		enzyme
RNF7	ring finger protein 7	-0.144	7.69E-02		enzyme
RPL14	ribosomal protein L14	-0.231	8.59E-02		other
RPS19	ribosomal protein S19	-0.218	5.43E-02	D	other
RPS19	ribosomal protein S19	-0.295	7.40E-02	D	other
RPS28	ribosomal protein S28	-0.317	4.52E-02		other
RSL24D1	ribosomal L24 domain containing 1	-0.389	7.07E-02		other
RSPO1	R-spondin 1	-0.125	8.43E-02		other
RUFY2	RUN and FYVE domain containing 2	0.188	5.79E-02		other
SEMA3F	sema domain. immunoglobulin domain (Ig). short basic domain. secreted. (semaphorin) 3F	-0.346	6.39E-02		other
SERAC1	serine active site containing 1	0.186	5.74E-02	D	other
SERAC1	serine active site containing 1	0.188	6.64E-02	D	other
SETD3	SET domain containing 3	0.219	9.94E-02		enzyme
SH3GL1	SH3-domain GRB2-like 1	-0.337	8.98E-02		other
SLTM	SAFB-like. transcription modulator	0.354	9.58E-02		other
SNF8	SNF8. ESCRT-II complex subunit	-0.111	8.43E-02	D	enzyme
SNF8	SNF8. ESCRT-II complex subunit	-0.178	9.67E-02	D	enzyme
SOCS1	suppressor of cytokine signaling 1	-0.827	4.52E-02		other
SPRY4	sprouty homolog 4 (Drosophila)	-0.497	6.11E-02	D	other
SPRY4	sprouty homolog 4 (Drosophila)	-0.569	6.37E-02	D	other
SPRYD3	SPRY domain containing 3	-0.353	4.52E-02		other
TOLLIP	toll interacting protein	-0.314	5.19E-02		other
TPD52	tumor protein D52	-0.221	9.17E-02		other
Tsc22d3	TSC22 domain family. member 3	-0.280	6.64E-02		other
TSKU	tsukushi. small leucine rich proteoglycan	-0.187	7.07E-02		other
TXNIP	thioredoxin interacting protein	0.902	2.04E-02	D	other
TXNIP	thioredoxin interacting protein	0.911	5.79E-02	D	other
UBR7	ubiquitin protein ligase E3 component n-recognin 7 (putative)	0.302	5.77E-02	D	enzyme
UBR7	ubiquitin protein ligase E3 component n-recognin 7 (putative)	0.350	7.01E-02	D	enzyme
WDR13	WD repeat domain 13	0.125	9.08E-02		other
WDR6	WD repeat domain 6	0.108	8.61E-02		other
YARS	tyrosyl-tRNA synthetase	-0.155	8.12E-02		enzyme
ZC3H11A	zinc finger CCCH-type containing 11A	0.183	5.77E-02		other
ZNF729	zinc finger protein 729	-0.158	9.47E-02		other
ZSWIM8	zinc finger. SWIM-type containing 8	-0.145	7.13E-02		other

Annex 18: Relative microgravity microarrays (1g) by entrez gene name.

Symbol	Entrez Gene Name	Log Ratio 1g	p-value	N	Type(s)
ABCF2	ATP-binding cassette. sub-family F (GCN20). member 2	-0.858	6.53E-02		transporter
ABCG2	ATP-binding cassette. sub-family G (WHITE). member 2	0.362	8.25E-02		transporter
ANXA6	annexin A6	-0.576	9.86E-02		ion channel
APOA4	apolipoprotein A-IV	-0.615	8.17E-02		transporter
ATP1A1	ATPase. Na+/K+ transporting. alpha 1 polypeptide	0.607	3.80E-02	D	transporter
ATP1A1	ATPase. Na+/K+ transporting. alpha 1 polypeptide	0.614	6.53E-02	D	transporter
ATP1B2	ATPase. Na+/K+ transporting. beta 2 polypeptide	-0.257	9.21E-02		transporter
ATP2B4	ATPase. Ca++ transporting. plasma membrane 4	-0.339	5.01E-02		transporter
ATP5G3	ATP synthase. H+ transporting. mitochondrial Fo complex. subunit C3 (subunit 9)	-0.185	7.86E-02		transporter
ATP6V1B2	ATPase. H+ transporting. lysosomal 56/58kDa. V1 subunit B2	0.249	9.37E-02		transporter
CACNA2D2	calcium channel. voltage-dependent. alpha 2/delta subunit 2	0.308	4.67E-02		ion channel
CACNG6	calcium channel. voltage-dependent. gamma subunit 6	0.166	5.50E-02		ion channel
EXOC7	exocyst complex component 7	0.315	8.39E-02		transporter
GABRG2	gamma-aminobutyric acid (GABA) A receptor. gamma 2	0.295	6.32E-02		ion channel
HNRNPU	heterogeneous nuclear ribonucleoprotein U (scaffold attachment factor A)	-0.310	5.52E-02		transporter
HSDL2	hydroxysteroid dehydrogenase like 2	-0.302	3.17E-02		transporter
KCTD12	potassium channel tetramerization domain containing 12	-0.105	9.84E-02	D	ion channel
KCTD12	potassium channel tetramerization domain containing 12	-0.150	3.96E-02	D	ion channel
NDUFA10	NADH dehydrogenase (ubiquinone) 1 alpha subcomplex. 10. 42kDa	-0.382	9.76E-02		transporter
PDZK1	PDZ domain containing 1	0.779	5.18E-02		transporter
SEC14L2	SEC14-like 2 (S. cerevisiae)	0.268	9.62E-02		transporter
SLC13A2	solute carrier family 13 (sodium-dependent dicarboxylate transporter). member 2	0.674	1.62E-02		transporter
SLC14A2	solute carrier family 14 (urea transporter). member 2	-0.237	9.37E-02		transporter
SLC15A1	solute carrier family 15 (oligopeptide transporter). member 1	0.380	9.30E-02		transporter
SLC16A3	solute carrier family 16 (monocarboxylate transporter). member 3	-0.414	3.17E-02	D	transporter
SLC16A3	solute carrier family 16 (monocarboxylate transporter). member 3	-0.476	4.16E-02	D	transporter
SLC1A3	solute carrier family 1 (glial high affinity glutamate transporter). member 3	0.154	8.39E-02		transporter
SLC22A2	solute carrier family 22 (organic cation transporter). member 2	0.481	3.05E-02	D	transporter
SLC22A2	solute carrier family 22 (organic cation transporter). member 2	0.507	3.80E-02	D	transporter
SLC22A5	solute carrier family 22 (organic cation/carnitine transporter). member 5	0.174	6.83E-02		transporter
SLC25A19	solute carrier family 25 (mitochondrial thiamine pyrophosphate carrier). member 19	-0.215	3.96E-02		transporter
SLC35D1	solute carrier family 35 (UDP-GlcA/UDP-GalNAc transporter). member D1	-0.147	7.04E-02		transporter
SLC37A4	solute carrier family 37 (glucose-6-phosphate transporter). member 4	-0.353	3.19E-02	D	transporter
SLC37A4	solute carrier family 37 (glucose-6-phosphate transporter). member 4	-0.365	3.80E-02	D	transporter
SLC6A19	solute carrier family 6 (neutral amino acid transporter). member 19	0.629	9.86E-02		transporter
SNX12	sorting nexin 12	-0.205	6.83E-02		transporter
SNX16	sorting nexin 16	0.444	4.09E-02		transporter
TAPBP	TAP binding protein (tapasin)	0.241	4.57E-02		transporter
TFRC	transferrin receptor	-0.184	3.29E-02		transporter
TIMM13	translocase of inner mitochondrial membrane 13 homolog (yeast)	-0.307	6.89E-02		transporter
TMED3	transmembrane emp24 protein transport domain containing 3	-0.193	7.04E-02		transporter
TMED9	transmembrane emp24 protein transport domain containing 9	-0.259	4.49E-02		transporter
USO1	USO1 vesicle transport factor	0.161	5.41E-02		transporter
VPS33A	vacuolar protein sorting 33 homolog A (S. cerevisiae)	-0.270	7.58E-02		transporter
ANKS4B	ankyrin repeat and sterile alpha motif domain containing 4B	0.313	9.11E-02		transcription regulator
ATF3	activating transcription factor 3	-0.319	6.83E-02		transcription regulator
BTG2	BTG family. member 2	-2.106	1.04E-02	D	transcription regulator
BTG2	BTG family. member 2	-2.024	1.35E-02	D	transcription regulator
C1QBP	complement component 1. q subcomponent binding protein	0.331	6.56E-02		transcription regulator
CEBPD	CCAAT/enhancer binding protein (C/EBP). delta	-0.193	5.92E-02		transcription regulator
DLX1	distal-less homeobox 1	-0.153	9.30E-02		transcription regulator
ECD	ecdysoneless homolog (Drosophila)	0.137	5.19E-02		transcription regulator
EEF2	eukaryotic translation elongation factor 2	0.180	9.76E-02		translation regulator
EGR1	early growth response 1	-0.388	3.99E-02		transcription

					regulator
EGR2	early growth response 2	-0.292	4.32E-02		transcription regulator
EGR3	early growth response 3	-0.305	6.08E-02		transcription regulator
EIF3C	eukaryotic translation initiation factor 3. subunit C	0.458	2.99E-02		translation regulator
EIF4A1	eukaryotic translation initiation factor 4A1	-0.742	2.89E-02	D	translation regulator
EIF4A1	eukaryotic translation initiation factor 4A1	-0.599	3.19E-02	D	translation regulator
FOS	FBJ murine osteosarcoma viral oncogene homolog	-2.530	2.89E-02		transcription regulator
FOSB	FBJ murine osteosarcoma viral oncogene homolog B	-2.124	9.40E-03		transcription regulator
FOXQ1	forkhead box Q1	-0.411	3.99E-02	D	transcription regulator
FOXQ1	forkhead box Q1	-0.577	3.05E-02	D	transcription regulator
GTF2H4	general transcription factor IIH. polypeptide 4. 52kDa	-0.181	5.08E-02		transcription regulator
HLTF	helicase-like transcription factor	0.234	6.53E-02		transcription regulator
HSF2	heat shock transcription factor 2	0.641	5.52E-02	D	transcription regulator
HSF2	heat shock transcription factor 2	0.624	6.53E-02	D	transcription regulator
KLF11	Kruppel-like factor 11	-0.386	3.05E-02	D	transcription regulator
KLF11	Kruppel-like factor 11	-0.518	6.30E-02	D	transcription regulator
L3MBTL2	l(3)mbt-like 2 (Drosophila)	-0.173	8.96E-02		transcription regulator
MED27	mediator complex subunit 27	-0.194	6.15E-02		transcription regulator
MYBL2	v-myb avian myeloblastosis viral oncogene homolog-like 2	-0.314	2.89E-02		transcription regulator
MYCL	v-myc avian myelocytomatosis viral oncogene lung carcinoma derived homolog	0.402	6.59E-02		transcription regulator
MYOG	myogenin (myogenic factor 4)	-0.359	9.26E-02		transcription regulator
NFIL3	nuclear factor. interleukin 3 regulated	-0.370	4.69E-02		transcription regulator
NFKBIA	nuclear factor of kappa light polypeptide gene enhancer in B-cells inhibitor. alpha	-0.468	5.67E-02		transcription regulator
NKX2-2	NK2 homeobox 2	-0.168	9.39E-02		transcription regulator
NMI	N-myc (and STAT) interactor	0.542	5.76E-02		transcription regulator
NPAS4	neuronal PAS domain protein 4	-1.722	3.86E-02		transcription regulator
OVOL1	ovo-like zinc finger 1	-0.217	3.17E-02		transcription regulator
PDLIM1	PDZ and LIM domain 1	0.235	9.37E-02		transcription regulator
Pou3f1	POU domain. class 3. transcription factor 1	-0.113	9.24E-02		transcription regulator
PPARG	peroxisome proliferator-activated receptor gamma	0.286	3.96E-02		ligand-dependent nuclear receptor
PTGES2	prostaglandin E synthase 2	-0.269	9.67E-02		transcription regulator
RXRG	retinoid X receptor. gamma	0.201	7.17E-02		ligand-dependent nuclear receptor
SOX14	SRY (sex determining region Y)-box 14	-0.248	5.62E-02		transcription regulator
SQSTM1	sequestosome 1	0.587	4.57E-02		transcription regulator
TAF7	TAF7 RNA polymerase II. TATA box binding protein (TBP)-associated factor. 55kDa	-0.124	8.25E-02		transcription regulator
TRIP13	thyroid hormone receptor interactor 13	-0.240	5.52E-02		transcription regulator
YWHAB	tyrosine 3-monooxygenase/tryptophan 5-monooxygenase activation protein. beta	-0.295	5.01E-02	D	transcription regulator

YWHAB	tyrosine 3-monooxygenase/tryptophan 5-monooxygenase activation protein. beta	-0.230	5.87E-02	D	transcription regulator
CXCR4	chemokine (C-X-C motif) receptor 4	-0.099	7.21E-02		G-protein coupled receptor
DRD3	dopamine receptor D3	-0.172	4.88E-02		G-protein coupled receptor
F3	coagulation factor III (thromboplastin. tissue factor)	-0.352	5.52E-02		transmembrane receptor
HMMR	hyaluronan-mediated motility receptor (RHAMM)	-0.471	9.96E-02		transmembrane receptor
IFNAR1	interferon (alpha. beta and omega) receptor 1	0.354	5.45E-02		transmembrane receptor
OPN1LW	opsin 1 (cone pigments). long-wave-sensitive	-0.484	3.19E-02	D	G-protein coupled receptor
OPN1LW	opsin 1 (cone pigments). long-wave-sensitive	-0.866	3.17E-02	D	G-protein coupled receptor
TNFRSF19	tumor necrosis factor receptor superfamily. member 19	0.287	3.99E-02		transmembrane receptor
C19orf10	chromosome 19 open reading frame 10	-0.161	7.06E-02		cytokine
CMTM3	CKLF-like MARVEL transmembrane domain containing 3	-0.156	9.53E-02		cytokine
EDN1	endothelin 1	-0.268	6.66E-02		cytokine
TNFSF10	tumor necrosis factor (ligand) superfamily. member 10	0.263	7.96E-02		cytokine
GAS6	growth arrest-specific 6	0.220	6.31E-02		growth factor
NOG	noggin	-0.221	3.45E-02		growth factor
ACP2	acid phosphatase 2. lysosomal	0.343	8.19E-02		phosphatase
ACVR1	activin A receptor. type I	-0.415	3.96E-02	D	kinase
ACVR1	activin A receptor. type I	-0.351	5.32E-02	D	kinase
AURKA	aurora kinase A	-0.248	9.47E-02		kinase
AURKB	aurora kinase B	-0.532	5.92E-02		kinase
BCKDK	branched chain ketoacid dehydrogenase kinase	-0.593	3.05E-02		kinase
CCNB1	cyclin B1	-0.258	5.30E-02		kinase
CDK2	cyclin-dependent kinase 2	-0.298	4.38E-02		kinase
CDK7	cyclin-dependent kinase 7	-0.174	6.83E-02		kinase
CKB	creatine kinase. brain	0.231	3.80E-02		kinase
CLK4	CDC-like kinase 4	0.413	5.92E-02		kinase
CMPK1	cytidine monophosphate (UMP-CMP) kinase 1. cytosolic	-0.184	5.52E-02		kinase
DAK	dihydroxyacetone kinase 2 homolog (S. cerevisiae)	0.279	3.17E-02		kinase
DUSP1	dual specificity phosphatase 1	-1.383	3.05E-02	D	phosphatase
DUSP1	dual specificity phosphatase 1	-1.311	3.80E-02	D	phosphatase
DUSP2	dual specificity phosphatase 2	-0.716	2.89E-02		phosphatase
DUSP27	dual specificity phosphatase 27 (putative)	0.782	3.78E-02		phosphatase
ILK	integrin-linked kinase	-0.562	1.04E-02	D	kinase
ILK	integrin-linked kinase	-0.577	1.04E-02	D	kinase
IMPA1	inositol(myo)-1(or 4)-monophosphatase 1	-0.279	5.17E-02		phosphatase
INPP5D	inositol polyphosphate-5-phosphatase. 145kDa	0.094	9.76E-02		phosphatase
MKNK2	MAP kinase interacting serine/threonine kinase 2	0.241	8.25E-02		kinase
MYO3A	myosin IIIA	0.301	5.01E-02	D	kinase
MYO3A	myosin IIIA	0.325	6.81E-02	D	kinase
PFKFB4	6-phosphofructo-2-kinase/fructose-2.6-biphosphatase 4	-0.355	6.83E-02		kinase
PLK1	polo-like kinase 1	-0.492	3.94E-02		kinase
PPP2R2D	protein phosphatase 2. regulatory subunit B. delta	-0.209	8.40E-02		phosphatase
PPP2R4	protein phosphatase 2A activator. regulatory subunit 4	-0.169	7.17E-02		phosphatase
PPP4C	protein phosphatase 4. catalytic subunit	-0.354	9.40E-02		phosphatase
SIK2	salt-inducible kinase 2	0.635	4.71E-02		kinase
SLK	STE20-like kinase	0.192	7.57E-02		kinase
SOCS3	suppressor of cytokine signaling 3	-2.498	2.89E-02	D	phosphatase
SOCS3	suppressor of cytokine signaling 3	-2.432	3.05E-02	D	phosphatase
STK39	serine threonine kinase 39	-0.295	3.80E-02		kinase
TEC	tec protein tyrosine kinase	0.546	1.30E-02		kinase
UBLCP1	ubiquitin-like domain containing CTD phosphatase 1	-0.384	5.36E-02		phosphatase
VRK1	vaccinia related kinase 1	-0.226	8.25E-02		kinase
ACAA2	acetyl-CoA acyltransferase 2	-0.475	6.82E-02		enzyme
ACE	angiotensin I converting enzyme	0.511	7.42E-02		peptidase
ACOX1	acyl-CoA oxidase 1. palmitoyl	0.109	9.31E-02		enzyme
ACTA2	actin. alpha 2. smooth muscle. aorta	-0.411	8.89E-02		other
ACTG1	actin. gamma 1	-0.309	9.37E-02		other
ACTR2	ARP2 actin-related protein 2 homolog (yeast)	-0.134	9.26E-02		other
AGXT	alanine-glyoxylate aminotransferase	0.572	5.55E-02		enzyme
AHSG	alpha-2-HS-glycoprotein	0.427	9.44E-02		other
AKAP17A	A kinase (PRKA) anchor protein 17A	0.258	9.73E-02		other
AKIRIN1	akirin 1	-0.124	5.38E-02		enzyme
AKR1A1	aldo-keto reductase family 1. member A1 (aldehyde reductase)	-0.149	6.52E-02		enzyme
ALDH2	aldehyde dehydrogenase 2 family (mitochondrial)	-0.401	9.11E-02		enzyme
ALG8	ALG8. alpha-1.3-glucosyltransferase	-0.181	5.52E-02		enzyme
AMD1	adenosylmethionine decarboxylase 1	0.373	3.94E-02	D	enzyme

AMD1	adenosylmethionine decarboxylase 1	0.360	6.69E-02	D	enzyme
AMY2A	amylase. alpha 2A (pancreatic)	0.757	3.96E-02	D	enzyme
AMY2A	amylase. alpha 2A (pancreatic)	0.822	5.33E-02	D	enzyme
AMY2A	amylase. alpha 2A (pancreatic)	0.841	4.89E-02	D	enzyme
AMY2B	amylase. alpha 2B (pancreatic)	1.047	3.80E-02		enzyme
ANLN	anillin. actin binding protein	-0.459	7.42E-02		other
API5	apoptosis inhibitor 5	-0.301	3.99E-02		other
Arf2	ADP-ribosylation factor 2	-0.325	8.25E-02		other
ARHGDIB	Rho GDP dissociation inhibitor (GDI) beta	-0.252	8.55E-02	D	other
ARHGDIB	Rho GDP dissociation inhibitor (GDI) beta	-0.309	9.95E-02	D	other
ARHGEF28	Rho guanine nucleotide exchange factor (GEF) 28	0.214	8.25E-02		other
ARHGEF39	Rho guanine nucleotide exchange factor (GEF) 39	-0.199	9.37E-02		other
ARR3	arrestin 3. retinal (X-arrestin)	1.025	4.16E-02		other
ASL	argininosuccinate lyase	-0.218	5.65E-02		enzyme
B4GALT1	UDP-Gal:betaGlcNAc beta 1.4- galactosyltransferase. polypeptide 1	0.200	6.83E-02		enzyme
BCL2L1	BCL2-like 1	0.218	7.66E-02		other
BCO1	beta-carotene oxygenase 1	0.387	3.19E-02		enzyme
BIN1	bridging integrator 1	0.183	7.97E-02		other
BOD1	biorientation of chromosomes in cell division 1	-0.164	4.69E-02		other
BTBD6	BTB (POZ) domain containing 6	-0.349	6.52E-02		other
C10orf54	chromosome 10 open reading frame 54	0.191	3.70E-02		other
C10orf88	chromosome 10 open reading frame 88	0.108	9.16E-02		other
C12orf65	chromosome 12 open reading frame 65	-0.106	7.73E-02		other
C1orf106	chromosome 1 open reading frame 106	0.180	9.30E-02		other
C2orf40	chromosome 2 open reading frame 40	-0.281	3.96E-02		other
CA10	carbonic anhydrase X	0.145	9.30E-02		enzyme
CALU	calumenin	-0.434	3.14E-02		other
CAMK2N2	calcium/calmodulin-dependent protein kinase II inhibitor 2	0.153	7.28E-02		other
CAPRIN1	cell cycle associated protein 1	0.335	2.89E-02	D	other
CAPRIN1	cell cycle associated protein 1	0.312	4.12E-02	D	other
CASQ1	calsequestrin 1 (fast-twitch. skeletal muscle)	-0.319	4.71E-02		other
CAV3	caveolin 3	-0.217	5.62E-02		enzyme
CBWD1	COBW domain containing 1	-0.190	6.31E-02		other
CCDC25	coiled-coil domain containing 25	-0.221	9.39E-02		other
CCNA2	cyclin A2	-0.493	3.94E-02		other
CCNB2	cyclin B2	-0.250	5.41E-02		other
CCNE2	cyclin E2	-0.203	9.37E-02		other
CCNF	cyclin F	-0.250	3.29E-02		other
CD2AP	CD2-associated protein	-0.154	4.66E-02		other
CD82	CD82 molecule	-0.237	8.80E-02		other
CDA	cytidine deaminase	0.294	5.55E-02		enzyme
CDC20	cell division cycle 20	-0.379	3.19E-02		other
CDC5L	cell division cycle 5-like	0.223	6.20E-02		other
CDC6	cell division cycle 6	-0.236	5.87E-02	D	other
CDC6	cell division cycle 6	-0.167	6.29E-02	D	other
CEL	carboxyl ester lipase	1.208	4.99E-02	D	enzyme
CEL	carboxyl ester lipase	1.219	5.32E-02	D	enzyme
CEL	carboxyl ester lipase	0.998	7.78E-02	D	enzyme
CETP	cholesteryl ester transfer protein. plasma	0.495	9.64E-02		enzyme
CFB	complement factor B	0.322	3.96E-02	D	peptidase
CFB	complement factor B	0.160	7.90E-02	D	peptidase
CFP	complement factor properdin	-0.313	5.32E-02		other
CGRRF1	cell growth regulator with ring finger domain 1	-0.089	9.76E-02		other
CHAC2	ChaC. cation transport regulator homolog 2 (E. coli)	-0.128	6.99E-02		other
CHCHD4	coiled-coil-helix-coiled-coil-helix domain containing 4	-0.275	3.17E-02		enzyme
CHIA	chitinase. acidic	0.357	3.96E-02		enzyme
CHODL	chondrolectin	-0.109	8.11E-02		other
CHPF	chondroitin polymerizing factor	0.125	7.04E-02		enzyme
CKAP2	cytoskeleton associated protein 2	-0.478	3.80E-02		other
CNN3	calponin 3. acidic	-0.302	3.24E-02		other
COL4A1	collagen. type IV. alpha 1	0.481	5.49E-02		other
COL9A3	collagen. type IX. alpha 3	-0.534	8.51E-02		other
COPS8	COP9 signalosome subunit 8	-0.122	7.51E-02	D	other
COPS8	COP9 signalosome subunit 8	-0.125	9.37E-02	D	other
CPA1	carboxypeptidase A1 (pancreatic)	1.029	5.65E-02	D	peptidase
CPA1	carboxypeptidase A1 (pancreatic)	0.545	6.29E-02	D	peptidase
CPB1	carboxypeptidase B1 (tissue)	0.731	4.50E-02		peptidase
CPT2	carnitine palmitoyltransferase 2	-0.372	8.55E-02		enzyme
CRIP2	cysteine-rich protein 2	-0.211	7.06E-02		other
CRY1	cryptochrome circadian clock 1	0.557	3.96E-02		enzyme
CRYGN	crystallin. gamma N	-0.456	4.86E-02		other
CTNNBIP1	catenin. beta interacting protein 1	-0.251	3.80E-02	D	other
CTNNBIP1	catenin. beta interacting protein 1	-0.227	8.37E-02	D	other
CTRB2	chymotrypsinogen B2	0.432	7.86E-02		peptidase
CTSS	cathepsin S	0.176	9.39E-02		peptidase

CYB5A	cytochrome b5 type A (microsomal)	0.150	6.33E-02		enzyme
Cyb5r3	cytochrome b5 reductase 3	-0.140	6.83E-02		enzyme
CYP24A1	cytochrome P450. family 24. subfamily A. polypeptide 1	1.264	3.97E-02		enzyme
CYP27A1	cytochrome P450. family 27. subfamily A. polypeptide 1	0.185	4.89E-02		enzyme
Cyp2ac1	cytochrome P450. family 2. subfamily ac. polypeptide 1	0.385	7.04E-02		other
CYP2J2	cytochrome P450. family 2. subfamily J. polypeptide 2	0.233	5.92E-02	D	enzyme
CYP2J2	cytochrome P450. family 2. subfamily J. polypeptide 2	0.379	5.18E-02	D	enzyme
CYP2J2	cytochrome P450. family 2. subfamily J. polypeptide 2	0.418	2.89E-02	D	enzyme
CYP2J2	cytochrome P450. family 2. subfamily J. polypeptide 2	0.750	3.17E-02	D	enzyme
CYP2J2	cytochrome P450. family 2. subfamily J. polypeptide 2	0.806	8.37E-02	D	enzyme
CYP2J2	cytochrome P450. family 2. subfamily J. polypeptide 2	0.282	3.45E-02	D	enzyme
CYR61	cysteine-rich. angiogenic inducer. 61	-0.797	1.35E-02		other
DBT	dihydrolipoamide branched chain transacylase E2	-0.470	3.80E-02		enzyme
DCAF13	DDB1 and CUL4 associated factor 13	-0.331	5.65E-02	D	other
DCAF13	DDB1 and CUL4 associated factor 13	-0.364	6.53E-02	D	other
DCHS1	dachsous cadherin-related 1	-0.113	9.98E-02		other
DCN	decorin	-0.293	7.13E-02		other
DCUN1D1	DCN1. defective in cullin neddylation 1. domain containing 1	-0.169	7.87E-02		other
DDB2	damage-specific DNA binding protein 2. 48kDa	0.300	9.57E-02		other
DDC	dopa decarboxylase (aromatic L-amino acid decarboxylase)	-0.212	6.38E-02		enzyme
DDX4	DEAD (Asp-Glu-Ala-Asp) box polypeptide 4	0.286	9.37E-02		enzyme
DHRS1	dehydrogenase/reductase (SDR family) member 1	0.176	9.20E-02		enzyme
DLST	dihydrolipoamide S-succinyltransferase (E2 component of 2-oxo-glutarate complex)	0.180	8.66E-02		enzyme
DNAJB11	DnaJ (Hsp40) homolog. subfamily B. member 11	-0.226	4.09E-02	D	other
DNAJB11	DnaJ (Hsp40) homolog. subfamily B. member 11	-0.230	4.12E-02	D	other
DPP7	dipeptidyl-peptidase 7	0.269	7.90E-02		peptidase
DSG2	desmoglein 2	-0.230	5.33E-02		other
DSP	desmoplakin	0.324	7.86E-02		other
EBAG9	estrogen receptor binding site associated. antigen. 9	-0.137	5.18E-02		other
ECI1	enoyl-CoA delta isomerase 1	-0.406	7.86E-02		enzyme
EEPD1	endonuclease/exonuclease/phosphatase family domain containing 1	0.200	8.37E-02		other
EIF2B3	eukaryotic translation initiation factor 2B. subunit 3 gamma. 58kDa	-0.109	9.21E-02		other
ELAC2	elaC ribonuclease Z 2	0.211	7.34E-02		enzyme
ELOVL4	ELOVL fatty acid elongase 4	-0.512	3.96E-02		enzyme
ELOVL7	ELOVL fatty acid elongase 7	-1.211	1.04E-02	D	enzyme
ELOVL7	ELOVL fatty acid elongase 7	-1.199	1.30E-02	D	enzyme
ELP6	elongator acetyltransferase complex subunit 6	-0.127	6.39E-02		other
EME1	essential meiotic structure-specific endonuclease 1	-0.179	9.76E-02		other
ENDOU	endonuclease. polyU-specific	0.845	3.17E-02		peptidase
ERRFI1	ERBB receptor feedback inhibitor 1	-0.417	5.74E-02		other
ETNPPL	ethanolamine-phosphate phospho-lyase	0.254	3.85E-02		enzyme
EXOSC2	exosome component 2	-0.269	3.05E-02		enzyme
EXT2	exostosin glycosyltransferase 2	0.162	6.69E-02		enzyme
FAAH2	fatty acid amide hydrolase 2	0.350	6.83E-02		enzyme
FAIM	Fas apoptotic inhibitory molecule	-0.119	9.16E-02		other
FAM212A	family with sequence similarity 212. member A	-0.155	8.74E-02		other
FARSA	phenylalanyl-tRNA synthetase. alpha subunit	0.410	6.33E-02		enzyme
FBL	fibrillarin	-0.287	4.38E-02		other
FBXO5	F-box protein 5	-0.113	7.23E-02		enzyme
FCGBP	Fc fragment of IgG binding protein	-0.335	6.08E-02		other
FEN1	flap structure-specific endonuclease 1	-0.258	6.53E-02	D	enzyme
FEN1	flap structure-specific endonuclease 1	-0.323	7.73E-02	D	enzyme
FGL2	fibrinogen-like 2	0.172	8.29E-02		peptidase
FKBP1B	FK506 binding protein 1B. 12.6 kDa	-0.280	3.70E-02		enzyme
FNIP1	folliculin interacting protein 1	0.278	7.17E-02		other
G2E3	G2/M-phase specific E3 ubiquitin protein ligase	-0.256	4.95E-02		enzyme
G3BP1	GTPase activating protein (SH3 domain) binding protein 1	-0.360	4.50E-02		enzyme
GADD45B	growth arrest and DNA-damage-inducible. beta	-0.636	5.76E-02		other
GDI2	GDP dissociation inhibitor 2	-0.419	5.08E-02		other
GINS4	GINS complex subunit 4 (Sld5 homolog)	-0.191	6.54E-02		other
GOLGA7	golgin A7	-0.317	3.94E-02		other
GPI	glucose-6-phosphate isomerase	-0.303	6.91E-02		enzyme
GPX7	glutathione peroxidase 7	-0.184	6.95E-02		enzyme
GTPBP4	GTP binding protein 4	0.334	7.59E-02		enzyme
GYG1	glycogenin 1	0.293	6.71E-02		enzyme
H1f0	H1 histone family. member 0	-0.399	4.29E-02	D	other
H1f0	H1 histone family. member 0	-0.408	6.33E-02	D	other
HADH	hydroxyacyl-CoA dehydrogenase	-0.407	8.04E-02		enzyme
HAUS4	HAUS augmin-like complex. subunit 4	-0.307	7.90E-02		other
HGD	homogentisate 1.2-dioxygenase	0.348	9.84E-02		enzyme
HIBADH	3-hydroxyisobutyrate dehydrogenase	-0.301	3.86E-02	D	enzyme
HIBADH	3-hydroxyisobutyrate dehydrogenase	-0.338	4.57E-02	D	enzyme
HIST2H2BE	histone cluster 2. H2be	-0.321	5.52E-02		other
HLCS	holocarboxylase synthetase (biotin-(proprionyl-CoA-carboxylase (ATP-	0.443	7.80E-02		enzyme

	hydrolysing)) ligase)				
HMBS	hydroxymethylbilane synthase	-0.213	6.83E-02		enzyme
HMGCL	3-hydroxymethyl-3-methylglutaryl-CoA lyase	-0.288	5.81E-02		enzyme
HMGCS1	3-hydroxy-3-methylglutaryl-CoA synthase 1 (soluble)	-0.372	8.25E-02		enzyme
HMGN3	high mobility group nucleosomal binding domain 3	-0.444	9.30E-02		other
HPRT1	hypoxanthine phosphoribosyltransferase 1	-0.138	7.87E-02		enzyme
HSD17B4	hydroxysteroid (17-beta) dehydrogenase 4	0.442	7.86E-02		enzyme
HSP90AA1	heat shock protein 90kDa alpha (cytosolic). class A member 1	0.382	4.50E-02		enzyme
HSP90B1	heat shock protein 90kDa beta (Grp94). member 1	-0.285	6.32E-02		other
IARS	isoleucyl-tRNA synthetase	0.736	8.66E-02		enzyme
IDH3A	isocitrate dehydrogenase 3 (NAD+) alpha	-0.307	4.95E-02		enzyme
IGFBP1	insulin-like growth factor binding protein 1	1.006	5.52E-02		other
IMP4	IMP4. U3 small nucleolar ribonucleoprotein	-0.154	4.71E-02		other
IMPDH1	IMP (inosine 5'-monophosphate) dehydrogenase 1	0.262	7.10E-02		enzyme
ING3	inhibitor of growth family. member 3	0.325	3.96E-02		other
INSIG1	insulin induced gene 1	0.307	4.32E-02		other
IRS2	insulin receptor substrate 2	0.266	2.89E-02		enzyme
KDELC2	KDEL (Lys-Asp-Glu-Leu) containing 2	-0.212	8.29E-02		other
KDM8	lysine (K)-specific demethylase 8	-0.206	4.86E-02		other
KIAA0196	KIAA0196	0.154	8.47E-02		other
KIAA1524	KIAA1524	-0.177	6.83E-02		other
KIAA1919	KIAA1919	0.203	7.18E-02		peptidase
KIF23	kinesin family member 23	-0.473	7.86E-02		other
KNTC1	kinetochore associated 1	-0.169	8.11E-02		other
KRT18	keratin 18	0.301	8.39E-02		other
LECT1	leukocyte cell derived chemotaxin 1	-1.097	9.40E-03	D	other
LECT1	leukocyte cell derived chemotaxin 1	-1.062	2.17E-02	D	other
LENG9	leukocyte receptor cluster (LRC) member 9	0.202	9.37E-02		other
LGSN	lengsin. lens protein with glutamine synthetase domain	-0.475	7.21E-02		enzyme
LIMCH1	LIM and calponin homology domains 1	0.710	3.80E-02		other
LMO7	LIM domain 7	0.281	3.86E-02		enzyme
LOX	lysyl oxidase	-0.117	9.11E-02		enzyme
LRIT1	leucine-rich repeat. immunoglobulin-like and transmembrane domains 1	0.613	3.80E-02		other
LRIT3	leucine-rich repeat. immunoglobulin-like and transmembrane domains 3	-0.232	6.91E-02		other
LRRC39	leucine rich repeat containing 39	-0.138	5.28E-02		other
LSM1	LSM1. U6 small nuclear RNA associated	-0.174	8.04E-02		other
LXN	latexin	0.312	6.83E-02		other
MANF	mesencephalic astrocyte-derived neurotrophic factor	-0.291	6.33E-02		other
MAPRE1	microtubule-associated protein. RP/EB family. member 1	-0.354	4.38E-02	D	other
MAPRE1	microtubule-associated protein. RP/EB family. member 1	-0.314	8.37E-02	D	other
MASP1	mannan-binding lectin serine peptidase 1 (C4/C2 activating component of Ra-reactive factor)	0.168	7.96E-02		peptidase
MATN1	matrilin 1. cartilage matrix protein	-0.391	4.58E-02		other
MCM10	minichromosome maintenance complex component 10	-0.152	5.78E-02		other
MCM2	minichromosome maintenance complex component 2	-0.163	4.38E-02		enzyme
MED28	mediator complex subunit 28	-0.171	9.26E-02		other
MFAP2	microfibrillar-associated protein 2	-0.287	8.11E-02		other
MOB3A	MOB kinase activator 3A	-0.119	6.53E-02		other
MOGAT1	monoacylglycerol O-acyltransferase 1	0.329	3.96E-02		enzyme
MON1A	MON1 secretory trafficking family member A	-0.298	3.05E-02		other
MOSPD2	motile sperm domain containing 2	0.201	7.51E-02		other
MPC2	mitochondrial pyruvate carrier 2	-0.326	4.50E-02	D	other
MPC2	mitochondrial pyruvate carrier 2	-0.230	9.76E-02	D	other
MSH2	mutS homolog 2	-0.303	8.51E-02		enzyme
MTFR2	mitochondrial fission regulator 2	-0.200	7.87E-02		other
MYBPH	myosin binding protein H	-0.244	4.66E-02		other
MYL6	myosin. light chain 6. alkali. smooth muscle and non-muscle	0.243	7.97E-02		other
MYL7	myosin. light chain 7. regulatory	-0.237	5.42E-02		enzyme
N6AMT1	N-6 adenine-specific DNA methyltransferase 1 (putative)	-0.256	8.47E-02		enzyme
NCAPG	non-SMC condensin I complex. subunit G	-0.275	8.11E-02		other
NCAPG2	non-SMC condensin II complex. subunit G2	-0.153	6.33E-02		other
NDC1	NDC1 transmembrane nucleoporin	-0.229	6.91E-02		other
NDC80	NDC80 kinetochore complex component	-0.224	4.34E-02		other
NDOR1	NADPH dependent diflavin oxidoreductase 1	-0.131	8.89E-02		enzyme
NDRG4	NDRG family member 4	-0.334	9.64E-02		other
NELFA	negative elongation factor complex member A	0.132	9.39E-02		other
NID1	nidogen 1	0.233	3.86E-02		other
NKAIN1	Na+/K+ transporting ATPase interacting 1	-0.259	3.71E-02		other
NOS1	nitric oxide synthase 1 (neuronal)	0.101	8.74E-02		enzyme
NPTN	neuroplastin	0.277	9.11E-02		other
NRAS	neuroblastoma RAS viral (v-ras) oncogene homolog	-0.195	4.32E-02		enzyme
NUDT18	nudix (nucleoside diphosphate linked moiety X)-type motif 18	0.182	9.96E-02		other
NUF2	NUF2. NDC80 kinetochore complex component	-0.358	5.94E-02		other
NXN	nucleoredoxin	-0.223	3.86E-02		enzyme
ORC6	origin recognition complex. subunit 6	-0.219	6.83E-02	D	other

ORC6	origin recognition complex. subunit 6	-0.243	7.04E-02	D	other
Otub1	OTU domain. ubiquitin aldehyde binding 1	-0.205	9.21E-02		enzyme
Otud5	OTU domain containing 5	0.197	7.06E-02		enzyme
PAH	phenylalanine hydroxylase	0.371	5.33E-02		enzyme
PAPD5	PAP associated domain containing 5	0.175	6.53E-02		enzyme
PC	pyruvate carboxylase	-0.226	3.05E-02	D	enzyme
PC	pyruvate carboxylase	-0.175	8.25E-02	D	enzyme
PDHX	pyruvate dehydrogenase complex. component X	0.230	8.17E-02		enzyme
PER3	period circadian clock 3	0.197	3.96E-02		other
PGM1	phosphoglucomutase 1	-0.322	4.65E-02		enzyme
PGP	phosphoglycolate phosphatase	-0.522	5.13E-02		enzyme
PGPEP1	pyroglutamyl-peptidase I	-0.124	5.52E-02		peptidase
PHF23	PHD finger protein 23	-0.151	7.04E-02		other
PIGQ	phosphatidylinositol glycan anchor biosynthesis. class Q	-0.111	8.74E-02		enzyme
PLA2G12B	phospholipase A2. group XIIB	0.153	9.85E-02		enzyme
PM20D1	peptidase M20 domain containing 1	0.460	7.34E-02		peptidase
POLR2H	polymerase (RNA) II (DNA directed) polypeptide H	-0.284	5.33E-02		enzyme
POSTN	periostin. osteoblast specific factor	-0.448	4.66E-02		other
PPP1R3B	protein phosphatase 1. regulatory subunit 3B	-0.340	6.33E-02		other
PRC1	protein regulator of cytokinesis 1	-0.247	6.91E-02		other
PRDM11	PR domain containing 11	-0.459	5.92E-02		other
PRIM1	primase. DNA. polypeptide 1 (49kDa)	-0.185	4.32E-02		enzyme
PRMT6	protein arginine methyltransferase 6	-0.242	4.32E-02		enzyme
PRPF31	pre-mRNA processing factor 31	0.118	7.42E-02		other
PRPH	peripherin	0.293	7.43E-02		other
PRRC1	proline-rich coiled-coil 1	-0.230	5.92E-02		other
PSMC6	proteasome (prosome. macropain) 26S subunit. ATPase. 6	-0.222	9.76E-02		peptidase
PSMD11	proteasome (prosome. macropain) 26S subunit. non-ATPase. 11	-0.154	8.33E-02		other
PSME3	proteasome (prosome. macropain) activator subunit 3 (PA28 gamma; Ki)	-0.354	3.29E-02		peptidase
PXMP2	peroxisomal membrane protein 2. 22kDa	-0.147	9.38E-02		other
PYGM	phosphorylase. glycogen. muscle	-0.265	4.29E-02		enzyme
RAB1A	RAB1A. member RAS oncogene family	-0.421	4.00E-02	D	enzyme
RAB1A	RAB1A. member RAS oncogene family	-0.306	6.81E-02	D	enzyme
RAC1	ras-related C3 botulinum toxin substrate 1 (rho family. small GTP binding protein Rac1)	-0.334	4.66E-02		enzyme
RAE1	ribonucleic acid export 1	-0.131	5.25E-02	D	other
RAE1	ribonucleic acid export 1	-0.156	7.10E-02	D	other
RALA	v-ral simian leukemia viral oncogene homolog A (ras related)	-0.226	8.29E-02		enzyme
RCC1	regulator of chromosome condensation 1	-0.449	6.83E-02		other
RDH13	retinol dehydrogenase 13 (all-trans/9-cis)	0.195	9.57E-02		enzyme
RGD1563307	similar to Set beta isoform	-0.302	4.88E-02	D	other
RGD1563307	similar to Set beta isoform	-0.197	7.46E-02	D	other
RGS1	regulator of G-protein signaling 1	-0.192	9.26E-02		other
RHOQ	ras homolog family member Q	-0.210	9.37E-02		enzyme
RMI2	RecQ mediated genome instability 2	-0.156	9.28E-02		other
RNASET2	ribonuclease T2	-0.369	7.80E-02		enzyme
RNF8	ring finger protein 8. E3 ubiquitin protein ligase	0.172	6.37E-02		enzyme
RNFT1	ring finger protein. transmembrane 1	-0.271	9.86E-02		other
RNLS	renalase. FAD-dependent amine oxidase	-0.519	8.29E-02		other
RPL31	ribosomal protein L31	0.236	5.52E-02		other
RPRM	reprimo. TP53 dependent G2 arrest mediator candidate	-0.207	3.80E-02		other
RPUSD2	RNA pseudouridylate synthase domain containing 2	-0.172	8.34E-02		enzyme
RRM1	ribonucleotide reductase M1	-0.398	4.81E-02		enzyme
RTCA	RNA 3'-terminal phosphate cyclase	-0.394	8.51E-02		enzyme
SAE1	SUMO1 activating enzyme subunit 1	-0.331	7.22E-02		enzyme
SAMM50	SAMM50 sorting and assembly machinery component	-0.186	5.01E-02	D	other
SAMM50	SAMM50 sorting and assembly machinery component	-0.285	7.87E-02	D	other
SCCPDH	saccharopine dehydrogenase (putative)	0.312	5.92E-02		other
SDAD1	SDA1 domain containing 1	0.250	8.39E-02		other
SEPHS1	selenophosphate synthetase 1	-0.283	4.50E-02		enzyme
SEPN1	selenoprotein N. 1	-0.394	5.91E-02		other
SERHL2	serine hydrolase-like 2	-0.181	8.80E-02		enzyme
SERPINB6	serpin peptidase inhibitor. clade B (ovalbumin). member 6	0.408	3.94E-02	D	other
SERPINB6	serpin peptidase inhibitor. clade B (ovalbumin). member 6	0.397	6.53E-02	D	other
SGPL1	sphingosine-1-phosphate lyase 1	0.324	9.26E-02		enzyme
Sh3bgr	SH3-binding domain glutamic acid-rich protein	-0.248	3.71E-02		other
SH3BGRL	SH3 domain binding glutamate-rich protein like	-0.207	3.91E-02		other
SIAE	sialic acid acetylesterase	-0.140	7.04E-02		enzyme
SLC25A47	solute carrier family 25. member 47	0.133	9.30E-02		other
SLMO2	slowmo homolog 2 (Drosophila)	-0.479	3.17E-02	D	other
SLMO2	slowmo homolog 2 (Drosophila)	-0.495	7.87E-02	D	other
SMARCAD1	SWI/SNF-related. matrix-associated actin-dependent regulator of chromatin. subfamily a. containing DEAD/H box 1	-0.414	6.56E-02		enzyme

SMPDL3B	sphingomyelin phosphodiesterase. acid-like 3B	0.280	9.11E-02		enzyme
SNRPA	small nuclear ribonucleoprotein polypeptide A	-0.213	8.74E-02		other
SNRPB2	small nuclear ribonucleoprotein polypeptide B	-0.220	3.17E-02		other
SPCS2	signal peptidase complex subunit 2 homolog (S. cerevisiae)	-0.519	5.08E-02		other
SPDL1	spindle apparatus coiled-coil protein 1	-0.360	4.66E-02		other
SRSF1	serine/arginine-rich splicing factor 1	-0.424	5.92E-02	D	other
SRSF1	serine/arginine-rich splicing factor 1	-0.368	9.28E-02	D	other
SRSF9	serine/arginine-rich splicing factor 9	-0.195	9.20E-02		enzyme
SSB	Sjogren syndrome antigen B (autoantigen La)	-0.334	9.76E-02		enzyme
ST7	suppression of tumorigenicity 7	0.268	2.89E-02		other
STARD10	StAR-related lipid transfer (START) domain containing 10	0.159	4.98E-02		other
STMN2	stathmin 2	-0.235	3.14E-02	D	other
STMN2	stathmin 2	-0.195	4.12E-02	D	other
STMN2	stathmin 2	-0.253	5.92E-02	D	other
STMN2	stathmin 2	-0.161	6.02E-02	D	other
STMN2	stathmin 2	-0.180	6.33E-02	D	other
STMN2	stathmin 2	-0.202	7.90E-02	D	other
SULT1A1	sulfotransferase family. cytosolic. 1A. phenol-preferring. member 1	0.222	4.65E-02	D	enzyme
SULT1A1	sulfotransferase family. cytosolic. 1A. phenol-preferring. member 1	0.226	5.41E-02	D	enzyme
SUMO3	small ubiquitin-like modifier 3	-0.376	7.97E-02		other
SYBU	syntabulin (syntaxin-interacting)	0.582	4.57E-02		other
TACC3	transforming. acidic coiled-coil containing protein 3	-0.500	5.67E-02		other
TAT	tyrosine aminotransferase	1.037	3.94E-02		enzyme
TCTA	T-cell leukemia translocation altered	-0.229	9.67E-02		other
TDG	thymine-DNA glycosylase	-0.372	9.83E-02		enzyme
TDO2	tryptophan 2.3-dioxygenase	0.538	6.33E-02		enzyme
TGFBI	transforming growth factor. beta-induced. 68kDa	-0.411	3.05E-02		other
TGM1	transglutaminase 1	-0.568	7.56E-02		enzyme
THOC6	THO complex 6 homolog (Drosophila)	-0.197	3.94E-02		other
THOP1	thimet oligopeptidase 1	-0.174	9.37E-02		peptidase
THYN1	thymocyte nuclear protein 1	-0.311	8.15E-02		other
TIAM1	T-cell lymphoma invasion and metastasis 1	0.150	5.65E-02		other
TMEM189	transmembrane protein 189	-0.266	2.99E-02		other
TMEM254	transmembrane protein 254	0.627	3.94E-02	D	other
TMEM254	transmembrane protein 254	0.638	5.58E-02	D	other
TMIGD1	transmembrane and immunoglobulin domain containing 1	0.365	3.29E-02		other
TMPRSS13	transmembrane protease. serine 13	0.277	7.42E-02		peptidase
TNKS	tankyrase. TRF1-interacting ankyrin-related ADP-ribose polymerase	0.151	7.09E-02		enzyme
TNR	tenascin R	0.221	5.01E-02	D	other
TNR	tenascin R	0.191	7.42E-02	D	other
TP53BP2	tumor protein p53 binding protein 2	0.365	6.89E-02		other
TRAM1	translocation associated membrane protein 1	0.319	5.41E-02		other
TRMT13	tRNA methyltransferase 13 homolog (S. cerevisiae)	-0.139	6.38E-02		other
TRMT61A	tRNA methyltransferase 61 homolog A (S. cerevisiae)	-0.149	8.37E-02		enzyme
TSPAN4	tetraspanin 4	0.635	3.94E-02		other
TSPAN6	tetraspanin 6	-0.452	6.20E-02		other
TTC5	tetratricopeptide repeat domain 5	-0.122	6.69E-02		other
TUBA1C	tubulin. alpha 1c	-0.329	8.29E-02	D	other
TUBA1C	tubulin. alpha 1c	-0.307	8.98E-02	D	other
TUBA8	tubulin. alpha 8	-0.715	5.91E-02		other
TUBB4B	tubulin. beta 4B class IVb	-0.301	2.89E-02		other
TXNDC12	thioredoxin domain containing 12 (endoplasmic reticulum)	-0.459	6.83E-02		enzyme
TYRP1	tyrosinase-related protein 1	-0.276	7.04E-02		enzyme
UCHL1	ubiquitin carboxyl-terminal esterase L1 (ubiquitin thiolesterase)	-0.184	3.96E-02		peptidase
UFL1	UFM1-specific ligase 1	0.352	6.53E-02		other
UGCG	UDP-glucose ceramide glucosyltransferase	-0.129	8.76E-02		enzyme
UGGT2	UDP-glucose glycoprotein glucosyltransferase 2	-0.273	7.94E-02		enzyme
USP13	ubiquitin specific peptidase 13 (isopeptidase T-3)	0.290	6.53E-02		peptidase
USP28	ubiquitin specific peptidase 28	0.426	4.15E-02		peptidase
USP48	ubiquitin specific peptidase 48	0.268	3.96E-02		peptidase
UTP11L	UTP11-like. U3 small nucleolar ribonucleoprotein (yeast)	-0.181	6.71E-02		other
VMP1	vacuole membrane protein 1	-0.232	4.15E-02		other
VWA5A	von Willebrand factor A domain containing 5A	0.413	9.40E-02		other
WDR5	WD repeat domain 5	-0.335	9.16E-02		other
WRNIP1	Werner helicase interacting protein 1	-0.209	9.30E-02		enzyme
XPOT	exportin. tRNA	-0.339	8.25E-02		other
YAE1D1	Yae1 domain containing 1	-0.336	5.40E-02		other
YWHAQ	tyrosine 3-monooxygenase/tryptophan 5-monooxygenase activation protein. theta	-0.314	7.87E-02	D	other
YWHAQ	tyrosine 3-monooxygenase/tryptophan 5-monooxygenase activation protein. theta	-0.384	7.97E-02	D	other
ZBTB11	zinc finger and BTB domain containing 11	0.335	3.85E-02		other
ZBTB49	zinc finger and BTB domain containing 49	0.234	3.29E-02		other
ZFYVE27	zinc finger. FYVE domain containing 27	-0.134	5.38E-02		other
ZMYND19	zinc finger. MYND-type containing 19	-0.138	8.98E-02		other

ZNF410	zinc finger protein 410	-0.198	8.25E-02		other
ZNF729	zinc finger protein 729	-0.278	3.34E-02	D	other
ZNF729	zinc finger protein 729	-0.158	5.74E-02	D	other
ZNF729	zinc finger protein 729	-0.280	5.28E-02	D	other
ZNF800	zinc finger protein 800	-0.177	5.16E-02	D	other
ZNF800	zinc finger protein 800	-0.196	6.83E-02	D	other

Annex 19: Relative microgravity microarrays (3g>axe) by entrez gene name.

Symbol	Entrez Gene Name	Log Ratio 3g>axe	p-value	N	Type(s)
AMBP	alpha-1-microglobulin/bikunin precursor	0.264	4.22E-02		transporter
APOA4	apolipoprotein A-IV	-0.574	9.90E-02		transporter
ATP1A1	ATPase. Na+/K+ transporting. alpha 1 polypeptide	-0.270	6.58E-02		transporter
ATP1B2	ATPase. Na+/K+ transporting. beta 2 polypeptide	-0.291	3.84E-02		transporter
ATP5J	ATP synthase. H+ transporting. mitochondrial Fo complex. subunit F6	0.179	9.90E-02		transporter
GLRB	glycine receptor. beta	0.127	9.81E-02		ion channel
GOLGA3	golgin A3	-0.113	9.10E-02		transporter
HBE1	hemoglobin. epsilon 1	0.429	9.61E-02		transporter
NSF	N-ethylmaleimide-sensitive factor	0.221	7.77E-02		transporter
RYR2	ryanodine receptor 2 (cardiac)	-0.218	9.04E-02		ion channel
SLC25A24	solute carrier family 25 (mitochondrial carrier; phosphate carrier). member 24	0.148	6.58E-02		transporter
SNX15	sorting nexin 15	0.098	9.81E-02		transporter
STX6	syntaxin 6	-0.266	9.32E-02		transporter
VPS33A	vacuolar protein sorting 33 homolog A (S. cerevisiae)	0.257	3.84E-02		transporter
BTG2	BTG family. member 2	-1.337	3.30E-02	D	transcription regulator
BTG2	BTG family. member 2	-1.504	4.80E-02	D	transcription regulator
CSHL1	chorionic somatomammotropin hormone-like 1	-0.434	5.73E-02		transcription regulator
EGR1	early growth response 1	-0.319	9.90E-02		transcription regulator
FOS	FBJ murine osteosarcoma viral oncogene homolog	-2.020	9.81E-02		transcription regulator
FOSB	FBJ murine osteosarcoma viral oncogene homolog B	-1.985	8.82E-02		transcription regulator
FOXM1	forkhead box M1	0.268	8.62E-02		transcription regulator
FOXQ1	forkhead box Q1	-0.719	3.37E-02		transcription regulator
HDAC4	histone deacetylase 4	-0.273	4.80E-02		transcription regulator
HES1	hes family bHLH transcription factor 1	-0.397	3.66E-02		transcription regulator
KLF2	Kruppel-like factor 2	-0.758	3.30E-02		transcription regulator
KLF2	Kruppel-like factor 2	-0.679	3.83E-02		transcription regulator
LHX1	LIM homeobox 1	-0.173	6.86E-02		transcription regulator
MSX2	msh homeobox 2	-0.310	3.84E-02		transcription regulator
NPAT	nuclear protein. ataxia-telangiectasia locus	0.233	6.58E-02		transcription regulator
ONECUT1	one cut homeobox 1	-0.133	6.86E-02	D	transcription regulator
ONECUT1	one cut homeobox 1	-0.126	9.17E-02	D	transcription regulator
PAX9	paired box 9	-0.226	5.32E-02		transcription regulator
PPARG	peroxisome proliferator-activated receptor gamma	0.339	9.90E-02		ligand-dependent nuclear receptor
PRPF6	pre-mRNA processing factor 6	0.130	9.39E-02		transcription regulator
SOX10	SRY (sex determining region Y)-box 10	0.120	9.21E-02		transcription regulator
TAF9	TAF9 RNA polymerase II. TATA box binding protein (TBP)-associated factor. 32kDa	-0.134	9.39E-02		transcription regulator

ACKR3	atypical chemokine receptor 3	-0.201	4.65E-02		G-protein coupled receptor
B2M	beta-2-microglobulin	-0.184	5.32E-02		transmembrane receptor
KTN1	kinectin 1 (kinesin receptor)	0.186	6.86E-02		transmembrane receptor
LGALS3BP	lectin. galactoside-binding. soluble. 3 binding protein	0.169	4.80E-02		transmembrane receptor
LRPAP1	low density lipoprotein receptor-related protein associated protein 1	0.175	6.74E-02		transmembrane receptor
OPN1LW	opsin 1 (cone pigments). long-wave-sensitive	0.198	9.55E-02		G-protein coupled receptor
TNFRSF14	tumor necrosis factor receptor superfamily. member 14	0.205	9.76E-02		transmembrane receptor
EDN1	endothelin 1	-0.175	7.78E-02	D	cytokine
EDN1	endothelin 1	-0.184	9.47E-02	D	cytokine
AGT	angiotensinogen (serpin peptidase inhibitor. clade A. member 8)	0.236	8.33E-02		growth factor
CAMK2G	calcium/calmodulin-dependent protein kinase II gamma	-0.412	3.30E-02		kinase
CKM	creatine kinase. muscle	-0.279	4.22E-02		kinase
DLG1	discs. large homolog 1 (Drosophila)	0.163	9.76E-02		kinase
GK5	glycerol kinase 5 (putative)	0.155	6.86E-02		kinase
GNE	glucosamine (UDP-N-acetyl)-2-epimerase/N-acetylmannosamine kinase	0.187	9.39E-02		kinase
MAP3K5	mitogen-activated protein kinase kinase kinase 5	-0.103	9.90E-02		kinase
NDRG1	N-myc downstream regulated 1	0.288	3.84E-02		kinase
PAK4	p21 protein (Cdc42/Rac)-activated kinase 4	-0.149	9.39E-02		kinase
PIM2	Pim-2 proto-oncogene. serine/threonine kinase	-0.451	9.61E-02		kinase
PTPN13	protein tyrosine phosphatase. non-receptor type 13 (APO-1/CD95 (Fas)-associated phosphatase)	0.174	6.67E-02		phosphatase
SOCS3	suppressor of cytokine signaling 3	-2.038	8.50E-02		phosphatase
TWF2	twinfilin actin-binding protein 2	-0.188	8.44E-02		kinase
2610028H24Rik	RIKEN cDNA 2610028H24 gene	-0.098	9.39E-02		other
ACAA1	acetyl-CoA acyltransferase 1	0.180	9.39E-02		enzyme
ACHE	acetylcholinesterase (Yt blood group)	-0.269	9.39E-02		enzyme
ACO1	aconitase 1. soluble	-0.405	4.38E-02		enzyme
ACTR10	actin-related protein 10 homolog (S. cerevisiae)	0.164	6.86E-02		other
AKTIP	AKT interacting protein	-0.098	9.61E-02		other
AMY2B	amylase. alpha 2B (pancreatic)	0.262	4.78E-02		enzyme
ANKRD9	ankyrin repeat domain 9	-0.290	8.47E-02		other
ARRDC3	arrestin domain containing 3	0.243	9.47E-02		other
ASL	argininosuccinate lyase	-0.176	4.80E-02		enzyme
ATL3	atlastin GTPase 3	-0.194	9.39E-02		other
BABAM1	BRISC and BRCA1 A complex member 1	0.184	5.29E-02		other
BCO1	beta-carotene oxygenase 1	0.189	8.01E-02		enzyme
BIN3	bridging integrator 3	-0.238	9.39E-02		other
BYSL	bystin-like	-0.147	9.39E-02		other
C14orf166	chromosome 14 open reading frame 166	0.119	9.44E-02		other
CA13	carbonic anhydrase XIII	0.174	9.39E-02		enzyme
CAP2	CAP. adenylate cyclase-associated protein. 2 (yeast)	-0.223	9.47E-02		other
CAPZA1	capping protein (actin filament) muscle Z-line. alpha 1	0.227	9.81E-02		other
CASP6	caspase 6. apoptosis-related cysteine peptidase	-0.377	3.84E-02		peptidase
CCDC93	coiled-coil domain containing 93	0.201	8.00E-02		other
CD2BP2	CD2 (cytoplasmic tail) binding protein 2	0.313	5.39E-02		other
CDC6	cell division cycle 6	0.149	9.39E-02		other
CKAP2	cytoskeleton associated protein 2	0.363	9.39E-02		other
CMTR1	cap methyltransferase 1	0.181	6.32E-02		enzyme
CRBN	cereblon	0.140	6.86E-02		enzyme
CRYL1	crystallin. lambda 1	0.338	7.15E-02		enzyme
CWC25	CWC25 spliceosome-associated protein homolog (S. cerevisiae)	0.175	6.32E-02		other
CYP26C1	cytochrome P450. family 26. subfamily C. polypeptide 1	-0.236	9.81E-02		enzyme
CYP2J2	cytochrome P450. family 2. subfamily J. polypeptide 2	-0.231	8.62E-02		enzyme
DBR1	debranching RNA lariats 1	0.142	7.63E-02		enzyme
DDX24	DEAD (Asp-Glu-Ala-Asp) box helicase 24	-0.255	3.84E-02		enzyme
DNAJA3	DnaJ (Hsp40) homolog. subfamily A. member 3	-0.330	9.53E-02		other
EFCAB14	EF-hand calcium binding domain 14	0.414	3.97E-02		other
EIF2B3	eukaryotic translation initiation factor 2B. subunit 3 gamma. 58kDa	-0.161	8.44E-02		other
ELAVL4	ELAV like neuron-specific RNA binding protein 4	-0.384	9.32E-02		other
ELOVL7	ELOVL fatty acid elongase 7	-1.122	6.86E-02	D	enzyme
ELOVL7	ELOVL fatty acid elongase 7	-1.130	8.00E-02	D	enzyme
ERGIC1	endoplasmic reticulum-golgi intermediate compartment (ERGIC) 1	0.347	4.65E-02		other
ERI1	exoribonuclease 1	0.165	8.82E-02		enzyme

ESF1	ESF1. nucleolar pre-rRNA processing protein. homolog (S. cerevisiae)	-0.274	6.37E-02	D	other
ESF1	ESF1. nucleolar pre-rRNA processing protein. homolog (S. cerevisiae)	-0.213	6.39E-02	D	other
ESF1	ESF1. nucleolar pre-rRNA processing protein. homolog (S. cerevisiae)	-0.239	6.37E-02	D	other
FAM195A	family with sequence similarity 195. member A	-0.179	5.32E-02		other
FBXL3	F-box and leucine-rich repeat protein 3	-0.157	9.39E-02		enzyme
FBXW11	F-box and WD repeat domain containing 11	0.109	9.39E-02		enzyme
FKBP5	FK506 binding protein 5	0.516	3.30E-02		enzyme
GADD45B	growth arrest and DNA-damage-inducible. beta	-0.313	9.76E-02		other
GRHL3	grainyhead-like 3 (Drosophila)	-0.152	7.15E-02		other
HES5	hes family bHLH transcription factor 5	-0.191	8.44E-02		other
HEXA	hexosaminidase A (alpha polypeptide)	-0.174	9.32E-02		enzyme
HS6ST2	heparan sulfate 6-O-sulfotransferase 2	0.175	9.39E-02		enzyme
HSP90AA1	heat shock protein 90kDa alpha (cytosolic). class A member 1	-0.233	9.04E-02		enzyme
HSPG2	heparan sulfate proteoglycan 2	-0.211	9.68E-02		enzyme
LETM2	leucine zipper-EF-hand containing transmembrane protein 2	-0.155	6.58E-02		other
LOX	lysyl oxidase	0.139	9.32E-02		enzyme
LRIT1	leucine-rich repeat. immunoglobulin-like and transmembrane domains 1	-0.257	9.88E-02		other
LSM12	LSM12 homolog (S. cerevisiae)	0.226	9.90E-02		other
MAB21L3	mab-21-like 3 (C. elegans)	0.134	6.58E-02		other
METAP1D	methionyl aminopeptidase type 1D (mitochondrial)	-0.252	9.39E-02		peptidase
METRN	meteorin. glial cell differentiation regulator	0.136	8.62E-02		other
MGME1	mitochondrial genome maintenance exonuclease 1	-0.281	6.86E-02		enzyme
MLF2	myeloid leukemia factor 2	-0.205	9.39E-02		other
MNAT1	MNAT CDK-activating kinase assembly factor 1	-0.139	8.00E-02		other
MVP	major vault protein	0.286	3.84E-02		other
NCKIPSD	NCK interacting protein with SH3 domain	-0.242	9.76E-02		other
NEIL3	nei endonuclease VIII-like 3 (E. coli)	-0.177	6.58E-02		enzyme
NIPAL4	NIPA-like domain containing 4	-0.237	9.39E-02		other
NPEPL1	aminopeptidase-like 1	0.114	9.39E-02		peptidase
Nrxn3	neurexin III	-0.228	4.16E-02		other
NUP205	nucleoporin 205kDa	0.178	4.80E-02		other
PARP1	poly (ADP-ribose) polymerase 1	0.224	8.00E-02		enzyme
PC	pyruvate carboxylase	0.205	4.65E-02		enzyme
PCDH11X	protocadherin 11 X-linked	-0.208	8.62E-02		other
PCDHA8	protocadherin alpha 8	0.506	6.22E-02	D	other
PCDHA8	protocadherin alpha 8	-0.196	9.39E-02	D	other
PDCD2L	programmed cell death 2-like	-0.158	9.39E-02		other
PDCL3	phosducin-like 3	-0.270	4.22E-02		other
PDHA1	pyruvate dehydrogenase (lipoamide) alpha 1	-0.224	7.77E-02		enzyme
PLA2G12B	phospholipase A2. group XIIB	0.222	4.78E-02		enzyme
PLA2G15	phospholipase A2. group XV	0.221	4.78E-02		enzyme
PLXDC2	plexin domain containing 2	-0.293	9.39E-02		other
POLR3B	polymerase (RNA) III (DNA directed) polypeptide B	-0.177	9.61E-02		enzyme
POPDC3	popeye domain containing 3	-0.125	7.15E-02		other
PPP1R37	protein phosphatase 1. regulatory subunit 37	0.149	7.78E-02		other
PRC1	protein regulator of cytokinesis 1	0.137	9.39E-02		other
PRPH	peripherin	0.157	8.01E-02		other
PSEN1	presenilin 1	0.176	6.46E-02		peptidase
RAB3C	RAB3C. member RAS oncogene family	0.276	7.14E-02		enzyme
RNF130	ring finger protein 130	0.196	4.80E-02		peptidase
RNF182	ring finger protein 182	-0.314	9.39E-02		enzyme
RNF34	ring finger protein 34. E3 ubiquitin protein ligase	-0.136	6.58E-02		enzyme
SCD	stearoyl-CoA desaturase (delta-9-desaturase)	-0.241	8.00E-02		enzyme
SEPT8	septin 8	0.137	6.58E-02		other
SERPINA10	serpin peptidase inhibitor. clade A (alpha-1 antiproteinase. antitrypsin). member 10	-0.463	5.25E-02		other
SERPINH1	serpin peptidase inhibitor. clade H (heat shock protein 47). member 1. (collagen binding protein 1)	-0.581	9.17E-02		other
SLBP	stem-loop binding protein	0.302	6.58E-02		other
SLMO2	slowmo homolog 2 (Drosophila)	-0.225	9.81E-02		other
SLTM	SAFB-like. transcription modulator	0.316	9.04E-02		other
SMYD5	SMYD family member 5	-0.190	4.30E-02		other
SPPL2A	signal peptide peptidase like 2A	0.202	4.22E-02		peptidase
SPTLC1	serine palmitoyltransferase. long chain base subunit 1	0.151	9.81E-02		enzyme
STC2	stanniocalcin 2	-0.358	4.78E-02		other
STMN2	stathmin 2	0.200	5.32E-02	D	other
STMN2	stathmin 2	0.134	8.91E-02	D	other
STRC	stereocilin	0.147	8.62E-02		other
TGM1	transglutaminase 1	-0.234	7.20E-02		enzyme

TMUB1	transmembrane and ubiquitin-like domain containing 1	-0.117	9.47E-02		other
TTC7A	tetratricopeptide repeat domain 7A	0.129	7.17E-02		other
TUBA1A	tubulin. alpha 1a	0.309	9.39E-02		other
UBE2QL1	ubiquitin-conjugating enzyme E2Q family-like 1	-0.672	9.39E-02		other
UGGT2	UDP-glucose glycoprotein glucosyltransferase 2	0.229	4.22E-02		enzyme
VIL1	villin 1	0.359	9.88E-02		other
VTN	vitronectin	0.274	4.22E-02	D	other
VTN	vitronectin	0.316	9.39E-02	D	other
XKR4	XK. Kell blood group complex subunit-related family. member 4	-0.230	9.32E-02		other
XPOT	exportin. tRNA	-0.119	9.57E-02		other
ZNF503	zinc finger protein 503	-0.199	9.04E-02		other
ZNF729	zinc finger protein 729	-0.123	9.39E-02		other

Annex 20: Relative microgravity microarrays (3g>1g) by entrez gene name.

Symbol	Entrez Gene Name	Log Ratio 3g>1g	p-value	N	Type(s)
ABCA1	ATP-binding cassette, sub-family A (ABC1), member 1	-0,346	8,67E-02		transporter
ABCA4	ATP-binding cassette, sub-family A (ABC1), member 4	0,297	6,97E-02		transporter
ABCB9	ATP-binding cassette, sub-family B (MDR/TAP), member 9	0,164	6,09E-02		transporter
ABCD3	ATP-binding cassette, sub-family D (ALD), member 3	0,180	7,68E-02		transporter
ABCE1	ATP-binding cassette, sub-family E (OABP), member 1	0,118	9,61E-02		transporter
ACTR6	ARP6 actin-related protein 6 homolog (yeast)	-0,183	7,54E-02		transporter
ANKH	ANKH inorganic pyrophosphate transport regulator	-0,221	3,25E-02		transporter
AQP3	aquaporin 3 (Gill blood group)	-0,254	9,64E-02		transporter
ATP6V1C1	ATPase, H+ transporting, lysosomal 42kDa, V1 subunit C1	0,103	8,42E-02		transporter
CACNG1	calcium channel, voltage-dependent, gamma subunit 1	-0,246	8,70E-02		ion channel
CACNG6	calcium channel, voltage-dependent, gamma subunit 6	-0,203	8,33E-02		ion channel
CDH17	cadherin 17, LI cadherin (liver-intestine)	0,171	8,36E-02		transporter
DDI2	DNA-damage inducible 1 homolog 2 (S. cerevisiae)	0,178	6,13E-02		transporter
FDX1L	ferredoxin 1-like	0,237	7,76E-02		transporter
GJB3	gap junction protein, beta 3, 31kDa	-0,185	8,08E-02		transporter
GPM6A	glycoprotein M6A	-0,485	9,71E-02		ion channel
GRID2	glutamate receptor, ionotropic, delta 2	0,142	8,69E-02		ion channel
HBE1	hemoglobin, epsilon 1	0,377	8,20E-02		transporter
HDLBP	high density lipoprotein binding protein	0,274	7,74E-02		transporter
HSDL2	hydroxysteroid dehydrogenase like 2	-0,188	2,44E-02		transporter
KCNC2	potassium voltage-gated channel, Shaw-related subfamily, member 2	0,183	6,03E-02		ion channel
KCNG4	potassium voltage-gated channel, subfamily G, member 4	0,189	6,03E-02		ion channel
LRRCC1	leucine rich repeat and coiled-coil centrosomal protein 1	0,175	4,25E-02		transporter
MCL1	myeloid cell leukemia 1	-0,595	3,78E-02		transporter
NPC1	Niemann-Pick disease, type C1	0,215	2,96E-02		transporter
NUP160	nucleoporin 160kDa	-0,365	6,05E-02		transporter
NUTF2	nuclear transport factor 2	-0,164	4,94E-02		transporter
RHBG	Rh family, B glycoprotein (gene/pseudogene)	-0,436	1,42E-02		transporter
RHCG	Rh family, C glycoprotein	-0,381	4,32E-02		transporter
SCAMP2	secretory carrier membrane protein 2	0,332	2,99E-02		transporter
SCARB1	scavenger receptor class B, member 1	0,110	5,13E-02		transporter
SCFD1	sec1 family domain containing 1	-0,111	7,15E-02		transporter
SCN8A	sodium channel, voltage gated, type VIII, alpha subunit	-0,224	7,81E-02		ion channel
SEC61A1	Sec61 alpha 1 subunit (S. cerevisiae)	0,183	2,85E-02		transporter
SEC63	SEC63 homolog (S. cerevisiae)	-0,144	8,09E-02		transporter
SFXN2	sideroflexin 2	-0,101	6,97E-02		transporter
SLC15A1	solute carrier family 15 (oligopeptide transporter), member 1	0,165	9,61E-02		transporter
SLC25A4	solute carrier family 25 (mitochondrial carrier; adenine nucleotide translocator), member 4	-0,279	6,78E-02		transporter
SLC43A2	solute carrier family 43 (amino acid system L transporter), member 2	-0,121	4,25E-02		transporter
SLC5A1	solute carrier family 5 (sodium/glucose cotransporter), member 1	0,645	4,25E-02		transporter
SLC6A1	solute carrier family 6 (neurotransmitter transporter), member 1	0,224	3,69E-02		transporter
SLC6A19	solute carrier family 6 (neutral amino acid transporter), member 19	0,350	6,30E-02		transporter
SMC1A	structural maintenance of chromosomes 1A	-0,141	5,83E-02		transporter
SRI	sorcin	-0,170	2,81E-02	D	transporter
SRI	sorcin	-0,268	7,17E-02	D	transporter
STAR	steroidogenic acute regulatory protein	0,159	7,52E-02		transporter
SYT12	synaptotagmin XII	0,219	5,16E-02		transporter
TAPBP	TAP binding protein (tapasin)	0,158	8,44E-02		transporter
TMED7	transmembrane emp24 protein transport domain containing 7	0,161	4,32E-02		transporter

TMEM38A	transmembrane protein 38A	-0,161	7,70E-02		ion channel
TRPC4AP	transient receptor potential cation channel, subfamily C, member 4 associated protein	0,172	6,97E-02		transporter
TRPM3	transient receptor potential cation channel, subfamily M, member 3	-0,081	7,77E-02		ion channel
TRPV1	transient receptor potential cation channel, subfamily V, member 1	0,171	2,56E-02		ion channel
TSPAN1	tetraspanin 1	-0,172	2,68E-02		transporter
TUSC3	tumor suppressor candidate 3	-0,225	2,53E-02		transporter
VDAC3	voltage-dependent anion channel 3	0,127	5,03E-02		ion channel
VPS13A	vacuolar protein sorting 13 homolog A (S. cerevisiae)	0,252	1,56E-02		transporter
VPS4B	vacuolar protein sorting 4 homolog B (S. cerevisiae)	-0,081	9,61E-02		transporter
XPO4	exportin 4	0,230	7,26E-02		transporter
ATF3	activating transcription factor 3	-0,321	1,42E-02	D	transcription regulator
ATF3	activating transcription factor 3	-0,347	3,25E-02	D	transcription regulator
BTAF1	BTAF1 RNA polymerase II, B-TFIID transcription factor-associated, 170kDa	0,141	6,24E-02		transcription regulator
BTG2	BTG family, member 2	-2,141	1,42E-02	D	transcription regulator
BTG2	BTG family, member 2	-2,186	3,04E-02	D	transcription regulator
CBX4	chromobox homolog 4	-0,152	5,61E-02		transcription regulator
CCAR1	cell division cycle and apoptosis regulator 1	0,254	1,98E-02		transcription regulator
CEBPD	CCAAT/enhancer binding protein (C/EBP), delta	-0,100	7,79E-02		transcription regulator
CLUH	clustered mitochondria (cluA/CLU1) homolog	0,190	7,24E-02		translation regulator
CNBP	CCHC-type zinc finger, nucleic acid binding protein	-0,208	6,03E-02	D	transcription regulator
CNBP	CCHC-type zinc finger, nucleic acid binding protein	-0,386	7,60E-02	D	transcription regulator
CTCF	CCCTC-binding factor (zinc finger protein)	-0,174	2,56E-02		transcription regulator
EED	embryonic ectoderm development	0,135	8,81E-02		transcription regulator
EGR1	early growth response 1	-0,406	7,41E-03		transcription regulator
EGR2	early growth response 2	-0,424	4,43E-02		transcription regulator
EGR3	early growth response 3	-0,350	8,40E-02		transcription regulator
EIF1AY	eukaryotic translation initiation factor 1A, Y-linked	-0,263	7,79E-02		translation regulator
EIF2B1	eukaryotic translation initiation factor 2B, subunit 1 alpha, 26kDa	-0,170	9,69E-02		translation regulator
EIF2S2	eukaryotic translation initiation factor 2, subunit 2 beta, 38kDa	-0,237	4,81E-02		translation regulator
EN2	engrailed homeobox 2	-0,096	7,68E-02		transcription regulator
ERCC6	excision repair cross-complementation group 6	0,565	1,04E-02		transcription regulator
ETV6	ets variant 6	0,219	3,25E-02		transcription regulator
FOS	FBJ murine osteosarcoma viral oncogene homolog	-2,902	2,28E-02		transcription regulator
FOSB	FBJ murine osteosarcoma viral oncogene homolog B	-2,076	3,61E-02		transcription regulator
FOXK1	forkhead box K1	0,084	8,54E-02		transcription regulator
FOXQ1	forkhead box Q1	-0,339	7,07E-02	D	transcription regulator
FOXQ1	forkhead box Q1	-0,598	5,07E-02	D	transcription regulator
GABPA	GA binding protein transcription factor, alpha subunit 60kDa	0,152	5,95E-02		transcription regulator
GFM2	G elongation factor, mitochondrial 2	0,165	7,27E-02		translation regulator
HES1	hes family bHLH transcription factor 1	-0,132	8,75E-02		transcription regulator
HEY1	hes-related family bHLH transcription factor with YRPW motif 1	-0,219	2,81E-02		transcription regulator

HLF	hepatic leukemia factor	-0,117	6,48E-02		transcription regulator
HNF4G	hepatocyte nuclear factor 4, gamma	0,177	3,37E-02		transcription regulator
HTATSF1	HIV-1 Tat specific factor 1	-0,166	3,31E-02		transcription regulator
ID1	inhibitor of DNA binding 1, dominant negative helix-loop-helix protein	-0,413	1,04E-02		transcription regulator
ID2	inhibitor of DNA binding 2, dominant negative helix-loop-helix protein	-0,270	1,84E-02		transcription regulator
IGF2BP1	insulin-like growth factor 2 mRNA binding protein 1	-0,484	7,54E-02		translation regulator
JUN	jun proto-oncogene	-0,462	3,01E-02	D	transcription regulator
JUN	jun proto-oncogene	-0,410	6,90E-02	D	transcription regulator
KCNIP3	Kv channel interacting protein 3, calsenilin	-0,173	5,63E-02		transcription regulator
KLF6	Kruppel-like factor 6	-0,185	5,16E-02		transcription regulator
KMT2C	lysine (K)-specific methyltransferase 2C	0,414	2,60E-02		transcription regulator
MED16	mediator complex subunit 16	0,267	5,01E-02		transcription regulator
MED24	mediator complex subunit 24	0,240	9,63E-02		transcription regulator
MTRF1	mitochondrial translational release factor 1	0,141	9,03E-02		translation regulator
MYC	v-myc avian myelocytomatosis viral oncogene homolog	-0,408	5,62E-02	D	transcription regulator
MYC	v-myc avian myelocytomatosis viral oncogene homolog	-0,273	7,24E-02	D	transcription regulator
MYC	v-myc avian myelocytomatosis viral oncogene homolog	-0,410	3,41E-02	D	transcription regulator
MYC	v-myc avian myelocytomatosis viral oncogene homolog	-0,377	5,09E-02	D	transcription regulator
MYOG	myogenin (myogenic factor 4)	-0,206	7,60E-02		transcription regulator
MYT1	myelin transcription factor 1	-0,224	5,13E-02		transcription regulator
NCOA4	nuclear receptor coactivator 4	0,164	7,59E-02		transcription regulator
NCOR1	nuclear receptor corepressor 1	0,276	2,68E-02		transcription regulator
NEO1	neogenin 1	0,242	5,22E-02		transcription regulator
NFKBIA	nuclear factor of kappa light polypeptide gene enhancer in B-cells inhibitor, alpha	-0,734	3,99E-02	D	transcription regulator
NFKBIA	nuclear factor of kappa light polypeptide gene enhancer in B-cells inhibitor, alpha	-0,606	1,67E-02	D	transcription regulator
NFKBIA	nuclear factor of kappa light polypeptide gene enhancer in B-cells inhibitor, alpha	-0,617	5,85E-02	D	transcription regulator
NFX1	nuclear transcription factor, X-box binding 1	0,284	1,98E-02		transcription regulator
NPAS4	neuronal PAS domain protein 4	-2,407	6,61E-02		transcription regulator
NPM1	nucleophosmin (nucleolar phosphoprotein B23, numatrin)	-0,238	8,05E-02		transcription regulator
NR4A1	nuclear receptor subfamily 4, group A, member 1	-0,646	3,61E-02		ligand-dependent nuclear receptor
PAX2	paired box 2	-0,100	9,43E-02	D	transcription regulator
PAX2	paired box 2	-0,107	6,07E-02	D	transcription regulator
PAX6	paired box 6	-0,250	7,52E-02		transcription regulator
PAX9	paired box 9	-0,144	5,13E-02		transcription regulator
PCID2	PCI domain containing 2	0,210	1,62E-02		transcription regulator
PER2	period circadian clock 2	0,133	5,46E-02		transcription regulator
PFDN5	prefoldin subunit 5	-0,297	4,25E-02		transcription regulator

PIAS4	protein inhibitor of activated STAT, 4	-0,076	9,63E-02		transcription regulator
PIR	pirin (iron-binding nuclear protein)	0,222	3,81E-02		transcription regulator
PITX2	paired-like homeodomain 2	-0,196	1,91E-02		transcription regulator
PPP1R27	protein phosphatase 1, regulatory subunit 27	-0,216	5,30E-02		transcription regulator
RAD54L2	RAD54-like 2 (S. cerevisiae)	0,251	4,83E-02		transcription regulator
RB1	retinoblastoma 1	-0,091	8,94E-02		transcription regulator
RUNX3	runt-related transcription factor 3	0,182	8,46E-02		transcription regulator
SCRT1	scratch family zinc finger 1	0,235	1,84E-02		transcription regulator
SIN3B	SIN3 transcription regulator family member B	0,308	8,70E-02		transcription regulator
SIX6	SIX homeobox 6	-0,105	5,80E-02		transcription regulator
SKP1	S-phase kinase-associated protein 1	-0,202	1,84E-02	D	transcription regulator
SKP1	S-phase kinase-associated protein 1	-0,189	4,30E-02	D	transcription regulator
SKP1	S-phase kinase-associated protein 1	-0,204	6,37E-02	D	transcription regulator
SKP1	S-phase kinase-associated protein 1	-0,139	9,10E-02	D	transcription regulator
SMARCE1	SWI/SNF related, matrix associated, actin dependent regulator of chromatin, subfamily e, member 1	0,450	1,98E-02		transcription regulator
SOX10	SRY (sex determining region Y)-box 10	0,146	3,25E-02		transcription regulator
SOX2	SRY (sex determining region Y)-box 2	-0,113	6,44E-02		transcription regulator
SOX3	SRY (sex determining region Y)-box 3	-0,154	6,14E-02	D	transcription regulator
SOX3	SRY (sex determining region Y)-box 3	-0,173	9,40E-02	D	transcription regulator
SP1	Sp1 transcription factor	0,331	1,17E-02		transcription regulator
SUPT5H	suppressor of Ty 5 homolog (S. cerevisiae)	0,184	4,25E-02		transcription regulator
TAF5	TAF5 RNA polymerase II, TATA box binding protein (TBP)-associated factor, 100kDa	0,311	7,52E-02		transcription regulator
TBX15	T-box 15	0,094	6,78E-02		transcription regulator
TEF	thyrotrophic embryonic factor	0,402	4,38E-02		transcription regulator
TFAP2C	transcription factor AP-2 gamma (activating enhancer binding protein 2 gamma)	-0,215	5,85E-02		transcription regulator
THRB	thyroid hormone receptor, beta	-0,241	9,55E-02		ligand-dependent nuclear receptor
TOB1	transducer of ERBB2, 1	-0,614	2,32E-02	D	transcription regulator
TOB1	transducer of ERBB2, 1	-0,562	3,25E-02	D	transcription regulator
TOB1	transducer of ERBB2, 1	-0,265	6,10E-02	D	transcription regulator
TSFM	Ts translation elongation factor, mitochondrial	0,216	2,35E-02		translation regulator
USF2	upstream transcription factor 2, c-fos interacting	-0,402	7,60E-02		transcription regulator
WDR77	WD repeat domain 77	0,193	5,71E-02		transcription regulator
YAP1	Yes-associated protein 1	-0,140	5,77E-02		transcription regulator
ZFP36L2	ZFP36 ring finger protein-like 2	-0,139	4,65E-02		transcription regulator
ZNF131	zinc finger protein 131	0,095	8,17E-02		transcription regulator
ADRB2	adrenoceptor beta 2, surface	-0,167	8,63E-02		G-protein coupled receptor
B2M	beta-2-microglobulin	-0,258	4,50E-02		transmembrane receptor

CALCRL	calcitonin receptor-like	-0,302	3,76E-02		G-protein coupled receptor
CCR9	chemokine (C-C motif) receptor 9	-0,251	1,91E-02		G-protein coupled receptor
CLDN3	claudin 3	-0,396	2,44E-02	D	transmembrane receptor
CLDN3	claudin 3	-0,365	3,42E-02	D	transmembrane receptor
F3	coagulation factor III (thromboplastin, tissue factor)	-0,357	7,73E-03		transmembrane receptor
FAM155B	family with sequence similarity 155, member B	0,217	6,44E-02		transmembrane receptor
GPR143	G protein-coupled receptor 143	0,209	6,49E-02		G-protein coupled receptor
GPR85	G protein-coupled receptor 85	-0,152	8,69E-02		G-protein coupled receptor
IFNAR1	interferon (alpha, beta and omega) receptor 1	0,236	2,63E-02		transmembrane receptor
ILDR1	immunoglobulin-like domain containing receptor 1	0,107	7,26E-02		transmembrane receptor
LGALS3BP	lectin, galactoside-binding, soluble, 3 binding protein	0,083	8,83E-02		transmembrane receptor
SFRP5	secreted frizzled-related protein 5	-0,086	7,79E-02		transmembrane receptor
TNFRSF19	tumor necrosis factor receptor superfamily, member 19	0,210	4,13E-02		transmembrane receptor
TNFRSF21	tumor necrosis factor receptor superfamily, member 21	0,196	6,17E-02		transmembrane receptor
CMTM7	CKLF-like MARVEL transmembrane domain containing 7	-0,232	4,71E-02		cytokine
CXCL14	chemokine (C-X-C motif) ligand 14	-0,327	3,67E-02		cytokine
EDN1	endothelin 1	-0,348	5,53E-02		cytokine
BMP2	bone morphogenetic protein 2	-0,194	3,25E-02		growth factor
CTGF	connective tissue growth factor	-0,539	3,68E-02		growth factor
GMFB	glia maturation factor, beta	-0,283	7,33E-02		growth factor
GRN	granulin	0,428	3,25E-02		growth factor
MST1	macrophage stimulating 1 (hepatocyte growth factor-like)	0,293	1,58E-02		growth factor
OGN	osteoglycin	-0,144	9,58E-02		growth factor
CKB	creatine kinase, brain	0,299	5,01E-02		kinase
DAK	dihydroxyacetone kinase 2 homolog (S. cerevisiae)	0,152	3,36E-02		kinase
Dclk1	doublecortin-like kinase 1	0,320	7,09E-02		kinase
DSTYK	dual serine/threonine and tyrosine protein kinase	0,326	8,62E-02		kinase
DUSP1	dual specificity phosphatase 1	-1,633	5,35E-03	D	phosphatase
DUSP1	dual specificity phosphatase 1	-1,561	2,28E-02	D	phosphatase
DUSP2	dual specificity phosphatase 2	-1,027	2,23E-02		phosphatase
DUSP5	dual specificity phosphatase 5	-0,605	7,44E-02		phosphatase
DUSP6	dual specificity phosphatase 6	-0,402	6,30E-02		phosphatase
FXN	frataxin	-0,109	4,86E-02		kinase
MAPK4	mitogen-activated protein kinase 4	0,233	1,84E-02		kinase
MINPP1	multiple inositol-polyphosphate phosphatase 1	0,083	9,74E-02		phosphatase
NT5C2	5'-nucleotidase, cytosolic II	-0,329	2,28E-02		phosphatase
NT5E	5'-nucleotidase, ecto (CD73)	0,230	3,78E-02	D	phosphatase
NT5E	5'-nucleotidase, ecto (CD73)	0,242	3,78E-02	D	phosphatase
PACSIN1	protein kinase C and casein kinase substrate in neurons 1	0,137	8,26E-02		kinase
PAK1	p21 protein (Cdc42/Rac)-activated kinase 1	0,162	4,37E-02		kinase
PANK4	pantothenate kinase 4	0,130	8,08E-02		kinase
PDK2	pyruvate dehydrogenase kinase, isozyme 2	-0,371	2,35E-02		kinase
PGK1	phosphoglycerate kinase 1	0,114	8,40E-02		kinase
PI4KA	phosphatidylinositol 4-kinase, catalytic, alpha	-0,149	7,79E-02		kinase
PIK3C2A	phosphatidylinositol-4-phosphate 3-kinase, catalytic subunit type 2 alpha	0,255	7,15E-02		kinase
PIM2	Pim-2 proto-oncogene, serine/threonine kinase	-0,282	6,61E-02		kinase
PPP1R3D	protein phosphatase 1, regulatory subunit 3D	0,197	8,33E-02		phosphatase
PPP2R4	protein phosphatase 2A activator, regulatory subunit 4	-0,091	8,33E-02		phosphatase
PPP3R1	protein phosphatase 3, regulatory subunit B, alpha	0,096	9,19E-02		phosphatase
PRKAG1	protein kinase, AMP-activated, gamma 1 non-catalytic subunit	-0,272	9,35E-02		kinase
PRKAR1A	protein kinase, cAMP-dependent, regulatory, type I, alpha	0,375	8,69E-02		kinase
PRKCE	protein kinase C, epsilon	-0,137	8,08E-02		kinase
RIPK4	receptor-interacting serine-threonine kinase 4	0,214	4,25E-02		kinase
ROCK2	Rho-associated, coiled-coil containing protein kinase 2	0,267	9,32E-02	D	kinase
ROCK2	Rho-associated, coiled-coil containing protein kinase 2	0,248	9,43E-02	D	kinase
SCYL3	SCY1-like 3 (S. cerevisiae)	-0,113	9,64E-02		kinase
SGK1	serum/glucocorticoid regulated kinase 1	-0,585	1,23E-02	D	kinase
SGK1	serum/glucocorticoid regulated kinase 1	-0,585	2,31E-02	D	kinase
SOCS3	suppressor of cytokine signaling 3	-2,729	3,84E-03	D	phosphatase
SOCS3	suppressor of cytokine signaling 3	-2,775	9,54E-03	D	phosphatase

SRPK1	SRSF protein kinase 1	0,131	6,03E-02		kinase
STK39	serine threonine kinase 39	-0,359	6,17E-02		kinase
TBK1	TANK-binding kinase 1	0,275	3,31E-02		kinase
TEC	tec protein tyrosine kinase	0,392	1,91E-02		kinase
UCK2	uridine-cytidine kinase 2	-0,096	7,52E-02		kinase
2010107G12Rik	RIKEN cDNA 2010107G12 gene	0,121	5,53E-02		other
ABAT	4-aminobutyrate aminotransferase	-0,636	5,20E-02		enzyme
ACACB	acetyl-CoA carboxylase beta	-0,082	8,03E-02		enzyme
ACE	angiotensin I converting enzyme	0,524	9,22E-02		peptidase
ACTA1	actin, alpha 1, skeletal muscle	-0,412	8,56E-02		other
ACTG1	actin, gamma 1	-14,161	2,61E00	D	other
ACTG1	actin, gamma 1	-14,128	1,46E00	D	other
ACTG1	actin, gamma 1	-12,414	4,61E-01	D	other
ACTG2	actin, gamma 2, smooth muscle, enteric	0,541	7,52E-02		other
ACTN4	actinin, alpha 4	0,279	2,50E-02	D	other
ACTN4	actinin, alpha 4	0,296	5,16E-02	D	other
ACTR10	actin-related protein 10 homolog (S. cerevisiae)	0,180	5,13E-02		other
ACTR8	ARP8 actin-related protein 8 homolog (yeast)	0,252	4,62E-02		other
ADCY8	adenylate cyclase 8 (brain)	0,413	1,04E-02		enzyme
AIG1	androgen-induced 1	0,130	2,99E-02		other
ALDH6A1	aldehyde dehydrogenase 6 family, member A1	-0,112	4,38E-02		enzyme
AMDHD1	amidohydrolase domain containing 1	0,177	7,06E-02		enzyme
ANKRD13C	ankyrin repeat domain 13C	0,284	8,58E-02		other
ANKRD9	ankyrin repeat domain 9	-0,574	6,98E-03		other
ANXA4	annexin A4	-0,375	1,92E-02		other
APC	adenomatous polyposis coli	0,095	7,91E-02		enzyme
API5	apoptosis inhibitor 5	-0,193	8,89E-02		other
ARIH2	ariadne RBR E3 ubiquitin protein ligase 2	-0,181	9,60E-02		enzyme
ARL3	ADP-ribosylation factor-like 3	-0,126	8,40E-02		enzyme
ARRDC2	arrestin domain containing 2	0,131	6,31E-02		other
ATPAF2	ATP synthase mitochondrial F1 complex assembly factor 2	-0,132	4,54E-02		other
ATXN3	ataxin 3	0,535	3,31E-02	D	peptidase
ATXN3	ataxin 3	0,374	3,86E-02	D	peptidase
BBS5	Bardet-Biedl syndrome 5	-0,133	5,13E-02		other
BCAT1	branched chain amino-acid transaminase 1, cytosolic	-0,123	6,46E-02		enzyme
BFSP2	beaded filament structural protein 2, phakinin	-0,876	4,83E-02		other
BTF3L4	basic transcription factor 3-like 4	-0,330	3,67E-02		other
BVES	blood vessel epicardial substance	-0,321	6,98E-03	D	other
BVES	blood vessel epicardial substance	-0,299	3,28E-02	D	other
C12orf66	chromosome 12 open reading frame 66	-0,086	7,43E-02		other
C14orf119	chromosome 14 open reading frame 119	-0,181	5,62E-02		other
C15orf27	chromosome 15 open reading frame 27	0,105	6,36E-02		other
C15orf59	chromosome 15 open reading frame 59	0,202	5,75E-02		other
C2orf47	chromosome 2 open reading frame 47	-0,124	7,49E-02		other
C3	complement component 3	0,275	5,47E-02	D	peptidase
C3	complement component 3	0,178	7,60E-02	D	peptidase
CA10	carbonic anhydrase X	0,118	4,25E-02		enzyme
CAPN1	calpain 1, (mu/I) large subunit	0,267	7,47E-02		peptidase
CAPN3	calpain 3, (p94)	-0,625	4,25E-02		peptidase
CAPNS1	calpain, small subunit 1	-0,400	4,25E-02		peptidase
CBWD1	COBW domain containing 1	-0,163	6,76E-02		other
CCBL2	cysteine conjugate-beta lyase 2	-0,167	8,91E-02		enzyme
CCDC28A	coiled-coil domain containing 28A	-0,233	2,56E-02		other
CCDC53	coiled-coil domain containing 53	-0,156	4,39E-02	D	other
CCDC53	coiled-coil domain containing 53	-0,129	6,79E-02	D	other
CCT4	chaperonin containing TCP1, subunit 4 (delta)	0,170	3,04E-02		other
CDC40	cell division cycle 40	0,121	9,27E-02		other
Cdc42	cell division cycle 42	-0,264	5,02E-02		enzyme
CDC5L	cell division cycle 5-like	0,277	8,59E-02		other
CDC6	cell division cycle 6	-0,129	9,09E-02		other
CDH8	cadherin 8, type 2	0,151	7,79E-02		other
CECR1	cat eye syndrome chromosome region, candidate 1	-0,139	3,31E-02		enzyme
CEL	carboxyl ester lipase	0,451	4,25E-02		enzyme
CETP	cholesteryl ester transfer protein, plasma	0,191	1,98E-02		enzyme
CHAC1	ChaC, cation transport regulator homolog 1 (E. coli)	-0,750	1,84E-02		other
CHMP1A	charged multivesicular body protein 1A	0,193	4,62E-02		peptidase
Chmp4b	charged multivesicular body protein 4B	-0,274	3,87E-02		other
CHMP5	charged multivesicular body protein 5	-0,216	2,49E-02		other
CHORDC1	cysteine and histidine-rich domain (CHORD) containing 1	-0,217	5,58E-02		other
CIAPIN1	cytokine induced apoptosis inhibitor 1	-0,182	7,31E-02		other
CISH	cytokine inducible SH2-containing protein	-0,424	2,86E-02		other
CLASP1	cytoplasmic linker associated protein 1	-0,125	5,25E-02		other
CLDN12	claudin 12	-0,188	4,32E-02		other

CLDN7	claudin 7	-0,164	5,38E-02		other
CLDN9	claudin 9	-0,361	7,41E-03	D	other
CLDN9	claudin 9	-0,201	1,71E-02	D	other
CLDN9	claudin 9	-0,312	3,99E-02	D	other
CLPX	caseinolytic mitochondrial matrix peptidase chaperone subunit	-0,175	6,25E-02		enzyme
CLTC	clathrin, heavy chain (Hc)	0,210	7,54E-02		other
COL10A1	collagen, type X, alpha 1	0,271	5,15E-02		other
COL15A1	collagen, type XV, alpha 1	0,434	7,84E-02		other
COL4A1	collagen, type IV, alpha 1	0,272	7,54E-02		other
COL6A6	collagen, type VI, alpha 6	0,090	8,60E-02		other
COQ2	coenzyme Q2 4-hydroxybenzoate polyprenyltransferase	-0,089	7,26E-02		enzyme
CPA2	carboxypeptidase A2 (pancreatic)	0,166	6,08E-02		peptidase
CPSF2	cleavage and polyadenylation specific factor 2, 100kDa	0,338	1,96E-02		other
CPXM2	carboxypeptidase X (M14 family), member 2	0,185	5,13E-02		peptidase
CRY1	cryptochrome circadian clock 1	0,796	9,03E-02		enzyme
CRYBA2	crystallin, beta A2	-0,764	5,78E-02		other
CRYGN	crystallin, gamma N	-0,161	5,13E-02		other
CSNK2A3	casein kinase 2, alpha 3 polypeptide	-0,311	5,53E-02	D	other
CSNK2A3	casein kinase 2, alpha 3 polypeptide	-0,314	7,74E-02	D	other
CSTB	cystatin B (stefin B)	-0,354	5,31E-02		peptidase
CTC1	CTS telomere maintenance complex component 1	0,316	3,42E-02		other
CTR9	CTR9, Paf1/RNA polymerase II complex component	0,188	3,96E-02		other
CTSS	cathepsin S	0,251	3,42E-02	D	peptidase
CTSS	cathepsin S	0,303	4,56E-02	D	peptidase
CYP27C1	cytochrome P450, family 27, subfamily C, polypeptide 1	0,257	4,90E-02		other
CYR61	cysteine-rich, angiogenic inducer, 61	-1,160	9,40E-03		other
DAB1	Dab, reelin signal transducer, homolog 1 (Drosophila)	0,361	3,68E-02		other
DARS	aspartyl-tRNA synthetase	-0,283	3,25E-02		enzyme
DCN	decorin	-0,191	7,16E-02	D	other
DCN	decorin	-0,304	9,79E-02	D	other
DDA1	DET1 and DDB1 associated 1	0,151	2,99E-02		other
DDB2	damage-specific DNA binding protein 2, 48kDa	0,154	6,63E-02		other
DDIT4	DNA-damage-inducible transcript 4	-0,558	9,35E-03	D	other
DDIT4	DNA-damage-inducible transcript 4	-0,546	2,44E-02	D	other
DDOST	dolichyl-diphosphooligosaccharide--protein glycosyltransferase subunit (non-catalytic)	0,251	2,60E-02		enzyme
DDX27	DEAD (Asp-Glu-Ala-Asp) box polypeptide 27	-0,149	3,36E-02		enzyme
DDX31	DEAD (Asp-Glu-Ala-Asp) box polypeptide 31	0,120	3,78E-02		enzyme
DDX39B	DEAD (Asp-Glu-Ala-Asp) box polypeptide 39B	0,079	1,01E-01		enzyme
DDX49	DEAD (Asp-Glu-Ala-Asp) box polypeptide 49	-0,159	7,64E-02		enzyme
DDX51	DEAD (Asp-Glu-Ala-Asp) box polypeptide 51	0,247	7,12E-02		enzyme
DEDD2	death effector domain containing 2	-0,090	9,74E-02		other
DENND5B	DENN/MADD domain containing 5B	0,289	8,74E-02		other
DEPTOR	DEP domain containing MTOR-interacting protein	-0,458	2,44E-02		other
DHX16	DEAH (Asp-Glu-Ala-His) box polypeptide 16	0,336	3,86E-02	D	enzyme
DHX16	DEAH (Asp-Glu-Ala-His) box polypeptide 16	0,229	6,24E-02	D	enzyme
DNAJA3	DnaJ (Hsp40) homolog, subfamily A, member 3	-0,150	5,53E-02		other
DSP	desmoplakin	0,241	3,17E-02		other
DTX2	deltex 2, E3 ubiquitin ligase	0,279	3,51E-02		other
EFCAB14	EF-hand calcium binding domain 14	0,422	8,67E-02		other
EGLN1	egl-9 family hypoxia-inducible factor 1	0,420	1,25E-02		other
EHBP1	EH domain binding protein 1	0,275	1,36E-02		other
EHHADH	enoyl-CoA, hydratase/3-hydroxyacyl CoA dehydrogenase	0,282	4,32E-02		enzyme
EIF2B3	eukaryotic translation initiation factor 2B, subunit 3 gamma, 58kDa	-0,232	6,79E-02		other
EIF4EBP3	eukaryotic translation initiation factor 4E binding protein 3	0,156	7,73E-02		other
ELMOD2	ELMO/CED-12 domain containing 2	-0,103	7,24E-02		other
ELOVL7	ELOVL fatty acid elongase 7	-1,400	1,48E-02	D	enzyme
ELOVL7	ELOVL fatty acid elongase 7	-1,377	1,84E-02	D	enzyme
EMC8	ER membrane protein complex subunit 8	-0,109	4,25E-02	D	other
EMC8	ER membrane protein complex subunit 8	-0,112	9,25E-02	D	other
ERGIC2	ERGIC and golgi 2	0,196	9,19E-02		other
ERRFI1	ERBB receptor feedback inhibitor 1	-0,522	1,39E-02		other
ESRP2	epithelial splicing regulatory protein 2	0,173	8,80E-02		other
EVPL	envoplakin	0,253	7,54E-02		other
EXT2	exostosin glycosyltransferase 2	0,491	5,85E-02		enzyme
EXTL3	exostosin-like glycosyltransferase 3	0,077	9,53E-02		enzyme
F11R	F11 receptor	-0,141	9,25E-02		other
F2	coagulation factor II (thrombin)	0,384	8,87E-02		peptidase
FAAH2	fatty acid amide hydrolase 2	0,179	3,78E-02	D	enzyme
FAAH2	fatty acid amide hydrolase 2	0,202	8,47E-02	D	enzyme
FAM135A	family with sequence similarity 135, member A	0,198	2,44E-02		enzyme
FAM173A	family with sequence similarity 173, member A	-0,148	8,33E-02		other
FAM195B	family with sequence similarity 195, member B	-0,266	9,43E-02		other
FAM212A	family with sequence similarity 212, member A	-0,123	8,70E-02		other

FAM213A	family with sequence similarity 213, member A	-0,196	9,09E-02		other
FAM213B	family with sequence similarity 213, member B	0,179	2,44E-02		enzyme
FAM43A	family with sequence similarity 43, member A	-0,355	2,44E-02		other
FAM57B	family with sequence similarity 57, member B	0,227	8,33E-02		enzyme
FAM91A1	family with sequence similarity 91, member A1	0,207	5,95E-02		other
FBLN2	fibulin 2	0,230	3,88E-02		other
FBXL4	F-box and leucine-rich repeat protein 4	0,102	7,24E-02		other
FBXO9	F-box protein 9	0,193	8,75E-02		enzyme
FEZ1	fasciculation and elongation protein zeta 1 (zygin I)	0,368	9,64E-02		other
FIBCD1	fibrinogen C domain containing 1	0,244	6,03E-02		other
FLCN	folliculin	-0,131	9,25E-02		other
FNBP4	formin binding protein 4	-0,225	8,26E-02		other
FNIP1	folliculin interacting protein 1	0,402	7,41E-03		other
Folh1	folate hydrolase 1	0,233	3,81E-02		peptidase
FSCN2	fascin actin-bundling protein 2, retinal	-0,117	4,90E-02		other
FST	follistatin	-0,136	7,07E-02		other
GADD45A	growth arrest and DNA-damage-inducible, alpha	-0,563	5,47E-02		other
GADD45B	growth arrest and DNA-damage-inducible, beta	-0,956	2,34E-02	D	other
GADD45B	growth arrest and DNA-damage-inducible, beta	-0,538	5,35E-03	D	other
GALNT6	polypeptide N-acetylgalactosaminyltransferase 6	0,316	5,75E-02		enzyme
GAREM	GRB2 associated, regulator of MAPK1	0,175	9,50E-02		other
GCSH	glycine cleavage system protein H (aminomethyl carrier)	-0,224	7,68E-02		enzyme
GDI1	GDP dissociation inhibitor 1	-0,162	7,57E-02		other
GDPD1	glycerophosphodiester phosphodiesterase domain containing 1	0,157	6,63E-02		enzyme
GMPR	guanosine monophosphate reductase	-0,187	7,47E-02		enzyme
GNPNAT1	glucosamine-phosphate N-acetyltransferase 1	-0,157	8,05E-02		enzyme
GOT2	glutamic-oxaloacetic transaminase 2, mitochondrial	-0,229	8,53E-02		enzyme
GPALPP1	GPALPP motifs containing 1	-0,151	4,26E-02		other
GPHN	gephyrin	-0,120	4,25E-02		enzyme
H1f0	H1 histone family, member 0	-0,611	8,33E-03		other
H2AFY	H2A histone family, member Y	0,171	2,28E-02		other
HABP2	hyaluronan binding protein 2	0,234	8,27E-02		peptidase
HAL	histidine ammonia-lyase	0,433	4,02E-02		enzyme
HECTD1	HECT domain containing E3 ubiquitin protein ligase 1	-0,100	9,32E-02		enzyme
HEMK1	HemK methyltransferase family member 1	-0,095	6,38E-02		enzyme
HES5	hes family bHLH transcription factor 5	-0,156	8,75E-02		other
HHIP	hedgehog interacting protein	0,212	9,74E-02		other
HIBADH	3-hydroxyisobutyrate dehydrogenase	-0,226	5,68E-02	D	enzyme
HIBADH	3-hydroxyisobutyrate dehydrogenase	-0,160	7,37E-02	D	enzyme
HIST2H2BE	histone cluster 2, H2be	-0,246	1,56E-02		other
HMBS	hydroxymethylbilane synthase	-0,101	5,77E-02		enzyme
HNRNPAB	heterogeneous nuclear ribonucleoprotein A/B	0,085	7,84E-02		enzyme
HPRT1	hypoxanthine phosphoribosyltransferase 1	-0,156	8,64E-02		enzyme
HPS3	Hermansky-Pudlak syndrome 3	0,147	5,27E-02		other
HS2ST1	heparan sulfate 2-O-sulfotransferase 1	-0,105	6,90E-02		enzyme
IARS	isoleucyl-tRNA synthetase	0,490	2,44E-02		enzyme
ICA1L	islet cell autoantigen 1,69kDa-like	0,108	4,77E-02		other
IDI1	isopentenyl-diphosphate delta isomerase 1	-0,262	5,13E-02		enzyme
IGFBP1	insulin-like growth factor binding protein 1	-0,606	1,33E-02		other
ISCU	iron-sulfur cluster assembly enzyme	-0,138	8,41E-02	D	other
ISCU	iron-sulfur cluster assembly enzyme	-0,162	2,44E-02	D	other
IST1	increased sodium tolerance 1 homolog (yeast)	-0,260	3,88E-02		other
ITM2C	integral membrane protein 2C	-0,239	1,39E-02		other
IVD	isovaleryl-CoA dehydrogenase	-0,186	9,35E-02		enzyme
JADE3	jade family PHD finger 3	0,169	9,69E-02		other
KDM2A	lysine (K)-specific demethylase 2A	0,179	9,16E-02		other
KDM4C	lysine (K)-specific demethylase 4C	0,182	9,43E-02		other
KIAA0196	KIAA0196	0,303	3,78E-02	D	other
KIAA0196	KIAA0196	0,301	4,81E-02	D	other
KIAA0907	KIAA0907	0,208	9,35E-02		other
KIAA1191	KIAA1191	0,138	8,08E-02		other
KIAA1429	KIAA1429	0,215	1,84E-02		other
KIAA2013	KIAA2013	0,108	5,34E-02		other
KLHL21	kelch-like family member 21	-0,253	2,44E-02		other
KLHL35	kelch-like family member 35	0,085	9,15E-02		other
KRT222	keratin 222	-0,117	9,09E-02		other
LAMA4	laminin, alpha 4	0,230	2,49E-02		enzyme
LAMB1	laminin, beta 1	-0,193	8,13E-02		other
LAPTM4B	lysosomal protein transmembrane 4 beta	-0,176	2,72E-02		other
LCP1	lymphocyte cytosolic protein 1 (L-plastin)	0,559	3,58E-02		other
LCTL	lactase-like	-0,436	4,32E-02		enzyme
LEPROT	leptin receptor overlapping transcript	-0,078	9,60E-02		other
LGSN	lengsin, lens protein with glutamine synthetase domain	-0,752	7,85E-02		enzyme
LOC10035	heterogeneous nuclear ribonucleoprotein K-like	0,312	4,04E-02		other

9916					
LRAT	lecithin retinol acyltransferase (phosphatidylcholine--retinol O-acyltransferase)	-0,091	7,95E-02		enzyme
LRIT1	leucine-rich repeat, immunoglobulin-like and transmembrane domains 1	-0,173	3,31E-02		other
LSM1	LSM1, U6 small nuclear RNA associated	-0,141	9,79E-02		other
LYSMD2	LysM, putative peptidoglycan-binding, domain containing 2	-0,098	6,03E-02		other
LYSMD4	LysM, putative peptidoglycan-binding, domain containing 4	0,082	7,54E-02		other
MAB21L1	mab-21-like 1 (C. elegans)	0,129	4,73E-02		other
MAF1	MAF1 homolog (S. cerevisiae)	-0,318	8,38E-02		other
Marcks	myristoylated alanine rich protein kinase C substrate	-0,313	3,42E-02		other
MCM3	minichromosome maintenance complex component 3	-0,137	9,31E-02		enzyme
MCTS1	malignant T cell amplified sequence 1	-0,110	7,55E-02		other
MED28	mediator complex subunit 28	-0,107	6,44E-02		other
METTL3	methyltransferase like 3	0,195	8,46E-02		enzyme
MFGE8	milk fat globule-EGF factor 8 protein	-0,153	3,78E-02		other
MGME1	mitochondrial genome maintenance exonuclease 1	-0,260	5,03E-02		enzyme
MGST1	microsomal glutathione S-transferase 1	-0,267	2,49E-02		enzyme
MKRN2	makorin ring finger protein 2	0,244	1,91E-02		other
MPC2	mitochondrial pyruvate carrier 2	-0,282	1,21E-02	D	other
MPC2	mitochondrial pyruvate carrier 2	-0,372	5,28E-02	D	other
MROH1	maestro heat-like repeat family member 1	-0,088	6,67E-02		other
MRPL15	mitochondrial ribosomal protein L15	-0,155	7,92E-02		other
MRPS18B	mitochondrial ribosomal protein S18B	-0,102	9,15E-02		other
MRPS27	mitochondrial ribosomal protein S27	-0,176	3,92E-02		other
MTHFD2	methylenetetrahydrofolate dehydrogenase (NADP+ dependent) 2, methenyltetrahydrofolate cyclohydrolase	0,174	4,54E-02		enzyme
MVP	major vault protein	0,255	7,52E-02		other
MYH10	myosin, heavy chain 10, non-muscle	0,364	4,49E-02		other
MYH11	myosin, heavy chain 11, smooth muscle	0,417	1,98E-02		other
MYH4	myosin, heavy chain 4, skeletal muscle	-0,294	3,25E-02	D	enzyme
MYH4	myosin, heavy chain 4, skeletal muscle	-0,357	8,26E-02	D	enzyme
MYL6	myosin, light chain 6, alkali, smooth muscle and non-muscle	0,201	3,11E-02		other
MYO15A	myosin XVA	0,216	7,60E-02		other
MYO1B	myosin IB	0,189	4,11E-02		other
NCF1	neutrophil cytosolic factor 1	0,310	8,69E-02		enzyme
NCKAP1L	NCK-associated protein 1-like	0,322	3,36E-02		other
NCOA5	nuclear receptor coactivator 5	0,413	3,31E-02		other
NDOR1	NADPH dependent diflavin oxidoreductase 1	0,125	5,04E-02		enzyme
NDUFAF1	NADH dehydrogenase (ubiquinone) complex I, assembly factor 1	-0,141	9,24E-02		other
NEDD1	neural precursor cell expressed, developmentally down-regulated 1	-0,220	3,76E-02		other
NIFK	nucleolar protein interacting with the FHA domain of MKI67	-0,188	3,50E-02		other
NLGN4X	neuroligin 4, X-linked	-0,226	2,29E-02		enzyme
NOL9	nucleolar protein 9	0,183	3,99E-02		other
NOP58	NOP58 ribonucleoprotein	-0,271	7,00E-02		enzyme
NSUN2	NOP2/Sun RNA methyltransferase family, member 2	-0,122	4,62E-02		enzyme
NUCB2	nucleobindin 2	0,096	8,83E-02		other
NUDCD1	NudC domain containing 1	0,134	4,30E-02		other
NUF2	NUF2, NDC80 kinetochore complex component	-0,099	9,19E-02		other
NUP205	nucleoporin 205kDa	0,350	6,48E-02		other
NVL	nuclear VCP-like	0,273	6,46E-02		other
OBSL1	obscurin-like 1	-0,120	4,84E-02		other
ODF3L1	outer dense fiber of sperm tails 3-like 1	0,144	4,32E-02		other
OLIG3	oligodendrocyte transcription factor 3	0,235	6,34E-02		other
OPTN	optineurin	0,115	8,46E-02		other
Otud5	OTU domain containing 5	0,241	9,10E-02		enzyme
PAPLN	papilin, proteoglycan-like sulfated glycoprotein	0,223	6,03E-02		other
PARN	poly(A)-specific ribonuclease	0,305	6,03E-02		enzyme
PDCD11	programmed cell death 11	-0,157	4,62E-02		other
PDCL3	phosducin-like 3	-0,107	4,56E-02		other
PDXDC1	pyridoxal-dependent decarboxylase domain containing 1	0,207	6,50E-02		other
PECAM1	platelet/endothelial cell adhesion molecule 1	0,173	5,81E-02		other
PEX26	peroxisomal biogenesis factor 26	-0,128	6,03E-02		other
PFDN4	prefoldin subunit 4	-0,131	7,52E-02		other
PHACTR3	phosphatase and actin regulator 3	0,126	7,26E-02		other
PICALM	phosphatidylinositol binding clathrin assembly protein	0,333	8,86E-02		other
PLAA	phospholipase A2-activating protein	0,280	6,30E-02		other
PLS1	plastin 1	-0,101	5,95E-02		other
PLS3	plastin 3	-0,151	4,02E-02		other
POLDIP2	polymerase (DNA-directed), delta interacting protein 2	0,145	6,18E-02		other
POLR1C	polymerase (RNA) I polypeptide C, 30kDa	-0,118	3,92E-02		enzyme
PON2	paraoxonase 2	-0,114	6,10E-02		enzyme
PRICKLE2	prickle homolog 2 (Drosophila)	0,101	7,79E-02		other

PROC	protein C (inactivator of coagulation factors Va and VIIIa)	0,266	4,61E-02		peptidase
PRPF39	pre-mRNA processing factor 39	0,190	5,26E-02		other
PRPH	peripherin	0,148	3,48E-02		other
Prps1l3	phosphoribosyl pyrophosphate synthetase 1-like 3	0,111	8,08E-02		other
PSD3	pleckstrin and Sec7 domain containing 3	0,144	9,74E-02		other
PSMB7	proteasome (prosome, macropain) subunit, beta type, 7	-0,172	5,13E-02		peptidase
PTCD3	pentatricopeptide repeat domain 3	-0,103	5,85E-02		other
PTGIS	prostaglandin I2 (prostacyclin) synthase	-0,126	8,56E-02		enzyme
Pwp2	PWP2 periodic tryptophan protein homolog (yeast)	-0,100	7,64E-02		other
QRICH1	glutamine-rich 1	0,240	5,25E-02		other
RAB28	RAB28, member RAS oncogene family	0,247	8,12E-02		enzyme
RAB37	RAB37, member RAS oncogene family	-0,118	7,54E-02	D	enzyme
RAB37	RAB37, member RAS oncogene family	-0,090	8,68E-02	D	enzyme
RAB3IP	RAB3A interacting protein	0,240	3,78E-02		other
RAB40C	RAB40C, member RAS oncogene family	0,207	3,79E-02		enzyme
RAB5A	RAB5A, member RAS oncogene family	-0,114	5,96E-02		enzyme
RAD23A	RAD23 homolog A (S. cerevisiae)	0,080	9,63E-02		other
RAD54L	RAD54-like (S. cerevisiae)	0,080	9,15E-02		enzyme
RANBP9	RAN binding protein 9	-0,207	8,62E-02		other
RARS	arginyl-tRNA synthetase	0,294	1,95E-02		enzyme
RASAL2	RAS protein activator like 2	0,203	4,83E-02		other
RASD1	RAS, dexamethasone-induced 1	-0,240	8,08E-02		enzyme
RBBP5	retinoblastoma binding protein 5	0,204	7,52E-02		other
RBM28	RNA binding motif protein 28	-0,344	2,04E-02		other
RDH12	retinol dehydrogenase 12 (all-trans/9-cis/11-cis)	0,132	9,95E-02		enzyme
REEP3	receptor accessory protein 3	-0,133	5,68E-02		other
RETSAT	retinol saturase (all-trans-retinol 13,14-reductase)	0,157	4,32E-02		enzyme
RFC2	replication factor C (activator 1) 2, 40kDa	-0,096	5,55E-02		other
RGS1	regulator of G-protein signaling 1	-0,213	6,03E-02		other
RGS14	regulator of G-protein signaling 14	0,158	6,64E-02	D	other
RGS14	regulator of G-protein signaling 14	0,100	7,89E-02	D	other
RGS16	regulator of G-protein signaling 16	-0,425	9,53E-02		other
RHOC	ras homolog family member C	-0,143	6,85E-02		enzyme
RNF103	ring finger protein 103	-0,126	4,81E-02		enzyme
RNF144B	ring finger protein 144B	-0,197	9,48E-02		enzyme
RNF20	ring finger protein 20, E3 ubiquitin protein ligase	0,158	3,72E-02		enzyme
RNF213	ring finger protein 213	0,230	2,99E-02		enzyme
RNF7	ring finger protein 7	-0,229	9,15E-02		enzyme
RP2	retinitis pigmentosa 2 (X-linked recessive)	-0,140	7,81E-02		enzyme
RPAP3	RNA polymerase II associated protein 3	0,174	9,15E-02		enzyme
RPP40	ribonuclease P/MRP 40kDa subunit	-0,106	9,35E-02		enzyme
RPS19	ribosomal protein S19	-0,331	9,60E-02		other
RRAD	Ras-related associated with diabetes	-0,216	2,57E-02	D	enzyme
RRAD	Ras-related associated with diabetes	-0,240	6,03E-02	D	enzyme
RRM1	ribonucleotide reductase M1	-0,152	8,84E-02		enzyme
RTTN	rotatin	0,159	5,18E-02		other
SAMSN1	SAM domain, SH3 domain and nuclear localization signals 1	0,090	7,50E-02		other
SAR1A	secretion associated, Ras related GTPase 1A	-0,356	5,22E-02		enzyme
SARDH	sarcosine dehydrogenase	0,212	7,48E-02		enzyme
SARS2	seryl-tRNA synthetase 2, mitochondrial	0,184	9,40E-02		enzyme
SCAPER	S-phase cyclin A-associated protein in the ER	0,228	3,37E-02		other
SCRN3	secernin 3	0,164	2,53E-02		other
SCUBE2	signal peptide, CUB domain, EGF-like 2	0,262	7,54E-02		other
SDHA	succinate dehydrogenase complex, subunit A, flavoprotein (Fp)	0,329	3,17E-02		enzyme
SEC23IP	SEC23 interacting protein	-0,130	4,88E-02		other
SECISBP2L	SECIS binding protein 2-like	-0,201	9,15E-02		other
SEPSECS	Sep (O-phosphoserine) tRNA:Sec (selenocysteine) tRNA synthase	0,124	7,75E-02		enzyme
Sept4	septin 4	0,172	4,84E-02		other
SERINC4	serine incorporator 4	0,292	6,42E-02		other
SERPINA9	serpin peptidase inhibitor, clade A (alpha-1 antiproteinase, antitrypsin), member 9	0,142	7,48E-02		other
SESTD1	SEC14 and spectrin domains 1	0,221	7,04E-02		other
SFSWAP	splicing factor, suppressor of white-apricot family	0,376	7,93E-02		other
SGPL1	sphingosine-1-phosphate lyase 1	0,280	8,46E-02		enzyme
SGSM3	small G protein signaling modulator 3	0,328	8,25E-02	D	other
SGSM3	small G protein signaling modulator 3	0,293	9,15E-02	D	other
SIRT6	sirtuin 6	0,124	5,13E-02		enzyme
SLC16A9	solute carrier family 16, member 9	-0,370	4,36E-02		other
SLMO2	slowmo homolog 2 (Drosophila)	-0,410	6,30E-02		other
SLTM	SAFB-like, transcription modulator	0,182	2,49E-02		other
SMAP1	small ArfGAP 1	0,195	9,63E-02		other
SNX27	sorting nexin family member 27	-0,108	7,38E-02		other
SOCS1	suppressor of cytokine signaling 1	-0,486	4,92E-02		other

SOCS7	suppressor of cytokine signaling 7	0,184	9,03E-02		other
SOGA3	SOGA family member 3	-0,206	4,26E-02		other
SORD	sorbitol dehydrogenase	0,286	5,79E-02		enzyme
SPAG7	sperm associated antigen 7	-0,154	5,90E-02		other
SPPL2A	signal peptide peptidase like 2A	0,308	8,08E-02		peptidase
SSFA2	sperm specific antigen 2	0,248	2,07E-02		other
STAU2	staufen double-stranded RNA binding protein 2	-0,511	8,36E-02	D	other
STAU2	staufen double-stranded RNA binding protein 2	-0,428	8,69E-02	D	other
STIP1	stress-induced phosphoprotein 1	-0,148	7,31E-02		other
STRC	stereocilin	0,128	9,35E-02		other
STRN	striatin, calmodulin binding protein	0,126	6,24E-02		other
STXBP4	syntaxin binding protein 4	-0,108	8,08E-02		other
SVIL	supervillin	0,228	2,44E-02		other
SYBU	syntabulin (syntaxin-interacting)	0,224	6,90E-02		other
SYMPK	symplekin	0,200	7,25E-02		other
SYNPO2L	synaptopodin 2-like	-0,148	7,54E-02		other
TAX1BP1	Tax1 (human T-cell leukemia virus type I) binding protein 1	0,205	4,81E-02		other
TCAP	titin-cap	-0,598	8,33E-02		other
TCTN2	tectonic family member 2	0,126	7,38E-02		other
TEX10	testis expressed 10	0,141	3,25E-02		other
TFIP11	tuftelin interacting protein 11	0,261	4,45E-02		other
THEM4	thioesterase superfamily member 4	-0,102	5,78E-02		enzyme
THNSL2	threonine synthase-like 2 (S. cerevisiae)	0,102	6,21E-02		other
THOC3	THO complex 3	-0,120	8,27E-02		other
TIPARP	TCDD-inducible poly(ADP-ribose) polymerase	-0,405	6,71E-03		enzyme
TKTL2	transketolase-like 2	0,444	2,85E-02		enzyme
TMBIM4	transmembrane BAX inhibitor motif containing 4	-0,236	6,46E-02		other
TMEM147	transmembrane protein 147	0,315	4,69E-02		other
TMEM183A	transmembrane protein 183A	-0,215	3,25E-02		other
TMEM223	transmembrane protein 223	-0,169	5,61E-02		other
TMEM237	transmembrane protein 237	0,084	8,12E-02		other
TMEM51	transmembrane protein 51	0,314	1,98E-02		other
TMOD4	tropomodulin 4 (muscle)	-0,215	2,44E-02		other
TMTC4	transmembrane and tetratricopeptide repeat containing 4	0,151	3,78E-02		other
TMX3	thioredoxin-related transmembrane protein 3	0,452	5,95E-02		enzyme
TPD52L2	tumor protein D52-like 2	0,298	4,99E-02		other
TPRKB	TP53RK binding protein	-0,115	8,08E-02		other
TREH	trehalase (brush-border membrane glycoprotein)	0,111	8,36E-02		enzyme
TRMT61B	tRNA methyltransferase 61 homolog B (S. cerevisiae)	0,169	3,42E-02		enzyme
Tsc22d3	TSC22 domain family, member 3	-0,261	8,80E-02		other
TSPAN12	tetraspanin 12	-0,179	3,61E-02		other
TSPAN4	tetraspanin 4	0,256	4,49E-02		other
TTC7A	tetratricopeptide repeat domain 7A	0,270	9,54E-03		other
TXNIP	thioredoxin interacting protein	-0,472	9,43E-02	D	other
TXNIP	thioredoxin interacting protein	-0,341	9,35E-02	D	other
TYRP1	tyrosinase-related protein 1	0,172	5,45E-02		enzyme
U2AF2	U2 small nuclear RNA auxiliary factor 2	0,093	9,79E-02		other
UBA1	ubiquitin-like modifier activating enzyme 1	0,106	9,09E-02		enzyme
UBE2G1	ubiquitin-conjugating enzyme E2G 1	0,192	3,04E-02		enzyme
UBE2H	ubiquitin-conjugating enzyme E2H	-0,176	3,25E-02		enzyme
UBE2I	ubiquitin-conjugating enzyme E2I	-0,200	2,44E-02		enzyme
UBE2Q2	ubiquitin-conjugating enzyme E2Q family member 2	0,362	8,33E-02		enzyme
UBE4B	ubiquitination factor E4B	-0,154	9,10E-02		enzyme
UBXN1	UBX domain protein 1	0,203	2,12E-02		other
UGGT2	UDP-glucose glycoprotein glucosyltransferase 2	0,132	7,47E-02		enzyme
UNC50	unc-50 homolog (C. elegans)	-0,191	6,79E-02		other
USP25	ubiquitin specific peptidase 25	0,302	6,69E-02	D	peptidase
USP25	ubiquitin specific peptidase 25	0,259	8,67E-02	D	peptidase
USP48	ubiquitin specific peptidase 48	0,135	2,86E-02		peptidase
USP5	ubiquitin specific peptidase 5 (isopeptidase T)	0,143	3,61E-02		peptidase
UTP11L	UTP11-like, U3 small nucleolar ribonucleoprotein (yeast)	-0,188	5,28E-02		other
VAMP3	vesicle-associated membrane protein 3	-0,315	2,07E-02		other
Vma21	VMA21 vacuolar H+-ATPase homolog (S. cerevisiae)	-0,106	6,12E-02		other
VPS8	vacuolar protein sorting 8 homolog (S. cerevisiae)	0,291	9,09E-02		other
WDR5	WD repeat domain 5	-0,151	6,34E-02		other
WDR6	WD repeat domain 6	0,119	4,81E-02		other
WDR62	WD repeat domain 62	0,223	6,86E-02		other
WDR74	WD repeat domain 74	-0,177	2,28E-02		other
WDR76	WD repeat domain 76	0,163	4,25E-02		other
WRAP73	WD repeat containing, antisense to TP73	0,160	6,24E-02		other
XKR9	XK, Kell blood group complex subunit-related family, member 9	-0,176	3,25E-02		other
XPC	xeroderma pigmentosum, complementation group C	0,447	5,46E-02		other
YAE1D1	Yae1 domain containing 1	-0,306	7,85E-02		other

YKT6	YKT6 v-SNARE homolog (S. cerevisiae)	-0,143	4,04E-02	enzyme
YTHDF3	YTH domain family, member 3	0,121	8,62E-02	other
ZMYM2	zinc finger, MYM-type 2	0,121	5,18E-02	other

Annex 21: Relative microgravity microarrays (1g, 3g>axe, 3g>1g) by category.

Category	1g p-value	N	3g > axe p-value	N	3g > 1g p-value	N
Cellular Growth and Proliferation	5.71^{E-11}-4.98^{E-03}	181	6.87^{E-07}-6.95^{E-03}	70	5.78^{E-09}-3.15^{E-03}	213
Cell Cycle	1.15^{E-10}-4.98^{E-03}	93	3.61^{E-05}-7.6^{E-03}	20	8.79^{E-06}-2.63^{E-03}	85
Organismal Survival	8.1^{E-09}-8.1^{E-09}	119	1.23^{E-04}-7.24^{E-03}	46	1.87^{E-06}-3.23^{E-03}	139
Cellular Development	4.9^{E-08}-4.98^{E-03}	156	6.89^{E-08}-8.09^{E-03}	60	2.17^{E-06}-3.31^{E-03}	205
Connective Tissue Development and Function	4.9^{E-08}-4.98^{E-03}	44	1.55^{E-04}-6.95^{E-03}	26	1.91^{E-05}-3.3^{E-03}	75
Tissue Development	4.9^{E-08}-4.6^{E-03}	104	6.89^{E-08}-8.11^{E-03}	65	2.26^{E-06}-3.31^{E-03}	177
Cell Death and Survival	1.79^{E-07}-4.99^{E-03}	157	6.01^{E-09}-8.25^{E-03}	59	1.49^{E-10}-3.35^{E-03}	203
DNA Replication. Recombination. and Repair	1.11^{E-06}-4.98^{E-03}	77	4.27^{E-03}-7.37^{E-03}	7	2.22^{E-03}-2.63^{E-03}	8
Cardiovascular System Development and Function	9.78^{E-06}-3.03^{E-03}	28	1.1^{E-05}-7.81^{E-03}	28	3.76^{E-06}-3.02^{E-03}	92
Hematological System Development and Function	9.78^{E-06}-4.98^{E-03}	57	4.53^{E-05}-8.11^{E-03}	32	6.3^{E-06}-3.31^{E-03}	114
Cellular Assembly and Organization	1.75^{E-05}-4.98^{E-03}	80	4.21^{E-06}-7.65^{E-03}	42	1.83^{E-05}-3.02^{E-03}	90
Cellular Movement	2.64^{E-05}-4.55^{E-03}	94	2.43^{E-04}-7.89^{E-03}	35	1.82^{E-06}-3.02^{E-03}	132
Cell Morphology	3.38^{E-05}-3.03^{E-03}	89	2.43^{E-04}-7.65^{E-03}	47	7.12^{E-08}-2.7^{E-03}	144
Amino Acid Metabolism	4.27^{E-05}-4.98^{E-03}	23	2.37^{E-03}-6.69^{E-03}	3	1.08^{E-05}-1.83^{E-03}	13
Small Molecule Biochemistry	4.27^{E-05}-4.98^{E-03}	100	1.6^{E-05}-7.6^{E-03}	36	1.08^{E-05}-2.74^{E-03}	72
Embryonic Development	4.66^{E-05}-4.98^{E-03}	83	6.89^{E-08}-7.81^{E-03}	52	2.46^{E-07}-3.22^{E-03}	141
Organismal Development	4.66^{E-05}-4.93^{E-03}	85	6.89^{E-08}-7.81^{E-03}	63	2.46^{E-07}-3.22^{E-03}	203
Cell-To-Cell Signaling and Interaction	7.89^{E-05}-4.39^{E-03}	27	6.44^{E-05}-7.6^{E-03}	17	2.07^{E-03}-2.07^{E-03}	7
Cellular Function and Maintenance	1.27^{E-04}-4.39^{E-03}	67	4.21^{E-06}-7.65^{E-03}	37	1.83^{E-05}-3.02^{E-03}	148
Energy Production	1.72^{E-04}-2.24^{E-03}	22	5.95^{E-03}-7.37^{E-03}	6		
Lipid Metabolism	1.72^{E-04}-4.98^{E-03}	60	6.84^{E-05}-7.6^{E-03}	30	4.52^{E-05}-2.74^{E-03}	58
Renal and Urological System Development and Function	1.72^{E-04}-2.93^{E-03}	25	2.04^{E-04}-7.6^{E-03}	5	2.56^{E-03}-2.56^{E-03}	2
Nucleic Acid Metabolism	1.74^{E-04}-3.03^{E-03}	36	1.6^{E-05}-7.37^{E-03}	15	2.63^{E-03}-2.63^{E-03}	3
Tissue Morphology	1.75^{E-04}-4.98^{E-03}	80	4.53^{E-05}-7.81^{E-03}	47	2.49^{E-06}-3.15^{E-03}	129
Cellular Compromise	2.25^{E-04}-9.79^{E-04}	13	5.37^{E-04}-7.6^{E-03}	15	4.79^{E-04}-9.19^{E-04}	9
Molecular Transport	2.25^{E-04}-4.98^{E-03}	89	1.6^{E-05}-7.6^{E-03}	41	4.52^{E-05}-2.74^{E-03}	106
Lymphoid Tissue Structure and Development	2.29^{E-04}-4.55^{E-03}	24	1.18^{E-03}-6.38^{E-03}	17	2.24^{E-05}-3.01^{E-03}	36
Gene Expression	4.45^{E-04}-4.39^{E-03}	83	2.04^{E-04}-7.81^{E-03}	37	6.97^{E-08}-2.28^{E-03}	134
Carbohydrate Metabolism	5.2^{E-04}-3.1^{E-03}	43	6.84^{E-05}-7.52^{E-03}	19	2.63^{E-03}-2.63^{E-03}	3
Cell-mediated Immune Response	5.21^{E-04}-1.54^{E-03}	5			8.71^{E-04}-3.01^{E-03}	9
Cellular Response to Therapeutics	5.21^{E-04}-4.98^{E-03}	3				
Hematopoiesis	5.21^{E-04}-4.55^{E-03}	10	2.78^{E-03}-7.76^{E-03}	14	6.3^{E-06}-3.31^{E-03}	70
Hair and Skin Development and Function	6.67^{E-04}-4.49^{E-03}	19	1.88^{E-03}-1.88^{E-03}	6	8.79^{E-06}-3.35^{E-03}	47
Nervous System Development and Function	8.28^{E-04}-4.98^{E-03}	40	8.72^{E-06}-7.6^{E-03}	46	2.37^{E-05}-2.7^{E-03}	76
Organ Morphology	8.73^{E-04}-3.03^{E-03}	18	3.32^{E-05}-6.97^{E-03}	33	4.58^{E-06}-3.11^{E-03}	87
Organ Development	1.06^{E-03}-4.24^{E-03}	33	1.25^{E-06}-7.6^{E-03}	35	2.26^{E-06}-3.01^{E-03}	109
Skeletal and Muscular System Development and Function	1.06^{E-03}-4.28^{E-03}	34	1.55^{E-04}-7.6^{E-03}	23	2.26^{E-06}-3.11^{E-03}	67
Immune Cell Trafficking	1.54^{E-03}-1.71^{E-03}	3	8.11^{E-03}-8.11^{E-03}	5	2.23^{E-04}-2.79^{E-03}	53
Reproductive System Development and Function	1.54^{E-03}-4.6^{E-03}	10	2.37^{E-03}-7.6^{E-03}	8	1.21^{E-03}-2.81^{E-03}	21
Visual System Development and Function	1.7^{E-03}-1.71^{E-03}	6	1.25^{E-06}-4.5^{E-03}	17	4.58^{E-06}-1.78^{E-03}	35
Post-Translational Modification	1.71^{E-03}-4.98^{E-03}	4	8.8^{E-05}-5.83^{E-03}	15	3.03^{E-04}-1.43^{E-03}	48
Digestive System Development and Function	2.64^{E-03}-4.24^{E-03}	8	1.17^{E-04}-8.04^{E-03}	24	6.28^{E-05}-1.79^{E-03}	52
Hepatic System Development and Function	2.64^{E-03}-4.24^{E-03}	6	2.04^{E-04}-6.95^{E-03}	15	1.02^{E-04}-7.51^{E-04}	28
Protein Synthesis	2.98^{E-03}-2.98^{E-03}	41	8.8^{E-05}-3.54^{E-03}	27	2.6^{E-04}-2.24^{E-03}	66
Vitamin and Mineral Metabolism	3.55^{E-03}-3.55^{E-03}	8	1^{E-03}-3.18^{E-03}	6	2.56^{E-03}-2.56^{E-03}	2
Organismal Functions	4.98^{E-03}-4.98^{E-03}	2	6.73^{E-04}-4.27^{E-03}	8	3.15^{E-03}-3.15^{E-03}	13
Protein Trafficking	4.98^{E-03}-4.98^{E-03}	2			2.45^{E-03}-2.45^{E-03}	19
Cell Signaling			8.8^{E-05}-5.02^{E-03}	14	6.4^{E-04}-1.05^{E-03}	46
Drug Metabolism			6.44^{E-05}-3.02^{E-03}	4	8.71^{E-04}-8.71^{E-04}	2
Protein Degradation			3.54^{E-03}-3.54^{E-03}	13	2.24^{E-03}-2.24^{E-03}	13
Behavior			3.61^{E-04}-3.82^{E-03}	22	5.52^{E-06}-3.15^{E-03}	77
Auditory and Vestibular System Development and Function			5.5^{E-04}-3.82^{E-03}	7		
Endocrine System Development and Function			1.2^{E-04}-6.16^{E-03}	9	4.52^{E-05}-2.56^{E-03}	16

Annex 22: Relative microgravity microarrays (1g, 3g>axe, 3g>1g) Heat map by category.

Canonical Pathway	1g	3g>axe	3g>1g	1g>3g
IGF-1 Signaling	2.77	0.72	3.87	3.59
Tight Junction Signaling	1.42	0.39	7.63	0.35
JAK/Stat Signaling	1.08	0.92	2.90	4.31
Mitotic Roles of Polo-Like Kinase	6.57	0.98	0.51	
Prolactin Signaling	1.07	0.91	3.54	2.36
ERK/MAPK Signaling	2.41	1.15	2.01	2.14
Glucocorticoid Receptor Signaling	2.55	1.66	1.06	2.00
Erythropoietin Signaling	1.17	0.97	2.45	2.49
ILK Signaling	2.42		3.87	0.62
GADD45 Signaling	3.10	0.83	0.97	1.90
PPAR Signaling	1.68	1.36	0.52	2.78
Remodeling of Epithelial Adherens Junctions	3.81	0.36	1.82	0.33
VEGF Signaling	1.24	0.27	3.46	1.30
Insulin Receptor Signaling	1.06	0.51	1.74	2.85
Sertoli Cell-Sertoli Cell Junction Signaling	1.65	0.73	3.05	0.65
Epithelial Adherens Junction Signaling	3.87		1.53	0.42
CDK5 Signaling	0.72	0.70	3.16	1.21
PI3K/AKT Signaling	3.28	0.57	0.31	1.59
Growth Hormone Signaling	0.33	2.59	1.79	0.89
Cell Cycle Control of Chromosomal Replication	3.49	0.70	0.72	0.66
Role of JAK2 in Hormone-like Cytokine Signaling	1.34	0.60	1.08	2.41
Integrin Signaling	2.61		1.77	0.95
FAK Signaling	1.31	0.29	2.38	1.35
Renin-Angiotensin Signaling	0.62	1.21	2.30	1.11
Cell Cycle: G2/M DNA Damage Checkpoint Regulation	4.86		0.37	
GNRH Signaling	0.47	2.35	1.42	0.95
Valine Degradation I	1.20		3.86	
Cellular Effects of Sildenafil (Viagra)	0.76		3.35	0.95
IL-2 Signaling	0.47	0.45	1.15	2.87
Telomerase Signaling	0.72	0.70	0.77	2.68
Gα12/13 Signaling	0.88	0.20	2.10	1.66
Agrin Interactions at Neuromuscular Junction	1.14	0.36	2.38	0.89
Neuregulin Signaling	1.29	0.78	0.58	2.07
Regulation of IL-2 Expression in Activated and Anergic T Lymphocytes	0.97	0.32	1.07	2.24
Notch Signaling		2.42	1.60	0.53
STAT3 Pathway	0.63	0.34	1.19	2.36
Cyclins and Cell Cycle Regulation	2.69	0.32	0.70	0.80
Mechanisms of Viral Exit from Host Cells	0.62		1.49	2.22
PDGF Signaling	1.00	0.32	0.71	2.28

TNFR1 Signaling	0.51	2.11	1.25	0.44
Gap Junction Signaling	0.84		2.19	1.28
Role of JAK1 and JAK3 in γc Cytokine Signaling	0.76	0.39	0.55	2.59
Huntington's Disease Signaling		0.90	2.06	1.23
TNFR2 Signaling	0.85	0.67	2.00	0.63
LXR/RXR Activation	0.84	2.47	0.32	0.52
FXR/RXR Activation	0.78	2.38		0.96
Leukocyte Extravasation Signaling	0.52		3.56	
Actin Cytoskeleton Signaling	0.90		2.28	0.87
Thyroid Cancer Signaling	1.20	0.55		2.25
Amyloid Processing		0.46	2.42	1.11
Mouse Embryonic Stem Cell Pluripotency			1.21	2.76
Urate Biosynthesis/Inosine 5'-phosphate Degradation	0.56		1.20	2.16
Small Cell Lung Cancer Signaling	2.25		0.80	0.87
IL-9 Signaling	0.74	0.61	1.11	1.42
Cell Cycle Regulation by BTG Family Proteins	2.09	0.60	1.08	
Tyrosine Degradation I	2.30			1.35
Fatty Acid β-oxidation I	2.34	0.66	0.65	
IL-1 Signaling		0.27	1.28	2.02
Protein Kinase A Signaling	0.42		0.97	2.07
Citrulline-Nitric Oxide Cycle	2.13	1.31		
Chronic Myeloid Leukemia Signaling		0.27	0.28	2.80
DNA damage-induced 14-3-3σ Signaling	3.10			
Protein Ubiquitination Pathway	1.83		0.87	0.39
β-alanine Degradation I			3.06	
Amyotrophic Lateral Sclerosis Signaling	0.73	0.25	2.07	
Acute Myeloid Leukemia Signaling		0.32	0.40	2.28
Tryptophan Degradation X (Mammalian, via Tryptamine)	2.13			0.82
Histidine Degradation III			2.89	
Glutathione Redox Reactions I	0.47		0.38	1.94
Superpathway of Methionine Degradation			0.22	2.56
Agranulocyte Adhesion and Diapedesis	0.36		2.38	
Oncostatin M Signaling	0.26			2.45
G Beta Gamma Signaling			0.58	2.07
nNOS Signaling in Neurons			2.61	
IL-4 Signaling	0.28			2.30
Xenobiotic Metabolism Signaling		1.12		1.43
EIF2 Signaling	0.38			2.16
Ethanol Degradation IV	1.20		0.38	0.82
Phenylalanine Degradation IV (Mammalian, via Side Chain)	0.56		0.46	0.92
Glutathione-mediated Detoxification			0.25	1.58
Melatonin Degradation I	0.90	0.44		0.41

Superpathway of Melatonin Degradation	0.82	0.41		0.38
PXR/RXR Activation		0.37	0.87	0.34
Complement System	0.76		0.20	0.58
Histamine Degradation	0.59			0.95
Nicotine Degradation III	0.49	0.46		0.43
Nicotine Degradation II	0.40	0.40		0.37
Thyroid Hormone Metabolism II (via Conjugation and/or Degradation)	0.78		0.21	
LPS/IL-1 Mediated Inhibition of RXR Function			0.49	0.49
Bile Acid Biosynthesis, Neutral Pathway	0.59			

Annex 23: Relative microgravity microarrays. Heat map by diseases and functions.

Diseases and Bio Functions	**3g**	**3g>axe**	**3g>1g**	**1g>3g**
proliferation of cells	10,24	4,95	8,24	3,30
apoptosis	5,95	5,48	9,83	3,64
cell death of tumor cell lines	4,41	8,22	5,51	3,76
organismal death	8,09	3,91	5,73	4,14
cell death	6,20	4,18	7,15	3,77
necrosis	5,38	5,71	6,78	3,00
apoptosis of tumor cell lines	3,27	7,03	5,58	4,32
differentiation of cells	3,53	3,72	5,66	5,12
proliferation of tumor cell lines	4,86	3,71	4,82	4,39
morphology of cells	3,75	3,47	7,15	2,69
colony formation of tumor cell lines	2,51	3,78	5,17	5,56
necrosis of epithelial tissue	6,01	2,49	6,24	2,14
development of body trunk	2,31	4,23	6,61	3,59
proliferation of connective tissue cells	4,91	2,53	5,60	3,46
proliferation of fibroblasts	7,31	2,20	3,80	2,96
transcription of RNA	3,07	2,39	6,57	4,14
differentiation of tumor cell lines	3,15	2,36	4,93	5,45
cell cycle progression	9,94		3,40	2,45
colony formation of cells	2,98	2,44	4,52	5,78
cell death of epithelial cells	6,75	2,79	6,13	
quantity of cells	2,43	3,50	5,60	3,70
apoptosis of epithelial cells	2,41	2,76	6,76	2,50
organization of cytoplasm	3,89	5,38	4,74	
expression of RNA		2,58	7,16	4,20
binding of DNA		3,51	5,83	4,08
cell movement of tumor cell lines	4,58	3,61	5,14	
transactivation	3,35	3,35	6,53	
differentiation of embryonic tissue		7,16	3,74	2,28
cell movement	2,59	2,37	5,74	2,46
interphase	5,13	4,44	3,35	
cell death of central nervous system cells	2,37	6,14	4,26	

apoptosis of cervical cancer cell lines	2,65	3,56	3,82	2,66
differentiation of epithelial cells		5,25	4,51	2,39
activation of DNA endogenous promoter		2,73	5,31	4,10
cell survival	3,22	2,79	2,92	3,14
colony formation	4,20	2,61	5,23	
organization of cytoskeleton	3,12	4,36	4,48	
mitosis	6,84		2,73	2,21
cell death of cervical cancer cell lines	3,03	3,29	2,73	2,45
transactivation of RNA	2,89	2,73	5,81	
transcription of DNA		2,51	5,25	3,52
transport of molecule	2,63	2,82	2,91	2,80
cell viability	3,48	2,66	2,56	2,43
arrest in interphase	4,63	3,65	2,85	
metabolism of protein	2,53	2,89	3,58	2,09
invasion of cells	2,60		5,12	3,36
G1 phase	3,46	3,95	3,66	
microtubule dynamics	2,56	3,89	4,41	
concentration of aldosterone		2,21	4,34	4,28
formation of cells	3,58	3,06	4,14	
concentration of lipid	3,28	2,22	2,58	2,52
differentiation of blood cells		2,21	5,04	3,34
development of cardiovascular system		2,81	5,43	2,32
apoptosis of prostate cancer cell lines		2,29	6,03	2,10
quantity of blood cells		3,48	4,16	2,57
eye development		5,90	4,24	
migration of tumor cell lines	3,97	2,53	3,55	
migration of cells		2,57	4,73	2,73
quantity of K+			3,52	6,42
abnormal morphology of digestive system		3,79	3,60	2,45
development of body axis		3,49	6,30	
development of neurons	2,63	2,47	4,62	
binding of DNA fragment		2,63	4,59	2,49
apoptosis of beta islet cells	2,58		3,39	3,64
cell viability of epithelial cell lines	3,18		2,47	3,93
quantity of filaments	2,91	3,83		2,80
development of sensory organ		5,16	4,36	
abnormal morphology of body cavity		2,97	4,38	2,14
abnormal morphology of abdomen		2,63	3,58	3,28
size of body		2,60	4,58	2,17
proliferation of muscle cells	2,37		4,57	2,26
proliferation of liver cells		2,77	3,86	2,55
differentiation of keratinocytes		2,73	3,15	3,27
cell death of breast cancer cell lines	3,37	2,93	2,73	

growth of epithelial tissue		2,10	4,68	2,13
arrest in G0/G1 phase transition	2,61	2,81	3,44	
abnormal morphology of eye		4,36	4,48	
cell death of bone marrow cells	3,76	2,59		2,45
behavior		3,44	5,26	
abnormal morphology of cells		2,12	4,37	2,20
cell death of connective tissue cells	2,72		2,60	3,36
development of head		3,24	5,22	
uptake of D-glucose	3,28	2,36		2,75
apoptosis of glomerular cells	5,00		3,37	
vasculogenesis		2,15	3,71	2,48
G1/S phase transition	2,73	2,59	3,02	
cell death of pancreatic cancer cell lines	2,73		2,50	3,08
cell death of kidney cells	5,59		2,64	
differentiation of connective tissue cells	2,45	2,21	3,53	
differentiation of leukocytes		2,11	2,69	3,36
development of muscle			5,65	2,51
apoptosis of kidney cells	4,49		3,58	
morphology of head		5,39	2,57	
development of epithelial tissue			5,20	2,54
cell death of brain cells		4,27	3,46	
development of lymphatic system component		2,93	4,65	
quantity of hematopoietic progenitor cells			5,20	2,38
myogenesis			5,31	2,26
differentiation of central nervous system cells		4,29	3,19	
abnormal morphology of head		4,77	2,58	
development of abdomen			3,85	3,48
metabolism of amino acids	4,37		2,74	
differentiation of connective tissue	2,40		4,68	
binding of synthetic promoter		2,11	4,94	
development of blood vessel		2,11	4,90	
differentiation of neural precursor cells		4,10	2,91	
development of digestive system		2,72	4,20	
quantity of leukocytes		3,92	3,00	
growth of organism	3,01		3,88	
fatty acid metabolism	3,62	3,24		
apoptosis of central nervous system cells		4,05	2,78	
differentiation of brain cells		3,66	3,15	
quantity of centrosome	4,11		2,65	
proliferation of colon cancer cell lines			4,27	2,49
apoptosis of epithelial cell lines	3,76		2,99	
pluripotency of cells				6,62

concentration of cholesterol	2,69	3,92		
differentiation of astrocytes		2,92	3,65	
cell viability of fibroblast cell lines			4,00	2,48
morphology of vessel		3,60	2,85	
development of muscle cells	2,98		3,44	
expression of DNA			6,40	
morphology of digestive system			3,74	2,65
differentiation of skin			2,87	3,50
metabolism of thymocytes	3,28		3,06	
immortalization			3,83	2,49
abnormal morphology of olfactory placode		3,69	2,59	
arrest in G2/M phase of bone marrow cells		3,69	2,59	
fate determination of hair cells		3,69	2,59	
apoptosis of leukocyte cell lines			4,21	2,07
development of thymus gland		2,68	3,59	
degradation of amino acids	3,12		3,15	
repression of RNA			3,76	2,51
morphogenesis of ventricular septum			3,32	2,94
metabolism of nucleoside triphosphate	2,87	3,39		
abnormal morphology of retina		2,35	3,90	
contraction of aortic ring tissue		3,93		2,29
skin development			3,18	3,03
arrest in cell cycle progression of keratinocytes			2,59	3,61
development of neuroglia	3,08		3,11	
abnormal morphology of hepatobiliary system		2,47	3,69	
cell viability of breast cancer cell lines	3,50	2,66		
fate determination of cells		2,63	3,52	
abnormal morphology of epithelial tissue		2,38	3,74	
assembly of protein-protein complex		3,08	2,98	
differentiation of embryonic cells		3,53	2,53	
neuronal cell death		3,18	2,88	
arrest in growth of fibroblast cell lines			3,52	2,52
proliferation of smooth muscle cells		2,31	3,72	
cytokinesis	3,02		3,00	
senescence of fibroblast cell lines	3,39		2,61	
perinatal death		3,16	2,83	
binding of gene	2,36	3,63		
G2 phase	3,42	2,54		
checkpoint control	5,95			
formation of hair cells		2,85	3,09	
size of animal		2,85	3,04	
proliferation of bone marrow cells	3,10	2,76		

accumulation of cells		2,15	3,69	
growth of lymphatic system component	3,64	2,20		
G1 phase of tumor cell lines		2,52	3,32	
growth of embryonic tissue		3,33	2,49	
synthesis of rRNA			5,80	
development of oligodendrocytes		2,49	3,23	
necrosis of kidney	5,70			
apoptosis of leukemia cell lines		2,30	3,29	
uptake of monosaccharide	3,17	2,41		
differentiation of lymphocytes			3,04	2,49
interphase of epithelial cells			3,16	2,34
apoptosis of B-lymphocyte derived cell lines			3,32	2,17
migration of smooth muscle cells	2,44		3,05	
quantity of steroid hormone			3,02	2,46
adipogenesis of mesenchymal cells	2,30	3,17		
oxygenation	2,30	3,17		
synthesis of DNA	3,25			2,21
catabolism of amino acids	2,65		2,77	
cell death of carcinoma cell lines	3,27			2,15
metabolism of carbohydrate	2,58			2,82
interphase of tumor cell lines		2,13	3,25	
differentiation of hematopoietic cells			3,05	2,33
quantity of carbohydrate		2,19		3,18
morphology of eye			5,34	
contraction of heart	3,06			2,23
arrest in G2 phase	3,04			2,22
growth of connective tissue			5,25	
heart rate	3,10			2,13
M phase	5,16			
arrest in mitosis	5,14			
proliferation of neuronal cells		5,06		
cell cycle progression of epidermal cells			5,06	
systolic pressure	5,01			
arrest in metaphase	4,99			
catabolism of neutral amino acid			4,97	
apoptosis of breast cell lines			4,97	
quantity of steroid	2,45	2,51		
vasoconstriction of afferent arterioles		4,96		
secretion of lipid		2,17	2,57	
concentration of acylglycerol			2,56	2,05
cellular homeostasis			4,60	
morphology of cardiovascular system			4,25	

influx of cholesterol				4,23
abnormal morphology of cardiovascular system			4,22	
elongation of mitotic spindle	3,94			
beta-oxidation of fatty acid	3,76			
cell viability of kidney cell lines	3,76			
synthesis of fatty acid		3,70		
proliferation of lung cancer cell lines				3,57
differentiation of trophoblast		3,48		
contraction of mesangial cells		3,39		
kidney development				3,33
beta-oxidation of docosahexaenoic acid	3,28			
beta-oxidation of tetracosahexaenoic acid	3,28			
leukocyte migration			3,24	
uptake of cholesterol ester			3,23	
metabolism of membrane lipid derivative	3,22			
concentration of sterol	3,20			
adipogenesis			3,15	
concentration of D-glucose				3,09
metabolism of glutamine family amino acid	3,07			
muscle contraction			2,99	
metabolism of vitamin				2,74
arrest in interphase of epithelial cell lines				2,74
concentration of triacylglycerol			2,73	
uptake of carbohydrate		2,73		
quantity of amino acids	2,67			
oxidation of polyunsaturated fatty acids	2,65			
efflux of cholesterol				2,64
abnormal quantity of lipid		2,63		
gluconeogenesis	2,51			
synthesis of lipid	2,50			
metabolism of sterol	2,45			
synthesis of amino acids				2,42
quantity of vldl triglyceride in blood				2,37
glucose tolerance				2,29

Bibliography

Abbink, W. and G. Flik (2007). "Parathyroid hormone-related protein in teleost fish." Gen Comp Endocrinol **152**(2-3): 243-251.

Aceto, J., M. Muller, R. Nourizadeh-Lillabadi, P. Alestrom, J. Van Loon, V. Schiller, R. Goerlich, J. Renn and C. Winkler (2008). "Small fish species as powerful model systems to study vertebrate physiology in space." J Gravit Physiol **15**: 111-112.

Aceto, J., R. Nourizadeh-Lilladadi, J. van Loon, P. Motte, P. Alestrom, J. A. Martial and M. Muller (2009). "Microgravity simulation comparison at genome level in Danio rerio and role of Sox4 transcription factors in cranial skeleton development." J Gravit Physiol **16**: in press.

Ahmed, C. M., J. Larkin, 3rd and H. M. Johnson (2015). "SOCS1 Mimetics and Antagonists: A Complementary Approach to Positive and Negative Regulation of Immune Function." Front Immunol **6**: 183.

Alderman, S. L. and N. J. Bernier (2009). "Ontogeny of the corticotropin-releasing factor system in zebrafish." Gen Comp Endocrinol **164**(1): 61-69.

Alexander, C., E. Zuniga, I. L. Blitz, N. Wada, P. Le Pabic, Y. Javidan, T. Zhang, K. W. Cho, J. G. Crump and T. F. Schilling (2011). "Combinatorial roles for BMPs and Endothelin 1 in patterning the dorsal-ventral axis of the craniofacial skeleton." Development **138**(23): 5135-5146.

Alexandre, C. (2001). " Microgravité et système ostéoarticulaire. ." Revue du rhumatisme **68**: 781-786.

Aliprantis, A. O., Y. Ueki, R. Sulyanto, A. Park, K. S. Sigrist, S. M. Sharma, M. C. Ostrowski, B. R. Olsen and L. H. Glimcher (2008). "NFATc1 in mice represses osteoprotegerin during osteoclastogenesis and dissociates systemic osteopenia from inflammation in cherubism." J Clin Invest **118**(11): 3775-3789.

Allen, D. L., E. R. Bandstra, B. C. Harrison, S. Thorng, L. S. Stodieck, P. J. Kostenuik, S. Morony, D. L. Lacey, T. G. Hammond, L. L. Leinwand, W. S. Argraves, T. A. Bateman and J. L. Barth (2009). "Effects of spaceflight on murine skeletal muscle gene expression." J Appl Physiol (1985) **106**(2): 582-595.

Alsop, D. and M. Vijayan (2009). "The zebrafish stress axis: molecular fallout from the teleost-specific genome duplication event." Gen Comp Endocrinol **161**(1): 62-66.

Alsop, D. and M. M. Vijayan (2008). "Development of the corticosteroid stress axis and receptor expression in zebrafish." Am J Physiol Regul Integr Comp Physiol **294**(3): R711-719.

Alsop, D. and M. M. Vijayan (2009). "Molecular programming of the corticosteroid stress axis during zebrafish development." Comp Biochem Physiol A Mol Integr Physiol **153**(1): 49-54.

Aluru, N. and M. M. Vijayan (2008). "Molecular characterization, tissue-specific expression, and regulation of melanocortin 2 receptor in rainbow trout." Endocrinology **149**(9): 4577-4588.

Aluru, N. and M. M. Vijayan (2009). "Stress transcriptomics in fish: a role for genomic cortisol signaling." Gen Comp Endocrinol **164**(2-3): 142-150.

Amling, M., M. Priemel, T. Holzmann, K. Chapin, J. M. Rueger, R. Baron and M. B. Demay (1999). "Rescue of the skeletal phenotype of vitamin D receptor-ablated mice in the setting of normal mineral ion homeostasis: formal histomorphometric and biomechanical analyses." Endocrinology **140**(11): 4982-4987.

Andersen, T. L., M. E. Abdelgawad, H. B. Kristensen, E. M. Hauge, L. Rolighed, J. Bollerslev, P. Kjaersgaard-Andersen and J. M. Delaisse (2013). "Understanding coupling between bone resorption and formation: are reversal cells the missing link?" Am J Pathol **183**(1): 235-246.

Anken, R. H. (2006). "On the role of the central nervous system in regulating the mineralisation of inner-ear otoliths of fish." Protoplasma **229**(2-4): 205-208.

Anken, R. H., M. Beier and H. Rahmann (2004). "Hypergravity decreases carbonic anhydrase-reactivity in inner ear maculae of fish." J Exp Zool A Comp Exp Biol **301**(10): 815-819.

Apschner, A., S. Schulte-Merker and P. E. Witten (2011). "Not all bones are created equal - using zebrafish and other teleost species in osteogenesis research." Methods Cell Biol **105**: 239-255.

Arfat, Y., W. Z. Xiao, S. Iftikhar, F. Zhao, D. J. Li, Y. L. Sun, G. Zhang, P. Shang and A. R. Qian (2014). "Physiological effects of microgravity on bone cells." Calcif Tissue Int **94**(6): 569-579.

Arias, J. L., O. Nakamura, M. S. Fernandez, J. J. Wu, P. Knigge, D. R. Eyre and A. I. Caplan (1997). "Role of type X collagen on experimental mineralization of eggshell membranes." Connect Tissue Res **36**(1): 21-33.

Ashurst, J. L., C. K. Chen, J. G. Gilbert, K. Jekosch, S. Keenan, P. Meidl, S. M. Searle, J. Stalker, R. Storey, S. Trevanion, L. Wilming and T. Hubbard (2005). "The Vertebrate Genome Annotation (Vega) database." Nucleic Acids Res **33**(Database issue): D459-465.

Avaron, F., L. Hoffman, D. Guay and M. A. Akimenko (2006). "Characterization of two new zebrafish members of the hedgehog family: atypical expression of a zebrafish indian hedgehog gene in skeletal elements of both endochondral and dermal origins." Dev Dyn **235**(2): 478-489.

Bacchetta, J., B. Ranchin, L. Dubourg and P. Cochat (2010). "[Vitamin D revisited: a cornerstone of health?]." Arch Pediatr **17**(12): 1687-1695.

Baek, W. Y., M. A. Lee, J. W. Jung, S. Y. Kim, H. Akiyama, B. de Crombrugghe and J. E. Kim (2009). "Positive regulation of adult bone formation by osteoblast-specific transcription factor osterix." J Bone Miner Res **24**(6): 1055-1065.

Balla, B., J. P. Kosa, J. Kiss, A. Borsy, J. Podani, I. Takacs, A. Lazary, Z. Nagy, K. Bacsi, G. Speer, L. Orosz and P. Lakatos (2008). "Different gene expression patterns in the bone tissue of aging postmenopausal osteoporotic and non-osteoporotic women." Calcif Tissue Int **82**(1): 12-26.

Barbazuk, W. B., I. Korf, C. Kadavi, J. Heyen, S. Tate, E. Wun, J. A. Bedell, J. D. McPherson and S. L. Johnson (2000). "The syntenic relationship of the zebrafish and human genomes." Genome Res **10**(9): 1351-1358.

Beier, M., R. H. Anken and H. Rahmann (2002). "Influence of hypergravity on fish inner ear otoliths: II. Incorporation of calcium and kinetotic behaviour." Space Life Sciences: Biological Research and Space Radiation **30**(4): 727-731.

Bellido, T., A. A. Ali, I. Gubrij, L. I. Plotkin, Q. Fu, C. A. O'Brien, S. C. Manolagas and R. L. Jilka (2005). "Chronic elevation of parathyroid hormone in mice reduces expression of sclerostin by osteocytes: a novel mechanism for hormonal control of osteoblastogenesis." Endocrinology **146**(11): 4577-4583.

Benjamini, Y. and M. C. Hochberg (1995). "Controlling the false discovery rate: A practical and powerful approach to multiple testing." J. R. Stat. Soc. Ser. B (Methodological) **57**: 289-300.

Beyer, C. and G. Schett (2010). "Pharmacotherapy: concepts of pathogenesis and emerging treatments. Novel targets in bone and cartilage." Best Pract Res Clin Rheumatol **24**(4): 489-496.

Beysens, D., L. Carotenuto, J. J. W. A. van Loon and M. Zell (2011). Laboratory Science with Space Data. Accessing and Using Space-Experiment Data., Springer.

Billiard, J., R. A. Moran, M. Z. Whitley, M. Chatterjee-Kishore, K. Gillis, E. L. Brown, B. S. Komm and P. V. Bodine (2003). "Transcriptional profiling of human osteoblast differentiation." J Cell Biochem **89**(2): 389-400.

Blaber, E., H. Marcal and B. P. Burns (2010). "Bioastronautics: the influence of microgravity on astronaut health." Astrobiology **10**(5): 463-473.

Blaker-Lee, A., S. Gupta, J. M. McCammon, G. De Rienzo and H. Sive (2012). "Zebrafish homologs of genes within 16p11.2, a genomic region associated with brain disorders, are active during brain development, and include two deletion dosage sensor genes." Dis Model Mech **5**(6): 834-851.

Bodine, P. V., M. Trailsmith and B. S. Komm (1996). "Development and characterization of a conditionally transformed adult human osteoblastic cell line." J Bone Miner Res **11**(6): 806-819.

Borst, A. G. and J. J. W. A. van Loon (2009). "Technology and Development for the Random Positioning Machine, RPM. ." Microgravity Sci Technol **21**: 287-292.

Boskey, A. L., L. Spevak, E. Paschalis, S. B. Doty and M. D. McKee (2002). "Osteopontin deficiency increases mineral content and mineral crystallinity in mouse bone." Calcif Tissue Int **71**(2): 145-154.

Boudin, E., I. Fijalkowski, E. Piters and W. Van Hul (2013). "The role of extracellular modulators of canonical Wnt signaling in bone metabolism and diseases." Semin Arthritis Rheum **43**(2): 220-240.

Bouillon, R. and T. Suda (2014). "Vitamin D: calcium and bone homeostasis during evolution." Bonekey Rep **3**: 480.

Bradshaw, A. D. and E. H. Sage (2001). "SPARC, a matricellular protein that functions in cellular differentiation and tissue response to injury." J Clin Invest **107**(9): 1049-1054.

Braemer W, B. H., editors (1957). "Orientation of fish to gravity." Symposium on fish behavior, AIBS Meetings; Stanford University.

Brekken, R. A. and E. H. Sage (2001). "SPARC, a matricellular protein: at the crossroads of cell-matrix communication." Matrix Biol **19**(8): 816-827.

Briegleb, W. (1992). "Some qualitative and quantitative aspects of the fast-rotating clinostat as a research tool." ASGSB Bull **5**(2): 23-30.

Britsch, S., D. E. Goerich, D. Riethmacher, R. I. Peirano, M. Rossner, K. A. Nave, C. Birchmeier and M. Wegner (2001). "The transcription factor Sox10 is a key regulator of peripheral glial development." Genes Dev **15**(1): 66-78.

Brown, J. R., H. Ye, R. T. Bronson, P. Dikkes and M. E. Greenberg (1996). "A defect in nurturing in mice lacking the immediate early gene fosB." Cell **86**(2): 297-309.

Brungs, S., J. Hauslage, R. Hilbig, R. Hemmersbach and R. Anken (2011). "Effects of simulated weightlessness on fish otolith growth: Clinostat versus Rotating-Wall Vessel." Advances in Space research **48**: 792-798.

Bucay, N., I. Sarosi, C. R. Dunstan, S. Morony, J. Tarpley, C. Capparelli, S. Scully, H. L. Tan, W. Xu, D. L. Lacey, W. J. Boyle and W. S. Simonet (1998). "osteoprotegerin-deficient mice develop early onset osteoporosis and arterial calcification." Genes Dev **12**(9): 1260-1268.

Bucking, C., C. M. Lemoine and P. J. Walsh (2013). "Waste nitrogen metabolism and excretion in zebrafish embryos: effects of light, ammonia, and nicotinamide." J Exp Zool A Ecol Genet Physiol **319**(7): 391-403.

Burgers, T. A. and B. O. Williams (2013). "Regulation of Wnt/beta-catenin signaling within and from osteocytes." Bone **54**(2): 244-249.

Caillot-Augusseau, A., M. H. Lafage-Proust, C. Soler, J. Pernod, F. Dubois and C. Alexandre (1998). "Bone formation and resorption biological markers in cosmonauts during and after a 180-day space flight (Euromir 95)." Clin Chem **44**(3): 578-585.

Caillot-Augusseau, A., L. Vico, M. Heer, D. Voroviev, J. C. Souberbielle, A. Zitterman, C. Alexandre and M. H. Lafage-Proust (2000). "Space flight is associated with rapid decreases of undercarboxylated osteocalcin and increases of markers of bone resorption without changes in their circadian variation: observations in two cosmonauts." Clin Chem **46**(8 Pt 1): 1136-1143.

Carmeliet, G. and R. Bouillon (1999). "The effect of microgravity on morphology and gene expression of osteoblasts in vitro." FASEB J **13 Suppl**: S129-134.

Carmeliet, G., L. Vico and R. Bouillon (2001). "Space flight: a challenge for normal bone homeostasis." Crit Rev Eukaryot Gene Expr **11**(1-3): 131-144.

Catalano, A., N. Morabito, G. Basile, S. Brancatelli, D. Cucinotta and A. Lasco (2013). "Zoledronic acid acutely increases sclerostin serum levels in women with postmenopausal osteoporosis." J Clin Endocrinol Metab **98**(5): 1911-1915.

Catchen, J. M., J. S. Conery and J. H. Postlethwait (2009). "Automated identification of conserved synteny after whole-genome duplication." Genome Res **19**(8): 1497-1505.

Cau, E., G. Gradwohl, S. Casarosa, R. Kageyama and F. Guillemot (2000). "Hes genes regulate sequential stages of neurogenesis in the olfactory epithelium." Development **127**(11): 2323-2332.

Chen, Y., B. S. Bal and J. P. Gorski (1992). "Calcium and collagen binding properties of osteopontin, bone sialoprotein, and bone acidic glycoprotein-75 from bone." J Biol Chem **267**(34): 24871-24878.

Chou, M. Y., C. H. Lin, P. L. Chao, J. C. Hung, S. A. Cruz and P. P. Hwang (2015). "Stanniocalcin-1 controls ion regulation functions of ion-transporting epithelium other than calcium balance." Int J Biol Sci **11**(2): 122-132.

Chun, R. F., E. Blatter, S. Elliott, S. Fitz-Gibbon, S. Rieger, A. Sagasti, J. S. Adams and M. Hewison (2014). "Cloning of a functional 25-hydroxyvitamin D-1alpha-hydroxylase in zebrafish (Danio rerio)." Cell Biochem Funct **32**(8): 675-682.

Close, R., S. Toro, J. A. Martial and M. Muller (2002). "Expression of the zinc finger Egr1 gene during zebrafish embryonic development." Mech Dev **118**(1-2): 269-272.

Cogoli, M. (1992). "The fast rotating clinostat: a history of its use in gravitational biology and a comparison of ground-based and flight experiment results." ASGSB Bull **5**(2): 59-67.

Collet, P., D. Uebelhart, L. Vico, L. Moro, D. Hartmann, M. Roth and C. Alexandre (1997). "Effects of 1- and 6-month spaceflight on bone mass and biochemistry in two humans." Bone **20**(6): 547-551.

Cools, M., S. Goemaere, D. Baetens, A. Raes, A. Desloovere, J. M. Kaufman, J. De Schepper, I. Jans, D. Vanderschueren, J. Billen, E. De Baere, T. Fiers and R. Bouillon (2015). "Calcium and bone homeostasis in heterozygous carriers of CYP24A1 mutations: A cross-sectional study." Bone **81**: 89-96.

Craig, T. A., S. Sommer, C. R. Sussman, J. P. Grande and R. Kumar (2008). "Expression and regulation of the vitamin D receptor in the zebrafish, Danio rerio." J Bone Miner Res **23**(9): 1486-1496.

Craig, T. A., Y. Zhang, M. S. McNulty, S. Middha, H. Ketha, R. J. Singh, A. T. Magis, C. Funk, N. D. Price, S. C. Ekker and R. Kumar (2012). "Research resource: whole transcriptome RNA sequencing detects multiple 1alpha,25-dihydroxyvitamin D(3)-sensitive metabolic pathways in developing zebrafish." Mol Endocrinol **26**(9): 1630-1642.

Crosnier, C., D. Stamataki and J. Lewis (2006). "Organizing cell renewal in the intestine: stem cells, signals and combinatorial control." Nat Rev Genet **7**(5): 349-359.

Cubbage, C. and P. Mabee (1996). "Development of the Cranium and Paired Fins in the Zebrafish Danio rerio (Ostariophysi, Cyprinidae)." Journal of Morphology. **229**: 121-160

Cubbage, C. C. and P. M. Mabee (1996). "Development of the Cranium and Paired Fins in the Zebrafish Danio rerio (Ostariophysi, Cyprinidae)." J. Morphol **229**: 121-160.

Dahm, R., R. Geisler and C. Nüsslein-Volhard (2005). Encyclopedia of Molecular Cell Biology and Molecular Medicine. .

Dalcq, J., V. Pasque, A. Ghaye, A. Larbuisson, P. Motte, J. A. Martial and M. Muller (2012). "RUNX3, EGR1 and SOX9B form a regulatory cascade required to modulate BMP-signaling during cranial cartilage development in zebrafish." PLoS One **7**(11): e50140.

Dallas, S. L., M. Prideaux and L. F. Bonewald (2013). "The osteocyte: an endocrine cell ... and more." Endocr Rev **34**(5): 658-690.

Dalle Carbonare, L., M. T. Valenti, M. Zanatta, L. Donatelli and V. Lo Cascio (2009). "Circulating mesenchymal stem cells with abnormal osteogenic differentiation in patients with osteoporosis." Arthritis Rheum **60**(11): 3356-3365.

Danks, J. A., D. G. D'Souza, H. J. Gunn, K. M. Milley and S. J. Richardson (2011). "Evolution of the parathyroid hormone family and skeletal formation pathways." Gen Comp Endocrinol **170**(1): 79-91.

Dattani, M. T. (2005). "Growth hormone deficiency and combined pituitary hormone deficiency: does the genotype matter?" Clin Endocrinol (Oxf) **63**(2): 121-130.

de Boer, J., R. Siddappa, C. Gaspar, A. van Apeldoorn, R. Fodde and C. van Blitterswijk (2004). "Wnt signaling inhibits osteogenic differentiation of human mesenchymal stem cells." Bone **34**(5): 818-826.

de Crombrugghe, B., V. Lefebvre and K. Nakashima (2001). "Regulatory mechanisms in the pathways of cartilage and bone formation." Curr Opin Cell Biol **13**(6): 721-727.

de Groot, R. P., P. J. Rijken, J. den Hertog, J. Boonstra, A. J. Verkleij, S. W. de Laat and W. Kruijer (1990). "Microgravity decreases c-fos induction and serum response element activity." J Cell Sci **97 (Pt 1)**: 33-38.

de Groot, R. P., P. J. Rijken, J. den Hertog, J. Boonstra, A. J. Verkleij, S. W. de Laat and W. Kruijer (1991). "Nuclear responses to protein kinase C signal transduction are sensitive to gravity changes." Exp Cell Res **197**(1): 87-90.

Dedolph, R. R. and M. H. Dipert (1971). "The physical basis of gravity stimulus nullification by clinostat rotation." Plant Physiol **47**(6): 756-764.

Denis, G. V., C. Vaziri, N. Guo and D. V. Faller (2000). "RING3 kinase transactivates promoters of cell cycle regulatory genes through E2F." Cell Growth Differ **11**(8): 417-424.

Denkers, N., P. Garcia-Villalba, C. K. Rodesch, K. R. Nielson and T. J. Mauch (2004). "FISHing for chick genes: Triple-label whole-mount fluorescence in situ hybridization detects simultaneous and overlapping gene expression in avian embryos." Dev Dyn **229**(3): 651-657.

Dirckx, N., M. Van Hul and C. Maes (2013). "Osteoblast recruitment to sites of bone formation in skeletal development, homeostasis, and regeneration." Birth Defects Res C Embryo Today **99**(3): 170-191.

Duncan, E. L., P. Danoy, J. P. Kemp, P. J. Leo, E. McCloskey, G. C. Nicholson, R. Eastell, R. L. Prince, J. A. Eisman, G. Jones, P. N. Sambrook, I. R. Reid, E. M. Dennison, J. Wark, J. B. Richards, A. G. Uitterlinden, T. D. Spector, C. Esapa, R. D. Cox, S. D. Brown, R. V. Thakker, K. A. Addison, L. A. Bradbury, J. R. Center, C. Cooper, C. Cremin, K. Estrada, D. Felsenberg, C. C. Gluer, J. Hadler, M. J. Henry, A. Hofman, M. A. Kotowicz, J. Makovey, S. C. Nguyen, T. V. Nguyen, J. A. Pasco, K. Pryce, D. M. Reid, F. Rivadeneira, C. Roux, K. Stefansson, U. Styrkarsdottir, G. Thorleifsson, R. Tichawangana, D. M. Evans and M. A. Brown (2011). "Genome-wide association study using extreme truncate selection identifies novel genes affecting bone mineral density and fracture risk." PLoS Genet **7**(4): e1001372.

Dutton, K., L. Abbas, J. Spencer, C. Brannon, C. Mowbray, M. Nikaido, R. N. Kelsh and T. T. Whitfield (2009). "A zebrafish model for Waardenburg syndrome type IV reveals diverse roles for Sox10 in the otic vesicle." Dis Model Mech **2**(1-2): 68-83.

Eames, B. F., A. Amores, Y. L. Yan and J. H. Postlethwait (2012). "Evolution of the osteoblast: skeletogenesis in gar and zebrafish." BMC Evol Biol **12**: 27.

Edsall, S. C. and T. A. Franz-Odendaal (2014). "An assessment of the long-term effects of simulated microgravity on cranial neural crest cells in zebrafish embryos with a focus on the adult skeleton." PLoS One **9**(2): e89296.

Eijken, M., I. M. Meijer, I. Westbroek, M. Koedam, H. Chiba, A. G. Uitterlinden, H. A. Pols and J. P. van Leeuwen (2008). "Wnt signaling acts and is regulated in a human osteoblast differentiation dependent manner." J Cell Biochem **104**(2): 568-579.

Elliott, J. and J. A. Johnston (2004). "SOCS: role in inflammation, allergy and homeostasis." Trends Immunol **25**(8): 434-440.

Farioli-Vecchioli, S., D. Saraulli, M. Costanzi, L. Leonardi, I. Cina, L. Micheli, M. Nutini, P. Longone, S. P. Oh, V. Cestari and F. Tirone (2009). "Impaired terminal differentiation of hippocampal granule neurons and defective contextual memory in PC3/Tis21 knockout mice." PLoS One **4**(12): e8339.

Feng, X. and J. M. McDonald (2011). "Disorders of bone remodeling." Annu Rev Pathol **6**: 121-145.

Ferla, S., A. S. Aboraia, A. Brancale, C. J. Pepper, J. Zhu, J. T. Ochalek, H. F. DeLuca and C. Simons (2014). "Small-molecule inhibitors of 25-hydroxyvitamin D-24-hydroxylase (CYP24A1): synthesis and biological evaluation." J Med Chem **57**(18): 7702-7715.

Fiaz, A. W., K. M. Leon-Kloosterziel, G. Gort, S. Schulte-Merker, J. L. van Leeuwen and S. Kranenbarg (2012). "Swim-training changes the spatio-temporal dynamics of skeletogenesis in zebrafish larvae (Danio rerio)." PLoS One **7**(4): e34072.

Fisher, S., P. Jagadeeswaran and M. E. Halpern (2003). "Radiographic analysis of zebrafish skeletal defects." Dev Biol **264**(1): 64-76.

Fitzgerald, J. and M. Hughes-Fulford (1996). "Gravitational loading of a simulated launch alters mRNA expression in osteoblasts." Exp Cell Res **228**(1): 168-171.

Fleming, A. and M. Sato (2004). "Continuous and intermittent treatment of zebrafish with recombinant human parathyroid hormone (1-34) have opposite effects on the growing fish skeleton." Journal of Bone and Mineral Research **19**: S334-S335.

Fleming, A., M. Sato and P. Goldsmith (2005). "High-throughput in vivo screening for bone anabolic compounds with zebrafish." J Biomol Screen **10**(8): 823-831.

Fleming, A., M. Sato and P. Goldsmith (2005). "High-throughput in vivo screening for bone anabolic compounds with zebrafish." Journal of Biomolecular Screening **10**(8): 823-831.

Flores, M. V., E. Y. Lam, P. Crosier and K. Crosier (2006). "A hierarchy of Runx transcription factors modulate the onset of chondrogenesis in craniofacial endochondral bones in zebrafish." Dev Dyn **235**(11): 3166-3176.

Fong, K. (2004). "The next small step." BMJ **329**(7480): 1441-1444.

Franz-Odendaal, T. A., B. K. Hall and P. E. Witten (2006). "Buried alive: how osteoblasts become osteocytes." Dev Dyn **235**(1): 176-190.

Fuentes, J., P. M. Guerreiro, T. Modesto, J. Rotllant, A. V. Canario and D. M. Power (2007). "A PTH/PTHrP receptor antagonist blocks the hypercalcemic response to estradiol-17beta." Am J Physiol Regul Integr Comp Physiol **293**(2): R956-960.

Fuentes, J., C. Haond, P. M. Guerreiro, N. Silva, D. M. Power and A. V. Canario (2007). "Regulation of calcium balance in the sturgeon Acipenser naccarii: a role for PTHrP." Am J Physiol Regul Integr Comp Physiol **293**(2): R884-893.

Fuentes, J., D. M. Power and A. V. Canario (2010). "Parathyroid hormone-related protein-stanniocalcin antagonism in regulation of bicarbonate secretion and calcium precipitation in a marine fish intestine." Am J Physiol Regul Integr Comp Physiol **299**(1): R150-158.

Fuller, C. A., D. M. Murakami, T. M. Hoban-Higgins and I. H. Tang (1994). "Changes in hypothalamic [correction of hypothalmic] staining for c-Fos following 2G exposure in rats." J Gravit Physiol **1**(1): P69-70.

Ganss, B. and A. Jheon (2004). "Zinc finger transcription factors in skeletal development." Crit Rev Oral Biol Med **15**(5): 282-297.

Gao, L., G. J. Wu, X. W. Liu, R. Zhang, L. Yu, G. Zhang, F. Liu, C. G. Yu, J. L. Yuan, H. Wang and L. B. Yao (2011). "Suppression of invasion and metastasis of prostate cancer cells by overexpression of NDRG2 gene." Cancer Lett **310**(1): 94-100.

Gavaia, P. J., D. C. Simes, J. B. Ortiz-Delgado, C. S. Viegas, J. P. Pinto, R. N. Kelsh, M. C. Sarasquete and M. L. Cancela (2006). "Osteocalcin and matrix Gla protein in zebrafish (Danio rerio) and Senegal sole (Solea senegalensis): comparative gene and protein expression during larval development through adulthood." Gene Expr Patterns **6**(6): 637-652.

Genc, K. O., R. Gopalakrishnan, M. M. Kuklis, C. C. Maender, A. J. Rice, K. D. Bowersox and P. R. Cavanagh (2010). "Foot forces during exercise on the International Space Station." J Biomech **43**(15): 3020-3027.

Gennero, I., P. Moulin, T. Edouard, F. Conte-Auriol, M. T. Tauber and J. P. Salles (2004). "[Bone mineral metabolism: recent data and perspectives related to osteogenesis]." Arch Pediatr **11**(12): 1473-1483.

Gensure, R. C., B. Ponugoti, Y. Gunes, M. R. Papasani, B. Lanske, M. Bastepe, D. A. Rubin and H. Juppner (2004). "Identification and characterization of two parathyroid hormone-like molecules in zebrafish." Endocrinology **145**(4): 1634-1639.

Gericke, A., C. Qin, L. Spevak, Y. Fujimoto, W. T. Butler, E. S. Sorensen and A. L. Boskey (2005). "Importance of phosphorylation for osteopontin regulation of biomineralization." Calcif Tissue Int **77**(1): 45-54.

Giannotti, S., V. Bottai, G. Dell'osso, G. De Paola, G. Bugelli, E. Pini and G. Guido (2013). "Disuse osteoporosis of the upper limb: assessment of thirty patients." Clin Cases Miner Bone Metab **10**(2): 129-132.

Gillette-Ferguson, I., D. G. Ferguson, K. D. Poss and S. J. Moorman (2003). "Changes in gravitational force induce alterations in gene expression that can be monitored in the live, developing zebrafish heart." Adv Space Res **32**(8): 1641-1646.

Goerlich, R., J. Renn, P. Alestrom, R. Nourizadeh-Lillabadi, M. Schartl, C. Winkler, M. Muller, P. J. Midtlyng, M. Eberius and K. Slenzka (2005). "European Network Using Fish as Osteoporosis Research Model (ENFORM)." J. Grav. Physiol. **12**(1): P279-P280.

Goldring, M. B., M. Otero, K. Tsuchimochi, K. Ijiri and Y. Li (2008). "Defining the roles of inflammatory and anabolic cytokines in cartilage metabolism." Ann Rheum Dis **67 Suppl 3**: iii75-82.

Goltzman, D. (2007). "Use of genetically modified mice to examine the skeletal anabolic activity of vitamin D." J Steroid Biochem Mol Biol **103**(3-5): 587-591.

Goodwin, T. J., J. M. Jessup and D. A. Wolf (1992). "Morphologic differentiation of colon carcinoma cell lines HT-29 and HT-29KM in rotating-wall vessels." In Vitro Cell Dev Biol **28A**(1): 47-60.

Granet, C., N. Boutahar, L. Vico, C. Alexandre and M. H. Lafage-Proust (2001). "MAPK and SRC-kinases control EGR-1 and NF-kappa B inductions by changes in mechanical environment in osteoblasts." Biochem Biophys Res Commun **284**(3): 622-631.

Graves, L. and B. P. Lukert (2004). "Glucocorticoid-Induced Osteoporosis." Clinical Reviews in Bone and Mineral Metabolism **2**(2): 79-90.

Gribble, S. L., H. S. Kim, J. Bonner, X. Wang and R. I. Dorsky (2009). "Tcf3 inhibits spinal cord neurogenesis by regulating sox4a expression." Development **136**(5): 781-789.

Grimm, D., M. Wehland, J. Pietsch, G. Aleshcheva, P. Wise, J. van Loon, C. Ulbrich, N. E. Magnusson, M. Infanger and J. Bauer (2014). "Growing tissues in real and simulated microgravity: new methods for tissue engineering." Tissue Eng Part B Rev **20**(6): 555-566.

Guerreiro, P. M., J. L. Renfro, D. M. Power and A. V. Canario (2007). "The parathyroid hormone family of peptides: structure, tissue distribution, regulation, and potential functional roles in calcium and phosphate balance in fish." Am J Physiol Regul Integr Comp Physiol **292**(2): R679-696.

Gustave Dit Duflo, S., C. Gestreau and M. Lacour (2000). "Fos expression in the rat brain after exposure to gravito-inertial force changes." Brain Res **861**(2): 333-344.

Hall, B. K. (2005). Bone and Cartilage: Developmental and evolutionary skeletal Biology.

Hammond, C. L. and S. Schulte-Merker (2009). "Two populations of endochondral osteoblasts with differential sensitivity to Hedgehog signalling." Development **136**(23): 3991-4000.

Hammond, T. G., E. Benes, K. C. O'Reilly, D. A. Wolf, R. M. Linnehan, A. Taher, J. H. Kaysen, P. L. Allen and T. J. Goodwin (2000). "Mechanical culture conditions effect gene expression: gravity-induced changes on the space shuttle." Physiol Genomics **3**(3): 163-173.

Hammond, T. G. and J. M. Hammond (2001). "Optimized suspension culture: the rotating-wall vessel." Am J Physiol Renal Physiol **281**(1): F12-25.

Hatakeyama, J., Y. Bessho, K. Katoh, S. Ookawara, M. Fujioka, F. Guillemot and R. Kageyama (2004). "Hes genes regulate size, shape and histogenesis of the nervous system by control of the timing of neural stem cell differentiation." Development **131**(22): 5539-5550.

Hauptmann, G. and T. Gerster (1994). "Two-color whole-mount in situ hybridization to vertebrate and Drosophila embryos." Trends Genet **10**(8): 266.

Henning, P. C., B. S. Park and J. S. Kim (2011). "Physiological decrements during sustained military operational stress." Mil Med **176**(9): 991-997.

Henriksen, K., M. A. Karsdal and T. J. Martin (2014). "Osteoclast-derived coupling factors in bone remodeling." Calcif Tissue Int **94**(1): 88-97.

Henrotin, Y. E., P. Bruckner and J. P. Pujol (2003). "The role of reactive oxygen species in homeostasis and degradation of cartilage." Osteoarthr. Cartilage **11**(10): 747-755.

Herranz, R., R. Anken, J. Boonstra, M. Braun, P. C. Christianen, M. de Geest, J. Hauslage, R. Hilbig, R. J. Hill, M. Lebert, F. J. Medina, N. Vagt, O. Ullrich, J. J. van Loon and R. Hemmersbach (2013). "Ground-based facilities for simulation of microgravity: organism-specific recommendations for their use, and recommended terminology." Astrobiology **13**(1): 1-17.

Heude, E., S. Shaikho and M. Ekker (2014). "The dlx5a/dlx6a genes play essential roles in the early development of zebrafish median fin and pectoral structures." PLoS One **9**(5): e98505.

Hillegass, J. M., C. M. Villano, K. R. Cooper and L. A. White (2007). "Matrix metalloproteinase-13 is required for zebra fish (Danio rerio) development and is a target for glucocorticoids." Toxicol Sci **100**(1): 168-179.

Hoare, S. R., D. A. Rubin, H. Juppner and T. B. Usdin (2000). "Evaluating the ligand specificity of zebrafish parathyroid hormone (PTH) receptors: comparison of PTH, PTH-related protein, and tuberoinfundibular peptide of 39 residues." Endocrinology **141**(9): 3080-3086.

Hogan, B. M., J. A. Danks, J. E. Layton, N. E. Hall, J. K. Heath and G. J. Lieschke (2005). "Duplicate zebrafish pth genes are expressed along the lateral line and in the central nervous system during embryogenesis." Endocrinology **146**(2): 547-551.

Holick, M. F. (1996). "Vitamin D and bone health." J Nutr **126**(4 Suppl): 1159S-1164S.

Holmen, S. L., T. A. Giambernardi, C. R. Zylstra, B. D. Buckner-Berghuis, J. H. Resau, J. F. Hess, V. Glatt, M. L. Bouxsein, M. Ai, M. L. Warman and B. O. Williams (2004). "Decreased BMD and limb deformities in mice carrying mutations in both Lrp5 and Lrp6." J Bone Miner Res **19**(12): 2033-2040.

Holzschuh, J., N. Wada, C. Wada, A. Schaffer, Y. Javidan, A. Tallafuss, L. Bally-Cuif and T. F. Schilling (2005). "Requirements for endoderm and BMP signaling in sensory neurogenesis in zebrafish." Development **132**(16): 3731-3742.

Hong, D., H. X. Chen, R. S. Ge and J. C. Li (2008). "The biological roles of extracellular and intracytoplasmic glucocorticoids in skeletal cells." J Steroid Biochem Mol Biol **111**(3-5): 164-170.

Hopwood, B., A. Tsykin, D. M. Findlay and N. L. Fazzalari (2007). "Microarray gene expression profiling of osteoarthritic bone suggests altered bone remodelling, WNT and transforming growth factor-beta/bone morphogenic protein signalling." Arthritis Res Ther **9**(5): R100.

Horn, E., J. J. W. A. van Loon, J. Aceto and M. Muller (2011). "Life Sciences: Animal Physiology." Laboratory Science with Space Data **Eds. D. Beysens, L. Carotenuto, J. J. W.A. van Loon, M. Zell; ISBN 978-3-642-21143-0 Springer Verlag Berlin Heidelberg 2011**: 123-129.

Horn, E. R. (2003). "The development of gravity sensory systems during periods of altered gravity dependent sensory input." Adv Space Biol Med **9**: 133-171.

Howe, K., M. D. Clark, C. F. Torroja, J. Torrance, C. Berthelot, M. Muffato, J. E. Collins, S. Humphray, K. McLaren, L. Matthews, S. McLaren, I. Sealy, M. Caccamo, C. Churcher, C. Scott, J. C. Barrett, R. Koch, G. J. Rauch, S. White, W. Chow, B. Kilian, L. T. Quintais, J. A. Guerra-Assuncao, Y. Zhou, Y. Gu, J. Yen, J. H. Vogel, T. Eyre, S. Redmond, R. Banerjee, J. Chi, B. Fu, E. Langley, S. F. Maguire, G. K. Laird, D. Lloyd, E. Kenyon, S. Donaldson, H. Sehra, J. Almeida-King, J. Loveland, S. Trevanion, M. Jones, M. Quail, D. Willey, A. Hunt, J. Burton, S. Sims, K. McLay, B. Plumb, J. Davis, C. Clee, K. Oliver, R. Clark, C. Riddle, D. Elliot, G. Threadgold, G. Harden, D. Ware, S. Begum, B. Mortimore, G. Kerry, P. Heath, B. Phillimore, A. Tracey, N. Corby, M. Dunn, C. Johnson, J. Wood, S. Clark, S. Pelan, G. Griffiths, M. Smith, R. Glithero, P. Howden, N. Barker, C. Lloyd, C. Stevens, J. Harley, K. Holt, G. Panagiotidis, J. Lovell, H. Beasley, C. Henderson, D. Gordon, K. Auger, D. Wright, J. Collins, C. Raisen, L. Dyer, K. Leung, L. Robertson, K. Ambridge, D. Leongamornlert, S. McGuire, R. Gilderthorp, C. Griffiths, D. Manthravadi, S. Nichol, G. Barker, S. Whitehead, M. Kay, J. Brown, C. Murnane, E. Gray, M. Humphries, N. Sycamore, D. Barker, D. Saunders, J. Wallis, A. Babbage, S. Hammond, M. Mashreghi-Mohammadi, L. Barr, S. Martin, P. Wray, A. Ellington, N. Matthews, M. Ellwood, R. Woodmansey, G. Clark, J. Cooper, A. Tromans, D. Grafham, C. Skuce, R. Pandian, R. Andrews, E. Harrison, A. Kimberley, J. Garnett, N. Fosker, R. Hall, P. Garner, D. Kelly, C. Bird, S. Palmer, I. Gehring, A. Berger, C. M. Dooley, Z. Ersan-Urun, C. Eser, H. Geiger, M. Geisler, L. Karotki, A. Kirn, J. Konantz, M. Konantz, M. Oberlander, S. Rudolph-Geiger, M. Teucke, C. Lanz, G. Raddatz, K. Osoegawa, B. Zhu, A. Rapp, S. Widaa, C. Langford, F. Yang, S. C. Schuster, N. P. Carter, J. Harrow, Z. Ning, J. Herrero, S. M. Searle, A. Enright, R. Geisler, R. H. Plasterk, C. Lee, M. Westerfield, P. J. de Jong, L. I. Zon, J. H. Postlethwait, C. Nusslein-Volhard, T. J. Hubbard, H. Roest Crollius, J. Rogers and D. L. Stemple (2013). "The zebrafish reference genome sequence and its relationship to the human genome." Nature **496**(7446): 498-503.

Hsu, H., D. L. Lacey, C. R. Dunstan, I. Solovyev, A. Colombero, E. Timms, H. L. Tan, G. Elliott, M. J. Kelley, I. Sarosi, L. Wang, X. Z. Xia, R. Elliott, L. Chiu, T. Black, S. Scully, C. Capparelli, S. Morony, G. Shimamoto, M. B. Bass and W. J. Boyle (1999). "Tumor necrosis factor receptor family member RANK mediates osteoclast differentiation and activation induced by osteoprotegerin ligand." Proc Natl Acad Sci U S A **96**(7): 3540-3545.

Hubbard, T., D. Barker, E. Birney, G. Cameron, Y. Chen, L. Clark, T. Cox, J. Cuff, V. Curwen, T. Down, R. Durbin, E. Eyras, J. Gilbert, M. Hammond, L. Huminiecki, A. Kasprzyk, H. Lehvaslaiho, P. Lijnzaad, C. Melsopp, E. Mongin, R. Pettett, M. Pocock, S. Potter, A. Rust, E. Schmidt, S. Searle, G. Slater, J. Smith, W. Spooner, A. Stabenau, J. Stalker, E. Stupka, A. Ureta-Vidal, I. Vastrik and M. Clamp (2002). "The Ensembl genome database project." Nucleic Acids Res **30**(1): 38-41.

Hughes-Fulford, M. (2011). "To infinity ... and beyond! Human spaceflight and life science." FASEB J **25**(9): 2858-2864.

Hughes-Fulford, M. and M. L. Lewis (1996). "Effects of microgravity on osteoblast growth activation." Exp Cell Res **224**(1): 103-109.

Hughes-Fulford, M., K. Rodenacker and U. Jutting (2006). "Reduction of anabolic signals and alteration of osteoblast nuclear morphology in microgravity." J Cell Biochem **99**(2): 435-449.

Hughes-Fulford, M., R. Tjandrawinata, J. Fitzgerald, K. Gasuad and V. Gilbertson (1998). "Effects of microgravity on osteoblast growth." Gravit Space Biol Bull **11**(2): 51-60.

Huijser, R. (2000). "Desktop RPM: New Small Size Microgravity Simulator for the Bioscience Laboratory Leiden, Netherlands: Fokker Space.".

Hwang, P. P. and M. Y. Chou (2013). "Zebrafish as an animal model to study ion homeostasis." Pflugers Arch **465**(9): 1233-1247.

Ijiri, K. (1995). "Fish mating experiment in space--what it aimed at and how it was prepared." Biol Sci Space **9**(1): 3-16.

Ijiri, K., L. F. Zerbini, H. Peng, R. G. Correa, B. Lu, N. Walsh, Y. Zhao, N. Taniguchi, X. L. Huang, H. Otu, H. Wang, J. F. Wang, S. Komiya, P. Ducy, M. U. Rahman, R. A. Flavell, E. M. Gravallese, P. Oettgen, T. A. Libermann and M. B. Goldring (2005). "A novel role for GADD45beta as a mediator of MMP-13 gene expression during chondrocyte terminal differentiation." J Biol Chem **280**(46): 38544-38555.

Inman, C. K. and P. Shore (2003). "The osteoblast transcription factor Runx2 is expressed in mammary epithelial cells and mediates osteopontin expression." J Biol Chem **278**(49): 48684-48689.

Inoue, K., S. Ozaki, T. Shiga, K. Ito, T. Masuda, N. Okado, T. Iseda, S. Kawaguchi, M. Ogawa, S. C. Bae, N. Yamashita, S. Itohara, N. Kudo and Y. Ito (2002). "Runx3 controls the axonal projection of proprioceptive dorsal root ganglion neurons." Nat Neurosci **5**(10): 946-954.

Jemtland, R., M. Holden, S. Reppe, O. K. Olstad, F. P. Reinholt, V. T. Gautvik, H. Refvem, A. Frigessi, B. Houston and K. M. Gautvik (2011). "Molecular disease map of bone characterizing the postmenopausal osteoporosis phenotype." J Bone Miner Res **26**(8): 1793-1801.

Jilka, R. L. (2007). "Molecular and cellular mechanisms of the anabolic effect of intermittent PTH." Bone **40**(6): 1434-1446.

Johnston, J. A. (2004). "Are SOCS suppressors, regulators, and degraders?" J Leukoc Biol **75**(5): 743-748.

Jongen, J. W., E. C. Willemstein-van Hove, J. M. van der Meer, M. P. Bos, H. Juppner, G. V. Segre, A. B. Abou-Samra, J. H. Feyen and M. P. Herrmann-Erlee (1996). "Down-regulation of the receptor for parathyroid hormone (PTH) and PTH-related peptide by PTH in primary fetal rat osteoblasts." J Bone Miner Res **11**(9): 1218-1225.

Kageyama, R. and T. Ohtsuka (1999). "The Notch-Hes pathway in mammalian neural development." Cell Res **9**(3): 179-188.

Kang, K., H. Jung, S. Nam and J. S. Lim (2011). "NDRG2 Promotes GATA-1 Expression through Regulation of the JAK2/STAT Pathway in PMA-stimulated U937 Cells." Immune Netw **11**(6): 348-357.

Kang, Y. J., A. K. Stevenson, P. M. Yau and R. Kollmar (2008). "Sparc protein is required for normal growth of zebrafish otoliths." J Assoc Res Otolaryngol **9**(4): 436-451.

Kanis, J. A., L. J. Melton, 3rd, C. Christiansen, C. C. Johnston and N. Khaltaev (1994). "The diagnosis of osteoporosis." J Bone Miner Res **9**(8): 1137-1141.

Karlsson, C., M. Jonsson, J. Asp, C. Brantsing, R. Kageyama and A. Lindahl (2007). "Notch and HES5 are regulated during human cartilage differentiation." Cell Tissue Res **327**(3): 539-551.

Karsenty, G. (2008). "Transcriptional control of skeletogenesis." Annu Rev Genomics Hum Genet **9**: 183-196.

Kato, M., M. S. Patel, R. Levasseur, I. Lobov, B. H. Chang, D. A. Glass, 2nd, C. Hartmann, L. Li, T. H. Hwang, C. F. Brayton, R. A. Lang, G. Karsenty and L. Chan (2002). "Cbfa1-independent decrease in osteoblast proliferation, osteopenia, and persistent embryonic eye vascularization in mice deficient in Lrp5, a Wnt coreceptor." J Cell Biol **157**(2): 303-314.

Kaufman, G. D. (2005). "Fos expression in the vestibular brainstem: what one marker can tell us about the network." Brain Res Brain Res Rev **50**(1): 200-211.

Kawane, T., J. Mimura, T. Yanagawa, Y. Fujii-Kuriyama and N. Horiuchi (2003). "Parathyroid hormone (PTH) down-regulates PTH/PTH-related protein receptor gene expression in UMR-106 osteoblast-like cells via a 3',5'-cyclic adenosine monophosphate-dependent, protein kinase A-independent pathway." J Endocrinol **178**(2): 247-256.

Kiefer, J. C. (2007). "Back to basics: Sox genes." Dev Dyn **236**(8): 2356-2366.

Kim, I. S., F. Otto, B. Zabel and S. Mundlos (1999). "Regulation of chondrocyte differentiation by Cbfa1." Mech Dev **80**(2): 159-170.

Kim, J. H. and N. Kim (2014). "Regulation of NFATc1 in Osteoclast Differentiation." J Bone Metab **21**(4): 233-241.

Kim, Y. I., S. Lee, S. H. Jung, H. T. Kim, J. H. Choi, M. S. Lee, K. H. You, S. Y. Yeo, K. W. Yoo, S. Kwak, J. N. Lee, R. Park, S. K. Choe and C. H. Kim (2013). "Establishment of a bone-specific col10a1:GFP transgenic zebrafish." Mol Cells **36**(2): 145-150.

Kimmel, C. B., W. W. Ballard, S. R. Kimmel, B. Ullmann and T. F. Schilling (1995). "Stages of embryonic development of the zebrafish." Dev. Dyn **203**(3): 253-310.

Kimmel, C. B., C. T. Miller, G. Kruze, B. Ullmann, R. A. BreMiller, K. D. Larison and H. C. Snyder (1998). "The shaping of pharyngeal cartilages during early development of the zebrafish." Dev Biol **203**(2): 245-263.

Kishi, S., J. Uchiyama, A. M. Baughman, T. Goto, M. C. Lin and S. B. Tsai (2003). "The zebrafish as a vertebrate model of functional aging and very gradual senescence." Exp Gerontol **38**(7): 777-786.

Klaus, D. M. (2001). "Clinostats and bioreactors." Gravit Space Biol Bull **14**(2): 55-64.

Knight, T. (1806). "On the Direction of the Radicle and Gernien during the Vegetation of Seeds.".

Kobayashi, T. and H. Kronenberg (2005). "Minireview: transcriptional regulation in development of bone." Endocrinology **146**(3): 1012-1017.

Komori, T. (2006). "Regulation of osteoblast differentiation by transcription factors." J Cell Biochem **99**(5): 1233-1239.

Komori, T., H. Yagi, S. Nomura, A. Yamaguchi, K. Sasaki, K. Deguchi, Y. Shimizu, R. T. Bronson, Y. H. Gao, M. Inada, M. Sato, R. Okamoto, Y. Kitamura, S. Yoshiki and T. Kishimoto (1997). "Targeted

disruption of Cbfa1 results in a complete lack of bone formation owing to maturational arrest of osteoblasts." Cell **89**(5): 755-764.

Krause, U. and C. A. Gregory (2012). "Potential of modulating Wnt signaling pathway toward the development of bone anabolic agent." Curr Mol Pharmacol **5**(2): 164-173.

Kronenberg, H. M. (2003). "Developmental regulation of the growth plate." Nature **423**(6937): 332-336.

Kurihara, Y., H. Kurihara, H. Suzuki, T. Kodama, K. Maemura, R. Nagai, H. Oda, T. Kuwaki, W. H. Cao, N. Kamada and et al. (1994). "Elevated blood pressure and craniofacial abnormalities in mice deficient in endothelin-1." Nature **368**(6473): 703-710.

Lacey, D. L., E. Timms, H. L. Tan, M. J. Kelley, C. R. Dunstan, T. Burgess, R. Elliott, A. Colombero, G. Elliott, S. Scully, H. Hsu, J. Sullivan, N. Hawkins, E. Davy, C. Capparelli, A. Eli, Y. X. Qian, S. Kaufman, I. Sarosi, V. Shalhoub, G. Senaldi, J. Guo, J. Delaney and W. J. Boyle (1998). "Osteoprotegerin ligand is a cytokine that regulates osteoclast differentiation and activation." Cell **93**(2): 165-176.

Lafont, A. G., Y. F. Wang, G. D. Chen, B. K. Liao, Y. C. Tseng, C. J. Huang and P. P. Hwang (2011). "Involvement of calcitonin and its receptor in the control of calcium-regulating genes and calcium homeostasis in zebrafish (Danio rerio)." J Bone Miner Res **26**(5): 1072-1083.

Laize, V., C. S. Viegas, P. A. Price and M. L. Cancela (2006). "Identification of an osteocalcin isoform in fish with a large acidic prodomain." J Biol Chem **281**(22): 15037-15043.

Larbuisson, A., J. Dalcq, J. A. Martial and M. Muller (2013). "Fgf receptors Fgfr1a and Fgfr2 control the function of pharyngeal endoderm in late cranial cartilage development." Differentiation **86**(4-5): 192-206.

Larbuisson, A., J. Dalcq, J. A. Martial and M. Muller (2013). "Fgf receptors Fgfr1a and Fgfr2 control the function of pharyngeal endoderm in late cranial cartilage development." Differentiation **86**: 192-206.

Lau, R. Y. and X. Guo (2011). "A review on current osteoporosis research: with special focus on disuse bone loss." J Osteoporos **2011**: 293808.

Lazner, F., M. Gowen, D. Pavasovic and I. Kola (1999). "Osteopetrosis and osteoporosis: two sides of the same coin." Hum Mol Genet **8**(10): 1839-1846.

Lee, A. P., S. Y. Kerk, Y. Y. Tan, S. Brenner and B. Venkatesh (2011). "Ancient vertebrate conserved noncoding elements have been evolving rapidly in teleost fishes." Mol Biol Evol **28**(3): 1205-1215.

Lee, S. L., Y. Sadovsky, A. H. Swirnoff, J. A. Polish, P. Goda, G. Gavrilina and J. Milbrandt (1996). "Luteinizing hormone deficiency and female infertility in mice lacking the transcription factor NGFI-A (Egr-1)." Science **273**(5279): 1219-1221.

Lerner, U. H. (2006). "Bone remodeling in post-menopausal osteoporosis." J Dent Res **85**(7): 584-595.

Levanon, D., D. Bettoun, C. Harris-Cerruti, E. Woolf, V. Negreanu, R. Eilam, Y. Bernstein, D. Goldenberg, C. Xiao, M. Fliegauf, E. Kremer, F. Otto, O. Brenner, A. Lev-Tov and Y. Groner (2002). "The Runx3 transcription factor regulates development and survival of TrkC dorsal root ganglia neurons." EMBO J **21**(13): 3454-3463.

Li, H., I. Marijanovic, M. S. Kronenberg, I. Erceg, M. L. Stover, D. Velonis, M. Mina, J. G. Heinrich, S. E. Harris, W. B. Upholt, I. Kalajzic and A. C. Lichtler (2008). "Expression and function of Dlx genes in the osteoblast lineage." Dev Biol **316**(2): 458-470.

Li, N., K. Felber, P. Elks, P. Croucher and H. H. Roehl (2009). "Tracking gene expression during zebrafish osteoblast differentiation." Dev Dyn **238**(2): 459-466.

Li, X., M. S. Ominsky, Q. T. Niu, N. Sun, B. Daugherty, D. D'Agostin, C. Kurahara, Y. Gao, J. Cao, J. Gong, F. Asuncion, M. Barrero, K. Warmington, D. Dwyer, M. Stolina, S. Morony, I. Sarosi, P. J. Kostenuik, D. L. Lacey, W. S. Simonet, H. Z. Ke and C. Paszty (2008). "Targeted deletion of the sclerostin gene in mice results in increased bone formation and bone strength." J Bone Miner Res **23**(6): 860-869.

Lian, J. B., G. S. Stein, A. Javed, A. J. van Wijnen, J. L. Stein, M. Montecino, M. Q. Hassan, T. Gaur, C. J. Lengner and D. W. Young (2006). "Networks and hubs for the transcriptional control of osteoblastogenesis." Rev Endocr Metab Disord **7**(1-2): 1-16.

Liang, J., D. Wang, G. Renaud, T. G. Wolfsberg, A. F. Wilson and S. M. Burgess (2012). "The stat3/socs3a pathway is a key regulator of hair cell regeneration in zebrafish. [corrected]." J Neurosci **32**(31): 10662-10673.

Lin, C. H., C. H. Su and P. P. Hwang (2014). "Calcium-sensing receptor mediates Ca(2+) homeostasis by modulating expression of PTH and stanniocalcin." Endocrinology **155**(1): 56-67.

Lin, C. H., C. H. Su, D. Y. Tseng, F. C. Ding and P. P. Hwang (2012). "Action of vitamin D and the receptor, VDRa, in calcium handling in zebrafish (Danio rerio)." PLoS One **7**(9): e45650.

Lin, C. H., I. L. Tsai, C. H. Su, D. Y. Tseng and P. P. Hwang (2011). "Reverse effect of mammalian hypocalcemic cortisol in fish: cortisol stimulates Ca2+ uptake via glucocorticoid receptor-mediated vitamin D3 metabolism." PLoS One **6**(8): e23689.

Lindsey, B. W., T. C. Dumbarton, S. J. Moorman, F. M. Smith and R. P. Croll (2011). "Effects of simulated microgravity on the development of the swimbladder and buoyancy control in larval zebrafish (Danio rerio)." J Exp Zool A Ecol Genet Physiol **315**(5): 302-313.

Lohr, H. and M. Hammerschmidt (2011). "Zebrafish in endocrine systems: recent advances and implications for human disease." Annu Rev Physiol **73**: 183-211.

Lu, B., A. F. Ferrandino and R. A. Flavell (2004). "Gadd45beta is important for perpetuating cognate and inflammatory signals in T cells." Nat Immunol **5**(1): 38-44.

Ma, Y. L., R. L. Cain, D. L. Halladay, X. Yang, Q. Zeng, R. R. Miles, S. Chandrasekhar, T. J. Martin and J. E. Onyia (2001). "Catabolic effects of continuous human PTH (1--38) in vivo is associated with sustained stimulation of RANKL and inhibition of osteoprotegerin and gene-associated bone formation." Endocrinology **142**(9): 4047-4054.

Malicki, J., A. F. Schier, L. Solnica-Krezel, D. L. Stemple, S. C. Neuhauss, D. Y. Stainier, S. Abdelilah, Z. Rangini, F. Zwartkruis and W. Driever (1996). "Mutations affecting development of the zebrafish ear." Development **123**: 275-283.

Marée, R., B. Stevens, L. Rollus, N. Rocks, X. Moles-Lopez, I. Salmon, D. Cataldo and L. Wehenkel (2013). A rich internet application for remote visualization and collaborative annotation of digital slide images in histology and cytology. Diagnostic Pathology. **8(S1):** S26-S29.

Marie, P. (2001). "Différenciation, fonction et contrôle de l'ostéoblaste." medecine/sciences. **17**: 1252-1259.

Marieb, E. N. (1999). Anatomie et physiologie humaines. .

Martin, T. J. (2014). "Bone biology and anabolic therapies for bone: current status and future prospects." J Bone Metab **21**(1): 8-20.

Matsubara, T., K. Kida, A. Yamaguchi, K. Hata, F. Ichida, H. Meguro, H. Aburatani, R. Nishimura and T. Yoneda (2008). "BMP2 regulates Osterix through Msx2 and Runx2 during osteoblast differentiation." J Biol Chem **283**(43): 29119-29125.

Mavropoulos, A., N. Devos, F. Biemar, E. Zecchin, F. Argenton, H. Edlund, P. Motte, J. A. Martial and B. Peers (2005). "sox4b is a key player of pancreatic alpha cell differentiation in zebrafish." Dev Biol **285**(1): 211-223.

McCarthy, E. F. (2011). "Perspective: skeletal complications of space flight." Skeletal Radiol **40**(6): 661-663.

Merlo, G. R., B. Zerega, L. Paleari, S. Trombino, S. Mantero and G. Levi (2000). "Multiple functions of Dlx genes." Int J Dev Biol **44**(6): 619-626.

Mesland, D. A. M., A. H. Anton, H. Willemsen and H. van den Ende (1996). "The Free Fall Machine – a facility for microgravity research in life sciences." Microgravity Sci. Technol. **9**: 10-14.

Meunier, F., M.-H. Deschamps, F. Lecomte and A. Kacem (2008). Le squelette des poissons téléostéens: structure, développement, physiologie, pathologie. , Bull Soc zool Fr. **133(1-3):** 9-32.

Miao, D., B. He, B. Lanske, X. Y. Bai, X. K. Tong, G. N. Hendy, D. Goltzman and A. C. Karaplis (2004). "Skeletal abnormalities in Pth-null mice are influenced by dietary calcium." Endocrinology **145**(4): 2046-2053.

Miller, C. T., T. F. Schilling, K. Lee, J. Parker and C. B. Kimmel (2000). "sucker encodes a zebrafish Endothelin-1 required for ventral pharyngeal arch development." Development **127**(17): 3815-3828.

Mithal, A., D. A. Wahl, J. P. Bonjour, P. Burckhardt, B. Dawson-Hughes, J. A. Eisman, G. El-Hajj Fuleihan, R. G. Josse, P. Lips, J. Morales-Torres and I. O. F. C. o. S. A. N. W. Group (2009). "Global vitamin D status and determinants of hypovitaminosis D." Osteoporos Int **20**(11): 1807-1820.

Monroe, D. G., M. E. McGee-Lawrence, M. J. Oursler and J. J. Westendorf (2012). "Update on Wnt signaling in bone cell biology and bone disease." Gene **492**(1): 1-18.

Moorman, S. J., N. Shimada, G. Sokunbi and C. Pfirrmann (2007). "Simulated-microgravity induced changes in gene expression in zebrafish embryos suggest that the primary cilium is involved in gravity transduction." Gravitational Space Biol. **20**(2): 79-86.

Morey-Holton, E. R. (2003). The impact of gravity on life. . Evolution on Planet Earth: The Impact of the Physical Environment:. R. L., Elsevier**:** 143-159.

Morey, E. R. and D. J. Baylink (1978). "Inhibition of bone formation during space flight." Science **201**(4361): 1138-1141.

Morgan, J. L., M. Heer, A. R. Hargens, B. R. Macias, E. K. Hudson, L. C. Shackelford, S. R. Zwart and S. M. Smith (2014). "Sex-specific responses of bone metabolism and renal stone risk during bed rest." Physiol Rep **2**(8).

Morvan, F., K. Boulukos, P. Clement-Lacroix, S. Roman Roman, I. Suc-Royer, B. Vayssiere, P. Ammann, P. Martin, S. Pinho, P. Pognonec, P. Mollat, C. Niehrs, R. Baron and G. Rawadi (2006). "Deletion of a single allele of the Dkk1 gene leads to an increase in bone formation and bone mass." J Bone Miner Res **21**(6): 934-945.

Muller, M., J. Aceto, J. Dalcq, P. Alestrom, R. Nourizadeh-Lillabadi, R. Goerlich, V. Schiller, C. Winkler, J. Renn, M. Eberius and K. Slenzka (2008). "Small Fish Species as Powerful Model Systems to Study Vertebrate Physiology in Space." J. Gravit. Physiol. **15**: 253-254.

Muller, M., J. Dalcq, J. Aceto, A. Larbuisson, V. Pasque, R. Nourizadeh-Lillidadi, P. Aleström and J. A. Martial (2010). "The function of the Egr1 transcrition factor in cartilage formation and adaptation to microgravity in *Danio rerio*." J. Appl. Ichthyol. **26**: 239-244.

Muller, M., J. Dalcq, V. Pasque, J. Aceto, P. Motte and J. A. Martial (2009). "The function of the Egr1 transcription factor in cartilage formation and adaptation to microgravity in Danio rerio." J Gravit Physiol **16**: in press.

Nabavi, N., A. Khandani, A. Camirand and R. E. Harrison (2011). "Effects of microgravity on osteoclast bone resorption and osteoblast cytoskeletal organization and adhesion." Bone **49**(5): 965-974.

Nagaraja, M. P. and D. Risin (2013). "The current state of bone loss research: data from spaceflight and microgravity simulators." J Cell Biochem **114**(5): 1001-1008.

Nakada, T., K. Hoshijima, M. Esaki, S. Nagayoshi, K. Kawakami and S. Hirose (2007). "Localization of ammonia transporter Rhcg1 in mitochondrion-rich cells of yolk sac, gill, and kidney of zebrafish and its ionic strength-dependent expression." Am J Physiol Regul Integr Comp Physiol **293**(4): R1743-1753.

Nakagawa, A., A. Uno, A. Horii, T. Kitahara, M. Kawamoto, Y. Uno, M. Fukushima, S. Nishiike, N. Takeda and T. Kubo (2003). "Fos induction in the amygdala by vestibular information during hypergravity stimulation." Brain Res **986**(1-2): 114-123.

Nakashima, K., X. Zhou, G. Kunkel, Z. Zhang, J. M. Deng, R. R. Behringer and B. de Crombrugghe (2002). "The novel zinc finger-containing transcription factor osterix is required for osteoblast differentiation and bone formation." Cell **108**(1): 17-29.

Neutelings, T., B. Nusgens, Y. Liu, S. Tavella, A. Ruggiu, R. Cancedda, M. Gabriel, A. Colige and C. Lambert (2015). "Skin physiology in microgravity: a 3-month stay aboard ISS induces dermal atrophy and affects cutaneous muscle and hair follicles cycling in mice." NPJ Microgravity **1**(15002): doi:10.1038/npjmgrav.2015.1032.

Nguyen-Yamamoto, L., I. Bolivar, S. A. Strugnell and D. Goltzman (2010). "Comparison of active vitamin D compounds and a calcimimetic in mineral homeostasis." J Am Soc Nephrol **21**(10): 1713-1723.

Nishio, Y., Y. Dong, M. Paris, R. J. O'Keefe, E. M. Schwarz and H. Drissi (2006). "Runx2-mediated regulation of the zinc finger Osterix/Sp7 gene." Gene **372**: 62-70.

Nissen-Meyer, L. S., R. Jemtland, V. T. Gautvik, M. E. Pedersen, R. Paro, D. Fortunati, D. D. Pierroz, V. A. Stadelmann, S. Reppe, F. P. Reinholt, A. Del Fattore, N. Rucci, A. Teti, S. Ferrari and K. M. Gautvik (2007). "Osteopenia, decreased bone formation and impaired osteoblast development in Sox4 heterozygous mice." J Cell Sci **120**(Pt 16): 2785-2795.

Nose, K. and M. Shibanuma (1994). "Induction of early response genes by hypergravity in cultured mouse osteoblastic cells (MC3T3-E1)." Exp Cell Res **211**(1): 168-170.

Nourizadeh-Lillabadi, R., J. L. Lyche, C. Almaas, B. Stavik, S. J. Moe, M. Aleksandersen, V. Berg, K. S. Jakobsen, N. C. Stenseth, J. U. Skare, P. Alestrom and E. Ropstad (2009). "Transcriptional regulation in liver and testis associated with developmental and reproductive effects in male zebrafish exposed to natural mixtures of persistent organic pollutants (POP)." J Toxicol Environ Health A **72**(3-4): 112-130.

Nüsslein-Volhard C, D. R. (2001). Zebrafish: A Practical Approach., Oxford University Press

Ohira, T., F. Kawano, T. Ohira, K. Goto and Y. Ohira (2015). "Responses of skeletal muscles to gravitational unloading and/or reloading." J Physiol Sci **65**(4): 293-310.

Okabe, M. and A. Graham (2004). "The origin of the parathyroid gland." Proc Natl Acad Sci U S A **101**(51): 17716-17719.

Ono, Y. (2014). "Multifunctional and potent roles of the 3-hydroxypropoxy group provide eldecalcitol's benefit in osteoporosis treatment." J Steroid Biochem Mol Biol **139**: 88-97.

Ormsby, R. T., D. M. Findlay, M. Kogawa, P. H. Anderson, H. A. Morris and G. J. Atkins (2014). "Analysis of vitamin D metabolism gene expression in human bone: evidence for autocrine control of bone remodelling." J Steroid Biochem Mol Biol **144 Pt A**: 110-113.

Ortega, M. T., N. Lu and S. K. Chapes (2012). "Evaluation of in vitro macrophage differentiation during space flight." Adv Space Res **49**(10): 1441-1455.

Orwoll, E. S., R. A. Adler, S. Amin, N. Binkley, E. M. Lewiecki, S. M. Petak, S. A. Shapses, M. Sinaki, N. B. Watts and J. D. Sibonga (2013). "Skeletal health in long-duration astronauts: nature, assessment, and management recommendations from the NASA Bone Summit." J Bone Miner Res **28**(6): 1243-1255.

Otto, F., A. P. Thornell, T. Crompton, A. Denzel, K. C. Gilmour, I. R. Rosewell, G. W. Stamp, R. S. Beddington, S. Mundlos, B. R. Olsen, P. B. Selby and M. J. Owen (1997). "Cbfa1, a candidate gene for cleidocranial dysplasia syndrome, is essential for osteoblast differentiation and bone development." Cell **89**(5): 765-771.

Panda, D. K., D. Miao, I. Bolivar, J. Li, R. Huo, G. N. Hendy and D. Goltzman (2004). "Inactivation of the 25-hydroxyvitamin D 1alpha-hydroxylase and vitamin D receptor demonstrates independent and interdependent effects of calcium and vitamin D on skeletal and mineral homeostasis." J Biol Chem **279**(16): 16754-16766.

Pardo, S. J., M. J. Patel, M. C. Sykes, M. O. Platt, N. L. Boyd, G. P. Sorescu, M. Xu, J. J. van Loon, M. D. Wang and H. Jo (2005). "Simulated microgravity using the Random Positioning Machine inhibits differentiation and alters gene expression profiles of 2T3 preosteoblasts." Am J Physiol Cell Physiol **288**(6): C1211-1221.

Peterson, M. C. and M. M. Riggs (2010). "A physiologically based mathematical model of integrated calcium homeostasis and bone remodeling." Bone **46**(1): 49-63.

Pfaffl, M. W. (2001). "A new mathematical model for relative quantification in real-time RT-PCR." Nucleic Acids Res **29**(9): 2002-2007.

Pinto, J. P., N. M. Conceicao, C. S. Viegas, R. B. Leite, L. D. Hurst, R. N. Kelsh and M. L. Cancela (2005). "Identification of a new pebp2alphaA2 isoform from zebrafish runx2 capable of inducing osteocalcin gene expression in vitro." J Bone Miner Res **20**(8): 1440-1453.

Piotrowski, T., T. F. Schilling, M. Brand, Y. J. Jiang, C. P. Heisenberg, D. Beuchle, H. Grandel, F. J. van Eeden, M. Furutani-Seiki, M. Granato, P. Haffter, M. Hammerschmidt, D. A. Kane, R. N. Kelsh, M. C. Mullins, J. Odenthal, R. M. Warga and C. Nusslein-Volhard (1996). "Jaw and branchial arch mutants in zebrafish II: anterior arches and cartilage differentiation." Development **123**: 345-356.

Pompeiano, O., P. d'Ascanio, C. Centini, M. Pompeiano and E. Balaban (2002). "Gene expression in rat vestibular and reticular structures during and after space flight." Neuroscience **114**(1): 135-155.

Provot, S. and E. Schipani (2005). "Molecular mechanisms of endochondral bone development." Biochem Biophys Res Commun **328**(3): 658-665.

Quintana, L., N. I. zur Nieden and C. E. Semino (2009). "Morphogenetic and regulatory mechanisms during developmental chondrogenesis: new paradigms for cartilage tissue engineering." Tissue Eng Part B Rev **15**(1): 29-41.

Quiroz, Y., M. Lopez, A. Mavropoulos, P. Motte, J. A. Martial, M. Hammerschmidt and M. Muller (2012). "The HMG-box transcription factor Sox4b is required for pituitary expression of gata2a and specification of thyrotrope and gonadotrope cells in zebrafish." Mol Endocrinol **26**(6): 1014-1027.

Rahmann, H. and R. H. Anken (2000). "Gravitational neurobiology of fish." Adv Space Res **25**(10): 1985-1995.

Rahmann, H. and R. H. Anken (2002). "Gravity related research with fishes--perspectives in regard to the upcoming International Space Station, ISS." Adv Space Res **30**(4): 697-710.

Regard, J. B., Z. Zhong, B. O. Williams and Y. Yang (2012). "Wnt signaling in bone development and disease: making stronger bone with Wnts." Cold Spring Harb Perspect Biol **4**(12).

Renn, J., B. Pruvot and M. Muller (2014). "Detection of nitric oxide by diaminofluorescein visualizes the skeleton in living zebrafish." J. Appl. Ichthyol. **30**: 701-706.

Renn, J., C. Winkler, M. Schartl, R. Fischer and R. Goerlich (2006). "Zebrafish and medaka as models for bone research including implications regarding space-related issues." Protoplasma **229**(2-4): 209-214.

Reppe, S., E. Rian, R. Jemtland, O. K. Olstad, V. T. Gautvik and K. M. Gautvik (2000). "Sox-4 messenger RNA is expressed in the embryonic growth plate and regulated via the parathyroid hormone/parathyroid hormone-related protein receptor in osteoblast-like cells." J Bone Miner Res **15**(12): 2402-2412.

Ritter, N. M., M. C. Farach-Carson and W. T. Butler (1992). "Evidence for the formation of a complex between osteopontin and osteocalcin." J Bone Miner Res **7**(8): 877-885.

Roberts, A. W., L. Robb, S. Rakar, L. Hartley, L. Cluse, N. A. Nicola, D. Metcalf, D. J. Hilton and W. S. Alexander (2001). "Placental defects and embryonic lethality in mice lacking suppressor of cytokine signaling 3." Proc Natl Acad Sci U S A **98**(16): 9324-9329.

Robledo, R. F., L. Rajan, X. Li and T. Lufkin (2002). "The Dlx5 and Dlx6 homeobox genes are essential for craniofacial, axial, and appendicular skeletal development." Genes Dev **16**(9): 1089-1101.

Rossini, M., D. Gatti and S. Adami (2013). "Involvement of WNT/beta-catenin signaling in the treatment of osteoporosis." Calcif Tissue Int **93**(2): 121-132.

Rotllant, J., D. Liu, Y. L. Yan, J. H. Postlethwait, M. Westerfield and S. J. Du (2008). "Sparc (Osteonectin) functions in morphogenesis of the pharyngeal skeleton and inner ear." Matrix Biol **27**(6): 561-572.

Sabatakos, G., G. C. Rowe, M. Kveiborg, M. Wu, L. Neff, R. Chiusaroli, W. M. Philbrick and R. Baron (2008). "Doubly truncated FosB isoform (Delta2DeltaFosB) induces osteosclerosis in transgenic mice and modulates expression and phosphorylation of Smads in osteoblasts independent of intrinsic AP-1 activity." J Bone Miner Res **23**(5): 584-595.

Salie, R., M. Kneissel, M. Vukevic, N. Zamurovic, I. Kramer, G. Evans, N. Gerwin, M. Mueller, B. Kinzel and M. Susa (2010). "Ubiquitous overexpression of Hey1 transcription factor leads to osteopenia and chondrocyte hypertrophy in bone." Bone **46**(3): 680-694.

Sambandam, Y., J. J. Blanchard, G. Daughtridge, R. J. Kolb, S. Shanmugarajan, S. N. Pandruvada, T. A. Bateman and S. V. Reddy (2010). "Microarray profile of gene expression during osteoclast differentiation in modelled microgravity." J Cell Biochem **111**(5): 1179-1187.

Samee, N., V. Geoffroy, C. Marty, C. Schiltz, M. Vieux-Rochas, P. Clement-Lacroix, C. Belleville, G. Levi and M. C. de Vernejoul (2009). "Increased bone resorption and osteopenia in Dlx5 heterozygous mice." J Cell Biochem **107**(5): 865-872.

Samee, N., V. Geoffroy, C. Marty, C. Schiltz, M. Vieux-Rochas, G. Levi and M. C. de Vernejoul (2008). "Dlx5, a positive regulator of osteoblastogenesis, is essential for osteoblast-osteoclast coupling." Am J Pathol **173**(3): 773-780.

Santamaria, N., G. Bello, C. Pousis, R. Vassallo-Agius, F. de la Gandara and A. Corriero (2015). "Fin spine bone resorption in atlantic bluefin tuna, Thunnus thynnus, and comparison between wild and captive-reared specimens." PLoS One **10**(3): e0121924.

Santos, A., A. D. Bakker and J. Klein-Nulend (2009). "The role of osteocytes in bone mechanotransduction." Osteoporos Int **20**(6): 1027-1031.

Sato, A., T. Hamazaki, T. Oomura, H. Osada, M. Kakeya, M. Watanabe, T. Nakamura, Y. Nakamura, N. Koshikawa, I. Yoshizaki, S. Aizawa, S. Yoda, A. Ogiso, M. Takaoki, Y. Kohno and H. Tanaka (1999). "Effects of microgravity on c-fos gene expression in osteoblast-like MC3T3-E1 cells." Adv Space Res **24**(6): 807-813.

Saura, M., C. Tarin and C. Zaragoza (2010). "Recent insights into the implication of nitric oxide in osteoblast differentiation and proliferation during bone development." TheScientificWorldJ **10**: 624-632.

Sbaihi, M., K. Rousseau, S. Baloche, F. Meunier, M. Fouchereau-Peron and S. Dufour (2009). "Cortisol mobilizes mineral stores from vertebral skeleton in the European eel: an ancestral origin for glucocorticoid-induced osteoporosis?" J Endocrinol **201**(2): 241-252.

Schein, V., J. C. Cardoso, P. I. Pinto, L. Anjos, N. Silva, D. M. Power and A. V. Canario (2012). "Four stanniocalcin genes in teleost fish: structure, phylogenetic analysis, tissue distribution and expression during hypercalcemic challenge." Gen Comp Endocrinol **175**(2): 344-356.

Schilling, T. F. (2002). "The morphology of larval and adult zebrafish." Zebrafish, a practical approach. Eds: Nüsslein-Volhard, C; Dahm, R. Oxford University Press: 59-94.

Schilling, T. F. and C. B. Kimmel (1994). "Segment and cell type lineage restrictions during pharyngeal arch development in the zebrafish embryo." Development **120**(3): 483-494.

Schmidt, W. (2004). "Quickly changing acceleration forces (QCAFs) vibration analysis on the A300 ZERO-G." Microgravity Sci Technol **15**(1): 42-48.

Sebastian, C., K. Esseling and E. Horn (2001). "Altered gravitational forces affect the development of the static vestibuloocular reflex in fish (Oreochromis mossambicus)." Journal of Neurobiology **46**(1): 59-72.

Seitz, S., C. Rendenbach, F. Barvencik, T. Streichert, A. Jeschke, J. Schulze, M. Amling and T. Schinke (2013). "Retinol deprivation partially rescues the skeletal mineralization defects of Phex-deficient Hyp mice." Bone **53**(1): 231-238.

Sepich, D. S., J. Wegner, S. O'Shea and M. Westerfield (1998). "An altered intron inhibits synthesis of the acetylcholine receptor alpha-subunit in the paralyzed zebrafish mutant nic1." Genetics **148**(1): 361-372.

Sharif, F., M. A. de Bakker and M. K. Richardson (2014). "Osteoclast-like Cells in Early Zebrafish Embryos." Cell J **16**(2): 211-224.

Shih, T. H., J. L. Horng, S. T. Liu, P. P. Hwang and L. Y. Lin (2012). "Rhcg1 and NHE3b are involved in ammonium-dependent sodium uptake by zebrafish larvae acclimated to low-sodium water." Am J Physiol Regul Integr Comp Physiol **302**(1): R84-93.

Shimada, N. and S. J. Moorman (2006). "Changes in gravitational force cause changes in gene expression in the lens of developing zebrafish." Developmental Dynamics **235**(10): 2686-2694.

Shimada, N., G. Sokunbi and S. J. Moorman (2005). "Changes in gravitational force affect gene expression in developing organ systems at different developmental times." BMC Dev Biol **5**: 10.

Shum, L. and G. Nuckolls (2002). "The life cycle of chondrocytes in the developing skeleton." Arthritis Res **4**(2): 94-106.

Sibonga, J. D. (2013). "Spaceflight-induced bone loss: is there an osteoporosis risk?" Curr Osteoporos Rep **11**(2): 92-98.

Sibonga, J. D., H. J. Evans, H. G. Sung, E. R. Spector, T. F. Lang, V. S. Oganov, A. V. Bakulin, L. C. Shackelford and A. D. LeBlanc (2007). "Recovery of spaceflight-induced bone loss: bone mineral density after long-duration missions as fitted with an exponential function." Bone **41**(6): 973-978.

Silverman, M. N. and E. M. Sternberg (2012). "Glucocorticoid regulation of inflammation and its functional correlates: from HPA axis to glucocorticoid receptor dysfunction." Ann N Y Acad Sci **1261**: 55-63.

Simeone, A., D. Acampora, M. Pannese, M. D'Esposito, A. Stornaiuolo, M. Gulisano, A. Mallamaci, K. Kastury, T. Druck, K. Huebner and et al. (1994). "Cloning and characterization of two members of the vertebrate Dlx gene family." Proc Natl Acad Sci U S A **91**(6): 2250-2254.

Simpson, E. R., C. Clyne, G. Rubin, W. C. Boon, K. Robertson, K. Britt, C. Speed and M. Jones (2002). "Aromatase--a brief overview." Annu Rev Physiol **64**: 93-127.

Slenzka, K., R. Appel and H. Rahmann (1995). "Development and altered gravity dependent changes in glucose-6-phosphate dehydrogenase activity in the brain of the cichlid fish Oreochromis mossambicus." Neurochem Int **26**(6): 579-585.

Smith, A., F. Avaron, D. Guay, B. K. Padhi and M. A. Akimenko (2006). "Inhibition of BMP signaling during zebrafish fin regeneration disrupts fin growth and scleroblasts differentiation and function." Dev Biol **299**(2): 438-454.

Smith, S. M., M. A. Heer, L. C. Shackelford, J. D. Sibonga, L. Ploutz-Snyder and S. R. Zwart (2012). "Benefits for bone from resistance exercise and nutrition in long-duration spaceflight: Evidence from biochemistry and densitometry." J Bone Miner Res **27**(9): 1896-1906.

Smith, S. M., M. E. Wastney, K. O. O'Brien, B. V. Morukov, I. M. Larina, S. A. Abrams, J. E. Davis-Street, V. Oganov and L. C. Shackelford (2005). "Bone markers, calcium metabolism, and calcium kinetics during extended-duration space flight on the mir space station." J Bone Miner Res **20**(2): 208-218.

Smith, S. M., S. R. Zwart, M. Heer, E. K. Hudson, L. Shackelford and J. L. Morgan (2014). "Men and women in space: bone loss and kidney stone risk after long-duration spaceflight." J Bone Miner Res **29**(7): 1639-1645.

Smyth, G. K., J. Michaud and H. S. Scott (2005). "Use of within-array replicate spots for assessing differential expression in microarray experiments." Bioinformatics **21**(9): 2067-2075.

Smyth, G. K. and T. Speed (2003). "Normalization of cDNA microarray data." Methods **31**(4): 265-273.

Sommerfeldt, D. W. and C. T. Rubin (2001). "Biology of bone and how it orchestrates the form and function of the skeleton." Eur Spine J **10 Suppl 2**: S86-95.

Spaink, H. P., H. J. Jansen and R. P. Dirks (2014). "Advances in genomics of bony fish." Brief Funct Genomics **13**(2): 144-156.

Spaulding, G. F., J. M. Jessup and T. J. Goodwin (1993). "Advances in cellular construction." J Cell Biochem **51**(3): 249-251.

Sperber, S. M., V. Saxena, G. Hatch and M. Ekker (2008). "Zebrafish dlx2a contributes to hindbrain neural crest survival, is necessary for differentiation of sensory ganglia and functions with dlx1a in maturation of the arch cartilage elements." Dev Biol **314**(1): 59-70.

Suzuki, N., J. A. Danks, Y. Maruyama, M. Ikegame, Y. Sasayama, A. Hattori, M. Nakamura, M. J. Tabata, T. Yamamoto, R. Furuya, K. Saijoh, H. Mishima, A. K. Srivastav, Y. Furusawa, T. Kondo, Y. Tabuchi, I. Takasaki, V. S. Chowdhury, K. Hayakawa and T. J. Martin (2011). "Parathyroid hormone 1 (1-34) acts on the scales and involves calcium metabolism in goldfish." Bone **48**(5): 1186-1193.

Swaminathan, R. (2001). "Biochemical markers of bone turnover." Clin Chim Acta **313**(1-2): 95-105.

Takayanagi, H., S. Kim, T. Koga, H. Nishina, M. Isshiki, H. Yoshida, A. Saiura, M. Isobe, T. Yokochi, J. Inoue, E. F. Wagner, T. W. Mak, T. Kodama and T. Taniguchi (2002). "Induction and activation of the transcription factor NFATc1 (NFAT2) integrate RANKL signaling in terminal differentiation of osteoclasts." Dev Cell **3**(6): 889-901.

Takeda, S., T. Yoshizawa, Y. Nagai, H. Yamato, S. Fukumoto, K. Sekine, S. Kato, T. Matsumoto and T. Fujita (1999). "Stimulation of osteoclast formation by 1,25-dihydroxyvitamin D requires its binding to vitamin D receptor (VDR) in osteoblastic cells: studies using VDR knockout mice." Endocrinology **140**(2): 1005-1008.

Tamma, R., G. Colaianni, C. Camerino, A. Di Benedetto, G. Greco, M. Strippoli, R. Vergari, A. Grano, L. Mancini, G. Mori, S. Colucci, M. Grano and A. Zallone (2009). "Microgravity during spaceflight directly affects in vitro osteoclastogenesis and bone resorption." FASEB J **23**(8): 2549-2554.

Tavella, S., A. Ruggiu, A. Giuliani, F. Brun, B. Canciani, A. Manescu, K. Marozzi, M. Cilli, D. Costa, Y. Liu, F. Piccardi, R. Tasso, G. Tromba, F. Rustichelli and R. Cancedda (2012). "Bone turnover in wild type and pleiotrophin-transgenic mice housed for three months in the International Space Station (ISS)." PLoS One **7**(3): e33179.

Teitelbaum, S. L. (2007). "Osteoclasts: what do they do and how do they do it?" Am J Pathol **170**(2): 427-435.

Topilko, P., S. Schneider-Maunoury, G. Levi, A. Trembleau, D. Gourdji, M. A. Driancourt, C. V. Rao and P. Charnay (1998). "Multiple pituitary and ovarian defects in Krox-24 (NGFI-A, Egr-1)-targeted mice." Mol Endocrinol **12**(1): 107-122.

Trahey, M. and I. L. Weissman (1999). "Cyclophilin C-associated protein: a normal secreted glycoprotein that down-modulates endotoxin and proinflammatory responses in vivo." Proc Natl Acad Sci U S A **96**(6): 3006-3011.

Tsuchimochi, K., M. Otero, C. L. Dragomir, D. A. Plumb, L. F. Zerbini, T. A. Libermann, K. B. Marcu, S. Komiya, K. Ijiri and M. B. Goldring (2010). "GADD45beta enhances Col10a1 transcription via the MTK1/MKK3/6/p38 axis and activation of C/EBPbeta-TAD4 in terminally differentiating chondrocytes." J Biol Chem **285**(11): 8395-8407.

Turner, R. T., G. L. Evans and G. K. Wakley (1995). "Spaceflight results in depressed cancellous bone formation in rat humeri." Aviat Space Environ Med **66**(8): 770-774.

Ulsamer, A., M. J. Ortuno, S. Ruiz, A. R. Susperregui, N. Osses, J. L. Rosa and F. Ventura (2008). "BMP-2 induces Osterix expression through up-regulation of Dlx5 and its phosphorylation by p38." J Biol Chem **283**(7): 3816-3826.

Unsworth, B. R. and P. I. Lelkes (1998). "Growing tissues in microgravity." Nat Med **4**(8): 901-907.

Van Loon, J. (2001). "Hypergravity studies in the Netherlands." J Gravit Physiol **8**: P139-P142.

Van Loon, J. (2007). "The Gravity Environment in Space Experiments." in “Biology in Space and Life on Earth”. Editor E. Brinckmann. Whiley, Weinheim, Germany.: 17-32.

Van Loon, J., E. Tanck, F. A. van Nieuwenhoven, L. H. E. H. Snoeckx, H. A. A. de Jong and R. J. Wubbels (2005). "A brief overview of animal hypergravity studies. ." J Gravit Physiol **12**: P5-P10.

Van Loon, J. J. (2007). "Some history and use of the random positioning machine, RPM, in gravity related research." Advances in Space research **39**(7): 1161-1165.

Van Loon, J. J., D. J. Bervoets, E. H. Burger, S. C. Dieudonne, J. W. Hagen, C. M. Semeins, B. Z. Doulabi and J. P. Veldhuijzen (1995). "Decreased mineralization and increased calcium release in isolated fetal mouse long bones under near weightlessness." J Bone Miner Res **10**(4): 550-557.

van Loon, J. J., E. H. Folgering, C. V. Bouten and T. H. Smit (2004). "Centrifuges and inertial shear forces." J Gravit Physiol **11**(1): 29-38.

van Loon, J. J., E. H. Folgering, C. V. Bouten, J. P. Veldhuijzen and T. H. Smit (2003). "Inertial shear forces and the use of centrifuges in gravity research. What is the proper control?" J Biomech Eng **125**(3): 342-346.

van Loon, J. J., M. C. van Laar, J. P. Korterik, F. B. Segerink, R. J. Wubbels, H. A. de Jong and N. F. van Hulst (2009). "An atomic force microscope operating at hypergravity for in situ measurement of cellular mechano-response." J Microsc **233**(2): 234-243.

van Loon, J. J. W. A., J. P. Veldhuijzen, J. Kiss, C. Wood, H. vd Ende, A. Guntemann, D. Jones, H. de Jong and R. Wubbels (1999). "Microgravity research starts on the ground! Apparatuses for long-term ground based hypo-and hypergravity studies." In Proceedings of the 2nd European Symposium on the Utilisation of the International Space Station, ESA SP-433, ESTEC, European Space Agency, Noordwijk, the Netherlands, **SP-433**: 415-419.

van Straaten, F., R. Muller, T. Curran, C. Van Beveren and I. M. Verma (1983). "Complete nucleotide sequence of a human c-onc gene: deduced amino acid sequence of the human c-fos protein." Proc Natl Acad Sci U S A **80**(11): 3183-3187.

Venkatesh, B., A. P. Lee, V. Ravi, A. K. Maurya, M. M. Lian, J. B. Swann, Y. Ohta, M. F. Flajnik, Y. Sutoh, M. Kasahara, S. Hoon, V. Gangu, S. W. Roy, M. Irimia, V. Korzh, I. Kondrychyn, Z. W. Lim, B. H. Tay, S. Tohari, K. W. Kong, S. Ho, B. Lorente-Galdos, J. Quilez, T. Marques-Bonet, B. J. Raney, P. W. Ingham, A. Tay, L. W. Hillier, P. Minx, T. Boehm, R. K. Wilson, S. Brenner and W. C. Warren (2014). "Elephant shark genome provides unique insights into gnathostome evolution." Nature **505**(7482): 174-179.

Vermot, J., A. S. Forouhar, M. Liebling, D. Wu, D. Plummer, M. Gharib and S. E. Fraser (2009). "Reversing blood flows act through klf2a to ensure normal valvulogenesis in the developing heart." PLoS Biol **7**(11): e1000246.

Vernikos, J. and V. S. Schneider (2010). "Space, gravity and the physiology of aging: parallel or convergent disciplines? A mini-review." Gerontology **56**(2): 157-166.

Verreijdt, L., M. Debiais-Thibaud, V. Borday-Birraux, C. Van der Heyden, J. Y. Sire and A. Huysseune (2006). "Expression of the dlx gene family during formation of the cranial bones in the zebrafish (Danio rerio): differential involvement in the visceral skeleton and braincase." Dev Dyn **235**(5): 1371-1389.

Versari, S., J. Klein-Nulend, J. van Loon and S. Bradamante (2013). "Influence of Oxygen in the Cultivation of Human Mesenchymal Stem Cells in Simulated Microgravity: An Explorative Study." Microgravity Sci. Technol. **25**: 59-66.

Versari, S., G. Longinotti, L. Barenghi, J. A. Maier and S. Bradamante (2013). "The challenging environment on board the International Space Station affects endothelial cell function by triggering oxidative stress through thioredoxin interacting protein overexpression: the ESA-SPHINX experiment." FASEB J **27**(11): 4466-4475.

Vico, L., D. Chappard, S. Palle, A. V. Bakulin, V. E. Novikov and C. Alexandre (1988). "Trabecular bone remodeling after seven days of weightlessness exposure (BIOCOSMOS 1667)." Am J Physiol **255**(2 Pt 2): R243-247.

Vico, L., P. Collet, A. Guignandon, M. H. Lafage-Proust, T. Thomas, M. Rehaillia and C. Alexandre (2000). "Effects of long-term microgravity exposure on cancellous and cortical weight-bearing bones of cosmonauts." Lancet **355**(9215): 1607-1611.

Vilardaga, J. P., G. Romero, P. A. Friedman and T. J. Gardella (2011). "Molecular basis of parathyroid hormone receptor signaling and trafficking: a family B GPCR paradigm." Cell Mol Life Sci **68**(1): 1-13.

Walker, M. B. and C. B. Kimmel (2007). "A two-color acid-free cartilage and bone stain for zebrafish larvae." Biotech Histochem **82**(1): 23-28.

Wang, L., P. Zhang, Y. Wei, Y. Gao, R. Patient and F. Liu (2011). "A blood flow-dependent klf2a-NO signaling cascade is required for stabilization of hematopoietic stem cell programming in zebrafish embryos." Blood **118**(15): 4102-4110.

Wang, Y. H., Y. Liu, K. Buhl and D. W. Rowe (2005). "Comparison of the action of transient and continuous PTH on primary osteoblast cultures expressing differentiation stage-specific GFP." J Bone Miner Res **20**(1): 5-14.

Wang, Z. Q., C. Ovitt, A. E. Grigoriadis, U. Mohle-Steinlein, U. Ruther and E. F. Wagner (1992). "Bone and haematopoietic defects in mice lacking c-fos." Nature **360**(6406): 741-745.

Wani, M. A., R. T. Means, Jr. and J. B. Lingrel (1998). "Loss of LKLF function results in embryonic lethality in mice." Transgenic Res **7**(4): 229-238.

Weinstein, R. S. (2012). "Glucocorticoid-induced osteoporosis and osteonecrosis." Endocrinol Metab Clin North Am **41**(3): 595-611.

Westerfield, M. (2007). "THE ZEBRAFISH BOOK, 5th Edition; A guide for the laboratory use of zebrafish (Danio rerio), Eugene, University of Oregon Press."

Whitfield, T. T., M. Granato, F. J. van Eeden, U. Schach, M. Brand, M. Furutani-Seiki, P. Haffter, M. Hammerschmidt, C. P. Heisenberg, Y. J. Jiang, D. A. Kane, R. N. Kelsh, M. C. Mullins, J. Odenthal and C. Nusslein-Volhard (1996). "Mutations affecting development of the zebrafish inner ear and lateral line." Development **123**: 241-254.

Williams, D., A. Kuipers, C. Mukai and R. Thirsk (2009). "Acclimation during space flight: effects on human physiology." CMAJ **180**(13): 1317-1323.

Windhausen, T., S. Squifflet, J. Renn and M. Muller (2015). "BMP Signaling Regulates Bone Morphogenesis in Zebrafish through Promoting Osteoblast Function as Assessed by Their Nitric Oxide Production." Molecules **20**(5): 7586-7601.

Witten, P. E., A. Hansen and B. K. Hall (2001). "Features of mono- and multinucleated bone resorbing cells of the zebrafish Danio rerio and their contribution to skeletal development, remodeling, and growth." J Morphol **250**(3): 197-207.

Witten, P. E. and A. Huysseune (2009). "A comparative view on mechanisms and functions of skeletal remodelling in teleost fish, with special emphasis on osteoclasts and their function." Biol Rev Camb Philos Soc **84**(2): 315-346.

Wohrle, F. U., R. J. Daly and T. Brummer (2009). "Function, regulation and pathological roles of the Gab/DOS docking proteins." Cell Commun Signal **7**: 22.

Wronski, T. J., E. R. Morey-Holton, S. B. Doty, A. C. Maese and C. C. Walsh (1987). "Histomorphometric analysis of rat skeleton following spaceflight." Am J Physiol **252**(2 Pt 2): R252-255.

Wronski, T. J. and E. R. Morey (1983). "Recovery of the rat skeleton from the adverse effects of simulated weightlessness." Metab Bone Dis Relat Res **4**(6): 347-352.

Wu, L., C. Timmers, B. Maiti, H. I. Saavedra, L. Sang, G. T. Chong, F. Nuckolls, P. Giangrande, F. A. Wright, S. J. Field, M. E. Greenberg, S. Orkin, J. R. Nevins, M. L. Robinson and G. Leone (2001). "The E2F1-3 transcription factors are essential for cellular proliferation." Nature **414**(6862): 457-462.

Xue, Y., A. C. Karaplis, G. N. Hendy, D. Goltzman and D. Miao (2005). "Genetic models show that parathyroid hormone and 1,25-dihydroxyvitamin D3 play distinct and synergistic roles in postnatal mineral ion homeostasis and skeletal development." Hum Mol Genet **14**(11): 1515-1528.

Yan, Y. L., P. Bhattacharya, X. J. He, B. Ponugoti, B. Marquardt, J. Layman, M. Grunloh, J. H. Postlethwait and D. A. Rubin (2012). "Duplicated zebrafish co-orthologs of parathyroid hormone-related peptide (PTHrP, Pthlh) play different roles in craniofacial skeletogenesis." J Endocrinol **214**(3): 421-435.

Yan, Y. L., C. T. Miller, R. M. Nissen, A. Singer, D. Liu, A. Kirn, B. Draper, J. Willoughby, P. A. Morcos, A. Amsterdam, B. C. Chung, M. Westerfield, P. Haffter, N. Hopkins, C. Kimmel and J. H. Postlethwait

(2002). "A zebrafish sox9 gene required for cartilage morphogenesis." Development **129**(21): 5065-5079.

Yan, Y. L., J. Willoughby, D. Liu, J. G. Crump, C. Wilson, C. T. Miller, A. Singer, C. Kimmel, M. Westerfield and J. H. Postlethwait (2005). "A pair of Sox: distinct and overlapping functions of zebrafish sox9 co-orthologs in craniofacial and pectoral fin development." Development **132**(5): 1069-1083.

Yang-Yen, H. F. (2006). "Mcl-1: a highly regulated cell death and survival controller." J Biomed Sci **13**(2): 201-204.

Yoshida, C. A., H. Yamamoto, T. Fujita, T. Furuichi, K. Ito, K. Inoue, K. Yamana, A. Zanma, K. Takada, Y. Ito and T. Komori (2004). "Runx2 and Runx3 are essential for chondrocyte maturation, and Runx2 regulates limb growth through induction of Indian hedgehog." Genes Dev **18**(8): 952-963.

You, L., S. Temiyasathit, P. Lee, C. H. Kim, P. Tummala, W. Yao, W. Kingery, A. M. Malone, R. Y. Kwon and C. R. Jacobs (2008). "Osteocytes as mechanosensors in the inhibition of bone resorption due to mechanical loading." Bone **42**(1): 172-179.

Zajac, J. D. and J. A. Danks (2008). "The development of the parathyroid gland: from fish to human." Curr Opin Nephrol Hypertens **17**(4): 353-356.

Zanotti, S. and E. Canalis (2010). "Notch and the skeleton." Mol Cell Biol **30**(4): 886-896.

Zanotti, S. and E. Canalis (2012). "Notch regulation of bone development and remodeling and related skeletal disorders." Calcif Tissue Int **90**(2): 69-75.

Zanotti, S. and E. Canalis (2013). "Notch signaling in skeletal health and disease." Eur J Endocrinol **168**(6): R95-103.

Zenmyo, M., A. Tanimoto, H. Sakakima, M. Yokouchi, S. Nagano, T. Yamamoto, Y. Ishido, S. Komiya and K. Ijiri (2010). "Gadd45beta expression in chondrosarcoma: a pilot study for diagnostic and biological implications in histological grading." Diagn Pathol **5**: 69.

Zhang, C. (2012). "Molecular mechanisms of osteoblast-specific transcription factor Osterix effect on bone formation." Beijing Da Xue Xue Bao **44**(5): 659-665.

Zheng, C. L., T. Sumizawa, X. F. Che, S. Tsuyama, T. Furukawa, M. Haraguchi, H. Gao, T. Gotanda, H. C. Jueng, F. Murata and S. Akiyama (2005). "Characterization of MVP and VPARP assembly into vault ribonucleoprotein complexes." Biochem Biophys Res Commun **326**(1): 100-107.

Zhou, X. and P. D. Vize (2004). "Proximo-distal specialization of epithelial transport processes within the Xenopus pronephric kidney tubules." Dev Biol **271**(2): 322-338.

Zhu, H. and A. J. Bendall (2009). "Dlx5 Is a cell autonomous regulator of chondrocyte hypertrophy in mice and functionally substitutes for Dlx6 during endochondral ossification." PLoS One **4**(11): e8097.

Zhu, H., J. Zhao, W. Zhou, H. Li, R. Zhou, L. Zhang, H. Zhao, J. Cao, X. Zhu, H. Hu, G. Ma, L. He, Z. Yao, L. Yao and X. Guo (2012). "Ndrg2 regulates vertebral specification in differentiating somites." Dev Biol **369**(2): 308-318.

Zobel, B. B., R. Del Vescovo, G. Oliva, V. Russo and R. Setola (2012). "Assessing bone loss in micro-gravity: a fuzzy approach." Comput Methods Programs Biomed **108**(3): 910-921.

Zuniga, E., M. Rippen, C. Alexander, T. F. Schilling and J. G. Crump (2011). "Gremlin 2 regulates distinct roles of BMP and Endothelin 1 signaling in dorsoventral patterning of the facial skeleton." Development **138**(23): 5147-5156.

Publications and Congress

Publications

1. Aceto, J., R. Nourizadeh-Lillabadi, S. Bradamante, J. Maier, P. Alestrom, J.J.W.A. van Loon, and M. Muller (2015). "Effects of microgravity simulation on zebrafish transcriptomes and bone physiology." *Submitted*

2. Aceto, J., R. Nourizadeh-Lillabadi, R. Marée, N. Dardenne, N. Jeanray, L. Wehenkel, P. Aleström, J. J.W.A. van Loon and M. Muller (2015). "Zebrafish bone and general physiology are differently affected by hormones or changes in gravity. " *PLoS ONE*: 10(6), 1-42.

3. D. Beyens, L. Carotenuto, J.J.W.A.van Loon, M.Zell (Eds) (2011). "Areas of Research: Life sciences: Animal Physiology. Laboratory Science with Space Data: Accessing and using space-experiment data". Springer Science & Business. p123-129: E. Horn, J.J.W.A. van Loon, J.Aceto and M.Muller.

4. O. Stern, R. Marée, J. Aceto, N. Jeanray, M. Muller, L. Wehenkel and P. Geurts (2011). "Automatic Localisation of interest points in Zebrafish images with tree-based methods." *Pattern Recognition in Bioinformatics* ; 7036.

5. Aceto, J., R. Nourizadeh-Lilladadi, J. van Loon, P. Motte, P. Alestrom, J. A. Martial and M. Muller (2009). "Microgravity simulation comparison at genome level in Danio rerio and role of Sox4 transcription factors in cranial skeleton development." J Gravit Physiol **16**: in press.

6. Muller, M., J. Dalcq, V. Pasque, J. Aceto, P. Motte and J. A. Martial (2009). "The function of the Egr1 transcription factor in cartilage formation and adaptation to microgravity in Danio rerio." J Gravit Physiol **16**: in press.

7. Aceto, J., M. Muller, R. Nourizadeh-Lillabadi, P. Alestrom, J. Van Loon, V. Schiller, R. Goerlich, J. Renn and C. Winkler (2008). "Small fish species as powerful model systems to study vertebrate physiology in space." J Gravit Physiol **15**: 111-112.

8. J. Aceto, P. Motte and al (2008). J. Aceto, P. Motte and al. "The function of the HMG-box transcription factors Sox4a and Sox4b in zebrafish bone development and homeostasis." *Journal of Gravitational Physiology: A journal of the International Society for Gravitational Physiology*, 15.

Congress

1. 2nd Interdisciplinary Approaches in Fish Skeletal Biology, 26-28/04/2011 in Tavira, Portugal. Poster presentation:"Microgravity Simulations and Hypergravity Effects on Skeleton Development in Zebrafish."

2. European Congress on Osteoporosis and Osteoarthritis, 23-26/03/2011 in Valence, Spain. Poster presentation: "The function of sox4 Transciption Factor in zebrafish Bone Development and Homeostasis."

3. ASBMR, 15-19/10/2010 in Toronto, Canada. Poster presentation: "The function of sox4 Transciption Factor in zebrafish Bone Development and Homeostasis."

4. Price poster at the ISGP, 24-29/05/2009 in Xi'an, Chine. "Whole Genome Expression Modulation by simulated Microgravity and sox4 Transciption Factor in Skeleton Development in *Danio rerio*."

5. Life in Space for life on Earth, 22-26/06/2008 in Angers, France.
Oral presentation: "Small Fish Species as Powerfull Model Systems to Study Physiology in Space".
Poster presentation: "The function of the HMG-box Transcription factor sox4a and sox4b in Zebrafish Bone Development and Homeostasis."